frontiers | Research Topics

Women in molecular and cellular oncology, volume II: 2022

Edited by
Sharon Prince, Shilpa S. Dhar and Erika Ruiz-Garcia

Published in
Frontiers in Oncology

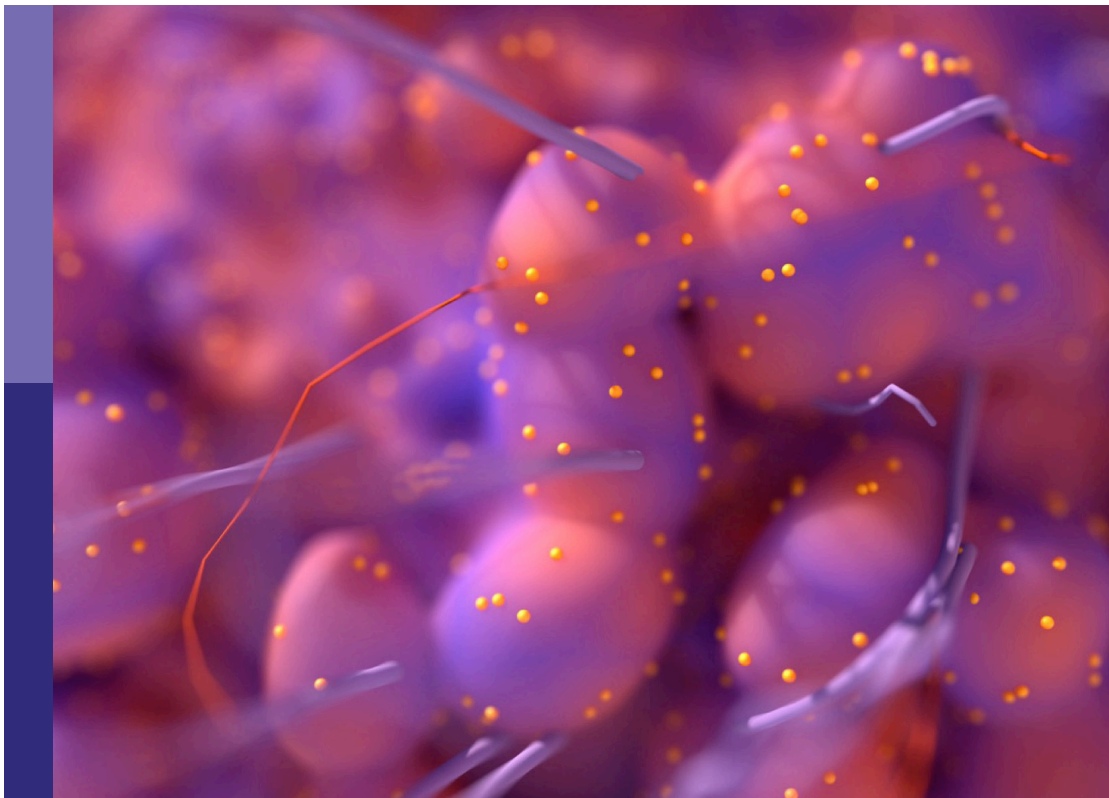

ISSN 1664-8714
ISBN 978-2-8325-2543-2
DOI 10.3389/978-2-8325-2543-2

About Frontiers

Frontiers is more than just an open access publisher of scholarly articles: it is a pioneering approach to the world of academia, radically improving the way scholarly research is managed. The grand vision of Frontiers is a world where all people have an equal opportunity to seek, share and generate knowledge. Frontiers provides immediate and permanent online open access to all its publications, but this alone is not enough to realize our grand goals.

Frontiers journal series

The Frontiers journal series is a multi-tier and interdisciplinary set of open-access, online journals, promising a paradigm shift from the current review, selection and dissemination processes in academic publishing. All Frontiers journals are driven by researchers for researchers; therefore, they constitute a service to the scholarly community. At the same time, the *Frontiers journal series* operates on a revolutionary invention, the tiered publishing system, initially addressing specific communities of scholars, and gradually climbing up to broader public understanding, thus serving the interests of the lay society, too.

Dedication to quality

Each Frontiers article is a landmark of the highest quality, thanks to genuinely collaborative interactions between authors and review editors, who include some of the world's best academicians. Research must be certified by peers before entering a stream of knowledge that may eventually reach the public - and shape society; therefore, Frontiers only applies the most rigorous and unbiased reviews. Frontiers revolutionizes research publishing by freely delivering the most outstanding research, evaluated with no bias from both the academic and social point of view. By applying the most advanced information technologies, Frontiers is catapulting scholarly publishing into a new generation.

What are Frontiers Research Topics?

Frontiers Research Topics are very popular trademarks of the *Frontiers journals series*: they are collections of at least ten articles, all centered on a particular subject. With their unique mix of varied contributions from Original Research to Review Articles, Frontiers Research Topics unify the most influential researchers, the latest key findings and historical advances in a hot research area.

Find out more on how to host your own Frontiers Research Topic or contribute to one as an author by contacting the Frontiers editorial office: frontiersin.org/about/contact

Women in molecular and cellular oncology, volume II: 2022

Topic editors

Sharon Prince — University of Cape Town, South Africa

Shilpa S. Dhar — University of Texas MD Anderson Cancer Center, United States

Erika Ruiz-Garcia — National Institute of Cancerology (INCAN), Mexico

Citation

Prince, S., Dhar, S. S., Ruiz-Garcia, E., eds. (2023). *Women in molecular and cellular oncology, volume II: 2022*. Lausanne: Frontiers Media SA.

doi: 10.3389/978-2-8325-2543-2

Table of contents

05 Editorial: Women in molecular and cellular oncology, volume II: 2022
Shilpa S. Dhar

08 FNC: An Advanced Anticancer Therapeutic or Just an Underdog?
Daria Fayzullina, Rajesh Kumar Kharwar, Arbind Acharya, Anton Buzdin, Nicolas Borisov, Peter Timashev, Ilya Ulasov and Byron Kapomba

16 CAR Co-Operates With Integrins to Promote Lung Cancer Cell Adhesion and Invasion
Claudia Owczarek, Elena Ortiz-Zapater, Jana Kim, Efthymia Papaevangelou, George Santis and Maddy Parsons

31 Heat Shock Proteins and HSF1 in Cancer
Anna M. Cyran and Anatoly Zhitkovich

52 RNA Demethylase ALKBH5 Prevents Lung Cancer Progression by Regulating EMT and Stemness *via* Regulating p53
Xiangli Liu, Ziyi Wang, Qiwei Yang, Xiaohai Hu, Qiang Fu, Xinyu Zhang and Wenya Li

66 Case Report: *GNAQ*- and *SF3B1* Mutations in an Aggressive Case of Relapsing Uveal Ring Melanoma
Michelle Prasuhn, Josephine Christin Freitag, Sabine Lüken, Vinodh Kakkassery, Hartmut Merz, Almuth Caliebe, Malte Spielmann, Mahdy Ranjbar and Felix Rommel

72 YY1 Is a Key Player in Melanoma Immunotherapy/Targeted Treatment Resistance
Dominika Kwiatkowska, Ewelina Mazur and Adam Reich

80 Mambalgin-2 Inhibits Lung Adenocarcinoma Growth and Migration by Selective Interaction With ASIC1/α-ENaC/γ-ENaC Heterotrimer
Anastasia V. Sudarikova, Maxim L. Bychkov, Dmitrii S. Kulbatskii, Vladislav I. Chubinskiy-Nadezhdin, Olga V. Shlepova, Mikhail A. Shulepko, Sergey G. Koshelev, Mikhail P. Kirpichnikov and Ekaterina N. Lyukmanova

97 Resistance Training Attenuates Activation of STAT3 and Muscle Atrophy in Tumor-Bearing Mice
Mayra Tardelli de Jesus Testa, Paola Sanches Cella, Poliana Camila Marinello, Fernando Tadeu Trevisan Frajacomo, Camila de Souza Padilha, Patricia Chimin Perandini, Felipe Arruda Moura, José Alberto Duarte, Rubens Cecchini, Flavia Alessandra Guarnier and Rafael Deminice

109 Non-Coding RNAs and Oral Cancer: Small Molecules With Big Functions
Leila Erfanparast, Mohammad Taghizadieh and Ali Akbar Shekarchi

140 Suppressor of fused associates with dissemination patterns in patients with glioma
María Peris-Celda, Josefa Carrión-Navarro, Irina Palacín-Aliana, Pilar Sánchez-Gómez, Ricardo Prat Acín, Noemi Garcia-Romero and Angel Ayuso-Sacido

150 Role of extracellular matrix architecture and signaling in melanoma therapeutic resistance
Ana Popovic and Sophie Tartare-Deckert

164 A major role for Nrf2 transcription factors in cell transformation by KSHV encoded oncogenes
Daiana Sapochnik, Ana R. Raimondi, Victoria Medina, Julian Naipauer, Enrique A. Mesri and Omar Coso

182 CDK7 is a prognostic biomarker for non-small cell lung cancer
Christiane Kuempers, Tobias Jagomast, Carsten Heidel, Finn-Ole Paulsen, Sabine Bohnet, Stefanie Schierholz, Eva Dreyer, Jutta Kirfel and Sven Perner

192 HLA-BAT1 alters migration, invasion and pro-inflammatory cytokines in prostate cancer
Aileen M. García-Vargas, Yarelis M. Roque-Reyes, Desiree M. Arroyo-Villegas, Daniel Santiago-Negron, María M. Sánchez-Vázquez, Alejandro Rivera-Torres, Andrea C. Reyes-Meléndez, Valerie Cardona-Berdecía, Miosotis García-Maldonado, Olga M. Víquez and Magaly Martínez-Ferrer

frontiers | Frontiers in Oncology

TYPE Editorial
PUBLISHED 01 September 2023
DOI 10.3389/fonc.2023.1272365

OPEN ACCESS

EDITED AND REVIEWED BY
Luisa Lanfrancone,
European Institute of Oncology (IEO), Italy

*CORRESPONDENCE
Shilpa S. Dhar
ssdhar@mdanderson.org

RECEIVED 03 August 2023
ACCEPTED 22 August 2023
PUBLISHED 01 September 2023

CITATION
Dhar SS (2023) Editorial: Women in molecular and cellular oncology, volume II: 2022.
Front. Oncol. 13:1272365.
doi: 10.3389/fonc.2023.1272365

Editorial: Women in molecular and cellular oncology, volume II: 2022

Shilpa S. Dhar*

Department of Molecular & Cellular Oncology, The University of Texas M. D. Anderson Cancer Center, Houston, TX, United States

KEYWORDS

women, molecular oncology, therapeutic targets, cancer, tumor microenvironment

Editorial on the Research Topic
Women in molecular and cellular oncology, volume II: 2022

The COVID-19 emergency has worsened existing inequalities, especially those related to sex and gender. Women have been disproportionately affected, experiencing increased violence and caregiving responsibilities during lockdowns, economic hardships, disrupted health services, and school closures (1). Unfortunately, progress toward gender equality has been eroded by early 2023 (2, 3). Therefore, it's crucial to prioritize gender in addressing global challenges to create a more equitable world. Women in oncology, including clinical trials, have made significant contributions, advancing cancer research and treatment on par with men. Despite facing historical biases, they excel in molecular and cellular oncology and foster diverse collaborations. Empowering women in this field requires promoting mentorship, supportive work environments, gender equality in funding, and leadership roles. By embracing the potential of all scientists, we can accelerate the fight against cancer and improve treatments. This article aims to highlight women scientists' diverse research in oncology. This impressive Research Topic highlights 14 distinguished articles on various forms of cancer, all of which were authored by remarkable women.

Lung cancer is the top cause of cancer deaths; it surpasses the combined deaths from breast, prostate, and pancreatic cancers (4). Liu et al. investigated the role of m6A demethylase ALKBH5 in non-small-cell lung cancer-derived cancer stem-like cells (CSCs). The study revealed that ALKBH5 is highly expressed in lung CSCs, positively correlated with p53. Knocking down ALKBH5 reduced stem markers and inhibited stemness, while p53 knockdown decreased ALKBH5 expression and malignancies. This p53/ALKBH5 axis may be a potential therapeutic target for NSCLC.

Moreover, CDK7 was significantly overexpressed in squamous cell carcinomas compared to adenocarcinomas, with high CDK7 levels linked to worse overall and disease-free survival in NSCLC patients. Kuempers et al. proposed CDK7 as a promising prognostic biomarker for NSCLC and a potential target for future anticancer therapies.

Furthermore, Owczarek et al. investigated that The CAR protein, highly expressed in lung cancer, promotes tumor growth through increased cell adhesion and enhanced b1 integrin activity, leading to invasion in 3D models. CAR forms a complex with focal adhesion proteins,

activating the GTPase Rap1, which mediates enhanced integrin activation and potentially contributes to lung cancer metastasis.

Targeted therapies are crucial for lung cancer with low survival rates. Ion channels called Acid sensors like ion channels (ASICs) are promising targets that detect changes in pH levels within the tumor microenvironment. Several types of ASICs and degenerin/epithelial Na+ channel (DEG/ENaC) and ENaC subunits can form different channels, influencing how cells respond to stimuli. Sudarikova et al. demonstrated that Mambalgin-2 inhibits the growth and migration of lung adenocarcinoma cells by inducing G2/M cell cycle arrest and apoptosis. It targets ASIC1a/α-ENaC/-γENaC heterotrimeric channels, bypassing resistance mechanisms in bulky tumors, thus holding potential for novel channel-targeting anticancer drugs.

Malignant melanoma, a highly aggressive skin malignancy causing significant global mortality, exhibits an intriguing duality. While it contributes to numerous deaths, it also sparks a robust anti-tumor immune response, one of the most immunogenic cancers. Kwiatkowska et al. has compiled data showing that the transcription factor Yin Yang 1 (YY1) is key in cancer progression. It controls genes related to cell death, immune response, and metastasis. It also affects melanoma survival, proliferation, and stem cell-related transcription factors. Focusing on YY1 and its pathways can lead to novel therapeutic strategies, improving melanoma treatment. More research is needed to determine its specific role in pathogenesis, progression, and drug resistance for potential therapeutic breakthroughs.

Another exciting review was presented by Popovic and Tartare-Decket about the extracellular matrix (ECM) as a critical component for tissue homeostasis. Changes in the ECM structure of melanoma tumors increase stiffness, promoting disease progression and poor survival rates. Melanoma cells interact with the ECM through receptors, secreted factors, or enzymes. Stromal fibroblasts deposit and remodel the ECM, enabling interactions with melanoma cells. Understanding ECM properties is critical to understanding melanoma progression and resistance. Targeting ECM abnormalities with therapies has the potential to improve treatment outcomes.

Prasuhn et al. describes a case report of a patient with malignant uveal melanoma and exudative retinal detachment, treated with plaque brachytherapy resulting in tumor regression. After one year, a ring-shaped recurrence with extraocular extension appeared, necessitating enucleation. Genetic analyses revealed GNAQ and SF3B1 mutations not previously reported in ring melanoma. Ring melanoma is a rare and aggressive variant of uveal melanoma with limited treatment options. Regular follow-up and genetic testing are essential to monitor disease progression and identify potential therapeutic targets. This case sheds light on the genetic background of ring melanoma, contributing to the development of personalized treatment strategies.

Prostate cancer (PCa) is a significant health concern for men, leading to numerous diagnoses and cancer-related deaths. Despite successful treatments, recurrence remains a challenge. Garcı´a-Vargas et al. explored the role of HLA-B-associated transcript 1 (BAT1) in PCa. BAT1 was found to be differentially expressed in patients with varying Gleason scores. This report suggests that BAT1 expression plays a role in prostate cancer. Reducing BAT1 increases cell migration and inflammation, while overexpression decreases these processes. By understanding BAT1's role, one can develop better treatments for recurrent PCa.

Erfanparast et al. presented a detailed review of Oral cancer and non-coding RNAs (ncRNAs). Despite advancements in treatment, the five-year survival rate remains low, and the molecular mechanisms underlying oral cancer development are not fully understood. Noncoding RNAs (ncRNAs), including microRNAs, long ncRNAs, and circular RNAs, play crucial roles in cancer cell development, including cell death processes such as apoptosis and autophagy. Understanding the regulatory relationships between ncRNAs and cell death pathways is critical in developing targeted therapies for oral cancer. Manipulating the expression of apoptosis-regulating ncRNAs may represent a strategy to combat carcinogenesis and enhance the response to chemotherapy and radiotherapy. Identifying and profiling ncRNAs in clinical samples can aid in predicting patient responses to treatments and designing personalized therapeutic strategies for oral cancer.

Gliomas, the most common brain tumors, are known for their poor prognosis due to tumor cell migration and invasion in the brain. Peris-Celda et al. found that high levels of SuFu, a molecular mediator in this pathway, were associated with increased dissemination patterns in glioma patients. Further experiments showed that SuFu overexpression increased cancer stemness properties and a migratory phenotype in Glioblastoma Cancer Stem Cells (GB CSCs). Further research is needed to confirm its role as a mediator of tumor spread and develop effective blocking agents for improved patient outcomes.

Resistance training (RT) in tumor-bearing mice can prevent cancer-induced muscle atrophy. Testa et al. investigated the role of signal transducers and activators of transcription (STAT3) in mediating muscle atrophy and the effects of RT on its activation. Resistance training can prevent muscle atrophy caused by cancer in mice by reducing STAT3 activation, downregulating key genes and proteins, and improving strength and locomotor capacity. This also leads to improved quality of life for cancer patients.

Sapochnik et al. have suggested that targeting Nrf2 and its associated proteins could be a promising therapeutic approach for treating Kaposi's sarcoma (KS), a frequently occurring tumor in individuals with AIDS.

Cyran and Zhitkovich conducted a detailed analysis of how heat-shock response (HSR) is activated to manage high levels of proteotoxic stress experienced by cancer cells because of gene mutations and dysregulation. This results in an increase in heat shock proteins (HSPs) and HSF1. High levels of HSR components are linked to drug resistance and poor clinical outcomes in cancer. Targeting the HSR pathway is a promising approach for treating human malignancies as it is a common vulnerability in cancer cells.

Fayzullina et al. described Azvudine (FNC) as a novel cytidine analog with antiviral and anticancer properties. Its inhibitory effects on RNA viruses and retroviruses, including HIV and SARS-COV-2, make it a promising antiviral agent. FNC can impede malignant cell growth and induce apoptosis as an anticancer drug. Further research is needed to understand its precise mechanisms of action. As a group of female scientists who have contributed 14 exciting articles to the Women in Molecular and Cancer Oncology 2022 edition, we strongly advocate for gender equality in oncology

research. By providing more opportunities for women to conduct research, we can enhance the quality and impact of our work, ultimately benefiting all cancer patients. Our goal is to promote progress toward gender equality in the field, and we are dedicated to making this a reality.

Author contributions

SD: Conceptualization, Visualization, Writing – original draft, Writing – review & editing.

Acknowledgments

I am grateful to the other editors for their invaluable contributions, especially Sharon Prince and Erika Ruiz-Garcia. Thanks to the authors for their dedicated work on this Research Topic.

Conflict of interest

The author declares that the research was conducted in the absence of any commercial or financial relationships that could be construed as a potential conflict of interest.

The author(s) declared that they were an editorial board member of Frontiers, at the time of submission. This had no impact on the peer review process and the final decision

Publisher's note

References

1. Ryan M, Tuke J, Hutchinson MR, Spencer SJ. Gender-specific effects of COVID-19 lockdowns on scientific publishing productivity: Impact and resilience. *Soc Sci Med* (2023) 320:115761. doi: 10.1016/j.socscimed.2023.115761

2. Bedi G, Van Dam NT, Munafo M. Gender inequality in awarded research grants. *Lancet* (2012) 380(9840):474. doi: 10.1016/S0140-6736(12)61292-6

3. Teixeira da Silva JA, Dobranszki J. Gender inequality or gender inversion? Gender comparison of several ethics and research integrity groups, ethics and research integrity journals, and sex and gender journals. *Arch Sex Behav* (2019) 48(7):1893–7. doi: 10.1007/s10508-019-01495-y

4. Viale PH. The american cancer society's facts & Figures: 2020 edition. *J Adv Pract Oncol* (2020) 11(2):135–6. doi: 10.6004/jadpro.2020.11.2.1

frontiers in Oncology

MINI REVIEW
published: 10 February 2022
doi: 10.3389/fonc.2022.820647

FNC: An Advanced Anticancer Therapeutic or Just an Underdog?

*Daria Fayzullina[1], Rajesh Kumar Kharwar[2], Arbind Acharya[3], Anton Buzdin[1], Nicolas Borisov[4], Peter Timashev[1], Ilya Ulasov[1] and Byron Kapomba[5]**

[1] World-Class Research Center "Digital Biodesign and Personalized Healthcare", Sechenov First Moscow State Medical University, Moscow, Russia, [2] Endocrine Research Lab, Department of Zoology, Kutir Post Graduate College, Chakkey, Jaunpur, India, [3] Tumor Immunology Lab, Department of Zoology, Institute of Science, Banaras Hindu University, Varanasi, India, [4] Department of Medical and Biological Physics, Moscow Institute of Physics and Technology, Dolgoprudny, Russia, [5] Department of General Surgery, Parirenyatwa Group of Hospitals, Harare, Zimbabwe

Azvudine (FNC) is a novel cytidine analogue that has both antiviral and anticancer activities. This minireview focuses on its underlying molecular mechanisms of suppressing viral life cycle and cancer cell growth and discusses applications of this nucleoside drug for advanced therapy of tumors and malignant blood diseases. FNC inhibits positive-stand RNA viruses, like HCV, EV, SARS-COV-2, HBV, and retroviruses, including HIV, by suppressing their RNA-dependent polymerase enzymes. It may also inhibit such enzyme (reverse transcriptase) in the human retrotransposons, including human endogenous retroviruses (HERVs). As the activation of retrotransposons can be the major factor of ongoing cancer genome instability and consequently higher aggressiveness of tumors, FNC has a potential to increase the efficacy of multiple anticancer therapies. Furthermore, FNC also showed other aspects of anticancer activity by inhibiting adhesion, migration, invasion, and proliferation of malignant cells. It was also reported to be involved in cell cycle arrest and apoptosis, thereby inhibiting the progression of cancer through different pathways. To the date, the grounds of FNC effects on cancer cells are not fully understood and hence additional studies are needed for better understanding molecular mechanisms of its anticancer activities to support its medical use in oncology.

Keywords: FNC, oncology, nucleoside (acid) analogues, azvudine, cancer

OPEN ACCESS

Edited by:
Massimiliano Berretta, University of Messina, Italy

Reviewed by:
Bryan E. Strauss, Universidade de São Paulo, Brazil

****Correspondence:***
Byron Kapomba
byronkaps@gmail.com

Specialty section:
This article was submitted to Molecular and Cellular Oncology, a section of the journal Frontiers in Oncology

Received: *23 November 2021*
Accepted: *13 January 2022*
Published: *10 February 2022*

Citation:
Fayzullina D, Kharwar RK, Acharya A, Buzdin A, Borisov N, Timashev P, Ulasov I and Kapomba B (2022) FNC: An Advanced Anticancer Therapeutic or Just an Underdog? Front. Oncol. 12:820647. doi: 10.3389/fonc.2022.820647

INTRODUCTION

Despite the best efforts of mankind, cancer remains one of the major causes of death worldwide (approximately 10 million deaths in 2020). Moreover, the proportion of cancer-associated deaths demonstrates a growing trend (https://www.who.int/ru/news-room/fact-sheets/detail/cancer, https://www.who.int/ru/news-room/fact-sheets/detail/the-top-10-causes-of-death). Many effective cancer drugs have been developed over the past decades, although none of them can guarantee to the patient long-lasting survival and protection against relapse (1). Different drugs have different molecular mechanisms, different clinical indications, and different response rates. In addition, cancers can frequently develop drug resistance, thus creating a barrier to effective tumor control (2).

This stresses the importance of finding novel cancer treatment approaches, their proper combination, and their personalization (3).

FNC (2'-deoxy-2'-β-fluoro-4'-azidocytidine) (**Figure 1**) also known as Azvudine is a recently developed cytidine analogue. It is a new experimental drug that has been shown to be active against viruses and retrotransposons with RNA-dependent polymerase enzymes, as well as against cancer cell lines and xenografts in animal models (4–6). Anticancer activities of FNC at least in part can be linked with its inhibition of retrotransposons which had formed about 30-40% of the human DNA (7, 8). The transcriptional activation of retrotransposons including HERVs has been reported to be a consequence of multiple systemic intracellular factors (9) such as the stress response, epigenetic reprogramming, and intracellular pathways triggered by the hormones, growth factors, and cytokines (10).

The expression of retrotransposons and HERVs is tightly controlled in a normal cell with most of the elements being transcriptionally repressed (11). However, in cancer cells due to an overall deregulated epigenetic and transcriptional control, there is a strong transcriptional reactivation of retrotransposons and HERVs, which also play a role of major genomic regulatory elements (12). Many cancer types were shown to be associated with the reactivation of retrotransposons and HERVs: breast cancer (13), prostate cancer (14), melanoma (15), ovarian cancer (16), hepatocelular carcinoma (17), germ cell tumors (18), renal cell carcinoma (19, 20), leukemia (21), glioblastoma (22), and osteosarcoma (23). Retrotransposons can drive tumorigenesis through different mechanisms.

Their life cycle comprises transcription of their genomic copy and further reverse transcription of the respective RNAs, *i.e.* generation of a cDNA copy on an RNA template (**Figure 2A**). The reverse-transcribed cDNA then integrates into a new genomic site to generate a new copy of retrotransposon. Most of such copies accumulated mutations and contain, if any, only interrupted/truncated non-functional open reading frames (24). However, there is a fraction of few hundred active human retrotransposons that harbor a functional reverse transcriptase (RT) gene (25) and, therefore, can mediate genomic insertion of new copies (25). Interestingly, most part of the active human retrotransposons is presented by the elements that don't code for RT but instead utilize for their proliferation reverse transcriptase from the other elements. Indeed, the number of active non-autonomous retrotransposons of the Alu and SVA families is one or two orders higher than the number of autonomous elements with fully functional RT (26). Their functional reactivation in cancer can result in a dramatic increase of retrotransposition events, *i.e.* generation of their novel genomic copies (27). Interestingly, similar effects were observed also in other long-term stress conditions such as the retroviral infection by HIV (28).

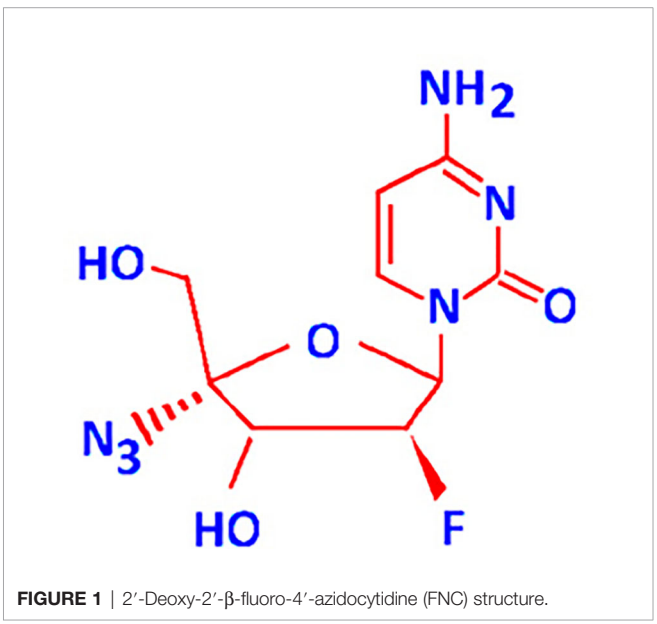

FIGURE 1 | 2′-Deoxy-2′-β-fluoro-4′-azidocytidine (FNC) structure.

It should be mentioned that all human retrotransposons are repetitive sequences presented in the genome by hundreds or thousands of copies (29). They totally occupy nearly 40% of the human DNA and may serve as the substrates for recombination, especially with the newly inserted copies (8). Such recombinations can occur especially frequently in cancers, where DNA repair mechanisms function abnormally (30). These recombinations lead to various genomic rearrangements and gene conversion events, including deletions, translocations, and amplifications (25).

Alternatively, transcriptional reactivation of retrotransposons in cancer can lead to expression of HERV-encoded oncogenic proteins that can influence passing through the cell cycle checkpoints, and possess fusogenic and immunosuppressive activities (31, 32). On the other hand, massive expression of multiple normally-silent retrotransposon copies may result in the appearance of novel antigens that are presented by the major histocompatibility complex (MHC) molecules. The latter can provoke specific immune response (33), which can be a specific anticancer protective mechanism.

Nowadays, there is a growing evidence that the expression of retrotransposons, especially HERVs, is connected with cancer manifestation (17). Moreover, cancer cells with stemness features and expressing HERVs may exhibit sensitivity to antiretroviral drugs treatment (10).

This review focuses on the potential action of FNC to treat aggressive tumors in combination with chemotherapeutic and/or immunotherapy regimens. We consider known and potential mechanisms of action of FNC as the anti-cancer therapeutic and their crosslinks with its antiviral activities.

STRUCTURE OF FNC

FNC is a recently developed nucleoside analogue (1). Nucleosides consist of a nucleobase and a ribose or deoxyribose sugar residue, thus showing considerable structural similarity to normal nucleotides. FNC is a 4′-C-substituted-2′-deoxynucleoside with a 3′-OH group. It mimics 2′-deoxynucleosides, and its 2′-fluoro

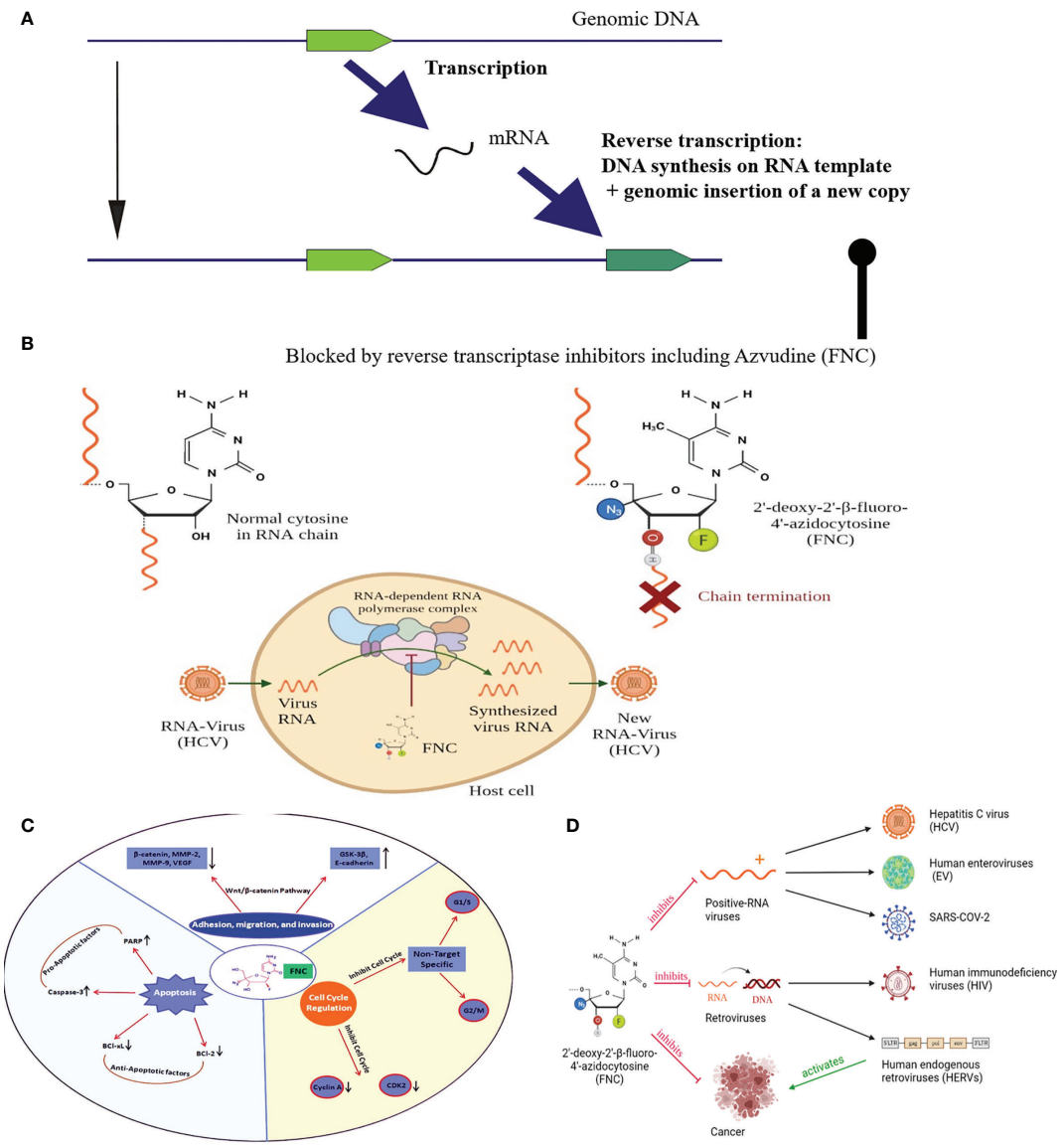

FIGURE 2 | **(A)** Schematic representation of retrotransposon/HERV life cycle; **(B)** Mechanism of FNC-triggered chain termination. The 3′-OH group of FNC is unlikely to be used by polymerases for elongation of proviral RNA synthesis.; **(C)** Representation of antitumor mehanisms of FNC through multiple molecular pathways. FNC promotes apoptosis by decreasing Bcl-xL and Bcl-2 and activation of caspase-3 which further regulates proteolytic cleavage of many key proteins such as PARP. FNC inhibits the adhesion, migration and invasion of Raji and JeKo-1 cell lines by up-regulating the expression of E-cadherin and GSK-3β proteins and down-regulating the expression of proteins such as β-catenin, VEGF, MMP-2 and MMP-9. Wnt/β-catenin signaling pathway has a crucial position in the development and promotion of a wide variety of cancers. Activated Wnt/β-catenin changing the E-cadherin-β-catenin complex expression is significantly coupled with the invasiveness of tumor cells. FNC is a cell cycle-nonspecific agent which causes G1/S or G2/M phase cell cycle arrest and induces apoptosis. It inhibits cell cycle checkpoint activation (e.g., Cyclin-A binding to CDK2 permits cells to complete S phase and enter to M phase); **(D)** Graphic Abstract, depicts the possible mechanisms of FNC anticancer and antiviral activities.

substituent improves its stability in acidic media (34). The 4′-C-substituted 2′-deoxynucleosides retain all functional groups of 2′-deoxynucleosides. Thus, FNC can compete with the cellular internally-generated nucleotides for the incorporation into DNA and RNA strands, which results in attenuated nucleotide synthesis, and interferes with cell growth and division (35). The modification in the second position makes viral RNA-dependent polymerases more sensitive to FNC. In this case, the molecule can be incorporated into both RNA and DNA – in the second position it has fluorine, and not the functional group that determines the sugar residue type (36). FNC is also a preferred substrate for deoxycytidine kinase, and it is phosphorylated with up to 3-fold higher efficiency than its prototype, deoxycytidine (36).

PHARMACOLOGICAL MECHANISMS OF FNC

FNC and Positive-Strand RNA Viruses

FNC was first synthesized in 2009 among many potential therapeutic molecules for screening more specific treatments of the Hepatitis C virus (HCV) (37). It showed up to 125 times greater efficacy than the previously used treatment, and the effect was more selective (38). Since HCV often cause chronic disease that may result in liver cirrhosis or hepatocellular carcinoma, it is important to detect this infection as early as possible to start treatment. The major antiviral mechanism of FNC is thought to be the inhibition of viral replication. When FNC is incorporated into viral RNA newly synthesized by the HCV RNA-dependent RNA polymerase NS5B, it causes preliminary chain termination and, therefore, nonfunctional viral genomic RNA (**Figure 2B**) .

Similarly, RNA synthesis by the RNA-dependent RNA polymerase can be interrupted for other viruses as well. For example, Na Xu et al. (6). showed for the first time that FNC can be used as an effective inhibitor for broad spectrum of human enterovirus (EV) pathogens. With high specificity and efficiency, the nucleoside analog is inserted into the positive or negative RNA strand by EV71 viral RNA-dependent RNA polymerase 3Dpol and results in truncated viral RNAs, as shown by quantitative real-time reverse transcription-PCR (RT-qPCR). The same mechanism is suggested also for the FNC antiviral activity on SARS-COV-2, another virus with the sense single-stranded RNA genome (39).

FNC and Retroviruses

FNC also may function as the nucleoside reverse transcriptase inhibitor (NRTI), being a potentially effective agent for the treatment of retroviral infections. Being preferred targets for cellular nucleotide kinases, fluoronucleosides can serve as the good substrates for RNA and DNA polymerases. The triphosphates of nucleoside analogs compete with the cellular endogenous deoxyribonucleotides for the incorporation into DNA during replication. FNC mimics dN, and both viral and cellular replication complexes can mistakenly include it in the newly synthesized chain. The 3′-OH group of FNC is unlikely to be used by polymerases for elongation of viral DNA synthesis, and may cause immediate chain termination of replication by blocking further addition of nucleotide residues (40). Due to its chemical modifications, FNC is targeted for viral RNA-dependent polymerases, which is why it has low cytotoxicity (6).

To date, FNC is at various stages of clinical and preclinical trials for many infectious agents, and is an approved anti-HIV drug – Azvudine (6). Emerging drug-resistant viral strains as well as long-term toxicity are the main problem in current antiviral chemotherapy (41). Unlike previous NRTIs (e.g., Lamivudine), development of drug resistance against FNC requires different kind of genetic mutations. Thus, FNC could be included in an anti-AIDS treatment pipeline to overcome drug resistance issues with other drugs (42).

In addition to nanomolar activity against NRTI-resistant and multi-resistant HIV strains, it was noted that FNC is extremely potent against HIV-1 wild-type strain without obvious cytotoxicity (43). Azvudine has been also shown to be effective against HIV-2 *in vitro* (44), and demonstrates a long-lasting inhibition of HIV infection. A possible mechanism has been proposed by Sun et al. (40): in FNC-treated HIV-1 patients, FNC can restore APOBEC3 (A3G) expression in CD4+ T cells. FNC binds to the Vif-E3 ubiquitin ligase complex, enabling APOBEC3 to avoid Vif-induced ubiquitination and degradation. In turn, APOBEC3 may effectively restrict viral replication (45). In addition, FNC showed selective entry and long-term retention in HIV-1 target cells.

Nearly one-tenth of the patients with HIV are also infected with the Hepatitis B virus (HBV) due to a similar transmission path. Importantly, FNC was shown both *in vitro* and *in vivo* to restrict proliferation of human and duck hepatitis B viruses (HBV and DHBV, respectively) (46). Moreover, FNC is effective against both wild-type and lamivudine-resistant HBV clinical isolates (47). At the same time FNC showed low cytotoxicity, thus implying acceptable side effects of the treatment. For example, cytotoxicity test on the human hepatoma cell line HepG2 showed that FNC could not cause a 50% reduction of cell viability even at the concentration of 1,000 μM, which is ~200 fold higher than its physiological concentration in some previous treatments (47). Histopathological analysis also demonstrated hepatoprotective effect of FNC – less virus-induced damage to the liver was observed (5).

FNC and Cancer

Cancer cells also can be specifically affected by FNC (**Table 1**). First, FNC, as an antiviral drug, suppresses the activity of many viruses with oncogenic effects. In addition, as a nucleotide analogue, FNC demonstrates suppression of cell growth and active proliferation of cancer cells, apparently, penetrating the synthesized nucleic acid chain and causing chain termination (49). The sensitivity to antiretroviral drugs treatment for tumor initiating (stem) cells, expressing HERVs, was demonstrated (10).Specifically, HERV-K was implemented in the maintenance and plasticity of CD133-positive melanoma stem cells. As shown by Giovavinazzo et al., treatment of lung adenocarcinoma cells A549 and hepatocarcinoma HepG2 with reverse transcriptase inhibitors such as azidothymidine (AZT) and efavirenz (EFV) decreased clonogenic, cell growth and induce apoptosis. Moreover, there are a lot of side effects on different signaling pathways of the cell, the mechanisms of which require additional research.

FNC can suppresses tumor progression by inhibiting adhesion, migration, and invasion of tumor cells in a dose-dependent manner (50). This has been shown *in vitro* and *in vivo* for non-small-cell lung cancer (NSCLC) cell line H460, and for two human aggressive non-Hodgkin lymphoma cell lines Raji and JeKo-1. Both series of experiments showed that following FNC treatment the expression levels of MMP-2, MMP-9, and VEGF were suppressed while E-cadherin expression level was increased. Later, Zhang and colleagues (51) also reported increased GSK-3β expression following FNC treatment and concluded that FNC may be considered an effective chemotherapeutic agent by regulating the invasion and

TABLE 1 | FNC nucleoside analogues and cancer.

Sr. No.	Tumor type	Specific cell line	IC-50 Value [μM]	Reference
1.	Non-Hodgkin lymphoma	Raji	0.2	(48)
2	Non-Hodgkin lymphoma	JeKo-1	0.29	(4)
3.	B-cell non-Hodgkin lymphoma	SUDHL-6	4.55	(1)
4.	B-cell non-Hodgkin lymphoma	RL	1.74	(1)
5.	B-cell non-Hodgkin lymphoma	Granta-519	0.95	(1)
6.	Human non-small cell lung cancer	A549	1.22	(1)
7.	Acute myeloid leukemia	HL60	3.30	(1)

metastasis of aggressive non-Hodgkin lymphomas *via* inhibition of the Wnt/β-catenin signaling pathway.

Most of the studied aspects of FNC effect on cancer cells occur in a dose- and time-dependent manner. It is thought to inhibit cell growth by suppressing expression of CDKN1A, PML, TP53INP1, TNF, SPN and LST1 proteins (4). FNC also regulates the cell cycle. It may cause cell cycle arrest of a different period at different concentrations. The gene expression assay showed that *PRNP, TP53INP1, PRKAG2, SESN2, SESN3, ERN1, CDKN1A, PML* and *TCF7L2* genes are linked with the cell cycle arrest in the G1/S or G2/M phase (4). FNC can also influence gene expression through the regulation of DNA methylation (50).

The growth and development of a tumor are regulated not only by the activity of proliferation and the rate of cell growth but also by the intensity of apoptotic processes. FNC was reported to induce apoptosis by triggering both the cell death receptor-mediated extrinsic pathway (4), and mitochondrial apoptotic pathway (50) for different types of cancers. In the first case, FNC treatment significantly increased the protein expression of Fas, FasL and TNF-α. In addition, Zhang et al. (4) found that FNC treatment also affects expression levels of some other genes that play a role in the apoptosis: *CDKN1A, PML, BIRC3, CASP10* and *TNF-α.* In the second case, treatment of H460 cells with FNC inhibited Bcl-2 expression and potentiated Cytochrome C (Cyt-C) release, Bax and caspase-3 expression.

Modulating the immune system may be another important anti-tumor mechanism of FNC and should be investigated. In a study comparing the gene-expression profiles with and without FNC treatment, significant changes in the expression of several genes associated with immunity were shown. The co-stimulatory signal during T-cell activation and genes associated with IL-2, IL-4, IL-7, IL-10 pathways has been shown based on Biocarta (4). In addition, some HERVs have proven effects on the immune system too: protein products of the translation of retroviral sequences, for example, the Gag of the HERV-K gene, affect the interaction of cancer cells with the immune system (14, 19). Retroviruses' activity and metabolites, secreted by tumor microenvironment, inducing immunosuppressive activity along with other properties of the stem of cancer cells (10). HERVs also induces local immune checkpoint activation (19). Therefore, suppression of retroviral activity by FNC can lead to an increase in the effectiveness of immunotherapeutic strategies. Actually, targeting of the HERV-K envelope protein by CAR-T cells has already been reported as a potential immunotherapeutic approach for melanoma and other tumors (52).

Those pleiotropic effects of FNC on the cell growth, cell cycle arrest and apoptosis can be mediated by the independent reasons, or by the common functional nodes. For example, PML and CDKN1A are related to all the above processes (4). This suggests that FNC could be a potent pleiotropic molecule for treatment of multiple pathological conditions in cancer (**Figure 2C**). However, those studies may be considered fragmentary as they don't provide comprehensive high-throughput gene expression analysis connected with the FNC effects. Therefore, a series of more in-depth studies of the FNC molecular mechanism of action on the cell cycle and apoptosis will be critical to support its potential applicability in cancer therapy.

Thus, FNC can inhibit adhesion, migration, invasion, and proliferation of tumor cells, is involved in the cell cycle arrest, immune system process and apoptosis, thereby suppressing the progression of cancer. Therefore, FNC may affect the occurrence and development of tumors through multiple molecular pathways. For most of these processes, it has been shown that the impact of FNC occurs in a dose- and time-dependent manner.

The effectiveness of FNC has been already demonstrated *in vitro* and *in vivo* for the cell lines of NSCLC and lung adenocarcinoma (50), non-Hodgkin lymphomas (49), acute myeloid leukemia (1), and for mouse xenograft models of hepatocarcinoma (H22), sarcoma (S180), and gastric carcinoma (SGC7901) (1).

At the same time, FNC has demonstrated relatively low toxicity. For example, in the experiments with mantle cell lymphoma in SCID mice (4) the low- and medium-dose FNC groups did not demonstrate significant body weight loss compared to the negative control group. Further histopathological examination of the liver and kidney tissues revealed no signs of drug toxicity.

CLINICAL TRIALS OF FNC

FNC has nanomolar activity against NRTI-resistant and multi-resistant HIV strains. This is most probably due to different mutations involved in the viral resistance against previously used NRTIs, and FNC. Indeed, Wang et al. analyzed HIV strains resistant to FNC-, or previous generation NRTI (3TC – lamivudine), and found that in 3TC-resistant viruses the dominant mutation was M184V (valine replacing methionine at position 184 in the reverse transcriptase gene), which was

detected in only ~2% of FNC-resistant strains (44). FNC-resistant clones, in turn, had increased M184I mutation rate (44).

In a trial "Azvudine vs HIV-infection/AIDS, phase II (NCT04109183)", FNC was administered in the form of a tablet medicine. This was a phase II multicenter, randomized, double-blind, double-simulation, positive control trial with 172 participants. The subjects were randomized to the treatment group of 3TC (positive control) or different doses (from 2 to 4 mg per tablet) of FNC. The background drugs (reverse transcriptase inhibitors therapy) were Efavirenz and Tenofovir disoproxil fumarate. FNC showed no serious adverse effects, exhibited desirable pharmacokinetics, and met the efficacy endpoints (39), thus forming the basis for the third phase trials.

One of such trials has started in March 2020 by HeNan Sincere Biotech in China (Phase III Clinical Study of Azvudine in Hiv-infected Treatment Naive Patients, NCT04303598). Based on the results of the previous phase, the optimal dose of 3 mg tablet of active ingredient was chosen. This is a randomized, double-blind, double-simulated, active-controlled phase III trial with 720 participants enrolled evaluating the efficacy and safety of Azvudine combined with tenofovir fumarate and efavirenz in HIV-infected treatment naive patients. FNC in combination therapy is compared with 3TC, estimated completion date is August 2022.

Alternatively, the third phase clinical trial evaluating the use of Azvudine against SARS-COV-2 started on April 2021 and was estimated to be completed in December 2021. FNC has been successful against this infection in preclinical trials (53). Later on in a randomized, open-label, controlled clinical trial of FNC in the treatment of mild and common COVID-19 (a Pilot Study) it was found that FNC treatment of mild and common COVID-19 patients may shorten the time of nucleic acid negativity conversion versus standard antiviral treatment according to the "Diagnosis and treatment program trial version 5 (or 6) guidelines" issued by the National Health Commission of China. The term was reduced by an average of 4.5 days. During phase 1 of the trial, the climbing testing showed that 6 mg of FNC was still a safe dose, and a dose of 5 mg per day was chosen for further evaluations. No drug-related adverse effects were observed in patients treated with FNC versus ~30% after treatment with standard antiviral drugs (53).

CONCLUSION

Taken overall, FNC is a novel nucleoside analogue that has both antiviral and anticancer activities (**Figure 2D**). It is an effective drug for viruses like HCV, EV and SARS-COV-2 with a positive strand RNA genome. On the other hand, it belongs to the nucleoside reverse transcriptase inhibitors (NRTIs) group and may suppress HIV and most probably other reverse transcriptase containing viruses and transposable elements, including retrotransposons and HERVs. Finally, FNC shows considerable anti-cancer activity, which theoretically can be due to both cell cycle attenuation and the suppression of retrotransposons/HERVs. Whether these effects can be improved by the possible combination of FNC treatment with TK/Gancyclovir or 5FC/CD prodrug systems need to be evaluated. However, basic mechanisms which laid a foundation for FNC application are not fully understood, and additional studies are needed to elucidate the FNC activities in cancer and healthy human cells to support its medical applications other than treating viral infections.

AUTHOR CONTRIBUTIONS

DF, Conceptualization, Methodology, Investigation, Writing - Original Draft, Writing - Review and Editing. RK, Conceptualization, Writing - Original Draft, Visualization. AA, Conceptualization, Writing - Original Draft, Visualization. AB, Writing - Original Draft, Writing - Review and Editing. NB, Writing, Conceptualization, Visualization. PT,-Review. IU, Conceptualization, Supervision, Writing – Review. BK, Review. All authors contributed to the article and approved the submitted version.

FUNDING

This work is supported by the Russian Science Foundation under grant № 21-15-00213 (IU, description of molecular mechanisms, antiviral activity of FNC, clinical trials) and grant 21-74-20066 (NB, anticancer activity of FNC).

REFERENCES

1. Wang Q, Liu X, Wang Q, Zhang Y, Jiang J, Guo X, et al. FNC, a Novel Nucleoside Analogue Inhibits Cell Proliferation and Tumor Growth in a Variety of Human Cancer Cells. *Biochem Pharmacol* (2011) 81(7):848–55. doi: 10.1016/j.bcp.2011.01.001
2. Gatenby RA, Brown JS. Integrating Evolutionary Dynamics Into Cancer Therapy. *Nat Rev Clin Oncol* (2020) 17: (11):675–86. doi: 10.1038/s41571-020-0411-1
3. Buzdin A, Sorokin M, Garazha A, Glusker A, Aleshin A, Poddubskaya E, et al. RNA Sequencing for Research and Diagnostics in Clinical Oncology. *Semin Cancer Biol* (2020) 60:311–23. doi: 10.1016/j.semcancer.2019.07.010
4. Zhang Y, Zhang R, Ding X, Peng B, Wang N, Ma F, et al. FNC Efficiently Inhibits Mantle Cell Lymphoma Growth. *PloS One* (2017) 12(3):e0174112. doi: 10.1371/journal.pone.0174112
5. Yang Q, Zhao X, Zang L, Fang X, Zhao J, Yang X, et al. Anti-Hepatitis B Virus Activities of α-DDB–FNC, a Novel Nucleoside–Biphenyldicarboxylate Compound in Cells and Ducks, and its Anti-Immunological Liver Injury Effect in Mice. *Antiviral Res* (2012) 96: (3):333–9. doi: 10.1016/j.antiviral.2012.10.003
6. Xu N, Yang J, Zheng B, Zhang Y, Cao Y, Huan C, et al. The Pyrimidine Analog FNC Potently Inhibits the Replication of Multiple Enteroviruses. *J Virol* (2020) 94(9):204–20. doi: 10.1128/JVI.00204-20
7. Schumann GG, Gogvadze EV, Osanai-Futahashi M, Kuroki A, Munk C, Fujiwara H, et al. Unique Functions of Repetitive Transcriptomes. *Int Rev Cell Mol Biol* (2010) 285:115–88. doi: 10.1016/B978-0-12-381047-2.00003-7
8. Jiang Y, Zong W, Ju S, Jing R, Cui M. Promising Member of the Short Interspersed Nuclear Elements (Alu Elements): Mechanisms and Clinical Applications in Human Cancers. *J Med Genet* (2019) 56(10):639–45. doi: 10.1136/jmedgenet-2018-105761

9. Buzdin AA, Prassolov V, Garazha AV. Friends-Enemies: Endogenous Retroviruses Are Major Transcriptional Regulators of Human DNA. *Front Chem* (2017) 5:35. doi: 10.3389/fchem.2017.00035
10. Giovinazzo A, Balestrieri E, Petrone V, Argaw-Denboba A, Cipriani C, Miele MT, et al. The Concomitant Expression of Human Endogenous Retroviruses and Embryonic Genes in Cancer Cells Under Microenvironmental Changes is a Potential Target for Antiretroviral Drugs. *Cancer Microenviron* (2019) 12(2-3):105–18. doi: 10.1007/s12307-019-00231-3
11. Suntsova M, Garazha A, Ivanova A, Kaminsky D, Zhavoronkov A, Buzdin A. Molecular Functions of Human Endogenous Retroviruses in Health and Disease. *Cell Mol Life Sci* (2015) 72(19):3653–75. doi: 10.1007/s00018-015-1947-6
12. Nikitin D, Kolosov N, Murzina A, Pats K, Zamyatin A, Tkachev V, et al. Retroelement-Linked H3K4me1 Histone Tags Uncover Regulatory Evolution Trends of Gene Enhancers and Feature Quickly Evolving Molecular Processes in Human Physiology. *Cells* (2019) 8(10):1219. doi: 10.3390/cells8101219
13. Jin X, Xu XE, Jiang YZ, Liu YR, Sun W, Guo YJ, et al. The Endogenous Retrovirus-Derived Long Noncoding RNA TROJAN Promotes Triple-Negative Breast Cancer Progression *via* ZMYND8 Degradation. *Sci Adv* (2019) 5(3):eaat9820. doi: 10.1126/sciadv.aat9820
14. Schulz WA. Does HERV-K Represent a Potential Therapeutic Target for Prostate Cancer? *Expert Opin Ther Targets* (2017) 21(10):921–4. doi: 10.1080/14728222.2017.1373095
15. Argaw-Denboba A, Balestrieri E, Serafino A, Cipriani C, Bucci I, Sorrentino R, et al. HERV-K Activation is Strictly Required to Sustain CD133+ Melanoma Cells With Stemness Features. *J Exp Clin Cancer Res* (2017) 36(1):1–17. doi: 10.1186/s13046-016-0485-x
16. Bannert N, Hofmann H, Block A, Hohn O. HERVs New Role in Cancer: From Accused Perpetrators to Cheerful Protectors. *Front Microbiol* (2018) 9:178. doi: 10.3389/fmicb.2018.00178
17. Grabski DF, Hu Y, Sharma M, Rasmussen SK. Close to the Bedside: A Systematic Review of Endogenous Retroviruses and Their Impact in Oncology. *J Surg Res* (2019) 240:145–55. doi: 10.1016/j.jss.2019.02.009
18. Chan SM, Sapir T, Park SS, Rual JF, Contreras-Galindo R, Reiner O, et al. The HERV-K Accessory Protein Np9 Controls Viability and Migration of Teratocarcinoma Cells. *PloS One* (2019) 14(2):e0212970. doi: 10.1371/journal.pone.0212970
19. Panda A, de Cubas AA, Stein M, Riedlinger G, Kra J, Mayer T, et al. Endogenous Retrovirus Expression is Associated With Response to Immune Checkpoint Blockade in Clear Cell Renal Cell Carcinoma. *JCI Insight* (2018) 3 (16):e121522. doi: 10.1172/jci.insight.121522
20. Siebenthall KT, Miller CP, Vierstra JD, Mathieu J, Tretiakova M, Reynolds A, et al. Integrated Epigenomic Profiling Reveals Endogenous Retrovirus Reactivation in Renal Cell Carcinoma. *EBioMedicine* (2019) 41:427–42. doi: 10.1016/j.ebiom.2019.01.063
21. Deniz O, Ahmed M, Todd CD, Rio-Machin A, Dawson MA, Branco MR. Endogenous Retroviruses are a Source of Enhancers With Oncogenic Potential in Acute Myeloid Leukaemia. *Nat Commun* (2020) 11(1):3506. doi: 10.1038/s41467-020-17206-4
22. Yuan Z, Yang Y, Zhang N, Soto C, Jiang X, An Z, et al. Human Endogenous Retroviruses in Glioblastoma Multiforme. *Microorganisms* (2021) 9(4):764. doi: 10.3390/microorganisms9040764
23. Ho XD, Nguyen HG, Trinh LH, Reimann E, Prans E, Kõks G, et al. Analysis of the Expression of Repetitive DNA Elements in Osteosarcoma. *Front Genet* (2017) 8:193. doi: 10.3389/fgene.2017.00193
24. Kazazian HHJr., Moran JV. Mobile DNA in Health and Disease. *N Engl J Med* (2017) 377(4):361–70. doi: 10.1056/NEJMra1510092
25. Hancks DC, Kazazian HHJr. Active Human Retrotransposons: Variation and Disease. *Curr Opin Genet Dev* (2012) 22(3):191–203. doi: 10.1016/j.gde.2012.02.006
26. Mills RE, Bennett EA, Iskow RC, Luttig CT, Tsui C, Pittard WS, et al. Recently Mobilized Transposons in the Human and Chimpanzee Genomes. *Am J Hum Genet* (2006) 78(4):671–9. doi: 10.1086/501028
27. Scott EC, Devine SE. The Role of Somatic L1 Retrotransposition in Human Cancers. *Viruses* (2017) 9(6):131. doi: 10.3390/v9060131
28. Jones RB, Song H, Xu Y, Garrison KE, Buzdin AA, Anwar N, et al. LINE-1 Retrotransposable Element DNA Accumulates in HIV-1-Infected Cells. *J Virol* (2013) 87(24):13307–20. doi: 10.1128/JVI.02257-13
29. Garazha A, Ivanova A, Suntsova M, Malakhova G, Roumiantsev S, Zhavoronkov A, et al. New Bioinformatic Tool for Quick Identification of Functionally Relevant Endogenous Retroviral Inserts in Human Genome. *Cell Cycle* (2015) 14(9):1476–84. doi: 10.1080/15384101.2015.1022696
30. Scott EC, Gardner EJ, Masood A, Chuang NT, Vertino PM, Devine SE. A Hot L1 Retrotransposon Evades Somatic Repression and Initiates Human Colorectal Cancer. *Genome Res* (2016) 26(6):745–55. doi: 10.1101/gr.201814.115
31. Kassiotis G, Stoye JP. Making a Virtue of Necessity: The Pleiotropic Role of Human Endogenous Retroviruses in Cancer. *Philos Trans R Soc Lond B Biol Sci* (2017) 372: (1732):20160277. doi: 10.1098/rstb.2016.0277
32. Lemaître C, Tsang J, Bireau C, Heidmann T, Dewannieux M. A Human Endogenous Retrovirus-Derived Gene That can Contribute to Oncogenesis by Activating the ERK Pathway and Inducing Migration and Invasion. *PLoS Pathog* (2017) 13: (6):. doi: 10.1371/journal.ppat.1006451
33. Smith CC, Selitsky SR, Chai S, Armistead PM, Vincent BG, Serody JS. Alternative Tumour-Specific Antigens. *Nat Rev Cancer* (2019) 19(8):465–78. doi: 10.1038/s41568-019-0162-4
34. Yang Q, Kang J, Zheng L, Wang XJ, Wan N, Wu J, et al. Synthesis and Biological Evaluation of 4-Substituted Fluoronucleoside Analogs for the Treatment of Hepatitis B Virus Infection. *J Med Chem* (2015) 58(9):3693–703. doi: 10.1021/jm5012963
35. Liu W, Zhang L, Zhou H, Yang C, Miao Z, Zhao Y. Synthesis of Novel Nucleoside Analogue Phosphorothioamidate Prodrugs and In Vitro Anticancer Evaluation Against RKO Human Colon Carcinoma Cells. *Nucleosides Nucleotides Nucleic Acids* (2013) 32(4):161–73. doi: 10.1080/15257770.2013.770523
36. Klumpp K, Kalayanov G, Ma H, Le Pogam S, Leveque V, Jiang WR, et al. 2'-Deoxy-4'-Azido Nucleoside Analogs are Highly Potent Inhibitors of Hepatitis C Virus Replication Despite the Lack of 2'-Alpha-Hydroxyl Groups. *J Biol Chem* (2008) 283(4):2167–75. doi: 10.1074/jbc.M708929200
37. Smith DB, Kalayanov G, Sund C, Winqvist A, Pinho P, Maltseva T, et al. The Design, Synthesis, and Antiviral Activity of 4'-Azidocytidine Analogues Against Hepatitis C Virus Replication: The Discovery of 4'-Azidoarabinocytidine. *J Med Chem* (2009) 52(1):219–23. doi: 10.1021/jm800981y
38. Smith DB, Kalayanov G, Sund C, Winqvist A, Maltseva T, Leveque VJ-P, et al. The Design, Synthesis, and Antiviral Activity of Monofluoro and Difluoro Analogues of 4′-Azidocytidine Against Hepatitis C Virus Replication: The Discovery of 4′-Azido-2′-Deoxy-2′-Fluorocytidine and 4′-Azido-2′-Dideoxy-2′, 2′-Difluorocytidine. *J med Chem* (2009) 52(9):2971–8. doi: 10.1021/jm801595c
39. Yu B, Chang JJST, Therapy T. Azvudine (FNC): A Promising Clinical Candidate for COVID-19 Treatment. *Signal Transduct Target Ther* (2020) 5: (1):1–2. doi: 10.1038/s41392-020-00351-z
40. Sun L, Peng Y, Yu W, Zhang Y, Liang L, Song C, et al. Mechanistic Insight Into Antiretroviral Potency of 2′-Deoxy-2′-β-Fluoro-4′-Azidocytidine (FNC) With a Long-Lasting Effect on HIV-1 Prevention. *J Med Chem* (2020) 63 (15):8554–66. doi: 10.1021/acs.jmedchem.0c00940
41. Wang Q, Li Y, Song C, Qian K, Chen C-H, Lee K-H, et al. Synthesis and Anti-HIV Activity of 2′-Deoxy-2′-Fluoro-4′-C-Ethynyl Nucleoside Analogs. *Bioorg Med Chem Lett* (2010) 20: (14):4053–6. doi: 10.1016/j.bmcl.2010.05.090
42. Wang Q, Li Y, Song C, Qian K, Chen CH, Lee KH, et al. Synthesis and Anti-HIV Activity of 2'-Deoxy-2'-Fluoro-4'-C-Ethynyl Nucleoside Analogs. *Bioorg Med Chem Lett* (2010) 20(14):4053–6. doi: 10.1016/j.bmcl.2010.05.090
43. Li H, Dou H, Zhang Y, Li Z, Wang R, Chang J, et al. Studies of the Interaction Between FNC and Human Hemoglobin: A Spectroscopic Analysis and Molecular Docking. *Spectrochim Acta A Mol Biomol Spectrosc* (2015) 136:416–22. doi: 10.1016/j.saa.2014.09.051
44. Wang R-R, Yang Q-H, Luo R-H, Peng Y-M, Dai S-X, Zhang X-J, et al. Azvudine, a Novel Nucleoside Reverse Transcriptase Inhibitor Showed Good Drug Combination Features and Better Inhibition on Drug-Resistant Strains Than Lamivudine. *vitro* (2014) 9(8):e105617. doi: 10.1371/journal.pone.0105617

45. Sadeghpour S, Khodaee S, Rahnama M, Rahimi H, Ebrahimi D. Human APOBEC3 Variations and Viral Infection. *Viruses* (2021) 13(7):1366. doi: 10.3390/v13071366
46. Zheng L, Wang Q, Yang X, Guo X, Chen L, Tao L, et al. Antiviral Activity of FNC, 2'-Deoxy-2'-Beta-Fluoro-4'-Azidocytidine, Against Human and Duck HBV Replication. *Antivir Ther* (2012) 17(4):679–87. doi: 10.3851/IMP2094
47. Zhou Y, Zhang Y, Yang X, Zhao J, Zheng L, Sun C, et al. Novel Nucleoside Analogue FNC is Effective Against Both Wild-Type and Lamivudine-Resistant HBV Clinical Isolates. *Antivir Ther* (2012) 17(8):1593–9. doi: 10.3851/IMP2292
48. Zhang Y, Cheng X, Huang G, Dong J, Wang C, Jiang H-h, et al. Effect of New Nucleoside Analogue FNC on Proliferation, Apoptosis and Expressions of Bcl-6, PRDM1, C-myc in Cell Line Raji. *J Zhengzhou University* (2013) 4, 450–4
49. Zhang Y, Wang C-P, Ding X-X, Wang N, Ma F, Jiang J-H, et al. FNC, a Novel Nucleoside Analogue, Blocks Invasion of Aggressive non-Hodgkin Lymphoma Cell Lines *via* Inhibition of the Wnt/β-Catenin Signaling Pathway. *Asian Pacific J Cancer Prev* (2014) 15(16):6829–35. doi: 10.7314/APJCP.2014.15.16.6829
50. Jing X, Niu S, Liang Y, Chen H, Wang N, Peng Y, et al. FNC Inhibits Proliferation and Metastasis of Non-Small-Cell Lung Cancer in Vivo and In Vitro. (2021). doi: 10.21203/rs.3.rs-219276/v1
51. Zhang Y, Wang CP, Ding XX, Wang N, Ma F, Jiang JH, et al. FNC, a Novel Nucleoside Analogue, Blocks Invasion of Aggressive non-Hodgkin Lymphoma Cell Lines via Inhibition of the Wnt/beta-Catenin Signaling Pathway. *Asian Pac J Cancer Prev* (2014) 15(16):6829–35. doi: 10.7314/apjcp.2014.15.16.6829
52. Balestrieri E, Argaw-Denboba A, Gambacurta A, Cipriani C, Bei R, Serafino A, et al. Human Endogenous Retrovirus K in the Crosstalk Between Cancer Cells Microenvironment and Plasticity: A New Perspective for Combination Therapy. *Front Microbiol* (2018) 9:1448. doi: 10.3389/fmicb.2018.01448
53. Ren Z, Luo H, Yu Z, Song J, Liang L, Wang L, et al. A Randomized, Open-Label, Controlled Clinical Trial of Azvudine Tablets in the Treatment of Mild and Common COVID-19, A Pilot Study. *Adv Sci (Weinh)* (2020) 7 (19):2001435. doi: 10.1002/advs.202001435

Conflict of Interest: Author AB is employed by OmicsWay Corp., Walnut, CA, 91789, USA.

The remaining authors declare that the research was conducted in the absence of any commercial or financial relationships that could be construed as a potential conflict of interest.

Publisher's Note: All claims expressed in this article are solely those of the authors and do not necessarily represent those of their affiliated organizations, or those of the publisher, the editors and the reviewers. Any product that may be evaluated in this article, or claim that may be made by its manufacturer, is not guaranteed or endorsed by the publisher.

frontiers in Oncology

ORIGINAL RESEARCH
published: 14 February 2022
doi: 10.3389/fonc.2022.829313

CAR Co-Operates With Integrins to Promote Lung Cancer Cell Adhesion and Invasion

*Claudia Owczarek[1], Elena Ortiz-Zapater[1,2], Jana Kim[2], Efthymia Papaevangelou[3], George Santis[3] and Maddy Parsons[1]**

[1] Randall Centre for Cell and Molecular Biophysics, King's College London, London, United Kingdom, [2] School of Biomedical Engineering and Imaging Sciences, King's College London, St Thomas Hospital, London, United Kingdom, [3] Peter Gorer Department of Immunobiology, School of Immunology and Microbial Science, King's College London, London, United Kingdom

The coxsackie and adenovirus receptor (CAR) is a member of the junctional adhesion molecule (JAM) family of adhesion receptors and is localised to epithelial cell tight and adherens junctions. CAR has been shown to be highly expressed in lung cancer where it is proposed to promote tumor growth and regulate epithelial mesenchymal transition (EMT), however the potential role of CAR in lung cancer metastasis remains poorly understood. To better understand the role of this receptor in tumor progression, we manipulated CAR expression in both epithelial-like and mesenchymal-like lung cancer cells. In both cases, CAR overexpression promoted tumor growth *in vivo* in immunocompetent mice and increased cell adhesion in the lung after intravenous injection without altering the EMT properties of each cell line. Overexpression of WTCAR resulted in increased invasion in 3D models and enhanced β1 integrin activity in both cell lines, and this was dependent on phosphorylation of the CAR cytoplasmic tail. Furthermore, phosphorylation of CAR was enhanced by substrate stiffness *in vitro*, and CAR expression increased at the boundary of solid tumors *in vivo*. Moreover, CAR formed a complex with the focal adhesion proteins Src, Focal Adhesion Kinase (FAK) and paxillin and promoted activation of the Guanine Triphosphate (GTP)-ase Ras-related Protein 1 (Rap1), which in turn mediated enhanced integrin activation. Taken together, our data demonstrate that CAR contributes to lung cancer metastasis *via* promotion of cell-matrix adhesion, providing new insight into co-operation between cell-cell and cell-matrix proteins that regulate different steps of tumorigenesis.

Keywords: cell-cell adhesion, cell-matrix adhesion, invasion, integrins, coxsackievirus adenovirus receptor (CAR), lung cancer

OPEN ACCESS

Edited by:
Yunfeng Feng,
Qinghai University Medical College, China

Reviewed by:
Teresita Padilla-Benavides, Wesleyan University, United States
Andrei Ivanov, Cleveland Clinic, United States

***Correspondence:**
Maddy Parsons
maddy.parsons@kcl.ac.uk

Specialty section:
This article was submitted to Molecular and Cellular Oncology, a section of the journal Frontiers in Oncology

Received: *05 December 2021*
Accepted: *19 January 2022*
Published: *14 February 2022*

Citation:
Owczarek C, Ortiz-Zapater E, Kim J, Papaevangelou E, Santis G and Parsons M (2022) CAR Co-Operates With Integrins to Promote Lung Cancer Cell Adhesion and Invasion. Front. Oncol. 12:829313. doi: 10.3389/fonc.2022.829313

Abbreviations: Ad5FK, Adenovirus 5 FiberKnob; CAR, Coxsackie and Adenovirus Receptor; ECM, ExtraCellular Matrix; EMT, Epithelial-Mesenchymal Transition; FAK, Focal Adhesion Kinase; FRAP, Fluorescence Recovery After Photobleaching; GEF, Guanine Nucleotide-Exchange Factor; GFP, Green Fluorescent Protein; GST, Glutathione S-transferase; GTP, Guanine Triphosphate; HSC70, Heat Shock Cognate 70kDa; JAM, Junctional Adhesion Molecule; MAGI-1, Membrane Associated Guanylate kinase with Inverted orientation 1; PD-L1, Programmed Death-Ligand 1; PKC, Protein Kinase C; Rap1, Ras-related Protein 1; RIAM, Rap1-GTP Interacting Adaptor Molecule; ROCK, Rho-associated Protein Kinase; SCID, Severe Combined ImmunoDeficiency; ZO-1, Zonula Occludens 1.

INTRODUCTION

Lung cancer is the leading cause of cancer death worldwide (1). Despite advances in treatment options, prognosis remains poor as lung cancer is mainly diagnosed at advanced stages (2). To metastasise, tumor cells must undergo a multi-step process defined as the metastatic cascade. Metastasis requires cell detachment from the primary tumor, local invasion, intravasation and survival in the vasculature, extravasation, and colonisation of a secondary site (3). Adhesion molecules play a crucial role in all the metastatic steps as they regulate adhesive properties and integrate extracellular cues with cell intrinsic signalling to regulate other cellular functions (4). Numerous previous studies have suggested that metastasis requires cancer cells to undergo epithelial to mesenchymal transition (EMT) whereby cell-cell adhesions are downregulated to promote a more pro-migratory phenotype. However, recent studies have highlighted the dynamic nature of these phenotypic transitions. Indeed, recent studies discovered the existence of a wide spectrum of intermediate states whereby a mix of epithelial and mesenchymal markers are expressed (5).

Members of the Junctional Adhesion Molecule (JAM) family are aberrantly expressed in several types of cancer where they play a dual role. JAMs are type I transmembrane glycoproteins characterised by the presence of two extracellular immunoglobulin (Ig)-like domains and include JAM-A, JAM-B, JAM-C and Coxsackie and Adenovirus Receptor (CAR) (6). CAR was originally identified as a docking receptor for adenovirus type 2 and 5 and coxsackie B virus and subsequently recognized as a key regulator of cell-cell adhesion (7, 8). CAR is comprised of an extracellular domain (containing D1 and D2 domains), a transmembrane region and an unstructured cytoplasmic tail (9). CAR is found at both tight and adherens junctions where it regulates cell-cell adhesion *via* homodimerization *in trans* between CAR D1 domains present on adjacent cells and/or *via* cytoplasmic interactions with other adhesion molecules such as Zonula Occludens 1 (ZO-1), E-cadherin and β-catenin (10–13). Phosphorylation at Ser290/Thr293 residues in the CAR cytoplasmic tail by Protein Kinase C δ (PKCδ) plays a crucial role in its CAR-dependent adhesion dynamics, leading to enhanced E-cadherin endocytosis (10). Moreover, CAR associates with β integrins, and this requires the CAR cytoplasmic domain (14). CAR has also been implicated in regulation of cell-extracellular matrix (ECM) adhesion as increased activation of β1 and β3 integrins was shown to be a direct consequence of CAR-induced p44/42 activation (14). CAR interactions with the actin cytoskeleton suggest that it might be involved in additional processes such as cell migration. Indeed, CAR binds actin and microtubules and it interacts with the F-actin regulatory kinase Rho-associated Protein Kinase (ROCK) (15–17).

In addition to regulating cell-cell homeostasis, CAR is emerging as a key player in disease states such as inflammation and cancer (8). Phosphorylation of the cytoplasmic tail of CAR promotes trans-epithelial migration of leukocytes in inflammation (18). CAR levels are altered at both early and late tumor stages and variability in its role in tumor progression may depend on pre-existing endogenous CAR levels (19, 20). Like other JAMs, CAR has a dual role as it presents both a tumor suppressive and tumor promoting role according to the type of cancer (17, 21). CAR expression is upregulated in lung squamous cell carcinoma and adenocarcinomas and CAR expression level is correlated with poorer prognosis (22, 23). This makes CAR an attractive target for cancer treatment. In line with this, inhibition of CAR expression in lung cancer cells decreases tumor volume in Severe Combined Immuno Deficiency (SCID) mice and high CAR expression promotes expression of mesenchymal markers, suggesting it could play a role in EMT (20). CAR depletion in human lung cancer cells results in reduced anchorage-independent growth and tumor growth in mice (24). CAR not only contributes to tumor development, but also to treatment resistance as it has been identified as a marker of cancer stem cells in non-small lung cancer (25).

In this study we aimed to define whether changes to CAR levels as observed in lung cancer, could contribute to the metastatic potential *via* regulation of cell-cell and cell-ECM adhesion. Our data demonstrate that CAR overexpression promotes cell adhesion to ECM proteins and cell invasion into 3D collagen gels without affecting classical epithelial to mesenchymal transition (EMT) markers. Overexpression of WTCAR promotes tumor growth *in vivo* and cell adhesion in the lung after intravenous injection. Mechanistically, we show that phosphorylation of CAR is responsive to increasing extracellular stiffness. Overexpression of WTCAR results in increased β1 integrin activity through activation of the GTPase Ras-related Protein 1 (Rap1), leading to enhanced CAR-dependent adhesion. Immunoprecipitation experiments further show that CAR forms a complex with the focal adhesion proteins Src, Focal Adhesion Kinase (FAK) and paxillin and that this requires phosphorylation of CAR. Taken together, these data suggest that CAR contributes to lung cancer metastasis *via* promotion of cell-matrix adhesion.

METHODS

Antibodies and Reagents

Anti-integrin β1 (12G10, Santa Cruz), anti-active β1 integrin (9EG7, Merck Millipore), anti β-catenin [Santa Cruz (IF) and BD Bioscience (WB)], anti-CAR antibody (Santa-Cruz), anti E-Cadherin (Abcam), anti-FAK (Cell signalling), anti-green fluorescent protein (GFP) (26), anti- Heat Shock Cognate 70kDa (HSC70) (Sigma-Aldrich), anti-paxillin (BD Bioscience), anti phospho-FAK (Y397, Cell signalling), anti-phospho-paxillin (Y118, Cell signalling), anti-phospho-src (Y418, Millipore), anti-rap1 A/B (R&D Systems) and anti-src (Millipore) antibodies were used for western blot. Adenovirus Type5 fiberknob (Ad5FK) was produced and purified as previously described (27). CAR thr290/ser293 polyclonal antibody was developed by Perbioscience (Thermofisher) using the peptide Ac-RTS (28)AR(pS)YIGSNH-C and was affinity purified before use. DAPI (Sigma Aldrich) was used as nuclear stain for immunofluorescence. Anti-mouse-HRP, anti-rabbit-HRP, anti-goat-HRP were from DAKO, anti-mouse-568, anti-rabbit-568, anti-goat-568 and phalloidin-647 were all obtained

from Invitrogen. Inhibitors to FAK (PF228), Rap1A (GGTI298) and src (PP2) were all obtained from Tocris.

Plasmids and Primers

CAR phospho-mutants (T290A & S293A, non-phosphorylated (AACAR) and T290D & S293D, phospho-mimetic (DDCAR) in both GFP lentiviral backbones and Glutathione S-transferase (GST) expression vectors were described previously (10). RalGDS-RBD-GST construct was kindly gifted by Dr Ritu Garg (King's College London). Luciferase-mStrawberry lentiviral plasmid and pMDL, RSV-Rev and CMV-VSVG packaging plasmids were kindly gifted by Dr Scott Lyons (Cold Spring Harbor Laboratories). The *CXADR* CRISPR Guide RNA targeting sequence TAGATACGCAGTTTCCCCTT cloned into pSpCas9 BB-2A-GFP (PX458) lentiviral construct and acquired from Genscript. The following primers were used for qPCR: CAR primer forward 5' AAGTGACGCGAGTTCACCTG 3'CAR primer reverse 5'AGATGTTCAAGACCTGTACACTG 3' 18S primer forward 5'-CCCATCACCATCTTCCAGGAGC -3' 18S primer reverse 5'-CCAGTGAGCTTCCCGTTCAGC -3'.

Cell Culture

LLC1 murine Lewis Lung Carcinoma epithelial cells (29), CMT-167 murine carcinoma alveogenic epithelial cells (30) were a kind gift from Prof K.Hodivala-Dilke (Barts Cancer Institute, QMUL, London) and Human Embryonic Kidney 293T (HEK293T) cells (purchased from ATCC) were cultured in high glucose DMEM containing 10% FCS, supplemented with 2mM glutamine. HEK293T packaging cells were used to generate lentiviral particles for CAR and GFP lentiviral expression using GFP, WTCAR-GFP and AACAR-GFP constructs. CAR-CRISPR cell lines were established *via* transient transfection of LLC and CMT parental cells with *CXADR* CRISPR Guide RNA vector carrying a GFP tag. The GFP-tagged cells were sorted 24 h post-transfection using flow cytometry to obtain a homogenous but non-clonal cell population. CMT and LLC cells were treated with Ad5 FK (100μg/mL for 2.5h), FAK inhibitor (PF228; 1μM for 4h), Rap1A inhibitor (GGTI298, 10μM for 30min) or Src inhibitor (PP2, 5μM for 4h). PP2 also inhibits Lck and Fyn members of the Src family of tyrosine kinases (31) but PP2 has been previously shown to effectively inhibit Src activity (32) at concentrations used here (33). Effective inhibition of Src was proven by reduced pY418Src. Ad5FK was used at concentrations previously shown to block CAR homodimerisation (18). GGTI298 has been effectively used to inhibit Rap1 processing (34, 35).

Generation of Lentiviral Virus From HEK-293T Cells

HEK-293T cells were plated at 40% confluency 24 hours prior to transfection. A transfection mixture containing a total of 7.5 μg DNA (2.1 μg pCMV8.91, 0.7 μg pMD.G and 3.75 μg of various lentiviral constructs) was mixed in 500 μL of OptiMEM. Subsequently, 22.5 μL of PEI transfection reagent was added in the transfection mixture (3:1 ratio to total DNA). The DNA-PEI mix was vortexed and incubated for 15 minutes at room temperature before being added to HEK-293T cells with OptiMEM. After incubation with the transfection mixture for 5 hours at 37°C, OptiMEM was replaced with complete media. Lentivirus was harvested after 48 hours by removing the media and centrifugation at 1200 rpm for 3 minutes to remove any HEK293T cells. Viruses were then filtered through 0.4 μm sterile filters and stored in 1 mL aliquots at -80°C.

Lentiviral Infection to Generate Stable Cell Lines

CMT and LLC cells were plated to 40% confluency 24 hours prior to viral infection. Polybrene (8 mg/mL) was added into normal growth media to increase the efficiency of viral infection. 1-4 mL of lentivirus were added to the cells and left to incubate at 37°C for 24-72 hours. Media was replaced 24-48 hours post-infection to remove the virus and cells were grown and passaged.

GFP-Trap Immunoprecipitation

LLC and CMT cells expressing GFP-tagged proteins were lysed in IP lysis buffer (pH 7.4, 50 mM Tris, 150 mM NaCl, 50mM NaF, 1 mM EDTA, 1% Triton X-100, 1% NP40, PI cocktail). Lysates were incubated with 1:1 of GFP-trap®beads (Chromotek) and agarose resin on a rotator at 4°C for 2 hours. Beads were washed with IP lysis buffer and immunocomplexes were separated using SDS-PAGE and immunoblotted for either β1 integrin, FAK, paxillin, Src or GFP.

GST Pulldown Assay

GST-fusion constructs were expressed in *E. coli* BL21 competent cells using conditions recommended by the manufacturer (Amersham Pharmacia Biotech). Pulldown assays were carried out using WTCAR-GST, AACAR-GST and DDCAR-GST cytoplasmic tail constructs as previously described (10). LLC and CMT cells were cultured in 10 cm dishes until 100% confluent and lysed in 500 μl IP buffer containing protease and phosphatase inhibitor cocktails (1:100). Cell lysate proteins were collected as supernatant after centrifuging at 13,000 rpm for 10 minutes at 4°C. 50 μl of each lysate was kept aside for use in loading controls while the rest were incubated with pre-washed GST or CAR-GST beads for 3 hours at 4°C on a rotator. Following incubation, the unbound fractions were removed and the beads washed three times with IP buffer before boiling for 5 minutes in 50 μl of 2X SDS sample loading buffer containing β-mercaptoethanol (1:50). 40 μl of samples were loaded onto 10% polyacrylamide gels and immunoblotted.

Western Blotting

CMT and LLC cells were lysed in RIPA buffer (pH 7.4, 10 mM Tris Base, 150 mM NaCl, 1mM EDTA, 1% Triton X- 100) containing β-mercaptoethanol (1:100). Lysates were subjected to SDS-PAGE and blotted using PVDF membrane. Blots were blocked and probed using 5% skimmed milk powder or Bovine Serum Albumin in TBS-0.1% Tween. Proteins were detected by ECL chemiluminescence kit (BioRad) and directly imaged using the BioRad imager digital imaging system.

Immunofluorescence

CMT and LLC cells were plated on 13mm coverslips and incubated overnight in normal growth media. Cells were

washed 1x with PBS and then fixed using 4%PFA in PBS for 10 minutes at room temperature and then washed three times with PBS. Cells were then stored or permeabilised using 0.25% TritonX-100 in PBS for 5 minutes and washed again three times with PBS. Following permeabilization, coverslips were blocked with 5% BSA/PBST for 1 hour at room temperature. Incubation of cells with primary antibody diluted in 5% BSA/PBST was then carried out in a dark humid chamber placed at 4°C overnight. Cells were incubated with secondary antibodies and DAPI diluted in 5% BSA/PBST for 1h at room temperature. Coverslips were mounted on slides using FluorSafe mounting media (Calbiochem).

Confocal Microscopy

The slides were analysed using a A1R laser scanning confocal microscope (Nikon) with a 60x/1.4Plan-APOCHROMAT oil immersion objective. Images were acquired in ND2 format, exported as TIFFs, and analysed in Image J. Confocal microscopy Images of fixed cells were acquired on a Nikon A1R inverted confocal microscope (Nikon Instruments UK) with an environmental chamber maintained at 37°C/5% CO2. Images were taken using a 40x or 60x Plan Fluor oil immersion objective (numerical aperture of 1 and 1.4, respectively). Excitation wavelengths of 488 nm (diode laser), 561 nm (diode laser) or 640 nm (diode laser) were used. In experiments where multiple cell lines were analysed from the same cell type, all images were acquired at identical laser settings to permit comparison of intensities. Images were acquired using NIS-Elements imaging software (v4) and were saved in Nikon Elements in the.ND2 format. Image processing was carried out in Fiji processing software (36).

Fluorescence Recovery Activated Photo Bleaching (FRAP)

CMT cells expressing WTCAR-GFP and AACAR-GFP were used for FRAP experiments. CMT cells expressing WTCAR-GFP were treated with DMSO/anti-src (PP2, for 4h) and used for FRAP experiments in presence of anti-Src/DMSO. Regions of interest (23) were drawn across CAR-positive cell-cell junctions and photobleached by a bleach pulse (0.5 second) at 80% laser intensity at 488 nm. Recovery of fluorescence within the ROI was monitored over 6 min. Background and reference ROIs were selected for background and reference correction. 10 cell-cell junctions were averaged to generate one FRAP curve for a single experiment. Fluorescence recovery of CAR-GFP was analysed using the NIS-Elements Advanced Research software. The experimental data were fitted using the one-phase decay in Graphpad Prism.

Cell Matrix Adhesion Assay

CMT and LLC cells were plated on Collagen (Rat Tail Type I) or Matrigel and allowed to adhere for 2h at 37°C. Cells were fixed with 4%PFA and nuclei were stained *via* incubation with DAPI (1:1000) for 10min. Fluorescent images were acquired on Evos FL Auto 2 fluorescent microscope (Invitrogen). Tile-scans were obtained using a 4x air objective with 3.2 MP CMOS camera. Excitation using DAPI LED light cube was used. Images were acquired using EVOS software (v2). Tiles were knitted into.TIFF files using FIJI software and total cell count was obtained by thresholding for nuclear stain followed by automated counting. 35mm low stiffness μ-dishes (1.5kPa and 28 kPa) were obtained from Ibidi.

Cell Proliferation Assay

LLC and CMT cells were fixed with 4% PFA/PBS for 10 min at 4h, 24h and 48h post-plating. Nuclei were stained with DAPI to enable cell quantification. Images were acquired as described for cell matrix adhesion assay.

Inverted Invasion Assay

Transwell inserts with 8 μm wide pores were filled with a gel comprised of Collagen (Rat Tail Type I 1.6 mg/mL), Fibronectin (10μg/mL) and FCS (2%). LLC and CMT cells plated on top of each transwell were left to invade through the gel for 72h following a FCS concentration gradient. Transwells were fixed with 4%PFA and nuclei stained with DAPI. Confocal sections were taken every 1.5 μm in 5 independent fields per transwell with a 20x dry objective in a Nikon Eclipse Ti-E inverted microscope with A1R Si Confocal system using Nikon Software Elements. To quantify invasion levels, images acquired in the DAPI channel were imported on Fiji software. Cell count was obtained by thresholding for nuclear stain followed by automated counting. The percentage of total invading cells present at each depth in the collagen gel was determined. This was done by dividing the number of cells present in each layer by the sum of invading cells present in all layers.

Spheroid Assays

CMT cells were re-suspended in DMEM supplemented with 0.5% FCS and methylcellulose (37) to generate spheroids *via* the hanging drop method. Spheroids were left to form for 48 h at 37°C. A collagen mix containing 2 mg/ml collagen (Rat Tail Type I collagen), 20 mM Hepes, 10 mM fibronectin, 17.5 mM NaOH and OptiMEM was made to embed the spheroids. Phase-contrast images were acquired using the Evos FL Auto 2 fluorescent microscope with a 10x objective at 0, 24 and 48 hours. Cell invasion was quantified using Fiji software. The acquired images (.TIFF format) were imported in Fiji, a region of interest was manually drawn around each spheroid and the area quantified. 0h post-embedding spheroids were only comprised of a spheroid core, whereas 24 and 48 h post-embedding cells started leaving the core and spheroids were comprised of invading cells in addition to a spheroid core. Regions of interest were drawn around the entire spheroid (including invading cells). Spheroid cell invasion was quantified by dividing the spheroid area at 24h or 48 h by the spheroid area measured at 0h post-embedding.

In-Vivo Experiments

The use of animals for this study was approved by the Ethical Review Committee at King's College London and the Home Office, UK. All animals were housed in the Biological Support Unit (BSU) located in New Hunt's House at King's College London. All experiments were carried out under project license no. P9672569A and personal license no. I83A1F143. For

subcutaneous tumors, $7.5x10^6$ CMT or LLC cells were re-suspended in 200 µl PBS. Cells were injected subcutaneously into the shaved flank of immunocompetent C57BL/6 mice (male, 7-8 weeks old, 20 g weight). Tumors were allowed to grow until they reached a maximum diameter of 20 mm. A Vernier caliper was used to measure perpendicular tumor diameter every three days and tumor volumes were calculated using the following formula: $V = (W(2) \times L)/2$. For experimental metastasis models, $7.5x10^5$ CMT or LLC cells expressing a luciferase mStrawberry-tagged construct were re-suspended in 150 µl of PBS and injected into the mouse tail vein of immunocompetent C57BL/6 mice (male, 7-8 weeks old, 20 g weight). To detect luminescent cells, each mouse was injected intra-peritoneally with 200 µl of D-luciferin (PerkinElmer, 0.15 mg Luciferin/g body weight) PBS solution before *in vivo* imaging. Mice were imaged at 4h and 24h post-injection using the IVIS spectrum imaging system (PerkinElmer) (38). A region of interest was drawn around each luminescent signal present in the lung and quantified using the Living Image® software and measured in Total Flux [= radiance (photons/sec) in each pixel summed over the ROI area (cm^2) x 4π].

Tissue Processing

Tumors extracted from mice were fixed with 4%PFA prior to paraffin wax embedding. 10 µm thick sections were obtained and used for DAB staining. Paraffin-embedded sections were dewaxed and antigen retrieval was carried out *via* 20min incubation with sodium citrate buffer (0.0874 M sodium citrate, 0.0126 M citric acid, pH 6) in a pressure cooker at 95°C. Endogenous peroxidase activity was blocked *via* 10 *min* incubation in hydrogen peroxide (3% in TBS). Non-specific binding was blocked *via* incubation with TBS-1%BSA-1%FBS blocking solution. Tissues were incubated with primary antibody at 4°C overnight. Secondary HRP-conjugated antibody was added for 1h at room temperature. DAB staining was visualised by adding DAB developing solution for up to 20 min (Dako, Liquid DAB+Substrate Chromogen system). Tissues were counterstained using haematoxylin for 1 sec. Tissues were dehydrated and mounted with DPX mounting medium (Sigma-Aldrich).

Statistical Analysis

Data values are expressed as mean ± standard error of mean (s.e.m). All statistical tests were performed using GraphPad Prism, version 8. Student's t-test was used for comparing two groups for statistical analysis. One or two-way analysis of variance (ANOVA) with *post hoc* test was used for multiple comparisons. Statistically significant values were taken as * = $p < 0.05$, ** = $p < 0.01$, *** = $p < 0.001$, **** = $p < 0.0001$ and were assigned in specific figures and experiments as shown.

RESULTS

CAR Regulates Lung Cancer Cell Invasion But Does Not Alter EMT Phenotypes

To explore whether CAR plays a role in tumorigenesis and EMT we generated a panel of epithelial-like CMT 167 mouse lung adenocarcinoma cells overexpressing WT or AACAR (**Figure 1A**) and where CAR is removed using CRISPR (**Figures 1B–E**). As a cell-cell adhesion molecule, CAR has previously been suggested to play a role in EMT. Notably we did not observe any changes in cell-cell adhesion behaviour under normal growth conditions. However, to more formally address whether changes to EMT may be occurring, we assessed expression of key characterised EMT markers E-Cadherin, β-catenin and vimentin in these cells. Confocal images demonstrated colocalization of both WTCAR and AACAR with E-Cadherin at cell-cell adhesion sites (**Supplementary Figure 1A**). Overexpression or deletion of CAR did not change levels or localisation of E-cadherin or β-catenin as quantified from confocal images and western blots (**Supplementary Figures 1A–C**). Moreover, vimentin was detected in CMT 167 cells, despite their epithelial-like appearance, but the expression of this protein was unaltered following manipulation of CAR levels (**Supplementary Figure 1D**), further indicating that CAR does not contribute to EMT changes. Whilst our data from fixed cells suggested that WTCAR and AACAR were similarly distributed at cell-cell adhesions, we postulated, based on our previous data in normal lung epithelial cells, that dynamics of CAR itself would be altered upon phosphorylation of the cytoplasmic tail (10). Analysis of CAR dynamics at the plasma membrane using fluorescence recovery after photobleaching (FRAP) revealed significantly slower recovery of AACAR compared to WTCAR at cell-cell adhesions (**Supplementary Figures 1E, F**) indicating phosphorylation promotes CAR movement at the membrane but that this does not result in a tangible change in cell-cell adhesion properties. Functional analysis of this panel of cells showed a doubling time of approximately 48 hours in parental cells that did not significantly change in CAR overexpressing or CRISPR cells over this time (**Figure 1F**). However, subcutaneous injection of cells into immunocompetent mice revealed a significant increase in tumor growth *in vivo* in WTCAR and AACAR cells, with WTCAR cells showing the highest proliferative potential (**Figure 1G**). This data demonstrates that higher levels of CAR promote tumor growth, and this may be specific to 3D microenvironments. To determine whether this enhanced proliferative capacity correlated with invasive potential, we analysed invasion as measured using 3D inverted invasion assays and 3D spheroids. In both cases, WTCAR and AACAR promoted invasion in CMT cells compared to controls (**Figures 1H–K**). Collectively these data demonstrate that enhancing CAR expression can drive a pro-tumorigenic phenotype within 3D environments.

CAR Expression Promotes Cell-Matrix Adhesion

As our data demonstrated no change in cell-cell adhesion but enhanced invasion when CAR is overexpressed, we next explored whether CAR may be mediating a pro-invasive phenotype through contributions to cell-matrix adhesion. We firstly explored whether initial attachment to ECM proteins was altered across the CMT cell panel with a particular focus on those ECM proteins within the stroma (collagen I) or surrounding the solid tumor (basement membrane). WTCAR

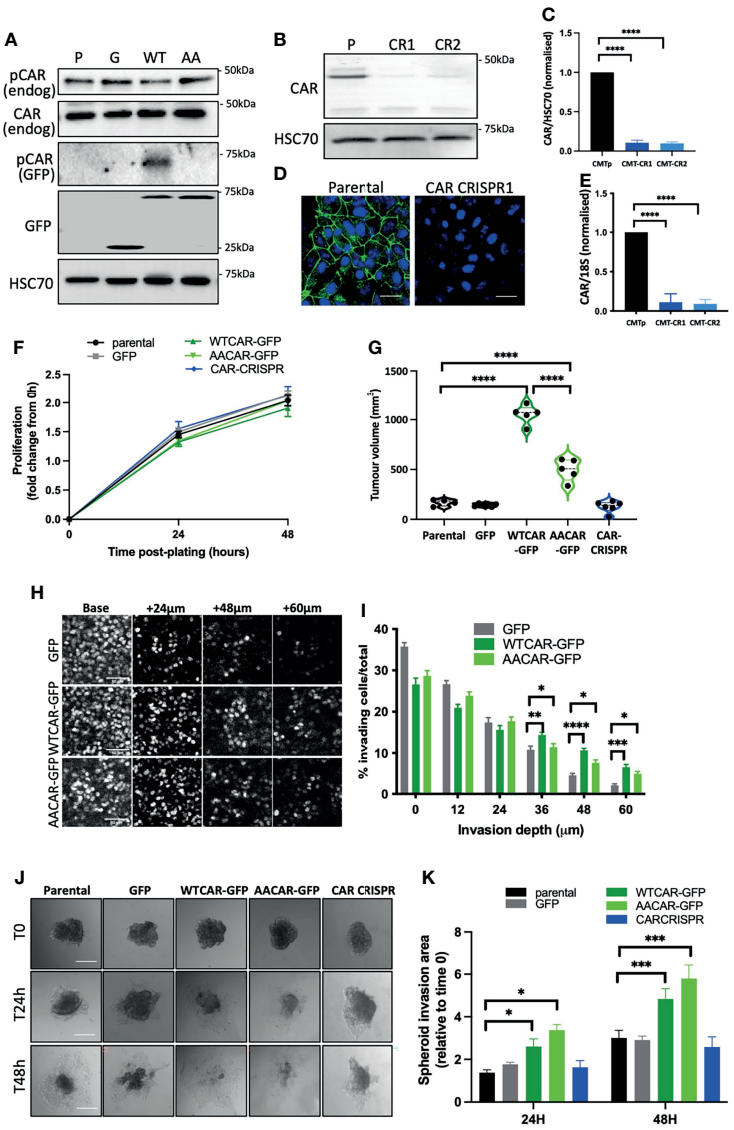

FIGURE 1 | CAR promotes lung cancer progression. **(A)** Representative Western blots of specified proteins in CMT 167 cells, parental (P), GFP expressing **(G)**, WTCAR-GFP (WT) and AACAR-GFP (36). **(B)** Representative Western blots of CAR levels in parental (P) and 2 different CAR CRISPR CMT 167 cell populations (CR1, CR2). **(C)** Graph shows quantification of CAR levels as in **(B)** from 4 independent experiments. **(D)** Representative confocal images of parental and CAR CRISPR cells stained for CAR (green) and DAPI (blue). Scale bars are 10 µm. **(E)** CAR transcript levels in parental and CRISPR cells by qPCR relative to 18S control. Pooled data from 3 independent experiments. **(F)** Proliferation in specified CMT 167 cells 24h and 48h post-plating. Data is representative of 3 independent experiments and from 4 replicates per cell line per time point. **(G)** Tumor volume in mice subcutaneously injected with specified CMT 167 cells. Violin plots shown with each point represents one animal (n=5 per group). **(H)** Representative confocal images of nuclei stained in specified CMT 167 cell lines at intervals through 3D inverted invasion assay. Scale bars are 50 µm. **(I)** Quantification of invasion data from **(H)** at different depth intervals, pooled from 4 different wells per condition, representative of 3 independent experiments. **(J)** Representative phase contrast widefield images of specified CMT 167 cell spheroids images over time. Scale bars are 100 µm. **(K)** Quantification of spheroid area over time relative to time 0. 10 spheroids per cell line analysed; representative of 3 independent experiments. All values are mean ± SEM. P values *p < 0.05,**p < 0.01, ***p < 0.0005, ****p < 0.0001.

overexpression promoted initial CMT cell attachment to both Collagen I and Matrigel as measured 2 hours post-plating (**Figure 2A**). To explore whether this phenotype was associated with higher levels of active β1 integrins, that are the major receptor family for these ECM proteins, cells were fixed and stained with an antibody that recognizes the active conformation of these receptors (9EG7). Images revealed that neither WTCAR-GFP nor AACAR-GFP localised to active integrin containing adhesions (**Figure 2B**). However, quantification of data revealed that WTCAR but not AACAR expressing cells showed a significant enhancement in larger activeβ1 integrin containing focal adhesions (**Figures 2C, D**).

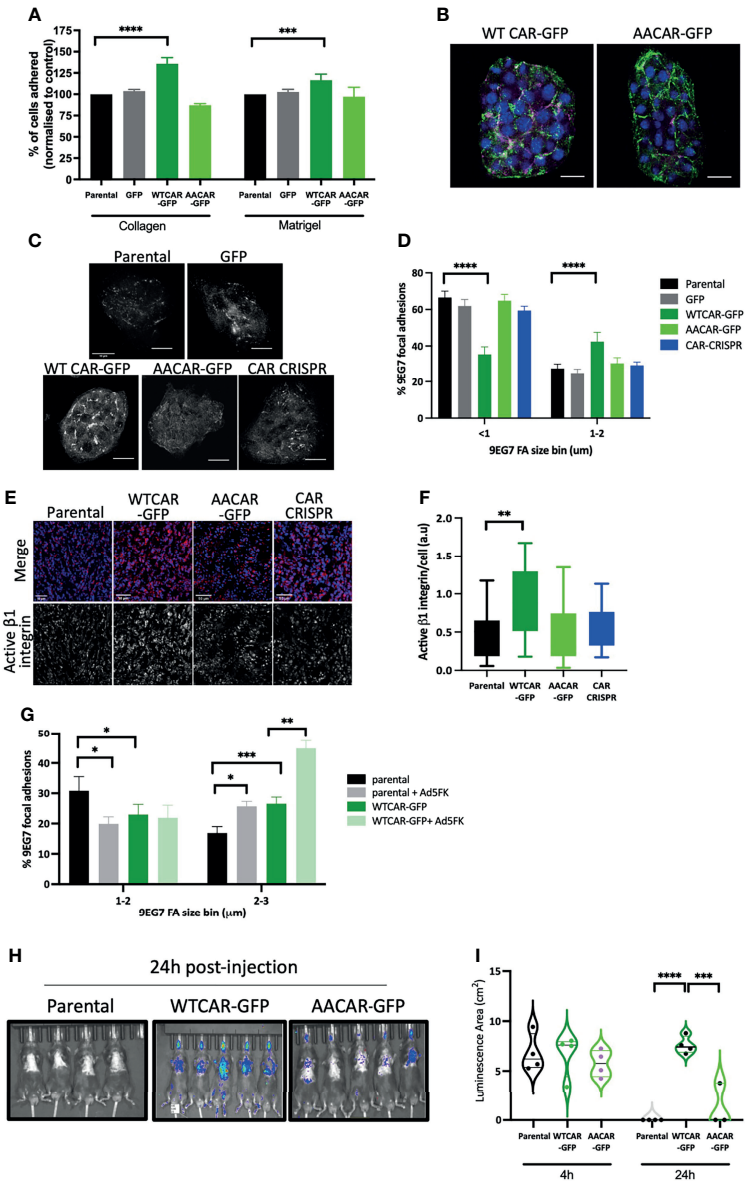

FIGURE 2 | CAR promotes cell-matrix adhesion. **(A)** Graphs showing % adhesion to collagen and Matrigel of indicated cell lines 2h post-plating. Data is from 3 wells per cell line, representative of 3 independent experiments. **(B)** Representative confocal images of WTCAR-GFP and AACAR-GFP CMT cells (CAR; green) stained for active β1 integrins (9EG7; magenta). Scale bars are 20 μm. **(C)** Representative confocal images of indicated cell lines stained for active β1 integrins (9EG7). Scale bars are 50 μm. **(D)** Quantification of images as in **(C)** from at least 10 different fields of view. Data is presented as % of active integrin adhesions categorised in sizes. Representative of 3 independent experiments. **(E)** Representative confocal images of tissues from subcutaneous tumors of indicated cell lines, stained for active integrins (9EG7, red) and DAPI (blue). Scale bars are 50 μm. **(F)** Quantification of images as shown in (D or E)?. Data is from 6 tumors per cell line, and 4 fields of view per tumor. **(G)** Quantification of 9EG7 staining as in (B,C what about 9eg7 fk images)? from parental or WTCAR-GFP cells with or without Ad5FK pre-incubation. Data is from at least 10 different fields of view per condition. Data is presented as % of active integrin adhesions categorised in sizes. Representative of 3 independent experiments. **(H)** Images of indicated cell lines expressing luciferase 24 hours after intravenous injection into animals. Representative of 2 independent experiments. **(I)** Quantification of data as in **(H)** Violin plots shown with each point represents one animal (n=4-5 per group). All values are mean ± SEM. P values *p < 0.05,**p < 0.01, ***p < 0.0005, ****p < 0.0001.

In agreement with this, we also observed significantly increased activeβ1 integrins in solid tumors following subcutaneous injection of WTCAR overexpressing cells (**Figures 2E, F**). To test whether CAR engagement *in trans* at cell-cell adhesions contributed to this integrin-based adhesion phenotype, we treated cells with recombinant Ad5FK to block CAR *in trans* binding as we have previously (18). Ad5FK enhanced active β1 integrins in both parental and WTCAR expressing CMT cells (**Figure 2G**), suggesting CAR-CAR homodimers need to be disengaged at cell-cell adhesions for CAR to promote cell-

matrix adhesion. To determine if this enhanced adhesion phenotype was also seen *in vivo*, we performed IV injections of CMT cells expressing a luciferase reporter and analysed retention of cells in the lung over 24 hours. Significantly enhanced retention of WTCAR cells in lung was seen after 24 hours (**Figures 2H, I**) suggesting enhanced cell-matrix stability leads to increased metastatic potential.

CAR Expression Promotes Adhesion and Invasion in Mesenchymal Cells

Our data show that CAR engagement at junctions negatively regulates the ability of epithelial-like carcinoma cells to activate integrins and undergo invasion. We therefore hypothesised that overexpressing CAR in mesenchymal lung cancer cells would promote adhesion and invasion. To test this, we generated LLC mouse lung carcinoma cells overexpressing WT and AACAR (**Figure 3A**), noting these cells express significantly reduced endogenous CAR compared to CMT 167 cells. Both WTCAR and AACAR localised to the membrane and was enriched at sites of transient cell-cell contact (**Figure 3B**). Analysis following subcutaneous injection of these cells revealed enhanced tumor growth in WTCAR overexpressing cells (**Figure 3C**), similar to that seen in CMT cells (**Figure 1G**). WTCAR overexpression also enhanced initial LLC cell attachment to Collagen I and Matrigel (**Figure 3D**). To determine whether CAR was associated with integrin-containing focal adhesions in mesenchymal lung cancer cells, WTCAR-GFP and AACAR-GFP overexpressing cells were stained with antibody to active β1 integrins. Images demonstrated no clear colocalisation of CAR and β1 integrins in either cell line (**Figure 3E**). However, significantly enhanced β1 integrin activation was measured in WTCAR-GFP overexpressing cells with a smaller increase seen in AACAR cells (**Figure 3F**) as also seen in CMT cells. WT and AACAR overexpression also enhanced LLC cell invasion in 3D inverted invasion assays (**Figure 3G**). Finally, WTCAR overexpression increased LLC cell retention in the lung following IV injection as measured using luciferase reporters (**Figures 3H, I**). These data suggest that overexpression of CAR in mesenchymal cancer cells enhances cell-matrix adhesion and invasion, suggesting CAR-dependent effects on these phenotypes do not require CAR localisation to adherens and tight junctions.

CAR Is Expressed Highly at Tumor Boundaries and Is Mechano-Responsive

Our data demonstrate that high expression of CAR positively regulates tumor cell-matrix adhesion, and this may be distinct from the known role of CAR at cell-cell adhesion sites. To determine whether CAR expression levels correlated with sites of cell-matrix adhesion in tumors, we stained for CAR in tissue sections from subcutaneous CMT and LLC cell tumors from immunocompetent mice. An increase in CAR levels was observed at the edge of solid tumors where cells contact the ECM in both cell types (**Figure 4A**). Moreover, phosphorylated CAR was also readily detected at the boundary of these tissues (**Figure 4B**). In addition to the biochemical properties of the ECM, the stiffness of the matrix surrounding the tumor is increasingly recognized as a key factor contributing to tumor growth and invasive potential (40). Enhanced stiffness in the tumor microenvironment is sensed through integrin-based focal adhesions and has been associated with increased invasion in several tumor types. Given our data demonstrating that CAR contributes to cell-matrix interactions in a phosphorylation-dependent manner, we next determined whether CAR phosphorylation was responsive to changes in the matrix properties. To define this, we analysed CAR phosphorylation in cells plated on substrates of differing biomechanical properties; 1.5kPa (normal lung tissue stiffness), 28kPa (stiffness detected in several lung cancers) or glass (>1Gpa, standard non-physiological substrate). We analysed levels of pCAR as a function of CAR expression on a cell-by-cell basis to control for any variation in CAR expression levels. Data revealed significantly enhanced levels of CAR phosphorylation in cells on stiffer ECM (**Figures 4C**) and this correlated with higher CAR:P-CAR colocalization co-efficient in both CMT and LLC cells (**Figure 4D**). These data show that properties of the surrounding ECM can lead to altered levels and localisation of phosphorylated CAR, potentially promoting CAR-dependent cell-matrix adhesion and invasion.

CAR Forms a Complex With Focal Adhesion Proteins and Promotes Rap1 Activity

In order to understand whether the observed CAR-dependent changes to cell-matrix adhesion were due to CAR physically engaging with focal adhesion proteins, we performed CAR immunoprecipitation experiments and probed for candidate proteins. We chose to focus on β1 integrins, Src, FAK and paxillin as these are core components of most focal adhesions formed in cells on collagen substrates and represent key regulatory elements to control of adhesion formation and dynamics. WTCAR, but not AACAR formed a complex with both β1 integrins (**Figure 5A**) and key focal adhesion components Src, FAK and paxillin (**Figure 5B**). Moreover, *in vitro* binding assays using the CAR cytoplasmic tail confirmed binding to FAK, Src and paxillin (**Figure 5C**) and further demonstrated dependence on phosphorylation of CAR at T290/S293 for these interactions as significantly lower binding was seen with AACAR vs WT or DD (phospho-mimic) CAR proteins (**Figure 5D**). To determine whether activity of these adhesion proteins may contribute to CAR-dependent cell-matrix adhesion, cells were treated with the Src inhibitor PP2 and the FAK inhibitor PF573228 (**Figures 5E, F**). Analysis of active β1 integrins revealed significantly reduced CAR-dependent β1 activation in the presence of both inhibitors (**Figure 5G**) indicating these proteins may be mediating CAR-dependent adhesion effects. To determine if Src activity might additionally play a role in controlling CAR mobility at the membrane, and thus its influence on cell-ECM adhesion, FRAP analysis was performed on WTCAR-GFP expressing cells in the presence of vehicle control or PP2. PP2 treatment resulted in significantly reduced CAR mobility at cell-cell adhesions (**Figure 5H**), supporting the notion that CAR-Src complex and Src activity

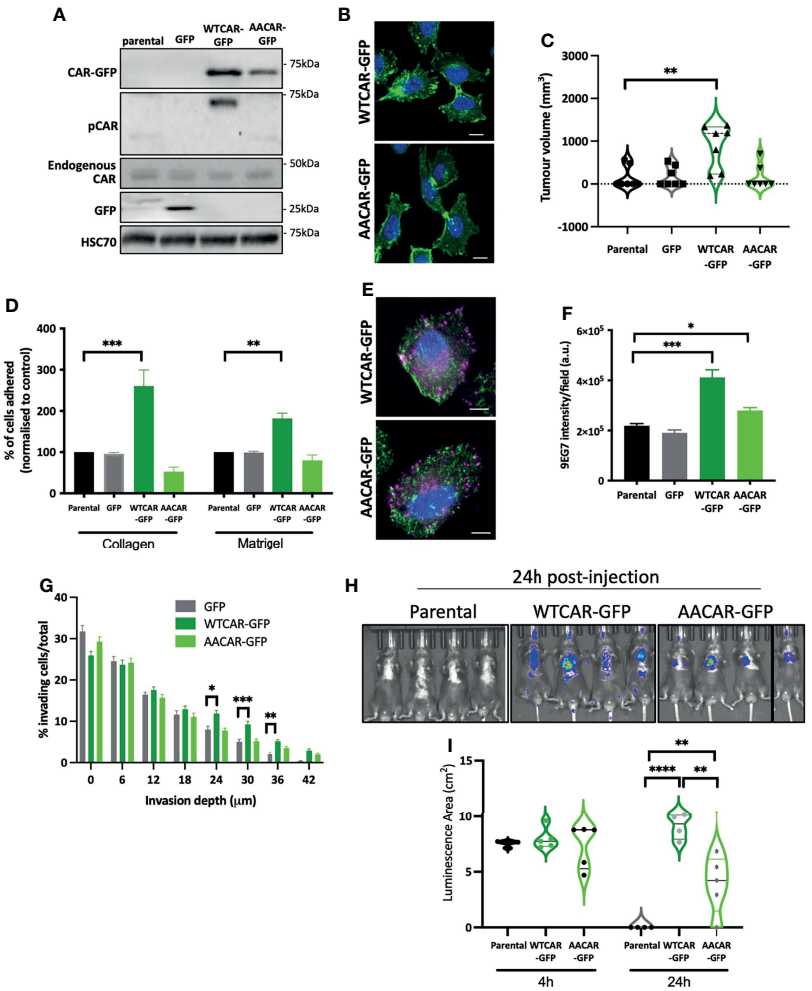

FIGURE 3 | CAR promotes adhesion and invasion in mesenchymal cells. **(A)** Representative Western blots of specified proteins in LLC cells, parental, GFP expressing, WTCAR-GFP and AACAR-GFP. **(B)** Representative confocal images of WTCAR-GFP and AACAR-GFP expressing LLC cells. CAR is shown in green and DAPI in blue. Scale bars are 10 μm. **(C)** Tumor volume in mice subcutaneously injected with specified CMT 167 cells. Violin plots shown with each point represents one animal (n=7-8 per group). **(D)** Graphs showing % adhesion to collagen and Matrigel of indicated cell lines 2h post-plating. Data is from 3 wells per cell line, representative of 3 independent experiments. **(E)** Representative confocal images of WTCAR-GFP and AACAR-GFP LLC cells (CAR; green) stained for active β1 integrins (9EG7; magenta). Scale bars are 10 μm. **(F)** Quantification of images of specified cell lines stained for active β1 integrins (9EG7). Data is from at least 10 fields of view (5-10 cells per field) per condition. Representative of 3 independent experiments. **(G)** Quantification of inverted invasion data from specified cell lines at different depth intervals, pooled from 4 different wells per condition, representative of 3 independent experiments. **(H)** Images of indicated cell lines expressing luciferase 24 hours after intravenous injection into animals. Representative of 2 independent experiments. **(I)** Quantification of data as in **(H)**. Violin plots shown with each point represents one animal (n=4-5 per group). All values are mean ± SEM. P values *p < 0.05, **p < 0.01, ***p < 0.0005, ****p < 0.0001.

may regulate the CAR-dependent effects on cell-ECM adhesion. Rap1 has also been previously shown to act downstream of the related family member JAM-A and controls integrin activation (41, 42). We therefore assessed Rap1 activity in the CMT 167 cell panel to understand if this GTPase may play a role downstream of CAR in driving integrin activity. WTCAR, but not AACAR overexpression led to significantly enhanced Rap1 activity as measured using pulldown assays, whereas depletion of CAR reduced Rap1 activity (**Figures 5I, J**). To further determine whether this enhanced activation of Rap1 contributed to CAR-dependent β1 integrin activation, cells were treated with the Rap1 inhibitor GGTI298 and adhesion to collagen I was tested as in previous experiments. Data revealed that treatment of cells with GGTI298 lead to suppression of CAR-induced adhesion (**Figure 5K**) indicating that enhanced integrin activation downstream of CAR is mediated by increased activity of Rap1. This data demonstrates that CAR acts to co-ordinate focal adhesion signalling through Src and Rap1.

DISCUSSION

Our study provides evidence that CAR contributes to several aspects of lung cancer progression including tumor growth,

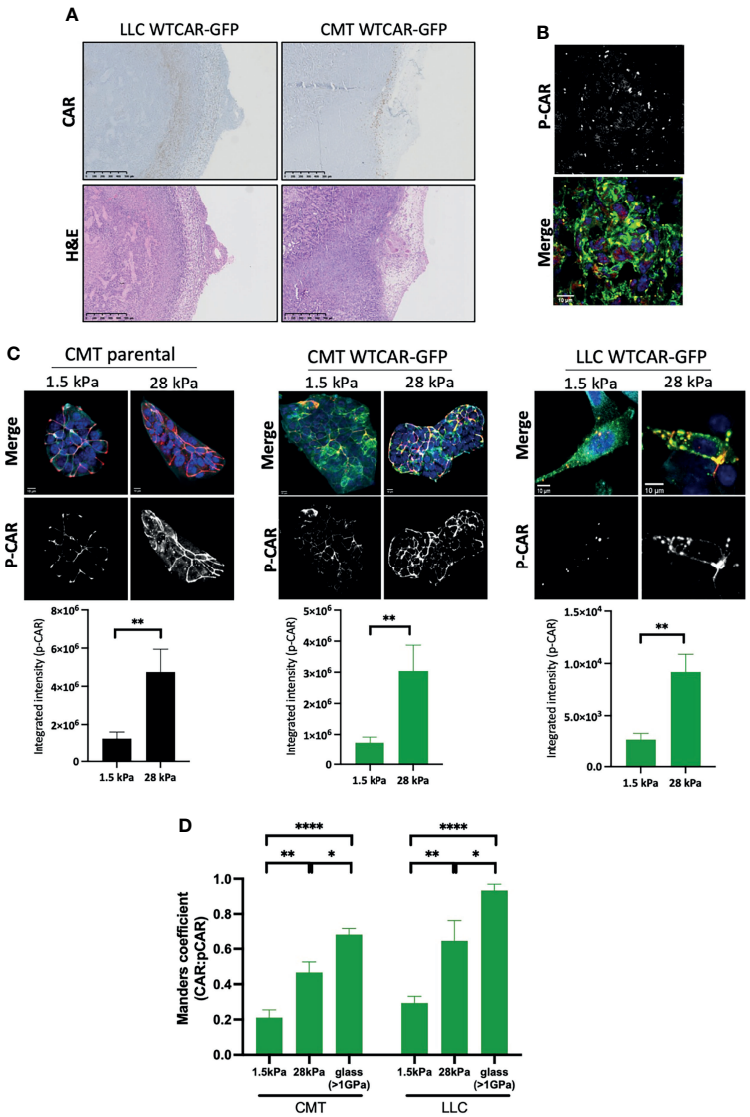

FIGURE 4 | CAR is a mechano-responsive protein. **(A)** Representative images of sections from tumors formed following subcutaneous injection of LLC or CMT cells stably expressing WTCAR-GFP, stained for CAR (top panels, brown) or H&E (bottom panels). **(B)** Representative images of P-CAR staining of frozen sections of tumors formed following subcutaneous injection of CMT WTCAR-GFP expressing cell. Top panel shows P-CAR alone, bottom panel P-CAR (39), CAR-GFP (green) and DAPI (blue). **(C)** Representative confocal images of indicated cell lines plated on 1.5 kPa or 28 kPa stiffness plates, stained for P-CAR (bottom panels) and DAPI (blue). CAR is shown in green. Graphs beneath each image set show quantification of P-CAR from at least 10 fields of view per cell line, representative of 3 independent experiments. **(D)** Quantification of colocalization between CAR and P-CAR from images as in **(C)** from CMT and LLC cells expressing WTCAR-GFP. All values are mean ± SEM. P values *p < 0.05, **p < 0.01, ****p < 0.0001.

adhesion and invasion. Importantly, we show these effects of CAR overexpression do not require formation of adherens or tight junctions, where CAR has been previously studied. Multiple studies have investigated the role of CAR in tumor growth; however, these reports did not analyse whether CAR homodimerization *in trans* and factors dictated by the tumor microenvironment influenced this phenotype. We propose a model based on our data (**Figure 6**) whereby CAR activates the integrin-regulator Rap1 and associates with focal adhesion molecules and β1 integrins to influence cell-matrix adhesion leading to enhanced tumor invasion and metastasis. CAR may undergo dimerization *in cis* to bring scaffold molecule MAGI-1 and Rap GEF PDZGEF-2 together to activate Rap1. We speculate that phospho-CAR is more mobile on the membrane, and under these conditions can distally regulate integrin activity, without localizing to focal adhesions, *via* recruitment of focal adhesion molecules and/or β1 integrins to the membrane.

CAR expression levels have been shown to differ depending on the stage of cancer progression. For example, CAR up-regulation has been implied to promote carcinogenesis in

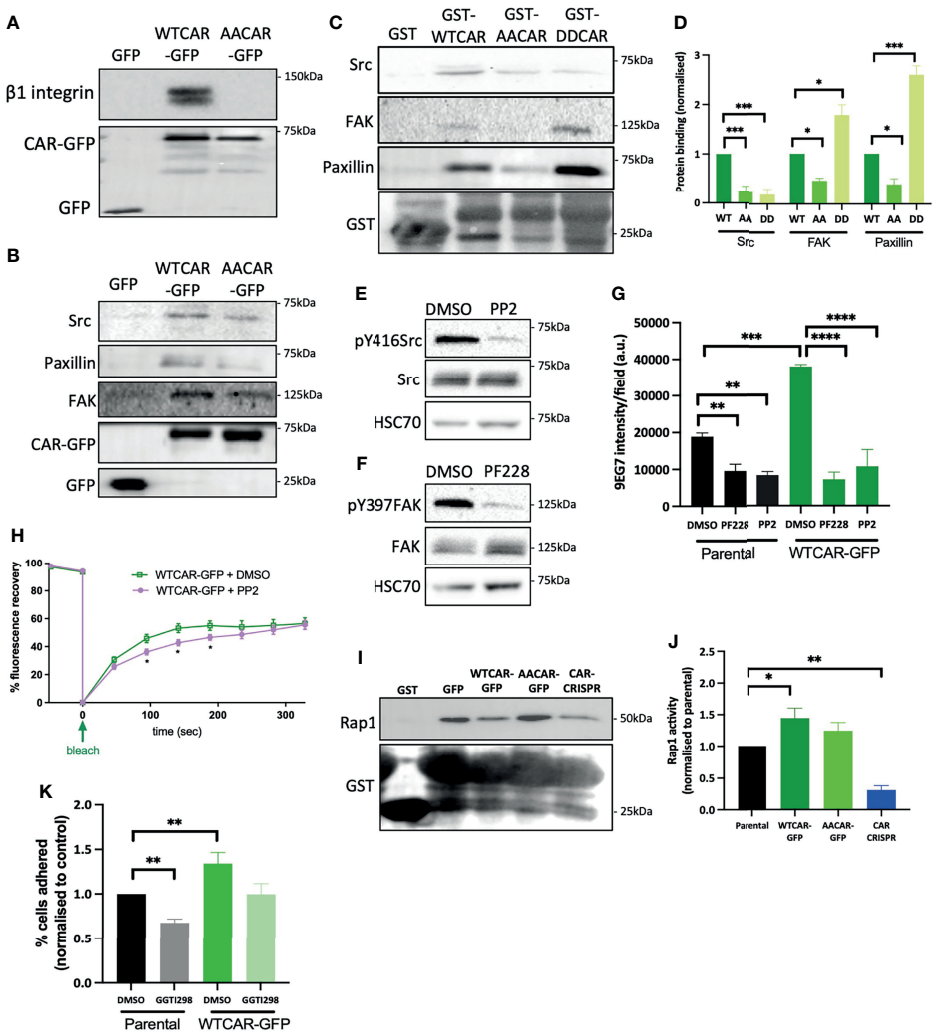

FIGURE 5 | CAR forms a complex with focal adhesion proteins. **(A)** Representative western blot of immunoprecipitation of β1 integrins from specified cell lines probed for β1 integrin and GFP. Representative of 5 independent experiments. **(B)** Western blots of immunoprecipitation of GFP or GFP-CAR from lysates from specified cell lines probed for indicated focal adhesion proteins and GFP. Representative of 5 independent experiments. **(C)** Western blots of GST pulldowns using GST only or GST-CAR cytoplasmic tail (WT, AA, DD) using from lysates from CMT parental cells probed for indicated focal adhesion proteins and GST. **(D)** Quantification of blots as in C from 5 independent experiments. **(E, F)** Western blot of lysates from CMT parental cells treated with Src inhibitor [PP2, 1μM, **(E)**] or FAK inhibitor [PF228, 1μM, **(F)**] probed for indicated proteins. **(G)** Quantification of active β1 integrins (9EG7) from images of specified CMT cell lines treated with DMSO, PP2 or PF228. Data is from at least 10 fields of view (5-10 cells per field) per condition. Representative of 3 independent experiments. **(H)** Quantification of recovery curves of fluorescence intensity for FRAP data from WTCAR-GFP CMT cells +/-PP2. Data is from at least 15 different ROIs per cell line, shown as mean +/-SEM, representative of 3 independent experiments. **(I)** Representative Western blots of lysates from Rap1 activity pulldown assays from specified CMT cell lines, probed for Rap1 and GST. **(J)** Quantification of data as in **(I)**, pooled from 5 independent experiments. **(K)** Quantification of CMT parental and WTCAR-GFP cell adhesion to Matrigel after 2h, following pre-treatment with DMSO or Rap1 inhibitor (GGTI298, 5μM) normalised to control. Data is from 3 wells per cell line, representative of 3 independent experiments. All values are mean ± SEM. P values *p < 0.05, **p < 0.01, ***p < 0.0005, ****p < 0.0001.

early-stage breast cancer and breast cancer precursor cells (43, 44). However, CAR is downregulated in advanced disease stages displaying loss of differentiation in several tumor types (21, 45–48). Similarly, CAR levels are high during early carcinogenesis in colon adenomas and decreased during cancer dissemination in colon cancer metastases (49). However, changes in expression and function of CAR during carcinogenesis may be tumor-specific and both positive and negative expression contribute to different aspects of tumor progression (19). Our data demonstrate that CAR expression levels are highest at the boundary between the tumor edge and the stroma, in agreement with another recent study (28). Moreover, we show that CAR is a mechanosensitive protein and undergoes enhanced phosphorylation in response to stiffness. This coupled with our discovery that CAR can promote integrin activation and enhanced adhesion both *in vitro* and *in vivo* suggests that CAR may be upregulated both in levels and activation status prior to invasion where it plays a role in enabling tumor cell escape into

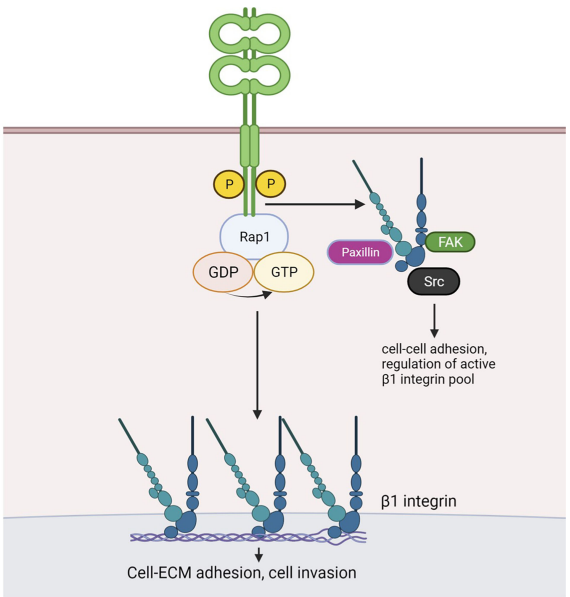

FIGURE 6 | Working model for CAR-dependent regulation of lung cancer cell adhesion. Phosphorylated CAR promotes β1 integrin and Rap1 activation. Similarly to JAM-A, dimerised CAR may promote interaction of scaffold protein MAGI-1 and the Rap1 GEF PDZ-GEF2, resulting in Rap1 activation. CAR-mediated Rap1 activation promotes cell-ECM adhesion and may enhanceβ1 integrin activity. The latter may in turn be involved in CAR-mediated promotion of cell invasion. Phosphorylated CAR may recruit β1 integrins and/or focal adhesion components Src, FAK and Paxillin to the membrane to regulate cell-cell adhesion and to distally control focal adhesion activity. Figure created with BioRender.com.

the stroma. Our data further suggest that this may be enhanced in tumors with stiffer extracellular matrix environments, as it has been shown for other proteins such as Programmed Death-Ligand 1 (PD-L1) (50). Whilst the precise mechanisms by which CAR levels and phosphorylation are controlled by mechanical properties of the matrix remain unclear, this does point towards a bi-directional interplay between integrins (as key membrane associated force-sensing molecules) and CAR in the control of tumor cell invasion.

Our identification of CAR in complex with several key focal adhesion proteins would indicate CAR-dependent adhesion and migration may operate through direct co-operation with integrin-associated proteins. We additionally demonstrated a dependence upon phosphorylation of the CAR cytoplasmic tail for formation of these complexes. However, CAR is not clearly or robustly localised to focal adhesions at the basal surface of adherent cells, either in CMT 167 or LLC cell lines. This suggests that this complex may form at cell-cell junctions or within intracellular endocytic compartments. Indeed, FAK and Src have been shown to localise to cell-cell contacts in other cell types and immuno-precipitate with E-cadherin, α-catenin and β-catenin (10, 51–53). Both α-catenin and β-catenin have been suggested as potential interacting partners of CAR and may therefore mediate formation of this multi-protein complex (54, 55). FAK, Src and paxillin also associate with integrins and recent work from our lab and others have shown that integrins localise to cell-cell contacts in several epithelial-like cells (32, 56, 57). Moreover, we show that Src activity can help to promote CAR stability at cell-cell adhesion sites, indicating formation of this complex may in turn control CAR localisation. Given that our data show CAR forms a complex with total β1 integrins, we postulate that FAK, Src and paxillin may be recruited to cell junctions by CAR *via* β1 integrins to regulate cell-cell adhesion, as well as controlling levels of active integrins at the cell-matrix interface. It would be interesting to investigate traffic of integrins in live cells, given that recent evidence also suggests integrins can remain as active signalling proteins in endocytic compartments in cancer cells (58).

Our data show that Rap1 mediates CAR-dependent increase in cell-ECM adhesion and that CAR over-expression increases Rap1 activity. Rap1 has been suggested to induce integrin-mediated cell-ECM adhesion through enhanced integrin avidity and affinity for extracellular ligands, possibly *via* Rap1-GTP Interacting Adaptor Molecule (RIAM)-mediated recruitment of talin to integrin complexes (42). Other junctional molecules such as JAM-A, Nectin and E-cadherin can also regulate Rap1 activity, and dimerised JAM-A can induce Rap1 activation by bringing Afadin and PDZ-Guanine Exchange Factor 2 (GEF2) in the same complex (41, 59–61). VE-cadherin-induced Rap1 activation was shown to occur *via* Membrane Associated Guanylate kinase with Inverted orientation 1 (MAGI-1) which localises to cell-cell junctions and forms a complex with PDZ-GEF2 (62). It is possible that CAR regulates Rap1 activity by creating a complex with MAGI-1 and PDZ-GEF2, and similar to JAM-A, this complex could be formed *via* dimerization of CAR molecules and binding of partners through CAR PDZ-binding domains. Taken together, these data suggest that CAR could facilitate the formation of a complex between the Rap GEF PDZ-GEF2 and the scaffold protein MAGI-1 to activate Rap1 and regulate β1 integrin activity and cell adhesion.

In summary, we have identified a new role for CAR in mediating cell-matrix adhesion and invasion of lung cancer cells through co-operation with integrin-based adhesions and mechanosensing. Our work paves the way for future studies to explore the relationship between organisation of the extracellular matrix and CAR levels/phosphorylation in human tumors to determine whether this receptor represents a potential therapeutic target to prevent lung cancer cell metastasis.

DATA AVAILABILITY STATEMENT

The original contributions presented in the study are included in the article/**Supplementary Material**. Further inquiries can be directed to the corresponding author.

ETHICS STATEMENT

The animal study was reviewed and approved by Ethical Review Committee at King's College London and the Home Office, UK.

AUTHOR CONTRIBUTIONS

CO, MP, GS, and EO-Z all designed the research. CO, MP, and EO-Z analyzed data. CO, EP, JK, and EO-Z performed research. CO and MP wrote the paper. All authors contributed to the article and approved the submitted version.

FUNDING

CO was supported by the National Institute for Health Research (NIHR) Biomedical Research Centre (BRC) based at Guy's and St Thomas' NHS Foundation Trust and King's College London. EO-Z was supported by funding from the Medical Research Council UK (MR/S009191/1, to MP).

ACKNOWLEDGMENTS

The authors would like to thank the Biological Service Unit at King's College London Guy's Hospital and St. Thomas' Hospital campuses for animal handling and care, James Rosekilly (King's Health Partners Cancer Biobank) for tumor embedding, sectioning and H&E staining and Debbie Finch (Comprehensive Cancer Centre, King's College London) for tissue scanning.

SUPPLEMENTARY MATERIAL

The Supplementary Material for this article can be found online at: https://www.frontiersin.org/articles/10.3389/fonc.2022.829313/full#supplementary-material

Supplementary Figure 1 | – Manipulation of CAR does not alter key EMT markers **(A)** Representative confocal images of specified cell lines fixed and stained for E-Cadherin (shown as single channel black and white, magenta in merged image) and DAPI (blue). GFP is shown in green in merged channel. Scale bars are 10 μm. **(B)** Quantification of E-cadherin intensity from line scans perpendicular to junctions in all cell lines from images as in **(A)**. Data from at least 30 junctions per cell line, representative of 3 independent experiments. **(C)** Western blots of lysates from indicated cell lines probed for E-cadherin, β-catenin and HSC70. Values shown beneath graph are from densitometry analysis of E-Cadherin blots normalised to parental cells from 4 independent experiments +/-SEM. **(D)** Western blots of lysates from indicated CMT cells probed for vimentin and HSC70. Representative of 4 independent experiments. **(E)** Representative confocal images of FRAP analysis of WTCAR-GFP vs AACAR-GFP over time. **(F)** Graph shows recovery curves of fluorescence intensity for each cell line from data as in **(E)**. Data is from at least 15 different ROIs per cell line, shown as mean +/-SEM, representative of 3 independent experiments. P values ***p < 0.0005, ****p < 0.0001.

REFERENCES

1. World Health Organisation. *Cancer Today*. (2020).
2. Lemjabbar-Alaoui H, Hassan OU, Yang YW, Buchanan P. Lung Cancer: Biology and Treatment Options. *Biochim Biophys Acta* (2015) 1856(2):189–210. doi: 10.1016/j.bbcan.2015.08.002
3. van Zijl F, Krupitza G, Mikulits W. Initial Steps of Metastasis: Cell Invasion and Endothelial Transmigration. *Mutat Res* (2011) 728(1-2):23–34. doi: 10.1016/j.mrrev.2011.05.002
4. Okegawa T, Pong RC, Li Y, Hsieh JT. The Role of Cell Adhesion Molecule in Cancer Progression and its Application in Cancer Therapy. *Acta Biochim Pol* (2004) 51(2):445–57. doi: 10.18388/abp.2004_3583
5. Lu W, Kang Y. Epithelial-Mesenchymal Plasticity in Cancer Progression and Metastasis. *Dev Cell* (2019) 49(3):361–74. doi: 10.1016/j.devcel.2019.04.010
6. Lauko A, Mu Z, Gutmann DH, Naik UP, Lathia JD. Junctional Adhesion Molecules in Cancer: A Paradigm for the Diverse Functions of Cell-Cell Interactions in Tumor Progression. *Cancer Res* (2020) 80(22):4878–85. doi: 10.1158/0008-5472.CAN-20-1829
7. Bergelson JM, Cunningham JA, Droguett G, Kurt-Jones EA, Krithivas A, Hong JS, et al. Isolation of a Common Receptor for Coxsackie B Viruses and Adenoviruses 2 and 5. *Science* (1997) 275(5304):1320–3. doi: 10.1126/science.275.5304.1320
8. Ortiz-Zapater E, Santis G, Parsons M. CAR: A Key Regulator of Adhesion and Inflammation. *Int J Biochem Cell Biol* (2017) 89:1–5. doi: 10.1016/j.biocel.2017.05.025
9. Cohen CJ, Shieh JT, Pickles RJ, Okegawa T, Hsieh JT, Bergelson JM. The Coxsackievirus and Adenovirus Receptor is a Transmembrane Component of the Tight Junction. *Proc Natl Acad Sci USA* (2001) 98(26):15191–6. doi: 10.1073/pnas.261452898
10. Morton PE, Hicks A, Nastos T, Santis G, Parsons M. CAR Regulates Epithelial Cell Junction Stability Through Control of E-Cadherin Trafficking. *Sci Rep* (2013) 3:2889. doi: 10.1038/srep02889
11. Huang K, Ru B, Zhang Y, Chan WL, Chow SC, Zhang J, et al. Sertoli Cell-Specific Coxsackievirus and Adenovirus Receptor Regulates Cell Adhesion and Gene Transcription *via* Beta-Catenin Inactivation and Cdc42 Activation. *FASEB J* (2019) 33(6):7588–602. doi: 10.1096/fj.201801584R
12. Garrido-Urbani S, Bradfield PF, Imhof BA. Tight Junction Dynamics: The Role of Junctional Adhesion Molecules (JAMs). *Cell Tissue Res* (2014) 355 (3):701–15. doi: 10.1007/s00441-014-1820-1
13. Matthaus C, Langhorst H, Schutz L, Juttner R, Rathjen FG. Cell-Cell Communication Mediated by the CAR Subgroup of Immunoglobulin Cell Adhesion Molecules in Health and Disease. *Mol Cell Neurosci* (2017) 81:32–40. doi: 10.1016/j.mcn.2016.11.009
14. Farmer C, Morton PE, Snippe M, Santis G, Parsons M. Coxsackie Adenovirus Receptor (CAR) Regulates Integrin Function Through Activation of P44/42 MAPK. *Exp Cell Res* (2009) 315(15):2637–47. doi: 10.1016/j.yexcr.2009.06.008
15. Fok PT, Huang KC, Holland PC, Nalbantoglu J. The Coxsackie and Adenovirus Receptor Binds Microtubules and Plays a Role in Cell Migration. *J Biol Chem* (2007) 282(10):7512–21. doi: 10.1074/jbc.M607230200
16. Huang KC, Yasruel Z, Guerin C, Holland PC, Nalbantoglu J. Interaction of the Coxsackie and Adenovirus Receptor (CAR) With the Cytoskeleton: Binding to Actin. *FEBS Lett* (2007) 581(14):2702–8. doi: 10.1016/j.febslet.2007.05.019
17. Saito K, Sakaguchi M, Iioka H, Matsui M, Nakanishi H, Huh NH, et al. Coxsackie and Adenovirus Receptor is a Critical Regulator for the Survival and Growth of Oral Squamous Carcinoma Cells. *Oncogene* (2014) 33 (10):1274–86. doi: 10.1038/onc.2013.66
18. Morton PE, Hicks A, Ortiz-Zapater E, Raghavan S, Pike R, Noble A, et al. TNFalpha Promotes CAR-Dependent Migration of Leukocytes Across Epithelial Monolayers. *Sci Rep* (2016) 6:26321. doi: 10.1038/srep26321
19. Reeh M, Bockhorn M, Gorgens D, Vieth M, Hoffmann T, Simon R, et al. Presence of the Coxsackievirus and Adenovirus Receptor (CAR) in Human Neoplasms: A Multitumour Array Analysis. *Br J Cancer* (2013) 109(7):1848–58. doi: 10.1038/bjc.2013.509
20. Veena MS, Qin M, Andersson A, Sharma S, Batra RK. CAR Mediates Efficient Tumor Engraftment of Mesenchymal Type Lung Cancer Cells. *Lab Invest* (2009) 89(8):875–86. doi: 10.1038/labinvest.2009.56
21. Anders M, Vieth M, Rocken C, Ebert M, Pross M, Gretschel S, et al. Loss of the Coxsackie and Adenovirus Receptor Contributes to Gastric Cancer Progression. *Br J Cancer* (2009) 100(2):352–9. doi: 10.1038/sj.bjc.6604876
22. Chen Z, Wang Q, Sun J, Gu A, Jin M, Shen Z, et al. Expression of the Coxsackie and Adenovirus Receptor in Human Lung Cancers. *Tumour Biol* (2013) 34(1):17–24. doi: 10.1007/s13277-012-0342-2
23. Wunder T, Schmid K, Wicklein D, Groitl P, Dobner T, Lange T, et al. Expression of the Coxsackie Adenovirus Receptor in Neuroendocrine Lung Cancers and its Implications for Oncolytic Adenoviral Infection. *Cancer Gene Ther* (2013) 20(1):25–32. doi: 10.1038/cgt.2012.80

24. Pike R, Ortiz-Zapater E, Lumicisi B, Santis G, Parsons M. KIF22 Coordinates CAR and EGFR Dynamics to Promote Cancer Cell Proliferation. *Sci Signal* (2018) 11(515). doi: 10.1126/scisignal.aaq1060
25. Zhang X, Fang B, Mohan R, Chang JY. Coxsackie-Adenovirus Receptor as a Novel Marker of Stem Cells in Treatment-Resistant Non-Small Cell Lung Cancer. *Radiother Oncol* (2012) 105(2):250–7. doi: 10.1016/j.radonc.2012.09.002
26. Li X, Stankovic M, Lee BP, Aurrand-Lions M, Hahn CN, Lu Y, et al. JAM-C Induces Endothelial Cell Permeability Through its Association and Regulation of {Beta}3 Integrins. *Arterioscler Thromb Vasc Biol* (2009) 29(8):1200–6. doi: 10.1161/ATVBAHA.109.189217
27. Kirby I, Davison E, Beavil AJ, Soh CP, Wickham TJ, Roelvink PW, et al. Mutations in the DG Loop of Adenovirus Type 5 Fiber Knob Protein Abolish High-Affinity Binding to its Cellular Receptor CAR. *J Virol* (1999) 73 (11):9508–14. doi: 10.1128/JVI.73.11.9508-9514.1999
28. McGraw JM, Thelen F, Hampton EN, Bruno NE, Young TS, Havran WL, et al. JAML Promotes CD8 and Gammadelta T Cell Antitumor Immunity and is a Novel Target for Cancer Immunotherapy. *J Exp Med* (2021) 218(10). doi: 10.1084/jem.20202644
29. Bertram JS, Janik P. Establishment of a Cloned Line of Lewis Lung Carcinoma Cells Adapted to Cell Culture. *Cancer Lett* (1980) 11(1):63–73. doi: 10.1016/0304-3835(80)90130-5
30. Franks LM, Carbonell AW, Hemmings VJ, Riddle PN. Metastasizing Tumors From Serum-Supplemented and Serum-Free Cell Lines From a C57BL Mouse Lung Tumor. *Cancer Res* (1976) 36(3):1049–55.
31. Hanke JH, Gardner JP, Dow RL, Changelian PS, Brissette WH, Weringer EJ, et al. Discovery of a Novel, Potent, and Src Family-Selective Tyrosine Kinase Inhibitor. Study of Lck- and FynT-Dependent T Cell Activation. *J Biol Chem* (1996) 271(2):695–701. doi: 10.1074/jbc.271.2.695
32. Howden JD, Michael M, Hight-Warburton W, Parsons M. Alpha2beta1 Integrins Spatially Restrict Cdc42 Activity to Stabilise Adherens Junctions. *BMC Biol* (2021) 19(1):130.
33. Kim NH, Park KS, Cha SK, Yoon JH, Yeh BI, Han KH, et al. Src Family Kinase Potentiates the Activity of Nicotinic Acetylcholine Receptor in Rat Autonomic Ganglion Innervating Urinary Bladder. *Neurosci Lett* (2011) 494(3):190–5. doi: 10.1016/j.neulet.2011.03.009
34. Ke Y, Karki P, Zhang C, Li Y, Nguyen T, Birukov KG, et al. Mechanosensitive Rap1 Activation Promotes Barrier Function of Lung Vascular Endothelium Under Cyclic Stretch. *Mol Biol Cell* (2019) 30(8):959–74. doi: 10.1091/mbc.E18-07-0422
35. Llavero F, Luque Montoro M, Arrazola Sastre A, Fernandez-Moreno D, Lacerda HM, Parada LA, et al. Epidermal Growth Factor Receptor Controls Glycogen Phosphorylase in T Cells Through Small GTPases of the RAS Family. *J Biol Chem* (2019) 294(12):4345–58. doi: 10.1074/jbc.RA118.005997
36. Schindelin J, Arganda-Carreras I, Frise E, Kaynig V, Longair M, Pietzsch T, et al. Fiji: An Open-Source Platform for Biological-Image Analysis. *Nat Methods* (2012) 9(7):676–82. doi: 10.1038/nmeth.2019
37. Haeger JD, Hambruch N, Dilly M, Froehlich R, Pfarrer C. Formation of Bovine Placental Trophoblast Spheroids. *Cells Tissues Organs* (2011) 193 (4):274–84. doi: 10.1159/000320544
38. Lim E, Modi KD, Kim J. *In Vivo* Bioluminescent Imaging of Mammary Tumors Using IVIS Spectrum. *J Vis Exp* (2009) 26. doi: 10.3791/1210
39. Calderwood DA, Fujioka Y, De Pereda JM, Garcia-Alvarez B, Nakamoto T, Margolis B, et al. Integrin Beta Cytoplasmic Domain Interactions With Phosphotyrosine-Binding Domains: A Structural Prototype for Diversity in Integrin Signaling. *Proc Natl Acad Sci USA* (2003) 100(5):2272–7. doi: 10.1073/pnas.262791999
40. Deville SS, Cordes N, Extracellular T. Cellular, and Nuclear Stiffness, a Trinity in the Cancer Resistome-A Review. *Front Oncol* (2019) 9:1376. doi: 10.3389/fonc.2019.01376
41. Severson EA, Lee WY, Capaldo CT, Nusrat A, Parkos CA. Junctional Adhesion Molecule A Interacts With Afadin and PDZ-GEF2 to Activate Rap1A, Regulate Beta1 Integrin Levels, and Enhance Cell Migration. *Mol Biol Cell* (2009) 20(7):1916–25. doi: 10.1091/mbc.e08-10-1014
42. Bos JL. Linking Rap to Cell Adhesion. *Curr Opin Cell Biol* (2005) 17(2):123–8. doi: 10.1016/j.ceb.2005.02.009
43. Anders M, Hansen R, Ding RX, Rauen KA, Bissell MJ, Korn WM. Disruption of 3D Tissue Integrity Facilitates Adenovirus Infection by Deregulating the Coxsackievirus and Adenovirus Receptor. *Proc Natl Acad Sci USA* (2003) 100 (4):1943–8. doi: 10.1073/pnas.0337599100
44. Bruning A, Stickeler E, Diederich D, Walz L, Rohleder H, Friese K, et al. Coxsackie and Adenovirus Receptor Promotes Adenocarcinoma Cell Survival and is Expressionally Activated After Transition From Preneoplastic Precursor Lesions to Invasive Adenocarcinomas. *Clin Cancer Res* (2005) 11 (12):4316–20. doi: 10.1158/1078-0432.CCR-04-2370
45. Rauen KA, Sudilovsky D, Le JL, Chew KL, Hann B, Weinberg V, et al. Expression of the Coxsackie Adenovirus Receptor in Normal Prostate and in Primary and Metastatic Prostate Carcinoma: Potential Relevance to Gene Therapy. *Cancer Res* (2002) 62(13):3812–8.
46. Sachs MD, Rauen KA, Ramamurthy M, Dodson JL, De Marzo AM, Putzi MJ, et al. Integrin Alpha(V) and Coxsackie Adenovirus Receptor Expression in Clinical Bladder Cancer. *Urology* (2002) 60(3):531–6. doi: 10.1016/S0090-4295(02)01748-X
47. Matsumoto K, Shariat SF, Ayala GE, Rauen KA, Lerner SP. Loss of Coxsackie and Adenovirus Receptor Expression is Associated With Features of Aggressive Bladder Cancer. *Urology* (2005) 66(2):441–6. doi: 10.1016/j.urology.2005.02.033
48. Wunder T, Schumacher U, Friedrich RE. Coxsackie Adenovirus Receptor Expression in Carcinomas of the Head and Neck. *Anticancer Res* (2012) 32 (3):1057–62.
49. Stecker K, Vieth M, Koschel A, Wiedenmann B, Rocken C, Anders M. Impact of the Coxsackievirus and Adenovirus Receptor on the Adenoma-Carcinoma Sequence of Colon Cancer. *Br J Cancer* (2011) 104(9):1426–33. doi: 10.1038/bjc.2011.116
50. Miyazawa A, Ito S, Asano S, Tanaka I, Sato M, Kondo M, et al. Regulation of PD-L1 Expression by Matrix Stiffness in Lung Cancer Cells. *Biochem Biophys Res Commun* (2018) 495(3):2344–9. doi: 10.1016/j.bbrc.2017.12.115
51. Koenig A, Mueller C, Hasel C, Adler G, Menke A. Collagen Type I Induces Disruption of E-Cadherin-Mediated Cell-Cell Contacts and Promotes Proliferation of Pancreatic Carcinoma Cells. *Cancer Res* (2006) 66(9):4662–71. doi: 10.1158/0008-5472.CAN-05-2804
52. Playford MP, Vadali K, Cai X, Burridge K, Schaller MD. Focal Adhesion Kinase Regulates Cell-Cell Contact Formation in Epithelial Cells *via* Modulation of Rho. *Exp Cell Res* (2008) 314(17):3187–97. doi: 10.1016/j.yexcr.2008.08.010
53. Palovuori R, Sormunen R, Eskelinen S. SRC-Induced Disintegration of Adherens Junctions of Madin-Darby Canine Kidney Cells is Dependent on Endocytosis of Cadherin and Antagonized by Tiam-1. *Lab Invest* (2003) 83 (12):1901–15. doi: 10.1097/01.LAB.0000107009.75152.03
54. Stecker K, Koschel A, Wiedenmann B, Anders M. Loss of Coxsackie and Adenovirus Receptor Downregulates Alpha-Catenin Expression. *Br J Cancer* (2009) 101(9):1574–9. doi: 10.1038/sj.bjc.6605331
55. Walters RW, Freimuth P, Moninger TO, Ganske I, Zabner J, Welsh MJ. Adenovirus Fiber Disrupts CAR-Mediated Intercellular Adhesion Allowing Virus Escape. *Cell* (2002) 110(6):789–99. doi: 10.1016/S0092-8674(02)00912-1
56. Chattopadhyay N, Wang Z, Ashman LK, Brady-Kalnay SM, Kreidberg JA. Alpha3beta1 Integrin-CD151, a Component of the Cadherin-Catenin Complex, Regulates PTPmu Expression and Cell-Cell Adhesion. *J Cell Biol* (2003) 163(6):1351–62. doi: 10.1083/jcb.200306067
57. Schoenenberger CA, Zuk A, Zinkl GM, Kendall D, Matlin KS. Integrin Expression and Localization in Normal MDCK Cells and Transformed MDCK Cells Lacking Apical Polarity. *J Cell Sci* (1994) 107(Pt 2):527–41. doi: 10.1242/jcs.107.2.527
58. Mana G, Valdembri D, Serini G. Conformationally Active Integrin Endocytosis and Traffic: Why, Where, When and How? *Biochem Soc Trans* (2020) 48(1):83–93. doi: 10.1042/BST20190309
59. Fukuyama T, Ogita H, Kawakatsu T, Fukuhara T, Yamada T, Sato T, et al. Involvement of the C-Src-Crk-C3G-Rap1 Signaling in the Nectin-Induced Activation of Cdc42 and Formation of Adherens Junctions. *J Biol Chem* (2005) 280(1):815–25. doi: 10.1074/jbc.M411099200
60. Guo XX, An S, Yang Y, Liu Y, Hao Q, Xu TR. Rap-Interacting Proteins Are Key Players in the Rap Symphony Orchestra. *Cell Physiol Biochem* (2016) 39 (1):137–56. doi: 10.1159/000445612
61. Asuri S, Yan J, Paranavitana NC, Quilliam LA. E-Cadherin Dis-Engagement Activates the Rap1 GTPase. *J Cell Biochem* (2008) 105(4):1027–37. doi: 10.1002/jcb.21902

62. Sakurai A, Fukuhara S, Yamagishi A, Sako K, Kamioka Y, Masuda M, et al. MAGI-1 is Required for Rap1 Activation Upon Cell-Cell Contact and for Enhancement of Vascular Endothelial Cadherin-Mediated Cell Adhesion. *Mol Biol Cell* (2006) 17(2):966–76. doi: 10.1091/mbc.e05-07-0647

Author Disclaimer: The views expressed are those of the author(s) and not necessarily those of the NHS, the NIHR or the Department of Health and Social Care.

Conflict of Interest: The authors declare that the research was conducted in the absence of any commercial or financial relationships that could be construed as a potential conflict of interest.

Publisher's Note: All claims expressed in this article are solely those of the authors and do not necessarily represent those of their affiliated organizations, or those of the publisher, the editors and the reviewers. Any product that may be evaluated in this article, or claim that may be made by its manufacturer, is not guaranteed or endorsed by the publisher.

frontiers in Oncology

REVIEW
published: 02 March 2022
doi: 10.3389/fonc.2022.860320

Heat Shock Proteins and HSF1 in Cancer

Anna M. Cyran and Anatoly Zhitkovich *

Legoretta Cancer Center, Department of Pathology and Laboratory Medicine, Brown University, Providence, RI, United States

Fitness of cells is dependent on protein homeostasis which is maintained by cooperative activities of protein chaperones and proteolytic machinery. Upon encountering protein-damaging conditions, cells activate the heat-shock response (HSR) which involves HSF1-mediated transcriptional upregulation of a group of chaperones – the heat shock proteins (HSPs). Cancer cells experience high levels of proteotoxic stress due to the production of mutated proteins, aneuploidy-induced excess of components of multiprotein complexes, increased translation rates, and dysregulated metabolism. To cope with this chronic state of proteotoxic stress, cancers almost invariably upregulate major components of HSR, including HSF1 and individual HSPs. Some oncogenic programs show dependence or coupling with a particular HSR factor (such as frequent coamplification of HSF1 and MYC genes). Elevated levels of HSPs and HSF1 are typically associated with drug resistance and poor clinical outcomes in various malignancies. The non-oncogene dependence ("addiction") on protein quality controls represents a pancancer target in treating human malignancies, offering a potential to enhance efficacy of standard and targeted chemotherapy and immune checkpoint inhibitors. In cancers with specific dependencies, HSR components can serve as alternative targets to poorly druggable oncogenic drivers.

Keywords: cancer, oncology, HSF1, heat shock protein, chaperone, proteotoxic stress

OPEN ACCESS

Edited by:
Sumitra Deb,
Virginia Commonwealth University, United States

Reviewed by:
Derek Brandon Oien,
Mayo Clinic, United States
Kevin Anthony Morano,
University of Texas Health Science Center at Houston, United States

***Correspondence:**
Anatoly Zhitkovich
anatoly_zhitkovich@brown.edu

Specialty section:
This article was submitted to Molecular and Cellular Oncology, a section of the journal Frontiers in Oncology

Received: *22 January 2022*
Accepted: *07 February 2022*
Published: *02 March 2022*

Citation:
Cyran AM and Zhitkovich A (2022) Heat Shock Proteins and HSF1 in Cancer. Front. Oncol. 12:860320. doi: 10.3389/fonc.2022.860320

1 INTRODUCTION

Eukaryotic cells rely on a tightly regulated state of protein homeostasis to carry out their functions. In physiological conditions, proteostasis depends on the cooperation of molecular chaperones, co-chaperones and proteolytic machinery. Proteins with hydrophobic residues and complex 3-dimensional structures require molecular chaperones to acquire their functional forms. Numerous co-chaperones further improve the specificity and selectivity of the process (1, 2). In stress conditions, the survival of cells depends on the activation of an elaborate cytoprotective mechanism known as the heat-shock response (HSR). The HSR has evolved as a rapid mechanism to upregulate selective gene transcription in response to the accumulation of damaged proteins in cells. It utilizes specific molecular chaperones - the heat shock proteins (HSPs) - as effectors to minimize the toxic effects of abnormal proteins. When confronted with hostile environmental and pathophysiological conditions (such as heat, free radicals, nutrient depletion, protein-reactive chemicals), HSPs act to prevent the aggregation of misfolded and malfunctional proteins. They promote protein refolding and/or direct them for degradation by the ubiquitin-proteasome or other

proteolytic systems (3). The HSR is driven by heat shock-inducible transcription factors (HSFs) which bind to the promoter regions of the HSPs and dramatically increase their transcription.

The human genome encodes six HSF isoforms, however, only HSF1, 2 and 4 contain confirmed DNA-binding domains (4). To date, three HSFs have been characterized in humans. HSF1 is expressed in all human tissues and acts as a master regulator for rapid and robust responses of cells to proteotoxic stress. In addition to HSPs, HSF1 also affects transcription of a much broader array of genes such as those involved in cell cycle control, protein synthesis, embryonic development, ribosome biogenesis and glucose metabolism (5, 6). Abnormalities in HSF1 are associated with stress sensitivity, aging, neurodegenerative diseases and oncogenesis (5). HSF2 was initially thought to play only a role in development. However, strong evidence has emerged pointing to its complex interactions with HSF1 and its ability to co-regulate HSR (5, 7, 8). HSF3 is solely a murine factor, and HSF4 is involved in lens development (9).

In this work, we review the role of HSF1 and HSPs in protein quality control in physiological conditions and in cancer. We then analyze the functions of HSF1 in cancer biology, links between its expression patterns and key oncogenic pathways, and clinical significance in specific types of cancer. Finally, we discuss why HSF1 is a suitable candidate for anticancer therapy and describe recent attempts of pharmacological targeting and potentially beneficial drug combinations.

2 PROTEOTOXIC STRESS AS A STRESS HALLMARK OF CANCER

A wide array of genetic alterations in cancers results in a set of common features described as hallmarks of cancer. In 2000, Hannan and Weinberg (10) named six classical hallmarks of cancer. Later they expanded this list by adding evasion of immune surveillance and reprogramming of metabolism (11) Luo et al. (12) proposed further characteristics shared across cancer types and contributing to tumor growth and maintenance of the malignant phenotype. These can be collectively described as cancer stress hallmarks and include genomic instability, proteotoxic, mitotic, metabolic and oxidative stress. Targeting of these attributes is a promising therapeutic strategy. Pervasive presence of mutator phenotype and aneuploidy in cancer create proteotoxic stress by producing abnormal proteins and nonstoichiometric amounts of the components of multiprotein complexes (12). Higher translation rates and abnormalities of cancer metabolism further increase the need for protein quality mechanisms. Thus, survival of cancer cells depends on the robust functioning of proteostatic processes which can be described as non-oncogene addiction. HSF1 itself is not tumorigenic (13) but its depletion restricts growth of diverse cancer lines while having little effect on normal cells (6). Dependence on protein quality mechanisms is more ubiquitous in most cancers than dependence on specific oncogenes and proteostasis represents a pan-cancer target for the development of new drugs.

3 HEAT SHOCK PROTEINS

HSPs have become synonymous with molecular chaperones but have a broad range of functions, including folding of newly translated proteins, assembly of protein complexes, protein trafficking, developmental processes and immunomodulation. They are classified according to their molecular masses; the five major groups include HSP110 (HSPH), HSP90 (HSPC), HSP70 (HSPA), HSP60 (HSPD), HSP40 (DNAJ) and small HSPs (HSPB) (14). HSPs can also be divided in accordance with their function in protein quality control into *holdases*, whose function is to bind and hold misfolded proteins to prevent the formation of toxic aggregates and *foldases* that actively assist substrates in assuming their functional conformation. Chaperones make up about 10% of the overall protein mass of immortalized human cells, half of which consists of HSP70 and the more abundant, HSP90. Although HSPs were first identified as proteins expressed in response to thermal stress, it was soon discovered that within each family, 2/3 of them are constitutively expressed, performing housekeeping functions (15). The specificity and selectivity of association with client proteins is modulated by co-chaperones (16).

3.1 HSP90

3.1.1 HSP90 Functions

The HSP90 family has five members: inducible cytosolic HSP90AA1 and HSP90AA2, constitutively expressed cytosolic HSP90AB1, mitochondrial TRAP1 and endoplasmic reticulum-localized HSP90B (Grp94). Cytosolic HSP90s are involved in many cellular functions, including protein folding, steroid signaling, DNA repair, protein trafficking, and immunity (17). HSP90 has several hundred client proteins and exerts profound effects on cellular regulatory pathways, with approximately 60% of kinases, 7% transcription factors and 30% ubiquitin ligases requiring its assistance (18). A comprehensive list of HSP90 client proteins is provided by the Picard lab[1]. HSF1 is both a transcriptional activator and client protein of HSP90 (19). HSPs feature different profiles of binding selectivity; HSP70 acts at an early stage of folding, associating with a wide range of protein regions, whereas HSP90 recognizes specific conformations. HSP90 and HSP70 are known to perform independently many of their protein chaperone activities and also to work together in execution of other protein structure-modifying functions (20). HSP90 is a comparatively specialized chaperone. Its substrates generally fall into three categories: (i) proteins with complex conformations in the last stage of the folding process, (ii) multiprotein complexes and (iii) proteins bound with their ligands (18). HSP90 activity is fine-tuned by numerous post-translational modifications, most notably phosphorylation and involvement of co-chaperones, such as AHA and p23 (21). Among many signaling pathways it influences are JAK-STAT, PI3K-AKT, BCR-ABL and NF-kB. Their regulatory aberrations have been linked to metastasis, angiogenesis, decreased apoptosis, EMT and cancer progression (22–24). HSP90 also stabilizes mutated forms of the tumor-suppressor p53 (TP53),

[1] https://www.picard.ch

hampering growth arrest and apoptosis in response to DNA damage (18).

3.1.2 HSP90 in Cancer

HSP90 has long been recognized as an attractive therapeutic target due to its frequent overexpression in various cancers and its importance in the maintenance of a proper conformation for components of various oncogenic pathways (17, 22). Transcripts of the two most abundant HSP90 members, HSP90AA1 or HSP90AB1, are elevated in 17 out of 21 major human cancers (**Figure 1**). Glioblastoma, renal clear cell (RCC) carcinoma and ovarian carcinoma exhibited approximately normal levels of HSP90 transcripts, whereas acute myeloid leukemia (AML) had lower gene expression of HSP90. High HSP90AA1 or HSP90AB1 expression was associated with a significantly lower survival in patients with breast carcinoma, cervical carcinoma, lung adenocarcinoma and head and neck carcinomas (**Figure 2A**). Overall survival was better for ovarian and RCC

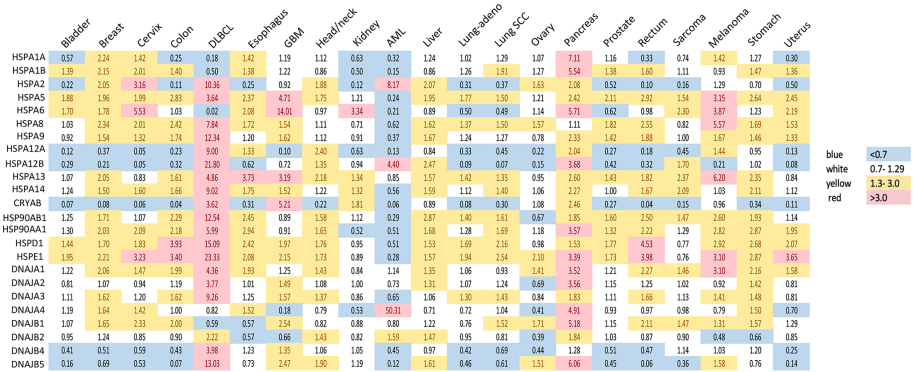

FIGURE 1 | Expression of heat shock genes across different types of human cancers. Shown are fold changes in gene expression of individual HSPs in cancers, which were calculated by dividing the number of transcripts per million in cancer tissue by that in the corresponding normal tissue. Transcript data were accessed through GEPIA (gepia.cancer-pku.cn) (25). Cancer types analyzed: bladder urothelial carcinoma, breast carcinoma, cervical squamous cell carcinoma and endocervical adenocarcinoma, colon adenocarcinoma, diffuse large B-cell lymphoma (DLBCL), esophageal carcinoma, glioblastoma multiforme (GBM), head and neck squamous cell carcinoma, renal clear cell carcinoma, acute myeloid leukemia (AML), hepatocellular carcinoma, lung adenocarcinoma (lung-adeno), lung squamous cell carcinoma (lung-SCC), ovarian serous cystadenocarcinoma, pancreatic adenocarcinoma, prostate adenocarcinoma, rectum adenocarcinoma, sarcoma, skin melanoma, stomach adenocarcinoma and uterine carcinosarcoma. The use of imperfectly matched cell populations as normal controls for hematological malignanies (bone marrow for DLBCL and blood for AML) potentially confounded patterns of normalized HSPs expression in these cancers.

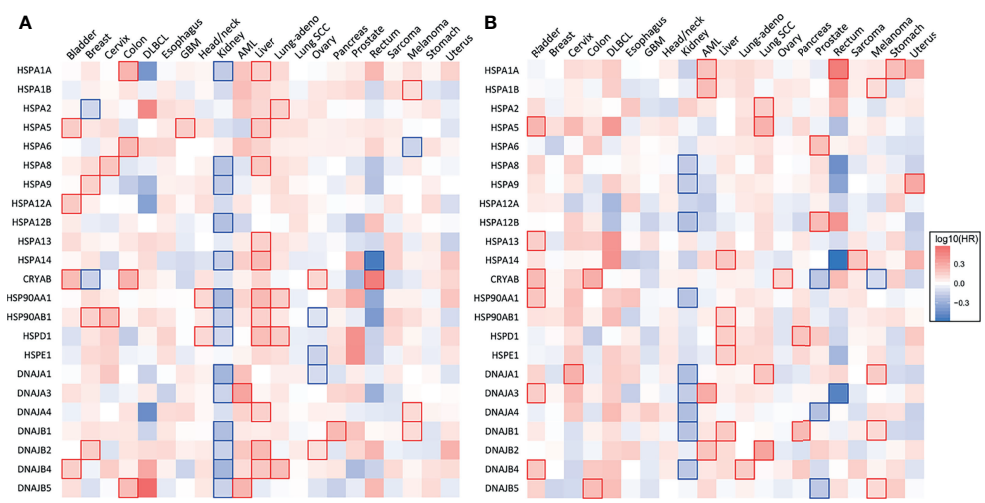

FIGURE 2 | Heat shock gene expression and survival across 21 types of human cancers. **(A)** Heatmap showing the relationship between heat shock gene expression and the overall survival and **(B)** disease-free survival of patients. Patients were divided into groups with high and low mRNA expression at median. Each heatmap cell corresponds to a $\log_{10}$ HR (hazard ratio) for respective cancer type. Cells marked with shades of red: HR>0, blue cells: HR<0. Statistically significant relationships are marked with blue or red cell borders. Significance level: p<0.05 in log-rank test. Data were accessed through GEPIA (gepia.cancer-pku.cn) (25).

cancers with higher HSP90AB1 or both HSP90 forms, respectively. However, high HSP90 expression did not alter disease-free survival of the majority of cancers that showed significantly different overall survival. Only RCC and liver cancers exhibited the same trend for both overall and disease-free survival (**Figure 2B**). Stronger effects of HSP90 expression on the overall survival than progression-free survival suggests that this chaperone may play a more important role in cancer progression/metastasis rather than in the initial therapy resistance. Problems with the accurate determination of the start of disease progression may also hamper analysis of its association with HSP90 and other HSR components.

3.1.3 Targeting HSP90 in Cancer

A multitude of compounds inhibiting HSP90 with promising anticancer properties in preclinical studies was described (26). However, in most cases, their clinical efficacy was modest. Geldanamycin, an ansamycin inhibitor of ATPase activity, showed promise in reducing tumor growth. However, it is poorly soluble and hepatotoxic, which precluded its introduction into clinical practice (27, 28). The synthetic derivative tanespimycin (17-AAG) was proven safe and effective in combination with trastuzumab for the treatment of refractory HER2-positive breast cancer (29). Nevertheless, further studies on prostate, renal, colorectal, head and neck and pancreatic cancers did not confirm the effectiveness of tanespimycin (30–32). The initial success led to the synthesis and testing of other inhibitors of HSP90 with improved bioavailability. For instance, KW-2478, a non-ansamycin, non-purine inhibitor, displayed a good safety profile and some antitumor activity in multiple myeloma *in vivo* with a synergistic action in combination with the proteasome inhibitor bortezomib (33). However, clinical trials with advanced solid tumors (prostate, melanoma, pancreas, gastrointestinal, NSCLC) showed either no significant improvement in survival or high toxicity (32). HSP90 inhibition leads to a compensatory response resulting in the increase of HSP70, which can serve as a biomarker for successful HSP90 blockade (34).

3.2 HSP70

3.2.1 HSP70 Functions

The human genome encodes 17 genes and 30 pseudogenes, generating 13 HSP70 gene products, which are subdivided into 7 phylogenetic families. The most abundant and well-studied members are in group VI comprising cytoplasmic and nuclear chaperones (HSPA1, HSPA8, and HSPA6) and group VII encompassing chaperones expressed in the endoplasmic reticulum (HSPA5) (35). Two major inducible forms HSPA1/HSP70-1 and HSPA1B/HSP70-2 differ by two amino acids and are collectively referred to as HSP70. HSPA8/HSP70-8/HSC72 is a constitutively expressed cytoplasmic protein, whereas HSPA6 is inducible and expressed in many types of immune cells (36). HSPA5/HSP70-5/GRP78 is an important facilitator of protein folding and transport across ER membrane (35).

Members of the HSP70 family are present in all cellular compartments and on cell membranes (37). There is some degree of tissue specificity in the expression pattern of HSP70 family members. For instance, HSPA8 and HSPA1A are especially highly expressed in blood vessels and spleen. Yet HSPA1A and HSPA1B, despite the very high degree of homology, are differentially expressed in some tissues (35). HSP70 family members perform crucial housekeeping functions such as nascent protein folding, import of proteins into organelles, protein de-aggregation and assembly of complexes (37). Their simultaneous deletion is lethal (38). Due to a low intrinsic ATPase activity, HSP70 never function alone. Their efficiency and specificity in protein folding are contingent on co-chaperones: HSP40/DNAJ proteins and nucleotide exchange factors (NEF). HSP40/DNAJ proteins are numerous, diverse and assist in the binding of client proteins. Their conserved J domain stimulates ATPase activity, which catalyzes conformational changes. In the next step, NEFs drive ADP and client protein dissociation. The HSP70 protein folding machinery functions in cycles, and its key components can be recycled (39). Proteins with complex structures, such as hormone receptors and transcription factors, undergo a series of folding events and are passed on from HSP40/DNAJ proteins to HSP70 where they are subject to repeated binding and folding. Complex proteins are ultimately delivered to HSP90 (40). NEFs are classified as *(i)* nucleotide releasing factors: HSP-BP-1 type and GRP-type factors; *(ii)* HSP110/HSPH, which are similar to HSP70, in some instances even stress-inducible and capable of preventing protein aggregation independently and *(iii)* less explored BAG family (BAG1-6) (41, 42). In physiological conditions, HSP70 is decidedly more abundant than its co-chaperones, yet their relative concentrations may have a regulatory effect (43).

3.2.2 HSP70 in Cancer

HSP70 transcript levels and their impact on the survival of patients show complex patterns and the extent of expression was not always predictive of the overall or disease-free survival among major human cancers. ER-localized HSPA5 (GRP78) was the most frequently overexpressed HSP70 member whose transcript levels were elevated in 18 out of 21 major human cancers (**Figure 1**). Melanoma, glioblastoma and diffuse B-cell lymphoma had the highest levels of GRP78 overexpression. High expression of this chaperone was predictive of poor overall survival only for three cancers: bladder, glioblastoma and liver (**Figure 2A**). Shorter disease-free survival was associated with higher amounts of GRP78 transcripts only for bladder and squamous cell lung carcinoma (**Figure 2B**). Inducible HSP70 forms are expressed in normal cells even in unstressed conditions, but their levels are elevated in many common human cancers such as melanoma and carcinomas of the breast, cervix, stomach, esophagus, prostate, rectum, pancreas and lung (**Figure 1**). The overexpression of both HSP70 forms was particularly high in pancreatic cancer. A significant association between high expression and lower overall survival was found only for melanoma, colon and liver cancers and no effects were detectable in pancreatic cancer (**Figure 2A**). Overall survival of patients with renal clear cell (RCC) carcinoma was better for the high expression group of HSP1A. High expression

of inducible HSP70 was predictive of a shorter disease-free survival only for AML, melanoma and stomach and rectal carcinomas (**Figure 2B**), which is consistent with the impact on the overall survival only for melanoma. HSPA2 and HSPA6 showed elevated gene expression in 9 and 10 out of 21 human cancers, respectively (**Figure 1**), which was predictive of a lower overall survival for one cancer for each chaperone. Other members of HSP70 family showed a less frequent overexpression among major human cancers and their significant impact on the overall survival was generally limited to one cancer. The most common change for HSP12A and HSP12B was downregulation. Collectively, major human cancers overexpressed at least one member of the HSP70 family, and this was associated with lower overall survival for 8 cancers. RCC carcinoma was a clear outlier with a significantly better overall and disease-free survival found for patients with higher mRNA levels of HSP70. RCC is a unique type of human cancer caused by the early loss of the VHL E3 ubiquitin ligase and the resulting constitutive activation of the transcription factor HIF2 (44). Thus, despite a frequent overexpression of HSP70 chaperones, which is indicative of beneficial functions in malignant cells, their abundance does not always associate with more aggressive cancers.

Mechanistic studies have shown that HSP70 downregulation impedes cancer cell growth, migration, invasion in various types of cancer, including colorectal, urothelial, hepatocellular carcinoma, renal cell carcinoma, pancreatic and breast cancers (45–50). While the exact mode of action for each of the HSP70 family members in this capacity has not yet been fully dissected, many molecular insights are available. The importance of HSP70 in cancer appears to center on cytoprotection, either through the HSR or by suppressing apoptotic pathways on many levels. HSP70 prevents BAX from translocating to mitochondria and associating with their outer membranes (51). It also indirectly inhibits the JNK/BIM axis (52). In a different study, HSP70 was found to prevent the release of apoptosis inducible factor (AIF) and cytochrome c from mitochondria and cathepsins from lysosomes by stabilizing their membranes (48, 53). The exact mechanism is not entirely clear, but it is possible that the two mechanisms are either complementary or upstream of one another. HSP70 was also found to inhibit the Apo-2L/TRAIL DISC assembly (54) and its knockdown sensitized cells to TRAIL-dependent apoptosis (55). On the other hand, HSP72 blocks the apoptosis-regulating kinase ASK by directly interacting with it (56). High constitutive transcription of HSP72 in cancer cells also impedes senescence pathways (57). HSP70 is important in tumorigenesis. This is illustrated well by a study using mice injected with cancer xenografts: overexpression of Her2 resulted in malignant transformation only when HSP72 expression was intact. HSP72 depletion inhibited transformation (58). Survival of both normal and malignant cells hinges on the presence of the constitutively expressed HSC70. Its depletion causes G2/M arrest. Knockdown of HSP70-2, the inducible chaperone, predominantly overexpressed in cancers, resulted in G1 arrest (49). There are many other reports detailing functional interactions between cancer hallmarks and HSP70 expression (59). Many substances blocking HSP70 activity have shown promise in human cancer cell lines and xenograft models (60, 61). However, no HSP70 inhibitors are currently in clinical trials, but attempts have been made to repurpose existing drugs with HSP70-inhibiting properties for new indications. This is the case with MKT-077, which exerts anticancer effects by binding to HSPA9 (mortalin). It was tested in phase 1 clinical trials on solid tumors but failed due to renal toxicity and unfavorable pharmacokinetics (62). Another example is methylene blue which showed suppression of HSPA1A and HSPB1 induction and sensitized melanoma cells to other chemotherapeutics (63). Ongoing clinical trials explore the diagnostic potential of HSP70 for the isolation of circulating tumor cells (ClinicalTrials.gov Identifier: NCT04628806) and in prevention where HSP70 DNA is a component of a dual vaccine for the treatment of lesions with increased risk of cervical cancer (ClinicalTrials.gov Identifier: NCT03911076).

3.3 HSP40

3.3.1 HSP40 Functions

The largest chaperone family, including over 40 members and 49 genes, some of which encoding several splice variants, is HSP40 (DNAJ). Their key role is partnering with HSP70 and HSP90 and participating in tasks related to the maintenance of proteostasis (64). HSP40 are present in all cellular compartments and partake in protein shuttling, endo- and exocytosis and hormone signaling. Diverse proteins are classified as DNAJ members based on the presence of a conserved J domain, whose role is to enable interaction with other chaperones, stimulate their ATPase and stabilize the client protein binding (65). Based on further structural characteristics, DNAJ are subdivided into 3 categories: DNAJA, DNAJB and DNAJC (66). The classification has functional consequences: DNAJA and DNAJB can bind to aberrant polypeptides independent of ATP to prevent their aggregation, the polypeptide chains they recognize are similar but distinct. An important functional difference is that DNAJA can work independently, whereas DNAJB necessitate HSP70 to prevent aggregation. DNAJC members have a specialized domain that recognizes distinct substrates and delivers them to different HSP70 members, making these highly versatile chaperones more specialized in certain contexts.

3.3.2 HSP40 in Cancer

Gene expression of HSP40 chaperones was elevated in 18 out of 21 major human cancers with particularly high levels of overexpression being found in diffuse B-cell lymphoma and pancreatic cancer, which represents a general trend for HSP expression in these two cancers (**Figure 1**). Bladder, prostate and RCC carcinomas did not show increases in the abundance of any of the HSP40 transcripts. High expression of specific HSP40 forms was associated with lower overall survival in 9 out of 21 major human cancers (**Figure 2A**). A poor survival prognosis in AML, liver carcinoma and melanoma was observed for more than one member of the HSP40 family. High expression of HSP40 was also predictive of shorter progression-free survival in 9 cancers, 8 of which were the same cancers that showed shorter overall survival. As discussed above, this consistency

between progression-free and overall survival was not observed for HSP70 and HSP90. As with other chaperones, RCC carcinoma was again a clear outlier that showed a much better overall and progression-free survival in patients with high expression of several HSP40 forms (**Figures 2A, B**). Interestingly, the overall survival of patients with ovarian carcinoma showed opposite trends for DNAJA1 and DNAJB2 expression, pointing to their involvement in different oncogenic programs in this malignancy.

On a protein level, HSP40 expression correlated with a less aggressive cancer phenotype in some studies. DNAJB4 abundance was associated with a better overall survival and lower recurrence rates in NSCLC (67–69). *In vitro*, it inhibited cell proliferation, motility, invasion and slowed cell cycle through STAT1/CDKN1A (70). Other studies in lung cancer provided evidence that overexpression of DNAJB4, mediated by the transcription factor YY1, hinders invasion *via* E-cadherin (71). Conversely, a low expression of DNAJB4 is a feature of highly malignant and metastatic breast and colon cancers (72). DNAJB4 suppresses activity of Src and the formation of oncogenic complexes, such as EGFR-Src, STAT3-Src and FAK-Src (73). It is known that mRNA levels do not always correlate with cellular protein levels (74). While there is a close correlation between the two for HSP90, HSPA5, HSPA8 and HSPB1, it is less clear for other HSP members. The relationship between mRNA and protein abundance varies greatly between tissues; one of the lowest correlation scores is seen in lung. In many cancer types, such as pancreatic, colonic, ovarian and urothelial, the transcript-protein correlation is much lower than in normal tissue (75).

3.4 HSP60

3.4.1 HSP60 Functions

HSP60 (HSPD) facilitates the folding, unfolding and degradation of mitochondrial proteins. While performing these classical functions, it is assisted by the co-chaperone HSP10/HSPE. HSP60 forms a double ring of seven subunits (a 14-mer complex) bound to a 7-unit ring formed by the co-chaperone. Together they create a compartment within which client proteins assume their conformation (76). A third of the HSP60 supply is located outside the mitochondria: in the cytosol, on the cell membrane and is secreted in extracellular vesicles (77) broadening its functions to include (among others) protein transport, peptide hormone signaling (78, 79). HSP60 also plays a role in both innate and adaptive immunity and the pathogenesis of autoimmune disorders (80). It induces cytokine release from lymphocytes, dendritic cells and macrophages and interacts with Toll-like receptors 2 and 4, fostering inflammatory response (80, 81).

3.4.2 HSP60 in Cancer

HSP60 (HSPD) transcript was found to be overexpressed in 17 out of 21 human cancers with especially high expression seen in diffuse large B-cell lymphoma and cancers of colon and rectum (**Figure 1**). The expression pattern of HSP60 cochaperone HSP10/HSPE showed a nearly identical trend for overexpression in the same cancers (elevated expression in 18 out of 21 cancers). High expression of HSP60 was predictive of a significantly lower survival in patients with head and neck cancers, liver carcinoma and lung adenocarcinoma (**Figure 2A**). Shorter progression-free survival was found in HSP60 high expression groups of patients with liver and pancreatic carcinomas (**Figure 2B**). As with all other families of HSP proteins, the overall survival of RCC patients was better in the HSP60-overexpressing group. Despite the presence of elevated transcript levels for HSP60 and its cochaperone in the same cancers, high expression of HSP10 was not associated with shorter overall survival in any cancers and in ovarian carcinoma, it was associated with better overall survival (**Figure 2A**). Thus, it appears that cochaperone-independent functions of HSP60 could be more important for disease aggressiveness in patients with head and neck cancers, liver carcinoma and lung adenocarcinoma. As seen with other HSP proteins, HSP60 expression had a more limited prediction potential for progression-free survival than for overall survival.

A multitude of HSP60 functions in cancer and their contributions to the progression and maintenance of specific malignant properties has been established in several cancer models. Mechanistic studies on liver (82), prostate (83), gastric (84), bladder (85), ovarian (86), pancreatic cancers (87), neuroblastoma (88) have shown its association with increased metastatic potential, risk of progression or recurrence and poor overall outcome. HSP60 was highly expressed in Hodgkin lymphoma as well as mitogen-stimulated B-, T- and NK-cells (80, 89). In colonic epithelium, HSP60 is highly expressed during early carcinogenesis and in preneoplastic lesions, suggesting a role in cancer progression (90). HSP60 interacts with major oncogenic pathways, leading to uncontrolled proliferation, resistance to cell death and senescence, and metastatic spread. Its transcription is directly activated by c-MYC, triggering malignant transformation (91). HSP60 is also important for the activity of multiple apoptosis-controlling processes. It promotes activation of IKK-NF-kB pathway, which is crucial for cancer cell survival (92). In pancreatic cancer, HSP60 depletion provokes a decrease in ERK1/2 phosphorylation, leading to cell arrest and apoptosis, ultimately decreasing tumor growth (87). HSP60 also regulates autocrine production of IL-8 *in vitro* and *in vivo via* its upstream regulator TGFβ, mediating resistance to apoptosis (93). HSP60 forms complexes with survivin (a potent inhibitor of apoptosis), stabilizing it and promoting oncogenesis. In experimental settings, HSP60 knockdown decreased the expression of survivin, disrupted mitochondrial homeostasis and led to BAX-mediated apoptosis. In the same study, HSP60 ablation released p53 from its complexes with the chaperone protein restraining its activity (94). Cancer-associated HSP60 overexpression was a prerequisite for a loss of replicative senescence, as p53 was sequestered from interacting with promoters of cell cycle arrest genes (95). A study by Chandra et al. (96) found that a cytosolic accumulation of HSP60 was a common feature of all cells in an early phase of apoptosis induction. The cytosolic accumulation of HSP60 was either of mitochondrial origin, in which case, upon release it interacts with procaspase 3, promoting its maturation

and activation. In this model, the chaperone was not available to counteract oxidative stress in the mitochondrion, rendering the cell particularly susceptible to apoptosis. In contrast, HSP60 accumulation of non-mitochondrial origin plays a cytoprotective role (96). As the primary role of HSP60 is to mitigate the effects of reactive oxygen species in mitochondria, its reduction and increased oxidative stress activate AMPK, which inhibits mTOR curbing cell proliferation (86, 97). In glioblastoma, this was accompanied by activation of integrin and WNT pathways and an elevation of EMT markers - key players in the process of metastatic spread (97). HSP60 also promoted metastasis by interacting with β-catenin and α3β1 integrin (98, 99). Interestingly, the latter can be prevented by mizoribine - a pharmacological inhibitor of HSP60 (99).

In some contexts, HSP60 can also assume an anticancer role, as evident by a better survival in RCC patients with high expression of this chaperone (**Figure 2A**). Its knockdown fostered cancer progression by promoting aerobic glycolysis *via* the AMPK pathway and enhanced EMT due to increased oxidative stress in mitochondria (100). In mice, increased tumor size of HSP60-depleted RCC xenografts was observed (100).

3.4.3 HSP60 as Cancer Biomarker and Drug Target

Because HSP60 is widely upregulated in cancer and is present in detectable quantities in blood serum, it was considered a potential biomarker to aid cancer diagnosis and monitor the disease course. Strong evidence exists to support its application for colonic adenocarcinoma, where a specific immunoassay detected increased HSP60 serum levels in cancer patients compared to healthy controls (90). Moreover, HSP60 was elevated already at an early stage of carcinogenesis - in tubular adenoma- raising hope for a tool for early detection (101). Another study on colonic carcinoma found that serum HSP60 had the same sensitivity as carcinoembryonic antigen and provided additional value by correlating with metastatic disease (102).

In HCC, HSP60 levels correlated with alpha-fetoprotein and differentiation grade and predicted favorable outcomes (103). In prostate cancer, HSP60 levels tracked Gleason score, prostate-specific antigen levels and were associated with the development of hormone-refractory disease, prompting further research into whether HSP60 could interact with the androgen receptor (83). Other potential uses for HSP60 as a biomarker include AML (104), lung adenocarcinoma (105, 106), differentiation between different subtypes of glioma (discussed in more detail by Nakamura et al.) (104). HSP60 was found to elicit a humoral response, and autoantibodies against it can have a diagnostic value in breast cancer, especially in DCIS (107) and osteosarcoma (108).

Several pharmacological modulators of HSP60 were described. Among the most promising is the immuno-suppressant mizoribine, which inhibits association with HSP10 and impedes ATPase activity (109, 110). However, given the molar dosage required to achieve biological effects, the compound necessitates further structural refinement. Epolactaene tertiary butyl ester (ETB) covalently binds to cysteine residues of HSP60, allosterically inhibiting its ATPase activity (111). Recently a known activator of apoptosis in cancer cells – myrtucommulone - was shown to interact directly with HSP60 reducing its activity more efficiently than ETB and inducing the intrinsic apoptotic pathway by interfering with mitochondrial functions (112, 113). Other potential HSP60-targeting drugs include carboranylphenoxyacetanilide, known primarily as HIF1 inhibitor, but its biological effects require further study (114). A detailed review of substances proposed to intervene pharmacologically with HSP60, and their activities can be found elsewhere (104, 115).

3.5 Small Heat Shock Proteins

Small heat shock proteins (sHSPs or HSPB) are defined by the presence of the α-crystallin domain. The family consists of 11 members, most notably HSPB1 (HSP27), HSPB4 (α-crystallin A) and HSPB5 (α-crystallin B). Their monomeric molecular masses range between 15-40 kDa; however, they usually exist in oligomeric form or as multimeric complexes of up to 40 units (116). sHSPs quickly bind to a large variety of client proteins to prevent the formation of large aggregates. However, they do not induce conformational changes alone. Instead, the unfolded protein chains are passed on to other chaperones for further processing. In contrast to other HSPs, their function is ATP-independent, i.e., client proteins can be released by association with another chaperone rather than by ATP hydrolysis (117). sHSPs are regulated by phosphorylation by multiple kinases, including MAPK2, MAPK3 and PKD (118, 119). They are highly expressed in colorectal (120), pancreatic, breast, ovarian, esophageal and some mesenchymal cancers (116). High expression of CRYAB (HSPB5) was associated with significantly lower disease-free and overall survival for bladder, colon and ovarian carcinomas (**Figures 2A, B**). HSPB1, by far the most researched sHSP member, is linked to tumor invasion and metastasis, epithelial-mesenchymal transition (EMT), reduced apoptosis, drug resistance. An antisense oligonucleotide inhibitor of HSPB1, apatorsen, was tested in phase II clinical trials in patients with prostate, NSCLC (121), pancreatic (122) and urothelial cancers (123), failing to improve the outcomes in all but one study (124).

4 HSF1

4.1 Structure and Function

HSF1 exists predominantly in the cytoplasm in a monomeric, inactive state. HSF1 monomer consists of the following functional modules: *(i)* N-terminal DNA-binding domain which can also interact with cofactors and modulate transactivation (4), *(ii)* leucine-zipper domains 1-3 (LZ1-3) collectively described as trimerization domain, facilitate interactions with other HSF monomers, *(iii)* regulatory domain which is subject to elaborate modifications, including phosphorylation, acetylation, SUMOylation, *(iv)* leucine-zipper LZ4, repressing oligomerization (9) and *(v)* activation domain located at the C-terminal side. The DBD and oligomerization domains are highly conserved between HSF1 and HSF2 (125).

The classical model of HSF1 activation posits that accumulation of misfolded proteins causes HSP70, HSP90 and likely other chaperones to dissociate from monomeric HSF1 and bind unfolded peptide chains (126, 127). This allows HSF1 to trimerize, translocate to the nucleus and bind to the heat shock elements in promoter regions of its gene targets (128). Trimeric HSF1 is capable of binding to DNA, but trimerization alone is not sufficient to transactivate target genes. HSF1 was shown to become active upon phosphorylation (125, 127). Each of the steps requires the assistance of multiple cofactors and different combinations of those fine-tune the overall HSR (4). Detailed studies of HSF1 structure indicate that elevated temperatures induce structural changes in HSF1, such as the unfolding of the regulatory domain and tighter packing of the trimerization region, resulting in increased trimer formation (129, 130). A ribonucleoprotein complex consisting of eEF1a and a non-coding RNA sequence HSR1 was found to promote HSF1 activation (131).

The DNA-binding sites for HSF1 feature inverted repeats of consensus sequence nGAAn. Multiple heat shock elements (HSE) may exist within one gene promoter, and the number of repeats and spatial orientation of bound sequences may vary (132). Attachment of HSF1 and its cofactors to HSE releases polymerase II elongation complex and enhances gene transcription (133). Deletion of HSF1 allows for basal expression of heat-shock proteins but abrogates the acute response (9). During HSR, HSF1 induces the expression of HSPs, co-chaperones and components of the ubiquitin-proteasome system to remove proteins damaged beyond repair (126). The cell cycle is halted to allow time for repair, while the transcription of genes unrelated to damage repair is globally repressed (134). Although short-term heat shock is well tolerated by *Hsf1*-/- animals, prolonged hyperthermia and additional inhibition of HSP90 are deleterious (135). In *Hsf1*-/- mice, heat shock upregulates ~40% of the genes activated in wild-type littermates (135). Mahat et al. (133) used precision run-on sequencing to look at the genome-wide transcriptional profile of HSF1 following heat shock. The study compared transcriptional response in wild-type mice with *Hsf1*-/- and double *Hsf1*-/- and *Hsf2*-/- gene knockouts and showed the HSR was dynamic and robust with approximately 1500 genes being activated and several thousand repressed. Overall, the proposed new model subdivides genes into *(a)* upregulated throughout the HSR, such as the HSPs, *(b)* genes upregulated transiently (only in the initial phase of HSR), such as certain cytoskeletal components, *(c)* large proportion of genes activated at a later timepoint, possibly by transcriptional factors activated by HSF1 and repressed genes. HSF1 can also apparently exert enhancer effects on some genes by regulating their expression from a distance (133, 136).

4.2 Regulation of HSF1

Transcription of HSF1 appears to be stable and transcript abundance may be subject to splicing regulation (137). HSF1 is also capable of augmenting its own protein abundance at the translation level. In stress, JNK phosphorylates mTORC1 at Ser567, inhibiting translation. HSF1 salvages mTORC1 from inactivation by binding JNK (138). Dampening of HSR occurs *via* a negative feedback loop exerted on HSF1 by HSP70, HSC70 and HSP40 (DNAJB1). The three chaperones aid monomerization and dissociation of HSF1 from DNA (139). Another mechanism involves overexpression of HSP70, which shifts the balance between HSF1 kinases and phosphatases (140).

HSF1 is subjected to a plethora of post-translational modifications. Phosphorylation occurs mainly within the regulatory domain on multiple serine and threonine residues and can exert both positive (Ser326, T142, Ser320) and negative regulatory effects (Ser303, Ser307, Ser363, T142) (141–143). The first systematic analysis of phosphorylation sites was carried out by Guettouche et al. (144) and identified 12 novel phosphorylated serine residues, including Ser326, which is considered crucial for HSF1 transcriptional activity. HSF1-targeting kinases include AKT1, members of the MAPK family (MEK1, MK2, p38), PLK, PKA, CK2 and mTORC (145, 146). AKT1 phosphorylates multiple sites and activates HSF1 transcriptional activity by fostering association with other co-factors (Ser326, Thr527, Ser230) and allowing trimerization (Thr142) (146). In metabolic stress, AMPK phosphorylates HSF1 at Ser121, suppressing HSR (147). Generally, serine and threonine residues can be modified by several kinases, and one kinase can modify residues with opposing functions. For example, Ser419 phosphorylation by PLK1 facilitates the nuclear translocation of HSF1 (148). In contrast, HSF1 phosphorylation by PLK1 at Ser216 during mitosis mediates its ubiquitination and degradation. This modification also serves another purpose unrelated to HSR - it enables CDC20 to be released from the complex with HSF1 and associate with CDC27, allowing mitosis to progress (149). The complete landscape of phosphorylation events, their timing and role in HSF1 activation is far from clear. However, an engineered HSF1 with 15 disrupted phosphorylation sites was still able to transactivate its gene targets. What is more, the transactivation properties of the mutant were stronger than that of wild-type protein (150). Hyperphosphorylation may regulate the sensitivity of HSF1 to transduced cues triggering activation. A more recent study suggested that phosphorylation at specific residues has an activating effect, whereas hyperphosphorylation results in dampening of HSR (146). Mathematical modeling and experimental work in budding yeast led to the formulation of a two-factor model of HSF1 activation where the key event is its dissociation from HSP70. Phosphorylation events augment the transcription activity and integrate signals from different cellular pathways (151, 152). Other post-translational modifications of HSF1 include its acetylation and SUMOylation.

Acetylation of lysine residues on HSF1 has a two-fold role. In the absence of stress, acetyltransferase p300 modifies Lys208 and Lys298 of HSF1, suppressing its degradation. In stress conditions, the same enzyme additionally acetylates Lys80, inhibiting the binding of HSF1 to the phosphate backbone of DNA (153). Downregulation of p300 results in decreased HSF1 protein levels, due to degradation (153). SIRT1 counteracts this effect by deacetylating HSF1 and promoting a longer association

with target gene promoters (154, 155). This form of regulation appears to play a role in pathologies and could be a target for intervention. SIRT1 is upregulated in many cancers, potentially contributing to a chronic hyperactivation of HSF1 in malignancy (154). A similar mechanism involving p300 and SIRT1 regulates HIF1 - a partner of HSF1 in activation of transcription in hypoxic conditions (156, 157). Also involved in the regulation of HSR are histone deacetylases HDAC7, HDAC9 and HDAC1, having both a positive and negative role. HDAC7 and HDAC9 act by removing the inhibitory acetyl group and increase the robustness of HSR. HDAC1, however, may sterically block the DBD of HSF1, diminishing its DNA binding activity (158). Histone deacetylases are a target for a new class of anticancer drugs, some of which have been approved for the treatment of hematological malignancies (159). Other modes of HSF1 regulation include its SUMOylation (160–162) and a production of its differentially spliced isoforms (137, 163).

5 HSF1 IN CANCER

Since the discovery of HSR, the understanding of the function of the heat shock factors has deepened. It is now clear that HSF1 is involved in many other processes independent of the HSR (164). Unsurprisingly, the cytoprotective properties of HSF1 are exploited by cancers to promote cell survival, proliferation, invasion and metastasis. HSF1 is infrequently mutated across cancer types, but copy number alterations, especially amplifications, are common (**Figure 3A**). The highest frequency of HSF1 gene amplification is found in ovarian, pancreatic, breast and liver carcinomas which also show elevated mRNA levels of HSF1 (**Figure 3B**). Increased HSF1 gene copy number was associated with significantly shorter survival in our pan-cancer analysis (**Figure 3C**). A robust upregulation of HSF1 mRNA in DLBC lymphoma (**Figure 3B**) can at least partially be responsible for strong increases in gene expression for most HSPs in this cancer (**Figure 1**). The cause for a broad decrease of HSPs expression accompanied by a potent induction of only three HSPs (HSPA2, HSPA12B and DNAJA4) in another hematological malignancy AML (**Figure 1**) is less clear as its HSF1 mRNA levels were not reduced (**Figure 3B**). It is possible that the use of peripheral blood cells as a normal tissue control for AML does not provide a good biological reference. In a meta-analysis of 10 studies, including 3159 patients, HSF1 protein abundance was also associated with shorter overall survival in esophageal squamous cell carcinoma, breast cancer, HCC, as well as non-small cell lung cancer (NSCLC) and pancreatic cancer (167). HSF1 expression also correlated with clinicopathological features of aggressiveness such as tumor, nodal and metastasis stage and histological grade (167). Cells with a more malignant phenotype have a higher abundance of HSF1 in the nucleus, and a higher amount of phosphorylated Ser326 (168). Strong nuclear staining for HSF1 was shown in cervix, colon, lung, pancreas, prostate, mesenchymal tumors (168). Association of HSF1 expression with unfavorable prognosis was also shown in oral squamous cell carcinoma (169), gastric (170) and esophageal cancer (171).

HSF1 supports carcinogenesis through a variety of pathways. Upon topical application of a mutagen, *Hsf1*-/- mice developed fewer tumors, had lower tumor burden and survived longer than their wild-type littermates (6). In this model of RAS-driven carcinogenesis, the overall incidence of tumors was much

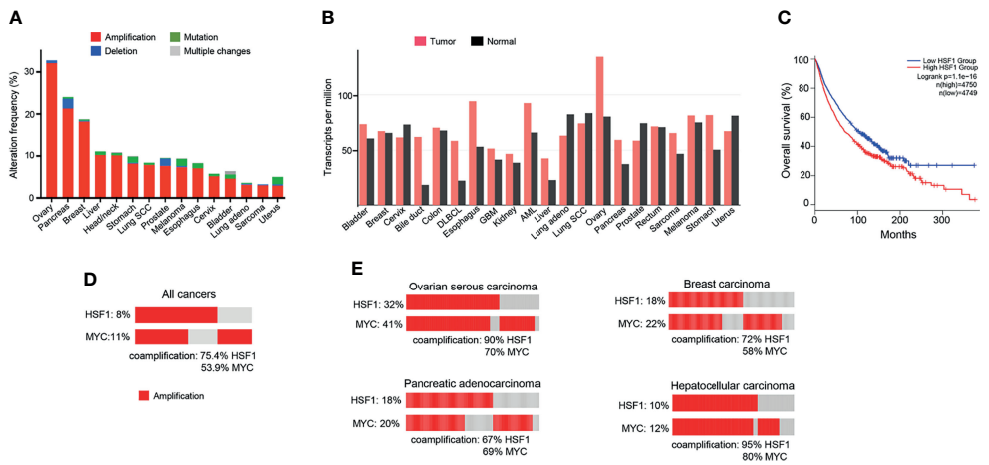

FIGURE 3 | HSF1 alterations in human cancers. **(A)** Frequency of *HSF1* gene alterations in major human cancers. *HSF1* gene is more commonly amplified than mutated in malignancies. Data source: curated set of all studies available (as of January 2022), accessed and analysed through cBioPortal (cbioportal.org) (165, 166). **(B)** HSF1 mRNA levels in cancer and corresponding normal tissue across common cancer types. Data was accessed and analysed through GEPIA (gepia.cancer-pku.cn) (25). **(C)** Kaplan-Meier graph demonstrating the impact of combined alterations in *HSF1* gene on overall survival in a pan-cancer analysis (log-rank p-value=1.1e^{-16}). Data were accessed and analysed through GEPIA (gepia.cancer-pku.cn) (25). **(D)** Oncoprint of genetic alterations in *HSF1* and *MYC* genes in a pancancer analysis (n=14107). **(E)** Amplification and coamplification of *HSF1* and *MYC* genes in ovarian serous carcinoma (n=311), invasive breast carcinoma (n=1169), hepatocellular carcinoma (n=596) and pancreatic adenocarcinoma (n=1846) (cbioportal.org) (165, 166).

lower when Hsf1 was deactivated, yet once a neoplasm was formed, the proportion of benign and malignant tumors was unchanged. In a separate set of experiments, the impact of Hsf1 deactivation in animals with a dominant p53 mutant was tested. Again, mice with intact Hsf1 function developed larger tumors and survived shortest. *Hsf1*-/+ littermates showed an intermediate phenotype, while the *Hsf1*-/- group was most resistant to carcinogenesis. Heterozygotes developed more carcinomas, while among *Hsf1* wild-type mice, sarcomas were more common. Several common human carcinogens, including a widespread water contaminant arsenic (172) and endogenous/exogenous carcinogen formaldehyde (173) are known to robustly activate HSF1 and HSR, which may play a pro-oncogenic role by promoting survival of damaged cells.

HSF1 fosters cancer cell to grow independently of growth signals (6). Mendillo et al. (168) demonstrated that HSF1 drives a transcriptional program, distinct from the HSR, which supports growth and development of malignant cells. The transcriptional signature involves 456 genes and correlates with poor patient outcomes across a variety of cancers. It encompasses pathways coordinating metabolism, cell cycle, DNA repair, apoptosis, adhesion, translation (168). HSF1 maintains ribosomal biogenesis and promotes glycolysis, which is the main energy-producing metabolic pathway from glucose in cancer cells (6). A bioinformatic analysis of over 10 000 cancer genomes showed that copy number alterations (CNA) of chromosome locus 8q24.3 was a common event across cancers and correlated with poor prognosis (174). Our pan-cancer analysis found that amplifications in HSF1 and MYC genes (both situated at this locus) co-occurred in a high percentage of cases (**Figure 3D**). For the top 4 cancers with the highest frequency of HSF1 amplification (ovarian, pancreatic, breast and liver – **Figure 3A**), the percentage of HSF1 co-amplification with MYC ranged from 67% to 90% (**Figure 3E**). Zhang et al. (175) report that about a third of top 100 most overexpressed genes constituting the HSF1 cancer signature are located at 8q21-24. The authors suggested that the co-expression of the genes cannot be fully explained by their co-localization and raised a possibility of a link to mRNA pre-processing (175).

5.1 HSF1 in Major Cancer Types

5.1.1 Breast Cancer

In our analysis of publicly available mRNA data (n=1903), high expression of HSF1 in breast adenocarcinoma correlates with poor prognosis (**Figures 4A–C**). Increased levels of HSF1 were associated with shorter overall survival and relapse-free survival. Samples with higher RNA expression of HSF1 also had higher histologic grade (X^2 test p-value<10^{-10}) and tumor stage (X^2-test p-value= $1.93e^{-3}$). While most patients with stage I breast cancer had low HSF1 expression, at more advanced stages elevated HSF1expression was more common. Negative ER, PR status and HER2 gain are also more likely in cases with high HSF1 transcripts (X^2-test p-values: $4.72e^{-8}$, 1.98^{e-10} and 7.56^{e-3} respectively). While mutations of *HSF1* gene were uncommon, gene amplifications were found in 18% of patients. Previously published meta-analyses of RNA data did not find a statistically significant correlation of HSF1 with prognosis or reported significance for ER-positive patients only, which likely results

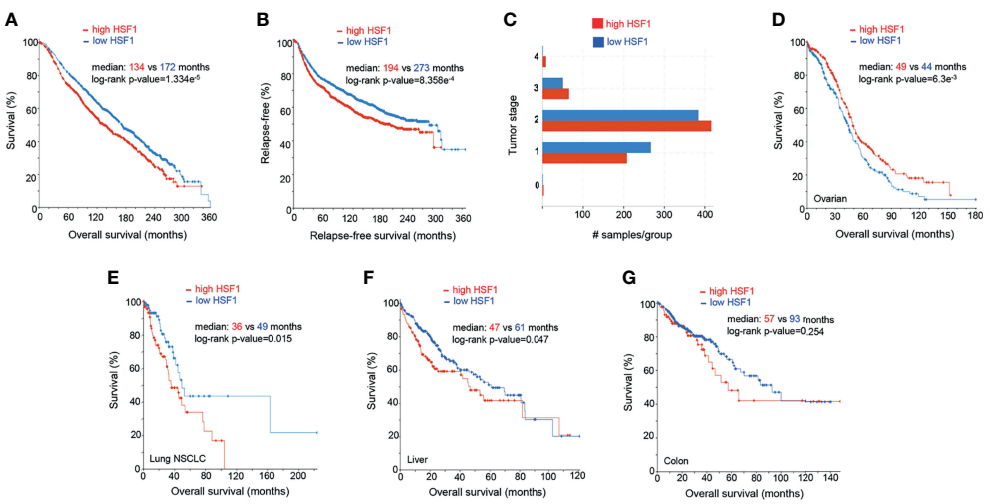

FIGURE 4 | Prognostic significance of HSF1 gene expression in selected human cancers. Patients were divided into groups with high and low expression of mRNA, significance level was defined as p-value<0.05 in log-rank test. Each sample corresponds to an individual patient. **(A)** HSF1 mRNA expression and overall survival in breast adenocarcinoma patients (n=1903). **(B)** Relapse-free survival in breast cancer patients. Cut-off point was set at median expression. **(C)** Tumor stage in relationship to the HSF1 transcript levels. Higher HSF1 expression was associated with more advanced tumor stages, X^2-test p-value= $1.93e^{-3}$. **(D)** Overall survival in patients with ovarian serous cystadenocarcinoma (n=537) in relation to HSF1 mRNA expression. Cut-off point was set at median expression. Microarray data used in panels A-D was sourced and analyzed *via* cBioPortal (cbioportal.org) (165, 166). **(E)** Overall survival in non-small cell lung cancer (NSCLC, n=211), **(F)** Hepatocellular carcinoma (n=373), cut-off point was set at 0.5 SD above the mean expression. **(G)** Colorectal adenocarcinoma (n=379), HSF1 mRNA is not associated with survival. RNA Seq data used in panels E-G was sourced and analyzed *via* cBioPortal (cbioportal.org) (165, 166).

from a lower number of cases studied (176, 177). Normal breast tissue typically shows no nuclear HSF1 staining, whereas HSF1 was commonly detectable in cancers, most abundantly in high-grade carcinoma (178). The increase in nuclear HSF1 was found at an early stage in carcinogenesis and was already seen in carcinoma *in situ*. Strong nuclear staining of HSF1 correlated with tumor stage and low differentiation (178). Estrogens can promote phosphorylation of HSF1 at S326 in ER-positive breast cancers. The activated HSF1 then fosters the transcription of several critical genes, including HSPB8, LHX4, PRKCE, WWC1, and GREB1 (179). Tumors with elevated HSF1 protein expression were also more likely to be ER-negative, HER2-positive and triple-negative (which typically have a more aggressive course) and were often diagnosed at more advanced stages (178). HSF1 appears to be involved in both ER and HER2 pathways. HSF1 associates with multiple proteins, including HDAC1, HDAC2 and metastasis-associated protein 1 (MTA1). These complexes accumulate in close proximity to promoters of estrogen-responsive genes, inhibiting their expression (180). The development of endocrine resistance involves multiple mechanisms, from overexpression of cytokines to transcription factors (STAT, NFkB, HIF1A, MYC). It is of great clinical interest to resolve the functions of HSF1 and HSPs in this process. HSF1 may decrease transcription and increase the degradation of ERα (181), while HSP70 and HSP90 can bind to steroid receptors and alter their activity (182).

HER2, overexpressed in up to 50% of breast carcinoma cases, is known to promote tumor cell growth. In HER2-positive breast cancer, HSF1 promotes malignant transformation and metastasis. Non-malignant HER2-expressing cells acquire malignant characteristics, manifested as the formation of transformed foci *in vitro* and tumors in mice only in the presence of functional HSF1 (183). HER2 also activates HSF1 and its effectors, including HSP90, which results in the activation of RAS-RAF-ERK1/2 axis. In $Hsf1^{+/-}$ mice, despite overexpression of HER2, tumorigenesis was significantly impaired, which was experimentally observed as decreased proliferation, invasion and EMT (184). Mechanistically, HER2 activated HSF1 *via* the PI3K-AKT-mTOR axis and inhibition of HER2, either pharmacological with lapatinib or transient knockdown, attenuated HSF1 activity (185). Consequently, a feedback loop exists, with HER2 activating HSF1, which in turn activates many of its classical effectors, such as HSP70 and HSP90, which further enhance HSF1 transcription (185). HSF1 and HSPs were consistently and very highly expressed in cells resistant to the tyrosine kinase inhibitor lapatinib, which disrupted both HER2 and EGFR pathways. In this context, targeting HSF1 decreased the expression of ERBB2, mut-p53 and components of several compensatory pathways implicated in resistance to this mode of therapy, suggesting that combination therapy with HSF1 inhibitor could be useful in preventing resistance to lapatinib (186).

5.1.2 Ovarian Cancer

Ovarian cancer is the most lethal female-specific cancer. Serous ovarian adenocarcinoma had elevated HSF1 mRNA expression in comparison to normal ovarian tissue (**Figure 3B**). A higher expression ovarian cancer group had a statistically better overall survival (**Figure 4D**). Gene CNA and chromosomal rearrangements were more prevalent in ovarian cancer than in any other human malignancy (**Figure 3A**). Intrachromosomal rearrangements in ovarian cancers were found to influence gene expression at loci distant from the aberration (187). A genome-wide search identified 8q24 (where HSF1 is situated) as high-risk loci in ovarian cancer (188). However, deletion of 8q24.3 increases 5-year mortality (174). On the protein level, malignant tumors express HSF1 more abundantly than benign ovarian tumors (189). HSF1 was barely detectable by IHC in normal ovarian tissue but high in different types of tumors: serous, mucinous, endometrioid, clear cell (190). Further, phosphorylation of HSF1 at Ser326 in ovarian cancer samples was associated with poor prognosis (191). HSF1 depletion triggered apoptosis in cancerous cells and suppressed carcinogenesis in nude mice implanted with xenografts (190). HSF1 was also linked to EMT in 3D cell culture model of ovarian carcinoma (192). Apart from HSF1 being a potential target of combinatory antitumor therapy, it could also be a useful diagnostic tool. Detection of autoantibodies against HSF1 in early-stage high-grade ovarian serous carcinoma (FIGO Ia-Ic) increased diagnostic accuracy of CA-125 (193). As 81% of ovarian cancers express the ERα (194), resolving the interactions of HSF1 and hormone receptor status could also be clinically important.

5.1.3 Lung Cancer

NSCLC is the most common type of human lung cancer. Higher levels of HSF1 mRNA were associated with lower overall survival in a cohort of NSCLC (**Figure 4E**). HSF1 gene amplifications were found in 11% of these aggressive tumors. On a protein level, a systematic meta-analysis confirmed the inverse relationship between HSF1 and overall survival in NSCLC (167). Moreover, in a study of 105 patients with NSCLC, 42.9% of tissue samples exhibited a high nuclear abundance of HSF1, correlating with poor overall survival, cancer stage and nodal metastasis (195). The same study suggested that nuclear accumulation of HSF1 may play a role in tumor neoangiogenesis (195). Further supporting its importance in malignant properties of NSCLC cells, HSF1 was a key factor allowing them to thrive independently of attachment to a surface. Although depletion of this transcription factor sensitized cancer cells to anoikis, HSF1 activation in normal bronchial epithelium did not confer the ability of anchorage-independent growth (196). HSF1 was also highly expressed in lung adenocarcinoma brain metastases (197). The ABL kinase-HSF1-E2F axis promotes cell cycle progression and cell survival. Its disruption by means of knockdown or targeted pharmacological inhibition provided a proof of concept for a therapeutic intervention (197). HSF1 also directs a malignancy-supporting program in surrounding stromal cells mediated by TGFβ and SD1. Higher expression of HSF1 in stromal cells from patients with stage I NSCLC was associated with significantly shorter disease-free survival (198). HSF1 was also an independent predictor of progression-free survival in NSCLC with positive KRAS and EGFR mutation status (198). A recent study identified HSF1 as a target for pharmacological intervention to overcome the resistance to the EGFR inhibitor erlotinib. The authors demonstrated the

effectiveness of this approach using the HSF1 inhibitor emetine to suppress tumor growth in mice (199). Yoon et al. (200) described a natural compound promoting the degradation of the active form of HSF1 through dephosphorylation at S326 in H460 cells, where it induced growth arrest, apoptosis and bolstered the effect of radiotherapy, paclitaxel and cisplatin. In line with the concept of targeting non-oncogene addiction, its effect was more pronounced in cancer cells (200). It would be interesting to see whether this strategy shows similar effectiveness *in vivo*.

5.1.4 Hepatocellular Carcinoma

HSF1 RNA transcripts were more abundant in tumors than neighboring normal liver tissue (**Figure 3B**) and correlated with adverse prognosis (**Figure 4F**). In immunohistochemistry, healthy liver cells showed faint immunoreactivity compared to strong staining seen in HCC cells (201). These observations were corroborated by another study, showing that high protein abundance of HSF1 and phospho-Ser326-HSF1 were increased in HCC and negatively correlated with tumor progression and survival (82). The role of HSF1 in oncogenesis and maintenance was well documented by ablation experiments. HSF1 knockout decreased cell proliferation and upregulated expression of the G1-S inhibitor Rb1 (82). HSF1 knockdown in human HCC cells suppressed cell proliferation and fostered apoptosis by disrupting the PI3K-AKT-mTOR axis (201). The relationship between HSF1 and mTOR, also seen in other cancer types, was demonstrated as a necessary component for MYC-driven HCC (202). Overexpression of cMYC is common in HCC. HSF1 and MYC were amplified in 10 and 12% of samples, respectively and co-occurred for >95% HSF1 cases (**Figure 3E**). Patients with overexpression of both genes had the shortest overall survival and higher-grade tumors. At the same time, human specimen of HCC often features an inactivation of either of the genes; in very rare cases of both (203). HSF1 knockdown downregulated cMYC and slowed the growth of cMYC-dependent HCC in mice. In turn, the silencing of cMYC in human HCC cells downregulated HSF1. In mice with dominant-negative HSF1, the growth of MYC-dependent tumors was completely halted (203). Specific biochemical mechanisms have not yet been demonstrated, but upon HSF1 knockdown, murine tumors overexpressing MYC experienced a dysregulation of its targets involved in metabolism and ribosome biogenesis (203).

5.1.5 Colorectal Cancer

HSF1 is highly expressed in colorectal adenocarcinoma on both transcript and protein level (204, 205). In our analysis, HSF1 RNA expression was not significantly associated with overall survival over 10 years, but patients with elevated HSF1 had lower 5-year survival (**Figure 4G**). HSF1stimulates glutaminolysis *via* GLS1 and activates mTOR in colorectal cancer cells; its knockdown restricts cell growth. Pharmacological inhibition or genetic abolishment of HSF1 suppressed carcinogenesis in mice (205). High expression of HSPs in inflammatory gut diseases and early stages of cancer are well documented (206). A recent study linked HSF1 to colitis-associated colon cancer through inflammatory remodeling of extracellular matrix (206).

5.1.6 Melanoma

HSF1 expression assessed by IHC was associated with greater disease severity as it was stronger in metastatic than in primary lesions. Strong nuclear staining also indicated shorter disease-free survival (207). The upregulation of HSF1 in melanoma likely resulted from its inefficient degradation due to frequent mutations or downregulation of the ubiquitin ligase FBXW7α (207). HSF1 depletion *in vitro* resulted in a reversible decrease in migration and invasion. HSF1 depletion markedly lowered the tumorigenic potential of melanoma cells in nude mice (208).

6 HEAT-SHOCK RESPONSE AND CANCER IMMUNOSURVEILLANCE

Tumors grow when the host immune system fails to recognize them as foreign. Cancer cells have evolved different strategies to achieve this, including downregulating the expression of MHC I, eliminating T cells within the tumor tissue and reduced antigen cross-presentation (209). It is well established that chaperones are involved in the immune response through their ability to stably bind polypeptide chains. HSPs bind tumor antigens, forming complexes recognized by monocytes, macrophages, B cells, dendritic cells, ultimately leading to cytotoxic T cell activation. All major HSPs interact with antigen-presenting cells *via* CD40, CD91 and LOX1 (210).

In recent years therapies with PD-1/PD-L1 inhibitors (also known as immune checkpoint inhibitors) have been widely introduced into clinical practice, yielding spectacular success in selected patients, but the overall response rate among all cancers remains around 12% (211). Based on this success, research efforts are invested into gaining a deeper understanding the mechanisms governing their expression and the links to patient outcomes. The binding of PD-1 with its ligand sends an inhibitory signal invoking decreased proliferation and activity of cytotoxic T cells, diminished cytokine production and differentiation of regulatory T cells, allowing cancer cells to escape the host immune surveillance (212). Yang et al. (213) have shown that HSF1 phosphorylation at Thr120 by PIM2 increased its transcriptional activity and promoted binding to HSE in the PD-L1 promoter, enhancing its expression. pThr120-HSF1 was associated with increased migration, invasion and proliferation in breast cancer cells *in vitro*. While targeted inhibition of PIM2 and HSF1 resulted in decreased tumor size in each case, combined treatment had a synergistic effect and arrested tumor growth entirely in murine xenografts (213). Similarly, previous studies show that blocking PIM kinases leads to a decreased PD-L1 expression (214). No studies combining HSF1 inhibitors and PD-L1 inhibitors have yet been published. Therapies targeting multiple HSPs are suggestive of an antitumor potential for a combined HSF1-targeted/immune checkpoint therapy. The effects of a multi-subtype HSP/peptide vaccine tested in murine osteosarcoma were potentiated by the addition of a PD-L1 inhibitor. The combination triggered elevated cytokine production, stimulated CD4+ and CD8+ T cells and mitigated lung metastasis better

than each therapeutic modality alone (215). Almost all HSP-inhibitors have been administered so far on intermittent dosage schemes. However, pharmacokinetics seems important, not only for the efficacy of HSF1-HSP axis inhibition but also for the accompanying immune effects. In comparison to a high acute dose regimen, a sustained low-dose inhibition of HSP90 slowed the progression of colon cancer in immunocompetent mice more effectively and produced a higher density of more diverse tumor-associated antigens. In the same experiment, additional administration of an immune adjuvant further improved tumor control and complete ablation of tumor in some cases (216).

HSE is present in the promoters of a plethora of genes, including those related to immune response such as FasL and HLA-G. Hyperthermia elevated the expression of a non-canonical MHC class I molecule HLA-G but did not affect other genes in this class (217). HLA-G is a low-polymorphism gene, generally expressed in tumors and fetal tissues, promoting immune tolerance. It inhibits the proliferation and cytotoxic activity of T cells and NK cells and is known to impair host immune responses against cancer cells (218, 219). Other stress-inducible genes containing HSE in the promoter region include major histocompatibility class I chain-related proteins A and B (MICA and MICB). MICA and MICB bind to NKG2D receptors, activating NK cells. HSF1 knockdown leads to a decrease in MICB only, whereas pharmacological inhibition by NZ28 depressed both MICA and MICB, causing a strong inhibition of NK cytotoxic activity (inhibition of HSP90 did not change MICA and MICB levels) (220). However, the effects of this inhibitor may be partially attributed to its non-specific mode of action and modulation of the NF-kB pathway. The family of NKG2D-ligands comprises six other members (ULBP1-6) whose promoters contain HSE, but their direct activation by HSF1 was not yet established.

7 HSF1 AND CANCER THERAPY

7.1 HSF1 and Drug Resistance

Another function of HSF1, independent of the heat shock response, is the promotion of drug resistance. Chemotherapy remains the mainstay of treatment for hematologic malignancies and metastatic cancers, and resistance to cytotoxic agents is common and often leads to therapy failure. One mechanism of multidrug resistance involves a superfamily of membrane transporters - the ATP-binding cassette (ABC) - which pump hydrophobic molecules out of the cell (221). Strong evidence exists that HSF1 contributes to the functioning of an ABC subgroup - ABCB1 (also referred to as P-glycoprotein and MDR1). Elevated P-glycoprotein drastically reduces prognosis in hematologic malignancies, solid and epithelial tumors and can transport a broad range of substrates across cellular membranes such as anthracyclines, taxanes, alkaloids, topoisomerase II inhibitors (221).

MDR1 gene features several HSE regulatory sequences, and its promoter is activated in response to stress (222). The increase in MDR1 expression is not associated with the accumulation of heat shock proteins, and the exact mode(s) of control over MDR1 expression exerted by HSF1 is less clear. Transfection with a constitutively active HSF1 led to increased MDR1 mRNA and protein levels and stimulated vinblastine efflux. The induction of the MDR phenotype was dependent on HSF1 recognizing and binding to binding the HSE in the MDR promoter (223). The concept of HSF1 transcriptional control is supported by the fact that inhibition of HSF1 binding to HSE by quercetin suppressed MDR-dependent drug resistance (224). However, in doxorubicin-resistant osteosarcoma cells, increased HSF1 expression was not coupled to elevated MDR1 transcription as has been shown in a luciferase reporter assay. Also, disruption of the HSE had no effect on induction of the MDR phenotype (225). Melanoma cells overexpressing mutant HSF1 with a deletion in the transcriptional activation domain were resistant to doxorubicin and paclitaxel (but not cisplatin, bortezomib and vinblastine), correlating with overexpression of several ABC transporters (ABCB1, ABCB8, ABCC1, ABCC2, ABCC5 and ABCD1) and increased drug efflux (226). The overabundance of the inactive mutant also suppressed heat shock response through the dominant-negative effect. In contrast, transfection with a constitutively active form of HSF1 elevated HSP expression in the absence of drug resistance (226). Overall, such observations suggest an involvement of HSF1 at a post-transcriptional level. Of note, although ABCs transport a broad array of substrates, the drug efflux induced by HSF1 transfections was selective and differed between cell lines. The reasons for the observed functional specificity remain to be elucidated.

HSF1 is a known regulator of autophagy - a cytoprotective response to stress - which when inhibited, sensitizes cells to radio- and chemotherapy (227). To this end, the transcriptional induction of autophagy *via* autophagy-related protein 7 (ATG7), fosters autophagosome formation and ultimately cell survival (228). Conversely, drug sensitivity was increased following HSF1 knockdown. Consistent with its cytoprotective role, ATG7 expression was associated with poor prognosis in breast cancer patients (229). A few members of the autophagy-related protein family also feature HSE regions, suggesting that these findings can be extrapolated to other proteins, for example, ATG4B, which attenuates the cytotoxicity of epirubicin in hepatocellular carcinoma cells (230). The mechanisms through which HSF1 and autophagy influence drug resistance are likely diverse. An interesting model of autophagy induction was proposed in a study on melanoma cells resistant to apoptosis by ER stress inducers (such as thapsigargin). Stress-induced transcriptional activation of RIPK1 *via* HSF1, downstream of XBP1, consequently promoting cell survival. No HSF1 activation occurred in cells sensitive to apoptosis by ER stress inducers (231).

7.2 Proteasome Inhibitors

Multiple myeloma is an example of a disease where a strategy for targeting the malignancy-associated proteotoxic state is successful. Myeloma cells experience elevated proteotoxic stress, not only due to rapid growth and dysbalanced metabolic conditions but also due to rampant immunoglobulin production.

This, in turn, leads to unfolded protein response and HSR activation (232). The molecular sequelae of proteasome inhibition involve a stark increase in HSP70, HSP27 and HSF1 expression (233). Silencing HSF1 in myeloma cells, as well as selective pharmacological inhibition of HSF1, strongly sensitizes cells to proteasome inhibition (234). In contrast, downregulation of individual HSPs in combination with proteasome inhibition was not as effective. This treatment was dependent on the basal HSP expression level and HSF1 suppression was less effective in cell lines with already elevated HSPs (235).

7.3 HSF1 as a Target for Pharmacotherapy

HSF1 is not an easily druggable molecule as it lacks a discernible binding site for small molecule inhibitors, its activation process is complex, and is subject to numerous posttranslational modifications in response to different forms and degrees of proteotoxic stress. Many potential inhibitors have been developed, often derivates of natural medicinal products, as well as products of *in silico* designs and large-scale screens of synthetic chemical libraries (236). Unfortunately, in many cases, the exact mechanism of action and drug specificity remain unknown. An ideal inhibitor would bind directly and with a high affinity to HSF1. Keeping in mind the potential future use as a clinical drug, the substance should exhibit its function at low concentrations and have favorable pharmacokinetics. To date, only three compounds with a known, on-target mode of action have been identified: KRIBB11, I_{HSF1}115, SchA and $iaRNA^{HSF1}$. A recent review by Dong et al. provides a detailed overview of the available compounds, their structure and mode of action (237).

The first direct inhibitor of HSF1, KRIBB11, was identified in a screen of over 6000 molecules (238). A luciferase reporter assay showed a decrease in HSP70 synthesis. Experimental evidence from affinity chromatography confirmed that KRIBB11 binds to HSF1 and abolishes the recruitment of pTEFb, which is necessary for the release of RNA polymerase II and continuation of transcription. KRIBB11 is highly effective with an IC_{50} = 1.2 μM and 10 μM, almost completely preventing the association of pTEFb to the HSP70-promoter. Experiments in nude mice revealed a 47% decrease in tumor volume and depletion of HSP70. This finding indicated a significant antitumor activity with limited general toxicity (238). Following a structure-activity analysis of HSF1 DBD (DNA-binding domain), I_{HSF1}115 was developed (239). Interestingly, despite binding to the DBD, it does not inhibit the HSF1 association with the HSE but rather modulates its transcriptional activity. The efficacy of I_{HSF1}115 was experimentally validated in several cancer cell lines. The structure targeted by I_{HSF1}115 is also present on HSF2. Therefore, it is possible that this inhibitor affects the function of both transcription factors (239). Salamanca et al. (240) utilized a different strategy and developed an RNA aptamer competing with HSE for binding with the DBD of HSF1. The inhibitory aptamer- $iaRNA^{HSF1}$- was evaluated in yeast, Drosophila and human cancer cells, where a reduction in colony-forming ability and an increase in apoptosis were noted. Difficulties with drug delivery *in vivo* currently hamper the application of this approach to pre-clinical studies (240). Recently, Chen et al. (241) reported HIF1-inibiting properties of deoxyschizandrin (also termed shizandrin A) which is a bioactive molecule derived from a Chinese medicinal plant *Schisandra chinensis*. Evidence from surface plasmon resonance and computer modeling suggested that deoxyschizandrin binds to HSF1 directly by inducing conformational changes to the binding site. The compound caused cell cycle arrest and death by apoptosis in human colorectal cancer cells *in vitro*. However, despite its direct binding to HSF1, deoxyschizandrin also appears to alter other functions in cells (241).

8 CONCLUDING REMARKS

Human cancers almost invariably overexpress main constituents of HSR, including individual HSPs and HSF1. Upregulation and its importance for maintenance of multiple oncogenic pathways identifies HSR as one of pan-cancer targets (**Figure 5**). Preclinical models and more limited clinical studies showed promising results with selected inhibitors of the HSR pathway. A new direction for exploration of antioncogenic effects of HSR inhibition, which has been impossible to detect in the classic tumor xenograft models in immunodeficient mice, is the modulation of immunosuppressive activity by cancers. Combinatory therapy including HSR-targeting drugs offers a potential to enhance the efficacy of clinically used drugs, including immune checkpoint inhibitors. The development of more specific inhibitors with better pharmacokinetic properties is needed for targeting of HSR components, including HSF1, for

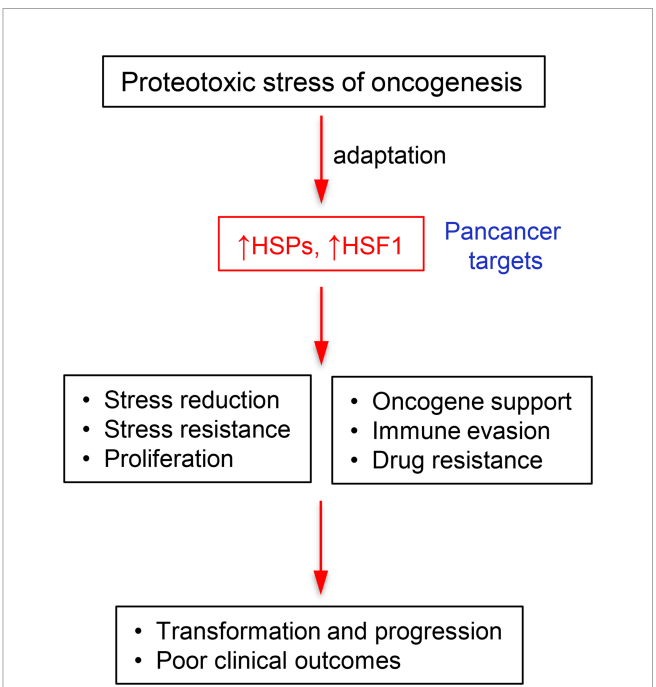

FIGURE 5 | Flow chart depicting the role of heat shock proteins and HSF1 in cancers.

successful cancer therapy. A strong association with poor prognosis or selective upregulation in malignancy are typically used as the initial screens to identify specific HSR proteins as clinically promising targets for drug development. Another approach for the selection of a drug target can involve identification of HSR components that exhibit a clear pattern of coexpression and/or dependency for a major oncogene that by itself is poorly druggable. Coamplification of HSF1 with a notoriously undruggable MYC oncogene points to HSF1 inhibition as a potential therapeutic strategy for numerous MYC-driven human malignancies. Higher translation activity is necessary to support a rapid growth of transformed cells, but the overabundance of nascent proteins also increases demand for the chaperone/HSR system, which is further exacerbated by aneuploidy-associated excesses in the production of unstable proteins. Thus, it is conceivable that cancers with activating mutations in the protein translation-controlling pathways such as AKT-mTOR can be particularly suitable for HSR-targeting therapies.

AUTHOR CONTRIBUTIONS

AC and AZ: conceptualization of the manuscript and editing of the final draft. AC: writing of the first draft. AZ: preparation of the final draft. All authors contributed to the article and approved the submitted version.

FUNDING

This work was supported by NIH grants ES031979, ES031002, and ES028072.

REFERENCES

1. Brancolini C, Iuliano L. Proteotoxic Stress and Cell Death in Cancer Cells. *Cancers* (2020) 12(9):2385. doi: 10.3390/cancers12092385
2. Hartl FU, Bracher A, Hayer-Hartl M. Molecular Chaperones in Protein Folding and Proteostasis. *Nature* (2011) 475(7356):324–32. doi: 10.1038/nature10317
3. Richter K, Haslbeck M, Buchner J. The Heat Shock Response: Life on the Verge of Death. *Mol Cell* (2010) 40(2):253–66. doi: 10.1016/j.molcel.2010.10.006
4. Akerfelt M, Morimoto RI, Sistonen L. Heat Shock Factors: Integrators of Cell Stress, Development and Lifespan. *Nat Rev Mol Cell Biol* (2010) 11 (8):545–55. doi: 10.1038/nrm2938
5. Vihervaara A, Sergelius C, Vasara J, Blom MAH, Elsing AN, Roos-Mattjus P, et al. Transcriptional Response to Stress in the Dynamic Chromatin Environment of Cycling and Mitotic Cells. *Proc Natl Acad Sci USA* (2013) 110(36):E3388–97. doi: 10.1073/pnas.1305275110
6. Dai C, Whitesell L, Rogers AB, Lindquist S. Heat Shock Factor 1 Is a Powerful Multifaceted Modifier of Carcinogenesis. *Cell* (2007) 130(6):1005–18. doi: 10.1016/j.cell.2007.07.020
7. Björk JK, Åkerfelt M, Joutsen J, Puustinen MC, Cheng F, Sistonen L, et al. Heat-Shock Factor 2 is a Suppressor of Prostate Cancer Invasion. *Oncogene* (2016) 35(14):1770–84. doi: 10.1038/onc.2015.241
8. Ostling P, Björk JK, Roos-Mattjus P, Mezger V, Sistonen L. Heat Shock Factor 2 (HSF2) Contributes to Inducible Expression of Hsp Genes Through Interplay With HSF1. *J Biol Chem* (2007) 282(10):7077–86. doi: 10.1074/jbc.M607556200
9. Gomez-Pastor R, Burchfiel ET, Thiele DJ. Regulation of Heat Shock Transcription Factors and Their Roles in Physiology and Disease. *Nat Rev Mol Cell Biol* (2018) 19(1):4–19. doi: 10.1038/nrm.2017.73
10. Hanahan D, Weinberg RA. The Hallmarks of Cancer. *Cell* (2000) 100(1):57–70. doi: 10.1016/S0092-8674(00)81683-9
11. Hanahan D, Weinberg RA. Hallmarks of Cancer: The Next Generation. *Cell* (2011) 144(5):646–74. doi: 10.1016/j.cell.2011.02.013
12. Luo J, Solimini NL, Elledge SJ. Principles of Cancer Therapy: Oncogene and non-Oncogene Addiction. *Cell* (2009) 136(5):823–37. doi: 10.1016/j.cell.2009.02.024
13. Weinstein IB. Cancer. Addiction to Oncogenes–the Achilles Heal of Cancer. *Science (New York NY)* (2002) 297(5578):63–4. doi: 10.1126/science.1073096
14. Kampinga HH, Hageman J, Vos MJ, Kubota H, Tanguay RM, Bruford EA, et al. Guidelines for the Nomenclature of the Human Heat Shock Proteins. *Cell Stress Chaperones* (2009) 14(1):105–11. doi: 10.1007/s12192-008-0068-7
15. Finka A, Goloubinoff P. Proteomic Data From Human Cell Cultures Refine Mechanisms of Chaperone-Mediated Protein Homeostasis. *Cell Stress Chaperones* (2013) 18(5):591–605. doi: 10.1007/s12192-013-0413-3
16. Saibil H. Chaperone Machines for Protein Folding, Unfolding and Disaggregation. *Nat Rev Mol Cell Biol* (2013) 14(10):630–42. doi: 10.1038/nrm3658
17. Trepel J, Mollapour M, Giaccone G, Neckers L. Targeting the Dynamic HSP90 Complex in Cancer. *Nat Rev Cancer* (2010) 10(8):537–49. doi: 10.1038/nrc2887
18. Schopf FH, Biebl MM, Buchner J. The HSP90 Chaperone Machinery. *Nat Rev Mol Cell Biol* (2017) 18(6):345–60. doi: 10.1038/nrm.2017.20
19. Prodromou C. Mechanisms of Hsp90 Regulation. *Biochem J* (2016) 473 (16):2439–52. doi: 10.1042/BCJ20160005
20. Genest O, Wickner S, Doyle SM. Hsp90 and Hsp70 Chaperones: Collaborators in Protein Remodeling. *J Biol Chem* (2019) 294(6):2109–20. doi: 10.1074/jbc.REV118.002806
21. Sahasrabudhe P, Rohrberg J, Biebl MM, Rutz DA, Buchner J. The Plasticity of the Hsp90 Co-Chaperone System. *Mol Cell* (2017) 67(6):947–61.e5. doi: 10.1016/j.molcel.2017.08.004
22. Whitesell L, Lindquist SL. HSP90 and the Chaperoning of Cancer. *Nat Rev Cancer* (2005) 5(10):761–72. doi: 10.1038/nrc1716
23. Schoof N, von Bonin F, Trümper L, Kube D. HSP90 is Essential for Jak-STAT Signaling in Classical Hodgkin Lymphoma Cells. *Cell Communication Signaling* (2009) 7(1):17. doi: 10.1186/1478-811X-7-17
24. Moulick K, Ahn JH, Zong H, Rodina A, Cerchietti L, Gomes DaGama EM, et al. Affinity-Based Proteomics Reveal Cancer-Specific Networks Coordinated by Hsp90. *Nat Chem Biol* (2011) 7(11):818–26. doi: 10.1038/nchembio.670
25. Tang Z, Li C, Kang B, Gao G, Li C, Zhang Z. GEPIA: A Web Server for Cancer and Normal Gene Expression Profiling and Interactive Analyses. *Nucleic Acids Res* (2017) 45(W1):W98–102. doi: 10.1093/nar/gkx247
26. Sanchez J, Carter TR, Cohen MS, Blagg BSJ. Old and New Approaches to Target the Hsp90 Chaperone. *Curr Cancer Drug Targets* (2020) 20(4):253–70. doi: 10.2174/1568009619666191202101330
27. Samuni Y, Ishii H, Hyodo F, Samuni U, Krishna MC, Goldstein S, et al. Reactive Oxygen Species Mediate Hepatotoxicity Induced by the Hsp90 Inhibitor Geldanamycin and its Analogs. *Free Radical Biol Med* (2010) 48 (11):1559–63. doi: 10.1016/j.freeradbiomed.2010.03.001
28. Shevtsov M, Multhoff G, Mikhaylova E, Shibata A, Guzhova I, Margulis B. Combination of Anti-Cancer Drugs With Molecular Chaperone Inhibitors. *Int J Mol Sci* (2019) 20(21):5284. doi: 10.3390/ijms20215284
29. Modi S, Sugarman S, Stopeck A, Linden H, Ma W, Kersey K, et al. Phase II Trial of the Hsp90 Inhibitor Tanespimycin (Tan) + Trastuzumab (T) in Patients (Pts) With HER2-Positive Metastatic Breast Cancer (MBC). *J Clin Oncol* (2008) 26(15_suppl):1027. doi: 10.1200/jco.2008.26.15_suppl.1027
30. Ronnen EA, Kondagunta GV, Ishill N, Sweeney SM, DeLuca JK, Schwartz L, et al. A Phase II Trial of 17-(Allylamino)-17-Demethoxygeldanamycin in Patients With Papillary and Clear Cell Renal Cell Carcinoma. *Invest New Drugs* (2006) 24(6):543–6. doi: 10.1007/s10637-006-9208-z

31. Heath EI, Hillman DW, Vaishampayan U, Sheng S, Sarkar F, Harper F, et al. A Phase II Trial of 17-Allylamino-17-Demethoxygeldanamycin in Patients With Hormone-Refractory Metastatic Prostate Cancer. *Clin Cancer Res* (2008) 14(23):7940–6. doi: 10.1158/1078-0432.CCR-08-0221
32. Talaei S, Mellatyar H, Asadi A, Akbarzadeh A, Sheervalilou R, Zarghami N. Spotlight on 17-AAG as an Hsp90 Inhibitor for Molecular Targeted Cancer Treatment. *Chem Biol Drug Design* (2019) 93(5):760–86. doi: 10.1111/cbdd.13486
33. Cavenagh J, Oakervee H, Baetiong-Caguioa P, Davies F, Gharibo M, Rabin N, et al. A Phase I/II Study of KW-2478, an Hsp90 Inhibitor, in Combination With Bortezomib in Patients With Relapsed/Refractory Multiple Myeloma. *Br J Cancer* (2017) 117(9):1295–302. doi: 10.1038/bjc.2017.302
34. Banerji U, Walton M, Raynaud F, Grimshaw R, Kelland L, Valenti M, et al. Pharmacokinetic-Pharmacodynamic Relationships for the Heat Shock Protein 90 Molecular Chaperone Inhibitor 17-Allylamino, 17-Demethoxygeldanamycin in Human Ovarian Cancer Xenograft Models. *Clin Cancer Res* (2005) 11(19):7023–32. doi: 10.1158/1078-0432.CCR-05-0518
35. Brocchieri L, Conway de Macario E, Macario AJL. Hsp70 Genes in the Human Genome: Conservation and Differentiation Patterns Predict a Wide Array of Overlapping and Specialized Functions. *BMC Evol Biol* (2008) 8 (1):19. doi: 10.1186/1471-2148-8-19
36. Nitika, Porter CM, Truman AW, Truttmann MC. Post-Translational Modifications of Hsp70 Family Proteins: Expanding the Chaperone Code. *J Biol Chem* (2020) 295(31):10689–708. doi: 10.1074/jbc.REV120.011666
37. Radons J. The Human HSP70 Family of Chaperones: Where do We Stand? *Cell Stress Chaperones* (2016) 21(3):379–404. doi: 10.1007/s12192-016-0676-6
38. Zorzi E, Bonvini P. Inducible Hsp70 in the Regulation of Cancer Cell Survival: Analysis of Chaperone Induction, Expression and Activity. *Cancers* (2011) 3(4):3921–56. doi: 10.3390/cancers3043921
39. Kampinga HH, Craig EA. The HSP70 Chaperone Machinery: J Proteins as Drivers of Functional Specificity. *Nat Rev Mol Cell Biol* (2010) 11(8):579–92. doi: 10.1038/nrm2941
40. Wandinger SK, Richter K, Buchner J. The Hsp90 Chaperone Machinery. *J Biol Chem* (2008) 283(27):18473–7. doi: 10.1074/jbc.R800007200
41. Finka A, Sharma SK, Goloubinoff P. Multi-Layered Molecular Mechanisms of Polypeptide Holding, Unfolding and Disaggregation by HSP70/HSP110 Chaperones. *Front Mol Biosci* (2015) 2:29. doi: 10.3389/fmolb.2015.00029
42. Bracher A, Verghese J. GrpE, Hsp110/Grp170, HspBP1/Sil1 and BAG Domain Proteins: Nucleotide Exchange Factors for Hsp70 Molecular Chaperones. *Sub Cellular Biochem* (2015) 78:1–33. doi: 10.1007/978-3-319-11731-7_1
43. Bracher A, Verghese J. The Nucleotide Exchange Factors of Hsp70 Molecular Chaperones. *Front Mol Biosci* (2015) 2:10. doi: 10.3389/fmolb.2015.00010
44. Shen C, Kaelin WGJr. The VHL/HIF Axis in Clear Cell Renal Carcinoma. *Semin Cancer Biol* (2013) 23(1):18–25. doi: 10.1016/j.semcancer.2012.06.001
45. Jagadish N, Parashar D, Gupta N, Agarwal S, Suri V, Kumar R, et al. Heat Shock Protein 70-2 (HSP70-2) is a Novel Therapeutic Target for Colorectal Cancer and is Associated With Tumor Growth. *BMC Cancer* (2016) 16:561. doi: 10.1186/s12885-016-2592-7
46. Garg M, Kanojia D, Seth A, Kumar R, Gupta A, Surolia A, et al. Heat-Shock Protein 70-2 (HSP70-2) Expression in Bladder Urothelial Carcinoma is Associated With Tumour Progression and Promotes Migration and Invasion. *Eur J Cancer (Oxford England: 1990)* (2010) 46(1):207–15. doi: 10.1016/j.ejca.2009.10.020
47. Singh S, Suri A. Targeting the Testis-Specific Heat-Shock Protein 70-2 (HSP70-2) Reduces Cellular Growth, Migration, and Invasion in Renal Cell Carcinoma Cells. *Tumour Biol* (2014) 35(12):12695–706. doi: 10.1007/s13277-014-2594-5
48. Aghdassi A, Phillips P, Dudeja V, Dhaulakhandi D, Sharif R, Dawra R, et al. Heat Shock Protein 70 Increases Tumorigenicity and Inhibits Apoptosis in Pancreatic Adenocarcinoma. *Cancer Res* (2007) 67(2):616–25. doi: 10.1158/0008-5472.CAN-06-1567
49. Rohde M, Daugaard M, Jensen MH, Helin K, Nylandsted J, Jäättelä M. Members of the Heat-Shock Protein 70 Family Promote Cancer Cell Growth by Distinct Mechanisms. *Genes Dev* (2005) 19(5):570–82. doi: 10.1101/gad.305405
50. Wang B, Lan T, Xiao H, Chen Z-H, Wei C, Chen L-F, et al. The Expression Profiles and Prognostic Values of HSP70s in Hepatocellular Carcinoma. *Cancer Cell Int* (2021) 21(1):286. doi: 10.1186/s12935-021-01987-9
51. Stankiewicz AR, Lachapelle G, Foo CPZ, Radicioni SM, Mosser DD. Hsp70 Inhibits Heat-Induced Apoptosis Upstream of Mitochondria by Preventing Bax Translocation. *J Biol Chem* (2005) 280(46):38729–39. doi: 10.1074/jbc.M509497200
52. Li H, Liu L, Xing D, Chen WR. Inhibition of the JNK/Bim Pathway by Hsp70 Prevents Bax Activation in UV-Induced Apoptosis. *FEBS Lett* (2010) 584 (22):4672–8. doi: 10.1016/j.febslet.2010.10.050
53. Nylandsted J, Gyrd-Hansen M, Danielewicz A, Fehrenbacher N, Lademann U, Høyer-Hansen M, et al. Heat Shock Protein 70 Promotes Cell Survival by Inhibiting Lysosomal Membrane Permeabilization. *J Exp Med* (2004) 200 (4):425–35. doi: 10.1084/jem.20040531
54. Guo F, Sigua C, Bali P, George P, Fiskus W, Scuto A, et al. Mechanistic Role of Heat Shock Protein 70 in Bcr-Abl-Mediated Resistance to Apoptosis in Human Acute Leukemia Cells. *Blood* (2005) 105(3):1246–55. doi: 10.1182/blood-2004-05-2041
55. Zhuang H, Jiang W, Zhang X, Qiu F, Gan Z, Cheng W, et al. Suppression of HSP70 Expression Sensitizes NSCLC Cell Lines to TRAIL-Induced Apoptosis by Upregulating DR4 and DR5 and Downregulating C-FLIP-L Expressions. *J Mol Med (Berlin Germany)* (2013) 91(2):219–35. doi: 10.1007/s00109-012-0947-3
56. Park H-S, Cho S-G, Kim CK, Hwang HS, Noh KT, Kim M-S, et al. Heat Shock Protein Hsp72 Is a Negative Regulator of Apoptosis Signal-Regulating Kinase 1. *Mol Cell Biol* (2002) 22(22):7721–30. doi: 10.1128/MCB.22.22.7721-7730.2002
57. Gabai VL, Yaglom JA, Waldman T, Sherman MY. Heat Shock Protein Hsp72 Controls Oncogene-Induced Senescence Pathways in Cancer Cells. *Mol Cell Biol* (2009) 29(2):559–69. doi: 10.1128/MCB.01041-08
58. Meng L, Hunt C, Yaglom JA, Gabai VL, Sherman MY. Heat Shock Protein Hsp72 Plays an Essential Role in Her2-Induced Mammary Tumorigenesis. *Oncogene* (2011) 30(25):2836–45. doi: 10.1038/onc.2011.5
59. Albakova Z, Armeev GA, Kanevskiy LM, Kovalenko EI, Sapozhnikov AM. HSP70 Multi-Functionality in Cancer. *Cells* (2020) 9(3):587. doi: 10.3390/cells9030587
60. Moradi-Marjaneh R, Paseban M, Marjaneh MM. Hsp70 Inhibitors: Implications for the Treatment of Colorectal Cancer. *IUBMB Life* (2019) 71:1834–45. doi: 10.1002/iub.2157
61. Goloudina AR, Demidov ON, Garrido C. Inhibition of HSP70: A Challenging Anti-Cancer Strategy. *Cancer Lett [Internet]* (2012) 325 (2):117–24. doi: 10.1016/j.canlet.2012.06.003
62. Li X, Srinivasan SR, Connarn J, Ahmad A, Young ZT, Kabza AM, et al. Analogs of the Allosteric Heat Shock Protein 70 (Hsp70) Inhibitor, MKT-077, as Anti-Cancer Agents. *ACS Medicinal Chem Lett* (2013) 4(11):1042–7. doi: 10.1021/ml400204n
63. Davis AL, Cabello CM, Qiao S, Azimian S, Wondrak GT. Phenotypic Identification of the Redox Dye Methylene Blue as an Antagonist of Heat Shock Response Gene Expression in Metastatic Melanoma Cells. *Int J Mol Sci* (2013) 14(2):4185–202. doi: 10.3390/ijms14024185
64. Qiu X-B, Shao Y-M, Miao S, Wang L. The Diversity of the DnaJ/Hsp40 Family, the Crucial Partners for Hsp70 Chaperones. *Cell Mol Life Sci* (2006) 63(22):2560–70. doi: 10.1007/s00018-006-6192-6
65. Fan C-Y, Lee S, Ren H-Y, Cyr DM. Exchangeable Chaperone Modules Contribute to Specification of Type I and Type II Hsp40 Cellular Function. *Mol Biol Cell* (2004) 15(2):761–73. doi: 10.1091/mbc.e03-03-0146
66. Cheetham ME, Caplan AJ. Structure, Function and Evolution of DnaJ: Conservation and Adaptation of Chaperone Function. *Cell Stress Chaperones* (1998) 3(1):28–36. doi: 10.1379/1466-1268(1998)003<0028:SFAEOD>2.3.CO;2
67. Tsai M-F, Wang C-C, Chen JJ. Tumour Suppressor HLJ1: A Potential Diagnostic, Preventive and Therapeutic Target in Non-Small Cell Lung Cancer. *World J Clin Oncol* (2014) 5(5):865–73. doi: 10.5306/wjco.v5.i5.865
68. Lin S-Y, Hsueh C-M, Yu S-L, Su C-C, Shum W-Y, Yeh K-C, et al. HLJ1 Is a Novel Caspase-3 Substrate and its Expression Enhances UV-Induced

Apoptosis in non-Small Cell Lung Carcinoma. *Nucleic Acids Res* (2010) 38 (18):6148–58. doi: 10.1093/nar/gkq412
69. Chen H-W, Lee J-Y, Huang J-Y, Wang C-C, Chen W-J, Su S-F, et al. Curcumin Inhibits Lung Cancer Cell Invasion and Metastasis Through the Tumor Suppressor HLJ1. *Cancer Res* (2008) 68(18):7428–38. doi: 10.1158/0008-5472.CAN-07-6734
70. Tsai M-F, Wang C-C, Chang G-C, Chen C-Y, Chen H-Y, Cheng C-L, et al. A New Tumor Suppressor DnaJ-Like Heat Shock Protein, HLJ1, and Survival of Patients With Non–Small-Cell Lung Carcinoma. *JNCI: J Natl Cancer Institute* (2006) 98(12):825–38. doi: 10.1093/jnci/djj229
71. Wang C-C, Tsai M-F, Hong T-M, Chang G-C, Chen C-Y, Yang W-M, et al. The Transcriptional Factor YY1 Upregulates the Novel Invasion Suppressor HLJ1 Expression and Inhibits Cancer Cell Invasion. *Oncogene* (2005) 24 (25):4081–93. doi: 10.1038/sj.onc.1208573
72. Acun T, Doberstein N, Habermann JK, Gemoll T, Thorns C, Oztas E, et al. HLJ1 (DNAJB4) Gene Is a Novel Biomarker Candidate in Breast Cancer. *Omics* (2017) 21(5):257–65. doi: 10.1089/omi.2017.0016
73. Chen C-H, Chang W-H, Su K-Y, Ku W-H, Chang G-C, Hong Q-S, et al. HLJ1 is an Endogenous Src Inhibitor Suppressing Cancer Progression Through Dual Mechanisms. *Oncogene* (2016) 35(43):5674–85. doi: 10.1038/onc.2016.106
74. Schwanhäusser B, Busse D, Li N, Dittmar G, Schuchhardt J, Wolf J, et al. Global Quantification of Mammalian Gene Expression Control. *Nature* (2011) 473(7347):337–42. doi: 10.1038/nature10098
75. Kosti I, Jain N, Aran D, Butte AJ, Sirota M. Cross-Tissue Analysis of Gene and Protein Expression in Normal and Cancer Tissues. *Sci Rep* (2016) 6:24799. doi: 10.1038/srep24799
76. Okamoto T, Ishida R, Yamamoto H, Tanabe-Ishida M, Haga A, Takahashi H, et al. Functional Structure and Physiological Functions of Mammalian Wild-Type HSP60. *Arch Biochem Biophys* (2015) 586:10–9. doi: 10.1016/j.abb.2015.09.022
77. Pace A, Barone G, Lauria A, Martorana A, Piccionello AP, Pierro P, et al. Hsp60, a Novel Target for Antitumor Therapy: Structure-Function Features and Prospective Drugs Design. *Curr Pharm Design* (2013) 19(15):2757–64. doi: 10.2174/1381612811319150011
78. Merendino AM, Bucchieri F, Campanella C, Marcianò V, Ribbene A, David S, et al. Hsp60 is Actively Secreted by Human Tumor Cells. *PLoS One* (2010) 5(2):e9247. doi: 10.1371/journal.pone.0009247
79. Cappello F, Conway de Macario E, Marasà L, Zummo G, Macario AJL. Hsp60 Expression, New Locations, Functions and Perspectives for Cancer Diagnosis and Therapy. *Cancer Biol Ther* (2008) 7(6):801–9. doi: 10.4161/cbt.7.6.6281
80. Quintana FJ, Cohen IR. The HSP60 Immune System Network. *Trends Immunol* (2011) 32(2):89–95. doi: 10.1016/j.it.2010.11.001
81. Cohen-Sfady M, Nussbaum G, Pevsner-Fischer M, Mor F, Carmi P, Zanin-Zhorov A, et al. Heat Shock Protein 60 Activates B Cells *via* the TLR4-MyD88 Pathway. *J Immunol (Baltimore Md: 1950)* (2005) 175(6):3594–602. doi: 10.4049/jimmunol.175.6.3594
82. Li S, Ma W, Fei T, Lou Q, Zhang Y, Cui X, et al. Upregulation of Heat Shock Factor 1 Transcription Activity is Associated With Hepatocellular Carcinoma Progression. *Mol Med Rep* (2014) 10(5):2313–21. doi: 10.3892/mmr.2014.2547
83. Castilla C, Congregado B, Conde JM, Medina R, Torrubia FJ, Japón MA, et al. Immunohistochemical Expression of Hsp60 Correlates With Tumor Progression and Hormone Resistance in Prostate Cancer. *Urology* (2010) 76 (4):1017. doi: 10.1016/j.urology.2010.05.045
84. Li X, Xu Q, Fu X, Luo W. Heat Shock Protein 60 Overexpression is Associated With the Progression and Prognosis in Gastric Cancer. *PLoS One* (2014) 9(9):e107507. doi: 10.1371/journal.pone.0107507
85. Lebret T, Watson RWG, Molinié V, O'Neill A, Gabriel C, Fitzpatrick JM, et al. Heat Shock Proteins HSP27, HSP60, HSP70, and HSP90. *Cancer* (2003) 98(5):970–7. doi: 10.1002/cncr.11594
86. Guo J, Li X, Zhang W, Chen Y, Zhu S, Chen L, et al. HSP60-Regulated Mitochondrial Proteostasis and Protein Translation Promote Tumor Growth of Ovarian Cancer. *Sci Rep* (2019) 9(1):12628. doi: 10.1038/s41598-019-48992-7
87. Zhou C, Sun H, Zheng C, Gao J, Fu Q, Hu N, et al. Oncogenic HSP60 Regulates Mitochondrial Oxidative Phosphorylation to Support Erk1/2 Activation During Pancreatic Cancer Cell Growth. *Cell Death Dis* (2018) 9 (2):161. doi: 10.1038/s41419-017-0196-z
88. Kim W, Ryu J, Kim J-E. CCAR2/DBC1 and Hsp60 Positively Regulate Expression of Survivin in Neuroblastoma Cells. *Int J Mol Sci* (2019) 20 (1):131. doi: 10.3390/ijms20010131
89. Hua Shu J, Tadashi Y, Takashi O, Keita K, Rie Y, Yi Xuan L, et al. Expression of Heat Shock Protein 60 in Normal and Neoplastic Human Lymphoid Tissues. *J Clin Exp Hematopathol* (2002) 42(1):25–32. doi: 10.3960/jslrt.42.25
90. Hamelin C, Cornut E, Poirier F, Pons S, Beaulieu C, Charrier J-P, et al. Identification and Verification of Heat Shock Protein 60 as a Potential Serum Marker for Colorectal Cancer. *FEBS J* (2011) 278(24):4845–59. doi: 10.1111/j.1742-4658.2011.08385.x
91. Tsai Y-P, Teng S-C, Wu K-J. Direct Regulation of HSP60 Expression by C-MYC Induces Transformation. *FEBS Lett* (2008) 582(29):4083–8. doi: 10.1016/j.febslet.2008.11.004
92. Chun JN, Choi B, Lee KW, Lee DJ, Kang DH, Lee JY, et al. Cytosolic Hsp60 is Involved in the NF-kappaB-Dependent Survival of Cancer Cells *via* IKK Regulation. *PLoS One* (2010) 5(3):e9422. doi: 10.1371/journal.pone.0009422
93. Kumar S, O'Malley J, Chaudhary AK, Inigo JR, Yadav N, Kumar R, et al. Hsp60 and IL-8 Axis Promotes Apoptosis Resistance in Cancer. *Br J Cancer* (2019) 121(11):934–43. doi: 10.1038/s41416-019-0617-0
94. Ghosh JC, Dohi T, Kang BH, Altieri DC. Hsp60 Regulation of Tumor Cell Apoptosis. *J Biol Chem* (2008) 283(8):5188–94. doi: 10.1074/jbc.M705904200
95. Marino Gammazza A, Campanella C, Barone R, Caruso Bavisotto C, Gorska M, Wozniak M, et al. Doxorubicin Anti-Tumor Mechanisms Include Hsp60 Post-Translational Modifications Leading to the Hsp60/p53 Complex Dissociation and Instauration of Replicative Senescence. *Cancer Lett* (2017) 385:75–86. doi: 10.1016/j.canlet.2016.10.045
96. Chandra D, Choy G, Tang DG. Cytosolic Accumulation of HSP60 During Apoptosis With or Without Apparent Mitochondrial Release: Evidence That its Pro-Apoptotic or Pro-Survival Functions Involve Differential Interactions With Caspase-3. *J Biol Chem* (2007) 282(43):31289–301. doi: 10.1074/jbc.M702777200
97. Tang H, Li J, Liu X, Wang G, Luo M, Deng H. Down-Regulation of HSP60 Suppresses the Proliferation of Glioblastoma Cells *via* the ROS/AMPK/mTOR Pathway. *Sci Rep* (2016) 6:28388. doi: 10.1038/srep28388
98. Tsai Y-P, Yang M-H, Huang C-H, Chang S-Y, Chen P-M, Liu C-J, et al. Interaction Between HSP60 and Beta-Catenin Promotes Metastasis. *Carcinogenesis* (2009) 30(6):1049–57. doi: 10.1093/carcin/bgp087
99. Barazi HO, Zhou L, Templeton NS, Krutzsch HC, Roberts DD. Identification of Heat Shock Protein 60 as a Molecular Mediator of Alpha 3 Beta 1 Integrin Activation. *Cancer Res* (2002) 62(5):1541–8.
100. Tang H, Chen Y, Liu X, Wang S, Lv Y, Wu D, et al. Downregulation of HSP60 Disrupts Mitochondrial Proteostasis to Promote Tumorigenesis and Progression in Clear Cell Renal Cell Carcinoma. *Oncotarget* (2016) 7 (25):38822–34. doi: 10.18632/oncotarget.9615
101. Rappa F, Pitruzzella A, Marino Gammazza A, Barone R, Mocciaro E, Tomasello G, et al. Quantitative Patterns of Hsps in Tubular Adenoma Compared With Normal and Tumor Tissues Reveal the Value of Hsp10 and Hsp60 in Early Diagnosis of Large Bowel Cancer. *Cell Stress Chaperones* (2016) 21(5):927–33. doi: 10.1007/s12192-016-0721-5
102. Vocka M, Langer D, Fryba V, Petrtyl J, Hanus T, Kalousova M, et al. Novel Serum Markers HSP60, CHI3L1, and IGFBP-2 in Metastatic Colorectal Cancer. *Oncol Lett* (2019) 18(6):6284–92. doi: 10.3892/ol.2019.10925
103. Zhang J, Zhou X, Chang H, Huang X, Guo X, Du X, et al. Hsp60 Exerts a Tumor Suppressor Function by Inducing Cell Differentiation and Inhibiting Invasion in Hepatocellular Carcinoma. *Oncotarget* (2016) 7(42):68976–89. doi: 10.18632/oncotarget.12185
104. Nakamura H, Minegishi H. HSP60 as a Drug Target. *Curr Pharm Design* (2013) 19(3):441–51. doi: 10.2174/138161213804143626
105. Xu X, Wang W, Shao W, Yin W, Chen H, Qiu Y, et al. Heat Shock Protein-60 Expression was Significantly Correlated With the Prognosis of Lung Adenocarcinoma. *J Surg Oncol* (2011) 104(6):598–603. doi: 10.1002/jso.21992
106. Ağababaoğlu İ, Önen A, Demir AB, Aktaş S, Altun Z, Ersöz H, et al. Chaperonin (HSP60) and Annexin-2 are Candidate Biomarkers for non-

Small Cell Lung Carcinoma. *Medicine* (2017) 96(6):e5903. doi: 10.1097/MD.0000000000005903
107. Desmetz C, Bibeau F, Boissière F, Bellet V, Rouanet P, Maudelonde T, et al. Proteomics-Based Identification of HSP60 as a Tumor-Associated Antigen in Early Stage Breast Cancer and Ductal Carcinoma in Situ. *J Proteome Res* (2008) 7(9):3830–7. doi: 10.1021/pr800130d
108. Trieb K, Gerth R, Windhager R, Grohs JG, Holzer G, Berger P, et al. Serum Antibodies Against the Heat Shock Protein 60 are Elevated in Patients With Osteosarcoma. *Immunobiology* (2000) 201(3–4):368–76. doi: 10.1016/S0171-2985(00)80091-1
109. Itoh H, Komatsuda A, Wakui H, Miura AB, Tashima Y. Mammalian HSP60 is a Major Target for an Immunosuppressant Mizoribine. *J Biol Chem* (1999) 274(49):35147–51. doi: 10.1074/jbc.274.49.35147
110. Tanabe M, Ishida R, Izuhara F, Komatsuda A, Wakui H, Sawada K, et al. The ATPase Activity of Molecular Chaperone HSP60 is Inhibited by Immunosuppressant Mizoribine. *Am J Mol Biol* (2012) 2:93–102. doi: 10.4236/ajmb.2012.22010
111. Nagumo Y, Kakeya H, Shoji M, Hayashi Y, Dohmae N, Osada H. Epolactaene Binds Human Hsp60 Cys442 Resulting in the Inhibition of Chaperone Activity. *Biochem J* (2005) 387(Pt 3):835–40. doi: 10.1042/BJ20041355
112. Izgi K, Iskender B, Jauch J, Sezen S, Cakir M, Charpentier M, et al. Myrtucommulone-A Induces Both Extrinsic and Intrinsic Apoptotic Pathways in Cancer Cells. *J Biochem Mol Toxicol* (2015) 29(9):432–9. doi: 10.1002/jbt.21716
113. Wiechmann K, Müller H, König S, Wielsch N, Svatoš A, Jauch J, et al. Mitochondrial Chaperonin HSP60 Is the Apoptosis-Related Target for Myrtucommulone. *Cell Chem Biol* (2017) 24(5):614–23. doi: 10.1016/j.chembiol.2017.04.008
114. Ban HS, Shimizu K, Minegishi H, Nakamura H. Identification of HSP60 as a Primary Target of O-Carboranylphenoxyacetanilide, an HIF-1alpha Inhibitor. *J Am Chem Society* (2010) 132(34):11870–1. doi: 10.1021/ja104739t
115. Meng Q, Li BX, Xiao X. Toward Developing Chemical Modulators of Hsp60 as Potential Therapeutics. *Front Mol Biosci* (2018) 5:35. doi: 10.3389/fmolb.2018.00035
116. Zoubeidi A, Gleave M. Small Heat Shock Proteins in Cancer Therapy and Prognosis. *Int J Biochem Cell Biol* (2012) 44(10):1646–56. doi: 10.1016/j.biocel.2012.04.010
117. Carra S, Alberti S, Arrigo PA, Benesch JL, Benjamin IJ, Boelens W, et al. The Growing World of Small Heat Shock Proteins: From Structure to Functions. *Cell Stress Chaperones* (2017) 22(4):601–11. doi: 10.1007/s12192-017-0787-8
118. Haslbeck M, Vierling E. A First Line of Stress Defense: Small Heat Shock Proteins and Their Function in Protein Homeostasis. *J Mol Biol* (2015) 427(7):1537–48. doi: 10.1016/j.jmb.2015.02.002
119. Kostenko S, Moens U. Heat Shock Protein 27 Phosphorylation: Kinases, Phosphatases, Functions and Pathology. *Cell Mol Life Sci* (2009) 66(20):3289–307. doi: 10.1007/s00018-009-0086-3
120. Yu Z, Zhi J, Peng X, Zhong X, Xu A. Clinical Significance of HSP27 Expression in Colorectal Cancer. *Mol Med Rep* (2010) 3(6):953–8. doi: 10.3892/mmr.2010.372
121. Spigel DR, Shipley DL, Waterhouse DM, Jones SF, Ward PJ, Shih KC, et al. A Randomized, Double-Blinded, Phase II Trial of Carboplatin and Pemetrexed With or Without Apatorsen (OGX-427) in Patients With Previously Untreated Stage IV Non-Squamous-Non-Small-Cell Lung Cancer: The SPRUCE Trial. *Oncol* (2019) 24(12):e1409–16. doi: 10.1634/theoncologist.2018-0518
122. Ko AH, Murphy PB, Peyton JD, Shipley DL, Al-Hazzouri A, Rodriguez FA, et al. A Randomized, Double-Blinded, Phase II Trial of Gemcitabine and Nab-Paclitaxel Plus Apatorsen or Placebo in Patients With Metastatic Pancreatic Cancer: The RAINIER Trial. *Oncol* (2017) 22(12):1427–e129. doi: 10.1634/theoncologist.2017-0066
123. Bellmunt J, Eigl BJ, Senkus E, Loriot Y, Twardowski P, Castellano D, et al. Borealis-1: A Randomized, First-Line, Placebo-Controlled, Phase II Study Evaluating Apatorsen and Chemotherapy for Patients With Advanced Urothelial Cancer. *Ann Oncol* (2017) 28(10):2481–8. doi: 10.1093/annonc/mdx400
124. Rosenberg JE, Hahn NM, Regan MM, Werner L, Alva A, George S, et al. Apatorsen Plus Docetaxel Versus Docetaxel Alone in Platinum-Resistant Metastatic Urothelial Carcinoma (Borealis-2). *Br J Cancer* (2018) 118(11):1434–41. doi: 10.1038/s41416-018-0087-9
125. Pirkkala L, Nykanen P, Sistonen L. Roles of the Heat Shock Transcription Factors in Regulation of the Heat Shock Response and Beyond. *FASEB J* (2001) 15(7):1118–31. doi: 10.1096/fj00-0294rev
126. Li J, Labbadia J, Morimoto RI. Rethinking HSF1 in Stress, Development, and Organismal Health. *Trends Cell Biol* (2017) 27(12):895–905. doi: 10.1016/j.tcb.2017.08.002
127. Guo Y, Guettouche T, Fenna M, Boellmann F, Pratt WB, Toft DO, et al. Evidence for a Mechanism of Repression of Heat Shock Factor 1 Transcriptional Activity by a Multichaperone Complex. *J Biol Chem* (2001) 276(49):45791–9. doi: 10.1074/jbc.M105931200
128. Anckar J, Sistonen L. Regulation of HSF1 Function in the Heat Stress Response: Implications in Aging and Disease. *Annu Rev Biochem* (2011) 80(1):1089–115. doi: 10.1146/annurev-biochem-060809-095203
129. Hentze N, Le Breton L, Wiesner J, Kempf G, Mayer MP. Molecular Mechanism of Thermosensory Function of Human Heat Shock Transcription Factor Hsf1. *eLife* (2016) 5:e11576. doi: 10.7554/eLife.11576.017
130. Ahn SG, Liu PC, Klyachko K, Morimoto RI, Thiele DJ. The Loop Domain of Heat Shock Transcription Factor 1 Dictates DNA-Binding Specificity and Responses to Heat Stress. *Genes Dev* (2001) 15(16):2134–45. doi: 10.1101/gad.894801
131. Shamovsky I, Ivannikov M, Kandel ES, Gershon D, Nudler E. RNA-Mediated Response to Heat Shock in Mammalian Cells. *Nature* (2006) 440(7083):556–60. doi: 10.1038/nature04518
132. Jaeger AM, Makley LN, Gestwicki JE, Thiele DJ. Genomic Heat Shock Element Sequences Drive Cooperative Human Heat Shock Factor 1 DNA Binding and Selectivity*. *J Biol Chem* (2014) 289(44):30459–69. doi: 10.1074/jbc.M114.591578
133. Mahat DB, Salamanca HH, Duarte FM, Danko CG, Lis JT. Mammalian Heat Shock Response and Mechanisms Underlying Its Genome-Wide Transcriptional Regulation. *Mol Cell* (2016) 62(1):63–78. doi: 10.1016/j.molcel.2016.02.025
134. Elsing AN, Aspelin C, Bjork JK, Bergman HA, Himanen SV, Kallio MJ, et al. Expression of HSF2 Decreases in Mitosis to Enable Stress-Inducible Transcription and Cell Survival. *J Cell Biol* (2014) 206(6):735–49. doi: 10.1083/jcb.201402002
135. Neueder A, Gipson TA, Batterton S, Lazell HJ, Farshim PP, Paganetti P, et al. HSF1-Dependent and -Independent Regulation of the Mammalian *In Vivo* Heat Shock Response and its Impairment in Huntington's Disease Mouse Models. *Sci Rep* (2017) 7(1):12556. doi: 10.1038/s41598-017-12897-0
136. Duarte FM, Fuda NJ, Mahat DB, Core LJ, Guertin MJ, Lis JT. Transcription Factors GAF and HSF Act at Distinct Regulatory Steps to Modulate Stress-Induced Gene Activation. *Genes Dev* (2016) 30(15):1731–46. doi: 10.1101/gad.284430.116
137. Neueder A, Achilli F, Moussaoui S, Bates GP. Novel Isoforms of Heat Shock Transcription Factor 1, HSF1γα and HSF1γβ, Regulate Chaperone Protein Gene Transcription. *J Biol Chem* (2014) 289(29):19894–906. doi: 10.1074/jbc.M114.570739
138. Su K-H, Cao J, Tang Z, Dai S, He Y, Sampson SB, et al. HSF1 Critically Attunes Proteotoxic Stress Sensing by Mtorc1 to Combat Stress and Promote Growth. *Nat Cell Biol* (2016) 18(5):527–39. doi: 10.1038/ncb3335
139. Kmiecik SW, Le Breton L, Mayer MP. Feedback Regulation of Heat Shock Factor 1 (Hsf1) Activity by Hsp70-Mediated Trimer Unzipping and Dissociation From DNA. *EMBO J* (2020) 39(14):e104096. doi: 10.15252/embj.2019104096
140. Ding XZ, Tsokos GC, Kiang JG. Overexpression of HSP-70 Inhibits the Phosphorylation of HSF1 by Activating Protein Phosphatase and Inhibiting Protein Kinase C Activity. *FASEB J* (1998) 12(6):451–9. doi: 10.1096/fasebj.12.6.451
141. Dayalan Naidu S, Sutherland C, Zhang Y, Risco A, de la Vega L, Caunt CJ, et al. Heat Shock Factor 1 Is a Substrate for P38 Mitogen-Activated Protein Kinases. *Mol Cell Biol* (2016) 36(18):2403–17. doi: 10.1128/MCB.00292-16
142. Xu Y-M, Huang D-Y, Chiu J-F, Lau ATY. Post-Translational Modification of Human Heat Shock Factors and Their Functions: A Recent Update by Proteomic Approach. *J Proteome Res* (2012) 11(5):2625–34. doi: 10.1021/pr201151a
143. Soncin F, Zhang X, Chu B, Wang X, Asea A, Ann Stevenson M, et al. Transcriptional Activity and DNA Binding of Heat Shock Factor-1 Involve

Phosphorylation on Threonine 142 by CK2. *Biochem Biophys Res Commun* (2003) 303(2):700–6. doi: 10.1016/S0006-291X(03)00398-X
144. Guettouche T, Boellmann F, Lane WS, Voellmy R. Analysis of Phosphorylation of Human Heat Shock Factor 1 in Cells Experiencing a Stress. *BMC Biochem* (2005) 6:4. doi: 10.1186/1471-2091-6-4
145. Murshid A, Chou S-D, Prince T, Zhang Y, Bharti A, Calderwood SK. Protein Kinase A Binds and Activates Heat Shock Factor 1. *PLoS One* (2010) 5(11):1–13. doi: 10.1371/annotation/5879464d-8556-4c3e-b11c-a96cbbff44a6
146. Lu WC, Omari R, Ray H, Wang J, Williams I, Jacobs C, et al. AKT1 Mediates Multiple Phosphorylation Events That Functionally Promote HSF1 Activation. *FEBS J* (2022). doi: 10.1111/febs.16375
147. Dai S, Tang Z, Cao J, Zhou W, Li H, Sampson S, et al. Suppression of the HSF1-Mediated Proteotoxic Stress Response by the Metabolic Stress Sensor AMPK. *EMBO J* (2015) 34(3):275–93. doi: 10.15252/embj.201489062
148. Kim S-A, Yoon J-H, Lee S-H, Ahn S-G. Polo-Like Kinase 1 Phosphorylates Heat Shock Transcription Factor 1 and Mediates Its Nuclear Translocation During Heat Stress*. *J Biol Chem* (2005) 280(13):12653–7. doi: 10.1074/jbc.M411908200
149. Lee Y-J, Kim E-H, Lee JS, Jeoung D, Bae S, Kwon SH, et al. HSF1 as a Mitotic Regulator: Phosphorylation of HSF1 by Plk1 Is Essential for Mitotic Progression. *Cancer Res* (2008) 68(18):7550–60. doi: 10.1158/0008-5472.CAN-08-0129
150. Budzyński MA, Puustinen MC, Joutsen J, Sistonen L. Uncoupling Stress-Inducible Phosphorylation of Heat Shock Factor 1 From Its Activation. *Mol Cell Biol* (2015) 35(14):2530–40. doi: 10.1128/MCB.00816-14
151. Krakowiak J, Zheng X, Patel N, Feder ZA, Anandhakumar J, Valerius K, et al. Hsf1 and Hsp70 Constitute a Two-Component Feedback Loop That Regulates the Yeast Heat Shock Response. *eLife* (2018) 7:e31668. doi: 10.7554/eLife.31668
152. Zheng X, Krakowiak J, Patel N, Beyzavi A, Ezike J, Khalil AS, et al. Dynamic Control of Hsf1 During Heat Shock by a Chaperone Switch and Phosphorylation. *eLife* (2016) 5:e18638. doi: 10.7554/eLife.18638
153. Raychaudhuri S, Loew C, Körner R, Pinkert S, Theis M, Hayer-Hartl M, et al. Interplay of Acetyltransferase EP300 and the Proteasome System in Regulating Heat Shock Transcription Factor 1. *Cell* (2014) 156(5):975–85. doi: 10.1016/j.cell.2014.01.055
154. Westerheide SD, Anckar J, Stevens SMJ, Sistonen L, Morimoto RI. Stress-Inducible Regulation of Heat Shock Factor 1 by the Deacetylase SIRT1. *Sci (New York NY)* (2009) 323(5917):1063–6. doi: 10.1126/science.1165946
155. Raynes R, Pombier KM, Nguyen K, Brunquell J, Mendez JE, Westerheide SD. The SIRT1 Modulators AROS and DBC1 Regulate HSF1 Activity and the Heat Shock Response. *PLoS One* (2013) 8(1):e54364. doi: 10.1371/journal.pone.0054364
156. Geng H, Liu Q, Xue C, David LL, Beer TM, Thomas GV, et al. Hif1α Protein Stability Is Increased by Acetylation at Lysine 709*. *J Biol Chem* (2012) 287 (42):35496–505. doi: 10.1074/jbc.M112.400697
157. Laemmle A, Lechleiter A, Roh V, Schwarz C, Portmann S, Furer C, et al. Inhibition of SIRT1 Impairs the Accumulation and Transcriptional Activity of HIF-1α Protein Under Hypoxic Conditions. *PLoS One* (2012) 7(3):1–12. doi: 10.1371/journal.pone.0033433
158. Zelin E, Freeman BC. Lysine Deacetylases Regulate the Heat Shock Response Including the Age-Associated Impairment of HSF1. *J Mol Biol* (2015) 427 (7):1644–54. doi: 10.1016/j.jmb.2015.02.010
159. Ceccacci E, Minucci S. Inhibition of Histone Deacetylases in Cancer Therapy: Lessons From Leukaemia. *Br J Cancer* (2016) 114(6):605–11. doi: 10.1038/bjc.2016.36
160. Kmiecik SW, Drzewicka K, Melchior F, Mayer MP. Heat Shock Transcription Factor 1 is SUMOylated in the Activated Trimeric State. *J Biol Chem* (2021) 296:100324. doi: 10.1016/j.jbc.2021.100324
161. Brunet Simioni M, de Thonel A, Hammann A, Joly AL, Bossis G, Fourmaux E, et al. Heat Shock Protein 27 is Involved in SUMO-2/3 Modification of Heat Shock Factor 1 and Thereby Modulates the Transcription Factor Activity. *Oncogene* (2009) 28(37):3332–44. doi: 10.1038/onc.2009.188
162. Anckar J, Hietakangas V, Denessiouk K, Thiele DJ, Johnson MS, Sistonen L. Inhibition of DNA Binding by Differential Sumoylation of Heat Shock Factors. *Mol Cell Biol* (2006) 26(3):955–64. doi: 10.1128/MCB.26.3.955-964.2006
163. Lecomte S, Reverdy L, le Quément C, le Masson F, Amon A, le Goff P, et al. Unraveling Complex Interplay Between Heat Shock Factor 1 and 2 Splicing Isoforms. *PLoS One* (2013) 8(2):e56085. doi: 10.1371/journal.pone.0056085
164. Barna J, Csermely P, Vellai T. Roles of Heat Shock Factor 1 Beyond the Heat Shock Response. *Cell Mol Life Sci* (2018) 75(16):2897–916. doi: 10.1007/s00018-018-2836-6
165. Cerami E, Gao J, Dogrusoz U, Gross BE, Sumer SO, Aksoy BA, et al. The Cbio Cancer Genomics Portal: An Open Platform for Exploring Multidimensional Cancer Genomics Data. *Cancer Discovery* (2012) 2 (5):401. doi: 10.1158/2159-8290.CD-12-0095
166. Gao J, Aksoy BA, Dogrusoz U, Dresdner G, Gross B, Sumer SO, et al. Integrative Analysis of Complex Cancer Genomics and Clinical Profiles Using the Cbioportal. *Sci Signaling* (2013) 6(269):pl1–1. doi: 10.1126/scisignal.2004088
167. Wan T, Shao J, Hu B, Liu G, Luo P, Zhou Y. Prognostic Role of HSF1 Overexpression in Solid Tumors: A Pooled Analysis of 3,159 Patients. *OncoTargets Ther* (2018) 11:383–93. doi: 10.2147/OTT.S153682
168. Mendillo ML, Santagata S, Koeva M, Bell GW, Hu R, Tamimi RM, et al. HSF1 Drives a Transcriptional Program Distinct From Heat Shock to Support Highly Malignant Human Cancers. *Cell* (2012) 150(3):549–62. doi: 10.1016/j.cell.2012.06.031
169. Wang Q, Zhang Y-C, Zhu L-F, Pan L, Yu M, Shen W-L, et al. Heat Shock Factor 1 in Cancer-Associated Fibroblasts is a Potential Prognostic Factor and Drives Progression of Oral Squamous Cell Carcinoma. *Cancer Sci* (2019) 110(5):1790–803. doi: 10.1111/cas.13991
170. Dai W, Ye J, Zhang Z, Yang L, Ren H, Wu H, et al. Increased Expression of Heat Shock Factor 1 (HSF1) is Associated With Poor Survival in Gastric Cancer Patients. *Diagn Pathol* (2018) 13(1):80. doi: 10.1186/s13000-018-0755-3
171. Tsukao Y, Yamasaki M, Miyazaki Y, Makino T, Takahashi T, Kurokawa Y, et al. Overexpression of Heat-Shock Factor 1 is Associated With a Poor Prognosis in Esophageal Squamous Cell Carcinoma. *Oncol Lett* (2017) 13 (3):1819–25. doi: 10.3892/ol.2017.5637
172. Salnikow K, Zhitkovich A. Genetic and Epigenetic Mechanisms in Metal Carcinogenesis and Cocarcinogenesis: Nickel, Arsenic, and Chromium. *Chem Res Toxicol* (2008) 21(1):28–44. doi: 10.1021/tx700198a
173. Ortega-Atienza S, Rubis B, McCarthy C, Zhitkovich A. Formaldehyde Is a Potent Proteotoxic Stressor Causing Rapid Heat Shock Transcription Factor 1 Activation and Lys48-Linked Polyubiquitination of Proteins. *Am J Pathol* (2016) 186(11):2857–68. doi: 10.1016/j.ajpath.2016.06.022
174. Brusselaers N, Ekwall K, Durand-Dubief M. Copy Number of 8q24.3 Drives HSF1 Expression and Patient Outcome in Cancer: An Individual Patient Data Meta-Analysis. *Hum Genomics* (2019) 13(1):54. doi: 10.1186/s40246-019-0241-3
175. Zhang CQ, Williams H, Prince TL, Ho ES. Overexpressed HSF1 Cancer Signature Genes Cluster in Human Chromosome 8q. *Hum Genomics* (2017) 11(1):35. doi: 10.1186/s40246-017-0131-5
176. Gökmen-Polar Y, Badve S. Upregulation of HSF1 in Estrogen Receptor Positive Breast Cancer. *Oncotarget* (2016) 7(51):84239–45. doi: 10.18632/oncotarget.12438
177. Chen F, Fan Y, Cao P, Liu B, Hou J, Zhang B, et al. Pan-Cancer Analysis of the Prognostic and Immunological Role of HSF1: A Potential Target for Survival and Immunotherapy. *Oxid Med Cell Longevity* (2021) 2021:5551036. doi: 10.1155/2021/5551036
178. Santagata S, Hu R, Lin NU, Mendillo ML, Collins LC, Hankinson SE, et al. High Levels of Nuclear Heat-Shock Factor 1 (HSF1) are Associated With Poor Prognosis in Breast Cancer. *Proc Natl Acad Sci USA* (2011) 108 (45):18378–83. doi: 10.1073/pnas.1115031108
179. Vydra N, Janus P, Toma-Jonik A, Stokowy T, Mrowiec K, Korfanty J, et al. 17beta-Estradiol Activates HSF1 *via* MAPK Signaling in ERalpha-Positive Breast Cancer Cells. *Cancers* (2019) 11(10):1533. doi: 10.3390/cancers11101533
180. Khaleque MA, Bharti A, Gong J, Gray PJ, Sachdev V, Ciocca DR, et al. Heat Shock Factor 1 Represses Estrogen-Dependent Transcription Through Association With MTA1. *Oncogene* (2008) 27(13):1886–93. doi: 10.1038/sj.onc.1210834
181. Silveira MA, Tav C, Bérube-Simard F-A, Cuppens T, Leclercq M, Fournier É, et al. Modulating HSF1 Levels Impacts Expression of the Estrogen Receptor

α and Antiestrogen Response. *Life Sci Alliance* (2021) 4(5):e202000811. doi: 10.26508/lsa.202000811
182. Hoter A, Naim HY. Heat Shock Proteins and Ovarian Cancer: Important Roles and Therapeutic Opportunities. *Cancers* (2019) 11(9):1389. doi: 10.3390/cancers11091389
183. Meng L, Gabai VL, Sherman MY. Heat-Shock Transcription Factor HSF1 has a Critical Role in Human Epidermal Growth Factor Receptor-2-Induced Cellular Transformation and Tumorigenesis. *Oncogene* (2010) 29(37):5204–13. doi: 10.1038/onc.2010.277
184. Xi C, Hu Y, Buckhaults P, Moskophidis D, Mivechi NF. Heat Shock Factor Hsf1 Cooperates With ErbB2 (Her2/Neu) Protein to Promote Mammary Tumorigenesis and Metastasis. *J Biol Chem* (2012) 287(42):35646–57. doi: 10.1074/jbc.M112.377481
185. Schulz R, Streller F, Scheel AH, Ruschoff J, Reinert M-C, Dobbelstein M, et al. HER2/ErbB2 Activates HSF1 and Thereby Controls HSP90 Clients Including MIF in HER2-Overexpressing Breast Cancer. *Cell Death Dis* (2014) 5:e980. doi: 10.1038/cddis.2013.508
186. Yallowitz A, Ghaleb A, Garcia L, Alexandrova EM, Marchenko N. Heat Shock Factor 1 Confers Resistance to Lapatinib in ERBB2-Positive Breast Cancer Cells. *Cell Death Dis* (2018) 9(6):621. doi: 10.1038/s41419-018-0691-x
187. Krzyzanowski PM, Sircoulomb F, Yousif F, Normand J, La Rose J, E Francis K, et al. Regional Perturbation of Gene Transcription is Associated With Intrachromosomal Rearrangements and Gene Fusion Transcripts in High Grade Ovarian Cancer. *Sci Rep* (2019) 9(1):3590. doi: 10.1038/s41598-019-39878-9
188. Coetzee SG, Shen HC, Hazelett DJ, Lawrenson K, Kuchenbaecker K, Tyrer J, et al. Cell-Type-Specific Enrichment of Risk-Associated Regulatory Elements at Ovarian Cancer Susceptibility Loci. *Hum Mol Genet* (2015) 24(13):3595–607. doi: 10.1093/hmg/ddv101
189. Chen Y-F, Dong Z, Xia Y, Tang J, Peng L, Wang S, et al. Nucleoside Analog Inhibits microRNA-214 Through Targeting Heat-Shock Factor 1 in Human Epithelial Ovarian Cancer. *Cancer Sci* (2013) 104(12):1683–9. doi: 10.1111/cas.12277
190. Chen Y-F, Wang S-Y, Yang Y-H, Zheng J, Liu T, Wang L. Targeting HSF1 Leads to an Antitumor Effect in Human Epithelial Ovarian Cancer. *Int J Mol Med* (2017) 39(6):1564–70. doi: 10.3892/ijmm.2017.2978
191. Yasuda K, Hirohashi Y, Mariya T, Murai A, Tabuchi Y, Kuroda T, et al. Phosphorylation of HSF1 at Serine 326 Residue is Related to the Maintenance of Gynecologic Cancer Stem Cells Through Expression of HSP27. *Oncotarget* (2017) 8(19):31540–53. doi: 10.18632/oncotarget.16361
192. Powell CD, Paullin TR, Aoisa C, Menzie CJ, Ubaldini A, Westerheide SD. The Heat Shock Transcription Factor HSF1 Induces Ovarian Cancer Epithelial-Mesenchymal Transition in a 3D Spheroid Growth Model. *PLoS One* (2016) 11(12):e0168389. doi: 10.1371/journal.pone.0168389
193. Wilson AL, Moffitt LR, Duffield N, Rainczuk A, Jobling TW, Plebanski M, et al. Autoantibodies Against HSF1 and CCDC155 as Biomarkers of Early-Stage, High-Grade Serous Ovarian Cancer. *Cancer Epidemiol Prev Biomarkers* (2018) 27(2):183–92. doi: 10.1158/1055-9965.EPI-17-0752
194. Sieh W, Köbel M, Longacre TA, Bowtell DD, deFazio A, Goodman MT, et al. Hormone-Receptor Expression and Ovarian Cancer Survival: An Ovarian Tumor Tissue Analysis Consortium Study. *Lancet Oncol* (2013) 14(9):853–62. doi: 10.1016/S1470-2045(13)70253-5
195. Cui J, Tian H, Chen G. Upregulation of Nuclear Heat Shock Factor 1 Contributes to Tumor Angiogenesis and Poor Survival in Patients With Non-Small Cell Lung Cancer. *Ann Thorac Surgery* (2015) 100(2):465–72. doi: 10.1016/j.athoracsur.2015.03.021
196. Carter JD. *Heat Shock Transcription Factor 1 (HSF1) Is a Novel Supporter of NSCLC Anoikis Resistance Independent of Heat Shock Proteins*. Philadelphia: University of the Sciences in Philadelphia (2017).
197. Hoj JP, Mayro B, Pendergast AM. The ABL2 Kinase Regulates an HSF1-Dependent Transcriptional Program Required for Lung Adenocarcinoma Brain Metastasis. *Proc Natl Acad Sci USA* (2020) 117(52):33486–95. doi: 10.1073/pnas.2007991117
198. Scherz-Shouval R, Santagata S, Mendillo ML, Sholl LM, Ben-Aharon I, Beck AH, et al. The Reprogramming of Tumor Stroma by HSF1 Is a Potent Enabler of Malignancy. *Cell* (2014) 158(3):564–78. doi: 10.1016/j.cell.2014.05.045
199. Lee S, Jung J, Lee Y-J, Kim S-K, Kim J-A, Kim B-K, et al. Targeting HSF1 as a Therapeutic Strategy for Multiple Mechanisms of EGFR Inhibitor Resistance in EGFR Mutant Non-Small-Cell Lung Cancer. *Cancers* (2021) 13(12):2987. doi: 10.3390/cancers13122987
200. Yoon T, Kang G-Y, Han A-R, Seo E-K, Lee Y-S. 2,4-Bis(4-Hydroxybenzyl) Phenol Inhibits Heat Shock Transcription Factor 1 and Sensitizes Lung Cancer Cells to Conventional Anticancer Modalities. *J Natural Products* (2014) 77(5):1123–9. doi: 10.1021/np4009333
201. Cigliano A, Wang C, Pilo MG, Szydlowska M, Brozzetti S, Latte G, et al. Inhibition of HSF1 Suppresses the Growth of Hepatocarcinoma Cell Lines *In Vitro* and AKT-Driven Hepatocarcinogenesis in Mice. *Oncotarget* (2017) 8 (33):54149–59. doi: 10.18632/oncotarget.16927
202. Liu P, Ge M, Hu J, Li X, Che L, Sun K, et al. A Functional Mammalian Target of Rapamycin Complex 1 Signaling is Indispensable for C-Myc-Driven Hepatocarcinogenesis. *Hepatol (Baltimore Md)* (2017) 66(1):167–81. doi: 10.1002/hep.29183
203. Cigliano A, Pilo MG, Li L, Latte G, Szydlowska M, Simile MM, et al. Deregulated C-Myc Requires a Functional HSF1 for Experimental and Human Hepatocarcinogenesis. *Oncotarget* (2017) 8(53):90638–50. doi: 10.18632/oncotarget.21469
204. Cen H, Zheng S, Fang Y-M, Tang X-P, Dong Q. Induction of HSF1 Expression is Associated With Sporadic Colorectal Cancer. *World J Gastroenterol* (2004) 10(21):3122–6. doi: 10.3748/wjg.v10.i21.3122
205. Li J, Song P, Jiang T, Dai D, Wang H, Sun J, et al. Heat Shock Factor 1 Epigenetically Stimulates Glutaminase-1-Dependent mTOR Activation to Promote Colorectal Carcinogenesis. *Mol Therapy* (2018) 26(7):1828–39. doi: 10.1016/j.ymthe.2018.04.014
206. Levi-Galibov O, Lavon H, Wassermann-Dozorets R, Pevsner-Fischer M, Mayer S, Wershof E, et al. Heat Shock Factor 1-Dependent Extracellular Matrix Remodeling Mediates the Transition From Chronic Intestinal Inflammation to Colon Cancer. *Nat Commun* (2020) 11(1):6245. doi: 10.1038/s41467-020-20054-x
207. Kourtis N, Moubarak RS, Aranda-Orgilles B, Lui K, Aydin IT, Trimarchi T, et al. FBXW7 Modulates Cellular Stress Response and Metastatic Potential Through HSF1 Post-Translational Modification. *Nat Cell Biol* (2015) 17 (3):322–32. doi: 10.1038/ncb3121
208. Nakamura Y, Fujimoto M, Fukushima S, Nakamura A, Hayashida N, Takii R, et al. Heat Shock Factor 1 is Required for Migration and Invasion of Human Melanoma In Vitro and *In Vivo*. *Cancer Lett* (2014) 354(2):329–35. doi: 10.1016/j.canlet.2014.08.029
209. Daniels GA, Sanchez-Perez L, Diaz RM, Kottke T, Thompson J, Lai M, et al. A Simple Method to Cure Established Tumors by Inflammatory Killing of Normal Cells. *Nat Biotechnol* (2004) 22(9):1125–32. doi: 10.1038/nbt1007
210. Taha EA, Ono K, Eguchi T. Roles of Extracellular HSPs as Biomarkers in Immune Surveillance and Immune Evasion. *Int J Mol Sci* (2019) 20(18):4588. doi: 10.3390/ijms20184588
211. Haslam A, Prasad V. Estimation of the Percentage of US Patients With Cancer Who Are Eligible for and Respond to Checkpoint Inhibitor Immunotherapy Drugs. *JAMA Netw Open* (2019) 2(5):e192535. doi: 10.1001/jamanetworkopen.2019.2535
212. Seliger B. Basis of PD1/PD-L1 Therapies. *J Clin Med* (2019) 8(12):2168. doi: 10.3390/jcm8122168
213. Yang T, Ren C, Lu C, Qiao P, Han X, Wang L, et al. Phosphorylation of HSF1 by PIM2 Induces PD-L1 Expression and Promotes Tumor Growth in Breast Cancer. *Cancer Res* (2019) 79(20):5233–44. doi: 10.1158/0008-5472.CAN-19-0063
214. Chatterjee S, Chakraborty P, Daenthanasanmak A, Iamsawat S, Andrejeva G, Luevano LA, et al. Targeting PIM Kinase With PD1 Inhibition Improves Immunotherapeutic Antitumor T-Cell Response. *Clin Cancer Res* (2019) 25 (3):1036–49. doi: 10.1158/1078-0432.CCR-18-0706
215. Li H, Sui X, Wang Z, Fu H, Wang Z, Yuan M, et al. A New Antisarcoma Strategy: Multisubtype Heat Shock Protein/Peptide Immunotherapy Combined With PD-L1 Immunological Checkpoint Inhibitors. *Clin Trans Oncol* (2021) 23(8):1688–704. doi: 10.1007/s12094-021-02570-4
216. Jaeger AM, Stopfer L, Lee S, Gaglia G, Sandel D, Santagata S, et al. Rebalancing Protein Homeostasis Enhances Tumor Antigen Presentation. *Clin Cancer Res* (2019) 25(21):6392–405. doi: 10.1158/1078-0432.CCR-19-0596

217. Ibrahim EC, Morange M, Dausset J, Carosella ED, Paul P. Heat Shock and Arsenite Induce Expression of the Nonclassical Class I Histocompatibility HLA-G Gene in Tumor Cell Lines. *Cell Stress Chaperones* (2000) 5(3):207–18. doi: 10.1379/1466-1268(2000)005<0207:HSAAIE>2.0.CO;2
218. Amodio G, Gregori S. HLA-G Genotype/Expression/Disease Association Studies: Success, Hurdles, and Perspectives. *Front Immunol* (2020) 11:1178. doi: 10.3389/fimmu.2020.01178
219. Morandi F, Rizzo R, Fainardi E, Rouas-Freiss N, Pistoia V. Recent Advances in Our Understanding of HLA-G Biology: Lessons From a Wide Spectrum of Human Diseases. *J Immunol Res* (2016) 2016:4326495. doi: 10.1155/2016/4326495
220. Schilling D, Kühnel A, Tetzlaff F, Konrad S, Multhoff G. NZ28-Induced Inhibition of HSF1, SP1 and NF-κb Triggers the Loss of the Natural Killer Cell-Activating Ligands MICA/B on Human Tumor Cells. *Cancer Immunol Immunother* (2015) 64(5):599–608. doi: 10.1007/s00262-015-1665-9
221. Nikolaou M, Pavlopoulou A, Georgakilas AG, Kyrodimos E. The Challenge of Drug Resistance in Cancer Treatment: A Current Overview. *Clin Exp Metastasis* (2018) 35(4):309–18. doi: 10.1007/s10585-018-9903-0
222. Kioka N, Yamano Y, Komano T, Ueda K. Heat-Shock Responsive Elements in the Induction of the Multidrug Resistance Gene (MDR1). *FEBS Lett* (1992) 301(1):37–40. doi: 10.1016/0014-5793(92)80205-U
223. Vilaboa NE, Galan A, Troyano A, de Blas E, Aller P. Regulation of Multidrug Resistance 1 (MDR1)/P-Glycoprotein Gene Expression and Activity by Heat-Shock Transcription Factor 1 (HSF1). *J Biol Chem* (2000) 275 (32):24970–6. doi: 10.1074/jbc.M909136199
224. Kim SH, Yeo GS, Lim YS, Kang CD, Kim CM, Chung BS. Suppression of Multidrug Resistance *via* Inhibition of Heat Shock Factor by Quercetin in MDR Cells. *Exp Mol Med* (1998) 30(2):87–92. doi: 10.1038/emm.1998.13
225. Tchénio T, Havard M, Martinez LA, Dautry F. Heat Shock-Independent Induction of Multidrug Resistance by Heat Shock Factor 1. *Mol Cell Biol* (2006) 26(2):580–91. doi: 10.1128/MCB.26.2.580-591.2006
226. Vydra N, Toma A, Glowala-Kosinska M, Gogler-Piglowska A, Widlak W. Overexpression of Heat Shock Transcription Factor 1 Enhances the Resistance of Melanoma Cells to Doxorubicin and Paclitaxel. *BMC Cancer* (2013) 13:504. doi: 10.1186/1471-2407-13-504
227. Dokladny K, Zuhl MN, Mandell M, Bhattacharya D, Schneider S, Deretic V, et al. Regulatory Coordination Between Two Major Intracellular Homeostatic Systems: Heat Shock Response and Autophagy. *J Biol Chem* (2013) 288(21):14959–72. doi: 10.1074/jbc.M113.462408
228. Luo T, Fu J, Xu A, Su B, Ren Y, Li N, et al. PSMD10/gankyrin Induces Autophagy to Promote Tumor Progression Through Cytoplasmic Interaction With ATG7 and Nuclear Transactivation of ATG7 Expression. *Autophagy* (2016) 12(8):1355–71. doi: 10.1080/15548627.2015.1034405
229. Desai S, Liu Z, Yao J, Patel N, Chen J, Wu Y, et al. Heat Shock Factor 1 (HSF1) Controls Chemoresistance and Autophagy Through Transcriptional Regulation of Autophagy-Related Protein 7 (ATG7). *J Biol Chem* (2013) 288 (13):9165–76. doi: 10.1074/jbc.M112.422071
230. Zhang N, Wu Y, Lyu X, Li B, Yan X, Xiong H, et al. HSF1 Upregulates ATG4B Expression and Enhances Epirubicin-Induced Protective Autophagy in Hepatocellular Carcinoma Cells. *Cancer Lett* (2017) 409:81–90. doi: 10.1016/j.canlet.2017.08.039
231. Luan Q, Jin L, Jiang CC, Tay KH, Lai F, Liu XY, et al. RIPK1 Regulates Survival of Human Melanoma Cells Upon Endoplasmic Reticulum Stress Through Autophagy. *Autophagy* (2015) 11(7):975–94. doi: 10.1080/15548627.2015.1049800
232. Parekh S. Targeting HSF1: A Prime Integrator of Proteotoxic Stress Response in Myeloma. *Clin Cancer Res* (2018) 24(10):2237–8. doi: 10.1158/1078-0432.CCR-18-0030
233. Manasanch EE, Orlowski RZ. Proteasome Inhibitors in Cancer Therapy. *Nat Rev Clin Oncol* (2017) 14(7):417–33. doi: 10.1038/nrclinonc.2016.206
234. Zaarur N, Gabai VL, Porco JA, Calderwood S, Sherman MY. Targeting Heat Shock Response to Sensitize Cancer Cells to Proteasome and Hsp90 Inhibitors. *Cancer Res* (2006) 66(3):1783–91. doi: 10.1158/0008-5472.CAN-05-3692
235. Shah SP, Nooka AK, Jaye DL, Bahlis NJ, Lonial S, Boise LH. Bortezomib-Induced Heat Shock Response Protects Multiple Myeloma Cells and Is Activated by Heat Shock Factor 1 Serine 326 Phosphorylation. *Oncotarget* (2016) 7(37):59727–41. doi: 10.18632/oncotarget.10847
236. Velayutham M, Cardounel AJ, Liu Z, Ilangovan G. Discovering a Reliable Heat-Shock Factor-1 Inhibitor to Treat Human Cancers: Potential Opportunity for Phytochemists. *Front Oncol* (2018) 8:97. doi: 10.3389/fonc.2018.00097
237. Dong B, Jaeger AM, Thiele DJ. Inhibiting Heat Shock Factor 1 in Cancer: A Unique Therapeutic Opportunity. *Trends Pharmacol Sci* (2019) 40(12):986–1005. doi: 10.1016/j.tips.2019.10.008
238. Yoon YJ, Kim JA, Shin KD, Shin D-S, Han YM, Lee YJ, et al. KRIBB11 Inhibits HSP70 Synthesis Through Inhibition of Heat Shock Factor 1 Function by Impairing the Recruitment of Positive Transcription Elongation Factor B to the Hsp70 Promoter. *J Biol Chem* (2011) 286 (3):1737–47. doi: 10.1074/jbc.M110.179440
239. Vilaboa N, Bore A, Martin-Saavedra F, Bayford M, Winfield N, Firth-Clark S, et al. New Inhibitor Targeting Human Transcription Factor HSF1: Effects on the Heat Shock Response and Tumor Cell Survival. *Nucleic Acids Res* (2017) 45(10):5797–817. doi: 10.1093/nar/gkx194
240. Salamanca HH, Antonyak MA, Cerione RA, Shi H, Lis JT. Inhibiting Heat Shock Factor 1 in Human Cancer Cells With a Potent RNA Aptamer. *PLoS One* (2014) 9(5):e96330. doi: 10.1371/journal.pone.0096330
241. Chen B-C, Tu S-L, Zheng B-A, Dong Q-J, Wan Z-A, Dai Q-Q. Schizandrin A Exhibits Potent Anticancer Activity in Colorectal Cancer Cells by Inhibiting Heat Shock Factor 1. *Biosci Rep* (2020) 40(3):BSR20200203. doi: 10.1042/BSR20200203

Conflict of Interest: The authors declare that the research was conducted in the absence of any commercial or financial relationships that could be construed as a potential conflict of interest.

frontiers | Frontiers in Oncology

ORIGINAL RESEARCH
published: 22 April 2022
doi: 10.3389/fonc.2022.858694

RNA Demethylase ALKBH5 Prevents Lung Cancer Progression by Regulating EMT and Stemness *via* Regulating p53

*Xiangli Liu, Ziyi Wang, Qiwei Yang, Xiaohai Hu, Qiang Fu, Xinyu Zhang and Wenya Li**

Department of Thoracic Surgery, The First Affiliated Hospital of China Medical University, Shenyang, China

OPEN ACCESS

Edited by:
Monica Fedele, Istituto per l'Endocrinologia e l'oncologia "Gaetano Salvatore" (CNR), Italy

Reviewed by:
Mohammad Imran Khan, King Abdulaziz University, Saudi Arabia
Yongye Huang, Northeastern University, China

***Correspondence:**
Wenya Li
saint5288@hotmail.com

Specialty section:
This article was submitted to Molecular and Cellular Oncology, a section of the journal Frontiers in Oncology

Received: *07 February 2022*
Accepted: *22 March 2022*
Published: *22 April 2022*

Citation:
Liu X, Wang Z, Yang Q, Hu X, Fu Q, Zhang X and Li W (2022) RNA Demethylase ALKBH5 Prevents Lung Cancer Progression by Regulating EMT and Stemness via Regulating p53. Front. Oncol. 12:858694. doi: 10.3389/fonc.2022.858694

Background: Although N6-methyladenosine (m^6A) RNA methylation is the most abundant reversible methylation of mRNA, which plays a critical role in regulating cancer processing, few studies have examined the role of m^6A in nonsmall-cell lung cancer-derived cancer stem-like cells (CSCs).

Methods: CSCs were enriched by culturing NSCLC cells in a serum-free medium, and stem factors, including CD24, CD44, ALDH1, Nanog, Oct4, and Sox2 were detected by Western blot. ALKBH5 expression was measured by employing a tissue array. Global m^6A methylation was measured after ALKBH5 knockdown. Malignances of CSCs were detected by performing CCK-8 assay, invasion assay, cell cycle analysis, and tumor formation *in vitro* and *in vivo*.

Results: m^6A demethylase ALKBH5 is highly expressed in CSCs derived from NSCLC. Knockdown of ALKBH5 increased global m^6A level, and also increased E-cadherin, decreased stem hallmarkers, Nanog and Oct4, and inhibited stemness of CSCs. In lung carcinoma, ALKBH5 is found to be positively correlated with p53 by using Gene Expression Profiling Interactive Analysis (GEPIA) online tool. P53 transcriptionally regulates ALKBH5 and subsequently regulates the global m^6A methylation level. Knockdown of p53 or inhibition of p53's transcriptional activity by addition of its specific inhibitor PFT-α decreased expression of ALKBH5 and CSCs' malignancies, including proliferation, invasion, and tumor formation ability, indicating that p53 may partially regulate CSC's malignancies *via* ALKBH5. Furthermore, we also found p53 transcriptionally regulates PRRX1, which is consistent with our previous report.

Conclusion: Collectively, our findings indicate the pivotal role of ALKBH5 in CSCs derived from NSCLC and highlight the regulatory function of the p53/ALKBH5 axis in modulating CSC progression, which could be a promising therapeutic target for NSCLC.

Keywords: nonsmall-cell lung cancer (NSCLC), N6-methyladenosine (m^6A) methylation, cancer stem-like cells (CSCs), ALKBH5, epithelial and mesenchymal transition (EMT)

INTRODUCTION

This small group of cells, known as cancer stem cells (CSCs), is characteristic of stem cells. The ability of CSCs to self-renew, multidifferentiate, transfer (1), and evade drug-induced cell death is mainly due to their dormant stem-like properties (2), which are characterized by clinical recurrence; the diffuse tumor cells remained inactive for long periods of time. This may occur in the early stages of the disease or after treatment interventions. Activation of these dormant cells contributes to tumor growth and recurrence. The self-protection of CSCs is achieved through asymmetric cell division cycles in which CSC populations are retained, resulting in heterogeneous tumor populations of CSCs and nonstem-like cancer cells (3). These nonstem-like cancer cells experienced rapid symmetric cell proliferation, making them susceptible to traditional cancer treatments and preserving the cancer stem cell population, vindicating treatment failure and cancer recurrence. These important clinical findings further stimulate strong interest in the further study of CSCs and their involvement in the treatment of drug-resistant lung cancer alternatives. CSCs exhibit high drug resistance and toughness due to prolonged telomere duration, initiation of apoptotic pathways, enhanced membrane transport protein activity, and enhanced mobility and metastasis.

The complete treatment of cancer depends on revealing its origin. Lung CSCs identify and demonstrate resistance to various lung cancer treatment regimens. These include conventional therapies, biomolecules, and targeted therapies. The elimination of lung cancer stem cells during therapeutic interventions is critical because it prevents tumor expansion, recurrence, and metastasis. Although little is known about the biology of pulmonary embolism, various markers of pulmonary embolism have been distinguished and considered. These markers were incorporated but not limited to ALDH1, CD133, side groups (Hoechst negative), CD44, CD87, and CD117. These markers are associated with chemoresistance in the treatment of various first-line diseases. Therefore, it is widely believed that CSC is closely related to pathological features, resulting in a poor clinical prognosis.

N6-methyladenosine (m^6A) is the most common internal chemical modification in eukaryotes. In mammals, m^6A installed by m^6A methyltransferase METTL3 and METTL14 is erased by fat mass and obesity-related proteins (FTO) or α-ketoglutaric acid-dependent dioxygenase homologs 5 (ALKBH5) (4–7). The effects of MRNA m^6A modification on cellular processes include changes in RNA stability (6, 8), translation efficiency (9, 10), secondary structure (11), subcellular localization (12), alternative polyadenylation, and splicing (13). m^6A methyltransferase is critical for the speed and differentiation of mouse embryonic stem cells and circadian clock. FTO is known to regulate fat production and energy homeostasis (14). ALKBH5 is overexpressed in testis but downregulated in the heart and brain, affecting nuclear RNA output and metabolism, gene expression, and mouse fertility (7). ALKBH5 knockout mice are viable, but significant changes in the expression of key genes required for spermatogenesis and maturation indicate a spermatogenesis disorder, although the overall increase in m^6A levels in the testes is modest (7). These studies suggest that key gene expression changes, which are sensitive to the function of m^6A regulators, can cause significant phenotypic changes. So far, however, the biological significance and key target genes of these m^6A modulators in human cancer remain elusive.

Regulation of ALKBH5 is manifested by multiple tumors (15, 16). A previous report shows when ALKBH5 is reduced in PC, the combination of P53 with ALKBH5 promoter was confirmed by genome analysis, microarray verification, and luciferase analysis, combined with bioinformatics prediction, indicating that P53 was transcriptionally activated on ALKBH5 gene. As a well-investigated transcriptional activator, p53 mutated about half of the malignant diseases and may explain the downregulation of ALKBH5 expression.

The molecular mechanism of RNA M6 methylation in regulating malignancies of different kinds of cancer has only recently begun to be elucidated. Dominissini and colleagues tried to explain the roles of m^6A methylation *via* regulating p53 signaling pathways, DNA mismatch repair, and RNA degradation (17). It is also reported that more than 7,000 human genes were sequenced using m^6A and found that silencing m^6A methyltransferase regulates the p53 signaling pathway-mediated apoptosis. Gabbert and Martin also reported that in gastric cancer, m^6A modification may exert critical regulatory roles *via* regulating p53 signaling pathway (18, 19).

In recent years, the carcinogenic or antitumor function of paired related homeobox 1 (PRRX1) has been reported in many kinds of tumors. In glioma and pancreatic cancer, PRRX1 is overexpressed in tumor-initiating cells and plays a regulatory role in tumor invasion and metastasis. In breast, lung, or hepatocellular carcinoma, PRRX1 inhibits the self-renewal and stem cell support of tumor-initiating cells (20, 21). In the field of sarcoma research, mice that eventually develop osteosarcoma p53 and Rb lack PRRX1-positive cells or osteoblasts (22–25), suggesting that PRRX1-positive cells play a key role in the development of osteosarcoma. However, the function of PRRX1 in human osteosarcoma has not been determined. In our previous report, it is presented that PRRX1 regulates the stemness phenotype and epithelial–mesenchymal transition (EMT) in CSCs enriched from nonsmall cell lung cancer (NSCLC) (26). However, the exact role of PRRX1 in regulating NSCLC is still largely unknown.

Here, we examined the correlation between m^6A methylation regulated by ALKBH5 and malignancies in human NSCLC-derived CSCs. We further investigated the modification of m^6A methylation on p53 using human NSCLC cell lines A549 and PC-9.

MATERIAL AND METHODS

Cell Culture and Enrichment of CSCs

Nonsmall cell lung cancer (NSCLC) cell lines A549 and PC-9 were all purchased from the American Type Culture Collection (ATCC). Cells were routinely maintained in Dulbecco's modified Eagle's medium (DMEM) supplemented with 10% fetal bovine

serum (FBS, Gibco, Ca, USA) and antibiotics (50 U/ml penicillin and 50 μg/ml streptomycin, Gibco) at 37°C in a humidified atmosphere containing 5% CO_2. To enrich CSCs from either cells, viable cells were seeded at a 6-well plate and cultured in DMEM/Ham Nutrient Mixture F-12 (F-12) (1:1) supplemented with epidermal growth factor (EGF, 20 ng/ml, Sigma-Aldrich, USA), human fibroblast growth factor basic (hFGFb, 10 ng/ml, Sigma-Aldrich, USA), and 2% B27 (Life Technologies, USA) for 14 days. Every 3 days, the medium was half-refreshed with the addition of relative supplements. For storage, cells were collected and suspended in DMEM/F-12 without the addition of serum and frozen in liquid nitrogen until use.

Cell Viability Analysis

Cells were suspended and adjusted to a concentration of 1 × 106 cells/ml. For each well of a 96-well plate, 2,500 cells were seeded and allowed to attach to the bottom of the plate overnight. To analyze cell viability, the Cell Counting Kit-8 (CCK-8, Sigma-Aldrich, St. Louis, MO, USA)-prepared solution was employed and 10 μl of CCK-8 solution was added into each well for a 4-h coincubation at 37°C away from light. OD450 was detected by a microplate reader (Synergy 2 Multi-Mode Microplate Reader, BioTek, Winooski, VT, USA) to determine the cell viability.

Reverse-Transcription Quantitative PCR

One microgram of total RNA was reverse transcripted following the instruction of the manufacturer, and complementary DNA (cDNA) was used as a template by using Reverse Transcriptase Kit (RIBOBIO, Guangzhou, China). The primers were listed as follow: CD24 sense primer 5′-CTCCTACCCACGCAGATTTATTC-3′ and antisense primer 5′-AGAGTGAGACCACGAAGAGAC-3′; CD44 sense primer 5′-CTGCCGCTTTGCAGGTGTA-3′ and antisense primer 5′-CATTGTGGGCAAGGTGCTATT-3′; ALDH1 sense primer 5′-GCACGCCAGACTTACCTGTC-3′ and antisense primer 5′-CCTCCTCAGTTGCAGGATTAAAG-3′; Nanog sense primer 5′-TTTGTGGGCCTGAAGAAAACT-3′ and antisense primer 5′-AGGGCTGTCCTGAATAAGCAG-3′; Oct4 sense primer 5′-CTGGGTTGATCCTCGGACCT-3′ and antisense primer 5′-CCATCGGAGTTGCTCTCCA-3′; Sox2 sense primer 5′–3′ and antisense primer 5′–3′; METTL3 sense primer 5′-TTGTCTCCAACCTTCCGTAGT-3′ and antisense primer 5′-CCAGATCAGAGAGGTGGTGTAG-3′; METTL14 sense primer 5′-AGTGCCGACAGCATTGGTG-3′ and antisense primer 5′-GGAGCAGAGGTATCATAGGAAGC-3′; YTHDF1 sense primer 5′-ACCTGTCCAGCTATTACCCG-3′ and antisense primer 5′-TGGTGAGGTATGGAATCGGAG-3′; WTAP sense primer 5′-CTTCCCAAGAAGGTTCGATTGA-3′ and antisense primer 5′-TCAGACTCTCTTAGGCCAGTTAC-3′; FTO sense primer 5′-ACTTGGCTCCCTTATCTGACC-3′ and antisense primer 5′–3′; ALKBH5 sense primer 5′-TGTGCAGTGTGAGAAAGGCTT-3′ and antisense primer 5′-CCACCAGCTTTTGGATCACCA-3′; β-actin sense primer 5′-CATGTACGTTGCTATCCAGGC-3′ and antisense primer 5′-CTCCTTAATGTCACGCACGAT-3′. PCR was then carried out using PowerUp SYBR™ Green Master Mix (Thermo Scientific, Waltham, MA, USA) following the manufacturer's instructions. mRNA levels were normalized against β-actin mRNA and expressed relative to the control conditions.

Western Blot

To detect specific protein levels, Western blot was carried out by using primary antibodies, which were all rabbit monoclonal and bought from Abcam (Cambridge, Britain). The primary antibodies used was listed as followed: anti-CD24 (Cat. No.: ab202073); anti-CD44 (Cat. No.: 189524); anti-ALDH1 (Cat. No.: ab227984); anti-Nanog (Cat. No.: ab109250); anti-Oct4 (Cat. No.: ab200834); anti-Sox2 (Cat. No.: ab92494); anti-β-actin (Cat. No.: ab115777); anti-METTL3 (Cat. No.: ab195352); anti-METTL14 (Cat. No.: ab252562); anti-YTHDF1 (Cat. No.: ab252346); anti-WTAP (Cat. No.: ab195380); anti-FTO (Cat. No.: ab126605); anti-ALKBH5 (Cat. No.: ab195377); anti-E-cadherin (Cat. No.: ab231303); anti-p53 (Cat. No.: ab32389); anti-PRRX1 (Cat. No.: ab211292). All antibodies were diluted at 1:1,000. Goat anti-rabbit IgG H&L antibody (HRP ladled, 1:10,000, #ab7090) was used as a secondary antibody. Blot bands were quantified *via* densitometry with Image J software (National Institutes of Health Baltimore, MD, USA). β-Actin was used as an internal reference.

Detection of m^{6}A Methylation Level

To quantitatively measure the m^{6}A methylation level, total RNA was extracted from tissue samples using TRIzol reagent (Thermo Scientific, USA) following the manufacturer's instruction, and then m^{6}A RNA methylation quantification kit (Thermo Scientific, USA) was employed for this purpose by following manufacturer's instruction. The percentage of m^{6}A-methylated mRNA in the total mRNA was calculated to access the m^{6}A methylation level. Briefly, 200 ng mRNA of each sample was loaded in the assay well. A capture antibody specific for m^{6}A (Synaptic Systems, catalog No. 202003, at dilution of 1:2,000) was then added to the wells. Two-hour incubation later, wells were washed three times using washing buffer, and a detection antibody (Abcam, Catalog. No. ab6747, at dilution of 1:5,000) was added to each well. The developer solution was added to each well following the wash steps to remove any liquid while protecting samples from light. The color was developed and captured using a 450-nm wavelength optical meter.

GEPIA Analysis

The online database gene expression profiling interactive analysis (GEPIA) (http://gepia.cancer-pku.cn/index.html) was used to investigate differential expression analysis, profiling according to pathological stages, patient survival analysis, and correlation analysis

PI Staining and Flow Cytometric Analysis

Cells were collected and adjusted to a concentration of 1 × 106 cells/ml and then fixed using 70% anhydrous ethanol overnight, stained with 50 μg/ml propidium iodide (PI, Sigma) for 30 min at 4°C, and then assessed with a Beckman Navios. The cell phase is represented by G0–G1, S, and G2–M.

Invasion

To assess invasive capacity, a 24-well Transwell insert system (Corning, NY) prelaid with Matrigel was used. For each well, 1 × 104 cells were plated in the top chamber containing a Matrigel-coated membrane (60 μg of Matrigel for each well). In the lower chamber, a medium containing 10% FBS was filled to be used as a chemoattractant. After 48-h incubation, cells on the lower surface of the membrane were fixed with methanol and stained with 0.1% crystal violet. The number of cells invading the membrane was counted under a microscope (Olympus, Tokyo, Japan).

Colony Formation

Cells at 2.5 × 103 were seeded in 0.3% low melting soft agar laid on 0.6% low melting soft agar support for 3-week incubation. Colonies were fixed with methanol and stained with 0.1% crystal violet in 20% methanol for 30 min. Each assay was performed in triplicate.

Tissue Microarray of ISH

Clinical Colorectal Cancer Tissue Microarray

Lung adenocarcinoma tissue microarrays (HLugS120CS01) and lung squamous cell carcinoma (HLuGA150CS03) were purchased from Outdo Biotech (Shanghai Outdo Biotech Co. Ltd., China). Completed clinicopathology data were collected for further analysis. The EnVision+detetion system (Dako) was employed to perform immunohistochemistry following the manufacturer's instructions. A semiquantitative scoring criterion for IHC of ALKBH5 staining was used (week or moderated was considered negative; strong was considered positive). Two independent pathologists, blinded to the clinicopathological information, performed the identification.

Human Protein Antibody Membrane Array Analysis

Fifteen different proteins were embedded on a human Protein Antibody Membrane Array (Cat. No.: ab211066, Abcam) according to the manufacturer's instructions. The experiments were performed following the manufacturer's instructions. Briefly, 650 μg total protein of each sample was used for 2-h incubation with membrane. Detection of proteins was performed by incubation with horseradish peroxidase(HRP)-conjugated streptavidin for 2 h. Signal intensities were detected by chemiluminescence, and the membranes (n = 2) were briefly exposed to x-ray films (GE Healthcare, Munich, Germany) for 30 s.

RNA Knockdown

To knockdown an inverted and self-complementary hairpin DNA oligonucleotide, encoding a short-hairpin RNA-targeting ALKBH5 mRNA was chemically synthesized (RIBOBIO, Guangzhou, China), aligned, and cloned into the lentiviral vector pLL3.7 (RIBOBIO, Guangzhou, China) that coexpresses the fluorescent protein GFP. As a control, we used shRNA-targeting Luciferase mRNA. Oligos used to construct the shRNA-targeting ALKBH5 a were as follows: 5′-CCTCATAGTCGCTGCGCTCG-3′; 5′-ATAGTTGTCCCGGGACGTCA-3′ (reverse). Oligos used as control shRNA were as follows: 5′-TTCTCCGAACGTGTCACGA-3′ (forward); 5′-ACGTGACACGTTCGGAGAATT-3′ (reverse).

Animal Experiment

All the animal experiments were conducted according to the ethics committee. All procedures in this section were approved by the Medical Ethics Committee of the Shanghai Outdo Biotech Company and performed according to the ethical guidelines (ethics No.: YB M-05-02). Four-week-old female BALB/c nude mice were purchased from Dashuo Experimental Animal Company (Chengdu, China) and raised in the SPF animal facilities.

Cells at 1 × 106 were subcutaneously injected into the mice similarly to nude mice. Twenty-eight days later, grafted tumors were collected and morphologically analyzed. The proliferating capacity was measured by Ki67 staining.

Statistical Analysis

Each experiment was performed at least three times. The software GraphPad Prism software was used for data analysis. Statistical analyses were performed using ANOVA (equal variance) or Welch's ANOVA (unequal variance). A statistically significant difference among groups was defined as $P < 0.05$.

RESULTS

ALKBH5 Is Upregulated in CSCs Compared With Those in Parental Cells and Leads to a Decrease in Global m^{6}A Methylation

Aiming to investigate the functional role of m^{6}A methylation in CSCs derived from lung adenocarcinoma cells, we firstly enriched spheres from A549 and PC9 cells by culturing in a serum-free medium (SFM) (**Figure 1A**). Ten days after being cultured in SFM, spheres (diameter >20 μm) were observed suspended in a medium, which is a characteristic of CSCs. Collected spheres present more vigorous viability from days 1 to 5 in a serum-supplemented medium (**Figure 1B**). We then accessed stem factors, including CD24, CD44, ALDH1, Nanog, Oct4, and Sox2 and expectedly found all these stem factors (**Figures 1C, D**).

By considering the critical roles of m^{6}A methylation in regulating CSCs, we tried to determine the expression levels of m^{6}A methylation in CSCs compared with that in relevant PCs. As shown in **Figure 2A**, CSCs present a relatively low level of m^{6}A methylation compared with that in relevant PCs. We then measured m^{6}A methylation regulatory genes, including METTL3, METLL14, YTHDF1, FTO, WTAP, and ALKBH5 by reverse-transcription quantitative PCR (RT-qPCR) and found that METTL3, FTO, and ALKBH5 were comparatively higher in CSCs normalized to PCs (**Figure 2B**). Consistent upregulation of METTL3, FTO, and ALKBH5 in CSCs were also observed by performing Western blot analysis (**Figure 2C**). By performing online database searching of the GEPIA database, although FTO

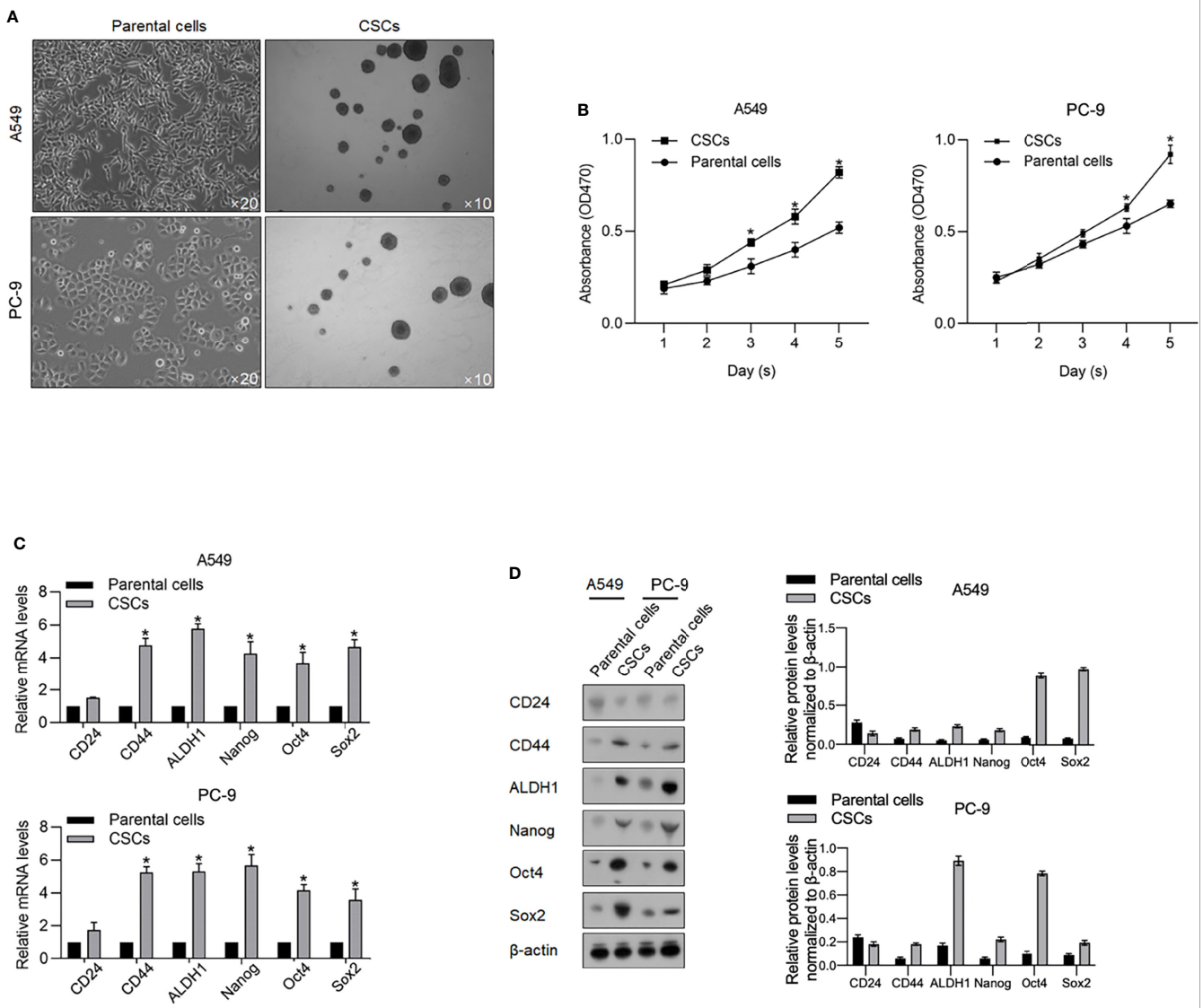

FIGURE 1 | Enrichment of CSCs from A549 and PC-9 cells. **(A)** After being cultured in a serum-free medium, spheres derived from A549 and PC-9 were imaged at an amplification of ×10. **(B)** By performing CCK-8 assay, the cell viability of CSCs and their parental cells from days 1 to 5 was measured. *$p < 0.05$ vs. the parental cell group. The mRNA **(C)** and protein levels **(D)** of stemness hallmarkers, including CD24, CD44, ALDH1, Nanog, Oct4, and Sox2 were measured by performing RT-qPCR and Western blot analysis. *$p < 0.05$ vs. parental cell group.

and ALKBH5 present no obvious difference between tumor and adjacent tissue, METTL3 significantly decreased in tumor tissues compared with adjacent tissues (**Figure 2D**).

ALKBH5 Is Upregulated in CSCs and Enhances Malignancies

To evaluate the effects of METTL3 and ALKBH5 on m^{6}A methylation in NSCLC CSCs, siRNAs targeting METTL3 or ALKBH5 were transfected efficiently into cells (**Figure 3A**). Seventy-two hours later after transfection, m^{6}A methylation level was measured, and, expectedly, results presented that knockdown of ALBKH5 significantly increased m^{6}A methylation, and oppositely, knockdown of METLL3 decreased m^{6}A methylation (**Figure 3B**). Knockdown of ALKBH5, but not METLL3, significantly inhibited malignant behaviors of CSCs, including cell proliferation (**Figure 3C**), cell cycle promotion (**Figure 3D**), invasion (**Figure 3E**), and colony formation (**Figure 3F**). These results indicate that ALKBH5, but not METLL3, plays a critical regulatory role in malignancies *via* regulating m^{6}A methylation in NSCLC CSCs. We then further employed a tissue array to evaluate the protein level of ALKBH5 in LUAD and LUSC. **Figures 4A, B** presents that, compared with adjacent tissues, tumor tissue presents obvious higher intensity of ALKBH5, which indicated that ALKBH5 may be upregulated in tumor tissues compared with adjacent tissues.

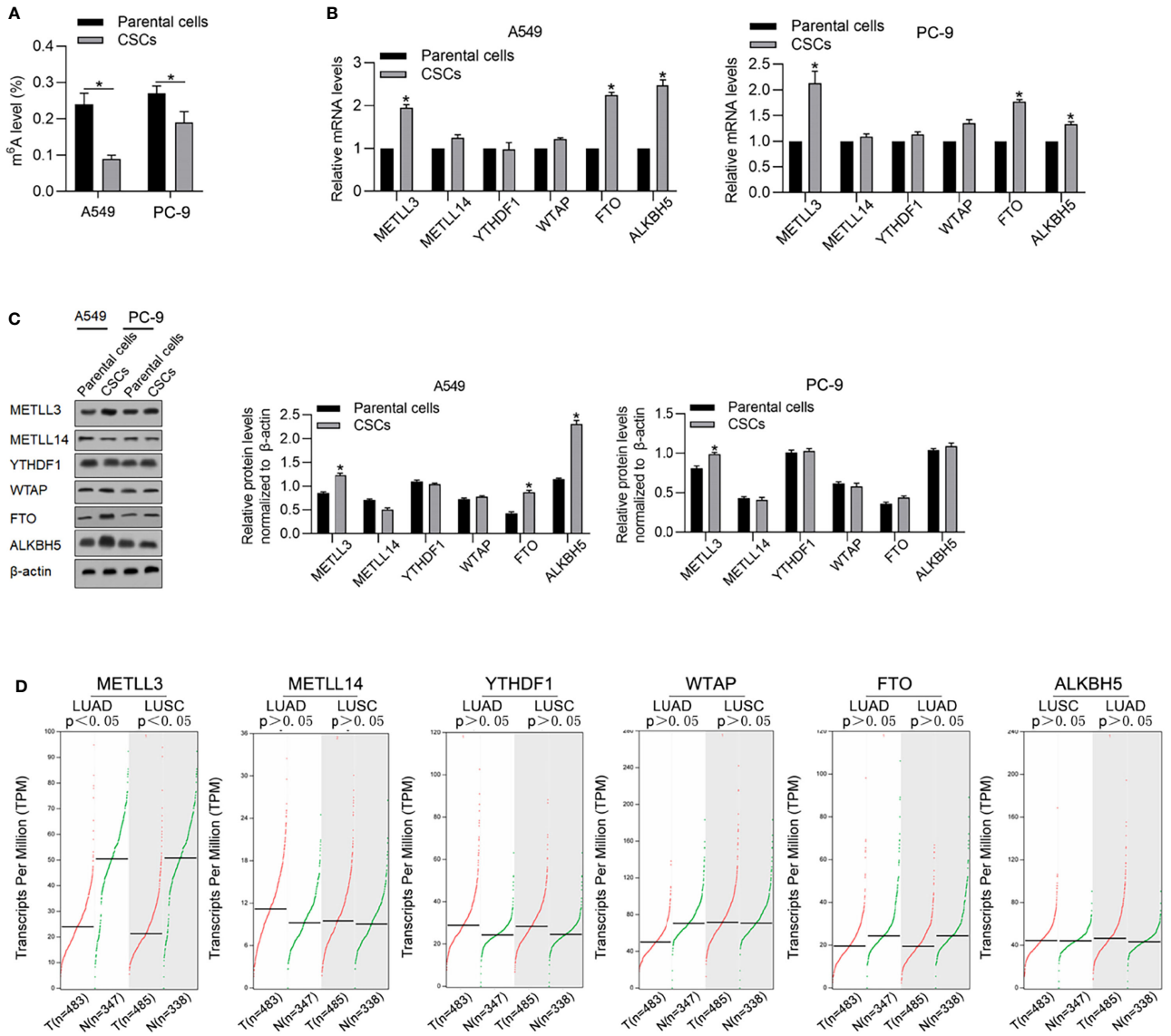

FIGURE 2 | CSCs present a relatively lower m^{6}A methylation level compared with their parental cells. **(A)** Global m^{6}A methylation was measured in CSCs and its parental cells of A549 and PC-9. *$p < 0.05$ vs. parental cells. m^{6}A methylation-relative gene expressions including METTL3, METTL14, YTHDF1, WTAP, FTO, and ALKBH5 were measured in mRNA **(B)** and protein levels **(C)**. **(D)** By employing the GEPIA database analysis tool, the relative mRNA levels of METTL3, METTL14, YTHDF1, WTAP, FTO, and ALKBH5 were compared between tumor samples and nontumor samples.

ALKBH5 Is Critical for Maintaining Stemness in CSCs

To determine the effects of METTL3 and ALKBH5 on the stem-like property of NSCLC CSCs, a stem factor protein array was employed after METTL3 or ALKBH5 knockdown. After METTL3 and ALKBH5 knockdown, E-cadherin protein level was significantly increased, and Nanog, Oct4, and Sox2 were decreased significantly (**Figure 5A**), indicating that knockdown of METTL3 or ALKBH5 potentially regulates stemness of NSCLC CSCs. Sphere formation was further performed to confirm their role in regulating stemness, and, expectedly, results presented that knockdown of either METTL3 or ALKBH5 inhibited sphere formation (**Figure 5B**). Changes in E-cadherin, Nanog, Oct4, and Sox2 indicated that these two proteins, especially ALKBH5 are critical for maintaining stemness (**Figure 5C**). Knockdown of ALKBH5 significantly modified hallmarkers of EMT, including E-cadherin, Nanog, Oct4, and Sox2, indicating its critical role in maintaining the stemness of CSCs.

P53 Transcriptionally Regulates ALKBH5 and Malignancies in CSCs

It is identified that ALKBH5 is a downstream target gene of p53, which is a key regulator of malignancies in various cancers. By searching the GEPIA database, it is illustrated that, both in

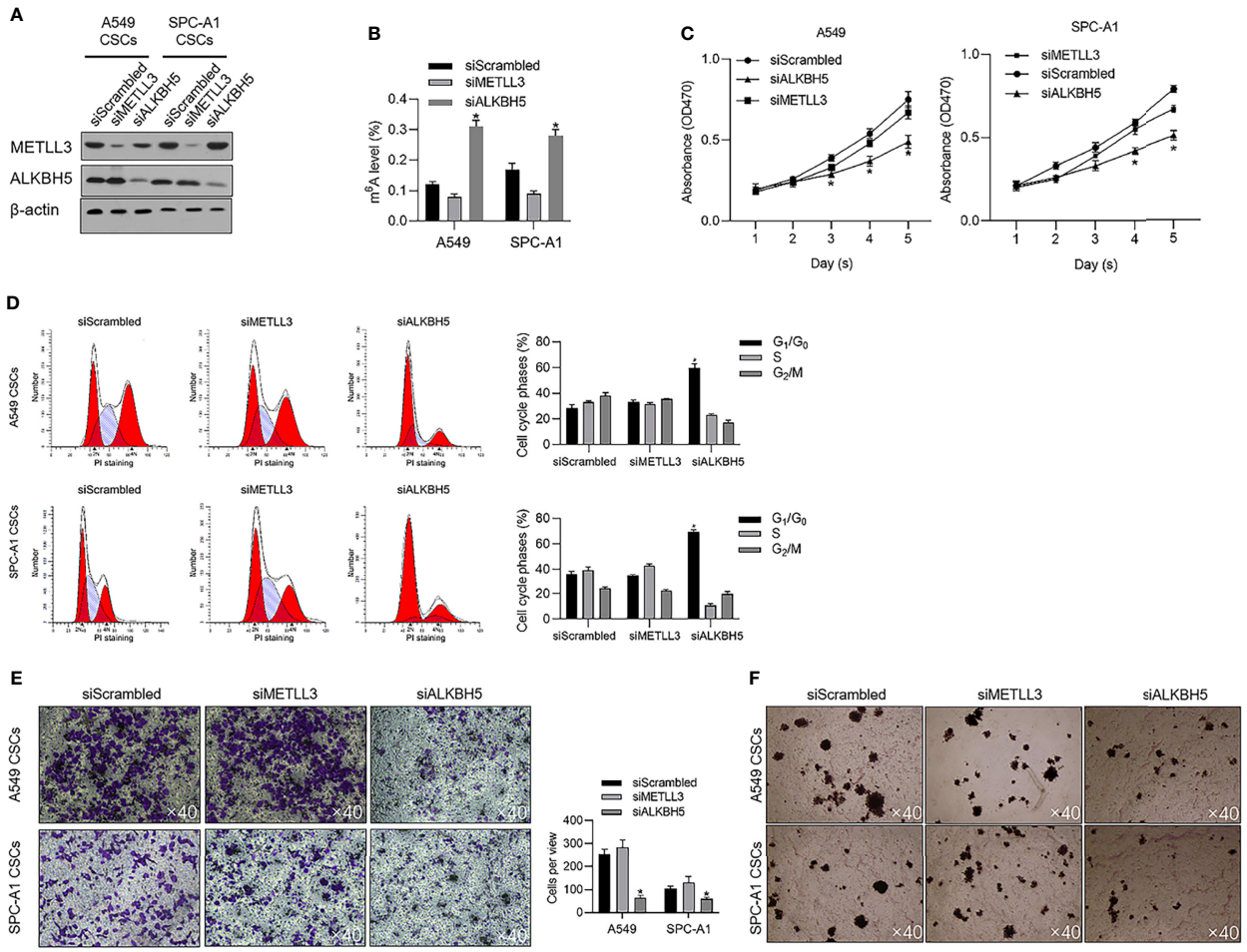

FIGURE 3 | ALKBH5 is tightly associated with global m^{6}A methylation level and promotes cell cycle progression and invasive capacity. **(A)** Efficient knockdown of METTL3 or ALKBH5 was confirmed by performing a Western blot analysis. **(B)** After METTL3 or ALKBH5 knockdown, the global m^{6}A methylation was measured. **(C)** After METTL3 or ALKBH5 knockdown, cell viability from days 1 to 5 was measured by performing CCK-8 assay. *$p < 0.05$ vs. the siScrambled group. **(D)** After METTL3 or ALKBH5 knockdown, the cell cycle distribution was measured by performing PI staining followed by flow cytometric analysis. *$p < 0.05$ vs. siScrambled group. After METTL3 or ALKBH5 knockdown, invasive capacity **(E)** or tumor formation in soft agar **(F)** was respectively analyzed.

LUAD and LUSA, mRNA levels of p53 are positively correlated with that of ALKBH5 (**Figure 6A**), which prompted us to identify the regulatory role of p53 on ALBKH5. To identify the effects of p53 on m^{6}A methylation, we efficiently knocked down p53 in A549 (**Figure 6B**) and overexpressed p53 in PC-9, which is a p53-null cell line (**Figure 6B**). After efficient knockdown of p53, ALKBH5 mRNA was significantly downregulated (**Figure 6C**), which was also observed after blockage of p53's transcriptional activity *via* inhibiting its DNA-binding activity (**Figure 6C**). We then further analyzed the m^{6}A methylation level after interfering with p53 activity. Expectedly, both p53 knockdown and inhibition of p53's transcriptional activity significantly increased the m^{6}A methylation in NSCLC CSCs (**Figure 6D**).

We further analyzed the roles of p53 on malignancies of NSCLC CSCs *via* regulating p53 transcriptional activity. Expectedly, in A549 CSCs, knockdown of p53 slightly inhibited malignancies, including cell proliferation, entry of cell cycle, invasion, and tumor formation *in vitro* (**Figures 7A–D**), which were achieved by the addition of PFT-α, indicating that the roles of p53 in regulating malignancies were due to its transcriptional activity. In PC-9 CSCs, overexpression of p53 significantly inhibited malignancies in PC-9 CSCs, which were reversed by the addition of PFT-α, indicating that p53 may, at least, partially regulates malignancies *via* ALKBH5 in NSCLC CSCs (**Figures 7A–D**).

P53 Potentially Regulates EMT and Stemness *via* PRRX1

It is reported that p53 functions as a transcriptional factor of PRRX1 and E-cadherin by targeting their upstream promoter region. In our previous study, PRRX1 was observed to be a negative regulator of E-cadherin, which is a marker of EMT. These results prompted us to detect the regulatory roles of p53

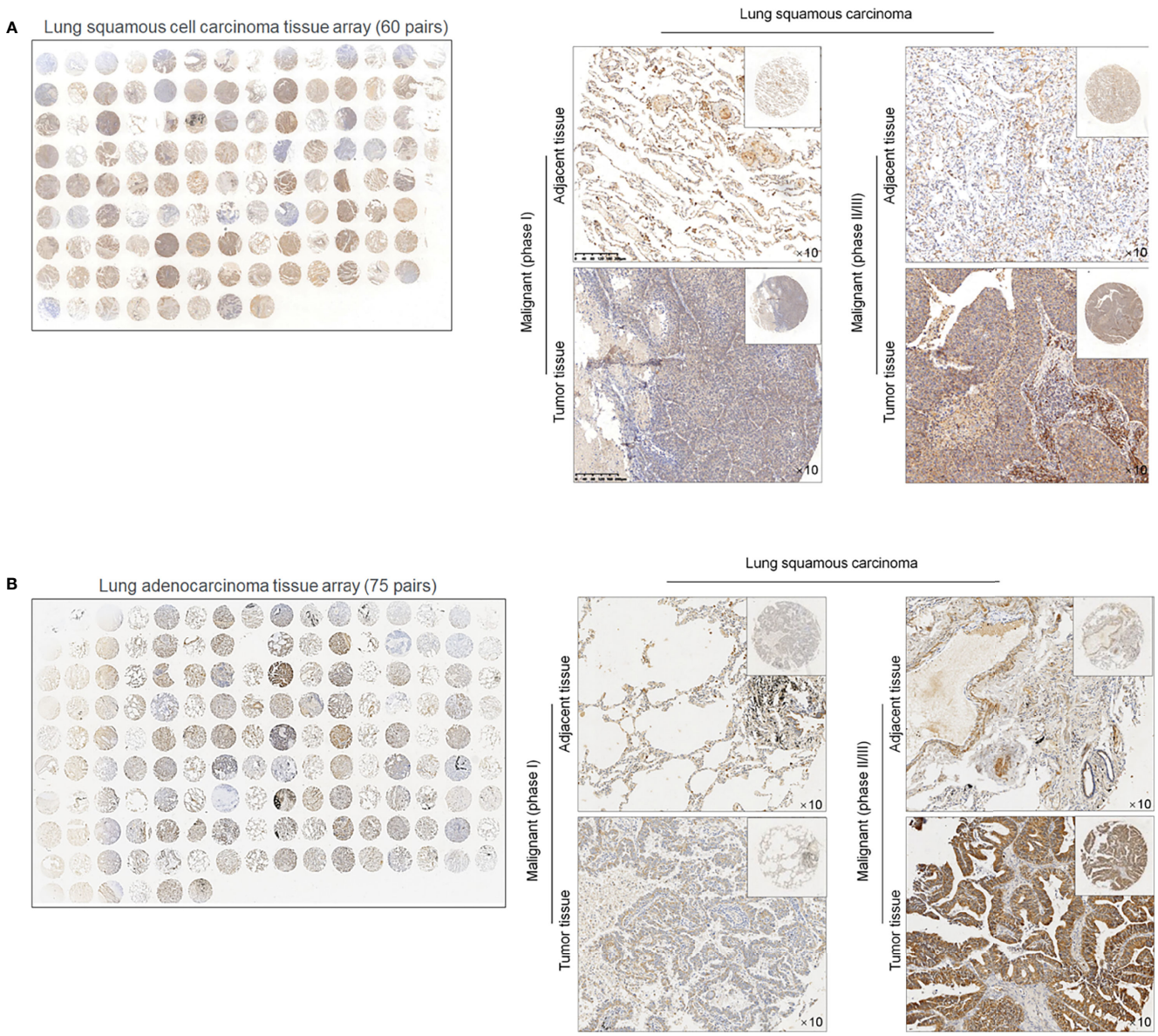

FIGURE 4 | ALKBH5 protein is expressed relatively higher in lung cancer tissues compared to adjacent non-tumor tissues60 paired lung squamous cell carcinoma (LUAD) tissue array **(A)** and 75 paried lung adenocarcinoma (LUSC) tissue array was employed for ISH staining of ALKBH5 **(B)**.

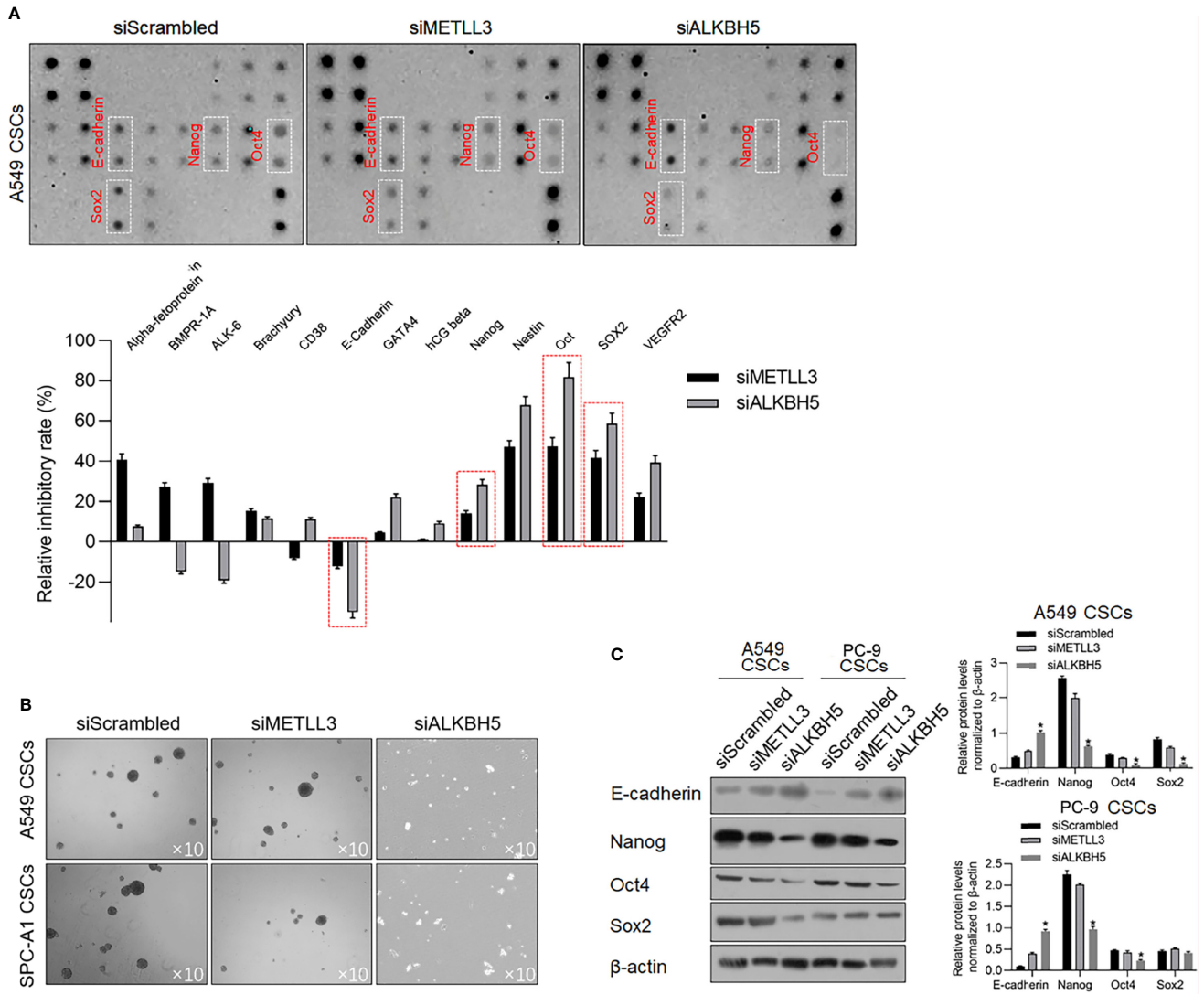

FIGURE 5 | ALKBH5 knockdown increased E-cadherin and decreased stemness. **(A)** To detect the changes of human stem cell hallmarkers after ALKBH5 knockdown, a human stem cell antibody array was performed. **(B)** After METTL3 or ALKBH5 knockdown, sphere formation was measured. **(C)** To confirm the effects of METLL3 or ALKBH5 knockdown on E-cadherin, Nanog, Oct4, and Sox2, a Western blot analysis was performed. *$p < 0.05$ vs. siScrambled group.

on PRRX1 and E-cadherin. As the results presented, knockdown of p53 significantly decreased PRRX1 mRNA and oppositely increased E-cadherin mRNA in A549 CSCs (**Figure 8A**). Overexpression of p53 in PC-9 CSCs increased PRRX1 mRNA and decreased E-cadherin mRNA, which were reversed by the addition of PFT-a, indicating that p53's transcriptional activity is critical for its regulatory roles on PRRX1 and E-cadherin (**Figure 8A**). These changes in protein levels were further confirmed by performing a Western blot analysis (**Figure 8B**). Taken together, p53 may act as a key regulator of PRRX1, ALKBH5, and E-cadherin.

To further confirm the roles of ALKBH5 in regulating tumor growth *in vivo*, A549 CSCs with knocked-down ALKBH5 were planted in nude mice. Twenty-eight days later, transplanted tumors in the ALKBH5 knockdown group were presented as significantly smaller than the control group (**Figures 9A, B**). By performing Ki67 staining to evaluate the proliferative capacity of tumors, expectedly, knockdown of Ki67 obviously decreased the Ki67-positive proportion in tumors (**Figure 9C**).

DISCUSSION

In this study, we presented that m^{6}A demethylase ALKBH5, which is transcriptionally regulated by p53, modifies the epithelial and mesenchymal transition process and maintenance of stemness of cancer stem-like cells derived from NSCLC. In our previous report, it is presented that PRRX1 regulates the stemness phenotype and EMT of CSCs derived from NSCLC *via* stabilizing Sox2 (7). **Figures 5**, **8** present that

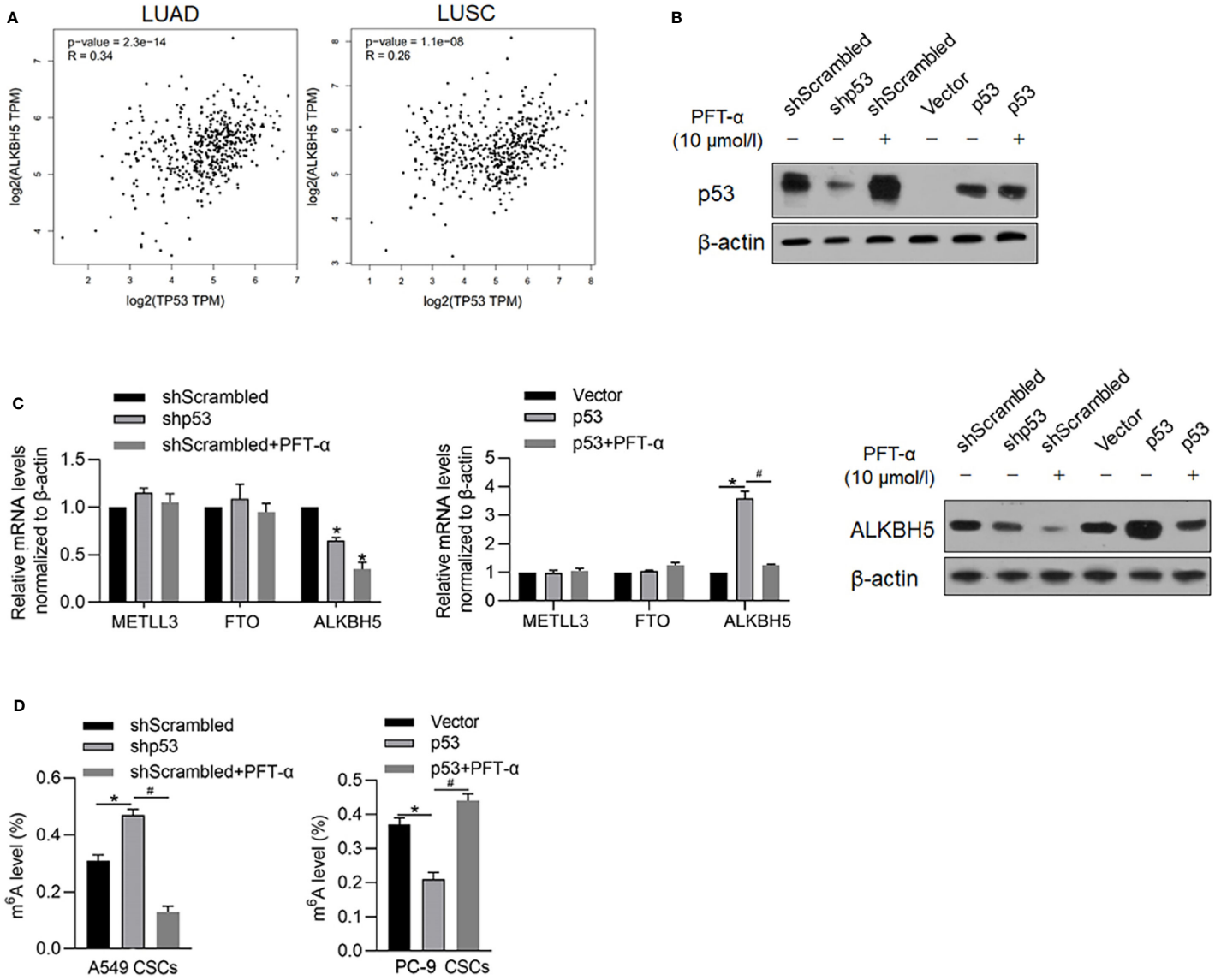

FIGURE 6 | p53 transcriptionally regulates ALKBH5 and subsequently decreased m^{6}A methylation. **(A)** GEPIA database analysis tool was used to compare the correlation between ALKBH5 and p53 in LUAD and LUSC. **(B)** In A549 and PC-9 CSCs, the efficiency of p53 knockdown or overexpression was measured by performing a Western blot analysis. **(C)** After modification of p53 with or without PFT-α, ALKBH5 mRNA and protein level were measured. $^*p < 0.05$ vs. shScrambled group; $^\#p < 0.05$ vs. p53 group. **(D)** After modification of p53 with or without PFT-α, m^{6}A methylation level was measured. $^*p < 0.05$ vs. shScrambled group; $^\#p < 0.05$ vs. shp53 group (left panel); $^*p < 0.05$, vs. vector group; $^\#p < 0.05$ vs. p53 group (right panel).

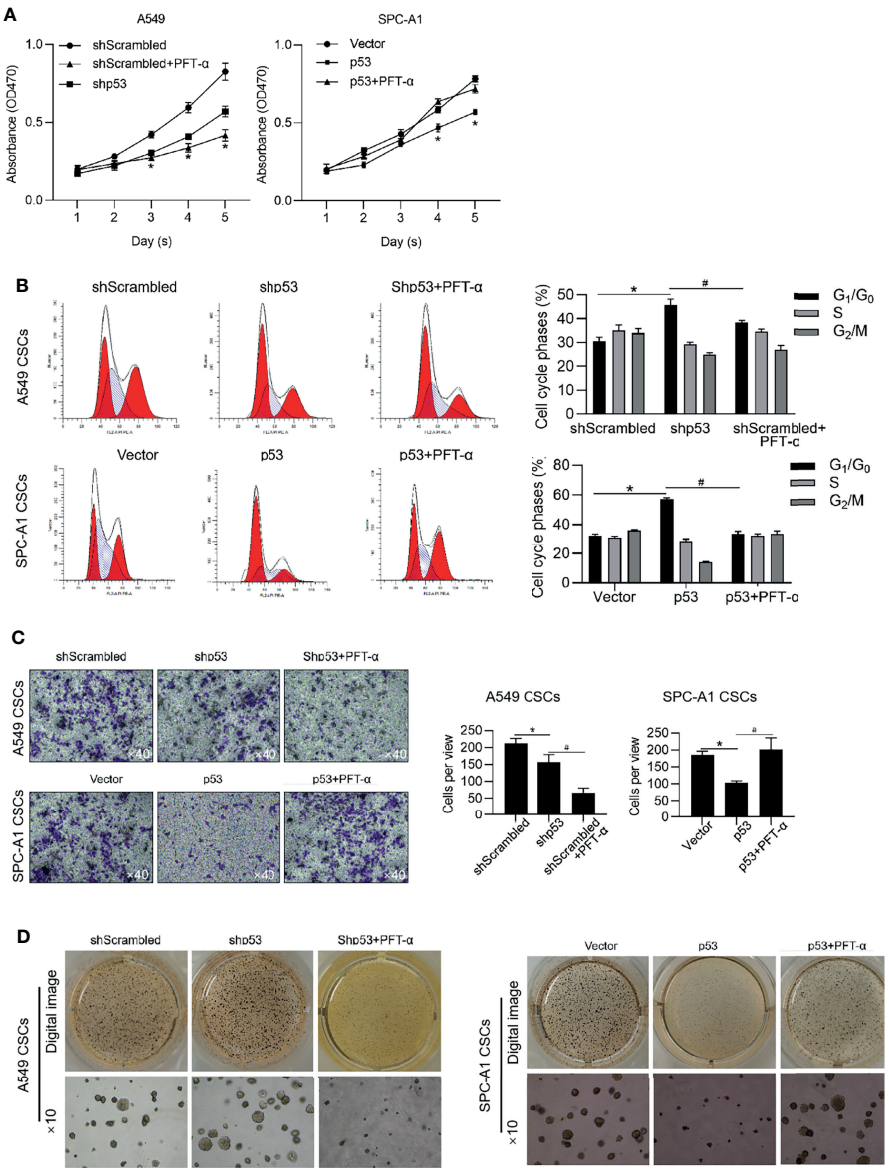

FIGURE 7 | p53 inhibits malignancies *via* exerting transcriptional activity. In A549 CSCs, p53 was efficiently knockdown by transfecting shRNA targeting to p53 mRNA. In PC-9 CSCs, p53 was efficiently overexpressed by transfecting p53-coding plasmid. Cell viability was then analyzed by performing CCK-8 assay **(A)**. $^{*}p <$ 0.05 vs. shScrambled group (left panel); $^{*}p < 0.05$ vs. vector group (right panel). **(B)** Cell cycle distribution was analyzed by performing PI staining followed by flow cytometry assay. $^{*}p < 0.05$ vs. shScrambled group; $^{\#}p < 0.05$ vs. shp53 group (left panel); $^{*}p < 0.05$ vs. vector group; $^{\#}p < 0.05$ vs. p53 group (right panel). **(C)** Cell invasion was analyzed by performing Transwell assay. $^{*}p<0.05$ vs. shScrambled group; $^{\#}p < 0.05$, vs. shp53 group (left panel); $^{*}p < 0.05$, vs. vector group; $^{\#}p <$ 0.05 vs. p53 group (right panel). **(D)** Tumor formation in soft agar was performed. $^{*}p < 0.05$ vs. shScrambled group; $^{\#}p < 0.05$ vs. shp53 group (left panel); $^{*}p <$ 0.05 vs. vector group; $^{\#}p < 0.05$ vs. p53 group (right panel).

downregulation of ALKBH5 or p53 significantly decreased Sox2 and increased E-cadherin protein levels, which is consistent with our previous findings and demonstrated the upstream regulating roles of ALKBH5 in modulating malignancies of CSCs derived from NSCLC.

PRRX1 is a member of the paired homeobox family, which plays an important role in tumors. EMT and mesenchymal–epithelial transition (MET) are two important mechanisms leading to tumor recurrence and metastasis. EMT can make tumor cells acquire the ability of invasion and migration, and promote the dissemination of tumor cells from the primary lesion, which is one of the initial steps of tumor recurrence and metastasis; MET can make tumor cells regain the ability of colonization and formation of tumor metastasis, then the cells resurge to complete tumor metastasis. At the same time, tumor IMT can make the tumor acquire stemness, and the two are correlated. PRRX1 is closely related to the occurrence of EMT, and it is an important transcription factor regulating EMT,

which plays an important role in tumor recurrence and metastasis and tumor stemness maintenance (27). Studies have shown that overexpressed PRRX1 can induce EMT in hepatoma cells by activating the TGF-β pathway to promote β-catenin entry into the nucleus, while downregulation of Prrx1 can inhibit the expression of Slug and TGF-β-R2 by upregulating Pitx2-microRNA pathway, then relieve the inhibition of Slug on E-cadherin, thus leading to the occurrence of MET in hepatoma cells, which is closely related to metastasis and recurrence of liver cancer (28). The role of PRRX1 varies in tumors of different systems and types. In liver cancer, downregulation of PRRX1 can promote tumors to produce stem cell-like features (29). However, it is found that overexpression of PRRX1 is closely related to tumor EMT, tumor stemness, tumor metastasis, and prognosis in pancreatic cancer (30), colorectal cancer (26), and papillary thyroid cancer (31). The above differences may be related to the differences in PRRX1's expression and function in different tumors.

In our previous report, main PRRX1 isoforms were investigated, and results found that PRRX1A, the main type of PRRX1 isoforms, promotes malignant behaviors *via* transcriptional activation of TGF-β depending on TGF-β/TGF-βR signaling pathway, and subsequently regulates EMT process (7). Meanwhile, PRRX1A tightly binds to and stabilizes Sox2, which may be the main cause of the decrease in stemness. Here, it is found that downregulation of ALKBH5, but not METLL3, significantly increased E-cadherin and decreased Oct4 and Sox2 proteins, which indicated its regulatory roles in the EMT process and maintenance of stemness. This indicates that ALKBH5 may be a direct regulator of PRRX1 and results in subsequent modification of EMT and stemness *via* PRRX1. However, we failed to evaluate the mRNA and protein levels of different isotypes of PRRX1, including PRRX1A and PRRX1B, which should be evaluated in further study.

m6A RNA methylation is involved in the phenotype of tumor stem cells by regulating gene expression. YTHDF2 is an m^6A reader, which has been proved to be associated with the prognosis of patients with hepatocellular carcinoma. Some studies suggest that YTHDF2 can promote the stemness phenotype of hepatoma cells by regulating the m^6A methylation of the Oct4 gene (32). At the same time, m^6A methylation can enhance the stemness of hepatoma cells by upregulating LINC00106 (33). In addition, m^6A methylation can also improve the stemness of hepatoma cells by regulating the stability of MGAT5 mRNA (34). In this study, we evaluated the protein levels of the main components of m^6A methylation, including METLL3, METLL14, YTHDF1, WTAP, FTO, and ALKBH5. Only METTL3 and ALKBH5 are upregulated in CSCs compared with that in parental cells. Moreover, only knockdown of ALKBH5 significantly regulates m^6A methylation, stemness, EMT, and malignancies together in NSCLC CSCs. ALKBH5 was reported to exert opposite roles in different kinds of cancers, indicating that it may regulate different m^6A methylation profiles in a different context.

P53, as a kind of tumor suppressor protein, can maintain the balance between self-renewal and differentiation, thus maintaining the stability of the internal environment of organs. In recent years, some studies have shown that the gain-of-function (GOF) mutation of p53 further improves the stemness of cancer cells (35). In addition to posttranslational regulation of p53 protein's stability and activity, p53 expression is also regulated by promoter methylation and m^6A RNA methylation at the transcriptional and posttranscriptional levels. Studies have shown that a food-borne mycotoxin FA can reduce P53 expression in human liver cancer cells by reducing the expression level of m^6A-p53 (36). In addition, the m^6A demethylase ALKBH5 can activate PER1 *via* an m^6A-ythdf2-dependent manner and reactivate the ATM-CHK2-P53 #CDC25C signaling pathway, inhibiting the growth of tumor cells. We presented that in LUAD and LUSC tissue samples, ALKBH5 is positively correlated with p53 and transcriptionally regulated by p53. Knockdown of p53 resulted in ALKBH5 decrease

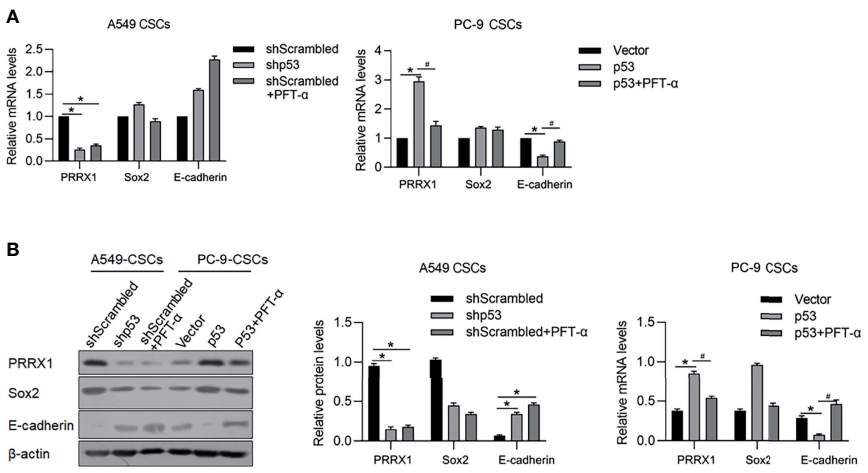

FIGURE 8 | p53 potentially regulates PRRX1, Sox2, and E-cadherin *via* ALKBH5. In A549 CSCs, p53 was efficiently knockdown by transfecting shRNA targeting p53 mRNA. In PC-9 CSCs, p53 was efficiently overexpressed by transfecting p53-coding plasmid. mRNA **(A)** and protein **(B)** of PRRX1, Sox2, and E-cadherin were measured. $^*p < 0.05$ shScrambled group (left panel); $^*p < 0.05$ vs. vector group; $^{\#}p < 0.05$ vs. p53 group (right panel).

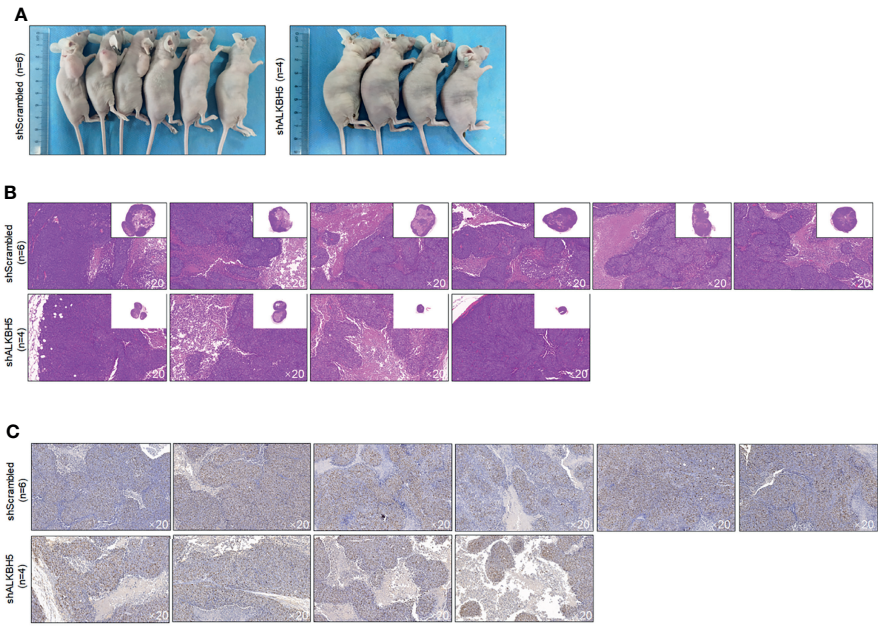

FIGURE 9 | ALKBH5 knockdown decreased tumor formation in nude mice. **(A)** Volume of CSCs formed tumors in nude mice after seeding 5 × 10^5 cells. Tumor formation was morphologically identified by H&E staining **(B)**, and cell proliferation marker Ki67 **(C)** were further measured.

and global m^{6}A methylation increase. These results demonstrated that ALKBH5 may be a downstream regulator of p53.

Our findings collectively show that ALKBH5 regulates EMT and maintenance of stemness of CSCs derived from NSCLC. P53 was found to act as an upstream regulator of ALKBH5 and exerts key roles in these processes. Targeting the p53-ALKBH5-PRRX1 axes may offer a promising therapeutic approach in curing metastatic NSCLC.

DATA AVAILABILITY STATEMENT

The original contributions presented in the study are included in the article/**Supplementary Material**. Further inquiries can be directed to the corresponding author.

ETHICS STATEMENT

The animal study was reviewed and approved by the medical ethics committee of the Shanghai Outdo Biotech Company.

AUTHOR CONTRIBUTIONS

XL, ZW, and WL designed the experiments and performed molecular-related experiments in this study. QY, XH, and QF performed experiments on processing cells. QY, QF, and XZ are responsible for data collection and performed statistical analysis. XL and WL wrote the manuscript. WL revised the manuscript. All authors read and approved the final manuscript.

ACKNOWLEDGMENTS

The authors would like to thank Mr. Wei Wang for language editing and providing suggestion in statistical analysis.

SUPPLEMENTARY MATERIAL

The Supplementary Material for this article can be found online at: https://www.frontiersin.org/articles/10.3389/fonc.2022.858694/full#supplementary-material

REFERENCES

1. Kreso A, Dick JE. Evolution of the Cancer Stem Cell Model. *Cell Stem Cell* (2014) 14(3):275–91. doi: 10.1016/j.stem.2014.02.006
2. Dembinski JL, Krauss S. Characterization and Functional Analysis of a Slow Cycling Stem Cell-Like Subpopulation in Pancreas Adenocarcinoma. *Clin Exp Metastasis* (2009) 26(7):611–23. doi: 10.1007/s10585-009-9260-0
3. Yoo YD, Kwon YT. Molecular Mechanisms Controlling Asymmetric and Symmetric Self-Renewal of Cancer Stem Cells. *J Anal Sci Technol* (2015) 6:28. doi: 10.1186/s40543-015-0071-4
4. Jia G, Fu Y, Zhao X, Dai Q, Zheng G, Yang Y, et al. N6- Methyladenosine in Nuclear RNA Is a Major Substrate of the Obesity-Associated FTO. *Nat Chem Biol* (2011) 7(12):885–7. doi: 10.1038/nchembio.687
5. Liu J, Yue Y, Han D, Wang X, Fu Y, Zhang L, et al. A METTL3- METTL14 Complex Mediates Mammalian Nuclear RNA N6-Adenosine Methylation. *Nat Chem Biol* (2014) 10(2):93–5. doi: 10.1038/nchembio.1432
6. Wang Y, Li Y, Toth JI, Petroski MD, Zhang Z, Zhao JC. N6-Methyladenosine Modification Destabilizes Developmental Regulators in Embryonic Stem Cells. *Nat Cell Biol* (2014) 16(2):191–8. doi: 10.1038/ncb2902

7. Zheng G, Dahl JA, Niu Y, Fedorcsak P, Huang CM, Li CJ, et al. ALKBH5 Is a Mammalian RNA Demethylase That Impacts RNA Metabolism and Mouse Fertility. *Mol Cell* (2013) 49(1):18–29. doi: 10.1016/j.molcel.2012.10.015
8. Wang X, Lu Z, Gomez A, Hon GC, Yue Y, Han D, et al. N6-Methyladenosine-Dependent Regulation of Messenger RNA Stability. *Nature* (2014) 505 (7481):117–20. doi: 10.1038/nature12730
9. Meyer KD, Patil DP, Zhou J, Zinoviev A, Skabkin MA, Elemento O, et al. 5′ UTR M(6)A Promotes Cap-Independent Translation. *Cell* (2015) 153(4):999–1010. doi: 10.1016/j.cell.2015.10.012
10. Wang X, Zhao BS, Roundtree IA, Lu Z, Han D, Ma H, et al. N(6)-Methyladenosine Modulates Messenger RNA Translation Efficiency. *Cell* (2015) 161(6):1388–99. doi: 10.1016/j.cell.2015.05.014
11. Liu N, Dai Q, Zheng G, He C, Parisien M, Pan T. N(6)-Methyladenosine-Dependent RNA Structural Switches Regulate RNA-Protein Interactions. *Nature* (2015) 518(7540):560–4. doi: 10.1038/nature14234
12. Fustin JM, Doi M, Yamaguchi Y, Hida H, Nishimura S, Yoshida M, et al. RNA-Methylation-Dependent RNA Processing Controls the Speed of the Circadian Clock. *Cell* (2013) 155(4):793–806. doi: 10.1016/j.cell.2013.10.026
13. Molinie B, Wang J, Lim KS, Hillebrand R, Lu ZX, Van Wittenberghe N, et al. M(6)A-LAIC-Seq Reveals the Census and Complexity of the M(6)A Epitranscriptome. *Nat Methods* (2016) 13(8):692–8. doi: 10.1038/nmeth.3898
14. Fischer J, Koch L, Emmerling C, Vierkotten J, Peters T, Bruning JC, et al. Inactivation of the Fto Gene Protects From Obesity. *Nature* (2009) 458 (7240):894–8. doi: 10.1038/nature07848
15. Zhang CZ, Samanta D, Lu HQ, Bullen J, Zhang HM, Chen I, et al. Hypoxia Induces the Breast Cancer Stem Cell Phenotype by HIF-Dependent and ALKBH5-Mediated M6a-Demethylation of NANOG mRNA. *Proc Natl Acad Sci* (2016) 113(14):E2047–56. doi: 10.1073/pnas.1602883113
16. Zhang SC, Zhao BS, Zhou AD, Lin KY, Zheng SP, Lu ZK, et al. M6a Demethylase ALKBH5 Maintains Tumorigenicity of Glioblastoma Stem-Like Cells by Sustaining FOXM1 Expression and Cell Proliferation Program. *Cancer Cell* (2017) 31(4):591–606. doi: 10.1016/j.ccell.2017.02.013
17. Dominissini D, Moshitch-Moshkovitz S, Schwartz S, Salmon-Divon M, Ungar L, Osenberg S, et al. Topology of the Human and Mouse M(6)A RNA Methylomes Revealed by M(6)A-Seq. *Nature* (2012) 485(7397):201–6. doi: 10.1038/nature11112
18. Gabbert HE, Muller W, Schneiders A, Meier S, Hommel G. The Relationship of P53 Expression to the Prognosis of 418 Patients With Gastric Carcinoma. *Cancer* (1995) 76(5):720–6. doi: 10.1002/1097-0142(19950901)76:5<720::AID-CNCR2820760503>3.0.CO;2-E
19. Martin HM, Filipe MI, Morris RW, Lane DP, Silvestre F. P53 Expression and Prognosis in Gastric Carcinoma. *Int J Cancer* (1992) 50(6):859–62. doi: 10.1002/ijc.2910500604
20. Chen ZT, Chen YH, Li Y, Lian WD, Zheng KH, Zhang YX, et al. Prrx1 Promotes Stemness and Angiogenesis *via* Activating TGF-β/Smad Pathway and Upregulating Proangiogenic Factors in Glioma. *Cell Death Dis* (2021) 12:615. doi: 10.1038/s41419-021-03882-7
21. Reichert M, Takano S, Von Burstin J, Kim SB, Lee JS, Ihida-Stansbury K, et al. The Prrx1 Homeodomain Transcription Factor Plays a Central Role in Pancreatic Regeneration and Carcinogenesis. *Genes Dev* (2013) 27:288–300. doi: 10.1101/gad.204453.112
22. Mutsaers AJ, Walkley CR. Cells of Origin in Osteosarcoma: Mesenchymal Stem Cells or Osteoblast Committed Cells? *Bone* (2014) 62:56–63. doi: 10.1016/j.bone.2014.02.003
23. Lin PP, Pandey MK, Jin FH, Raymond AK, Akiyama H, Lozano G. Targeted Mutation of P53 and Rb in Mesenchymal Cells of the Limb Bud Produces Sarcomas in Mice. *Carcinogenesis* (2009) 30(10):1789–95. doi: 10.1093/carcin/bgp180
24. Berman SD, Calo E, Landman AS, Danielian PS, Miler ES, West JC, et al. Metastatic Osteosarcoma Induced by Inactivation of Rb and P53 in the Osteoblast Lineage. *Proc Natl Acad Sci USA* (2008) 105(33):11851–6. doi: 10.1073/pnas.0805462105
25. Quist T, Jin H, Zhu JF, Smith-Fry K, Capecchi MR, Jones KB. The Impact of Osteoblastic Differentiation on Osteosarcomagenesis in the Mouse. *Oncogene* (2015) 34(32):4278–84. doi: 10.1038/onc.2014.354
26. Sun L, Han T, Zhang XY, Liu XL, Li PW, Shao MR, et al. PRRX1 Isoform PRRX1A Regulates the Stemness Phenotype and Epithelia-Mesenchymal Transition (EMT) of Cancer Stem-Like Cells (CSCs) Derived From Non-Small Cell Lung Cancer (NSCLC). *Trans Lung Cancer Res* (2020) 9(3):731–44. doi: 10.21037/tlcr-20-633
27. Chen WB, Wu JY, Shi WW, Zhang G, Chen XM, Ji A, et al. PRRX1 Deficiency Induces Mesenchymal-Epithelial Transition Through PITX2/miR-200-Dependent SLUG/CTNNB1 Regulation in Hepatocellular Carcinoma. *Cancer Sci* (2021) 112(6):2158–72. doi: 10.1111/cas.14853
28. Hirata H, Sugimachi K, Takahashi Y, Ueda M, Sakimura S, Uchi R, et al. Downregulation of PRRX1 Confers Cancer Stem Cell—Like Properties and Predicts Poor Prognosis in Hepatocellular Carcinoma. *Ann Surg Oncol* (2015) 22(S3):1402–9. doi: 10.1245/s10434-014-4242-0
29. Reichert M, Takano S, yon Burstin J, Kim SB, Lee JS, Stansbury K, et al. The PRRX1 Homedomain Transcription Factor Plays a Central Role in Pancreatic Re—Generation and Carcinogenesis. *Genes Dev* (2013) 27(3):288–300. doi: 10.1101/gad.204453.112
30. Takahashi Y, Sawada G, Kurashige J, Uchi R, Matsumura T, Ueo H, et al. Paired Related Homoeobox 1, A New EMT Inducer, Is Involved in Metastasis and Pooprognosis in Coloreetal Cancer. *Br J Cancer* (2013) 109(2):307–11. doi: 10.1038/bjc.2013.339
31. Zhang CZ, Huang SZ, Zhuang HK, Ruan SY, Zhou ZX, Huang KJ, et al. YTHDF2 Promotes the Liver Cancer Stem Cell Phenotype and Cancer Metastasis by Regulating OCT4 Expression *via* M6a RNA Methylation. *Oncogene* (2020) 39(23):4507–18. doi: 10.1038/s41388-020-1303-7
32. Liang WJ, Wang Y, Zhang QY, Gao M, Zhou HZ, Wang ZR. M6A-Mediated Upregulation of LINC00106 Promotes Stemness and Metastasis Properties of Hepatocellular Carcinoma *via* Sponging Let7f. *Front Cell Dev Biol* (2021) 9:781867. doi: 10.3389/fcell.2021.781867
33. Yang YC, Wu J, Liu FQ, He J, Wu F, Chen J, et al. IGF2BP1 Promotes the Liver Cancer Stem Cell Phenotype by Regulating MGAT5 mRNA Stability by M6a RNA Methylation. *Stem Cells Dev* (2021) 30(22):1115–25. doi: 10.1089/scd.2021.0153
34. Ghatak D, Ghosh DD, Roychoudhury S. Cancer Stemness: P53 at the Wheel. *Front Oncol* (2021) 10:604124. doi: 10.3389/fonc.2020.604124
35. Ghazi T, Nagiah S, Chuturgoon AA. Fusaric Acid Decreases P53 Expression by Altering Promoter Methylation and M6a RNA Methylation in Human Hepatocellular Carcinoma (HepG2) Cells. *Epigenetics* (2021) 16(1):79–91. doi: 10.1080/15592294.2020.1788324
36. Guo XY, Li K, Jiang WL, Hu YY, Xiao WQ, Huang YS, et al. RNA Demethylase ALKBH5 Prevents Pancreatic Cancer Progression by Posttranscriptional Activation of PER1 in an M6a-YTHDF2-Dependent Manner. *Mol Cancer* (2020) 19(1):91. doi: 10.1186/s12943-020-01158-w

Conflict of Interest: The authors declare that the research was conducted in the absence of any commercial or financial relationships that could be construed as a potential conflict of interest.

frontiers | Frontiers in Oncology

CASE REPORT
published: 25 May 2022
doi: 10.3389/fonc.2022.873252

Case Report: *GNAQ*- and *SF3B1* Mutations in an Aggressive Case of Relapsing Uveal Ring Melanoma

Michelle Prasuhn[1], Josephine Christin Freitag[1], Sabine Lüken[1], Vinodh Kakkassery[1], Hartmut Merz[2], Almuth Caliebe[3], Malte Spielmann[3], Mahdy Ranjbar[1] and Felix Rommel[1]*

[1] Department of Ophthalmology, University Hospital Schleswig-Holstein, University of Lübeck, Lübeck, Germany,
[2] Hämatopathologie Lübeck, Reference Centre for Lymph Node Pathology andHematopathology, Lübeck, Germany,
[3] Institute of Human Genetics, University Hospital of Schleswig-Holstein, University of Lübeck, Lübeck, Germany

OPEN ACCESS

Edited by:
Anna Maria Di Giacomo,
Siena University Hospital, Italy

Reviewed by:
Bo Liu,
Memorial Sloan Kettering Cancer Center, United States
Luca Falzone,
G. Pascale National Cancer Institute Foundation (IRCCS), Italy

***Correspondence:**
Michelle Prasuhn
michelle.prasuhn@uksh.de

Specialty section:
This article was submitted to Molecular and Cellular Oncology, a section of the journal Frontiers in Oncology

Received: *10 February 2022*
Accepted: *18 April 2022*
Published: *25 May 2022*

Citation:
Prasuhn M, Freitag JC, Lüken S, Kakkassery V, Merz H, Caliebe A, Spielmann M, Ranjbar M and Rommel F (2022) Case Report: GNAQ- and SF3B1 Mutations in an Aggressive Case of Relapsing Uveal Ring Melanoma. Front. Oncol. 12:873252. doi: 10.3389/fonc.2022.873252

The molecular mechanisms for uveal ring melanoma are still unclear until today. In this case report, we describe a patient with a malignant uveal melanoma with exudative retinal detachment that had been treated with plaque brachytherapy, resulting in successful tumor regression. After 1 year, a ring-shaped recurrence with extraocular extension appeared, and the eye required enucleation. Histological and molecular genetic analyses revealed an epithelioid-cell-type melanoma with complete circumferential involvement of the ciliary body and, so far, unreported GNAQ and SF3B1 mutations in ring melanoma. Therefore, this report gives new genetic background information on this ocular tumor usually leading to enucleation.

Keywords: uveal melanoma, ring melanoma, GNAQ, SF3B1, brachytherapy, case report

INTRODUCTION

Uveal melanomas represent the most frequently diagnosed primary intraocular malignant tumor in adults and are potentially life-threatening (1). Among uveal melanomas, the variant ring melanoma is a very rare entity and comprises around 0.3% of all uveal melanomas (2). It was first introduced as "ring sarcoma" by Ewetzky et al. to describe an unusual circumferential growth pattern of uveal melanoma involving the ciliary body and the iris (3). Ring melanomas are summarized as uveal melanomas manifesting as a circumferential growth pattern around the eye that can present in the choroid, ciliary body, anterior chamber angle, and iris with different features (2).

Here we describe a rare case of ring melanoma that manifested as a relapse of a uveal melanoma after plaque brachytherapy. The molecular genetic assessment revealed a unique and, so far, unreported mutation status.

BACKGROUND

Patient Information

A 72-year-old female patient was referred to our clinic with a suspicious, prominent choroidal lesion on her left eye that was noticed by her ophthalmologist in a routine checkup. The patient did not report any symptoms, and further ophthalmological medical history was unremarkable. General medical history revealed type 2 diabetes and hypertension treated with metformin, hydrochlorothiazide, nitrendipine, and candesartan. The patient did not report any prior malignancies, and the family health history concerning cancer or ophthalmological conditions was unremarkable as well.

Case Presentation

The best-corrected visual acuity (BCVA) on both eyes was 20/30, and the intraocular pressure was normal (15/18 mmHg). Upon slit-lamp examination, we found a moderate cataract on both eyes and an otherwise normal anterior segment, including any alterations of the iris. Fundoscopy of the left eye revealed a prominent melanocytic proliferation in the inferior hemisphere with surrounding subretinal fluid extending towards the inferior arcade (**Figure 1**). Another small, flat melanocytic lesion was visible next to the optic disk. Using ultrasound B-scans, we recognized a medium reflective tumor with a base of 13.6 × 10.8 mm and a thickness of 6.0 mm, with surrounding tumor-related retinal detachment (**Figure 1**). We carried out an ultrasound biomicroscopy (UBM), which showed a little swelling of the inferior ciliary body (max. 2.5 mm) but no infiltration of the surrounding structures. Upon these findings, the clinically suspected diagnosis was a uveal melanoma. Staging analyses including magnetic resonance imaging of the head, computed tomography (chest and abdomen), and ultrasound of the abdomen (dermatological and gynecological assessment) revealed no metastases or other suspicious lesions. The blood tests were unremarkable, especially for liver enzymes and S100. We discussed with the patient the option of taking a biopsy before therapy initiation, but since the tumor showed clinically distinct features for uveal melanoma, we decided on immediate therapeutic intervention. Therefore, we performed brachytherapy of the tumor with ruthenium-106 only shortly after the first visit. Intraoperatively, the diaphanoscopy showed that the tumor expanded even further anteriorly and along the ciliary body than we preoperatively suspected in UBM. Therefore, we first applied the ruthenium-106 plaque above the main part of the tumor (tumor apex dose 150 Gy, scleral dose 1,004 Gy) and relocated the plaque "edge to edge" after 7 days and above the minor part for another 6 days (tumor apex dose, 125 Gy; scleral dose, 850). During plaque removal, we additionally applied triamcinolone intravitreally to reduce the subretinal fluid surrounding the tumor as previously described by Parrazzoni et al. (4).

In the subsequent visits over 6 months, we noted a continuous decrease in tumor size until there was no uveal thickening detectable on ultrasound and no more subretinal fluid. At 7 months after the therapy with ruthenium-106, we confirmed a good local tumor control. However, the patient developed a radiation retinopathy with macular edema and deterioration of BCVA to 20/80, so we decided to inject triamcinolone intravitreally. When we saw the patient in our clinic 4 weeks after the injection, she had developed a posterior pole cataract which decreased the vision to hand motion and did not enable us to perform a fundus examination anymore. Therefore, we soon carried out cataract surgery without complications, which improved the patient's vision. Only a few weeks afterward, we noticed a suspicious melanotic lesion of the iris with vascularization that was not present before. The UBM revealed thickening of the ciliary body, measuring 1.5 × 1.5mm. Furthermore, we saw a still active radiation retinopathy, and a new exudative retinal detachment has formed. Suspecting a toxic tumor syndrome, we decided to perform a vitrectomy with

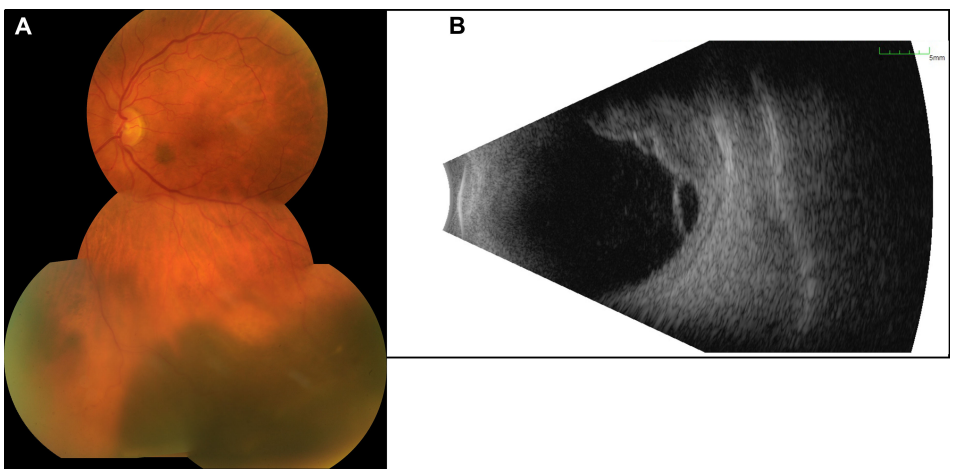

FIGURE 1 | Presentation of the initial tumor. **(A)** The image of the posterior pole illustrates a melanotic tumor with subretinal fluid. **(B)** The B-scan ultrasound reveals a multilobulated tumor with a size of 13.6 × 10.8 mm and a thickness of 6.0 mm and with surrounding subretinal fluid.

endoresection of the original melanoma, reattachment of the retina with silicone oil tamponade, and biopsy of the new iridial lesion. The latter unveiled histopathological findings that are typical of uveal melanoma with an epithelioid cell type (increased expression of HMB45 and MelanA and high proliferative activity in Ki67 staining). With the biopsy of the iris and the resected melanoma, we carried out additional molecular genetic analyses. Fluorescence *in situ* hybridization (FISH) of the iris biopsy disclosed monosomy 3, heterozygous deletion in 1p36, and excessive copies of *MYC* in 8q24. In next-generation sequencing [the targeted gene panel including *GNA22*: codon p.Arg625 and p.Gln209 (NM_002067); *GNAQ*: codon p.Arg183 and p.Gln209 (NM_002072); *SF3B1*: codon p.Arg625 (NM_012433) and MiSeq sequencing by synthesis (Illumina; coverage 250, average reads per exon >1,000), both probes revealed c.626A>T in *GNAQ* (encoding G Protein Subunit Alpha Q), leading to p.Gln209Leu, and c.1874G>A in *SF3B1* (encoding splicing factor 3B subunit 1), leading to p.Arg625His. Analyses concerning *GNA11* (encoding G Protein Subunit Alpha 11) showed a wild-type status. Soon after vitrectomy and endoresection, we noticed that the iridial lesions had increased in number and size, along with severe iridial vascularization and a prominent episcleral (sentinel) vessel (**Figure 2**). In UBM, we saw a circumferential infiltration of the iris and ciliary body, leading to the diagnosis of a ring melanoma (**Figure 2**). Considering the aggressiveness of the tumor progression to a ring melanoma and taking into account the toxic tumor syndrome with vision loss to hand motion, we had to decide on the enucleation of the left eye in agreement with the patient. The enucleation took place without complications, and the histopathological analyses of the enucleated eye confirmed the annular growth of the tumor around the iris (**Figure 3**).

Figure 4 illustrates and summarizes the chronology of the case.

The patient returns to our clinic for regular follow-up visits, during which we did not detect any signs of a local recurrence until today at 1 year after enucleation.

Over the disease course, the patient had received regular aftercare examinations to exclude metastases, including ultrasound imaging of the abdomen, serum liver enzyme levels, and chest X-rays. There were no suspicious lesions at any time.

DISCUSSION

Ring melanomas represent a very rare variant of uveal melanomas that are associated with a poor prognosis and often result in the enucleation of the affected eye (2). Detailed epidemiological studies are hampered by the rarity of this entity. Demirci et al. studied 8,800 patients with uveal melanoma and detected 23 cases with ciliary body ring melanoma (0.3%). In this study, all of the cases were managed with enucleation (2). It is often impossible to identify the site of primary growth, which can be the ciliary body, the base of the iris, or the iridociliary junction.

To our knowledge, so far, there are only two case descriptions of patients in which a relapse of a treated localized uveal melanoma presented as a ring melanoma. Meyer et al. described a patient diagnosed with ring melanoma 3 years after a proton beam treatment for a ciliary body melanoma (5). Tay et al. reported a ring-shaped recurrence with extrascleral extension of a ciliary body melanoma after plaque brachytherapy (6). In their case, the tumor relapsed 14 years after brachytherapy, shortly after performing trabeculectomy. In all published cases, it remains unclear whether these findings are real tumor recurrences or subclinical remaining tumor cells in the iridociliary junction.

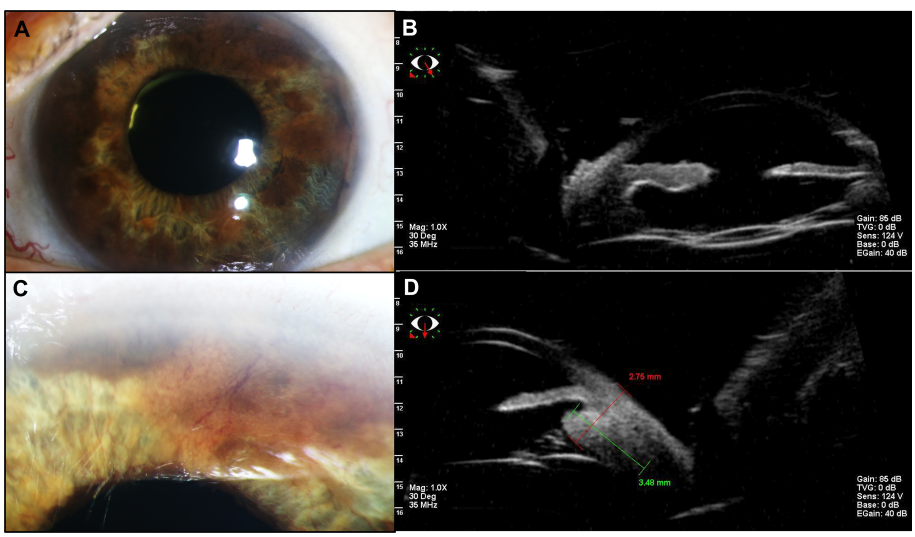

FIGURE 2 | Presentation of the recurrence. **(A)** The slit-lamp examination of the anterior segment shows an episcleral sentinel vessel and vascularized, melanotic lesions infiltrating the iris circumferentially. **(B)** Close-up image focusing on the iridial lesions with vascularization. **(C)** The ultrasound biomicroscopy (UBM) of the temporal–inferior iridociliary junction illustrates the thickening of the iris. **(D)** The UBM of the inferior–anterior segment reveals ciliary body infiltration, measuring 2.75 × 3.84 mm at this site. With UBM, iridial and ciliary body thickening was unveiled circumferentially.

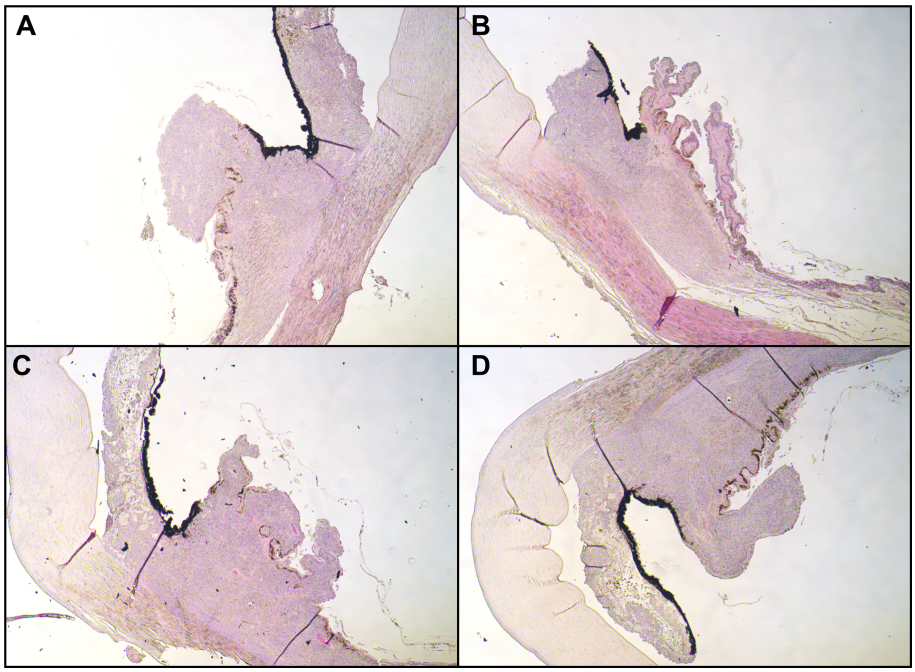

FIGURE 3 | Histopathological examination. Hematoxylin and eosin stain of the iridociliary junction, magnification: ×10. **(A)** Superior, **(B)** nasal parts of the iris were missing due to paraffin embedding; **(C)** inferior; **(D)** temporal. All images expose infiltration of an epithelioid-cell-type tumor infiltrating the ciliary body.

Our case represents a highly aggressive disease course of uveal melanoma which recurred after brachytherapy. The preoperatively present exudative retinal detachment is a known predictive factor for recurrence after radiation therapy (7, 8). In our patient, after plaque brachytherapy, we were able to observe a very good response with tumor remission until there was no more tumor prominence noticeable on ultrasound. The first signs of a recurrence presented only 1 year after brachytherapy with new melanotic iridial lesions.

Clinically, the differential diagnoses of a multilocular melanoma and a *de novo* melanoma after brachytherapy must be taken into consideration. Since we were able to illustrate a continuous circumferential tumor growth infiltrating the iris and ciliary body in UBM and later in the histopathological assessment, the diagnosis of a ring melanoma can be made. It can be speculated that the partial thickening of the ciliary body that we noticed before brachytherapy was already the beginning of a ring melanoma, which would represent a typical course in ring melanomas (2).

The histopathological and genetic analyses revealed the same characteristics in the treated uveal melanoma, and the latter detected iridial lesions, suggesting the ring melanoma to be most likely a relapse of the primary uveal melanoma. However, it cannot be completely excluded that the ring melanoma formed *de novo*.

Our histopathological analyses revealed an epithelioid cell type, which is a rather rare form of uveal melanoma and is associated with a poorer prognosis (9, 10).

Ring melanomas have not been systematically reviewed concerning their genetic features. However, molecular genetic analyses gain more and more importance as they provide us with information that are of increasing clinical relevance, especially concerning prognosis and personalized therapy options. This case reports a unique genetic pattern that has not been shown in ring melanoma yet.

Utilizing FISH, we detected 23% chromosomal aberrations concerning monosomy 3 (complete loss of one chromosome 3). Monosomy 3 is a significant predictor for a higher relapse rate and lower overall survival rates (11, 12). All analyzed nuclei showed changes of p1, which is a common feature of uveal melanoma (13). The amplification of *MYC*, as in this case, occurs in about 40% of all uveal melanoma (14).

Using next-generation sequencing, we investigated *GNA11*, *GNAQ*, and *SF3B1*. The activating hotspot mutation c.626A>T in *GNAQ*, which leads to an amino acid change from glutamine to leucine, has already been described and occurs in approximately 45% of primary uveal melanomas and 22% of uveal metastases (15). The mutations lead to the constitutive activation of the Gαq and Gα11 subunits by decreasing their GTPase activity, which is required to return them to an inactive state. This results in the constitutive activation of G-protein-coupled signaling pathways, such as MAPK, PI3K, PKC, Akt/mTOR, Rac/Rho, Wnt/β-catenin, and Hippo (13, 16). *GNAQ* mutations occur early in uveal melanoma as tumor-initiating mutations and do not seem to have a prognostic value (17).

Moreover, we were able to find a mutation in *SF3B1* that leads to an amino acid exchange of arginine to histidine (c.1874G>A; p.Arg625His). The mutations of codon 625 in *SF3B1* can be identified in 20% of uveal melanomas (18). They result in an aberrant splicing pattern of important apoptotic genes through the usage of an alternative 3′ splice site upstream

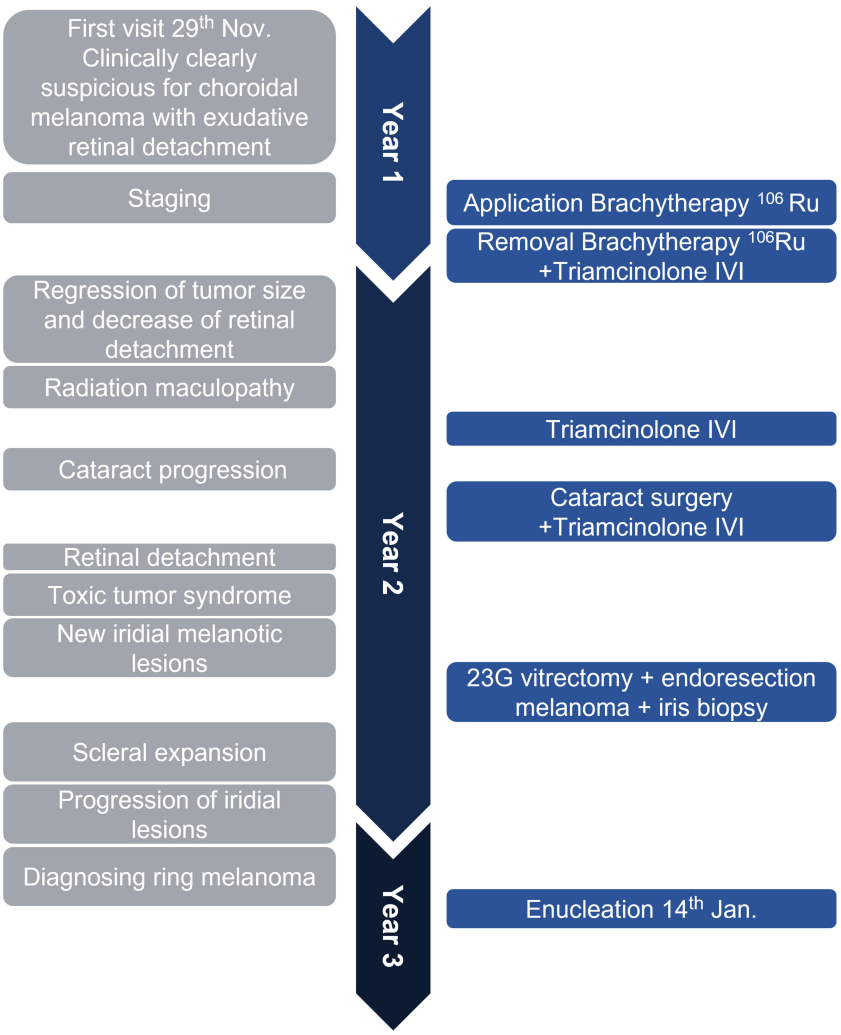

FIGURE 4 | The timeline illustrates the rapid disease course in this case. In about 1 year and 2 months, the patient received the primary diagnosis of uveal melanoma, underwent brachytherapy with good tumor regression, was treated for radiation retinopathy, then diagnosed with a ring-shaped relapse, and underwent enucleation of the eye. The left gray side lists important clinical features, and the right blue side demonstrates surgical interventions. IVI, intravitreal injection; Ru^{106}, ruthenium-106; 23G, 23-gauge.

of the canonical 3′ splice site (16). The mutation c.1874G>A has so far only been described by Hou et al. in 19 of 85 examined uveal melanomas (19). The clinical significance of this variant concerning disease course and prognosis is still unclear. However, information on the mutation status in uveal melanoma are crucial as more and more individual therapeutic concepts are emerging. Since *SF3B1* is involved in splicing, there has been growing interest in splicing modulators. Additionally, *SF3B1* mutations may also be sensitive to nonsense-mediated mRNA decay inhibitors or protein arginine methyltransferase 5 inhibitors (13, 20, 21).

To date, the management options for ring melanomas are still limited. Based on the large tumor dimension, enucleation is usually the preferred treatment option. The tumor in our case has certain characteristics that limit our patient's prognosis. First, ring melanomas have a poorer prognosis than localized uveal melanomas, with a metastatic rate of 52% after 5 years of follow-up (2). Additionally, ciliary body infiltration, monosomy 3, epithelioid cell type, and extrascleral extension are limiting factors. The patient regularly returns to our clinic and attends aftercare examinations. So far, no signs of a local recurrence or metastatic disease could be detected.

With this case report, we want to emphasize the importance of regular follow-up visits of patients with uveal melanoma, without and with pupil dilation. The interindividual disease course is highly variable, and in cases like this, disease progression and the possibility to intervene could be missed if follow-up intervals are extended. Additionally, we would like to encourage the genetic testing of biopsies of uveal melanoma and especially ring melanoma. Even though this entity is very rare, genetic testing is crucial to gain further insights into the pathomechanisms and could have therapeutic relevance as individualized treatment strategies emerge.

CONCLUDING REMARKS

This case illustrates a particularly aggressive local disease course in a uveal melanoma that relapsed as a ring melanoma. We detected hotspot mutations in *GNAQ* and *SF3B1* that have been described in uveal melanoma, but not ring melanoma. Molecular genetic analyses like in this case provide valuable insights into the disease entity that form the base for future therapeutic concepts as personalized medicine gains more and more importance.

DATA AVAILABILITY STATEMENT

The original contributions presented in the study are included in the article/supplementary material. Further inquiries can be directed to the corresponding author.

ETHICS STATEMENT

Written informed consent was obtained from the patients/participants for the publication of this case report.

AUTHOR CONTRIBUTIONS

JCF, MP, VK, MR, SL, and FR were responsible for the patient during clinical visits. VK and FR performed surgeries. Genetic analyses were performed and evaluated by MS and AC. Histopathological assessment was done by HM. JCF and MP took the microscopic and clinical images and created the figures. MP, VK, MR, and FR wrote the sections of the manuscript. All authors contributed to the article and approved the submitted version.

REFERENCES

1. Branisteanu DC, Bogdanici CM, Branisteanu DE, Maranduca MA, Zemba M, Florian B, et al. Uveal Melanoma Diagnosis and Current Treatment Options (Review). *Exp Ther Med* (2021) 22:1428. doi: 10.3892/etm.2021.10863
2. Demirci H, Shields CL, Shields JA, Honavar SG, Eagle RCJr. Ring Melanoma of the Ciliary Body: Report on Twenty-Three Patients. *Retina* (2002) 22:698–706. doi: 10.1097/00006982-200212000-00003
3. Ewetzky T. Weitere Studien Uber Intraoculare Sarkome. III. Flachensarkome Des Uvealtractus. *Von Graefes Arch Ophthalmol* (1898), 45(3):563–612. doi: 10.1007/BF01994790
4. Parrozzani R, Pilotto E, Dario A, Miglionico G, Midena E. Intravitreal Triamcinolone Versus Intravitreal Bevacizumab in the Treatment of Exudative Retinal Detachment Secondary to Posterior Uveal Melanoma. *Am J Ophthalmol* (2013) 155:127–133.e2. doi: 10.1016/j.ajo.2012.06.026
5. Meyer A, D'Hermies F, Korobelnik JF, Morel X, Elmaleh C, Renard G. Ring Recurrence of Ciliary Body Melanoma After Proton-Beam Therapy. *J Fr Ophtalmol* (1997) 20:697–700.
6. Tay E, Cree IA, Hungerford J, Franks W. Recurrence of Treated Ciliary Body Melanoma Following Trabeculectomy. *Clin Exp Ophthalmol* (2009) 37:503–5. doi: 10.1111/j.1442-9071.2009.02069.x
7. Egan KM, Gragoudas ES, Seddon JM, Glynn RJ, Munzenreider JE, Goitein M, et al. The Risk of Enucleation After Proton Beam Irradiation of Uveal Melanoma. *Ophthalmology* (1989) 96:1377–82. doi: 10.1016/S0161-6420(89)32738-2
8. Foss A, Whelehan I, Hungerford J, Anderson D, Errington R, Kacperek A, et al. Predictive Factors for the Development of Rubeosis Following Proton Beam Radiotherapy for Uveal Melanoma. *Br J Ophthalmol* (1997) 81:748–54. doi: 10.1136/bjo.81.9.748
9. Fallico M, Raciti G, Longo A, Reibaldi M, Bonfiglio V, Russo A, et al. Current Molecular and Clinical Insights Into Uveal Melanoma (Review). *Int J Oncol* (2021) 58:10. doi: 10.3892/ijo.2021.5190
10. Kaliki S, Shields CL, Shields JA. Uveal Melanoma: Estimating Prognosis. *Indian J Ophthalmol* (2015) 63:93–102. doi: 10.4103/0301-4738.154367
11. Prescher G, Bornfeld N, Hirche H, Horsthemke B, Jöckel KH, Beche R. Prognostic Implications of Monosomy 3 in Uveal Melanoma. *Lancet* (1996) 347:1222–5. doi: 10.1016/S0140-6736(96)90736-9
12. Schoenfield L, Pettay J, Tubbs RR, Singh AD. Variation of Monosomy 3 Status Within Uveal Melanoma. *Arch Pathol Lab Med* (2009) 133:1219–22. doi: 10.5858/133.8.1219
13. Seedor RS, Orloff M, Sato T. Genetic Landscape and Emerging Therapies in Uveal Melanoma. *Cancers (Basel)* (2021) 13:5503. doi: 10.3390/cancers13215503
14. Parrella P, Caballero OL, Sidransky D, and Merbs SL. Detection of C-Myc Amplification in Uveal Melanoma by Fluorescent *In Situ* Hybridization. *Invest Ophthalmol Vis Sci* (2001) 42:1679–84.
15. Van Raamsdonk CD, Griewank KG, Crosby MB, Garrido MC, Vemula S, Wiesner T, et al. Mutations in GNA11 in Uveal Melanoma. *N Engl J Med* (2010) 363:2191–9. doi: 10.1056/NEJMoa1000584
16. Vivet-Noguer R, Tarin M, Roman-Roman S, and Alsafadi S. Emerging Therapeutic Opportunities Based on Current Knowledge of Uveal Melanoma Biology. *Cancers (Basel)* (2019) 11:E1019. doi: 10.3390/cancers11071019
17. Terai M, Shimada A, Chervoneva I, Hulse L, Danielson M, Swensen J, et al. Prognostic Values of G-Protein Mutations in Metastatic Uveal Melanoma *Cancers (Basel)* (2021) 13:5749.
18. Harbour JW, Roberson EDO, Anbunathan H, Onken MD, Worley LA, Bowcock AM. Recurrent Mutations at Codon 625 of the Splicing Factor SF3B1 in Uveal Melanoma. *Nat Genet* (2013) 45:133–5. doi: 10.1038/ng.2523
19. Hou C, Xiao L, Ren X, Tang F, Guo B, Zeng W, et al. Mutations of GNAQ, GNA11, SF3B1, EIF1AX, PLCB4 and CYSLTR in Uveal Melanoma in Chinese Patients. *Ophthalmic Res* (2020) 63:358–68. doi: 10.1159/000502888
20. Leeksma AC, Derks IAM, Haidar Kasem M, Kilic E, de Klein A, Jager MJ, et al. The Effect of SF3B1 Mutation on the DNA Damage Response and Nonsense-Mediated mRNA Decay in Cancer. *Front Oncol* (2020) 10:609409. doi: 10.3389/fonc.2020.609409
21. Hamard PJ, Santiago GE, Liu F, Karl DL, Martinez C, Man N, et al. Abstract 1137: PRMT5 Inhibition Regulates Alternative Splicing and DNA Damage Repair Pathways in SF3B1 R625G Expressing Uveal Melanoma Cells. *Cancer Res* (2021) 81:1137–7. doi: 10.1158/1538-7445.AM2021-1137

Conflict of Interest: The authors declare that the research was conducted in the absence of any commercial or financial relationships that could be construed as a potential conflict of interest.

frontiers | Frontiers in Oncology

REVIEW
published: 01 June 2022
doi: 10.3389/fonc.2022.856963

YY1 Is a Key Player in Melanoma Immunotherapy/Targeted Treatment Resistance

Dominika Kwiatkowska, Ewelina Mazur and Adam Reich *

Department of Dermatology, Institute of Medical Sciences, Medical College of Rzeszow University, Rzeszow, Poland

Malignant melanoma, with its increasing incidence and high potential to form metastases, is one of the most aggressive types of skin malignancies responsible for a significant number of deaths worldwide. However, melanoma also demonstrates a high potential for induction of a specific adaptive anti-tumor immune response being one of the most immunogenic malignancies. Yin Yang 1 (YY1) transcription factor is essential to numerous cellular processes and the regulation of transcriptional and posttranslational modifications of various genes. It regulates programmed cell death 1 (PD1) and lymphocyte-activation gene 3 (LAG3) by binding to its promoters, as well as suppresses both Fas and TRAIL by negatively regulating DR5 transcription and expression and interaction with the silencer region of the Fas promoter, rendering cells resistant to apoptosis. Moreover, YY1 is considered a master regulator in various stages of embryogenesis, especially in neural crest stem cells (NCSCs) survival and proliferation as it acts as transcriptional repressor on cancer stem cells-related transcription factors. In addition, YY1 increases the metastatic potential of melanoma through negative regulation of microRNA-9 (miR-9) expression, acts as a cofactor of transcription factor EB (TFEB) and contributes to autophagy regulation, mainly due to increased transcription of genes related to autophagy and lysosome biogenesis. Therefore, focusing on the detailed biology and administration of therapies that directly target YY1 or crosstalk pathways in malignant melanoma could facilitate the development of new and more effective treatment strategies and improve patients' outcomes.

Keywords: malignant melanoma, immunotherapy, treatment resistance, YY1, PD1

OPEN ACCESS

Edited by:
Stéphane Terry,
Institut Gustave Roussy, France

Reviewed by:
Sivakumar Vallabhapurapu,
Indian Institute of Science Education and Research, Tirupati, India
Benjamin Bonavida,
University of California, Los Angeles, United States
William J. Magner,
University at Buffalo, United States

***Correspondence:**
Adam Reich
adamandrzejreich@gmail.com

Specialty section:
This article was submitted to Molecular and Cellular Oncology, a section of the journal Frontiers in Oncology

Received: *01 February 2022*
Accepted: *25 April 2022*
Published: *01 June 2022*

Citation:
Kwiatkowska D, Mazur E and Reich A (2022) YY1 Is a Key Player in Melanoma Immunotherapy/ Targeted Treatment Resistance. Front. Oncol. 12:856963. doi: 10.3389/fonc.2022.856963

INTRODUCTION

Malignant melanoma is one of the most aggressive types of skin malignancy, presenting high potential to form metastases. The incidence of melanoma has significantly increased all over the world within the last decades (1). Many factors can contribute to the malignant transformation of melanocytes and melanocytic lesions, among which one can distinguish a complex interaction between environmental and genetic factors (2). Oncogenic mutations in genes are widely observed in melanoma, with MEK, BRAF, NRAS, and NF1 being the most common ones (2).

The first step of the therapeutic management of cutaneous melanoma is surgical excision of the primary lesion with adequate margins. In a case of melanoma *in situ* or very thin melanomas (<0.8 mm), surgery is considered sufficient, whereas patients with more advanced stages often require adjuvant therapy (3). Malignant melanoma is a neoplasm which often shows resistance to standard cytotoxic treatments. However, it demonstrates a high potential for induction of a specific adaptive anti-tumor immune response being one of the most immunogenic malignancies (4). In recent years, the knowledge regarding the molecular biology of malignant melanoma has been expanding, and, thus, a huge progress in the field of immunotherapy (with its many innovative therapeutics) in the treatment of malignant melanoma has been observed. However, achieving disease remission or at least stabilization in patients with poor response to immunotherapy is almost impossible. Therefore, a better understanding of processes by which malignant cells evade immune surveillance is needed to increase treatment efficacy or reverse resistance. Recently, the possible role of the Yin Yang 1 (YY1) transcription factor in the pathogenesis and drug resistance of malignant melanoma is considered.

YY1, also known as a nuclear factor-E1 (NF-E1), is a GLI-Kruppel class of zinc finger protein transcription factors (5). YY1 is ubiquitously expressed, and its expression is on the same level within all tissues of the human body (6). This multifunction protein is essential to numerous cellular processes and the regulation of transcriptional and posttranslational modifications of various genes (7–9). The transcription factor YY1 has been studied in many cancers. To date, it was shown that YY1 exerts a role in tumorigenesis, mainly through alteration in cell cycle signaling pathways, the process of epithelial-mesenchymal transition, resistance to immunotherapy and targeted therapy, as well as the formation of metastasis (10–13). Moreover, the role of YY1 in modulating chronic inflammation, apoptosis evasion, angiogenesis, and genome instability have been previously described in the literature (14–16).

In the present review, we have highlighted the importance of the overexpression of the transcription factor YY1 in malignant melanoma tumorigenesis and its possible role in tumor surveillance and treatment resistance.

THE STRUCTURE AND FUNCTION OF YIN YANG 1 PROTEIN

The human YY1 consists of 414 amino acids and was first described as a transcriptional repressor that interacts with the P5 promoter for the adeno-associated virus (5, 17). However, YY1 can either positively or negatively regulate its target genes, acting as both a transcriptional activator and repressor. YY1 recognizes and binds to specific DNA sequences through the four zincs fingers, forming the DNA-binding domain (18). Both DNA binding-dependent and independent functions of YY1 have been already described. A recent study showed that YY1 also controls gene expression by binding to active enhancers and promoter-proximal elements (19). Furthermore, the pattern of this control varies due to the many interactions with versatile proteins. YY1 can also act indirectly, by affecting the chromatin state *via* the recruitment of histone methylases, acetylases, and deacetylases (20–22). These findings could enlighten the variety of YY1's functions including gene activation and repression. YY1 might impact positive or negative effects on transcription by influencing the positioning of other transcription factors in enhancers and promoters.

YY1 AND IMMUNE CELLS

The expression of YY1 influences the development of B and T cells on every stage (23). Germinal centers are vitally important for humoral immunity. During germinal center development, B cells depend strictly on YY1 expression (24). It was shown that the deletion of the YY1 gene reduces the amount of germinal center B cells and decreases survival. Interestingly, YY1 possesses dual functions, either as an activator or repressor. YY1 induces Th2 cells differentiation and, contrarily, blocks Treg cell differentiation and function. To control Th2 cytokine genes, YY1 mediates chromatin remodeling and chromosomal lopping of the Th2 cytokine locus (25). The primary function of Treg cells is the prevention of excessive immune response through inhibition of differentiation and proliferation of other T cells subpopulations, such as Th1, Th2, Th17, and Tfh cells (26). YY1 inhibits the differentiation and function of Treg cells by blocking Foxp3 – a transcription factor for Treg cells (27). Since melanomas are infiltrated by large numbers of Tregs to evade immune response, downregulation of the Treg cells' function in tumor microenvironment may enhance protective immunity against this cancer. On the other hand, the YY1 seems to promote T cell exhaustion by repressing IL-2 and upregulating checkpoint inhibitors. Exploring the exact role of YY1 on the molecular riddles of the melanoma microenvironment may shed light on new and better treatment strategies against this cancer.

MALIGNANT MELANOMA EVADES AND INHIBITS IMMUNE RESPONSES

Malignant melanoma may evade the host's cellular regulatory and immune system. Chronic inflammation can lead to exhaustion of the immune system, and inhibitory receptors and their ligands play a crucial role in this process (28). The persistent antigen exposure by melanoma cells is dependent on the up-regulation of immune checkpoints, such as programmed cell death 1 (PD1), cytotoxic T lymphocyte antigen 4 (CTLA4), T-cell immunoglobulin, and mucin-domain containing-3 (TIM3) or lymphocyte-activation gene 3 (LAG3) and results in negative feedback for the cytotoxic T-cells. Thus, blocking the different immune checkpoints has become a cornerstone of modern immunotherapy and the usefulness of CTLA-4, PD-1 and PD-L1/2 blockers in advanced melanoma therapy has been most widely studied to date (29, 30). However, there is still a large

group of patients in whom treatment with checkpoint inhibitors proved to be unsuccessful. In addition, prolonged treatment with the same medication could potentially lead to cross-resistance to a variety of therapies.

REGULATION OF PD1 AND LAG3 BY YY1

Interestingly, YY1 regulates PD1 and LAG3 by binding to the promoters of PD1 and LAG3. In the study provided by Balkhi et al. (31), mutation of the YY1's binding sites elicits increased transcription with repeat T-cell stimulation, which proves that both PD1 and LAG3 are positively regulated by YY1 (**Figure 1**). In melanoma, functional exhaustion with increased fractions of PD1+ CD4 cells were found to be associated with a high level of YY1. On the other hand, downregulation of YY1 in repeatedly stimulated cells causes a reduction of PD1 and LAG3. Moreover, in the aforementioned study, 15 human melanoma samples and 10 normal skin biopsies were examined. Exhaustion of tumor-infiltrating lymphocytes was mostly tied with overexpression of PD1, along with YY1-cofactor Ezh2. In normal skin, no exhaustion markers were found. Human melanoma sections stained by immunofluorescence showed activation of the p38MAPK/JNK pathway in tumor-infiltrating lymphocytes, which drives YY1 expression, leading to PD1 upregulation. These findings significantly improved our knowledge of the relevance of T-cell activation through a p38MAPK/JNK/YY1 pathway.

The specific tumor microenvironment uses several mechanisms to defend itself from cell death mediated by cytotoxic T-cells (32). One of them is an upregulation of PD-L1 expression. Multiple pathways have been identified by which YY1 could be involved in regulating PD-L1 expression. Recent findings indicate that therapies directly targeting YY1 or cross talk pathways could improve patients' outcomes due to the downregulation of PD-L1 expression on tumor cells.

YY1 REGULATES DRUG RESISTANCE IN MELANOMA

During tumorigenesis, pathways that regulate cell survival and apoptosis, become dysregulated. Bonavida et al. proposed a model of a dysregulated circuit consisting of the NF-κB/Snail/YY1/PTEN/RKIP loop, which may be crucial for melanoma cell growth, survival, and drug resistance (33, 34). Upon activation, the NF-κB signaling pathway (via autophagosomes, p62 and JNK signaling leading to the expression of their target genes HIF-1α, IL-8, BCL2 and BCLXL) regulates the transcription of YY1 and Snail 1 (35). In response to stimulation, these target genes further negatively regulate the phosphatase, and tensin homolog (PTEN), and RKIP which in turn activates the AKT/mTOR-C1 pathway and its interaction with LC3. Contrarily, the induction of RKIP downregulates NF-κB signaling and thus inhibits YY1 and Snail 1. At the same time, the expression of PTEN inhibits the PI3K/AKT (phosphoinositide-3-kinase/AKT) pathway (**Figure 2**) leading to a significant inhibition of AKT-mediated

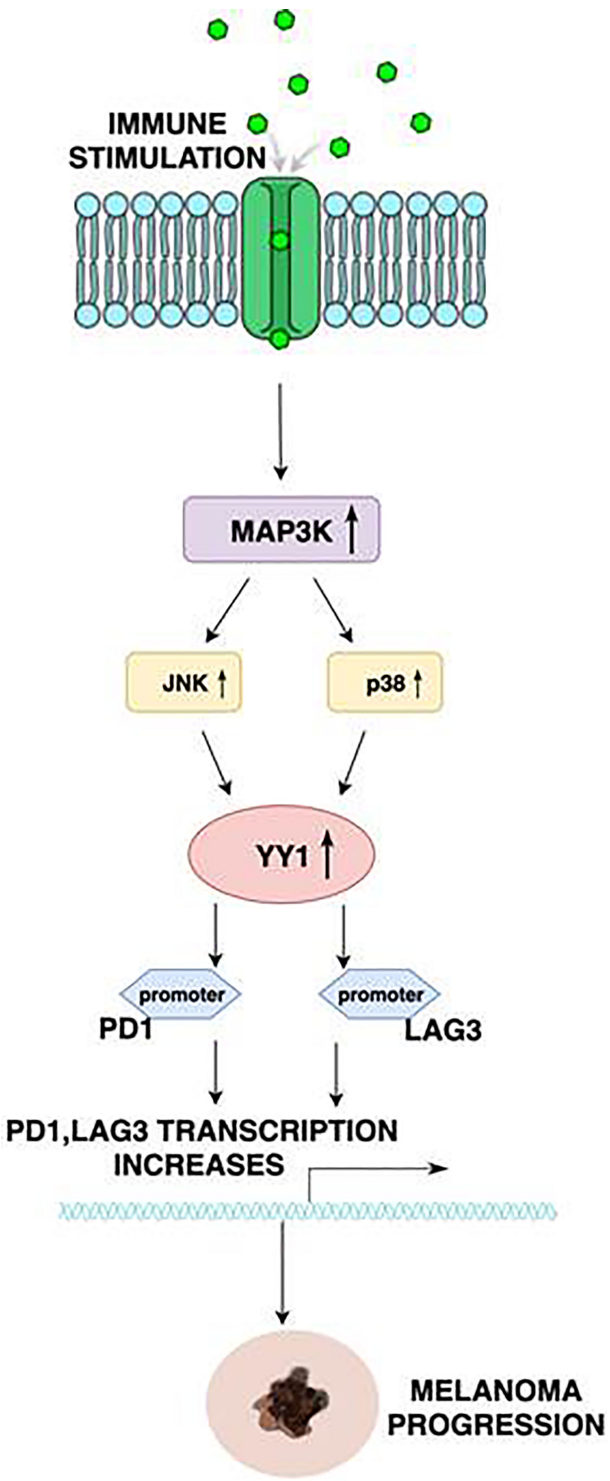

FIGURE 1 | Schematic diagram illustrating the regulation of PD1 and LAG3 by YY1. Stimulation of receptors on the immune cells results in the activation of the MAP3K, leading to the upregulation of JNK and p38. p38 and JNK, in turn, activate YY1. YY1 bind to the PD1 and LAG3 promoters to initiate transcription. This mechanism is correlated with the exhaustion of tumor infiltrating T lymphocytes, and thus assists melanoma progression.

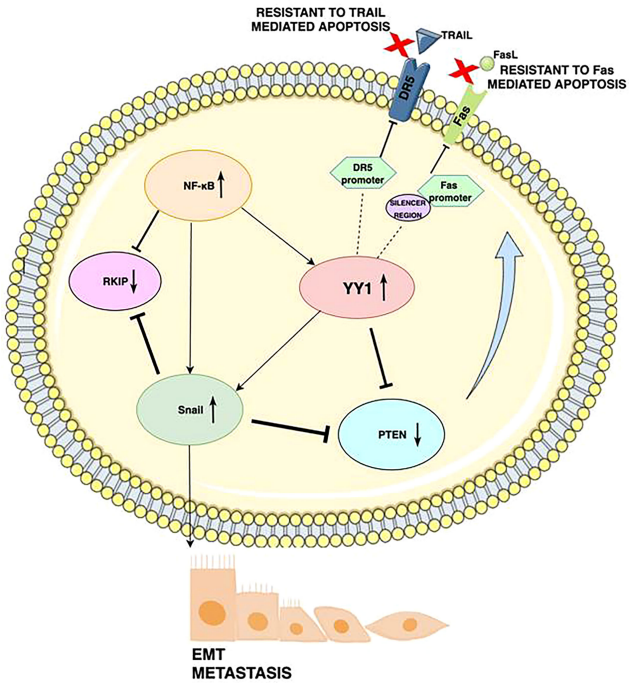

FIGURE 2 | Schematic diagram illustrating the mechanism by which YY1 regulates drug resistance in cancers: Activation of the YY1 negatively regulates DR5 transcription by binding to the DR5 promoter region, which elicits resistance to TRAIL-induced apoptosis. YY1 binds to the silencer region of the Fas promoter, blocks Fas expression and further leads to downregulation of Fas expression and resistance of cancerous cells to Fas-mediated apoptosis. High NF-kB expression corresponds to low RKIP expression, as well as NF-kB induces YY1 expression, which then represses PTEN. The underexpression of Fas is also caused by NF-κB's activation of YY1. YY1 induces SNAIL, the repressor of RKIP. Expression of YY1 and Snail is participating in downregulation of PTEN and DR5. As a result, YY1 promotes epithelial to mesenchymal transition (EMT) and metastasis through upregulation of Snail.

signaling pathway, but also to autophagy proteins such as LC3-I/II, LAMP, cathepsin B, and PI3K-AKT-MTOR. Increased PI3K/AKT activity appears to have a major role in resistance to BRAF inhibitors (36).

The regulation of various processes in cancer cells is strongly dependent on the different expression levels of each of the gene products. There is evidence revealing that YY1 is involved in melanoma resistance to apoptosis (37, 38). The extrinsic pathway of apoptosis involves death ligands on the surface of cytotoxic cells, which bind corresponding receptors on target cells. The molecular pathways by which Fas and TRAIL activate both the extrinsic and intrinsic apoptosis pathways have been well characterized (39). However, the exact mechanisms of resistance to TRAIL and Fas have not yet been fully elucidated. YY1 may play a role in this process, as YY1 can suppress both Fas and TRAIL, rendering cells resistant to apoptosis. Expression of Fas is negatively regulated by the interaction of YY1 with the silencer region of the Fas promoter (40). In another mechanism, YY1 negatively regulates DR5 transcription and expression, inducing resistance to TRAIL-induced apoptosis (41). Fas and TRAIL-mediated apoptosis can be restored by inhibiting YY1, which can reverse the resistance to many drugs.

The studies of new and more effective treatment strategies for melanoma are of great interest as still many patients with advanced melanomas demonstrate poor outcomes. As already mentioned, YY1 strongly contributes to the pathogenesis of this malignancy. The research above describes numerous melanoma oncogenes, several of which seem to be a good target for future therapies. Patients with melanoma may benefit from the inhibition of EMT. This approach aims to target miRNAs to downregulate YY1 expression and result in the inhibition of EMT in cancer cells (42). Previous findings demonstrated that YY1 is inhibited by nitric oxide. In the NF-κB/SNAIL/YY1/RKIP/PTEN loop, nitric oxide donors downregulate YY1 through S-nitrosylation and subsequently lead to inhibition of EMT. Inhibiting YY1 by nitric oxide may also sensitize melanoma cells to immunotherapies, like Fas-L, TRAIL, and anti-PDL1-dependent treatment (32, 41, 43). Moreover, YY1 activity is reduced significantly by rituximab, which results in up-regulation of Fas-induced apoptosis. Therefore, combined treatment with YY1 inhibitors may help overcome the problem of tumor cells' resistance (39). Finally, YY1 promotes melanoma angiogenesis, acting as a positive regulator of VEGF. A therapeutic intervention involving this mechanism may reduce neoangiogenesis and tumor growth

Still, many questions arise regarding the exact role of YY1 in melanoma pathogenesis, progression, and drug resistance. A deeper characterization of YY1 molecular pathways of action may help define novel biomarkers useful in the prognosis of melanoma.

YY1 AND CANCER STEM CELLS

Malignant melanoma originates from differentiated melanocytes that arise from neural crest stem cells (NCSCs) (44). However, a multitude of biochemical data suggests that it could also originate from cancer stem cells (CSCs) called tumor-initiating cells (TICs). CSCs are pluripotent cells with self-renewal potential, allowing cell proliferation without losing its differentiation potential. They are proved to be associated with worse clinical outcomes. The multilineage differentiation abilities can contribute to melanoma diversity and heterogeneity (45, 46). Assuming that melanoma formation is related to the CSC population, identifying molecular targets in these cells could help to provide new treatment modalities. It seems that YY1 may be associated with melanoma CSCs.

Overexpression of many transcription factors such as SRY-Box Transcription Factor 2 (SOX2), octamer-binding transcription factor 4 (OCT4), B lymphoma Mo-MLV insertion region 1 homolog (BMI1), and Nanog Homeobox protein (NANOG) have been identified as key players in CSCs-related tumor initiation and metastasis formation. Interestingly, YY1 expression may also depend on Sox2, OCT4, BMI1, and NANOG's activities (47). The study by Kaufhold et al. (47) has identified YY1 as a possible transcriptional repressor that acts on CSCs-related transcription factors. The correlation between expression levels of YY1 and Sox2 was observed among all cancer types. Subsequently, the four groups

of cancers were distinguished. The highest expression of YY1 and Sox2 proteins represented the group assembled by melanoma, colorectal cancer, and lymphomas. In addition, the study showed the presence of putative YY1 binding sites on all regulatory regions of the transcription factors. However, none of the putative transcription binding sites for BMI1, SOX2, and OCT4 were found on the YY1 or each other's regulatory regions, suggesting a multi-dynamic regulatory control of expression.

The invasiveness of malignant melanoma is attributed by some authors to SOX2 overexpression. Conversely, recent studies revealed that malignant melanoma initiation and progression are not affected by complete inhibition of SOX2 function (48). It can be explained by different study designs, as well as the aforementioned melanoma heterogeneity. Another set of data suggests that melanoma formation *in vitro* and *in vivo* is counteracted by the inactivation of neural crest stem cell factor SOX10. Furthermore, a subset of genes bound by YY1 is also co-bound by SOX10, which strongly suggests a connection between YY1-dependent metabolic processes and SOX10 (48). YY1 is considered a master regulator in various stages of embryogenesis, especially in NCSCs survival and proliferation.

YY1 plays a crucial role in metabolic reprogramming that converts a normal melanocyte into a melanoma-competent cell. This transition is achieved *via* binding and regulation of a subset of genes responsible for glucose metabolism, mitochondrial electron transfer chain, tricarboxylic acid cycle, one carbon metabolism, nucleotide metabolism, and protein synthesis. Varum et al. have found that the loss of YY1 leads to, among others, a reduction in basal oxygen consumption rates, maximal respiratory capacity, and ATP turnover, essential for cancer proliferation. These findings were especially expressed in melanoma cells, suggesting their particular sensitiveness to YY1 knockdown. They also reported that YY1 not only co-binds in different combinations with SOX10 and MITF (Melanocyte Inducing Transcription Factor) but also controls a MITF and c-MYC-regulated gene set. Therefore, it affects cancer stem cells metabolism in melanoma (49, 50).

THE ROLE OF YY1 IN TUMOR ANGIOGENESIS

Angiogenesis is crucial in the growth of various cancers, including malignant melanoma. This process allows to supply nutrients and oxygen to tumor cells. Studies have shown that without angiogenesis, the growth of a tumor larger than 1 mm is restricted, as diffusion of oxygen from blood vessels is not sufficient (51). To date, the family of vascular endothelial growth factors (VEGFs) turned out to be the major mediator of tumor angiogenesis. VEGF family consists of structurally related molecules including VEGF-A, VEGF-B, VEGF-C, VEGF-D, among which VEGF-A is typically referred to as VEGF (52). Through interaction with the VEGF receptor (VEGFR), VEGF promotes endothelial cell proliferation, which further mediates sprouting of angiogenesis. YY1 may participate in this process through positive regulation of VEGF transcription (53, 54). Moreover, YY1 regulates the increase of VEGF by suppressing HIF-1α proteasomal degradation which causes its accumulation (**Figure 3**). HIF-1α plays a pivotal role in the adaptation of cancer cells to hypoxia, as well as promotes tumor angiogenesis through contribution to endothelial cell proliferation and migration (55). A fraction of cells that can survive hypoxia exhibit a more invasive phenotype and refraction to anticancer therapies. In another mechanism, YY1 can influence tumor angiogenesis by increasing the expression of angiopoietin factors ANG-1 and ANG-2, which are mediators of microvascular remodeling and capillary maturation (**Figure 3**). Current findings suggest that YY1 regulates the expression of angiogenic genes that are critical for proper vascular development and maintaining homeostasis. The study conducted by Zhang et al. showed that endothelial cell specific YY1 deletion in mice causes embryonic lethality due to abnormal angiogenesis (56). Extensive research also revealed that YY1 deletion in the tamoxifen-inducible endothelial cell-specific YY1 deficient mouse model inhibited angiogenesis and the melanoma growth (57). A high level of YY1 expression was noted in tumor cells and tumor-associated endothelial cells in human melanoma tissues. These findings suggest that silencing endothelial YY1 could decline melanoma angiogenesis and thus can be a potential effective treatment option. Future research should focus on the usefulness of nitric oxide and rituximab to decrease tumor angiogenesis, as those drugs can potentially inhibit YY1 expression (39, 40).

YY1 AND MELANOMA METASTASIS

Tumor metastasis is an intricate process involving various signaling pathways. Genetic alterations enable the cancer cells to acquire the

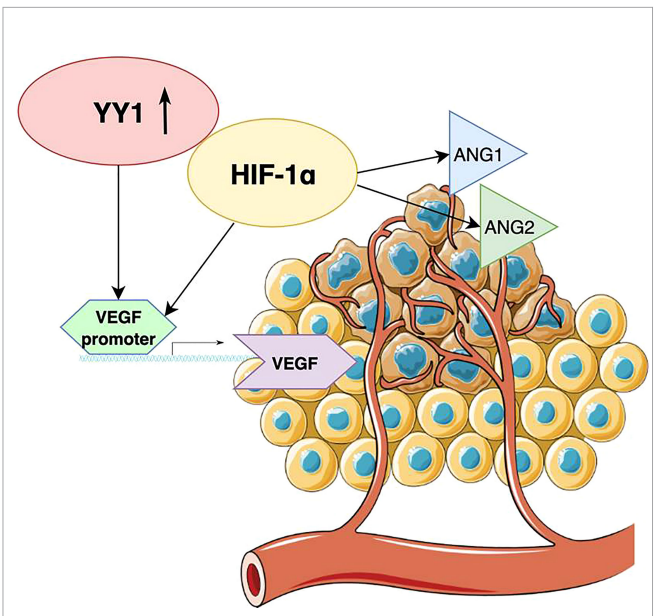

FIGURE 3 | Schematic diagram illustrating the role of YY1 in tumor angiogenesis. YY1 regulates the increase of VEGF by suppressing HIF-1α, which also upregulates the expression of angiopoietin factors ANG-1 and ANG-2.

biological properties essential for forming distinct metastasis. Zhao et al. discovered that YY1 increases the metastatic potential of melanoma through negative regulation of microRNA-9 (miR-9) expression (58). MiR-9 acts as a NF-κB-Snail1 pathway suppressor, therefore, inhibits migration and invasion of malignant melanoma cells (59, 60). MiR-9 directly binds to RING1 and YY1 binding protein (RYBP) 3′ untranslated region (3'UTR), thus leading to mRNA degradation. These findings demonstrated a potential role of RYBP as an oncogene by identification of a novel and vital YY1 ~ miR-9 ~ RYBP axis (58).

YY1 expression is closely related to tumor metastasis. YY1 directly binds the snail 3' enhancer, which regulates snail transcription. To change the chromatin structure of the 3' enhancer, YY1 participates in the recruitment of histone modification enzymes. It is well known that the migratory capacity of cancers is defined by snail overexpression. The regulation of the Snail gene is crucial for the epithelial-mesenchymal transitions (EMT), a process in which epithelial cells acquire invasive properties by transformation into migrating mesenchymal cells. EMT is essential for cancer invasiveness. As mentioned before, YY1 is an integral part of the NF-κB/Snail/YY1/RKIP axis, which in turn is the positive EMT regulator. However, the exact regulation of the *Snail* gene by the YY1 is not yet fully understood.

YY1 AND AUTOPHAGY

The importance of autophagy in the regulation of cancer cell biology and its response to various therapies is now intensively investigated. Autophagy is an intracellular degradative process. This mechanism requires the formation of autophagosomes and then fusion with lysosomes. Some studies to date have shown that the resistance of cancer cells to anticancer drugs can increase through the upregulation of autophagy (61, 62). It was recently introduced that YY1 acts as a cofactor of TFEB and contributes to autophagy regulation, mainly due to increased transcription of genes related to autophagy and lysosome biogenesis (63, 64). These authors also investigated whether YY1 mediated autophagy could modulate the activity of one of the commonly used in melanoma patients BRAF inhibitors – vemurafenib (63). Interestingly, the research showed that suppression of YY1 contributes to increased antitumor efficacy of vemurafenib (63).

Therefore, YY1 directs the apoptosis-anti-apoptosis balance in favor of tumor cells survival, protecting the cells from damage and activating autophagy-mediated survival (65). Protein kinase inhibitor - sorafenib was shown to block human receptor tyrosine kinase (c-Kit), platelet-derived growth factor receptor (PDGFR), vascular endothelial growth factor receptor (VEGFR), BRAF, and c-RAF signaling pathways both *in vitro* and *in vivo*. It prevents the tumor growth of hepatocellular, breast, and pancreatic cancer types and suppresses tumor growth and metastasis in melanoma by c-Kit inhibition (66). Interestingly, sorafenib may sensitize melanoma to vemurafenib through activation of oxidative stress (upregulated reactive oxygen species production, malondialdehyde, and iron, but decreased glutathione concentration). Moreover, sorafenib strongly promoted vemurafenib-mediated cell death (67).

YY1 AS A PROGNOSTIC MARKER OF MELANOMA

YY1 is characterized by a multifunctional mechanism of action, as it can act as an initiator, activator, or repressor of transcription. Increased levels of YY1 have been observed in both primary and metastatic melanoma (58). The overexpression of YY1 might be associated with melanoma progression, as it is involved in many biological processes, including modulation of the immune response, apoptosis, epithelial to mesenchymal transition, angiogenesis, and metastasis formation. Given that YY1 is essential for many biological processes, it may be an interesting prognostic target for melanoma.

Bioinformatics analyses on the expression of YY1 in melanomas seem to confirm the relevant role of this transcription factor in melanoma development and progression (68). It was revealed that an increased level of YY1 positively correlates with mRNA expression of the nectin like molecule-5 (*NECL-5*) gene (69). NECL-5 is a cell adhesion molecule, the decrease of which reduces migration, proliferation, and metastasis of cancer cells. The study conducted by Bevelacqua et al. suggests that NECL-5 may be a potential marker of melanoma progression (69). Additional bioinformatics studies also suggested an association between YY1 and MITF in melanoma progression (70). MITF activity strongly influences the phenotype of melanoma cells and determines its invasiveness (70). YY1 is one of the transcription factors that regulate MITF-dependent genes. Moreover, both MITF and YY1 are localized in the area of promoters of genes important in melanocyte differentiation. Besides MITF, transcription factor activator protein 2 A (TFAP2A) and SOX10 have also been identified to be localized alongside YY1. Furthermore, MITF interacts with PBAF (polybromo-associated BRG1/BRM-associated factor) chromatin remodelling complex comprising BRG1 and CHD7 (chromodomain helicase DNA binding protein 7) (71). BRG1 is essential for melanoma cell proliferation *in vitro* and for normal melanocyte development *in vivo* and combinations of MITF, SOX10, TFAP2A, and YY1 bind between two BRG1-occupied nucleosomes thus defining both a signature of transcription factors essential for the melanocyte lineage and a specific chromatin organization of the regulatory elements they occupy (71). Finally, recently published data of genome wide association study identified about 20 melanoma susceptibility loci, one of which was *MX2* – the HIV-1 restriction gene (72). It was shown that the level of *MX2* expression is critically mediated by YY1 further underlying the role of YY1 in melanoma (72).

However, still many questions arise regarding the exact role of YY1 in melanoma pathogenesis, progression, and drug resistance. A deeper characterization of YY1 molecular pathways of action may help to define novel biomarkers useful in melanoma prognosis. Future studies must investigate those molecular pathways to find more putative targets to develop innovative therapeutic approaches.

CONCLUSIONS

In summary, YY1 seems to play a crucial role in many of the metabolic processes. Therefore, focusing on the detailed biology and administration of therapies that directly target YY1 or crosstalk pathways in malignant melanoma could facilitate the development of new and more effective treatment strategies and improve patients' outcomes.

AUTHOR CONTRIBUTIONS

DK and AR contributed to the conception and design of the study. DK and EM performed the literature search. DK and EM wrote the first draft of the manuscript. AR finalized the manuscript. All authors contributed to manuscript revision, read, and approved the submitted version.

REFERENCES

1. Siegel RL, Miller KD, Fuchs HE, Jemal A. Cancer Statistics, 2021. *CA Cancer J Clin* (2021) 71:7–33. doi: 10.3322/caac.21654
2. Bandarchi B, Jabbari CA, Vedadi A, Navab R. Molecular Biology of Normal Melanocytes and Melanoma Cells. *J Clin Pathol* (2013) 66:644–8. doi: 10.1136/jclinpath-2013-201471
3. Garbe C, Amaral T, Peris K, Hauschild A, Arenberger P, Bastholt L, et al. European Consensus-Based Interdisciplinary Guideline for Melanoma. Part 1: Diagnostics - Update 2019. *Eur J Cancer* (2020) 126:141–58. doi: 10.1016/j.ejca.2019.11.014
4. Passarelli A, Mannavola F, Stucci LS, Tucci M, Silvestris F. Immune System and Melanoma Biology: A Balance Between Immunosurveillance and Immune Escape. *Oncotarget* (2017) 8:106132–42. doi: 10.18632/oncotarget.22190
5. Shi Y, Seto E, Chang LS, Shenk T. Transcriptional Repression Byyy1, a Human GLI Kruppel-Related Protein, and Relief of Repression by Adenovirus E1A Protein. *Cell* (1991) 67:377–88. doi: 10.1016/0092-8674(91)90189-6
6. Austen M, Luscher B, Luscher-Firzlaff JM. Characterization of the Transcriptional Regulator YY1. The Bipartite Transactivation Domain Is Independent of Interaction With the TATA Box Binding Protein, Transcription Factor IIB, TAFII55, or cAMP-Responsive Element-Binding Protein (CPB)-Binding Protein. *J Biol Chem* (1997) 272:1709–17. doi: 10.1074/jbc.272.3.1709
7. Kim JD, Yu S, Kim J. YY1 Is Autoregulated Through Its Own DNA-Binding Sites. *BMC Mol Biol* (2009) 10:85. doi: 10.1186/1471-2199-10-85
8. Yao YL, Yang WM, Seto E. Regulation of Transcription Factor YY1 by Acetylation and Deacetylation. *Mol Cell Biol* (2001) 21:5979–91. doi: 10.1128/MCB.21.17.5979-5991.2001
9. Atchison M, Basu A, Zaprazna K, Papasani M. Mechanisms of Yin Yang 1 in Oncogenesis: The Importance of Indirect Effects. *Crit Rev Oncog* (2011) 16:143–61. doi: 10.1615/CritRevOncog.v16.i3-4.20
10. Shi Y, Lee JS, Galvin KM. Everything You Have Ever Wanted to Know About Yin Yang 1. *Biochim Biophys Acta* (1997) 1332:F49–66. doi: 10.1016/S0304-419X(96)00044-3
11. Gordon S, Akopyan G, Garban H, Bonavida B. Transcription Factor YY1: Structure, Function, and Therapeutic Implications in Cancer Biology. *Oncogene* (2006) 25:1125–42. doi: 10.1038/sj.onc.1209080
12. Donohoe ME, Zhang X, McGinnis L, Biggers J, Li E, Shi Y. Targeted Disruption of Mouse Yin Yang 1 Transcription Factor Results in Peri-Implantation Lethality. *Mol Cell Biol* (1999) 19:7237–44. doi: 10.1128/MCB.19.10.7237
13. Cho AA, Bonavida B. Targeting the Overexpressed YY1 in Cancer Inhibits EMT and Metastasis. *Crit Rev Oncog* (2017) 22:49–61. doi: 10.1615/CritRevOncog.2017020473
14. Meliala ITS, Hosea R, Kasim V, Wu S. The Biological Implications of Yin Yang 1 in the Hallmarks of Cancer. *Theranostics* (2020) 1:4183–200. doi: 10.7150/thno.43481
15. Sarvagalla S, Kolapalli SP, Vallabhapurapu S. The Two Sides of YY1 in Cancer: A Friend and a Foe. *Front Oncol* (2019) 9:1230. doi: 10.3389/fonc.2019.01230
16. Wang W, Li D, Sui G. YY1 Is an Inducer of Cancer Metastasis. *Crit Rev Oncog* (2017) 22:1–11. doi: 10.1615/CritRevOncog.2017021314
17. Kim JD, Faulk C, Kim J. Retroposition and Evolution of the DNA Binding Motifs of YY1, YY2 and REX1. *Nucleic Acids Res* (2007) 35:3442–52. doi: 10.1093/nar/gkm235
18. Wai DC, Shihab M, Low JK, Mackay JP. The Zinc Fingers of YY1 Bind Single-Stranded RNA With Low Sequence Specificity. *Nucleic Acids Res* (2016) 44:9153–65. doi: 10.1093/nar/gkw590
19. Weintraub AS, Li CH, Zamudio AV, Sigova AA, Hannett NM, Day DS, et al. YY1 Is a Structural Regulator of Enhancer-Promoter Loops. *Cell* (2017) 171:1573–88.e1528. doi: 10.1016/j.cell.2017.11.008
20. Yang WM, Inouye C, Zeng Y, Bearss D, Seto E. Transcriptional Repression by YY1 Is Mediated by Interaction With a Mammalian Homolog of the Yeast Global Regulator RPD3. *Proc Natl Acad Sci* (1996) 93:12845–50. doi: 10.1073/pnas.93.23.12845
21. Lee JS, Galvin KM, See RH, Eckner R, Livingston D, Moran E, et al. Relief of YY1 Transcriptional Repression by Adenovirus E1A Is Mediated by E1A-Associated Protein P300. *Genes Dev* (1995) 9:1188–98. doi: 10.1101/gad.9.10.1188
22. Kim JD, Hinz AK, Bergmann A, Huang JM, Ovcharenko I, Stubbs L, et al. Identification of Clustered YY1 Binding Sites in Imprinting Control Regions. *Genome Res* (2006) 16:901–11. doi: 10.1101/gr.5091406
23. Kleiman E, Jia H, Loguercio S, Su AI, Feeney AJ. YY1 Plays an Essential Role at All Stages of B-Cell Differentiation. *Proc Natl Acad Sci* (2016) 113(27):E3911–20.x. doi: 10.1073/pnas.1606297113
24. Banerjee A, Sindhava V, Vuyyuru R, Jha V, Hodewadekar S, Manser T, et al. YY1 Is Required for Germinal Center B Cell Development. *PloS One* (2016) 11(5):e0155311. doi: 10.1371/journal.pone.0155311
25. Hwang SS, Kim YU, Lee S, Jang SW, Kim MK, Koh BH, et al. Transcription Factor YY1 Is Essential for Regulation of the Th2 Cytokine Locus and for Th2 Cell Differentiation. *Proc Natl Acad Sci* (2013) 110(1):276–81. doi: 10.1073/pnas.1214682110
26. Josefowicz SZ, Lu LF, Rudensky AY. Regulatory T Cells: Mechanisms of Differentiation and Function. *Annu Rev Immunol* (2012) 30:531–64. doi: 10.1146/annurev.immunol.25.022106.141623
27. Hwang SS, Jang SW, Kim MK, Kim LK, Kim BS, Kim HS, et al. YY1 Inhibits Differentiation and Function of Regulatory T Cells by Blocking Foxp3 Expression and Activity. *Nat Commun* (2016) 7:10789. doi: 10.1038/ncomms10789
28. Mahmoud F, Shields B, Makhoul I, Avaritt N, Wong HK, Hutchins LF, et al. Immune Surveillance in Melanoma: From Immune Attack to Melanoma Escape and Even Counterattack. *Cancer Biol Ther* (2017) 18:451–69. doi: 10.1080/15384047.2017.1323596
29. Seidel JA, Otsuka A, Kabashima K. Anti-PD-1 and Anti-CTLA-4 Therapies in Cancer: Mechanisms of Action, Efficacy, and Limitations. *Front Oncol* (2018) 8:86. doi: 10.3389/fonc.2018.00086
30. Kwiatkowska D, Kluska P, Reich A. Beyond PD-1 Immunotherapy in Malignant Melanoma. *Dermatol Ther (Heidelb)* (2019) 9:243–57. doi: 10.1007/s13555-019-0292-3
31. Balkhi MY, Wittmann G, Xiong F, Junghans RP. YY1 Upregulates Checkpoint Receptors and Downregulates Type I Cytokines in Exhausted, Chronically Stimulated Human T Cells. *Iscience* (2018) 2:105–22. doi: 10.1016/j.isci.2018.03.009
32. Hays E, Bonavida B. YY1 Regulates Cancer Cell Immune Resistance by Modulating PD-L1 Expression. *Drug Resist Update* (2019) 43:10–28. doi: 10.1016/j.drup.2019.04.001
33. Bonavida B, Baritaki S. Dual Role of NO Donors in the Reversal of Tumor Cell Resistance and EMT: Downregulation of the NF-κb/Snail/YY1/RKIP Circuitry. *Nitric Oxide* (2011) 24:1–7. doi: 10.1016/j.niox.2010.10.001
34. Bonavida B, Baritaki S. The Novel Role of Yin Yang 1 in the Regulation of Epithelial to Mesenchymal Transition in Cancer *via* the Dysregulated NF-κb/Snail/YY1/RKIP/PTEN Circuitry. *Crit Rev Oncog* (2011) 16:211–26. doi: 10.1615/CritRevOncog.v16.i3-4.50
35. Xia L, Tan S, Zhou Y, Lin J, Wang H, Oyang L, et al. Role of the Nfκb-Signaling Pathway in Cancer. *Onco Targets Ther* (2018) 11:2063–73. doi: 10.2147/OTT.S161109

36. Villanueva J, Vultur A, Lee JT, Somasundaram R, Fukunaga-Kalabis M, Cipolla AK, et al. Acquired Resistance to BRAF Inhibitors Mediated by a RAF Kinase Switch in Melanoma can be Overcome by Cotargeting MEK and IGF-1r/PI3K. *Cancer Cell* (2010) 18:683–95. doi: 10.1016/j.ccr.2010.11.023
37. Huerta-Yepez S, Vega M, Garban H, Bonavida B. Involvement of the TNF-Alpha Autocrine Paracrine Loop, *via* NF-KappaB and YY1, in the Regulation of Tumor Cell Resistance to Fas Induced Apoptosis. *Clin Immunol* (2006) 120:297–309. doi: 10.1016/j.clim.2006.03.015
38. Thomas WD, Hersey P. TNF-Related Apoptosis-Inducing Ligand (TRAIL) Induces Apoptosis in Fas Ligand-Resistant Melanoma Cells and Mediates CD4 T Cell Killing of Target Cells. *J Immunol* (1998) 161:2195–200.
39. Kumar R, Herbert PE, Warrens AN. An Introduction to Death Receptors in Apoptosis. *Int J Surg* (2005) 3:268–77. doi: 10.1016/j.ijsu.2005.05.002
40. Vega MI, Jazirehi AR, Huerta-Yepez S, Bonavida B. Rituximab-Induced Inhibition of YY1 and Bcl-xL Expression in Ramos Non-Hodgkin's Lymphoma Cell Line *via* Inhibition of NF-κb Activity: Role of YY1 and Bcl-xL in Fas Resistance and Chemoresistance, Respectively. *J Immun* (2005) 175:2174–83. doi: 10.4049/jimmunol.175.4.2174
41. Huerta-Yepez S, Vega M, Escoto-Chavez SE, Murdock B, Sakai T, Baritaki S, et al. Nitric Oxide Sensitizes Tumor Cells to TRAIL-Induced Apoptosis *via* Inhibition of the DR5 Transcription Repressor Yin Yang 1. *Nitric Oxide* (2009) 20:39–52. doi: 10.1016/j.niox.2008.08.001
42. Hosseinahli N, Aghapour M, Duijf PHG, Baradaran B. Treating Cancer With microRNA Replacement Therapy: A Literature Review. *J Cell Physiol* (2018) 233(8):5574–88. doi: 10.1002/jcp.26514
43. Hongo F, Garban H, Huerta-Yepez S, Vega M, Jazirehi AR, Mizutani Y, et al. Inhibition of the Transcription Factor Yin Yang 1 Activity by S-Nitrosation. *Biochem Biophys Res Commun* (2005) 336(2):692–701. doi: 10.1016/j.bbrc.2005.08.150
44. Shackleton M. Normal Stem Cells and Cancer Stem Cells: Similar and Different. *Semin Cancer Biol* (2010) 20:85–92. doi: 10.1016/j.semcancer.2010.04.002
45. Fang D, Nguyen TK, Leishear K, Finko R, Kulp AN, Hotz S, et al. A Tumorigenic Subpopulation With Stem Cell Properties in Melanomas. *Cancer Res* (2005) 65:9328–37. doi: 10.1158/0008-5472.CAN-05-1343
46. Brinckerhoff CE. Cancer Stem Cells (CSCs) in Melanoma: There's Smoke, But Is There Fire? *J Cell Physiol* (2017) 232:2674–8. doi: 10.1002/jcp.25796
47. Kaufhold S, Garbán H, Bonavida B. Yin Yang 1 Is Associated With Cancer Stem Cell Transcription Factors (SOX2, OCT4, BMI1) and Clinical Implication. *J Exp Clin Cancer Res* (2016) 35:84. doi: 10.1186/s13046-016-0359-2
48. Schaefer SM, Segalada C, Cheng PF, Bonalli M, Parfejevs V, Levesque MP, et al. Sox2 Is Dispensable for Primary Melanoma and Metastasis Formation. *Oncogene* (2017) 36:4516–24. doi: 10.1038/onc.2017.55
49. Varum S, Baggiolini A, Zurkirchen L, Atak ZK, Cantù C, Marzorati E, et al. Yin Yang 1 Orchestrates a Metabolic Program Required for Both Neural Crest Development and Melanoma Formation. *Cell Stem Cell* (2019) 24(4):637–53. doi: 10.1016/j.stem.2019.03.011
50. Martinez-Ruiz GU, Morales-Sanchez A, Pacheco-Hernandez AF. Roles Played by YY1 in Embryonic, Adult and Cancer Stem Cells. *Stem Cell Rev Rep* (2021) 17:1590–606. doi: 10.1007/s12015-021-10151-9
51. Kim JY, Lee JY. Targeting Tumor Adaption to Chronic Hypoxia: Implications for Drug Resistance, and How It Can Be Overcome. *Int J Mol Sci* (2017) 18:9. doi: 10.3390/ijms18091854
52. Ferrara N. VEGF and the Quest for Tumour Angiogenesis Factors. *Nat Rev Cancer* (2002) 2:795–803. doi: 10.1038/nrc909
53. deNigris F, Rossiello R, Schiano C, Arra C, Williams-Ignarro S, Barbieri A, et al. Deletion of Yin Yang 1 Protein in Osteosarcoma Cells on Cell Invasion and CXCR4/angiogenesis and Metastasis. *Cancer Res* (2008) 68:1797–808. doi: 10.1158/0008-5472.CAN-07-5582
54. Fu CY, Wang PC, Tsai HJ. Competitive Binding Between Seryl-tRNA Synthetase/YY1 Complex and NFKB1 at the Distal Segment Results in Differential Regulation of Human Vegfa Promoter Activity During Angiogenesis. *Nucleic Acids Res* (2017) 45:2423–37. doi: 10.1093/nar/gkw1187
55. LaGory EL, Giaccia AJ. The Ever-Expanding Role of HIF in Tumour and Stromal Biology. *Nat Cell Biol* (2016) 18:356–65. doi: 10.1038/ncb3330
56. Zhang S, Kim JY, Xu S, Liu H, Yin M, Koroleva M, et al. Endothelial-Specific YY1 Governs Sprouting Angiogenesis Through Directly Interacting With RBPJ. *Proc Natl Acad Sci USA* (2020) 117(9):4792–801. doi: 10.1073/pnas.1916198117
57. Liu H, Qiu Y, Pei X, Chitteti R, Steiner R, Zhang S, et al. Endothelial Specific YY1 Deletion Restricts Tumor Angiogenesis and Tumor Growth. *Sci Rep* (2020) 10:20493. doi: 10.1038/s41598-020-77568-z
58. Zhao G, Li Q, Wang A, Jiao J. YY1 Regulates Melanoma Tumorigenesis Through a MIR 9∈~∈RYBP Axis. *J Exp Clin Cancer Res* (2015) 34:66. doi: 10.1186/s13046-015-0177-y
59. Liu S, Kumar SM, Lu H, Liu A, Yang R, Pushparajan A, et al. MicroRNA-9 Up-Regulates E-Cadherin Through Inhibition of NF-κb1-Snail1 Pathway in Melanoma. *J Pathol* (2012) 226:61–72. doi: 10.1002/path.2964
60. Palmer MB, Majumder P, Cooper JC, Yoon H, Wade PA, Boss JM. Yin Yang 1 Regulates the Expression of Snail Through a Distal Enhancer. *Mol Cancer Res* (2009) 7:221–9. doi: 10.1158/1541-7786.MCR-08-0229
61. Bhutia SK, Mukhopadhyay S, Sinha N, Das DN, Panda PK, Patra SK, et al. Autophagy: Cancer's Friend or Foe? *Adv Cancer Res* (2013) 118:61–95. doi: 10.1016/B978-0-12-407173-5.00003-0
62. Chang H, Zou Z. Targeting Autophagy to Overcome Drug Resistance: Further Developments. *J Hematol Oncol* (2020) 13:159. doi: 10.1186/s13045-020-01000-2
63. Du J, Ren W, Yao F, Wang H, Zhang K, Luo M, et al. YY1 Cooperates With TFEB to Regulate Autophagy and Lysosomal Biogenesis in Melanoma. *Mol Carcinog* (2019) 58:2149–60. doi: 10.1002/mc.23105
64. Kwiatkowska D, Reich A. YY1 Is a Potential Key Player in the Pathogenesis of Malignant Melanoma. In: Bonavida B, editor. *YY1 in the Control of the Pathogenesis and Drug Resistance of Cancer*. London: Academic Press, Elsevier (2021). p. 163–9.
65. Meliala ITS, Hosea R, Kasim V, Wu S.12:47 pm 26/05/2022 The Biological Implications of Yin Yang 1 in the Hallmarks of Cancer. *Theranostics* (2020) 10:4183–200. doi: 10.7150/thno.43481
66. Takeda T, Tsubaki M, Kato N, Genno S, Ichimura E, Enomoto A, et al. Sorafenib Treatment of Metastatic Melanoma With C-Kit Aberration Reduces Tumor Growth and Promotes Survival. *Oncol Lett* (2021) 22:827. doi: 10.3892/ol.2021.13089
67. Tang F, Li S, Liu D, Chen J, Han C. Sorafenib Sensitizes Melanoma Cells to Vemurafenib Through Ferroptosis. *Transl Cancer Res* (2020) 9:1584–93. doi: 10.21037/tcr.2020.01.62
68. Bonavida B, Kaufhold S. Prognostic Significance of YY1 Protein Expression and mRNA Levels by Bioinformatics Analysis in Human Cancers: A Therapeutic Target. *Pharmacol Ther* (2015) 150:149–68. doi: 10.1016/j.pharmthera.2015.01.011
69. Bevelacqua V, Bevelacqua Y, Candido S, et al. Nectin Like-5 Overexpression Correlates With the Malignant Phenotype in Cutaneous Melanoma. *Oncotarget* (2012) 3:882–92. doi: 10.18632/oncotarget.594
70. Seberg HE, Van Otterloo E, Cornell RA. Beyond MITF: Multiple Transcription Factors Directly Regulate the Cellular Phenotype in Melanocytes and Melanoma. *Pigment Cell Melanoma Res* (2017) 30:454–66. doi: 10.1111/pcmr.12611
71. Laurette P, Strub T, Koludrovic D, Keime C, Le Gras S, Seberg H, et al. Transcription Factor MITF and Remodeller BRG1 Define Chromatin Organisation at Regulatory Elements in Melanoma Cells. *Elife* (2015) 4: e06857. doi: 10.7554/eLife.06857.025
72. Choi J, Zhang T, Vu A, Ablain J, Makowski MM, Colli LM, et al. Massively Parallel Reporter Assays of Melanoma Risk Variants Identify MX2 as a Gene Promoting Melanoma. *Nat Commun* (2020) 11:2718. doi: 10.1038/s41467-020-16590-1

Conflict of Interest: The authors declare that the research was conducted in the absence of any commercial or financial relationships that could be construed as a potential conflict of interest.

Publisher's Note: All claims expressed in this article are solely those of the authors and do not necessarily represent those of their affiliated organizations, or those of the publisher, the editors and the reviewers. Any product that may be evaluated in this article, or claim that may be made by its manufacturer, is not guaranteed or endorsed by the publisher.

frontiers | Frontiers in Oncology

ORIGINAL RESEARCH
published: 28 June 2022
doi: 10.3389/fonc.2022.904742

Mambalgin-2 Inhibits Lung Adenocarcinoma Growth and Migration by Selective Interaction With ASIC1/α-ENaC/γ-ENaC Heterotrimer

Anastasia V. Sudarikova[1,2†], Maxim L. Bychkov[1†], Dmitrii S. Kulbatskii[1†], Vladislav I. Chubinskiy-Nadezhdin[1,2], Olga V. Shlepova[1,3], Mikhail A. Shulepko[1], Sergey G. Koshelev[4], Mikhail P. Kirpichnikov[1,5] and Ekaterina N. Lyukmanova[1,3,5]*

[1] Laboratory of Bioengineering of Neuromodulators and Neuroreceptors, Shemyakin-Ovchinnikov Institute of Bioorganic Chemistry, Russian Academy of Sciences, Moscow, Russia, [2] Group of Ionic Mechanisms of Cell Signaling, Department of Intracellular Signaling and Transport, Institute of Cytology, Russian Academy of Sciences, St. Petersburg, Russia, [3] Phystech School of Biological and Medical Physics, Moscow Institute of Physics and Technology (National Research University), Dolgoprudny, Russia, [4] Laboratory of Neuroreceptors and Neuroregulators, Shemyakin-Ovchinnikov Institute of Bioorganic Chemistry, Russian Academy of Sciences, Moscow, Russia, [5] Interdisciplinary Scientific and Educational School of Moscow University «Molecular Technologies of the Living Systems and Synthetic Biology», Faculty of Biology, Lomonosov Moscow State University, Moscow, Russia

OPEN ACCESS

Edited by:
Nguan Soon Tan,
Nanyang Technological University, Singapore

Reviewed by:
Qiang Chen,
University of Macau, China
Mintu Pal,
All India Institute of Medical Sciences, India

***Correspondence:**
Ekaterina N. Lyukmanova
ekaterina-lyukmanova@yandex.ru

[†]These authors have contributed equally to this work and share first authorship

Specialty section:
This article was submitted to Molecular and Cellular Oncology, a section of the journal Frontiers in Oncology

Received: 25 March 2022
Accepted: 24 May 2022
Published: 28 June 2022

Citation:
Sudarikova AV, Bychkov ML, Kulbatskii DS, Chubinskiy-Nadezhdin VI, Shlepova OV, Shulepko MA, Koshelev SG, Kirpichnikov MP and Lyukmanova EN (2022) Mambalgin-2 Inhibits Lung Adenocarcinoma Growth and Migration by Selective Interaction With ASIC1/α-ENaC/γ-ENaC Heterotrimer. Front. Oncol. 12:904742. doi: 10.3389/fonc.2022.904742

Lung cancer is one of the most common cancer types in the world. Despite existing treatment strategies, overall patient survival remains low and new targeted therapies are required. Acidification of the tumor microenvironment drives the growth and metastasis of many cancers. Acid sensors such as acid-sensing ion channels (ASICs) may become promising targets for lung cancer therapy. Previously, we showed that inhibition of the ASIC1 channels by a recombinant analogue of mambalgin-2 from *Dendroaspis polylepis* controls oncogenic processes in leukemia, glioma, and melanoma cells. Here, we studied the effects and molecular targets of mambalgin-2 in lung adenocarcinoma A549 and Lewis cells, lung transformed WI-38 fibroblasts, and lung normal HLF fibroblasts. We found that mambalgin-2 inhibits the growth and migration of A549, metastatic Lewis P29 cells, and WI-38 cells, but not of normal fibroblasts. A549, Lewis, and WI-38 cells expressed different ASIC and ENaC subunits, while normal fibroblasts did not at all. Mambalgin-2 induced G2/M cell cycle arrest and apoptosis in lung adenocarcinoma cells. In line, acidification-evoked inward currents were observed only in A549 and WI-38 cells. Gene knockdown showed that the anti-proliferative and anti-migratory activity of mambalgin-2 is dependent on the expression of ASIC1a, α-ENaC, and γ-ENaC. Using affinity extraction and immunoprecipitation, mambalgin-2 targeting of ASIC1a/α-ENaC/γ-ENaC heteromeric channels in A549 cells was shown. Electrophysiology studies in *Xenopus* oocytes revealed that mambalgin-2 inhibits the ASIC1a/α-ENaC/γ-ENaC channels with higher efficacy than the ASIC1a channels, pointing on the heteromeric channels as a primary target of the toxin in cancer cells. Finally, bioinformatics analysis showed that the increased expression of ASIC1 and γ-ENaC correlates with a worse

survival prognosis for patients with lung adenocarcinoma. Thus, the ASIC1a/α-ENaC/γ-ENaC heterotrimer can be considered a marker of cell oncogenicity and its targeting is promising for the design of new selective cancer therapeutics.

Keywords: acid-sensing ion channel, degenerin/epithelial Na^+ channel, lung adenocarcinoma, mambalgin-2, lung cancer therapy

INTRODUCTION

Lung cancer is one of the most common cancer types in the world with the highest frequency of disease-associated morbidity and mortality. According to the cancer statistics from the Global Cancer Observatory (GLOBOCAN) in 2020, lung cancer accounts for 2.2 million newly diagnosed cases and 1.8 million deaths (18% of total cancer deaths) (1). Approximately 85% of all lung cancer diagnostic cases are non–small cell lung cancer (NSCLC), such as lung adenocarcinoma (2). Despite the existing treatment strategies for this disease such as chemotherapy, radiotherapy, and surgery, the overall patient survival rate remains low. Therefore, it is important to develop novel therapies and to search for specific targets to substantially improve the treatment and survival prognosis for patients with lung adenocarcinoma.

Tumor progression is accompanied by inflammatory processes, immunosuppression, hypoxia, and acidification of the microenvironment (3, 4). Acidosis of the microenvironment induced by local hypoxia and enhanced glycolytic activity is one of the biochemical characteristics of tumors. The local extracellular pH value may drop to 6.2–6.9 in solid tumors (4, 5) and to pH 5.5 or lower in chronic inflammatory conditions (6). Low extracellular pH was shown to promote progression, invasion, and metastasis of the tumors (5, 7, 8).

Different types of ion channels are involved in the regulation of many physiological and pathological functions in cells and tissues. Among them, acid-sensing ion channels (ASICs) contribute to cellular response to the altered pH in the tumor environment due to their ability to be activated by low extracellular pH. ASICs are proton-gated cation channels and belong to the degenerin/epithelial Na^+ channel (DEG/ENaC) superfamily (9). Currently, at least four genes encoding six types of the ASIC subunits are known: ASIC1a, ASIC1b, ASIC2a, ASIC2b, ASIC3, ASIC4 (10). ENaCs are sodium-selective channels that are expressed in a variety of epithelial and non-epithelial cells and tissues (11). Currently, the four subunits (α-ENaC, β-ENaC, γ-ENaC, and δ-ENaC) are identified. Usually they form the heteromeric channels (12, 13). ASIC subunits alone or in combination with ENaC subunits can form functionally active homo- or heterotrimeric channels with different physiological and biophysical properties. For example, the hybrid channels formed by ASIC1 and ENaCs were reported (14). In addition to a high level of ASIC expression in the nervous system, where they are involved in physiological processes such as pain perception, synaptic plasticity, learning, and memory, most ASIC and ENaC subunits are present in different non-excitable tissues, and the channels formed by them can also be implicated in tumor pathogenesis. Our previous results and literature data point on the possible ASIC1 and ENaC expressions in leukemia (15), glioma (16), melanoma (17), breast cancer (18), and pancreatic (19), lung (3), and hepatocellular carcinoma cells (20), where the ASIC1-containing channels participate in the regulation of cancer cell proliferation, migration, and invasion. In particular, the ASIC1a-containing channels affect the proliferation and migration of lung adenocarcinoma A549 cells induced by extracellular acidosis (3). However, the detailed molecular mechanisms of the ASIC1 oncogenic effects in lung adenocarcinoma as well as the prospects of the selective ASIC1 targeting for lung cancer therapy remain unclear.

Amiloride and psalmotoxin from the venom of the tarantula *Psalmopoeus cambridgei* (PcTx1) are the best known inhibitors of ASIC1a (21), and their antiproliferative effects on several types of tumor cells, including glioma (22) and carcinoma (3, 18), were reported. PcTx1 is the only specific inhibitor of the homomeric ASIC1a channel, but it is not suitable for clinical use, since it can inhibit and potentiate the heteromeric ASIC1a/ASIC2a channels upon different conditions, and its action is dependent on the pH value (23). Amiloride, which is widely used to inhibit the ASIC1 channels, demonstrates low selectivity and is more specific for the ENaC channels (24). Mambalgins isolated from the venom of black mamba *Dendroaspis polylepis* are three-finger small proteins from the Ly6/uPAR family (25), which reversibly selectively inhibit both the homomeric (ASIC1a) and heteromeric (ASIC1a /2a, ASIC1a /2b) channels containing the ASIC1a subunit (26). Previously, we demonstrated that the selective blocking of the amiloride-sensitive ASIC1a-containing channels by recombinant mambalgin-2 inhibits the proliferation of leukemia (15) and glioblastoma cells (16) causing the cell cycle arrest in the G1 phase and apoptosis, without affecting the proliferation of normal astrocytes.

Here, we studied mambalgin-2's effects on the growth and migration of human lung adenocarcinoma A549 cells, murine parental and metastatic lung adenocarcinoma Lewis cells, human lung immortalized fibroblasts WI-38, and human lung primary normal fibroblasts HLF-140. Also, we analyzed the expression profile of various ASIC and ENaC subunits and activation of the acid-sensitive channels in the cells in the absence and presence of mambalgin-2. Results obtained together with the affinity purification data and electrophysiology study in *X. laevis* oocytes allowed us to identify and characterize the new selective target of mambalgin-2 in cancer cells—the heteromeric ASIC1a/α-ENaC/γ-ENaC channels. Bioinformatic analysis revealed a correlation between the increased expression of mRNAs coding the ASIC1 and γ-ENaC subunits with the

worse survival prognosis for the patients with lung adenocarcinoma. Data obtained point on the heteromeric ASIC1a/α-ENaC/γ-ENaC channels as a promising target for new lung cancer therapies.

MATERIALS AND METHODS

Mambalgin-2 Production and Characterization

Recombinant mambalgin-2 was produced in *E. coli* as described previously (27). The purity and homogeneity of the recombinant protein (> 95%) were confirmed by HPLC, MALDI-MS, and SDS-PAGE. Disulfide bond formation was confirmed in the reaction with Ellman's reagent (Sigma-Aldrich, Saint-Louis, MO, USA). The correct spatial structure of the recombinant protein was confirmed by 1D ^{1}H-NMR-spectroscopy.

Cell Cultures

Human lung carcinoma A549 cell line and pseudo-normal human embryonic lung fibroblasts WI-38 VA 13 subline 2RA (transformed by SV-40 to increase the number of passages) were obtained from the shared research facility "Vertebrate cell culture collection" (Institute of Cytology, St. Petersburg, Russia). A549 cells were cultured in DMEM medium from Biolot (St. Petersburg, Russia), 10% FBS (Biowest, Nuaillé, France), and 80 mg/mL gentamicin, and WI-38 in EMEM medium (Biolot, St. Petersburg, Russia) supplemented with 1% non-essential amino acids (NEAA, Thermo Fisher Sci, Waltham, MA, USA), 10% FBS, and 80 mg/mL gentamycin. Primary normal embryo human lung fibroblasts HLF-104 (designated below as HLF) cells (Biolot) were passaged in EMEM medium (Biolot) containing 10% FBS and 80 mg/mL gentamycin. Murine Lewis lung adenocarcinoma cells and its metastatic subline P29 were a kind gift from Dr. B.S. Akopov and were cultivated in DMEM supplemented with 10% FBS. Cells were maintained at 37°C in a humidified atmosphere with 5% CO_2. All types of the cells were subcultured twice per week. Cells were passaged no more than 40 times and regularly tested for the absence of mycoplasma contamination by the PCR kit (MycoReport, Evrogen, Moscow, Russia).

Cell and Spheroid Proliferation Assay

To assay the influence of the medium acidification on the cell growth, the cells were seeded in 96-well culture plates (5×10^3 cells per well) and grown for 24 h. After that, the medium was aspirated and changed to the fresh one with pH 7.4 (normal medium) or 5.5 (containing 10 mM MES, acidic medium) and cells were incubated for 72 h without the medium change. To study mambalgin-2's influence on the cell proliferation, the cells were seeded in 96-well cell culture plates (5×10^3 cells/per well) in the normal or acidic medium and grown for 24 h. Thereafter, mambalgin-2 (from the 10 mM stock solution in 100% DMSO) was dissolved in the normal or acidic medium and added to the cells at concentrations from 10^{-11} to 10^{-5} M for further incubation during 72 h without the medium change. The maximal DMSO concentration did not exceed 0.1%. The added DMSO did not influence the cell growth as was established in additional experiments. For spheroid reconstruction, A549 cells (1×10^3 cells per well) were seeded on 96-well plates treated by poly(2-hydroxyethyl methacrylate) (Sigma-Aldrich) at pH 5.5 and incubated with 1 μM of mambalgin-2 for 24 h.

To analyze the cell viability of cells and spheroids, we used the WST-1 colorimetric test as described earlier (28). Briefly, WST-1 (water-soluble tetrazolium salt 1; Santa Cruz, Dallas, TX, USA) and 1-m-PMS (1-methoxy-5-methylphenazinium methyl sulfate, Santa Cruz) were added to the cells in concentrations of 0.25 mM and 5 μM, respectively, for 1 h, and formation of the colored product was measured at 450 nm with background subtraction at 655 nm on microplate reader Bio-Rad 680 (Bio-Rad, Hercules, CA, USA). The data were normalized to averaged readout from the control wells containing the cells without added compounds. The concentration–effect curves were fitted in the GraphPad Prism 8.0 software (GraphPad Software, San Diego, CA, USA). For investigation of the influence of medium acidification on the cells' viability, the cells cultivated at pH 7.4 (normal medium) were used as control. For visualization of spheroids, they were aspirated from wells, stained with 0.4% Trypan Blue (PanEco, Moscow, Russia), and imaged using the CellDrop Brightfield Cell Counter (DeNovix, Wilmington, DE, USA).

Gene Silencing

To block the expression of native ASIC1a, α-ENaC, and γ-ENaC, A549 cells were transfected with corresponding siRNA (**Table S1**, Synthol, Russia). Cells were seeded in six-well culture plates (2×10^5 cells/well) and grown for 24 h. Then, three siRNAs to different parts of the corresponding genes were mixed (1 μg per well), and the mixture was diluted in 100 μl of the transfection buffer (Pan-Biotech, Aidenbach, Germany), incubated for 5 min, and mixed with 15 μl of the pre-diluted PANFect A-plus transfection reagent (Pan-Biotech). The final mixture was incubated for 30 min and added to A549 cells. The cells were incubated in a CO_2 incubator for 4 h, and the cell media were replaced by the fresh one. After 96 h of incubation, the cells were detached by Versene and divided into two parts. The first part was incubated with ASIC1a (sheep, 1:1,000, ABIN350049, Antibodies-Online, Aachen, Germany), α-ENaC (rabbit, 1:1,000, ABIN1841945, Antibodies-Online), or γ-ENaC (mouse, 1:1,000, ABIN1865926, Antibodies-Online), washed, and incubated with the secondary TRITC-conjugated antibodies (713-025-003, 111-025-003, and 615-025-214, Jackson ImmunoResearch, West Grove, USA, for ASIC1a, α-ENaC, and γ-ENaC, respectively). The expression of the surface receptors was analyzed using the Attune NxT Flow Cytometer (Life Technologies, Carlsbad, CA, USA) for confirmation of gene knockdown (**Figure S1**). The second part of the cells was seeded in 96-well culture plates (5×10^4 cells per well) at pH 7.4 or 5.5 and incubated with different concentrations of mambalgin-2 for 72 h without media change, and the WST-1 assay was performed as described above.

"Wound-Healing" Migration Assay

To form the experimental wounds, cells were seeded into Ibidi Culture-Inserts 2 Well (Ibidi, Gräfelfing, Germany, 4–5 × 10^4 cells/well) installed in 24-well culture plates. The cells were placed in a cell culture incubator with 37°C and 5% CO_2 overnight to allow spreading. Before the experiments, the inserts were removed, and the culture medium was replaced with the normal or acidic fresh medium with or without 1 μM of mambalgin-2 (from the 10 mM stock solution in 100% DMSO) or equal DMSO amount. The phase-contrast images of the initial gaps were captured under an inverted microscope (10× objective, MicroMed, St. Petersburg, Russia) using the Toupcam 5.1 MPix CMOS Camera (ToupTek Photonics, Hangzhou, China) controlled by the ToupView 3.7 software (ToupTek Photonics). Then, the images of the same gaps were captured after 24 h from the start of the experiment. The gap sizes were calculated manually using the "Measure Area" tool in the ImageJ software (NIH, Bethesda, MD, USA) and normalized to the size of the initial gap (0 h). The area occupied by the migrated cells (in % from the initial gaps) was compared between groups.

Real-Time PCR

Total RNA was isolated using the Bio-Rad Aurum RNA isolation kit (Bio-Rad) according to the manufacturer's instructions. cDNA was synthesized by the Mint reverse transcriptase kit (Evrogen). After that, qPCR was performed with the ready-to-use SYBR Green HS mix (Evrogen) and primers specific to the *ACCN2* (coding the ASIC1a isoform, PubMed Gene ID NM_020039.4), *ACCN1*, *ACCN3*, *ACCN4*, *SCNN1A*, and *SCNN1G* genes (**Table S2**) using the Roche LightCycler 96 amplifier (Roche, Basel Switzerland). Data were analyzed by the ΔΔCt method and LightCycler SW software (Roche), and the gene expression was normalized to the expression of *β-ACTIN*, *GPDH*, and *RPL13a* housekeeping genes.

Cell Cycle Analysis

For analysis of mambalgin-2's influence on the cell cycle, the A549 and metastatic Lewis cells were seeded in six-well culture plates (2 × 10^5 cells per well) at pH 5.5, grown for 24 h, and incubated with 1 μM mambalgin-2 for 72 h without the media change. Then the cells were detached from the wells by 0.5% trypsin-EDTA, washed with Earle's Balanced Salt Solution (EBSS), and fixed in ice-cold 70% ethanol for 24 h at -20°C. After fixation, the cells were washed twice with EBSS, and DNA was extracted by 5 min of incubation with the DNA extraction buffer (200 mM Na_2HPO_4 with 0.004% Triton X-100, pH 7.8). Then the cells were washed with EBSS, resuspended in the DNA staining solution (EBSS, 50 mg/ml propidium iodide, 0.2 mg/mL DNAse-free RNAse A), and analyzed using the Attune NxT flow cytometer (Life Technologies). The data were analyzed using the Attune NxT flow cytometer Software (Life Technologies).

Analysis of Phosphatidylserine Externalization

To investigate apoptosis in A549 and Lewis cells, we used Annexin V for detection of phosphatidylserine externalization —one of the early apoptosis markers. Briefly, cells were seeded in six-well culture plates (2 × 10^5 cells per well) at pH 5.5, grown for 24 h, and incubated with 1 μM mambalgin-2 for 72 h without the media change. After incubation, the cells were detached using the Versene solution and washed with annexin-binding buffer (V13246, Thermo Fisher Scientific). Then, the cells were incubated with Annexin V conjugated to Alexa 488 (A13201, Thermo Fisher Scientific) for 20 min, washed with the annexin-binding buffer, and analyzed using the Attune NxT flow cytometer (Life Technologies). The data were analyzed using the Attune NxT Software (Life Technologies).

Patch-Clamp Recordings

Electrophysiological experiments on different cell lines (A549, WI-38, and HLF) were performed using the whole-cell configuration of the patch-clamp technique. Cells were placed (passaged) on sterile 4 × 4-mm coverslips in 35-mm Petri dishes 1–2 days before the experiment. Ion current records were acquired with the Axopatch 200B amplifier (Molecular Devices, San Jose, CA, USA), the analog–digital interface Digidata 1550A and PC running the Clampex software (Molecular Devices). Borosilicate micropipettes (BF-150-110-10, Sutter Instruments, Novato, CA, USA) were pulled at a P-97 puller (Sutter Instrument) to a resistance of 3–6 MΩ when filled with a relevant intracellular solution containing (in mM) 140 K-Aspartate, 5 NaCl, 1 $MgCl_2$, 2 EGTA/KOH, 20 HEPES/TRIS, and 0.176 $CaCl_2$ to establish free ionized calcium concentration $[Ca^{2+}]i$ at 0.01 μM. Typical bath solution (in the chamber) contained (in mM) 145 NaCl, 2 $CaCl_2$, 1 $MgCl_2$, and 10 HEPES/TRIS (pH 7.4). For bath extracellular solution with pH 5.5, HEPES/TRIS was replaced by MES. Gap-free ion currents were recorded at holding membrane potential -50 mV. Data were low-pass filtered at 200 Hz and analyzed using Axon pClamp 10.5 software suite (Molecular Devices).

Immunoprecipitation, Affinity Purification, and Western Blotting

For investigation of the mambalgin-2 targets in A549 cells, mambalgin-2 (1 mg/ml) was coupled to NHS-activated Sepharose 4 Fast Flow (Cat #17-0906-01, GE Healthcare, Chicago, IL, USA) according to the manufacturer's instructions. The resin blocked by 500 mM ethanolamine without any protein coupled was used as a negative control. The membrane fraction of A549 cells (5 × 10^7 cells per sample) was solubilized in 2% Triton X-100 (Cat# A4975, Panreac, Barcelona, Spain), diluted 10 times with TBS buffer (100 mM TRIS, 150 mM NaCl, pH 8.0), and incubated with the resin for 16 h at 4°C in TBS. After that, non-specifically bound proteins were sequentially washed out from the resin with five volumes of TBS, five volumes of TBS + 1 M NaCl + 0.5% Triton X-100, and five volumes of TBS + 0.5% Triton X-100. The specifically bound proteins were eluted by five volumes of 200 mM glycine (pH 2.6), diluted in the loading buffer (120 mM Tris–HCl, 20% [v/v] glycerol, 10% [v/v] mercaptoethanol, 4% [w/v] sodium dodecyl sulfate, and 0.05% [w/v] bromophenol blue, pH 6.8), submitted to gel electrophoresis, blotted onto nitrocellulose membranes (GE Healthcare), and blocked for 2 h in 5% skim milk

(Sigma-Aldrich) in TBS (50 mM Tris, 150 mM NaCl, pH 7.4) buffer + 0.1% Tween-20 (AppliChem, Darmstadt, Germany). The membranes were then incubated overnight at 4°C with primary antibodies against ASIC1a (mouse, 1:1,000, SMC-427, StressMarq Biosciences, Victoria, Canada), α-ENaC (rabbit, 1:1,000, ABIN1841945, Antibodies-Online), or γ-ENaC (mouse, 1:1,000, ABIN1865926, Antibodies-Online), washed three times with TBS + 0.1% Tween-20, and incubated with HRP-conjugated secondary anti-rabbit antibody (1:5,000, 111-035-003, Jackson ImmunoResearch), in the case of α-ENaC or anti-mouse antibody (1:5,000, 715-035-150, Jackson ImmunoResearch) in the cases of ASIC1a or γ-ENaC for 1 h (20°C). After that, membranes were washed four times with TBS + 0.1% Tween-20, and an HRP signal was detected by ECL substrate (Bio-Rad) using the ImageQuant LAS 500 chemidocumenter (GE Healthcare).

To study the formation of the ASIC1/α-ENaC/γ-ENaC heterotrimers in A549 cells, 100 μg of ASIC1a antibody (sheep, final concentration 1 mg/ml ABIN350049, Antibodies-Online) was conjugated to Protein-A agarose (Cat #10037259, Roche) in accordance with the manufacturer's protocols. The membrane fraction of A549 cells (5×10^7 cells per sample) was solubilized in 2% Triton X-100 (Panreac) and diluted 10 times with TBS buffer (100 mM Tris, 150 mM NaCl, pH 8.0). After that, the lysates were pre-cleared by empty Protein A-conjugated agarose (Roche) for 4 h at RT to avoid non-specific binding and then incubated with the ASIC1a antibody-coupled agarose for 16 h at 4°C in TBS. The empty agarose blocked with 1% skim dry milk (Sigma-Aldrich) was used as a negative control. After that, non-specifically bound proteins were sequentially washed out from the resin with five volumes of TBS, five volumes of TBS + 1 M NaCl + 0.5% Triton X-100, and five volumes of TBS + 0.5% Triton X-100. The specifically bound proteins were eluted by 10 min of heating in the loading buffer (120 mM Tris–HCl, 20% [v/v] glycerol, 10% [v/v] mercaptoethanol, 4% [w/v] sodium dodecyl sulfate, and 0.05% [w/v] bromophenol blue, pH 6.8), submitted to gel electrophoresis, blotted onto nitrocellulose membranes (GE Healthcare), and blocked for 2 h with 5% skim milk (Sigma-Aldrich) in TBS buffer (50 mM Tris, 150 mM NaCl, pH 7.4) + 0.1% Tween-20. The membranes were incubated overnight at 4°C with the primary antibodies against α-ENaC (rabbit, 1:1,000, ABIN1841945, Antibodies-Online) or γ-ENaC (mouse, 1:1,000, ABIN1865926, Antibodies-Online), washed three times with TBS + 0.1% Tween-20, and incubated with the HRP-conjugated secondary anti-rabbit antibody (1:5,000, 111-035-003, Jackson ImmunoResearch), in the case of α-ENaC or anti-mouse antibody (1:5,000, 715-035-150, Jackson ImmunoResearch) in the case of γ-ENaC for 1 h (20°C). After that, the membranes were washed four times with TBS + 0.1% Tween-20, and an HRP signal was detected by ECL substrate (Bio-Rad) using the ImageQuant LAS 500 chemidocumenter (GE Healthcare).

Expression of ASICs/ENaCs in *X. laevis* Oocytes

For expression of the human homomeric ASIC1a (hASIC1a) and human heteromeric ASIC1a/α-ENAC/γ-ENAC (hASIC1a/α-ENAC/γ-ENAC) channels in *Xenopus laevis* oocytes, the linearized plasmids were transcribed using the T7 mMESSAGE-mMACHINE Transcription Kit (Thermo Fischer Scientific). Oocytes were defolliculated and injected with 2.5–10 ng of mRNA. mRNA transcripts of hASIC1a, hENACα, and hENACγ were synthesized by the mMESSAGE-mMACHINE T7 kit (Cat# AM1344, Thermo Fisher Scientific) according to the protocol for capped transcripts supplied by the manufacturer. For hASIC1a/ENACα/ENACγ expression, the corresponding mRNAs were mixed at the 1:1:1 molar ratio. The preparation of *Xenopus* oocytes at defolliculated stages V–VI was done as previously described (29). Non-injected defolliculated oocytes were used as the control for an absence of endogenous ASIC expression. After injection, the oocytes were kept for 2–3 days at 19°C and then up to 7 days at 15°C in ND-96 medium supplemented with gentamycin (Cat# G1264, Merck, Darmstadt, Germany) (50 μg/ml) and containing (in mM) 96 NaCl, 2 KCl, 1.8 $CaCl_2$, 1 $MgCl_2$, and 10 HEPES, pH 7.4. Plasmids bearing hASIC1a, hα-ENAC, and hγ-ENAC were kindly provided by Dr. Alexander Staruschenko (University of South Florida, Tampa, FL, USA).

Electrophysiological Recordings in *X. laevis* Oocytes

Two-electrode voltage-clamp recordings were performed using the GeneClamp500 amplifier (Axon Instruments, Inverurie, UK) at the holding potential of -50 mV as described previously (29). The output signal was filtered at 20 Hz and digitized at 100 Hz using the L780 AD converter (L-Card, Moscow, Russia). Microelectrodes were filled with 3 M KCl. The external perfusion solution of oocytes was ND-96 with pH 7.4 for both hASIC1a and hASIC1a/α-ENAC/γ-ENAC, and it was fed to a perfusion chamber (volume ~50 μl) by a gravity-flow system at 2.5 ml/min. The currents were stimulated by a pH drop to 5.0 for both hASIC1a and hASIC1a/α-ENAC/γ-ENAC.

The pH drop was done by fast perfusion solution exchange for 0.1 s to ND-96 containing 10 mM MES instead of HEPES and adjusted to the target pH. The pH drop was kept for 7 s, and the solution was exchanged to ND-96 with pH 7.4 afterward. The treatment of oocytes with the mambalgin-2-containing solution was performed by solution exchange in the recording chamber for 15 s before the current stimulation. Lyophilized mambalgin-2 was dissolved in 100% DMSO to a 10-mM stock solution and then diluted to a target concentration with ND-96 right before the experiment. Amiloride (Sigma-Aldrich) was diluted in ND-96 (pH 7.4) from the 500-mM stock in 100% DMSO. The concentration of DMSO in the recording solution was kept below 1% in the all experiments. The exchange of extracellular solutions was performed using a computer-controlled valve system.

The dose–response curves for mambalgin-2 were recorded in the 0–10-μM concentration range. Each oocyte was tested with all concentrations of mambalgin-2. Dose–response curves were fitted using the Hill equation: $Y = 100\%/(1 + 10\text{^}((\text{Log}IC_{50} - X) *nH))$, where Y is the normalized current amplitude (the normalization was done independently for each oocyte), X is

the ligand concentration in the logarithmic scale, and nH is the Hill coefficient (slope factor).

TCGA Database Analysis

Data of the TCGA GTEX (healthy lung biopsies) and LUAD (lung adenocarcinoma) studies were accessed *via* the UCSC Xena platform (30). For comparison of the ASIC and ENaC expressions in normal lungs, adenocarcinomas, and adenocarcinoma-surrounding tissues, the data on the mRNA expression of the genes *ACCN2*, *ACCN1*, *ACCN3*, *ACCN4*, *SCNN1A*, and *SCNN1G* coding the ASIC1, ASIC2, ASIC3, ASIC4, α-ENaC, and γ-ENaC subunits, respectively, were downloaded from the GTEX and LUAD studies and analyzed by the GraphPad Prism 8.0 software (GraphPad Software). Please note that the genes coding the ASIC1 and ASIC2 subunits are designated as *ACCN2* and *ACCN1*, respectively. For analysis of the relationships between the ASIC/ENaC mRNA expression and lung adenocarcinoma patients' survival, the patients with lung adenocarcinoma on the I stage and on the II–IV stages were subdivided into two groups with the *ACCN2*, *ACCN1*, *ACCN3*, *ACCN4*, *SCNN1A*, and *SCNN1G* expression above (high) or below (low) the median value. Overall survival curves were analyzed according to the Kaplan–Meier method for estimation of the survival function from the lifetime data, and lifetime functions were compared using the log-rank test directly in the UCSC Xena platform interface.

Statistical Analysis

Data are presented as mean ± SEM. Sample numbers (n) are indicated in the figure legends. No exclusion criteria were applied for the experimental data. The absence of the outliers in each dataset was confirmed by the Grubbs' test (alpha = 0.05). Before the comparisons, the data were tested for normality (Shapiro–Wilk test, at $p = 0.05$) and for the homogeneity of variances (Levene's test, at $p = 0.05$). The data were analyzed using the one-way ANOVA with appropriate multiple-comparison *post-hoc* test, one-sample t-test, two-tailed t-test for normally-distributed data, and Welch's unequal variance t-test for data without the variance homogeneity as indicated in the figure legends. For comparison of the patients' survival with the different mRNA expressions of ASICs and ENaCs, the log-rank test was used. Differences in the data were considered statistically significant at $p < 0.05$. Analysis was performed using the GraphPad Prism 8.0 software (GraphPad Software).

RESULTS

Mambalgin-2 Inhibits the Growth and Migration of Lung Adenocarcinoma Cells

Previously, we showed that the recombinant analogue of mambalgin-2 inhibits the growth of leukemia (15) and glioma cells (16) and the growth and migration of melanoma cells (17). Here, we tested mambalgin-2's effect on lung adenocarcinoma A549 and Lewis cells, lung transformed WI-38 fibroblasts, and lung normal HLF fibroblasts. As the acidification of the cell media results in stimulation of the growth, migration, and invasion of melanoma cells and influences the expression pattern of the ASIC and ENac subunits (17), we studied mambalgin-2's activity in cells cultivated in the normal (pH 7.4) and acidic (pH 5.5) media.

WST-1 assay revealed that mambalgin-2 reduced the proliferation of A549 cells cultivated in both the normal and acidic media up to ~75% of the control (untreated cells) upon 72 h of incubation with the toxin. Mambalgin-2 demonstrated a dose-dependent activity with EC_{50} 9.29 ± 0.9 nM and 0.59 ± 0.1 nM in A549 cells cultivated at pH 7.4 and 5.5, respectively (**Figure 1A**). The maximal antiproliferative effect of mambalgin-2 on A549 cells was observed at the 1 μM concentration (**Figure 1A**). Mambalgin-2 did not affect the growth of Lewis lung adenocarcinoma (Lewis cells) at any pH but inhibited the growth of Lewis metastatic subline P29 (Lewis-P29 cells) at pH 5.5 with EC_{50} 17.47 ± 5.3 μM (**Figures S2A, B**).

Mambalgin-2 did not affect the viability of WI-38 fibroblasts cultivated in the normal media up to the 1 μM concentration but suppressed their growth up to ~65% upon cultivation in the acidic medium with EC_{50} significantly higher than that found for A549 cells (276.5 ± 14.3 nM, **Figure 1B**). Notably, no significant effect of mambalgin-2 on the growth of HLF fibroblasts cultivated at either pH 7.4 or 5.5 was observed (**Figure 1C**).

Study of 1 μM mambalgin-2's influence on the migration of A549 cells by wound healing assay revealed the toxin's inhibitory activity only at acidic conditions (**Figure 2**). Incubation with mambalgin-2 for 24 and 48 h at pH 5.5 resulted in 2- and 3-fold decreases in the cell motility, respectively (**Figures 2B, C**). Similarly, 1 μM mambalgin-2 affected the migration of Lewis-P29 cells only at pH 5.5 (**Figure S3**). Thus, we can conclude that mambalgin-2's effect on A549 cells observed by wound healing assay is most likely related with influence on the cell migration rather than on their growth, while the toxin action on the growth and migration of Lewis-P29 cells was equal.

Media acidification per se significantly inhibited the migration of A549, WI-38, and HLF cells upon 24 h of incubation with the most prominent effect in HLF cells even in the absence of mambalgin-2 (**Figures S4A–F**). The inhibition effect of acidification was increased in the series A549 < WI-38 < HLF. However, incubation of A549 cells upon 48 h at acidic conditions restored the cell migratory activity (**Figure 2B**), pointing on the successful adaptation of the cells to the acidic media. The media acidification did not influence the viability of A549 and WI-38 cells, while it significantly reduced the proliferation of HLF cells (**Figure S4G**). In contrast, mamblagin-2 inhibited the growth of A549 and WI-38 cells, and no effect was found in normal fibroblasts (**Figure 1**). Thus, we can conclude that the effects observed in the studied cells in the presence of mambalgin-2 are conditioned by the toxin's interaction with its targets.

To translate mambalgin-2's effects on a 3D cell model, we used multicellular spheroids reconstructed from A549 cells. Analysis with Trypan Blue showed that the control spheroids (in the absence of mambalgin-2) were composed of viable cells as they were impermeable for Trypan Blue. However, the spheroids

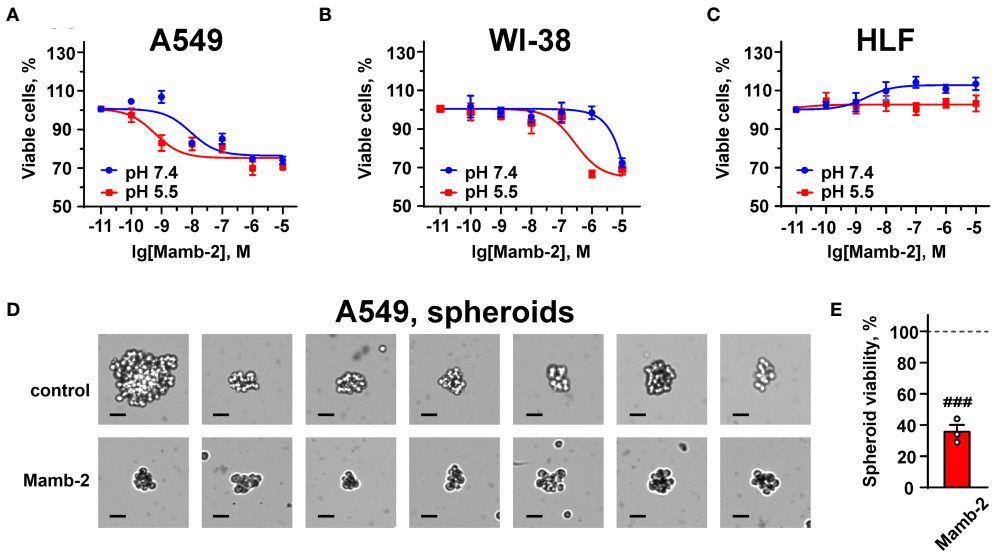

FIGURE 1 | Dose–response effects of mambalgin-2 on viability of A549 **(A, D, E)**, WI-38 **(B)**, and HLF **(C)** cells. **(A–C)** Cells were cultured at pH 7.4 and at pH 5.5. Data are presented as % of the control (untreated cells) ± SEM (n = 4). **(D)** Examples of the spheroids reconstructed from A549 cells incubated in the absence or presence of 1 μM of mambalgin-2 after staining by Trypan Blue, scale bar = 25 μm. **(E)** Influence of 1 μM of mambalgin-2 on the viability of the spheroids reconstructed from A549 cells. Data are presented as % of the control (untreated spheroids) ± SEM (n = 3). $^{###}$($p < 0.001$) indicates difference between untreated and treated spheroids according to one-sample t-test.

incubated with 1 μM mambalgin-2 for 24 h became permeable for Trypan Blue (**Figure 1D**). This points on the loss of cell membrane integrity of the spheroids upon mambalgin-2 treatment. WST-1 assay confirmed that mambalgin-2 inhibited the viability of cells in the spheroids up to ~37% from the control level (untreated spheroids, **Figure 1E**).

Mambalgin-2 Induces G2/M Cell Cycle Arrest and Apoptosis in Lung Adenocarcinoma Cells

Previously, we showed that mambalgin-2 induces the cell cycle arrest and apoptosis in leukemia and glioma cells (15, 16). Here,

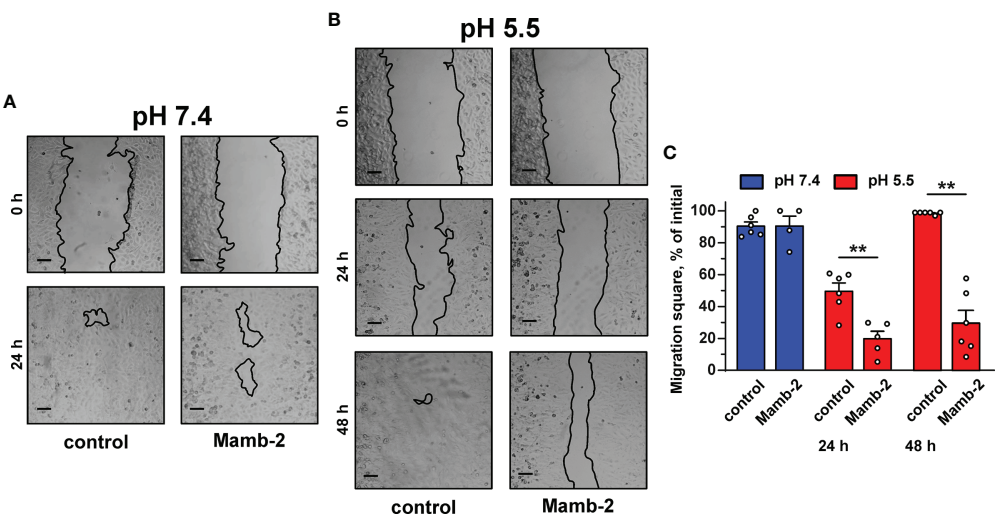

FIGURE 2 | Influence of mambalgin-2 on migration of A549 cells cultivated at pH 7.4 and 5.5. **(A, B)** Representative pictures of wounds for A549 cells incubated at pH 7.4 **(A)** and at pH 5.5 **(B)** in the absence or presence of 1 μM of mambalgin-2. Cells were incubated with mambalgin-2 at pH 7.4 for 24 h and at pH 5.5 for 48 h. Scale bar = 100 μm. **(C)** Wound area occupied by migrating A549 cells. Data are presented as % of the wound surface, occupied by migrating cells ± SEM (n = 6), **($p < 0.01$) indicates significant difference between the data groups by two-tailed t-test.

we analyzed the toxin's action in A549 and Lewis-P29 cells at pH 5.5. Flow cytometry analysis revealed that in A549 cells, mambalgin-2 reduces the cell number in the G1 phase from ~54% to ~38% and increases the cell number in the G2/M phase from ~23% to ~34% (**Figures 3A, B**), pointing on the cell cycle arrest in the G2/M phase. A significant increase in the sub-G1 population (from ~2.7% to 8.8%, **Figure 3B**) is characteristic for apoptosis (31). Indeed, the analysis by flow cytometry revealed that the number of A549 cells with externalized phosphatidylserine significantly increased upon the incubation with 1 μM mambalgin-2 from ~3.6% to ~25.2% (**Figures 3C, D**). Moreover, ~9.4% of A549 cells possessed not only externalized phosphatidylserine but also bound propidium iodide upon mambalgin-2 treatment (**Figures 3C, D**). This points to the membrane integrity loss and the late apoptosis induction. An even more profound G2/M cell cycle arrest was observed in Lewis-P29 cells upon incubation with 1 μM mambalgin-2 (**Figures S5A, B**), although the apoptosis induction was not so prominent as in the case of A549 cells (~ 12% of early apoptotic cells) (**Figures S5C, D**).

Expression of mRNAs Coding ASIC and ENaC Subunits in Lung Transformed and Normal Cells

As mambalgin-2's action in A549 and Lewis-P29 cells was pH-dependent (**Figures 1A**, **2C**, **S2B**, **S3C**), we proposed that it can be connected with the expression of some ASIC and/or ENaC subunits. In order to elucidate the expression pattern of the DEG/ENaC channels and to explain the reason of the mambalgin-2 selectivity in different lung-derived cells, we analyzed the expression of the *ACCN2*, *ACCN1*, *ACCN3*, *ACCN4*, *SCNN1A*, and *SCNN1G* genes coding the ASIC1a isoform, ASIC2, ASIC3, ASIC4, α-ENaC, and γ-ENaC subunits, respectively, in A549, Lewis, WI-38, and HLF cells by real-time PCR. We found that mRNAs of all the investigated channels except ASIC3 were presented in A549 cells. WI-38 fibroblasts demonstrated a higher expression of mRNA coding the ASIC1a, ASIC2, ASIC4, and γ-ENaC subunits than in A549 cells. In contrast, the expression of mRNA coding α-ENaC was significantly down-regulated in WI-38 cells in comparison with A549 cells (**Figure 4**). Surprisingly, HLF cells demonstrated little expression only of mRNA coding γ-ENaC, while the expression of the genes coding other ASIC and ENaC subunits was not found at all (**Figure 4**). Parental Lewis cells did not express ASIC1a at all and demonstrated the significantly lower expression of α-ENaC than metastatic Lewis-P29 cells, while all the studied ASIC and ENaC genes were presented in Lewis-P29 cells (**Figure S6**). As mambalgin-2 did not affect the proliferation of parental Lewis cells (**Figure S2**), we propose that the toxin's influence on the lung cancer cell growth is related at least with the ASIC1a expression.

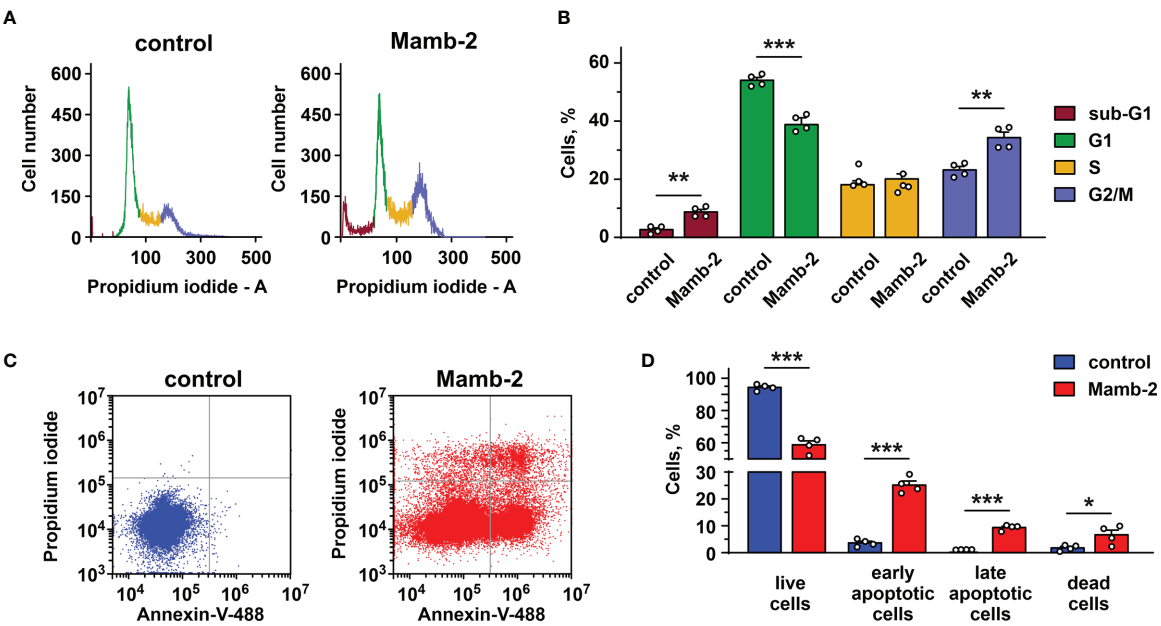

FIGURE 3 | Analysis of cell cycle and apoptosis induction by mambalgin-2 in A549 cells. **(A)** Representative nucleus population distribution of A549 cells incubated in the absence (control) or presence of 1 μM mambalgin-2. **(B)** % of cells in each cell cycle phase. Data are presented as % of cells in each cell cycle phase ± SEM (n = 4). ** ($p < 0.01$) and *** ($p < 0.001$) indicate significant difference between the data groups by two-tailed t-test. **(C)** Representative pictures of phosphatidylserine externalization analysis upon the 1 μM mambalgin-2 treatment of A549 cells by flow cytometry with Annexin V-488 and propidium iodide (control is in absence of mambalgin-2). **(D)** Percentage of A549 cells with externalized phosphatidylserine and bound propidium iodide in the absence (control) or presence of 1 μM mambalgin-2. The data are presented as % of live, early apoptotic, late apoptotic, and dead cells ± SEM (n = 4). * ($p < 0.05$) and *** ($p < 0.001$) indicate the significant difference between data groups by a two-tailed t-test.

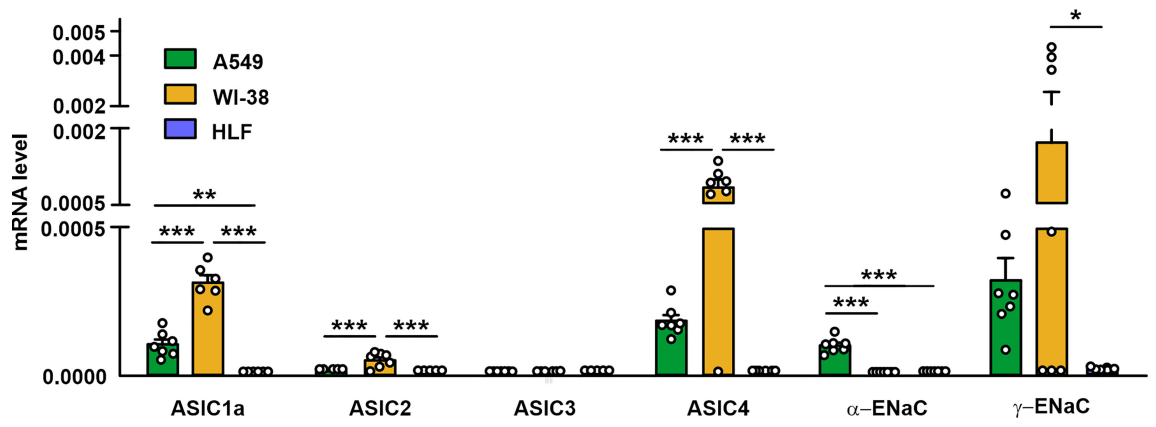

FIGURE 4 | qPCR analysis of the *ACCN2*, *ACCN1*, *ACCN3*, *ACCN4*, *SCNN1A*, and *SCNN1G* expression in A549, WI-38, and HLF cells. Gene expression was normalized to the *β-ACTIN*, *GPDH*, and *RPL13a* housekeeping genes and presented as relative mRNA level ± SEM (n = 6). * ($p < 0.05$), ** ($p < 0.01$), and *** ($p < 0.001$) indicate significant difference between the data groups according to one-way ANOVA followed Tukey's *post-hoc* test, n.s. - no significant difference ($p>0.05$).

Functional Expression of DEG/ENaC Channels in Lung Adenocarcinoma Cells and Immortalized Lung Fibroblasts

To determine the presence of the functionally active ASIC-like channels in lung cancer and normal cells, electrophysiological experiments in A549, WI-38, and HLF cells were carried out using the patch-clamp technique in the whole-cell configuration (**Figure 5A**). It was found that a rapid change in the pH value of the external (bath) solution from 7.4 to 5.5 in most cases activated the inward transmembrane currents in A549 cells with a peak amplitude from 12.8 to 109 pA (**Figures 5B, C**). A decrease in pH led to the rapid increase in the current amplitude to a maximum followed by the slower decrease in the course of desensitization to a stationary level, which is typical for the acid-sensing ion channel ASIC1a. The addition of 10 μM benzamil [analogue of amiloride with IC_{50} ~ 3.50 μM at the ASIC1 channels (24)] to the extracellular solution caused the suppression of the inward currents activated by acidification of the extracellular solution to pH 5.5 up to ~25% of the initial value (**Figure 5B**). Subsequent replacement of the extracellular solution with the solutions without benzamil (with pH 7.4 and 5.5) led to the reactivation of the ASIC channels (**Figure 5B**). The data obtained indicate the expression of the functionally active ASIC1a channels in the membrane of A549 cells. Similar to A549 cells, in the whole-cell experiments in immortalized WI-38 fibroblasts, we also recorded the currents induced by the rapid drop in the pH value of the extracellular solution from 7.4 to pH 5.5 with the kinetic parameters, which are characteristic for the ASIC1a-containing channels. The amplitude of the currents was in the range from 54.7 to 479.1 pA (**Figures 5E, F**). In line with nearly zero expression of the ASIC genes (**Figure 4**) and absence of mambalgin-2's effect on HLF cells (**Figure 1C**), the whole-cell experiments in lung primary fibroblasts did not reveal the presence of any acidification-induced currents (**Figure 5H**).

Finally, we studied the effect of 1 μM mambalgin-2 on the acid-sensing ion currents in A549 and WI-38 cells. The addition of mambalgin-2 to the extracellular solution fully inhibited the channel activity at pH 5.5 in both types of cells (**Figures 5D, G**). Thus, mambalgin-2 selectively inhibits the growth of the cells, which express the functional ASIC1a containing channels on their plasma membrane.

Mambalgin-2 Binds to ASIC1a/α-ENaC/γ-ENaC Heterotrimer in Lung Adenocarcinoma Cells

Different mambalgin-2 effects (**Figures 1A, B**) and expression patterns of the genes coding the ASIC and ENaC subunits (**Figure 4**) in A549 and WI-38 cells allowed us to hypothesize that mambalgin-2 has another acid-sensitive target in cancer cells than the described earlier homomeric ASIC1a channels (26).

Recently, we have proposed that the target of mambalgin-2 in melanoma cells could be the heteromeric acid-sensitive channels ASIC1/α-ENaC/γ-ENaC (17). To investigate whether mambalgin-2 interacts with the ASIC1a, α-ENaC, and γ-ENaC subunits in A549 cells, we performed an extraction of these subunits from the membrane fraction of A549 cells by affinity chromatography using an N-hydroxysuccinimide resin coupled with mambalgin-2. The empty resin blocked by 500 mM ethanolamine was used as a negative control. Analysis by Western blotting revealed that mambalgin-2 extracted detectable amounts of the ASIC1a, α-ENaC, and γ-ENaC subunits from the membrane fraction of A549 cells (**Figures 6A–C** and **S7**). To confirm the formation of the ASIC1a/α-ENaC/γ-ENaC heterotrimers, we performed the immunoprecipitation of the ASIC1a partners from the membrane fraction of A549 cells using the protein A-agarose coupled with the antibody against ASIC1a. Western blotting revealed extraction of the α-ENaC and γ-ENaC subunits (**Figures 6D, E** and **S8**) pointing on the direct interaction of ASIC1a with α-ENaC and γ-ENaC. Altogether, our data point on the formation of the ASIC1a/α-ENaC/γ-ENaC heterotrimers in

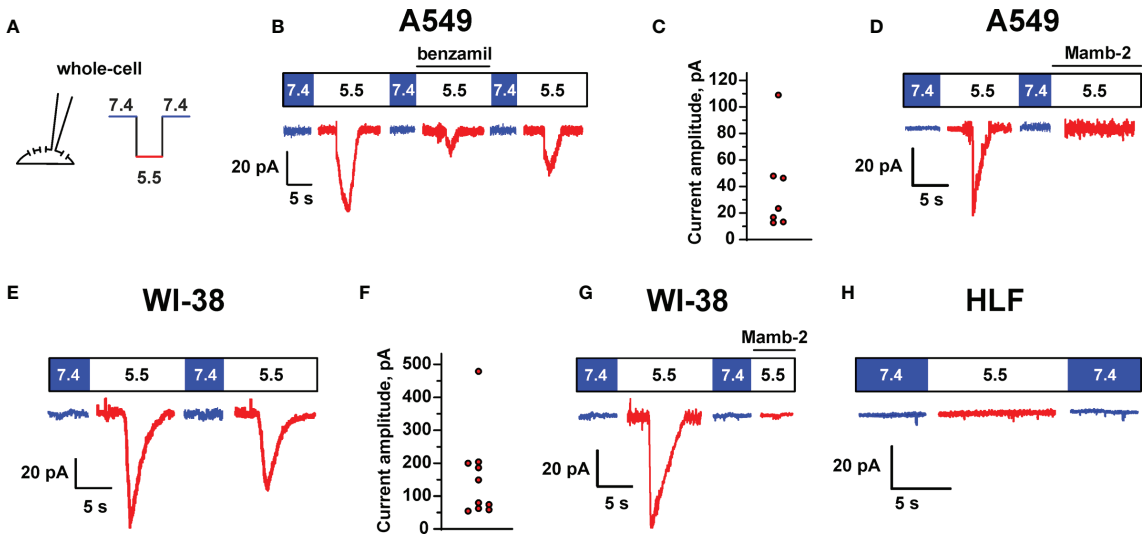

FIGURE 5 | ASIC channel activity in A549, WI-38, and HLF cells. **(A)** Whole-cell configuration of the patch clamp technique and protocol of experiments. Membrane voltage was clamped at −50 mV in all patches. **(B)** Representative traces showing ASIC1a-like currents activated by a rapid drop of extracellular pH from 7.4 to 5.5, the currents were reversibly inhibited by 10 μM benzamil (derivative of amiloride). **(C)** Distribution of transient peak amplitudes at pH 5.5 elicited ASIC1a-like currents in A549 cells. **(D)** The effect of mambalgin-2 on ASIC1a-like currents in A549 cells. **(E)** ASIC1a-like currents in WI-38 cells. **(F)** Distribution of transient peak amplitudes in WI-38 cells at pH 5.5 elicited ASIC1a-like currents. **(G)** The effect of mambalgin-2 on ASIC1a-like currents in WI-38 cells. **(H)** An absence of acidification-evoked currents in HLF cells.

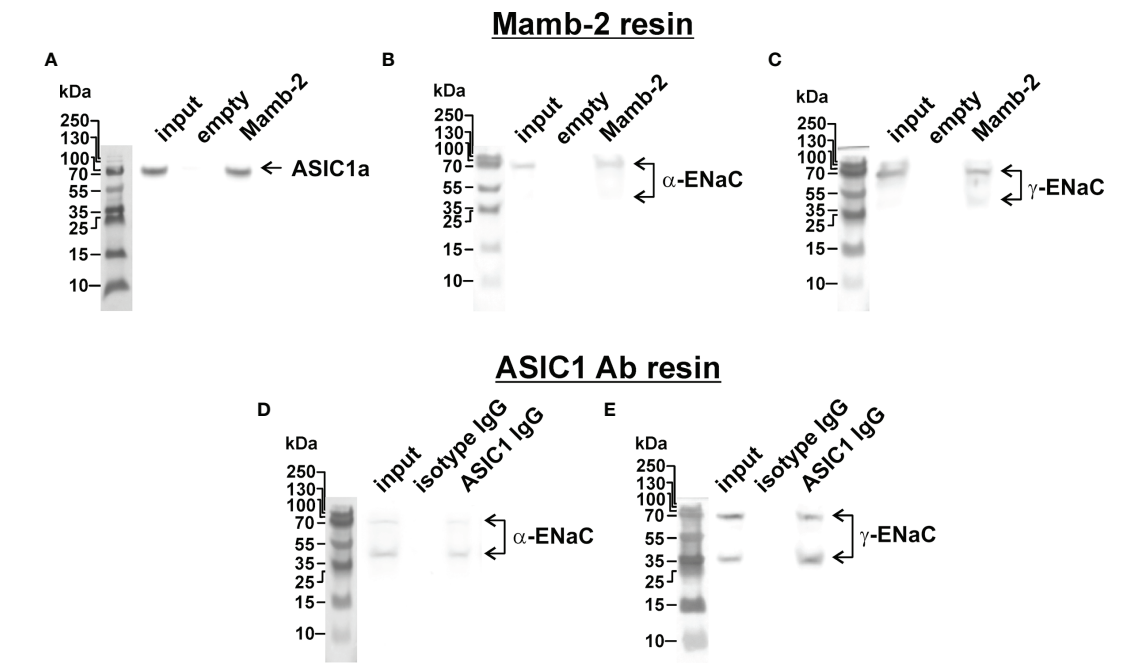

FIGURE 6 | Investigation of mambalgin-2 interaction with ASIC1, α-ENaC, and γ-ENaC subunits in A549 cells. Western blot analysis of the ASIC1 **(A)**, α-ENaC **(B)**, and γ-ENaC **(C)** subunits extraction from the membrane fraction of A549 cells by affinity chromatography using NHS-Sepharose resin coupled with mambalgin-2 (n = 4). Whole Western blotting membranes are shown in **Figure S7**. Western blot analysis of the α-ENaC **(D)** and γ-ENaC **(E)** subunits extracted from the membrane fraction of A549 cells after its precipitation using Protein A-agarose conjugated with ASIC1-antibody (n = 4). Whole Western blotting membranes are shown in **Figure S8**.

A549 cells and on the possible interaction of mambalgin-2 with these heteromeric channels.

Mambalgin-2 Inhibits ASIC1a/α-ENaC/γ-ENaC Heterotrimer Much More Effectively Than ASIC1a Homotrimer

To finally prove that the ASIC1a/α-ENaC/γ-ENaC heterotrimers can be the target of mambalgin-2, we studied the toxin's ability to modulate the acidification-induced currents in *X. laevis* oocytes expressing the human ASIC1a, α-ENAC, and γ-ENAC subunits in a ratio 1:1:1 using the two-electrode voltage clamp technique (**Figure 7A**). We have observed the current responses stimulated by the pH drop from 7.4 to 5.0, which could be reversibly inhibited by the mambalgin-2 treatment before the stimulation (**Figures 7B, C**). No currents were elicited by the pH drop in non-injected oocytes, confirming that the observed responses could be attributed only to heterologous expression (**Figure S9**). Surprisingly, mambalgin-2 inhibited the heterotrimeric hASIC1a/α-ENAC/γ-ENAC channels with significantly higher efficacy than the hASIC1a homotrimeric channels (**Figure 7D**). The inhibitory action of mambalgin-2 on both receptor types is described by the single-component Hill's equation, characterized by the following parameters: IC_{50} = 79 ± 5 nM, n_H = 2.9 ± 0.5, bottom = 0.23 ± 0.02 and IC_{50} = 0.59 ± 0.13 μM, n_H = 1.6 ± 0.5, bottom = 0.18 ± 0.06 for hASIC1a/α-ENAC/γ-ENAC and hASIC1a, respectively. Notably, the dose–response curves for amiloride were identical at the hASIC1a and hASIC1a/α-ENAC/γ-ENAC channels (F-test F m 3, 32 = 1.009; **Figure 7E**). Thus, we confirmed that mambalgin-2 is an inhibitor of the ASIC1a/α-ENaC/γ-ENaC heterotrimeric channels.

Anti-Proliferative and Anti-Migratory Activity of Mambalgin-2 at Low pH Is Dependent on the Expression of ASIC1a, α-ENaC, and γ-ENaC

In order to confirm the implication of the members of DEG/ENac superfamily in the anti-proliferative activity of mambalgin-2, we performed the knockdown of the genes coding the ASIC1a, α-ENaC, and γ-ENaC subunits by siRNA in A549 cells. ASIC1 knockdown completely abolished the mambalgin-2 activity at pH 7.4 and significantly decreased it at pH 5.5 (**Figure 8A**, **Table 1**). However, the down-regulation of the α-ENaC and γ-ENaC expression significantly decreased the mambalgin-2 activity only at pH 5.5 and even slightly increased it at pH 7.4 (**Figures 8B, C**). These results mean that mambalgin-2 can regulate the growth of A549 cells even at neutral pH, and this effect is mediated by ASIC1. Notably, the ASIC1a, α-ENaC, and γ-ENaC knockdown did not affect the A549 cell growth per se both at 7.4 and 5.5 pH (**Figure S1E**).

The migration assay revealed that knockdown of the α-ENaC expression impaired the migration of A549 cells at pH 5.5, while knockdown of the ASIC1a and γ-ENaC expression did not

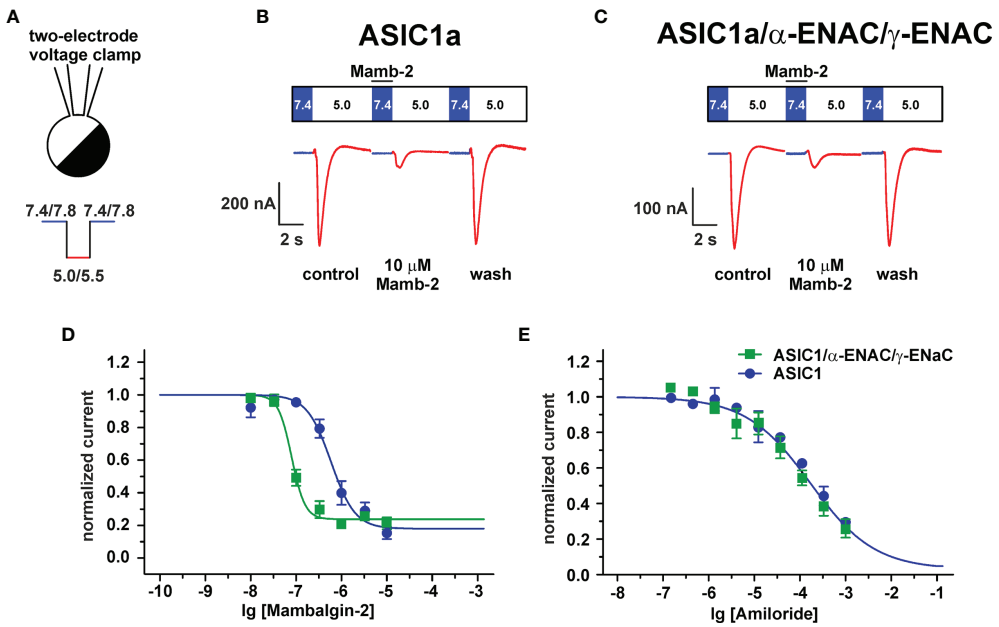

FIGURE 7 | Analysis of mambalgin-2 and amiloride action at ASIC1a and ASIC1a/α-ENaC/γ-ENaC channels in *Xenopus laevis* oocytes. **(A)** Two-electrode configuration of the patch-clamp technique and protocol of experiments. Representative current traces recorded in *X. laevis* oocytes expressing the hASIC1a **(B)** and hASIC1a/α-ENAC/γ-ENAC **(C)** channels; traces for non-injected oocytes were used as control and are shown in **Figure S9**. The pre-incubation with mambalgin-2 was 15 s (shown off time scale), the stimulation phase (pH 5.0) was 7 s, and the recovery phase is not shown. **(D)** Dose–response curves for mambalgin-2 inhibitory effect. For each mambalgin-2 concentration, the current response was normalized to the control experiment. Each data point represents an average from independent experiments in different oocytes ± SEM (n =11 for both channels). The fitted curves are described by single-component Hill's equation. **(E)** Dose–response curves for amiloride inhibitory effect. The data points are shown as normalized average ± SEM (n = 3 for both channels).

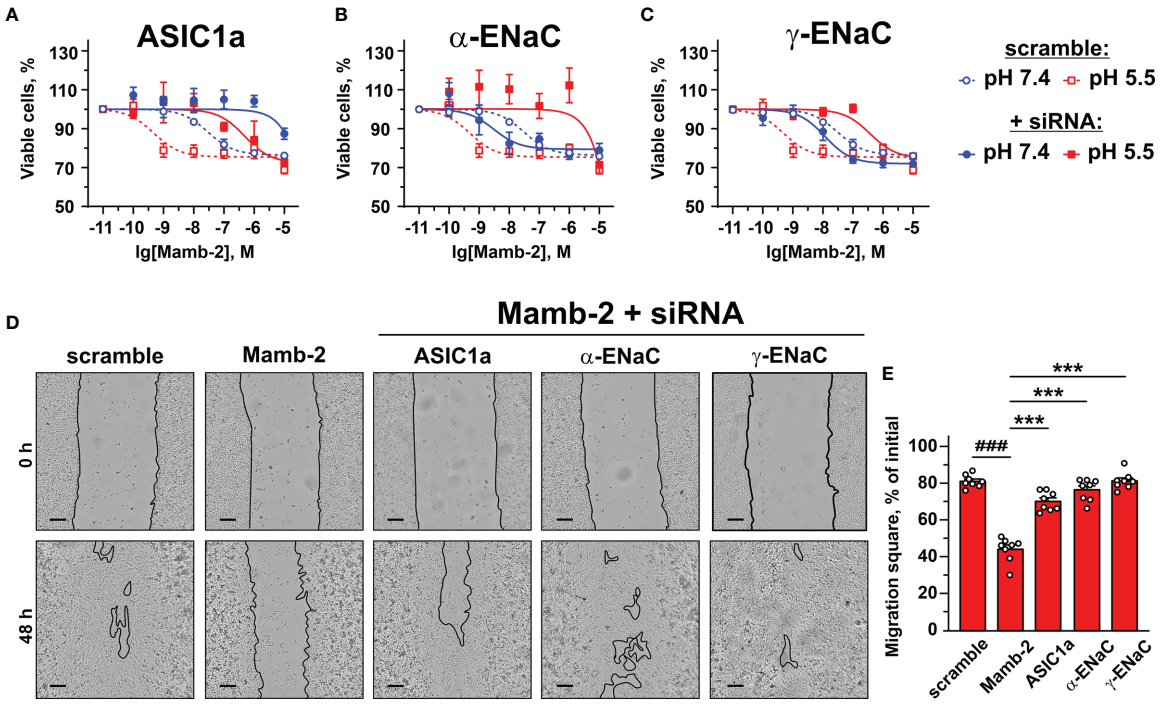

FIGURE 8 | Influence of knockdown of ASIC1, α-ENaC, and γ-ENaC expression on mambalgin-2 activity in A549 lung cancer cells. Dose–response effects of mambalgin-2 on viability of A549 cells after cell transfection with scramble siRNA or siRNA specific for ASIC1a **(A)**, α-ENaC **(B)**, and γ-ENaC. **(C)** Data are presented as % of the control (untreated cells) ± SEM (n = 4). The gene knockdown confirmation is shown in **Figures S1A–E**, and the analysis of dose–response curves is given in **Table 1**. **(D)** Representative pictures of wounds for A549 cells incubated at pH 5.5 in the presence of 1 μM of mambalgin-2 upon knockdown of ASIC1a, α-ENaC, and γ-ENaC genes. Scale bar = 100 μm. Analysis of gene knockdown influence on the migration of A549 cells in the absence of mambalgin-2 is given in **Figures S1F, G**. **(E)** Wound area occupied by migrating A549 cells. Data are presented as % of the wound surface, occupied by migrating cells ± SEM (n = 8); $^{###}$($p < 0.001$) and *** ($p < 0.001$) indicate significant difference between the data groups by one-way ANOVA followed by Tukey's *post-hoc* test.

(**Figure S1G**). In line with the data on the proliferation at pH 5.5 (**Figures 8A–C**), knockdown of any genes coding the ASIC1a, α-ENaC, and γ-ENaC subunits significantly impaired the anti-migration activity of mambalgin-2 at pH 5.5 (**Figures 8D, E**). Thus, all three ASIC1, α-ENaC, and γ-ENaC subunits are necessary for the mambalgin-2 function in A549 cells at acidic conditions.

Elevated Expression of ASIC1 in Lung Adenocarcinoma Correlates With Worse Survival Prognosis for Patients

To evaluate the physiological role of the different members of the DEG/ENaC family in the lung adenocarcinoma progression, we performed a comparative analysis of the expression of the *ACCN2*, *ACCN1, ACCN3, ACCN4, SCNN1A*, and *SCNN1G* genes in human lung adenocarcinoma tissues, tissues surrounding lung adenocarcinoma, and human healthy lung samples from TCGA LUAD and GTEX databases. We found that the *ACCN2* and *ACCN1* expression was elevated in lung adenocarcinoma in comparison to normal lung samples and lung adenocarcinoma surrounding tissue (**Figure 9A**). The expression levels of *ACCN3* and *ACCN4* were significantly lower in adenocarcinoma and surrounding tissue than in healthy lung samples (**Figure 9A**). The expression of mRNA coding the α-ENaC and γ-ENaC subunits was up-regulated in adenocarcinoma-surrounding tissue, but the expression of these mRNAs was up- and down-regulated, respectively, in adenocarcinoma in comparison to normal tissue (**Figure 9A**).

To study the correlation between the expression of the ASIC and ENaC subunits and survival prognosis for the patients with lung adenocarcinoma at different stages of the disease, we performed the Kaplan–Meier analysis of the patient biopsies from the TCGA LUAD database. No correlation was found between the expression of the studied ASIC and ENAC subunits and the survival prognosis for the patients with lung adenocarcinoma at stage I (**Figure 9B**). Analysis of the samples from the patients with adenocarcinoma at stages II–IV by the Kaplan–Meier method showed that the patients with a lower expression of mRNA coding the ASIC1 and γ-ENaC subunits demonstrated the better survival prognosis (**Figure 9C**). In contrast, a lower expression of mRNA coding ASIC4 correlated with the worse survival prognosis (**Figure 9C**). The expression of all other investigated genes did not correlate with the survival prognosis of the patients with lung adenocarcinoma at the stages II–IV. Thus, both ASIC1 and γ-ENaC may be implicated in the lung adenocarcinoma progression. It should be noted that mRNA

TABLE 1 | Parameters describing the effect of ASIC1a, α-ENaC, and γ-ENaC knockdown on the anti-proliferative activity of mambalgin-2 in A549 cells.

Gene knockdown	pH 7.4		pH 5.5	
	A_1, %	EC_{50}, nM	A_1, %	EC_{50}, nM
Scramble	76.63 ± 1.2	26 ± 1.9	75.42 ± 1.7	0.4 ± 0.02
ASIC1a	n.d.	n.d.	72.35 ± 6.5	507.4 ± 27.7[a]
α-ENaC	79.44 ± 2.7	3.5 ± 0.4	n.d.	n.d.
γ-ENaC	71.61 ± 1.8	14.15 ± 2.36	74.69 ± 2.6	375.3 ± 25.3[a]

[a]*Significant difference between EC_{50} values of mambalgin-2 upon and without knockdown of the corresponding gene according to F-test ($p < 0.001$, $n = 4$).*

expression does not necessarily correlate with the protein expression, so we cannot conclude that the ASIC1 and γ-ENaC subunits are really involved in lung adenocarcinoma progression, but the demonstrated phenomenon may point on the existence of a new class of molecular targets for lung cancer therapy.

DISCUSSION

Acidification of the tumor and its microenvironment drives the growth and metastasis of cancer cells (32). ASICs, the acid-sensitive channels from the DEG/ENaC family, are one of the most abundant sensors of acidification on the plasma membrane and participate in the pathogenesis of many cancers including lung, breast, pancreatic, and hepatocellular carcinomas (3, 18–20). Thus, these channels can be considered prospective targets for cancer therapy. However, a lack of selective and effective inhibitors hampers the targeting of these receptors. Previously, we demonstrated that mambalgin-2 from black mamba *Dendroaspis polylepis* controls the progression of leukemia (15), glioma (16), and melanoma cells (17). Here we studied

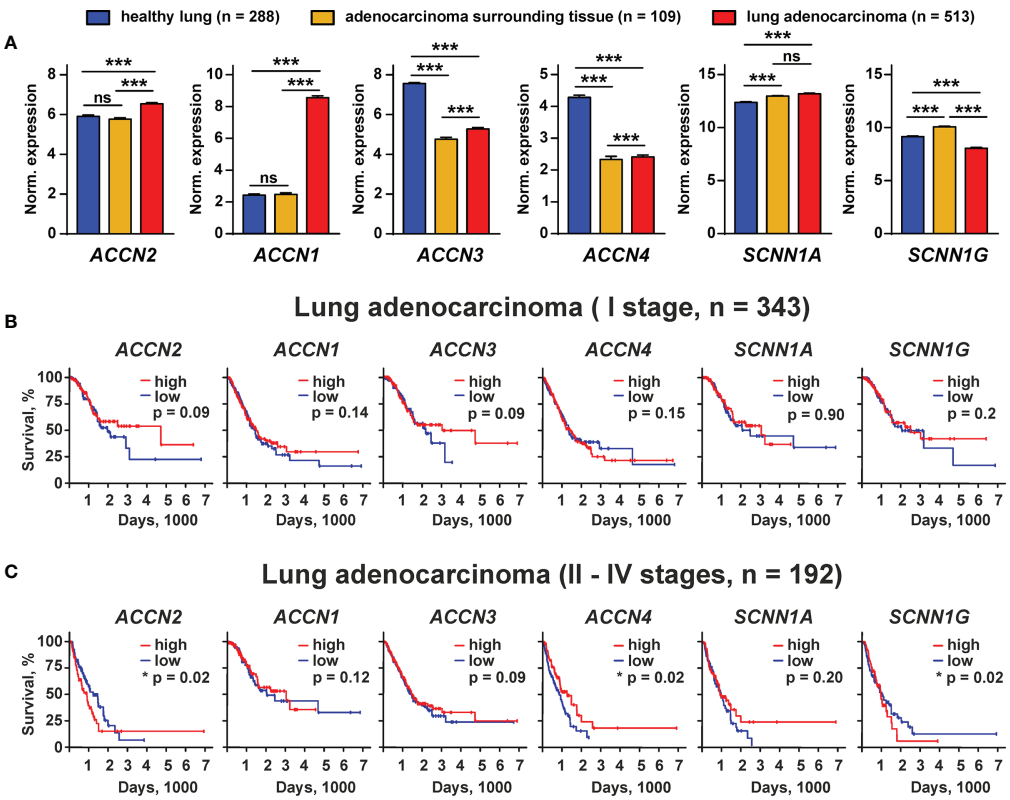

FIGURE 9 | Bioinformatic analysis of the *ACCN2*, *ACCN1*, *ACCN3*, *ACCN4*, *SCNN1A*, and *SCNN1G* expression in healthy people and patients with lung adenocarcinoma from the GTEX and TCGA LUAD databases. **(A)** Analysis of the gene expression in healthy lung biopsies (GTEX study) and in samples of lung adenocarcinoma surrounding tissue, and lung adenocarcinoma specimen (TCGA LUAD study). Data are presented as normalized gene expression ± SEM; *** ($p < 0.001$) indicates significant difference between the data groups by one-way ANOVA followed by Tukey's *post-hoc* test. **(B, C)** Kaplan–Meier analysis of the correlation between survival of the patients with lung adenocarcinoma at I **(B)** and II–IV stages **(C)** and different expressions of the *ACCN2*, *ACCN1*, *ACCN3*, *ACCN4*, *SCNN1A*, and *SCNN1G* genes. * ($p < 0.05$) indicates significant difference between the overall survival prognosis for patients with the high (above median) and low (below median) gene expressions according to the log-rank test, n.s. - no significant difference ($p > 0.05$).

the effects and molecular targets of mambalgin-2 in lung adenocarcinoma cells and normal lung fibroblasts.

Mambalgin-2 inhibited the growth and migration of A549 and Lewis-P29 cells and growth of WI-38 cells, and more pronounced effects were observed at low pH (**Figures 1A**, **2A, B**, **S2B**, **S3**). No toxin effect in normal HLF fibroblasts is consistent with the previously reported selective action of mambalgin-2 in glioma and melanoma cells, but not in normal astrocytes and keratinocytes (16, 17). This difference in the action points on the existence of a "pharmacological window"—the concentration range—in which mambalgin-2 inhibits the growth of cancer cells without a toxicity for normal ones. This selectivity of the action allowed us to propose the different presentations of the mambalgin-2 targets on the plasma membrane surface of the cancer and normal cells. Indeed, the study of the expression repertoire of the genes coding the ASIC and ENaC subunits revealed that in contrast to lung adenocarcinoma cells, lung normal fibroblasts do not express ASICs and α-ENaCs at all (**Figure 4**). A similar situation is observed in Lewis cells: the parental Lewis lung carcinoma cells resistant to mambalgin-2 do not express ASIC1, while metastatic Lewis cells sensitive to mambalgin-2 express very high amounts of ASIC1. Study of the functionally active acid-sensitive channels in A549, WI-38, and HLF cells confirmed the absence of these channels only in lung normal fibroblasts (**Figures 5B, E, H**). Notably, WI-38 cells, in spite of their common use as a model of normal cells, are transformed by the SV40 virus to increase the possible number of passages, and this transformation may lead to appearance of tumorigenicity by inactivation of the tumor-suppressing p53 and Rb proteins important for the cell cycle control in epithelial cells (33). Thus, this cell line occupies a middle position sharing some properties of cancer and normal cells.

In glioblastoma cells, the ASIC1 subunit can form the heterotrimer with the α- and γ-ENaC subunits (14, 34). Extracellular microenvironment acidification leads to the recruitment of the ASIC1/ENaC channels into the cell membrane (14), and the inward cation current mediated by these heteromeric channels may drive the glioma cell growth and migration (35). Previously, we demonstrated that mambalgin-2 extracts the ASIC1a and α-/γ-ENaC subunits from the membrane fraction of the patient-derived melanoma cells (17). Here, we showed the mambalgin-2 binding to the ASIC1a, α-ENaC, and γ-ENaC subunits extracted from the membrane fraction of A549 cells (**Figures 6A–C**) and the formation of the ASIC1a/α-ENaC/γ-ENaC complex (**Figures 6D, E**). Analysis using siRNA confirmed that the all three subunits are important for mambalgin-2's effect on the viability and migration of A549 cells at pH 5.5 (**Figure 8**).

For the first time, we studied the mambalgin-2 influence on the acidification-evoked currents through the ASIC1a/α-ENaC/γ-ENaC heterotrimeric channels (**Figure 7**). It was revealed that the toxin inhibits the heteromeric channels much more effectively than ASIC1a homomeric ones, while amiloride inhibits both types of the channels with the same efficacy (**Figures 7D, E**). Our results are consistent with the previously published data on the properties of the heterotrimeric ASIC/ENaC complexes (36). It was proposed that the different pharmacological properties of the homomeric and heterotrimeric channels can be explained by the formation of new inter-subunit interactions. No difference in the amiloride inhibitory effect at these channels (**Figure 7E**) also agrees with those data, which suggest that the amiloride binding site within the pore is formed by the single ASIC subunit (36). Interestingly, PcTx1 was shown to be a valuable tool for a functional discrimination between the heteromeric channels with different combinations of the ASIC1a/ASIC2a subunits (37). Here we demonstrated that mambalgin-2, similar to PcTx1, can be used in the same way to discriminate between the homomeric ASIC1a and heteromeric ASIC1a/α-ENaC/γ-ENaC channels.

A stronger interaction with the ASIC1a/α-ENaC/γ-ENaC heterotrimers can explain the more pronounced antiproliferative effect of mambalgin-2 in A549 than in WI-38 cells (**Figures 1A, B**). Indeed, mRNAs coding the ASIC1a, α-ENaC, and γ-ENaC subunits were found in A549 cells, while mRNA for α-ENaC was absent in WI-38 cells. We propose that mambalgin-2 targets the homomeric ASIC1 channels in WI-38 cells, while the toxin effect in A549 cells can be related both with the homomeric ASIC1 and heteromeric ASIC1a/α-ENaC/γ-ENaC channels. In line with it, inhibition of ASIC1 by PcTx or the *ACCN2* gene knock-down both significantly reduced the migration of A549 cells (3).

Previously, we showed that mambalgin-2 causes the cell cycle arrest in the G1 and S phases for leukemia and glioma cells (15, 16), but in A549 and Lewis-P29 cells it causes the cell cycle arrest in the G2/M phase (**Figures 3A, B**). This points on the possible implication of different intracellular mechanisms for control of the growth of leukemia/glioma and carcinoma cells. Moreover, mambalgin-2 promotes the more prominent cell cycle arrest but less severe apoptosis in Lewis-P29 cells in comparison with A549 cells (**Figures 3** and **S5**), which can also indicate the existence of different intracellular pathways and/or molecular targets in cancer cells modulated by mambalgin-2. Additionally, mambalgin-2 inhibited the proliferation of A549 cells even at pH 7.4 (**Figure 1A**) and the knockdown only of the ASIC1 expression abolished the toxin effect at normal pH (**Figure 8A**). Possibly, mambalgin-2 can bind to the ASIC1a channels in the closed or desensitized states (26, 38) and activate the metabotropic signaling through the channel without the pore opening. In line with this suggestion, it was shown that the intracellular domain of the ASIC channels can interact with different intracellular signaling messengers (39).

Bioinformatic analysis of the gene expression in the tissues from the patients with lung adenocarcinoma revealed possible implications of ASIC1, ASIC2, ASIC3, ASIC4, α-ENaC, and γ-ENaC in the disease progression (**Figure 9A**). Indeed, all these channels are involved in acidosis-induced tumor progression: ASIC1 and α-ENaC mediate the epithelial–mesenchymal transition of pancreatic cancer (19, 40), while ASIC2 promotes the invasion and metastasis of colorectal cancer (41). Interestingly, ASIC3, which is down-regulated in lung adenocarcinoma samples, may also drive the migration of pancreatic cancer cells (19), so its role in cancer progression

may depend on the carcinoma type. Notably, ASIC4 may down-regulate the ASIC1a expression on the cell surface (42). Thus, its down-regulation in lung carcinoma samples may be linked with the up-regulation of ASIC1. In line, the low expression of the gene coding ASIC1 and the high expression of the gene coding ASIC4 are correlated with better survival prognosis for the patients with lung adenocarcinoma at II–IV stages (**Figure 9C**). Overexpression of γ-ENaC was previously described for cervical cancers (43). Observed here, the lower expression of γ-ENaC in lung adenocarcinoma in comparison with normal lungs (**Figure 9A**) and the correlation of the increased γ-ENaC expression with worse survival prognosis (**Figure 9C**) may reflect the need to maintain the proper ratio between the ASIC homomers and ASIC1/α-ENaC/γ-ENaC heteromers in tumors and requires an additional detailed study. Notably, the bioinformatic analysis only points on the ASIC1- and γ-ENaC-containing channels as on promising targets for lung cancer, but further study is required to confirmthe actual implication of these channels in lung carcinoma progression.

The behavior of cells in a monolayer is significantly different from that of cells in bulky tumors. This is due to intercellular interactions, differences in pH, and different expression levels of the molecules responsible for the cell proliferation inside and outside the tumor (44). Moreover, signaling pathways can differ in bulky tumors and cell monolayers, which leads to the development of resistance to chemotherapeutic substances (45). Here, we showed that mambalgin-2 inhibits the growth of the multicellular spheroids reconstructed from A549 cells (**Figures 1D, E**). Thus, it can bypass the resistance mechanisms of the bulky tumors at least in *in vitro* experiments. Interestingly, previously we showed that another three-finger protein SLURP-1 inhibits the growth of the spheroids reconstructed from A549 cells (46). Probably, a three-finger fold can be used for the design of novel channel-targeting anticancer drugs.

In summary, the selective inhibition of the growth and migration of lung adenocarcinoma cells by mambalgin-2 was shown. For the first time, interaction of mambalgin-2 with the ASIC1a/α-ENaC/γ-ENaC heterotrimeric channels was confirmed by both the affinity chromatography in lung adenocarcinoma cells and electrophysiology experiments in *X. laevis* oocytes. Relations between the ASIC1a, α-ENaC, and γ-ENaC expression and mambalgin-2 effects in cancer cells were revealed. The expression of the heteromeric ASIC1a/α-ENaC/γ-ENaC channels can be considered a marker of the cell oncogenicity.

DATA AVAILABILITY STATEMENT

The original contributions presented in the study are included in the article/**Supplementary Material**. Further inquiries can be directed to the corresponding author.

AUTHOR CONTRIBUTIONS

Conceptualization: AS, MB, EL; data curation: AS, VC-N, MB, DK, EL; formal analysis: AS, VC-N, MB, DK, EL; funding acquisition: EL, MK; investigation: AS, VC-N, MB, DK, MS, OS; methodology: AS, VC-N, MB, DK, SK, MS, OS, EL; project administration: EL, MK; resources: AS, EL, MK; software: AS, VC-N, MB, DK, SK, MS; supervision: EL, visualization: AS, VC-N, MB, EL; writing—original draft preparation: AS, MB, EL; writing—review and editing: VC-N, DK, SK, MS, MK. All authors contributed to the article and approved the submitted version.

FUNDING

This research was funded by the grant from the Ministry of Science and Higher Education of Russian Federation (project № 075-15-2020-773).

SUPPLEMENTARY MATERIAL

The Supplementary Material for this article can be found online at: https://www.frontiersin.org/articles/10.3389/fonc.2022.904742/full#supplementary-material

REFERENCES

1. Sung H, Ferlay J, Siegel RL, Laversanne M, Soerjomataram I, Jemal A, et al. Global Cancer Statistics 2020: GLOBOCAN Estimates of Incidence and Mortality Worldwide for 36 Cancers in 185 Countries. *CA Cancer J Clin* (2021) 71:209–49. doi: 10.3322/caac.21660
2. Molina JR, Yang P, Cassivi SD, Schild SE, Adjei AA. Non-Small Cell Lung Cancer: Epidemiology, Risk Factors, Treatment, and Survivorship. *Mayo Clin Proc* (2008) 83:584–94. doi: 10.4065/83.5.584
3. Wu Y, Gao B, Xiong Q-J, Wang Y-C, Huang D-K, Wu W-N. Acid-Sensing Ion Channels Contribute to the Effect of Extracellular Acidosis on Proliferation and Migration of A549 Cells. *Tumour Biol* (2017) 39:1010428317705750. doi: 10.1177/1010428317705750
4. Pethő Z, Najder K, Carvalho T, McMorrow R, Todesca LM, Rugi M, et al. pH-Channeling in Cancer: How pH-Dependence of Cation Channels Shapes Cancer Pathophysiology. *Cancers (Basel)* (2020) 12:E2484. doi: 10.3390/cancers12092484
5. Wang L, Fan Z, Zhang J, Changyi Y, Huang C, Gu Y, et al. Evaluating Tumor Metastatic Potential by Imaging Intratumoral Acidosis *via* pH-Activatable Near-Infrared Fluorescent Probe. *Int J Cancer* (2015) 136:E107–116. doi: 10.1002/ijc.29153
6. Shi Q, Maas L, Veith C, Van Schooten FJ, Godschalk RW. Acidic Cellular Microenvironment Modifies Carcinogen-Induced DNA Damage and Repair. *Arch Toxicol* (2017) 91:2425–41. doi: 10.1007/s00204-016-1907-4
7. Gatenby RA, Gillies RJ. Why do Cancers Have High Aerobic Glycolysis? *Nat Rev Cancer* (2004) 4:891–9. doi: 10.1038/nrc1478
8. Estrella V, Chen T, Lloyd M, Wojtkowiak J, Cornnell HH, Ibrahim-Hashim A, et al. Acidity Generated by the Tumor Microenvironment Drives Local Invasion. *Cancer Res* (2013) 73:1524–35. doi: 10.1158/0008-5472.CAN-12-2796
9. Kellenberger S, Schild L. International Union of Basic and Clinical Pharmacology. XCI. Structure, Function, and Pharmacology of Acid-Sensing Ion Channels and the Epithelial Na+ Channel. *Pharmacol Rev* (2015) 67:1–35. doi: 10.1124/pr.114.009225

10. Foster VS, Rash LD, King GF, Rank MM. Acid-Sensing Ion Channels: Expression and Function in Resident and Infiltrating Immune Cells in the Central Nervous System. *Front Cell Neurosci* (2021) 15:738043. doi: 10.3389/fncel.2021.738043
11. Kleyman TR, Eaton DC. Regulating Enac's Gate. *Am J Physiol Cell Physiol* (2020) 318:C150–62. doi: 10.1152/ajpcell.00418.2019
12. Canessa CM, Merillat AM, Rossier BC. Membrane Topology of the Epithelial Sodium Channel in Intact Cells. *Am J Physiol* (1994) 267:C1682–1690. doi: 10.1152/ajpcell.1994.267.6.C1682
13. Giraldez T, Rojas P, Jou J, Flores C, Alvarez de la Rosa D. The Epithelial Sodium Channel δ-Subunit: New Notes for an Old Song. *Am J Physiol Renal Physiol* (2012) 303:F328–338. doi: 10.1152/ajprenal.00116.2012
14. Kapoor N, Lee W, Clark E, Bartoszewski R, McNicholas CM, Latham CB, et al. Interaction of ASIC1 and ENaC Subunits in Human Glioma Cells and Rat Astrocytes. *Am J Physiol Cell Physiol* (2011) 300:C1246–1259. doi: 10.1152/ajpcell.00199.2010
15. Bychkov ML, Shulepko MA, Vasileva VY, Sudarikova AV, Kirpichnikov MP, Lyukmanova EN. ASIC1a Inhibitor Mambalgin-2 Suppresses the Growth of Leukemia Cells by Cell Cycle Arrest. *Acta Naturae* (2020) 12:101–16. doi: 10.32607/actanaturae.10949
16. Bychkov M, Shulepko M, Osmakov D, Andreev Y, Sudarikova A, Vasileva V, et al. Mambalgin-2 Induces Cell Cycle Arrest and Apoptosis in Glioma Cells *via* Interaction With ASIC1a. *Cancers* (2020) 12:1837. doi: 10.3390/cancers12071837
17. Bychkov ML, Kirichenko AV, Shulepko MA, Mikhaylova IN, Kirpichnikov MP, Lyukmanova EN. Mambalgin-2 Inhibits Growth, Migration, and Invasion of Metastatic Melanoma Cells by Targeting the Channels Containing an ASIC1a Subunit Whose Up-Regulation Correlates With Poor Survival Prognosis. *Biomedicines* (2021) 9:1324. doi: 10.3390/biomedicines9101324
18. Gupta SC, Singh R, Asters M, Liu J, Zhang X, Pabbidi MR, et al. Regulation of Breast Tumorigenesis Through Acid Sensors. *Oncogene* (2016) 35:4102–11. doi: 10.1038/onc.2015.477
19. Zhu S, Zhou H-Y, Deng S-C, Deng S-J, He C, Li X, et al. ASIC1 and ASIC3 Contribute to Acidity-Induced EMT of Pancreatic Cancer Through Activating Ca 2+ /RhoA Pathway. *Cell Death Dis* (2017) 8:e2806–:e2806. doi: 10.1038/cddis.2017.189
20. Zhang Y, Zhang T, Wu C, Xia Q, Xu D. ASIC1a Mediates the Drug Resistance of Human Hepatocellular Carcinoma *via* the Ca2+/PI3-Kinase/AKT Signaling Pathway. *Lab Invest* (2017) 97:53–69. doi: 10.1038/labinvest.2016.127
21. Osmakov DI, Khasanov TA, Andreev YA, Lyukmanova EN, Kozlov SA. Animal, Herb, and Microbial Toxins for Structural and Pharmacological Study of Acid-Sensing Ion Channels. *Front Pharmacol* (2020) 11:991. doi: 10.3389/fphar.2020.00991
22. Hegde M, Roscoe J, Cala P, Gorin F. Amiloride Kills Malignant Glioma Cells Independent of its Inhibition of the Sodium-Hydrogen Exchanger. *J Pharmacol Exp Ther* (2004) 310:67–74. doi: 10.1124/jpet.103.065029
23. Liu Y, Hagan R, Schoellerman J. Dual Actions of Psalmotoxin at ASIC1a and ASIC2a Heteromeric Channels (ASIC1a/2a). *Sci Rep* (2018) 8:1–11. doi: 10.1038/s41598-018-25386-9
24. Leng T-D, Si H-F, Li J, Yang T, Zhu M, Wang B, et al. Amiloride Analogs as ASIC1a Inhibitors. *CNS Neurosci Ther* (2016) 22:468–76. doi: 10.1111/cns.12524
25. Vasilyeva NA, Loktyushov EV, Bychkov ML, Shenkarev ZO, Lyukmanova EN. Three-Finger Proteins From the Ly6/uPAR Family: Functional Diversity Within One Structural Motif. *Biochem (Moscow)* (2017) 82:1702–15. doi: 10.1134/S0006297917130090
26. Diochot S, Baron A, Salinas M, Douguet D, Scarzello S, Dabert-Gay A-S, et al. Black Mamba Venom Peptides Target Acid-Sensing Ion Channels to Abolish Pain. *Nature* (2012) 490:552–5. doi: 10.1038/nature11494
27. Shulepko MA, Lyukmanova EN, Shenkarev ZO, Dubovskii PV, Astapova MV, Feofanov AV, et al. Towards Universal Approach for Bacterial Production of Three-Finger Ly6/uPAR Proteins: Case Study of Cytotoxin I From Cobra N. *oxiana*. *Protein Expr Purif* (2017) 130:13–20. doi: 10.1016/j.pep.2016.09.021
28. Lyukmanova E, Bychkov M, Sharonov G, Efremenko A, Shulepko M, Kulbatskii D, et al. Human Secreted Proteins SLURP-1 and SLURP-2 Control the Growth of Epithelial Cancer Cells *via* Interactions With Nicotinic Acetylcholine Receptors: Actions of Human SLURP Proteins on Cancer Cells. *Br J Pharmacol* (2018) 175:1973–86. doi: 10.1111/bph.14194
29. Shenkarev ZO, Shulepko MA, Bychkov ML, Kulbatskii DS, Shlepova OV, Vasilyeva NA, et al. Water-Soluble Variant of Human Lynx1 Positively Modulates Synaptic Plasticity and Ameliorates Cognitive Impairment Associated With α7-NachR Dysfunction. *J Neurochem* (2020) 155:45–61. doi: 10.1111/jnc.15018
30. Goldman MJ, Craft B, Hastie M, Repečka K, McDade F, Kamath A, et al. Visualizing and Interpreting Cancer Genomics Data *via* the Xena Platform. *Nat Biotechnol* (2020) 38:675–8. doi: 10.1038/s41587-020-0546-8
31. Kajstura M, Halicka HD, Pryjma J, Darzynkiewicz Z. Discontinuous Fragmentation of Nuclear DNA During Apoptosis Revealed by Discrete "Sub-G1" Peaks on DNA Content Histograms. *Cytometry A* (2007) 71:125–31. doi: 10.1002/cyto.a.20357
32. Corbet C, Feron O. Tumour Acidosis: From the Passenger to the Driver's Seat. *Nat Rev Cancer* (2017) 17:577–93. doi: 10.1038/nrc.2017.77
33. Pipas JM. SV40: Cell Transformation and Tumorigenesis. *Virology* (2009) 384:294–303. doi: 10.1016/j.virol.2008.11.024
34. Kapoor N, Bartoszewski R, Qadri YJ, Bebok Z, Bubien JK, Fuller CM, et al. Knockdown of ASIC1 and Epithelial Sodium Channel Subunits Inhibits Glioblastoma Whole Cell Current and Cell Migration. *J Biol Chem* (2009) 284:24526–41. doi: 10.1074/jbc.M109.037390
35. Rooj AK, McNicholas CM, Bartoszewski R, Bebok Z, Benos DJ, Fuller CM. Glioma-Specific Cation Conductance Regulates Migration and Cell Cycle Progression. *J Biol Chem* (2012) 287:4053–65. doi: 10.1074/jbc.M111.311688
36. Meltzer RH, Kapoor N, Qadri YJ, Anderson SJ, Fuller CM, Benos DJ. Heteromeric Assembly of Acid-Sensitive Ion Channel and Epithelial Sodium Channel Subunits*. *J Biol Chem* (2007) 282:25548–59. doi: 10.1074/jbc.M703825200
37. Joeres N, Augustinowski K, Neuhof A, Assmann M, Gründer S. Functional and Pharmacological Characterization of Two Different ASIC1a/2a Heteromers Reveals Their Sensitivity to the Spider Toxin Pctx1. *Sci Rep* (2016) 6:27647. doi: 10.1038/srep27647
38. Baron A, Diochot S, Salinas M, Deval E, Noël J, Lingueglia E. Venom Toxins in the Exploration of Molecular, Physiological and Pathophysiological Functions of Acid-Sensing Ion Channels. *Toxicon* (2013) 75:187–204. doi: 10.1016/j.toxicon.2013.04.008
39. Couch T, Berger K, Kneisley DL, McCullock TW, Kammermeier P, Maclean DM. Topography and Motion of Acid-Sensing Ion Channel Intracellular Domains. *Elife* (2021) 10:e68955. doi: 10.7554/eLife.68955
40. Chang J, Hu X, Nan J, Zhang X, Jin X. HOXD9–induced SCNN1A Upregulation Promotes Pancreatic Cancer Cell Proliferation, Migration and Predicts Prognosis by Regulating Epithelial–Mesenchymal Transformation. *Mol Med Rep* (2021) 24:819. doi: 10.3892/mmr.2021.12459
41. Zhou Z-H, Song J-W, Li W, Liu X, Cao L, Wan L-M, et al. The Acid-Sensing Ion Channel, ASIC2, Promotes Invasion and Metastasis of Colorectal Cancer Under Acidosis by Activating the Calcineurin/NFAT1 Axis. *J Exp Clin Cancer Res* (2017) 36:130. doi: 10.1186/s13046-017-0599-9
42. Donier E, Rugiero F, Jacob C, Wood JN. Regulation of ASIC Activity by ASIC4–new Insights Into ASIC Channel Function Revealed by a Yeast Two-Hybrid Assay. *Eur J Neurosci* (2008) 28:74–86. doi: 10.1111/j.1460-9568.2008.06282.x
43. Song C, Lee Y, Kim S. Bioinformatic Analysis for the Prognostic Implication of Genes Encoding Epithelial Sodium Channel in Cervical Cancer. *Int J Gen Med* (2022) 15:1777–87. doi: 10.2147/IJGM.S346222
44. Duval K, Grover H, Han L-H, Mou Y, Pegoraro AF, Fredberg J, et al. Modeling Physiological Events in 2D vs. 3D Cell Culture. *Physiol (Bethesda)* (2017) 32:266–77. doi: 10.1152/physiol.00036.2016
45. Riedl A, Schlederer M, Pudelko K, Stadler M, Walter S, Unterleuthner D, et al. Comparison of Cancer Cells in 2D vs 3D Culture Reveals Differences in AKT-mTOR-S6K Signaling and Drug Responses. *J Cell Sci* (2017) 130:203–18. doi: 10.1242/jcs.188102
46. Bychkov ML, Shulepko MA, Shlepova OV, Lyukmanova EN, Kirpichnikov MP. Recombinant Analogue of the Human Protein SLURP-1 Inhibits the Growth of Multicellular Spheroids Reconstructed From Carcinoma Cells. *Dokl Biochem Biophys* (2019) 489:392–5. doi: 10.1134/S1607672919060103

Conflict of Interest: The authors declare that the research was conducted in the absence of any commercial or financial relationships that could be construed as a potential conflict of interest.

the publisher, the editors and the reviewers. Any product that may be evaluated in this article, or claim that may be made by its manufacturer, is not guaranteed or endorsed by the publisher.

frontiers | Frontiers in Oncology

ORIGINAL RESEARCH
published: 01 July 2022
doi: 10.3389/fonc.2022.880787

Resistance Training Attenuates Activation of STAT3 and Muscle Atrophy in Tumor-Bearing Mice

Mayra Tardelli de Jesus Testa[1], *Paola Sanches Cella*[1], *Poliana Camila Marinello*[1,2], *Fernando Tadeu Trevisan Frajacomo*[3], *Camila de Souza Padilha*[1,4], *Patricia Chimin Perandini*[1], *Felipe Arruda Moura*[1], *José Alberto Duarte*[5], *Rubens Cecchini*[2], *Flavia Alessandra Guarnier*[2] *and Rafael Deminice*[1]*

[1] Department of Physical Education, State University of Londrina, Londrina, Brazil, [2] Department of General Pathology, State University of Londrina, Londrina, Brazil, [3] Program of Molecular Carcinogenesis, Brazilian National Institute of Cancer, Rio de Janeiro, Brazil, [4] Department of Physical Education, State University of São Paulo (UNESP), Presidente Prudente, Brazil, [5] Faculty of Sport, University of Porto, CIAFEL, Porto, Portugal

Purpose: Although the role of signal transducers and activators of transcription (STAT3) in cachexia due to the association of circulating IL-6 and muscle wasting has been extensively demonstrated, the effect of resistance training on STAT3 in mediating muscle atrophy in tumor-bearing mice is unknown. The aim of this study is to investigate the effects of resistance exercise training on inflammatory cytokines and oxidative-mediated STAT3 activation and muscle loss prevention in tumor-bearing mice.

Methods: Male Swiss mice were inoculated with Ehrlich tumor cells and exposed or not exposed to resistance exercise protocol of ladder climbing. Skeletal muscle STAT3 protein content was measured, compared between groups, and tested for possible association with plasma interleukins and local oxidative stress markers. Components of the ubiquitin-proteasome and autophagy pathways were assessed by real-time PCR or immunoblotting.

Results: Resistance training prevented STAT3 excessive activation in skeletal muscle mediated by the overabundance of plasma IL-6 and muscle oxidative stress. These mechanisms contributed to preventing the increased key genes and proteins of ubiquitin-proteasome and autophagy pathways in tumor-bearing mice, such as Atrogin-1, LC3B-II, and Beclin-1. Beyond preventing muscle atrophy, RT also prevented strength loss and impaired locomotor capacity, hallmarks of sarcopenia.

Conclusion: Our results suggest that STAT3 inhibition is central in resistance exercise protective effects against cancer-induced muscle atrophy and strength loss.

Keywords: autophagy, cancer cachexia, muscle wasting, strength, ubiquitin-proteasome

OPEN ACCESS

Edited by:
Peti Thuwajit,
Mahidol University, Thailand

Reviewed by:
Viviana Moresi,
National Research Council (CNR), Italy
Paola Costelli,
University of Turin, Italy
Anirban Roy,
University of Houston, United States
Hualin Sun,
Nantong University, China

***Correspondence:**
Rafael Deminice
rdeminice@uel.br
orcid.org/0000-0002-9246-1079

Specialty section:
This article was submitted to Molecular and Cellular Oncology, a section of the journal Frontiers in Oncology

Received: *21 February 2022*
Accepted: *06 June 2022*
Published: *01 July 2022*

Citation:
Testa MTdJ, Cella PS, Marinello PC, Frajacomo FTT, Padilha CdS, Perandini PC, Moura FA, Duarte JA, Cecchini R, Guarnier FA and Deminice R (2022) Resistance Training Attenuates Activation of STAT3 and Muscle Atrophy in Tumor-Bearing Mice. Front. Oncol. 12:880787. doi: 10.3389/fonc.2022.880787

INTRODUCTION

Muscle wasting and cachexia are recognized as important and preeminent complications in cancer development and treatment (1). Cachexia, and in particular skeletal muscle wasting and weakness, leads to decreased functional capacity that negatively impacts the cancer patient's quality of life, treatment adherence, and survival (2). Indeed, muscle wasting and cachexia development have been demonstrated to increase the length of stay (6 vs. 3 days), hospitalization cost (44%), and thereby, risk of mortality in cachectic compared to non-cachectic cancer patients (3).

Despite the relevance of cachexia syndrome to cancer patient outcomes, anti-cachexia treatments are still lacking. The currently available standard-of-care for cachectic cancer patients is limited to nutritional support, while there are still no specific drugs available to counteract muscle wasting and cancer cachexia. In this scenario, resistance exercise training (RT) emerges as an anti-cachexia strategy. Recent pre-clinical studies have demonstrated that RT counteracted muscle wasting and functional decline (4–6). However, the mechanism by which RT protects against cancer-induced muscle wasting and strength loss is still debated.

Skeletal muscle loss during cancer occurs due to an imbalance between muscle protein synthesis and degradation (7). Such imbalance has been demonstrated to be driven by the tumor that releases proteolysis induction factors and promotes a sort of modification that, in turn, causes increased reactive oxygen species (ROS) formation and chronic inflammatory state, both key triggers for proteolytic pathway up-regulation in skeletal muscle (8). Indeed, excessive ROS formation and inflammatory cytokines release (i.e., tumoral necrosis factor-alpha [TNF-α], interleukin- 6, and 1β [IL-6 and IL-1β]) are master mediators of proteolytic systems and muscle atrophy during cancer (9). Signal transducer and activator of transcription 3 (STAT3) is a member of the STAT protein family in humans that is markedly phosphorylated in response to cytokines and ROS formation, acting as a transcriptional activator of proteolytic pathways such as ubiquitin-proteasome system (UPS), the major contractile proteins degradation system in skeletal muscle (10). Recently, some studies have also indicated that STAT3 participates in the process of autophagy during cancer (11, 12). Among other related cytokines, IL-6 is a potent STAT3 activator. Indeed, pre-clinical studies have demonstrated that STAT3 is activated in muscle mediated by IL-6 excess and significantly contributes to muscle wasting during cancer (13–17). Despite the importance of STAT3 to mediate muscle wasting and the emerging anti-atrophy protective effect of RT during cancer, the effect of RT on STAT3-mediated muscle atrophy in tumor-bearing mice is unknown.

This study aimed to investigate the effects of RT on STAT3 activation by increased inflammatory cytokines and oxidative damage during tumor-induced muscle atrophy and strength loss. We hypothesized that RT may protect against the excessive activation of STAT3 by the overabundance of IL-6 and oxidative stress during cancer-induced muscle atrophy and strength loss. RT protective effects against the excessive activation of STAT3 may attenuate key targets of major proteolytic pathways, such as UPS and autophagy in skeletal muscle. Given its position downstream of a variety of cachexia-promoting factors, STAT3 would be indicated as a potential key node for future therapeutic treatments.

METHODS

Animals and Study Design

Forty male *Swiss* mice, aged 6-7 weeks old, were obtained from our institutional animal facilities. The animals were housed in collective cages under controlled temperature (22± 10C), on a regular dark-light cycle (12h light/dark), and with free access to food (Nuvilab CR-1, Nuvital Nutrients Ltda., Curitiba, Brazil) and water during the whole experimental period. All procedures were approved by the Ethics Committee for Animal Use of the State University of Londrina (# 28336.2014.38) and followed the Guidelines of the Brazilian College of Animal Experimentation (COBEA) recommendations. Animals were placed in individual cages during the experiment to avoid confounders. Only two researchers (PSC and FTF) were responsible for group allocation at the different stages of the experiment. This study was conducted in accordance with the ARRIVE guidelines (Animal Research: Reporting of *In Vivo* Experiments).

Mice were randomly allocated in one of the following four groups: control (C, n=10), tumor-bearing (T, n= 10), exercised (E, n=10), and tumor-bearing exercised (TE, n=10). The number of animals was based on a previous study of our group (18), based on the number needed to generate cachexia (5% reduced body weight and muscle atrophy) considering an effect size of 0.90, power of 80%, and significance of 5%. There was no animal exclusion during the experiment.

Ehrlich breast carcinoma cells were inoculated two days before starting the resistance exercise training in the T and TE groups. Animals from groups C and E were injected with phosphate buffer solution (PBS). Both groups E and TE were submitted to a progressive resistance training for four weeks. Meanwhile, the physical activity of the animals in groups C and T was restricted to the space of their cages. Body weight and tumor volume were measured three times a week. The animals were euthanized 48 h after the last session of RT and fasted for 6 h; thus, the experimental design lasted 28 days of RT, 32 days of tumor growth.

Tumor Cells Inoculation

Ehrlich breast carcinoma cells were inoculated into the right flank of T and TE mice, as previously described by Frajacomo et al. (18). Tumor cells were obtained from the ascitic intraperitoneal cavity (2.0x106 cells in 0.5ml PBS) from host animals, in a phosphate buffer (PBS, pH 7.4) with 8 μL/mL of 5,000 IU/mL heparin and centrifuged at 1,000 *g*. In a Neubauer chamber, the percentage of viable cells was then determined using trypan blue dye exclusion, in which non-viable cells were stained blue. Animals from the T and TE groups were inoculated with a suspension of Ehrlich tumor cells (1 x 106 in 100μl PBS), subcutaneously into the right

flank, after which tumors were left to develop for 32 days. The inoculation of tumor cells occurred just once, and animals from the C and E groups received 100µl of PBS.

RT Protocol

RT was performed as previously described in a ladder-climbing protocol for rats (5, 6, 19) adapted to mice. RT consisted of a set of ladder-climbing (0.5m, 0.01m grid, 900 incline) projected so it favored 8-12 dynamic movements per climb. At the top of the ladder, a dark, covered chamber was placed so the mice could rest between the climbing bouts. One week after adapting to the climbing apparatus, the mice were subjected to four to eight ladder climbs with loads attached to their tails that progressively increased in weight according to their daily performance. Thus, the maximum load achieved by each mouse in the previous training session served as a parameter to determine the subsequent training load of that mouse. The procedure was repeated three times per week for 28 days, for 12 training sessions total. Mice in the C and T-groups performed movements that were restricted to their space in their cages, except on days one and 28, when all animals were submitted to an RT protocol to determine their maximal load-carrying ability.

Grip Strength, Locomotion, and Exploratory Activity

Once a week, the grip strength of the mice was determined using a dynamometer EEF 305 Grip Strength Meter (Insight R, Ribeirão Preto, Brazil) as previously described by Voltarelli et al. (20). The quantitative data used corresponds to the mean strength of three attempts performed by the animals. Data were reported as percentage changes from the control group. All tests were carried out under the same experimental conditions for all mice.

Locomotion and exploratory activity were determined using an open field arena (60 × 60 cm) as previously described by Voltarelli et al. (20). Briefly, the animals were recorded (digital camera, Logitech, C920, 30 Hz, fixed 90 cm above the arena) for a total of five minutes while they freely explored the open field arena. Using an automatic tracking method *via* DVideo software interface (21), the total distance traveled was measured and used as a locomotion and exploration parameter. Center crosses was calculated and used as a fragility index, since decreased exploration in the center of the open-field by the rodents is interpreted as a tendency for absence of novelty-seeking and risk-taking behavior (22).

Euthanasia and Tissue Preparation

Forty-eight hours after the last RT session (32 days after tumor cells inoculation), the mice were anesthetized with isoflurane (5%) and euthanized by exsanguination. Blood was collected by cardiac puncture and placed into heparinized tubes, centrifuged at 1,000 *g*, and the plasma separated and stored at -80°C for further analysis. Soleus and extensor digitorum skeletal muscles (EDL) were dissected, weighed, and fixed in 4% paraformaldehyde for histological analysis. Tumors, spleen, gastrocnemius skeletal muscle, and retroperitoneal fat were also removed and weighed; gastrocnemius was quickly frozen in liquid nitrogen and then stored at -80°C for further analysis. The sum of the weights of the gastrocnemius, soleus, and EDL was used as muscle mass parameter.

Histological Analysis

For optical microscopy analysis, soleus and EDL were fixed in 4% paraformaldehyde for 24 hours, dehydrated with graded ethanol, and embedded in paraffin blocks. Semi-thin sections of 5µm thickness were performed in a microtome, placed on glass slides, and subsequently stained with picrosirius red (H&E). For the determination of the fiber cross-sectional area (CSA) of skeletal muscles, images were captured on an optical microscope at a magnification of 100x, and the CSA of muscle fibers was quantified in six animals per group using ImageJ software (National Institutes of Health, Bethesda, MD, USA).

Cytokines and Oxidative Stress Response Analysis

Plasma TNF-α (Ref: #88-7340-88) and IL-6 (Ref: #88-7064-88) were determined using the ELISA Ready-SET-Go kit from eBioscience (San Diego, CA, USA). Skeletal muscle samples were homogenized in 500µL PBS containing protease inhibitor. Lipid peroxidation was determined by the quantification of malondialdehyde on a thiobarbituric acid reaction substances (TBARS) as previously described by Spirlandeli et al. (23). Advanced oxidation protein products (AOPP) were determined according to Witko-Sarsat et al. (24). Reduced and oxidized glutathione levels (GSH and GSSG, respectively) were measured as described by Rahman et al. (25).

Determination of mRNA Expression

RNA was isolated from 50 mg of frozen gastrocnemius using a RiboPure Kit (part no. AM 1924; Ambion, Austin, TX, USA) according to the manufacturer's instructions, after which total RNA was quantified by spectrophotometry at an optical density of 260/280 (NanoDrop 2000c; Thermo Scientific, Waltham, MA, USA). An additional DNase I treatment (DNA-free kit, part no. AM1906; Ambion, Austin, TX, USA) was performed to remove contaminating genomic DNA from the isolated RNA. Next, complementary DNA (cDNA) was synthesized from 1000 ng of total RNA using a high-capacity cDNA reverse transcription kit (part no. 4374966; Applied Biosystems, Foster City, CA, USA). A quantitative polymerase chain reaction (PCR) was performed using the ViiA7 Real-Time PCR System (Applied Biosystems, Foster City, CA, USA). The following Taqman® gene expression assays (Applied Biosystems, Foster City, CA, USA) were used in this study: FOXO1, FOXO3, Atrogin-1, and PGC-1α. PCR cycles were as follows: one cycle of 500C for 2 minutes, one cycle of 95°C for 20 seconds, 40 cycles of 01 second at 95°C, 20 seconds at 60°C. All amplification reactions were performed in triplicate, and peptidylprolyl isomerase A and beta-actin were used as a reference gene to normalize reactions. The relative expression was determined by the 2-ΔΔCT method.

Immunoblotting

Proteins from gastrocnemius muscle samples were extracted using the extraction buffer [50 mM of HEPES, 40 mM of NaCl, 2 mM of EDTA, 1.5 mM of Na3VO4, 50 mM of NaF, 0.1% sodium dodecyl

sulfate (SDS), 0.1% Triton X-100, and a protease and phosphatase inhibitor cocktail (#5872 Cell Signaling Technology, Danvers, MA, USA)] at 1:10 proportion. The total protein was determined by BCA assay (QPRO BCA protein assay, Cyanogen, Bologna, Italy), and equivalent amounts of 20–80 µg protein were electrophoresed on 10% SDS-PAGE in running buffer with 25 mM of Tris-base, 1.92 M of glycine (pH 8.6), and 1% SDS. Gels were blotted into a polyvinylidene difluoride (Immun-Blot® PVDF Membrane, Bio-Rad, Hercules, CA, USA) in transfer buffer containing 25 mM of Tris, 192 mM of glycine (pH 8.3), and 20% methanol. Non-specific binding was blocked with 5% (w/v) dry nonfat milk in TBS-T (anti-Fbx32/atrogin-1 1:1,000 Abcam catalog #ab74023, anti-MuRF-1 1:1,000 Abcam catalog #ab172479, anti-Phospho-Stat3 (Tyr705) 1:1,000 Cell Signaling catalog #9131, anti-Stat3 1:1,000 Cell Signaling catalog #12640; Anti SQSTM1/p62 1:1,000 Cell Signaling catalog #5114; Anti-Beclin-1 1:1,100 Invitrogen Catalog #PA1-18857; Anti-LC3B 1:1,100 Invitrogen Catalog #PA5-32254) overnight at 4°C, washed, and incubated with a secondary horseradish peroxidase-conjugated anti-rabbit antibody (anti-rabbit IgG 1:4,000 Bio-Rad, Hercules, CA, USA). Immunoreactivity bands were detected by enhanced chemiluminescence ECL (GE Healthcare, Chicago, IL, USA) according to the manufacturer's instructions. Total protein determined using a Ponceau buffer was used for normalization. Band quantification was performed by optical densitometry using Image Studio Lite Ver 5.2 (Li-Cor Biosciences, Lincoln, NE, USA).

Statistical Analyses

All data were expressed as mean ± standard deviation except CSA that was presented in dispersion data and frequency distribution. The data normality was checked using Shapiro-Wilk and D'Agostino-Pearson tests. Two-way analysis of variance (ANOVA) was applied for parametric group comparisons. When an *F* ratio was significant, Tukey's *post hoc* test was used to identify significant differences. The Kruskal-Wallis test compared the CSA muscles, followed by Dunn's *post hoc* test. The Pearson's correlation coefficient was used to determine the association among STAT3 protein content and interleukins and oxidative damage parameters. The significance level was significant when $P< 0.05$ in all cases. GraphPad Prism 5 and Origin 12.0 were used for statistical analysis and graphic production.

RESULTS

Resistance Training Prevented Tumor-Induced Muscle Wasting

Tumor grew progressively, reaching 15.5 ± 3.2% of the body weight of the mice 32 days after tumor cell inoculation in both T and TE groups. No changes in tumor volume or weight were demonstrated between T and TE groups (**Figures 1A, B**). Tumor-bearing mice exhibited significantly (P <.05) less weight (6.5 ± 1.1%) when compared to the controls (**Figure 1C**). Tumor-bearing mice also presented splenomegaly, significantly less retroperitoneal fat and a significant 16.1% reduction in muscle mass compared to control mice (**Figures 1E–J**). RT partially mitigated muscle wasting (P <.05) but did not prevent body weight and fat loss, tumor growth or splenomegaly. No changes in food intake emerged among the groups (**Figure 1D**).

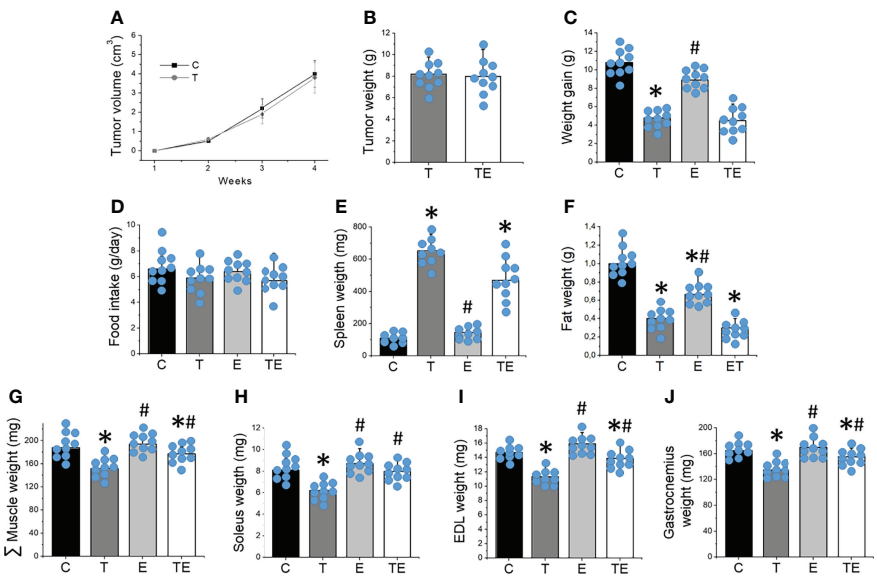

FIGURE 1 | Resistance training prevented tumor-induced muscle wasting. **(A)** tumor volume over the 4 weeks (n = 10) and **(B)** tumor mass (n = 10), **(C)** weight gain (n = 10), **(D)** food intake (n = 10), **(E)** spleen and **(F)** fat weight (n = 10), **(G)** sum of skeletal muscle mass (n = 10), **(H)** soleus (n = 10), **(I)** EDL (n = 10) and **(J)** gastrocnemius (n = 10) mass after 4 weeks of experiment for groups control, tumor-bearing, exercised and tumor-bearing exercised. Results are mean ± standard deviation. *p < .05, compared with control; #p < .05, compared with Tumor-bearing group (by ANOVA two-way followed by Tukey post-hoc test). C, control group; E, exercised; T, tumor-bearing; TE, tumor-bearing exercised.

Resistance Training Attenuated Tumor-Induced Muscle Atrophy, Strength Loss, and Impaired Locomotor Capacity

The tumor development provoked EDL and soleus muscle atrophy compared to the control group, as demonstrated by muscle fiber CSA (**Figure 2**). By contrast, RT mitigated the muscle atrophy in both EDL and soleus muscles (P <.05). Tumor development also impaired muscle strength measured by grip strength and maximal training load (**Figures 3A, B**) and locomotion and exploration capacity in tumor-bearing mice (**Figures 3C, D**). RT prevented muscle strength loss and impaired mice locomotion and exploration capacity (P <.05) (**Figure 3**). Notably, the maximal training load was greater in tumor-bearing exercised mice than in the healthy sedentary control group (**Figure 3B**).

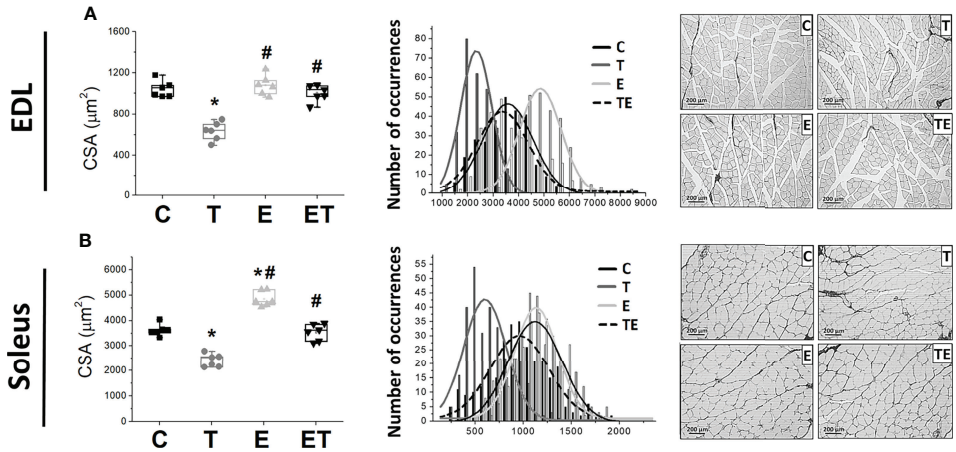

FIGURE 2 | Resistance exercise attenuates tumor-induced muscle loss. Scatter plot of the median cross-sectional area (left) and cross-sectional area distribution by occurrence number (right) of **(A)** soleus muscle (n = 6) and **(B)** EDL muscles (n = 6); representative images of cross-sectional area of soleus muscle (C) in groups control, tumor bearing, exercised and tumor-bearing exercised. *$p < .05$, compared with control group; #$p < .05$, compared with Tumor-bearing group (by Kruskal-Wallis test followed by Dunn's *post-hoc)*. C, control group; CSA, Cross Sectional Area; E, exercised; EDL, extensor digitorum longus; T, tumor-bearing; TE, tumor-bearing exercised.

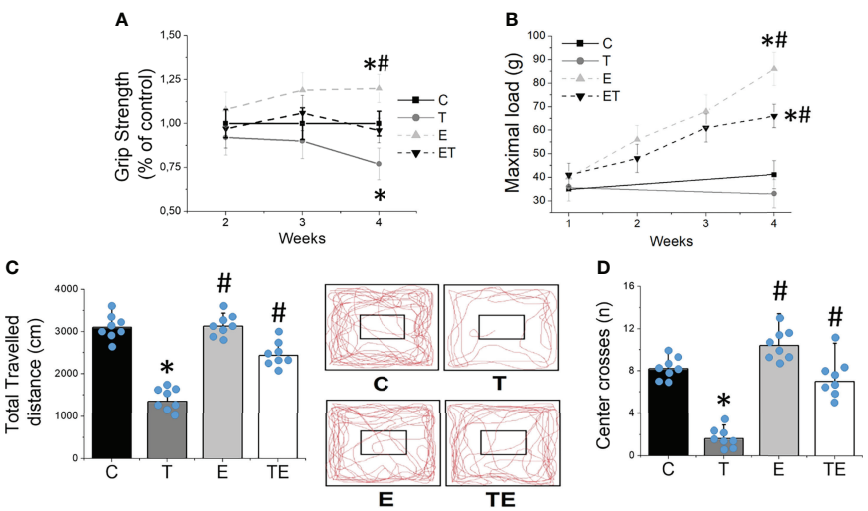

FIGURE 3 | Resistance exercise preclude impaired muscle function provoked by tumor growth. **(A)** grip strength gain (n = 10) and **(B)** maximal carrying load (n = 10) over 4 weeks. **(C)** locomotor/exploratory capacity demonstrated by total travelled distance (n = 8) and **(D)** number of center crosses (n = 8) in groups control, tumor-bearing, exercised and tumor-bearing exercised. Results are mean ± standard deviation. *$p < .05$, compared with control; #$p < .05$, compared with Tumor-bearing group (by ANOVA two-way followed by Tukey *post-hoc* test). C, control group; E, exercised; T, tumor-bearing; TE, tumor-bearing exercised.

RT Attenuated Muscle Atrophy by Preventing STAT3 Phosphorylation Mediated by Decreasing IL-6 and Muscle Lipid Peroxidation

STAT3-phosphorylated protein content was markedly elevated in the skeletal muscle of tumor-bearing mice compared to the controls (**Figure 4A**). In agreement with previous studies using different cancer cachexia models (5, 6, 18), Ehrlich tumor development presented characteristics of pro-inflammatory scenario, as demonstrated by significant (P <.05) elevated TNF-α and IL-6 in plasma of tumor-bearing mice compared to the control group (**Figures 4B, C**). Tumor-bearing mice also presented skeletal muscle oxidative damage, as demonstrated by elevated levels (P <.05) of the lipid peroxidation evaluated by TBARS, protein oxidation evaluated by AOPP, and redox imbalance demonstrated by elevated skeletal muscle GSSG concentration and reduced GSH/GSSG ratio (**Figures 4D–F**). Notably, STAT3-phosphorylated protein content was significantly correlated with plasma IL-6 and muscle TBARS concentrations (**Figures 4G, H**). These data demonstrated that STAT3 activated in skeletal muscle is strictly associated with elevated IL-6 and lipid peroxidation and significantly contributes to muscle wasting during tumor growth. By contrast, RT prevented tumor-induced elevation on IL-6 plasma concentration and oxidative damage markers on skeletal muscle, which attenuated STAT3 phosphorylation (**Figure 4**), all events that play a key role in skeletal muscle protein degradation.

RT Prevents the Increase of Key Genes and Proteins of Ubiquitin-Proteasome and Autophagy Pathways in Tumor-Bearing Mice

Expression of the RNA for FoXO1, FoXO3, and Atrogin-1, key genes in skeletal muscle proteolysis, were elevated along with the tumor development (**Figure 5A**). We also observed markedly elevated expression of muscle-specific ubiquitin ligases Atrogin-1 and Murf-1 (**Figures 5B, C**), as well as autophagy pathway proteins such as LC3B-II and Beclin-1 (**Figures 5D, E**) in tumor-bearing mice compared to the control. The expression of p62 was also elevated in tumor-bearing mice compared to the control, similar to demonstrated in previous studies (26–28). Consistent with the protective effect of RT on muscle atrophy, RT prevented elevated RNA levels of FoXO1 and FoXO3, and RNA and protein levels of Atrogin-1, master regulators and a key element of skeletal muscle proteolysis on the ubiquitin-proteasome system, respectively. RT also protected skeletal muscle against tumor-induced elevated autophagy proteins LC3B-II, Beclin-1 and p62. Heathy exercised mice (E group)

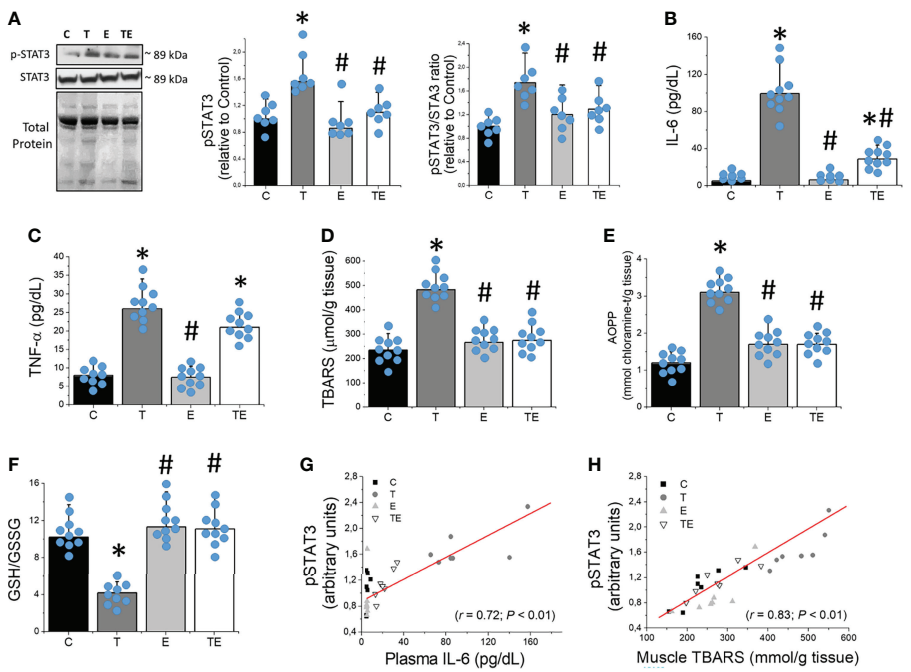

FIGURE 4 | Resistance exercise prevents tumor growth-induced STAT3 phosphorylation associated to elevated IL-6 and skeletal muscle oxidative stress. **(A)** Skeletal muscle protein levels of STAT3 (n = 7), **(B)** plasmatic concentration of IL-6 (n = 10) and **(C)** TNF-α (n = 10), **(D)** skeletal muscle concentration of TBARS (n = 10), **(E)** AOPP (n = 10) and **(F)** GSH/GSSG ratio (n = 10). **(G)** Association between skeletal muscle protein levels of STAT3 and IL-6 plasma concentration and **(H)** skeletal muscle TBARS concentration (n = 7) for groups control, tumor-bearing, exercised and tumor-bearing exercised groups. Results are mean ± standard deviation. *$p < .05$, compared with control; #$p < .05$, compared with Tumor-bearing group (by ANOVA two-way followed by Tukey *post-hoc* test). AOPP, advanced oxidation protein products; C, control group; E, exercised; GSH, Glutathione; GSSG, Glutathione disulfide; pSTAT-3, Signal transducers of transcription- phosphorylated; STAT-3, Signal transducers of transcription; T, tumor-bearing; TBARS, Thiobarbituric acid reactive substances; TE, tumor-bearing exercised; TNF-α, tumor necrosis factor-alpha.

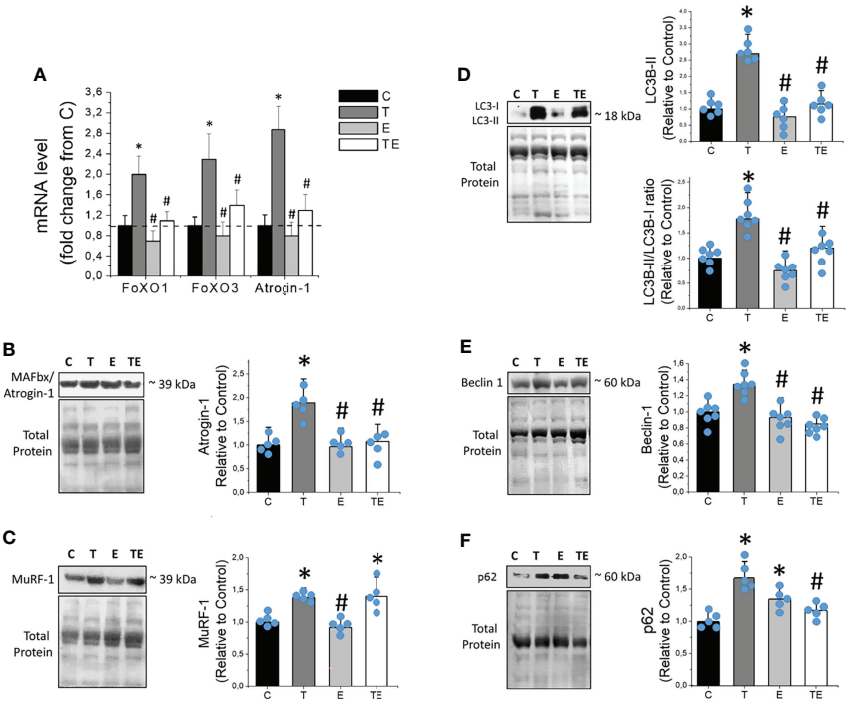

FIGURE 5 | Resistance exercise prevents tumor-induced elevation of proteolytic key genes and proteins linked to ubiquitin-proteasome and autophagy system. **(A)** Skeletal muscle mRNA levels of FoXO1, FoXO3 and Atrogin-1 (n = 6). **(B)** Skeletal muscle protein levels of MAFbx/Atrogin-1(n = 5), **(C)** MuRF-1 (n = 5), **(D)** LC3B-II and LC3B-II/LC3B-I ratio (n = 6), **(E)** Beclin-1 (n = 6) and **(F)** p62, of control, tumor-bearing, exercised and tumor-bearing exercised groups. Results are mean ± standard deviation. $^{*}p < .05$, compared with control; $^{\#}p < .05$, compared with Tumor-bearing group (by ANOVA two-way followed by Tukey *post-hoc* test). C, control group; E, exercised; FoXO, Forkhead box protein; LC3B-II, Light Chain 3B phosphatidylethanolamine conjugate; MAFbx, Muscle atrophy F-box; mRNA, messenger ribonucleuc acid; Murf-1, Muscle-specific RING finger protein 1; T, tumor-bearing; TE, tumor-bearing exercised.

did not presented any changes in muscle-specific ubiquitin ligases or autophagy proteins, except for modest elevated p62 (**Figure 5F**).

DISCUSSION

Given the emerging data demonstrating the protective effects of RT and the importance of STAT3 on mediating muscle wasting during cachexia, we sought to determine if the protective effects of RT on tumor-induced muscle atrophy and strength loss are associated with the STAT3 signaling mechanism in skeletal muscle. Specifically, we hypothesized that STAT3 changes mediated by RT play a central role in the protective effects of RT during cancer-induced muscle atrophy and strength loss. Indeed, our results show that STAT3 activation mediated by elevated IL-6 plasma concentration and oxidative damage in skeletal muscle plays a key role in tumor-induced muscle atrophy. In contrast and remarkably, RT attenuated muscle atrophy by preventing STAT3 phosphorylation-mediated decreasing IL-6 and muscle lipid peroxidation. This protection contributed to preventing the increase of key genes and proteins of ubiquitin-proteasome and autophagy pathways in tumor-bearing mice, such as Atrogin-1, LC3B-II, Beclin-1 and p62.

Considering the invasiveness of acquiring human muscle tissue from biopsies, we used Ehrlich´s animal model to investigate the mechanisms responsible for the protective effect of exercise during cancer cachexia. We used the Ehrlich solid tumor, a model extensively used as a tool to investigate antineoplastic drugs (29, 30). We recently demonstrated that the Ehrlich tumor model reproduces functional and biological characteristics of cancer cachexia, 28 days after Ehrlich tumor cells inoculation, such as loss of body weight and muscle mass, loss of strength, and muscle atrophy (18), as our data confirmed (**Figures 1** and **2**). Regarding exercise training, ladder climbing was chosen as the RT model because it has been previously demonstrated to be an efficient model to promote muscle hypertrophy in healthy rodents (19) and in the prevention of muscle loss during cancer using different tumor models (5, 6). We also choose ladder climbing as it consists of a voluntary model of RT, the exercise suggested by a meta-analysis and some institutional consensus, to be included in the exercise routine of cancer survivors (31–33).

Chronic inflammation and ROS formation are key drivers of muscle wasting during cancer, as they are important triggers of proteolytic pathways (7). More recently, studies have demonstrated that STAT3 activation, mediated by cytokines and oxidative stress, plays a central role in regulating skeletal

muscle mass during cancer progression (13–15, 17). Among inflammatory cytokines, IL-6 is a key player in STAT3 activation in skeletal muscle. Indeed, the elevated serum levels of IL-6 or IL-6 family ligands (e.g., IL-11, Leukemia Inhibitory Factor) associated with robust activation of the STAT3 pathway in skeletal muscle has been demonstrated in different cancer models in advanced stages, such as C26 (13, 15), ApcMin mice (14), and Lewis lung adenocarcinoma (17). Consistent with those, our data showed excessive activation of STAT3, demonstrated by STAT3 phosphorylation, in response to elevated IL-6 plasma concentration in Ehrlich tumor-bearing mice compared to controls. Notably, we demonstrated that STAT3 phosphorylated protein content was strictly associated with elevated IL-6 plasma concentration. This seems particularly relevant, as IL-6 is produced not only by the immune system but also directly by the tumor (34), which makes cancer a unique and severe form of muscle loss and cachexia.

Along with elevated IL-6 plasma concentration, we also demonstrated increased skeletal muscle lipid peroxidation (TBARS) and protein oxidation (AOPP) markers, combined with imbalanced skeletal muscle redox state, demonstrated by decreased GSH and GSSG ratio in tumor-bearing mice compared to control. Remarkably, TBARS concentration was significantly correlated with STAT3-phosphorylated protein content in skeletal muscle. Although some studies have already demonstrated that oxidative stress induced by hydrogen peroxide (H2O2) or ultraviolet radiation can activate STAT3 in the absence of cytokine stimulation (35, 36), the combination of both elevated inflammatory cytokine and oxidative stress may potentialize muscle wasting during tumor growth. in an *in vitro* model system of murine embryonic fibroblasts, Ng et al. (37) demonstrated that simultaneous exposure to the interleukin-6 family cytokine Leukemia Inhibitory Factor (LIF) and H2O2 drives a striking and persistent phosphorylation of STAT3, whereas STAT3 phosphorylation was only transiently increased in response to LIF alone.

Notably, our data demonstrated that RT provided protection against the activation of STAT3, overabundance of IL-6, and oxidative stress-mediated muscle atrophy in tumor-bearing mice. Although the anti-inflammation and antioxidant effects of exercise are disseminated (38, 39), our study is the first to demonstrate that the protective effects of RT against muscle atrophy during cancer are strictly related to its capacity to attenuate STAT3 phosphorylation and activation. It may seem contradictory, as resistance exercise has been demonstrated to acutely activate STAT3, a mechanism linked to muscle hypertrophy (40, 41). Guerci et al. (42) demonstrated that the IL-6-dependent activation of STAT3 is required for satellite cell proliferation in response to muscle overloading. However, the relation between resistance exercise and IL-6-dependent activation of STAT3 for skeletal atrophy/hypertrophy should consider that IL-6-dependent activation of STAT3 linked to muscle hypertrophy in response to exercise is transient (40–42), while persistent increased IL-6 and STAT3 phosphorylation and activation are linked to muscle atrophy during pro-inflammatory conditions such as cancer cachexia (13–15, 17). Indeed, cancer cachexia patients are exposed to elevated circulating IL-6 levels for weeks, while circulating IL-6 increases punctually after acute exercise. Otherwise, others accompanying our study demonstrated that exercise training inhibits STAT3 phosphorylation-mediated attenuation of pro-inflammatory condition in chronic diseases (43). Thus, when debating the role of IL-6 and reactive species-dependent STAT3 activation promoted by exercise, we should take in account that downstream target activation and its consequences for skeletal muscle might be different considering health versus disease conditions.

Beyond prevention of muscle atrophy, we demonstrated that RT was also able to prevent strength loss and impaired locomotor capacity. This is relevant given that strength loss and physical dysfunction are the hallmarks of sarcopenia, a musculoskeletal disease associated with higher mortality rates in the general population (44) and cancer survivors (45, 46). Indeed, our data demonstrated that RT-trained tumor-bearing mice presented a maximal training load greater than the healthy sedentary controls, also demonstrating that RT protects against sarcopenia. These data support the idea that RT may be part of the standard in oncology treatment, as proposed by some institutions' positions (31, 32).

Consistent with elevated IL-6, oxidative stress, STAT3 phosphorylation, and muscle wasting, we demonstrated elevated expression of key genes and protein levels of UPS and autophagy pathways in tumor-bearing mice compared to controls. Specifically, FoXO1, FoXO3, and Atrogin-1 mRNA levels and protein Murf-1 and Atrogin-1 were markedly increased in tumor-bearing mice compared to control. The same was observed for autophagy-related proteins such as LC3B-II and Beclin-1. Indeed, STAT3 acts as a transcriptional activator of the UPS proteolytic pathway (10) and has been demonstrated to trigger autophagy during cancer (11, 12). Notably, RT was able to prevent the elevation of some important proteolytic transcriptional factors (p-STAT3, FoXO1, FoXO3) and key proteins in UPS and autophagy pathways, conferring protection against muscle wasting in tumor-bearing mice. It may seem paradoxical given that the RT is an exercise modality known to promote hypertrophy and muscle growth. Therefore, studies from our group have demonstrated that in healthy rats, RT promotes the activation of mTORC1 signaling by increasing the phosphorylation of p70S6K, which is associated with skeletal muscle hypertrophy (6). In tumor-bearing rats, however, the RT-induced attenuation of myofiber atrophy was independent of the activation of anabolic mTORC1 activation; RT prevented muscle atrophy during cancer, which was associated with reduced inflammation, oxidative damage, and UPS proteins expression (6). Coherently, White et al. (47) demonstrated that IL-6 signaling inhibition after the initiation of cancer cachexia suppresses the progression of cachexia by sparing muscle mass independently of changes in muscle protein synthesis. These results suggest that proteolysis inhibition is central in the protective effects of RT against cancer-induced muscle atrophy and strength loss. In addition, beyond the ability to confer

intrinsic local skeletal muscle protective phenotype, RT is also able to confer a systemic organic response against tumor growth and the released muscle proteolytic factors such as inflammatory interleukins (5, 48), mechanisms that contribute to protection against cancer-induced muscle wasting.

Autophagy operates a massive amount of proteolysis in different tissues, including skeletal muscle (12). Indeed, altered lysosomal function has also been reported in several myopathies (47), including muscle wasting and cachexia in cancer patients (49) and in pre-clinical models (26–28). The role of STAT3 on autophagy activation is less known. Studies have proposed divergent effects of STAT3 phosphorylation on autophagy; reports have indicated that phosphorylation of STAT3 promotes autophagy activation (50), while others have indicated that p-STAT3 has an inhibitory effect on autophagy flux (12, 51). Our study demonstrated that STAT3 phosphorylation coincides with enhanced autophagy, demonstrated by increased protein expression of LC3B-II and Beclin-1. Indeed, both the lipidated form of microtubule-associated protein 1 light chain 3B (LC3B-II) and the ratio between II and I LC3B isoforms, which are considered reliable markers of autophagosome formation, are significantly elevated in the muscle of tumor-bearing mice compared to controls. In the same way, Beclin-1, a main upstream regulator of autophagic sequestration, was also elevated in tumor-bearing mice compared to controls. Important to note moreover, that increased p62 was also demonstrated in tumor-bearing mice compared to controls, results that, at first glance, contrast with the observation that autophagy is clearly enhanced. These results however, are compatible with previously studies using different cancer cachexia models (26–28). Indeed, p62 accumulation can be the result of either increased autophagic sequestration or reduced autophagosome clearance (52). Penna et al. (26) demonstrated elevated skeletal muscle LC3-II after colchicine administration – a microtubule-destabilizing agent that interacts with tubulin – demonstrating that autophagy is activated in the muscle of cancer cachectic animals even with elevated p62. Notably, we demonstrated that RT inhibited STAT3 phosphorylation, which was accompanied by the prevention of increased autophagic activation. Therefore, our study only suggests, in the absence of an autophagic flux experiment, that the phosphorylation of STAT3 in response to exacerbated IL-6 and ROS formation seems to be associated with autophagy activation during cancer cachexia. In addition, key autophagy protein inhibition seems to play an important role in the protective effects of RT on tumor-induced muscle atrophy since it is directly associated with persistent IL-6 production and phosphorylation of STAT3.

Of note, heathy exercised mice presented elevated p62 compared to controls, despite no changes in LC3B-II and Beclin-1, which, on the surface, seems paradoxal given that the levels of p62 binds LC3 and substrates marked for degradation by ubiquitylation. However, the effects of resistance training on p62 levels in muscle of healthy rodents and humans appear to be controversial. In fact, studies have shown elevated (53), reduced (54, 55) or unchanged (27, 56) p62 muscle levels promoted by RT. That controversy may be explained due to the multifunctional role of p62, protein involved in many signal transduction pathways, including nutrition sensing (*via* mTORC1), inflammation and apoptosis (*via* NF-κB), antioxidant response (*via* Nrf2) (57), in addition to autophagy regulation. In fact, studies have demonstrated p62 and Nrf2 are essential for exercise-mediated enhancement of antioxidant protein expression in skeletal muscle (58). Yamada et al. (58) demonstrated Nrf2 translocation into nuclei is a key event in exercise-mediated increase in antioxidant capacity of skeletal muscle; exercise-induced Nrf2 nuclei translocation can enhance the expression of p62 at the transcription level by directly binding to the promoter region of *p62* gene, forming a positive feedback loop. These authors also demonstrated that the loss of p62 in muscle significantly reduced regular exercise-mediated increase of antioxidant enzyme expression (*i.e.*, CuZnSOD and EcSOD), mimicking observations in Nrf2 mKO mice. Thus, we speculate that the slight increase in p62 without changes in the LC3-II/I ratio we found in heathy mice is compatible with the multifunctional action on this protein, such as exercise induced antioxidant activity. This however, must be further investigated in future studies.

It is important to mention that STAT3 is a transcriptional factor demonstrated to (co-)activate various metabolic pathways beyond the FoXO superfamily, UPS, and autophagy in skeletal muscles. Indeed, studies have demonstrated a vast diversity of assigned functions and other tissues not examined in our study, including tumors (59). In addition, studies have demonstrated that acute phosphorylation level of STAT3 imposed by IL-6 addition (12) or physical exercise (40, 41) is associated with muscle growth and may cause inhibited UPS and autophagy signaling (12). This response differs from that demonstrated during persistent inflammation, as the model we used in the present study. Thus, the STAT3 pathway's complexity warrants attention when considering its roles in RT-induced protection against cancer-induced muscle atrophy. Other pathways, functions, and targets of STAT3 should be considered in the future. It is also important to mention that some limitations must be considered in the present research. The absence of additional experiments using STAT3-modulating agents, as well as the absence of autophagy flux assessment can be considered limitations of the present study. These could bring new and important data about the role of STAT3 and autophagy on cancer cachexia and RT-protection effects.

In conclusion, our data demonstrated that RT prevents against STAT3 excessive activation in skeletal muscle mediated by the overabundance of plasma IL-6 and muscle oxidative stress, a key role to attenuate cancer-induced muscle atrophy. These mechanisms contributed to preventing the increase of key genes and proteins of ubiquitin-proteasome and autophagy pathways in tumor-bearing mice, such as Atrogin-1, LC3B-II, and Beclin-1. Beyond preventing muscle atrophy, RT also prevented strength loss and impaired locomotor capacity, conditions associated with higher mortality rates and better life quality in cancer patients.

DATA AVAILABILITY STATEMENT

The raw data supporting the conclusions of this article will be made available by the authors, without undue reservation.

ETHICS STATEMENT

The animal study was reviewed and approved by Ethics Committee for Animal Use of the State University of Londrina (# 28336.2014.38) and followed the Guidelines of the Brazilian College of Animal Experimentation (COBEA) recommendations.

AUTHOR CONTRIBUTIONS

MT designed the study, participated in data collection, contributed to analysis and interpretation of data and wrote the final version of the manuscript. PC participated in data collection, contributed to analysis and interpretation of data and wrote the final version of the manuscript. PM participated in data collection, contributed to analysis and interpretation of data. FF designed the study, participated in data collection, contributed to analysis and interpretation of data and wrote the final version of the manuscript. CP participated in data collection, contributed to analysis and interpretation of data and assisted in the preparation of the manuscript. PP contributed to analysis and interpretation of data and assisted in the preparation of the manuscript. JD designed the study, contributed to analysis and interpretation of data and wrote the final version of the manuscript. RC provided specialized technical assistance to the project. FG contributed to analysis and interpretation of data and assisted in the preparation of the manuscript. RD designed the study and wrote the final version of the manuscript. All authors contributed to the article and approved the submitted version.

FUNDING

This study was supported by Coordenação de Aperfeiçoamento de Pessoal de Niível Superior – Brazil (CAPES) and Fundação Araucaíria. RD is supported by CNPq-Brazil #306842/2021-1 and #403232-2021-0.

REFERENCES

1. Fearon K, Arends J, Baracos V. Understanding the Mechanisms and Treatment Options in Cancer Cachexia. *Nat Rev Clin Oncol* (2013) 10:90–9. doi: 10.1038/nrclinonc.2012.209
2. Swellengrebel HA, Marijnen CA, Verwaal VJ, Vincent A, Heuff G, Gerhards MF, et al. Toxicity and Complications of Preoperative Chemoradiotherapy for Locally Advanced Rectal Cancer. *Br J Surg* (2011) 98:418–26. doi: 10.1002/bjs.7315
3. Arthur ST, Van Doren BA, Roy D, Noone JM, Zacherle E, Blanchette CM. Cachexia Among US Cancer Patients. *J Med Econ* (2016) 19:874–80. doi: 10.1080/13696998.2016.1181640
4. Donatto FF, Neves RX, Rosa FO, Camargo RG, Ribeiro H, Matos-Neto EM, et al. Resistance Exercise Modulates Lipid Plasma Profile and Cytokine Content in the Adipose Tissue of Tumour-Bearing Rats. *Cytokine* (2013) 61:426–32. doi: 10.1016/j.cyto.2012.10.021
5. Padilha CS, Borges FH, Costa Mendes da Silva LE, Frajacomo FTT, Jordao AA, Duarte JA, et al. Resistance Exercise Attenuates Skeletal Muscle Oxidative Stress, Systemic Pro-Inflammatory State, and Cachexia in Walker-256 Tumor-Bearing Rats. *Appl Physiol Nutr Metab* (2017) 42:916–23. doi: 10.1139/apnm-2016-0436
6. Padilha CS, Cella PS, Chimin P, Voltarelli FA, Marinello PC, Testa MTJ, et al. Resistance Training's Ability to Prevent Cancer-Induced Muscle Atrophy Extends Anabolic Stimulus. *Med Sci Sports Exerc* (2021) 53:1572–82. doi: 10.1249/MSS.0000000000002624
7. Argilés JM, Busquets S, Stemmler B, López-Soriano FJ. Cancer Cachexia: Understanding the Molecular Basis. *Nat Rev Cancer* (2014) 14:754–62. doi: 10.1038/nrc3829
8. Hussey HJ, Todorov PT, Field WN, Inagaki N, Tanaka Y, Ishitsuka H, et al. Effect of a Fluorinated Pyrimidine on Cachexia and Tumour Growth in Murine Cachexia Models: Relationship With a Proteolysis Inducing Factor. *Br J Cancer* (2000) 83:56–62. doi: 10.1054/bjoc.2000.1278
9. Onesti JK, Guttridge DC. Inflammation Based Regulation of Cancer Cachexia. *BioMed Res Int* (2014) 2014:168407. doi: 10.1155/2014/168407
10. Bilodeau PA, Coyne ES, Wing SS. The Ubiquitin Proteasome System in Atrophying Skeletal Muscle: Roles and Regulation. *Am J Physiol - Cell Physiol* (2016) 311:C392–403. doi: 10.1152/ajpcell.00125.2016
11. Yoon S, Woo SU, Kang JH, Kim K, Kwon MH, Park S, et al. STAT3 Transcriptional Factor Activated by Reactive Oxygen Species Induces IL6 in Starvation-Induced Autophagy of Cancer Cells. *Autophagy* (2010) 6:1125–38. doi: 10.4161/auto.6.8.13547
12. Qin B, Zhou Z, He J, Yan C, Ding S. IL-6 Inhibits Starvation-Induced Autophagy *via* the STAT3/Bcl-2 Signaling Pathway. *Sci Rep* (2015) 5:1–10. doi: 10.1038/srep15701
13. Bonetto A, Aydogdu T, Kunzevitzky N, Guttridge DC, Khuri S, Koniaris LG, et al. STAT3 Activation in Skeletal Muscle Links Muscle Wasting and the Acute Phase Response in Cancer Cachexia. *PloS One* (2011) 6(7):e22538. doi: 10.1371/journal.pone.0022538
14. Baltgalvis KA, Berger FG, Peña MM, Davis JM, White JP, Carson JA, et al. Muscle Wasting and Interleukin-6-Induced Atrogin-I Expression in the Cachectic ApcMin/+Mouse. *Pflugers Arch Eur J Physiol* (2009) 457:989–1001. doi: 10.1007/s00424-008-0574-6
15. Bonetto A, Aydogdu T, Jin X, Zhang Z, Zhan R, Puzis L, et al. JAK/STAT3 Pathway Inhibition Blocks Skeletal Muscle Wasting Downstream of IL-6 and in Experimental Cancer Cachexia. *Am J Physiol - Endocrinol Metab* (2012) 303 (3):E410–21. doi: 10.1152/ajpendo.00039.2012
16. Chen L, Yang Q, Zhang H, Wan L, Xin B, Cao Y, et al. Cryptotanshinone Prevents Muscle Wasting in CT26-Induced Cancer Cachexia Through Inhibiting STAT3 Signaling Pathway. *J Ethnopharmacol* (2020) 260:113066. doi: 10.1016/j.jep.2020.113066
17. Zhang G, Jin B, Li Y-P. C/EBPb Mediates Tumour-Induced Ubiquitin Ligase Atrogin1/MAFbx Upregulation and Muscle Wasting THE. *EMBO J* (2011) 30:4323–35. doi: 10.1038/emboj.2011.292
18. Frajacomo FTT, de Souza Padilha C, Marinello PC, Guarnier FA, Cecchini R, Duarte JA, et al. Solid Ehrlich Carcinoma Reproduces Functional and Biological Characteristics of Cancer Cachexia. *Life Sci* (2016) 162:47–3. doi: 10.1016/j.lfs.2016.08.009
19. Padilha CS, Cella PS, Ribeiro AS, Voltarelli FA, Testa MTJ, Marinello PC, et al. Moderate vs High-Load Resistance Training on Muscular Adaptations in Rats. *Life Sci* (2019) 238:116964. doi: 10.1016/j.lfs.2019.116964
20. Voltarelli FA, Frajacomo FT, Padilha CS, Testa MTJ, Cella PS, Ribeiro DF, et al. Syngeneic B16F10 Melanoma Causes Cachexia and Impaired Skeletal Muscle Strength and Locomotor Activity in Mice. *Front Physiol* (2017) 8:6–13. doi: 10.3389/fphys.2017.00715

21. Figueroa PJ, Leite NJ, Barros RML. Background Recovering in Outdoor Image Sequences: An Example of Soccer Players Segmentation. *Image Vis Comput* (2006) 24:363–74. doi: 10.1016/j.imavis.2005.12.012
22. Valvassori SS, Varela RB, Quevedo J. Chapter 38 - Animal Models of Mood Disorders: Focus on Bipolar Disorder and Depression. In: *Conn M. Animals Models for Study of Human Disease, 2nd ed.* (2017). p. 991–1001. doi: 10.1016/B978-0-12-809468-6.00038-3
23. Spirlandeli AL, Deminice R, Jordao AA. Plasma Malondialdehyde as Biomarker of Lipid Peroxidation: Effects of Acute Exercise. *Int J Sports Med* (2014) 35:14–8. doi: 10.1055/s-0033-1345132
24. Witko-Sarsat V, Friedlander M, Capeillère-Blandin C, Nguyen-Khoa T, Nguyen AT, Zingraff J, et al. Advanced Oxidation Protein Products as a Novel Marker of Oxidative Stress in Uremia. *Kidney Int* (1996) 49:1304–13. doi: 10.1038/ki.1996.186
25. Rahman I, Kode A, Biswas SK. Assay for Quantitative Determination of Glutathione and Glutathione Disulfide Levels Using Enzymatic Recycling Method. *Nat Protoc* (2006) 1(6):3159–65. doi: 10.1038/nprot.2006.378
26. Penna F, Costamagna D, Pin F, Camperi A, Fanzani A, Chiarpotto EM, et al. Autophagic Degradation Contributes to Muscle Wasting in Cancer Cachexia. *Am J Pathol* (2013) 182:1367–78. doi: 10.1016/j.ajpath.2012.12.023
27. Ranjbar K, Ballarò R, Bover Q, Pin F, Beltrà M, Penna F, et al. Combined Exercise Training Positively Affects Muscle Wasting in Tumor-Bearing Mice. *Med Sci Sports Exerc* (2019) 51(7):1387–95. doi: 10.1249/MSS.0000000000001916
28. Pigna E, Berardi E, Aulino P, Rizzuto E, Zampieri S, Carraro U, et al. Aerobic Exercise and Pharmacological Treatments Counteract Cachexia by Modulating Autophagy in Colon Cancer. *Sci Rep* (2016) 6:26991. doi: 10.1038/srep26991
29. Elmorsi YM, El-Haggar SM, Ibrahim OM, Mabrouk MM. Effect of Ketoprofen and Indomethacin on Methotrexate Pharmacokinetics in Mice Plasma and Tumor Tissues. *Eur J Drug Metab Pharmacokinet* (2013) 38:27–32. doi: 10.1007/s13318-012-0113-x
30. Kabel AM, Omar MS, Balaha MF, Borg HM. Effect of Metformin and Adriamycin on Transplantable Tumor Model. *Tissue Cell* (2015) 47:498–505. doi: 10.1016/j.tice.2015.07.003
31. Hayes SC, Newton RU, Spence RR, Galvão DA. The Exercise and Sports Science Australia Position Statement: Exercise Medicine in Cancer Management. *J Sci Med Sport* (2019) 22:1175–99. doi: 10.1016/j.jsams.2019.05.003
32. Patel AV, Friedenreich CM, Moore SC, Hayes SC, Silver JK, Campbell KL, et al. American College of Sports Medicine Roundtable Report on Physical Activity, Sedentary Behavior, and Cancer Prevention and Control. *Med Sci Sports Exerc* (2019) 51:2391–402. doi: 10.1249/MSS.0000000000002117
33. Padilha CS, Marinello PC, Galvão DA, Newton RU, Borges FH, Frajacomo F, et al. Evaluation of Resistance Training to Improve Muscular Strength and Body Composition in Cancer Patients Undergoing Neoadjuvant and Adjuvant Therapy: A Meta-Analysis. *J Cancer Surviv* (2017) 11:339–49. doi: 10.1007/s11764-016-0592-x
34. Briukhovetska D, Dörr J, Endres S, Libby P, Dinarello CA, Kobold S, et al. Interleukins in Cancer: From Biology to Therapy. *Nat Rev Cancer* (2021) 21:481–99. doi: 10.1038/s41568-021-00363-z
35. Millonig G, Ganzleben I, Peccerella T, Casanovas G, Brodziak-Jarosz L, Breitkopf-Heinlein K, et al. Sustained Submicromolar H2O2 Levels Induce Hepcidin *via* Signal Transducer and Activator of Transcription 3 (STAT3). *J Biol Chem* (2012) 287:37472–82. doi: 10.1074/jbc.M112.358911
36. Bito T, Sumita N, Masaki T, Shirakawa T, Ueda M, Yoshiki R, et al. Ultraviolet Light Induces Stat3 Activation in Human Keratinocytes and Fibroblasts Through Reactive Oxygen Species and DNA Damage. *Exp Dermatol* (2010) 19:654–60. doi: 10.1111/j.1600-0625.2010.01084.x
37. Ng IH, Yeap YY, Ong LS, Jans DA, Bogoyevitch MA. Oxidative Stress Impairs Multiple Regulatory Events to Drive Persistent Cytokine-Stimulated STAT3 Phosphorylation. *Biochim Biophys Acta - Mol Cell Res* (2014) 1843:483–94. doi: 10.1016/j.bbamcr.2013.11.015
38. Gleeson M, Bishop NC, Stensel DJ, Lindley MR, Mastana SS, Nimmo MA, et al. The Anti-Inflammatory Effects of Exercise: Mechanisms and Implications for the Prevention and Treatment of Disease. *Nat Rev Immunol* (2011) 11:607–10. doi: 10.1038/nri3041
39. Powers SK, Deminice R, Ozdemir M, Yoshihara T, Bomkamp MP, Hyatt H, et al. Exercise-Induced Oxidative Stress: Friend or Foe? *J Sport Heal Sci* (2020) 9:415–25. doi: 10.1016/j.jshs.2020.04.001
40. Begue G, Douillard A, Galbes O, Rossano B, Vernus B, Candau R, et al. Early Activation of Rat Skeletal Muscle IL-6/STAT1/STAT3 Dependent Gene Expression in Resistance Exercise Linked to Hypertrophy. *PloS One* (2013) 8:1–12. doi: 10.1371/journal.pone.0057141
41. Trenerry MK, Carey KA, Ward AC, Cameron-Smith D. STAT3 Signaling is Activated in Human Skeletal Muscle Following Acute Resistance Exercise. *J Appl Physiol* (2007) 102:1483–9. doi: 10.1152/japplphysiol.01147.2006
42. Guerci A, Lahoute C, Hébrard S, Collard L, Graindorge D, Favier M, et al. Srf-Dependent Paracrine Signals Produced by Myofibers Control Satellite Cell-Mediated Skeletal Muscle Hypertrophy. *Cell Metab* (2012) 15:25–37. doi: 10.1016/j.cmet.2011.12.001
43. Rodrigues Brandao-Rangel MA, Bachi ALL, Oliveira-Junior MC, Abbasi A, Silva-Renno A, Aparecida de Brito A, et al. Exercise Inhibits the Effects of Smoke-Induced COPD Involving Modulation of STAT3. *Oxid Med Cell Longev* (2017) 2017:6572714. doi: 10.1155/2017/6572714
44. Chang SF, Lin PL. Systematic Literature Review and Meta-Analysis of the Association of Sarcopenia With Mortality. *Worldviews Evidence-Based Nurs* (2016) 13:153–62. doi: 10.1111/wvn.12147
45. Zhang XM, Dou QL, Zeng Y, Yang Y, Cheng ASK, Zhang WW. Sarcopenia as a Predictor of Mortality in Women With Breast Cancer: A Meta-Analysis and Systematic Review. *BMC Cancer* (2020) 20:1–11. doi: 10.1186/s12885-020-6645-6
46. Trejo-Avila M, Bozada-Gutiérrez K, Valenzuela-Salazar C, Herrera-Esquivel J, Moreno-Portillo M. Sarcopenia Predicts Worse Postoperative Outcomes and Decreased Survival Rates in Patients With Colorectal Cancer: A Systematic Review and Meta-Analysis. *Int J Colorectal Dis* (2021) 36:1077–96. doi: 10.1007/s00384-021-03839-4
47. White JP, Baynes JW, Welle SL, Kostek MC, Matesic LE, Sato S, et al. The Regulation of Skeletal Muscle Protein Turnover During the Progression of Cancer Cachexia in the Apc Min/+ Mouse. *PloS One* (2011) 6(9):e24650. doi: 10.1371/journal.pone.0024650
48. Padilha CS, Testa MT, Marinello PC, Cella PS, Voltarelli FA, Frajacomo FT, et al. Resistance Exercise Counteracts Tumor Growth in Two Carcinoma Rodent Models. *Med Sci Sport Exerc* (2019) 51:2003–11. doi: 10.1249/MSS.0000000000002009
49. Aversa Z, Pin F, Lucia S, Penna F, Verzaro F, Fazi M, et al. Autophagy is Induced in the Skeletal Muscle of Cachectic Cancer Patients. *Sci Rep* (2016) 6:1–11. doi: 10.1038/srep30340
50. Kang R, Loux T, Tang D, Schapiro NE, Vernon P, Livesey KM, et al. The Expression of the Receptor for Advanced Glycation End Products (RAGE) is Permissive for Early Pancreatic Neoplasia. *Proc Natl Acad Sci U S A* (2012) 109:7031–6. doi: 10.1073/pnas.1113865109
51. Yamada E, Bastie CC, Koga H, Wang Y, Cuervo AM, Pessin JE, et al. Mouse Skeletal Muscle Fiber-Type Specific Macroautophagy and Muscle Wasting is Regulated by a Fyn/STAT3/Vps34 Signaling Pathway. *Cell Rep* (2012) 1(5):557–69. doi: 10.1016/j.celrep.2012.03.014
52. Klionsky DJ, Abdalla FC, Abeliovich H, Abraham RT, Acevedo-Arozena A, Adeli K, et al. Guidelines for the Use and Interpretation of Assays for Monitoring Autophagy. *Autophagy* (2012) 8(4):445–544. doi: 10.4161/auto.19496
53. Kwon I, Jang Y, Cho JY, Jang YC, Lee Y. Long-Term Resistance Exercise-Induced Muscular Hypertrophy Is Associated With Autophagy Modulation in Rats. *J Physiol Sci* (2018) 68(3):269–80. doi: 10.1007/s12576-017-0531-2
54. Cui D, Drake JC, Wilson RJ, Shute RJ, Lewellen B, Zhang M, et al. A Novel Voluntary Weightlifting Model in Mice Promotes Muscle Adaptation and Insulin Sensitivity With Simultaneous Enhancement of Autophagy and mTOR Pathway. *FASEB J* (2020) 34(6):7330–44. doi: 10.1096/fj.201903055R
55. Mejías-Peña Y, Estébanez B, Rodriguez-Miguelez P, Fernandez-Gonzalo R, Almar M. Impact of Resistance Training on the Autophagy-Inflammation-Apoptosis Crosstalk in Elderly Subjects. *Aging (Albany NY)* (2017) 9:408–18. doi: 10.18632/aging.101167
56. Zeng Z, Liang J, Wu L, Zhang H, Lv J, Chen N, et al. Exercise-Induced Autophagy Suppresses Sarcopenia Through Akt/mTOR and Akt/FoxO3a Signal Pathways and AMPK-Mediated Mitochondrial Quality Control. *Front Physiol* (2020) 11:583478. doi: 10.3389/fphys.2020.583478
57. Gong L, Wang K, Wang M, Hu R, Li H, Gao D, et al. CUL5-ASB6 Complex Promotes P62/SQSTM1 Ubiquitination and Degradation to Regulate Cell

Proliferation and Autophagy. *Front Cell Dev Biol* (2021) 9:684885. doi: 10.3389/fcell.2021.684885
58. Yamada M, Iwata M, Warabi E, ishi H, Lira VA, Okutsu M, et al. P62/SQSTM1 and Nrf2 are Essential for Exercise-Mediated Enhancement of Antioxidant Protein Expression in Oxidative Muscle. *FASEB J* (2019) 33:8022–32. doi: 10.1096/fj.201900133R
59. Lee H, Jeong AJ, Ye SK. Highlighted STAT3 as a Potential Drug Target for Cancer Therapy. *BMB Rep* (2019) 52:415–23. doi: 10.5483/BMBRep.2019.52.7.152

Conflict of Interest: The authors declare that the research was conducted in the absence of any commercial or financial relationships that could be construed as a potential conflict of interest.

Publisher's Note: All claims expressed in this article are solely those of the authors and do not necessarily represent those of their affiliated organizations, or those of the publisher, the editors and the reviewers. Any product that may be evaluated in this article, or claim that may be made by its manufacturer, is not guaranteed or endorsed by the publisher.

frontiers | Frontiers in Oncology

REVIEW
published: 11 July 2022
doi: 10.3389/fonc.2022.914593

Non-Coding RNAs and Oral Cancer: Small Molecules With Big Functions

Leila Erfanparast[1], *Mohammad Taghizadieh*[2*] *and Ali Akbar Shekarchi*[3]

[1] Department of Pediatric Dentistry, Faculty of Dentistry, Tabriz University of Medical Sciences, Tabriz, Iran, [2] Department of Pathology, Faculty of Medicine, Tabriz University of Medical Sciences, Tabriz, Iran, [3] Department of Pathology, Tabriz University of Medical Sciences, Tabriz, Iran

Oral cancer remains a major public concern with considerable socioeconomic impact in the world. Despite substantial advancements have been made in treating oral cancer, the five-year survival rate for oral cancer remained undesirable, and the molecular mechanisms underlying OSCC carcinogenesis have not been fully understood. Noncoding RNAs (ncRNAs) include transfer RNAs (tRNAs), as well as small RNAs such as microRNAs, and the long ncRNAs such as HOTAIR are a large segment of the transcriptome that do not have apparent protein-coding roles, but they have been verified to play important roles in diverse biological processes, including cancer cell development. Cell death, such as apoptosis, necrosis, and autophagy, plays a vital role in the progression of cancer. A better understanding of the regulatory relationships between ncRNAs and these various types of cancer cell death is therefore urgently required. The occurrence and development of oral cancer can be controlled by increasing or decreasing the expression of ncRNAs, a method which confers broad prospects for oral cancer treatment. Therefore, it is urgent for us to understand the influence of ncRNAs on the development of different modes of oral tumor death, and to evaluate whether ncRNAs have the potential to be used as biological targets for inducing cell death and recurrence of chemotherapy. The purpose of this review is to describe the impact of ncRNAs on cell apoptosis and autophagy in oral cancer in order to explore potential targets for oral cancer therapy.

Keywords: oral cancer, non-coding RNAs, microRNAs, long non-coding RNAs, circular RNAs

OPEN ACCESS

Edited by:
Horacio Cabral,
The University of Tokyo, Japan

Reviewed by:
Federico Perche,
UPR4301 Centre de biophysique moléculaire (CBM), France
Shihori Tanabe,
National Institute of Health Sciences (NIHS), Japan

****Correspondence:***
Mohammad Taghizadieh
MohammadTaghizadieh@gmail.com

Specialty section:
This article was submitted to Molecular and Cellular Oncology, a section of the journal Frontiers in Oncology

Received: *07 April 2022*
Accepted: *16 June 2022*
Published: *11 July 2022*

Citation:
Erfanparast L, Taghizadieh M and Shekarchi AA (2022) Non-Coding RNAs and Oral Cancer: Small Molecules With Big Functions. Front. Oncol. 12:914593. doi: 10.3389/fonc.2022.914593

INTRODUCTION

Oral cancer is a common and fatal malignancy among head and neck malignant neoplasms; the number of new cases of oral cancer globally was 354,864 in 2018 (1). At present, principal treatments of oral cancer include extensive exeresis of the primary carcinoma, with or without neck dissection, and pre-or postoperative adjuvant chemotherapy and radiotherapy (2). However, the overall 5-year survival rate of patients with oral cancer was 65%, and the overall 5-year survival rate of patients with advanced oral cancer was as low as 27% between 2007 and 2013 in the USA (3). Despite the application of reconstructive radical resection and postoperative radiotherapy or chemotherapy, the 5-year survival rate of patients with terminal oral cancer has not improved effectively over the past years (4–6). Furthermore, the dysphagia, maxillofacial malformation and dysarthria induced by the aforementioned

therapies negatively affect the quality of life and psychology of patients (7). Therefore, there is a requirement to identify more effective treatment strategies to improve the survival rate and reduce complications of patients with oral cancer.

Programmed cell death (PCD) may balance cell death with the survival of normal cells; the equilibrium becomes disturbed and PCD plays key roles in ultimate decisions of cancer cell fate. Of note, apoptosis, autophagy, and programmed necrosis are the three main forms of PCD, easily distinguished by their morphological differences (8). Apoptosis, or type I PCD, was first described by Kerr et al. (9), and is characterized by specific morphological and biochemical changes of dying cells, including cell shrinkage, nuclear condensation and fragmentation, dynamic membrane blebbing, and loss of adhesion to neighbors or to extracellular matrix (8). Biochemical changes include chromosomal DNA cleavage into internucleosomal fragments, phosphatidylserine externalization, and a number of intracellular substrate cleavages by specific proteolysis (10, 11). Autophagy, or type II PCD, is an evolutionarily conserved catabolic process beginning with the formation of autophagosomes, double membrane-bound structures surrounding cytoplasmic macromolecules and organelles, destined for recycling (12). In general, autophagy plays a crucial pro-survival role in cell homeostasis, required during periods of starvation or stress due to growth factor deprivation (13). However, there is accumulating evidence that autophagic cells may commit suicide by undergoing cell death and coping with excessive stress, which differs from apoptosis and programmed necrosis (14). As 'the Janus role', autophagy controls a myriad of physiological processes including starvation, cell differentiation, cell survival and death. Besides apoptosis and autophagy, there exists a type III PCD termed programmed necrosis, which involves cell swelling, organelle dysfunction and cell lysis (15). Thus, PCD may play an important role during the preservation of tissue homoeostasis and elimination of damaged cells, – this has profound effects on malignant tissues (8).

Non-coding RNAs (ncRNAs) are transcripts that do not code for proteins, which can be roughly divided into small non-coding RNAs (smaller than 200 nt) and long non-coding RNAs (lncRNAs, longer than 200 nt) (16–25). NcRNAs account for the majority of transcriptome, interestingly the amount of ncRNAs correlates with organismal complexity (26). Emerging evidence showed that ncRNAs have regulatory roles in diverse cellular processes both in biological and pathological conditions including cancer (25, 27–33). Their roles in cancer progression are being appreciated (29, 34, 35). Among them, microRNAs (miRNAs), long non-coding RNAs (lncRNAs) and circular RNAs (circRNAs) are actively studied in recent years. Research is accelerating to decipher the underlying mechanism of ncRNA-regulated oral cancer progression (36, 37). **Table 1** shows classification of non-coding RNAs is given in.

Alterations in the molecular mechanisms of cell death are a common feature of oral cancer, like other cancer types. These alterations enable malignant cells to survive intrinsic death signaling leading to the accumulation of genetic aberrations and helping them to cope with adverse conditions (42). Although pharmacological targeting of cell death pathways has been the subject of intensive efforts in recent decades with a dominant focus on targeting apoptosis, the identification of factors like ncRNAs that regulates death pathways can open novel avenues for intervention in oral cancer cells and the immune system. In this mini-review, we discuss the importance of ncRNAs in the regulation of two key cell death processes, apoptosis, and necroptosis, of oral cancer cells and

TABLE 1 | Classification of non-coding RNAs.

Non-coding RNAs		Definition
1. Structural non-coding RNAs	tRNA and rRNA	A) The tRNA, 70–87 nucleotides in length, plays critical roles in translation by transferring amino acids to initialize and elongate peptides (38). B) In eukaryotes the cytoplasmic ribosomal RNAs (rRNAs) are the 5S (~120 nucleotides), the 5.8S (~150 nucleotides), the 18S (~1800 nucleotides) and the 28S (~4000 to 5000 nucleotides). Play critical role in protein synthesis (39).
2. Regulatory non-coding RNA	**2.1. small non-coding RNAs**: microRNA (miRNA), Piwi-interacting RNA (piRNA), Small interfering RNA (siRNA), Centromere repeat associated small interacting RNA (crasiRNAs), telomere-specific small RNA (telsRNAs) (40).	Size between 20–50 nucleotides, play critical roles in multiple regulatory processes, including transcription, post-transcription, and translation. miRNAs: are small non-coding RNAs that span between 18-24 nucleotides. miRNAs regulate gene expression on a post-transcriptional level. miRNAs modulate and orchestrate cellular pathways, including cell growth, autophagy, apoptosis, autophagy, and migration pathway (18, 41).
	2.2. medium non-coding RNA: small nucleolar RNA (snoRNA), transcription initiation RNA (tiRNA), small nuclear RNA (snRNA), small cytoplasmic RNA (scRNA), PROMPTs (40).	Size between 50–200 nucleotides (40).
	2.3. long non-coding RNAs: **2.3.1. Biogenesis**: Intronic RNA, Enhancer RNA, Promoter RNA, Antisense RNA, Sense RNA, Intergenic RNA, Bidirectional RNA (40). **2.3.2. Structure**: a) Linear lncRNA, b) Circular lncRNA, c) Long intergenic noncoding RNAs (lincRNA), enhancer-derived RNAs (eRNAs), transcribed ultraconserved RNAs (TUCRNAs), Natural antisense transcript (NATs) (40). **2.3.3. Action**: cis-acting long non coding RNA (cis-lncRNA), competing endogenous RNA (ceRNA), trans-acting long non coding RNA (trans-lncRNA) (40).	Size greater than 200 nucleotides (40).

delineate the role of ncRNAs in controlling the molecular networks of these forms of cell death during oral carcinogenesis.

ORAL CANCER

Oral cancer is a subcategory of head and neck cancers that initiates inside the mouth involving anterior two-thirds of the tongue, gingivae, mucosal lining of lips and cheeks, sublingual floor of the mouth, the hard palate and the small retromolar area (43, 44). Signs and symptoms associated with oral cancer include a lump or non-healing sore/ulcer present for more than 14 days, presence of soft red, white or speckled (red and white) patches in the mouth, difficulty in swallowing, chewing, speaking, jaw or tongue movements, malocclusion or ill-fitting dentures and sudden weight loss (45). Oral cancers are the 6th leading cancer by incidence in the world and 90% of these are histologically squamous cell carcinoma (46). The 5-year survival rate is <50% in advanced cases with women having a more favorable outcome (47). The prognosis of these patients is always reliant on age, lymph node involvement and primary tumor size and location (42, 48). The most common risk factors include the premalignant conditions, consumption of tobacco, betel nut, alcohol along with poor oral hygiene, UV radiations, Epstein Barr Virus (EBV) and Human Papilloma Virus (HPV) especially HPV 16 and 18 (49).

Accumulating evidence supports the idea that human microbiome are strongly associated with several tumor types. Oral squamous cell carcinoma(OSCC) is the most frequently studied oral malignancy and it is also the most prevalent head and neck cancer overally. However, there is debate considering the potent role of oral microbiome in the development of OSCC. A distinctive composition of oral microbiome associated with OSCC was not found in previous studies. Individual oral microbiome have the capability to enhance different tumor-promoting mutations in the pathogenesis of OSCC,however a direct casusal relationship has not been yet verified (50, 51). Fusobacterium nucleatum and Porphyromonas gingivalis, the two main oral microorganisms, have been shown to enhance tumorigenesis in mice. Infection with P. gingivalis was associated with tumors of the oro-digestive tract, enhanced invasiveness of oral cancer and increase proliferation of related stem cells (50). Previous studies have shown that periodontal inflammation may enhance inflammation in the gut *in vivo* through transferring oral pathobionts to the gut, which activates colonic mononuclear phagocytes inflammasome and promotes inflammation (52, 53). Moreover, periodontitis leads to formation of reactive Th17 cells against oral pathogens. These reactive Th17 cells then migrate to the gut. In the gut, these orally-based Th17 cells become activated by oral pathobionts translocated from the oral cavity and initiate colitis, mweanwhile the micribiota of the gut do not activate these cells (50). Whether inflammation of the gut may exert similar effect on the oral cavity environment and increases the severity of inflammatory reactions and head and neck cancers, has not been yet elucidated. There are few studies on the impact of the gut microbiome on the immune response to oral cavity cancer, but they may be worthwhile to pursue.

The extent of oral cancer spread is estimated by staging the cancer. The commonly used staging system for oral cancer is TNM system, where T (for tumor) defines the size of the primary tumor. It is further categorized from 1 to 4 on the basis of tumor size, a higher number indicates larger size. N (for lymph nodes) shows extend of cancer spread to lymph nodes in the vicinity of the organ. It is further categorized to N0 (no spread), N1, N2, or N3. The N1-N3 shows the number of lymph nodes involved alongside their location and size. M (for metastasis) describes cancer spread to other parts of the body *via* lymph or blood. It is further classified to M0 (no spread) and M1 (spread). Overall oral cancer staging is given as **Table 2** (42):

In addition, classification of tumors of the oral cavity and mobile tongue based on WHO classification is summarized in ***below***:

(A) Malignant Surface Epithelial Tumors: the major modification in this group is the oropharynx exclusion. Different OSCC(oral squamous cell carcinoma) subtypes are adenosquamous carcinoma,spindle cell carcinoma, basaloid SCC, papillary SCC, carcinoma cuniculatum, verrucous carcinoma, acantholytic SCC, and lymphoepithelial SCC (55). **(B)** Oral Potentially Malignant Disorders and Oral Epithelial Dysplasia: this group has been renamed from combining sections entitled Epithelial precursor lesions and Proliferative verrucous leukoplakia and precancerous lesions. A recently described type of dysplasia which is positive for high-risk HPV with characteristic histology (HPV-associated oral dysplasia) was added to the 4th edition, however the clinical significance of this finding is not clearly known as malignant transformation risk is poorly determined. **(C)** Papillomas : Condyloma acuminatum, Squamous cell papilloma, Verruca vulgaris, and Multifocal epithelial hyperplasia. **(D)** Tumours of uncertain histogenesis: Congenital granular cell epulis, and Ectomesenchymal chondromyxoid tumour. **(E)** Soft tissue and neural tumors: Rhbadomyoma, Granular cell tumour, Haemangioma, Lymphangioma, Kaposi sarcoma, Schwannoma, Myofibroblastic sarcoma and neurofibroma. **(F)** Oral mucosal melanoma, **(G)** Salivary type tumors: Mucoepidermoid carcinoma and Pleomorphic adenoma, and **(H)** Haematolymphoid tumours: CD30-positive T-cell lymphoproliferative disorder, Langerhans cell histiocytosis, plasmablastic lymphoma and extramedullary myeloid sarcoma (55–57).

The stage of the disease usually determines the primary option for the treatment of oral cancer. The treatment options include surgical resection, chemotherapy, radiotherapy, immunotherapy alone or in combination. Despite favorable advancements in the conventional therapeutic modalities, many disadvantages still need to be addressed; surgical resection may lead to long-lasting disfigurements, multiple corrective surgeries usually cause considerable deformities that leaves patients in psycho-social stress and isolation, whereas radio- or chemo- therapies end up with significant toxicities or treatment resistance, all compromising the patients' quality of life and well-being (58, 59). Also, locoregional relapse may occur after years of the treatment leading to recurrent growth of the

TABLE 2 | TNM classification of carcinomas of the lip and oral cavity (54).

Stage	Explanation
Primary Tumor	
T0	No evidence of primary tumor
TIS	Carcinoma in situ
T1	Tumor size 2cm or smaller, 5mm deep or less
T2	Tumor ≤ 2cm, >5mm and ≥ 10mm depth of invasion or tumor> 2cm but ≤ 4cm and depth of invasion ≤ 10mm
T3	Larger than 4cm, or deeper than 10mm
T4a	Extrinsic muscle of the tongue removed, included extensive tumors with bilateral tongue involvement and/or DOI>20 mm.
T4b	Very advanced locally disease definition; tumor invades masticator space, pterygoid plates, skull base, and/or encases the internal carotid artery.
Regional lymph nodes (N)	
N0	The lymph nodes don't contain cancer cells.
N1	Metastases to the single lymph node. The node is no larger than 3cm across. Node must be extranodal extension negative.
N2a	Metastases to multiple ipsilateral nodes, and the node is between 3cm and 6cm across. Nodes must be extranodal extension negative or single ipsilateral or node 3cm or smaller with extranodal extension.
N2b	Metastases to multiple ipsilateral nodes, and the node is between 3cm and 6cm across. The Nodes must be extranodal extension negative.
N2c	metastases to bilateral nodes or contralateral nodes none >6 cm. Nodes must be extranodal extension negative
N3	Metastases to nodes >6 cm
N3a	Metastases to nodes >6 cm but extranodal extension negative. single ipsilateral nodes in machine learning >3 cm in greatest dimension with extranodal extension or multiple ipsilateral, contralateral, or bilateral nodes, any with extranodal extension or single contralateral node 3cm or smaller and with extranodal extension.

cancers (60). The effectiveness of different therapeutic modalities is largely dependent on the mutational profile of tumors as genetic alterations confer new oncogenic potential to cancer cells. The precise targeting of these alterations together with treatment regimen modifications decreases therapeutic resistance and may result in countless lives being saved from potential morbidity and mortality (42).

PROGRAMMED CELL DEATH AND CANCER

Cancer, a complex genetic disease resulting from mutation of oncogenes or tumor suppressor genes, can be developed due to alteration of signaling pathways; it has been well known to have numerous links to PCD (61). Apoptosis (type I PCD) is the major type of cell death that occurs when DNA damage is irreparable. Two core pathways exist to induce apoptosis, the extrinsic – death receptor pathway and intrinsic – mitochondrial pathway (62, 63). The extrinsic pathway is triggered by binding of Fas (and other similar receptors such as tumor necrosis receptor 1 and its relatives) plasma-membrane death receptor with its extracellular ligand, Fas-L. When death stimuli occur, Fas-L combines with Fas to form a death complex. The Fas/Fas-L composite recruits death domain-containing protein (FADD) and pro-caspase-8, aggregating to become the death-inducing signaling complex (DISC). Consequently, the protein complex activates its pro-caspase-8, which proceeds to trigger pro-caspase-3, the penultimate enzyme for execution of the apoptotic process (9). The intrinsic pathway also leads to apoptosis but under the control of mitochondrial pro-enzymes. In both cases if a cell becomes initiated by either extracellular stimuli or intracellular signals, outer mitochondrial membranes become permeable to internal cytochrome c, which is then released into the cytosol. Cytochrome c recruits Apaf–1 and pro-caspase-9 to compose the apoptosome, which downstream triggers a caspase 9/3 signaling cascade, culminating (as concludes the extrinsic pathway) in apoptosis (64). Accumulating evidence has shown that abnormal expression of some key regulatory factors may lead to cancer, indicating the intricate relationships between apoptosis and cancer.

Autophagy is a major, regulated, catabolic mechanism with many links to processes that occur in malignant cells, and highly regulated by some autophagy-related genes (ATGs). It is a crucial mechanism that responds to either extra- or intracellular stress, and can result in cell survival under certain circumstances; however, over-activation of autophagy may result in autophagic cell death (65). When analyzing relationships between autophagy and cancer, a common challenge is to determine whether autophagy protects cell survival or contributes to cell death. Autophagy is well known to be crucial for cell survival under extreme conditions, and degradation of intracellular macromolecules provides energy required for minimal cell functioning when nutrients are scarce. Consequently, autophagic activation can play a protective role in early stages of cancer progression. On the other hand, however, autophagy can perform as a tumor suppressor by activating pro-autophagic genes and blocking anti-autophagic genes in oncogenesis (65, 66). However, reminiscent of the Roman god Janus, autophagy can also play the reverse part – a pro-tumor role in carcinogenesis – by regulating a number of pathways involving Beclin-1, Bcl-2, Class III and I PI3K, mTORC1/C2 and p53 (67).

BIOGENESIS AND FUNCTION OF MICRORNAS AND THEIR ROLES IN PROGRAMMED CELL DEATH OF ORAL CANCER

MicroRNAs (miRNAs) are small (20–23 nts) and non-coding RNA molecules that negatively influence gene expression by

binding to mRNAs and thereby promoting degradation of the target mRNA or blocking its translation into protein (19, 68–79).

MiRNA biogenesis is initiated from the nucleus similar to other RNAs (80–83). These non-coding RNAs are primarily synthesized as primary transcripts or pri-miRNAs by RNA polymerase II (RNA pol II), which are processed by the RNAse III, Drosha into pre-miRNAs with long hairpin precursors of ∼70–100 nucleotides. After Drosha processing, pre-miRNAs are transferred for cytoplasmic maturation. The protein exportin 5 combines with the pre-miRNA and GTP-binding nuclear protein RAN GTP and forms a transport complex (84). Following movement through the nuclear pore complex, GTP is degraded and leads to disassembly of the complex and release of the pre-miRNA into the cytoplasm (85, 86). Pre-miRNAs are then degraded by Dicer in the cytoplasm to generate mature miRNAs, leading to the production of a double-stranded ∼22-nt product, made up of the the mature miRNA guide strand and miRNA* passenger strand. This mature miRNA is subsequently loaded into the RISC(RNA-induced silencing complex). Accumulating evidence has found that the passenger strand may be loaded into the RISC complex in certain thermodynamic conditions (87, 88). RISC complex can detect target mRNA based on base-pair complementarity and lead to cleavage of the mRNA and/or suppression of the mRNA.

In addition, two strands comprise the miRNA duplex, known as the suffix -3p or -5p (26). One of these strands, is typically discarded (the passenger strand; annotated *), while the oher strand plays part in guiding eventual target selection of mRNA (the guide strand). Strand selection is mainly dependent on the thermodynamic characteristics of the duplex; the strand that is more loosely bound to the 5′-end of the duplex is likely to function as the guide strand. Additional features of miRNA guide strands include an excess of a purines (A/G rich) at the 5′-end and a U-bias, while the passenger strands contain excess pyrimidines (U/C rich) and a C-bias at the 5′-end. Meanwhile, the guide strand can be modified through different processes, such as duplex post-transcriptional modification, single point mutation in the duplex and specific proteins related to the Ago2 in the RISC complex(protein activator of dsRNA-dependent protein kinase versus trans-activation response RNA-binding protein) (89–92). Consequently, both arms comprising a pre-miRNA hairpin can guide miRNAs (93) that are biologically functional (19).

MicroRNAs act as key regulators of a wide variety of cellular mechanisms and physiological processes, such as cell cycle progression, cell division, apoptosis and necroptosis (62, 62, 94–102). Recent studies have demonstrated that numerous miRNAs can strongly affect the expression of pro- and anti-apoptotic genes, oncogenes, ER stress- and/or necroptosis-related genes (20, 103). Aberrations involving miRNAs implicated in apoptosis or necroptosis could also impact physiological conditions and promote disease, including carcinogenesis and infection diseases (19, 104–106). Numerous studies have demonstrated that miRNAs usually target multiple mRNAs and they could act as so-called apopto-miRs, oncomiR or tumor suppressor miRNAs in different cancers. Apopto-miRs are miRNAs involved in apoptosis, whereas oncomiRs promote tumor development (107). Elucidating the roles of oncomiRs and apopto-miRs in particular types of cancers can aid in their utility as tumor biomarkers for diagnosis, prognosis and selecting the most suitable treatment option for cancer patients.

MiRNAs can be used as treatment options in two different strategies. One approach is mediated by a gain of function and acts to suppress proto-oncogenic miRNAs through administering antagonists of miRNAs, including such as antagomiRs, locked-nucleic acids (LNA) and anti-miRs. The second approach, is directed by replacing a tumor-suppressor miRNA analogue to aim a loss of function. Among these strategies, the inhibitory approach is more generally and theoretically acceptable as it is in harmony with short interfering RNAs(siRNA) and small molecule inhibitors, however, the replacement strategy provides a novel opportunity to identify the therapeutic potential for tumor suppressors (108). Mimics of miRNA are synthetic oligonucleotides of two strands processed into single-stranded miRNA to control target genes expression in target cells (109). Gene therapy has been used in the past to therapeutically recover tumor suppressor levels in tumor tissues; however, a practical application of this strategy is still awaiting. MiRNAs bring in new opportunities, as in contrast to tumor-suppressor proteins, miRNA mimics are significantly smaller and do not usually require entery to the target cells to become activated and can be administered by systemic routes and technologies frequently also used by siRNAs. As a result, the delivery barrier for miRNA mimics appears to be lower than it is for protein-encoding DNA. Moreover, numerous different observations encourage the strategy of miRNA replacement therapy: (i)The majority of differentially expressed miRNAs are decreased in tumor tissue compared to normal tissue, suggesting that miRNAs are more likely to act as tumor suppressors than oncogenes (108, 110).; and (ii) suppression of the processing of endogenous miRNA leads to an oncogenic transformation and accentuates tumor formation, indicating that the miRNA tumor-suppressive role dominates against its oncogenic role (111). Another benefit of miRNA mimics is that it has a similar sequence to the naturally occurring miRNA, and thus is considered to target the same mRNAs, which is also regulated by natural miRNAs. Non-specific unusual effects are not frequent as miRNA mimics are thought to act as the naturally occurring counterpart of interactions between miRNA-mRNA, which have evolved over a billion years. However, the main reason to identify the therapeutic potentials of miRNAs is dependent on the fact that several oncogenes and oncogenic processes commonly dys-regulated in cancer, can be regulated by a single miRNA (112).As a result, miRNAs function in harmony with our previous observations of cancer as a “pathway disease”, which may only be effectively treated with modifying several oncogenic pathways (108, 113).

The imbalance between proliferation and apoptosis is one of the most remarkable features of cancer cells. Therefore, investigating the regulatory mechanisms of proliferation and apoptosis is of great importance for cancer research. It has

been well documented that resistance to apoptosis caused by several genetic aberrations may promote the uncontrolled growth, invasion, and metastasis of cancer cells (114). Apoptosis, as programmed cell death, is mainly mediated by two pathways: The mitochondrial pathway and the death receptor pathway (62, 115). It has been confirmed that the release of cytochrome c from the mitochondria into the cytosol may trigger the apoptosis *via* promoting the pro-apoptotic protein Bax expression, followed by the downstream activation of caspase-9 and caspase-3 (116, 117). Subsequently, PARP, as a substrate of caspase-3, is cleaved and activated to induce apoptosis (118). Recently, Cui et al. (119) investigated the regulation of miR-378 in the mitochondrial-mediated apoptotic signaling pathway of oral squamous carcinoma cells (OSCC). The results of their study showed that overexpression of miR-378 suppressed the proliferation and induced apoptosis of OSCC cells, while knockdown of miR-378-3p/5p led to the opposite results. Besides, miR-378 overexpression promoted the release of cytochrome c from the mitochondria into the cytosol, up-regulated the Bax/Bcl-2 ratio, and raised the cleaved caspase-9, cleaved caspase-3, and cleaved PARP levels in OSCC cells. Conversely, inhibition of miR-378-3p/5p expression obtained the opposite results. These results suggested that miR-378 participated in the dysregulation of proliferation and apoptosis in OSCC cells (119).

PI3K/AKT is an important signaling pathway, which regulates progression in numerous different types of tumors. The PI3K/AKT pathway is closely associated with apoptosis. This pathway controls cell proliferation, growth, translation, migration, and survival, and overactivation of this signaling pathway is associated with poor prognosis (120, 121). Activated PI3K may activate downstream protein kinase AKT; Activated AKT is able to phosphorylate Bax, inactivate Bax, and inhibit Bax and Bcl-2 to form dimers, thereby resulting in Bcl-2 dissociation and an anti-apoptotic effect (122, 123). Reportedly, miRNAs by regulating the PI3K/AKT signaling pathway can lead to modulation of oral cancer cell apoptosis. For example, miR-21-5p targeting PDCD4 suppresses apoptosis *via* regulating the PI3K/AKT/FOXO1 signaling pathway in tongue squamous cell carcinoma (TSCC). Also, inhibition of miR21-5p suppressed the PI3K/AKT/FOXO1 signaling pathway, suggesting that inhibiting the activation of the PI3K/AKT/FOXO1 signaling pathway may be a potential strategy for the treatment of TSCC (124). In addition, miR-378 overexpression was resulted in a decreased p-AKT level, whereas miR-378-3p/5p silencing could raise the p-AKT level in OSCC cells. Therefore, the PI3K/AKT signaling pathway was involved in the regulatory mechanisms of miR378 in OSCC (119). In addition, as shown in **Figure 1**, miR-29b suppresses proliferation, migration, and induces apoptosis of tongue squamous cell carcinoma through PTEN–AKT signaling pathway by targeting Sp1.

MiR-21 is commonly upregulated in toungue squamous cell carcinoma and carries an unfavorable prognosis by suppressing cellular apoptosis.On the other hand, its reduced expression was found to be associated with resistance to chemotherapy (125). In TSCC, high expression of miR-21 was associated with reduced expression of PTEN(phosphatase tensin homologue) and TPM1 (tropomyosin1) (126). Several other important tumor suppressor and oncogenic targets were detected for miR-21 in tumors of the head and neck, including Ras, HNRPK, reversion inducing cysteine rich protein with kazal motifs (RECK)andprogrammed cell death 4 (PDCD4) (125). Furthermore, Zhang et al. (127), found that miR-21

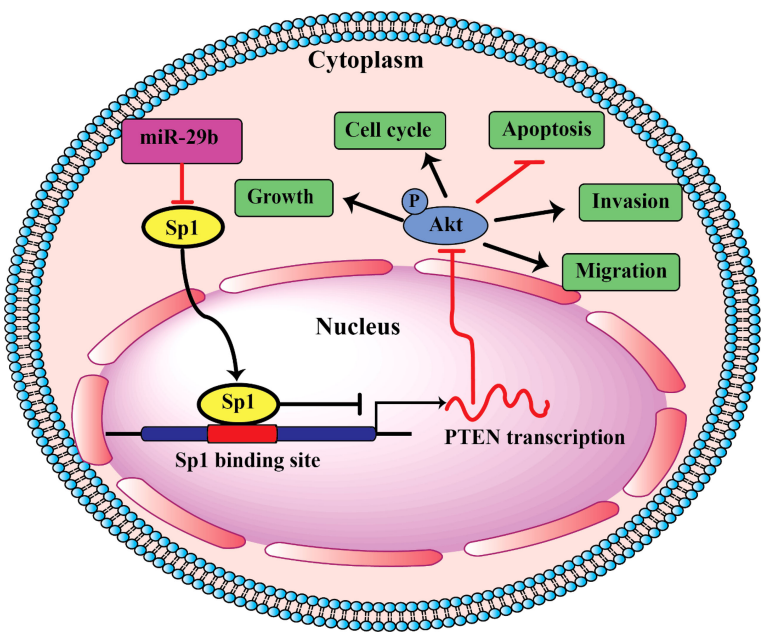

FIGURE 1 | Schematic of pathways involved in the tumor-suppressor role of miR-29b in TSCC cells.

can affect generation of ROS (reactive oxygen species) through direct mitigating the activity of SOD3 (superoxide dismutase family member 3), and through indirect attenuating the production of the pro-inflammatory mediator, tumor necrosis factor (TNF)-α, thus decreasing levels of SOD2 to facilitate carcinogenesis. Similarly, high expression of miR-2463 and miR-18462 is associated with decreased cellular apoptosis and augmented cellular proliferation (128). Upregulation of miR-184 exerts anti-apoptotic effects by targeting c-Myc and the apoptosis-related gene, TNFAIP2 (129, 130). Another study suggests that ectopic production of miR-184 inhibits the Akt pathway, which is linked to increased cell apoptosis and death, explaining the effects of miR-184 on epithelial cells and cancer cell lines *via* Akt signaling (131). Highly expressed miR-24 in oral squamous cell carcinoma appears to directly target DND1(RNA binding protein dead end 1), which leads to resistance to apoptosis.

p27Kip1 is a cyclin-dependent kinase inhibitor that regulates the progression of cells from G1 into the S phase in a cell cycle. p27Kip1 knockdown both inhibited G1 phase arrest and enhanced ER stress-induced cell apoptosis (132). Thus, deregulation of p27Kip1 has been associated with disease progression and an unfavorable outcome in several malignancies (133). Kudo et al. (134) demonstrated that Skp2 siRNA apparently inhibited p27Kip1 protein degradation, thus restraining oral cancer cell proliferation. It indicated that p27Kip1 upregulation played a role in weakening the malignancy of oral cancer cells (134). Fu et al. (135) exhibited that miR-155 targeted p27Kip1 gene and suppression of miR-155 lead to upregulated p27Kip1 level, reduced cell proliferation, and blocked cell cycle, which was similar to Kudo (134). In addition, Fu and colleagues (135) observed that antagomiR-155 transfection upregulated the CDC73 level in oral cancer cell line KB, thus promoting cell apoptosis and weakening the tumorigenicity in nude mice. This study revealed the role of miR-155 upregulation in reducing p27Kip1 expression and OSCC oncogenesis (135). As result, miR-155 regulates OSCC cells (Tca8113 cell) proliferation, cycle, and apoptosis *via* regulating p27Kip1.

Bmi-1, a polycomb ring finger oncogene, is highly expressed in multiple cancer cells and is involved in cancer cell proliferation, invasion, and apoptosis (136). Bmi-1 was first shown to collaborate with c-MYC in tumorigenesis in mice by suppressing the INK4A locus, which encodes (both p16Ink4a and p14ARF), two proteins that function to suppress cell proliferation and promote apoptosis (137). Recently, several studies have shown evidence for miRNA-mediated regulation of Bmi-1. miR-128a increases intracellular reactive oxygen species levels by targeting Bmi-1, which inhibits the growth of medulloblastoma cells (138) and miR-218 inhibits cell proliferation and cell cycle progression and promotes apoptosis by downregulating Bmi-1 in colorectal cancer cells (139). KIM et al. (140) suggested that the miR-203-induced apoptosis in YD-38 oral cancer cells was related to the suppression of Bmi-1. The result of this study demonstrated that miR-203 expression was significantly down-regulated in YD-38 cells compared to expression levels in normal human oral keratinocytes. miR-203 can decrease the viability of YD-38 cells in a time- and dose-dependent manner. In addition, over-expression of miR-203 significantly increased not only DNA segmentation but also the apoptotic population of YD-38 cells. These results indicate that miR-203 overexpression induces apoptosis in YD-38 cells. In addition, they found that both mRNA and protein levels of Bmi-1 were significantly reduced in YD-38 cells transfected with miR-203. These results indicate that Bmi-1 is a target gene of miR-203. miR-203 induces apoptosis in YD-38 cells by directly targeting Bmi-1, which suggests its possible application as an anti-cancer therapeutic. Although Bmi-1 is an important target of miR-203-induced apoptosis in YD-38 human oral cancer cells, they also suggested that miR-203 might regulate other genes (140).

Transforming growth factor (TGF)-β1 is known to regulate various cellular responses, including apoptosis, metastasis, cell proliferation, and differentiation (141). In the TGF-β1 pathway, Smad2 and Smad3 are receptor-regulated effector proteins, and TGF-β induces apoptosis through Smad-mediated expression of death-associated protein kinase (141). Recently, Huang and colleagues (142) investigated the role and mechanism of miR−18a-5p in OSCC and it was revealed that miR−18a-5p was highly expressed in SCC9 cells compared with normal cells. Then the effect of miR−18a-5p upregulation and miR−18a-5p downregulation was investigated on SCC9 cell viability, migration, invasion and apoptosis. They found that overexpression of miR−18a-5p could promote SCC9 cell viability, migration, invasion and inhibit cell apoptosis. While miR−18a-5p downregulation inhibited SCC9 cell viability, migration, invasion and induced cell apoptosis. These results indicated that miR−18a-5p acts as an oncogene to participate in OSCC progression and tumorigenesis by regulating the TGF-β1/Smad2 pathway (142). Also, several studies have shown miR-18a-5p was upregulated in several cancers such as (143, 144), hepatocellular carcinoma, prostate cancer and other cancers and can be act as oncomiR by inhibiting apoptosis of cancer cells (145–147). Also, in OSCC cells, miR−18a-5p acts as an oncogene by targeting tumor suppressor genes related to apoptosis.

HOX genes belong to a superfamily of homeobox genes that encodes transcription factors with important effects on modulating primary cellular processes, including cell recognition, growth, and differentiation, which was recently discovered to be regulated by miRNAs (148). Genes of the HOX family are highly expressed in leukemias, melanomas, and in breast, ovarian, cervical, esophageal, and prostate cancers (149–152). In addition, the aberrant expression of HOX genes was observed in OSCC (153). HOXB7, a member of the HOX family of homeodomain transcription factors, is a critical developmental regulator which influences the proliferation and survival of progenitor cells. However, its upregulation has been reported in several malignancies which contributed to tumorigenesis (154). Accumulating evidence has shown that HOXB7 was crucial to promoting cell proliferation and migration to participate in tumorigenesis and inhibit cell apoptosis (155, 156). Wang et al. (157) reported miR-376c-3p directly targeted HOXB7 and reduced the expression of HOXB7.

They found that the expression level of MiR-376c-3p was down-regulated while HOXB7 was up-regulated in OSCC tissues and cells than the normal ones. Moreover, the overexpression level of miR-376c-3p suppressed proliferation, viability, migration, and invasion and induced G1/G0 arrest and cell apoptosis of SCC-25 cells. As result, they reported that miR-376c-3p induced cell apoptosis of OSCC *via* targeting HOXB7 and suggested it useful to replenish the expression of miR-376c-3p for the therapy of OSCC (157). miRNAs as regulators of apoptotic pathways are listed in **Table 3**.

Human Herpesviruses (HHV), which are a group of large enveloped DNA viruses, have been found in several oral inflammatory diseases, indicating their role in progression of the disease. However, the viral components that cause oral illness are unknown. Interestingly, HHV also leads to expression of numerous miRNAs, known as viral miRNAs, which may be significantly involved in regulating pathogen-host interaction by regulating both the viral life cycle and host biological pathways. Viral miRNAs(v-miRs) have been detected in diseaded biopsies of the oral tissue and show their immunoregulatory roles. Accumulation of v-miRs in tumors of the oral cavity was observed in several studies (158, 159). For instance, nasopharyngeal carcinoma (NPC) due to EBV is a well-known oral cancer. Higher levels of seven EBV miRNAs were found in tissues from NPC and non-cancerous patients, with ebv-miR-BART7-3p being the most significantly enhanced (160). Ectopic expression of ebv-miR-BART7-3p in EBV-negative NPC cells causes a significant rise in metastases in mice, indicating that viral miRNAs play a role in tumor growth. Downregulation of PTEN induced by ebv-miR-BART7-3p, causes accumulation of the β-catenin and Snail.This leads to promoted EMT (epithelial-to-mesenchymal transition) and progression. An elevated EBV BART cluster miRNAs was also found in tissue samples of nasopharyngeal carcinoma (161). Additionally, ebv-miR-BART1 expression is significantly associated with distinct pathological features. In terms of mechanism of action, ebv-miR-BART1 (similar to miR-BART-7-3p) leads to direct downregulation of the PTEN levels and increased level of phosphorylated FAK,AKT, Shc,130Cas and ERK1/2. Accordingly, numerous miRNAs in herpes viruses cause synergistic regulation of the same gene/pathway to modulate pathological results. High expression of ebv-miR-BART7 was associated with resistance to treatment with cisplatin and increased cellular proliferation, migration and invasion *in vitro*. Using viral miRNAs as new markers of diagnosis in the progression of the disease course and treatment target in conjunction with pre-existing therapeutic modalities may bring a reliable and potent strategy for tumors and inflammatory diseases of the oral tract (158).

It has been shown that miRNAs may be applied as potent biomarkers in oral tumors. For instance, Maclellan et al. (162) explored the level of expression of different circulating miRNAs in patients with advanced oral lesions (high risk lesions is identified as oral cancer or carcinoma in situ). Their study found that 15 miRNAs were overexpressed and 5 miRNAs were prominently lowly expressed based on the clinical status of the disease.Therefore, their study confirmed that five miRNAs (miR-29a,miR-16, miR-223,let-7b and miR-338-3p)provide diagnostic potential as non-invasive markers for high-grade oral lesions or oral cancers (162) and that serum miRNA profiles combined with additional screening techniques may significantly enhance the sensitivity for detecting oral cancer.

BIOGENESIS AND FUNCTION OF LNCRNAS AND LNCRNAS-MEDIATED PROGRAMMED CELL DEATH OF ORAL CANCER

LncRNA is a special RNA type defined as transcripts over 200 nucleotides long, but is not translated into proteins (28, 70, 163–166). LncRNAs are numerous and abundant, and were originally considered to be biologically non-functional transcriptional noise.

In previous years, achievements in sequencing and analysis of genome facilitated the discovery of multiple lncRNAs and biogenesis of lncRNAs became unraveled (167). The majority of the lncRNAs are transcribed from exonic, intergenic and distal protein-encoding loci of the genome through the function of the enzyme RNA polymerase II, and only a tiny portion of these non-coding RNAs are generated by the RNA polymerase III (Pol III) complex or the single-polypeptide nuclear RNA polymerase IV complex. Then the pre-mature lncRNA becomes polyadenylated at the 3`-end and capped with methyl-guanosine at the 5′-end (168). It is usually modified by alternative splicing necessary to produce protein diversity (169). Alternative splicing can be categorized in three ways. Firstly, lncRNAs make interaction with certain splicing factors and then generate RNA-RNA duplexes with molecules of pre-mRNAs, and eventually, they affect the remodeling of chromatins, and thus accomplishing target genes splicing process (170). For instance, LINC-HELLP, a 205 kb-lncRNA, is found to be involved in regulating splicing and the pathogenesis of HELLP syndrome related to pregnancy.The mass spectrometry and purification experiments found that components of splicing such as the splicing-related factors Y-Box Binding Protein 1 (YBX1), Poly(RC) Binding Proteins 1 and 2 in addition to the the ribosomal machinery,can detect this lncRNA. The exact mechanism of regulating this splicing process by this lncRNA is poorly understood,however, it was shown that some protein (5′-end up to the middle) of the LINC-HELLP transcript loses its potential to make interactions with its protein partners due to the presence of mutation in patients with HELLP. On the contrary, mutations at the far 3′-end enhances the binding potential (170). Antisense, 'as-Oct4-pg5', and brain-associated'BC200' are examples of functional lncRNAs that are not polyadenylated (171, 172).Ovrall, genes encoding lncRNAs have their unique promoters and DNA motifs and transcription factors(TFs) (173).

Epigenetic modification plays a major role in biogenesis of lncRNAs. Methylation of histone has a key role in regulating transcription. Methylation of histone H3 lysine 4 (H3K4) represents activation of transcription, while tri-methylated

TABLE 3 | microRNA can regulate cell death pathways in oral cancer.

miRNAs	Expression	Cancer cell	Target of miRNA	Inhibition/ Induction of Cell Death	Sample type	Note	Ref
miR-486-3p	Down	Oral squamous cell carcinoma (OSCC)	DDR1	Induction of apoptosis	Human (OSCC tissue, n= 40), *In vitro* (OEC-M1 and TW2.6 cells)	Overexpression of miR-486-3p can induces apoptosis by regulating DDR1 expression.	(1)
miR-4282	Down	OSCC	LIN28B	Induction of apoptosis	Human (OSCC tissue, n=72), *In vivo* (mice), *In vitro* (SCC15 and TSCCA cells)	miR-4282 induces the apoptosis of OSCC cells through a decreased expression level of ZBTB2 *via* targeting LIN28B.	(2)
miR-17	–	Human tongue squamous cell carcinoma (TSCC)	–	Inhibition of apoptosis	*In vitro* (CAL-27 cells), *In vivo* (Xenograft tumor model (BALB/c nude mice))	MiR-17 suppresses the induction of cisplatin-induced apoptosis. Suppression of miR-17 causes induction apoptosis and autophagy by STAT3 signaling.	(3)
miR-17-5p	–	OSCC	–	–	*In vitro* (OC3 cells)	miR-17-5p increases (TRAIL R1, HIF-1α and cIAP-1) or decreases (p53, p21, FADD and TNF RI) apoptosis-related proteins in irradiated OC3 cell.	(4)
miR-27a	Up	TSCC	–	Inhibition of apoptosis	*In vitro* (Cal-27 cells and Clinical TSCC sample)	Decrease expression level of miR-27a lead to promote cell apoptosis in Cal-27 cells.	(5)
miR-145-5p	Down	TSCC and Oral cancer	–	Induction of apoptosis	Human (TSCC tissues), *In vitro* (SCC9 and Cal27 cell)	Upregulation of miR-145-5p levels cause promote cell apoptosis.	(6, 7)
miR-183	Up	TSCC	–	Inhibition of apoptosis	*In vitro* (SCC25 cell)	Downregulation of miR-183 levels lead to induction of apoptosis through decrease and increase expression level of casase-3 and BCL-xL, respectively.	(8)
miR-146a-5p	Up	OSCC	–	Inhibition of apoptosis	*In vitro* (SCC-9 cell)	The downregulation of miR-146a-5p levels leads to induces apoptosis in OSCC cells.	(9)
miR-149	Down	OSCC	–	Induction of apoptosis	*In vitro* (PECAPJ41 and HSC-4 cells)	Inhibition of miR-149 significantly suppresses apoptosis and autophagy.	(10)
miR-155	Up	Oral cancer cells	FoxO3a	Inhibition of apoptosis	*In vitro* (KB and KB/DDP cell line)	Inhibition of miR-155 significantly promotes apoptosis	(11)
miR-155	Up	OSCC	p27Kip1	Inhibition of apoptosis	Human (OSCC tissues, n=46), *In vitro* (Tca8113 cells)	Inhibition of miR-155 significantly promotes apoptosis od OSCC cells.	(12)
miR-378-3p/5p	Down	OSCC	KLK4	Induction of apoptosis	Human (OSCC tissues, n=30), *In vitro* (KB and Tca8113 cells)	miR-378-3p/5p promotes apoptosis of OSCC through targeting KLK4	(13)
miR-101-3p, miR-199b-5p	Down	Oral cancer	BICC1	Induction of apoptosis	Human (oral cancer tissues, n=62), *In vitro* (Tca8113, CAL-27, TSCCA, SCC-9) and *In vivo* (mice)	Overexpression of miR-199b-5p and miR-101-3p levels induces apoptosis by targeting BICC1 expression.	(14)
miR-214	Up	Oral cancer	MAPK/ ERK signaling pathway	Inhibition of apoptosis	*In vitro* (HB cell lines)	miR-214 suppresses apoptosis by MAPK/ERK signaling pathway.	(15)
miR-214	Up	Oral cancer	RASSF5	Inhibition of apoptosis	*In vitro* (KB cell)	Downregulation of miR-214 expression lead to inhibition of apoptosis by targeting RASSF5.	(16)
miR-139	Down	Oral cancer	Akt signaling pathway	Induction of apoptosis	*In vitro* (Tca8113 cell)	Overexpression of miR-139 levels cause promote apoptosis through Akt signaling pathway.	(17)
miR-21 –5p	Up	TSCC	PDCD4	Inhibition of apoptosis	Human (TSCC, n= 40), *In vitro* (Cal 27 and SCC9 cells)	miR-21-5p inhibits apoptosis by targeting PDCD4 and regulating the PI3K/AKT/FOXO1 signaling pathway.	(18)
miR-21	–	OSCC	–	Inhibition of apoptosis	*In vitro* (SCC15 and SCC25 cell)	miR-21 can inhibit apoptosis by up-regulating PTEN expression	(19)
miR-9	Down	OSCC	–	Induction of apoptosis	Human (OSCC, n= 21), *In vitro* (Tca8113 cells)	Overexpression of miR-9 levels cause induction of apoptosis	(20)
miR-203	Down	Oral cancer	Bmi-1	Induction of apoptosis	*In vitro* (YD-38 cells)	Upregulation of miR-203 levels cause induction of apoptosis by targeting Bmi-1.	(21)
miR-203	Down	Oral cancer	SEMA6A	Induction of apoptosis	*In vitro* (YD-38 cells)	miR-203 promotes apoptosis by targeting SEMA6A.	(22)
miR-4513	Up	OSCC	CXCL17	Inhibition of apoptosis	*In vitro* (Tca8113 and CAL-27)	Downregulation of miR-4513 levels promotes apoptosis.	(23)
miR-376c-3p	Down	OSCC	HOXB7	Induction of apoptosis	Human (OSCC, n= 49), *In vitro* (SCC-25 cells)	Overexpression of miR-376c-3p induces the apoptosis of SCC-25 cells by targeting HOXB7.	(24)

(Continued)

TABLE 3 | Continued

miRNAs	Expression	Cancer cell	Target of miRNA	Inhibition/ Induction of Cell Death	Sample type	Note	Ref
miR-375	Down	OSCC	IGF-1R	Induction of apoptosis	Human (OSCC, n= 44), *In vitro* (SCC-4)	miRNA-375 enhances apoptosis by targeting IGF-1R.	(25)
miR-124	–	OSCC	–	Induction of apoptosis	*In vitro* (KB and SCC9 cell)	Icaritin promotes mitochondrial apoptosis *via* increasing expression level of miR-124.	(26)
miR-26a	–	Oral cancer cells	Mcl-1	Induction of apoptosis	*In vitro* (KB cell)	Metformin promotes apoptosis through decreasing Mcl-1 expression by miR-26a.	(27)
miR –221/ 222	Up	OSCC	PTEN	Inhibition of apoptosis	*In vitro* (CAL27 and HSC6 cell)	miR–221/222 inhibits apoptosis by targeting PTEN.	(25)
miR-448	Up	OSCC	MPPED2	Inhibition of apoptosis	Human (OSCC, n= 15), *In vitro* (Cal–27 and Scc–9)	miR–448 inhibits apoptosis by targeting MPPED2.	(28)
miR-29a	Down	OSCC	MMP-2	Induction of apoptosis	Human (OSCC, n= 15), *In vitro* (SCC-4)	miR–29a induces apoptosis by targeting MMP-2.	(29)
miR-29b	Down	TSCC	Sp1	Induction of apoptosis	Human (OSCC, n= 40), *In vitro* (CAL27 cells)	Upregulation of miR-29b level cause promotes apoptosis in TSCC cells by regulating PTEN–AKT signaling pathway	(30)
miR-29a	Down	TSCC	Wnt/β-catenin pathway	Induction of apoptosis	Human (OSCC, n= 103), *In vitro* (HOK, SCC-25 cells)	Overexpression of miR–29a induces apoptosis by regulating Wnt/β-catenin pathway.	(31)
miR-9	Down	OSCC	CXCR4	Induction of apoptosis	*In vitro* (Tca8113 and SCC-9 cell)	Upregulation of miR-9 level cause promotes apoptosis in OSCC cells by targeting CXCR4	(27)
miR-218	–	OSCC	mTOR pathway	Induction of apoptosis	*In vitro* (OSCC cell line)	Overexpression of miR-218 reduces OSCC cell growth by caspase-mediated apoptosis.	(32)
miR-17-5p	Down	OSCC	p21	Induction of apoptosis	*In vitro* (OC3 cells)	Overexpression of miR-17-5p mediated by radiation treatment leads to induction of apoptosis by downregulation of p21 levels.	(33)
miR-1179	Up	Oral cancer cells	–	Inhibition of autophagy	*In vitro* (SCC-4, SCC-9, SCC-15 and SCC-25)	Inhibition of miR-1179 induces autophagy by regulation of MEK/ERK and PI3K/AKT signaling pathways.	(29)
miR-617	Down	OSCC	SERPINE1	Induction of apoptosis	*In vitro* (SCC-090 and PE/CA-PJ41)	Overexpression of miR-617 induces apoptosis of OSCC cells by negative regulation of SERPINE1.	(34)
miR-133a	Down	OSCC	CTBP2	Induction of apoptosis	Human (OSCC, n= 40), *In vitro* (UT-SCC-15 and CAL-27)	Overexpression of miR-133a induces apoptosis of OSCC cells by the suppression of CTBP2.	(35)
miR-149-3p	Down	OSCC	AKT2	Induction of apoptosis	*In vitro* (Cal27 and SCC-9)	miR-149-3p combined with Fluorouracil shows an additive effect on the OSCC cells apoptosis through targeting AKT2.	(36)
miR-198	Down	OSCC	–	Induction of apoptosis	*In vivo* (mice), *In vitro* (Cal-27 and SCC-9 cells)	Overexpression of miR-198 induces the apoptosis of OSCC cells.	(37)
miR-487-3p	Down	OSCC	PPM1A	Induction of apoptosis	Human (OSCC, n= 20), *In vitro* (CAL-27 and TCA8113)	miR-487-3p induces apoptosis of OSCC cell by targeting PPM1A.	(38)
miR –196a	Up	OSCC	FOXO1	Inhibition of apoptosis	*In vitro* (SCC9 cell)	Decrease the expression level of miR-196a induces apoptosis of SCC9 cell *via* regulating FOXO1 expression.	(39)
miR-103a-3p	Up	OSCC	RCAN1	Inhibition of apoptosis	*In vitro* (TSCCA and TCA8113 cells)	Inhibition of miR-103a-3p induces the apoptosis of OSCC cells by targeting RCAN1.	(40)
miR-195	Down	OSCC	–	Induction of apoptosis	*In vitro* (OSCC-15/DDP cells)	Overexpression of miR-195 induces apoptosis of OSC-15/DDP cells by regulating MEK1.	(18)
miR-92b	Up	OSCC	–	Inhibition of apoptosis	*In vitro* (CAL-27)	Inhibition of miR-92b induces the apoptosis of OSCC cells.	(41)
miR-101	Down	OSCC	TGF-βR1	Inhibition of apoptosis	*In vitro* (SCC-9 and Tca8113)	miR-101 induces apoptosis of OSCC cells through targeting TGF-βR1.	(42)
miR-22	Down	OSCC	WNT1	Induction of apoptosis	Human (OSCC, n=50) *In vitro* (Tca8113 and SAS)	miR-22 promotes apoptosis of OSCC cells *via* targeting WNT1.	(43)
miR-18a-5p	Up	OSCC	TGF-β1/ Smad2 pathway.	Inhibition of apoptosis	*In vitro* (SCC9 cell)	Downregulation of miR-18a-5p promotes apoptosis of SCC9 cell by regulation of TGF-β1/Smad2 pathway.	(44)
miR –543	Up	OSCC	–	Inhibition of apoptosis	*In vitro* (SCC9, SCC25 and CAL27 cells)	miR–543 inhibits apoptosis of OSCC cell.	(45)

(Continued)

TABLE 3 | Continued

miRNAs	Expression	Cancer cell	Target of miRNA	Inhibition/ Induction of Cell Death	Sample type	Note	Ref
miR −199a −5p	Down	OSCC	IKKβ/NF −κB pathway	Induction of apoptosis	Human (OSCC, n= 60), *In vitro* (Tca8113 and SCC–4 cells)	miR-199a-5p promoted apoptosis of OSCC cells through regulation of the NF−κB pathway *via* targeting IKKβ.	(46)
miR-16	Down	OSCC	AKT3 and BCL2L2	Induction of apoptosis	*In vitro* (SCC-25 and CAL-27 cells)	miR-16 can induce apoptosis of OSCC cells by decreasing AKT3 and BCL2L2 levels.	(47)
miR-186	Down	OSCC	SHP2	Induction of apoptosis	Human (OSCC tissue, n=14), *In vitro* (Tca8113 and SCC-25 cells)	Overexpression of miR-186 induces apoptosis of OSCC cells through ERK and AKT pathways by targeting SHP2.	(48)
miR-1-3p	Down	OSCC	DKK1	Induction of apoptosis	*In vitro* (SCC-4 cells)	miR-1-3p promotes apoptosis of SCC-4 cells by regulating DKK1.	(49)
miR-626	Up	OSCC	RASSF4	Inhibition of apoptosis	Human (OSCC tissue, n=94), *In vitro* (f Ca9-22 and HSC2 cells)	miR-626 can inhibit apoptosis of OSCC cells by targeting RASSF4.	(50)

H3K27 symbolizes gene silencing. Several lncRNAs such as XIST, HOTTIP and FIRRE, etc. play role in activation of transcriptional genes and organizing 3D nuclear architecture (173). On the contrary, lncRNA decoys such as lncRNA-DNA triplex or Alu transcripts can suppress regulation of the transcription by binding to RNA pol II (174). Different transcription factors may bind to lncRNAs and produce a nascent transcript that eventually alters processing of the mRNA molecule through alternative splicing. Binding of the lncRNAs to mRNA can enhance or suppress protein translation or can facilitate mRNA decay (175). Small RNA deep sequencing (Srna-Seq) experiments have found that lncRNAs have also the potential to encode small functional RNAs (176). Mature lncRNAs are also present in the cell cytoplasm and/or nucleus (177). Although the cytoplasmic lncRNAs do not go under translation, small peptides were detected that were produced from lncRNAs due to their association with ribosomes (178). According to some studies, pseudogenes transcriptionally active may also generate these molecules or they can be formed through transcription of the promoter or intergenic loci (179).

Because of enhanced technologies for lncRNA functioning, structure, and interacting partners, our present understanding of lncRNA is more thorough. LncRNAs have major role in maintaining pluripotency of stem cells, differentiation and related human disorders caused by their dysfunction, and recently identified lncRNAs were shown to maintain pluripotency of stem cells and regulate cellular lineage differentiation. Importantly,the structure and location of the lncRNAs appears to forecast their function. LncRNAs can regulate reprogramming of somatic cells and differentiation of stem cells, thus their manipulation allows more efficient strategies for stem cell differentiation nd reprogramming of somatic cells (180). Accordingly, lncRNAs regulate different stages of human or mice reprogramming through several exogenous factors. lncRNA-Xist is involved in the development of an epithelial phenotype during the early stages of conversion from somatic cells to reprogramming intermediates, whereas LNCrna-ladr86/91 is implicated in the metabolic transition from aerobic to anaerobic energy generation (181). lincRNA-p21 plays role in both the early and late phases(reactivation of the pluripotency gene network) in reprogramming by inhibiting cellular proliferation and activation of pluripotency genes, respectively. Likewise, lincRNA-RoR modulates the initial phases of reprogramming through inhibition of p53, which is negative regulator of cell survival, as well as the late phase of reprogramming *via* sponging for miR-145, targeting several pluripotency gene transcripts. lincRNA-1526 and lincRNA-1463 are associated with inverse regulation of the activation of the pluripotency genes in reprogramming, while lincRNA-1307 and ladr49/83 can positively regulate the pluripotency genes. LNCPRESS1, Snhg14, Gas5 and Peblr20 are positive regulators of the pluripotency genes in reprogramming and/or embryonic stem cells(ESCs) (182). Moreover, there are novel approaches to comprehend regulation of the lncRNAs. For instance, RAT-seq allows for the discovery of the genome-wide chromatin binding sites for each specific lncRNA (183, 184). More significant functions and fresh mechanistic insights into how lncRNAs influence biological processes and illnesses will be discovered using these methods. These new findings might potentially lead to the discovery of novel therapeutic targets and the development of new treatments for human diseases (185).

LncRNAs can be divided into three different categories based on their location in the genome: natural antisense transcripts (NATs), long gene non-coding RNAs (lincRNAs) and intron lncRNAs. Upon increasing the binding of UCHL1 mRNA to the polymer, antisense lncRNA UCHL1 enhances the UCHL1 mRNA translation. On the other hand, other lncRNAs, such as lincRNA-p21, inhibit the translation of their target mRNAs after binding to them (186). SINEUPs comprises a novel and functional family of synthetic and natural antisense lncRNAs that can promote target mRNAs translation without producing any effect on the circulating level of mRNAs (187). This lncRNA is comprised of an SINE element (effector domain) embedded into its structure and a binding domain exerting target specificity (188). AS-Uchl1comprises a classic example of the natural SINEUPs. Carrieri et al. observed that AS-Uchl1 had the potential to enhance the translation of sense Uchl1 mRNA in dopaminergic neuronal cells in mice by promoting association of Uchl1 mRNA to heavy polysomes. This process is dependent on the AS-Uchl1 inverted SINEB2 element, which does not affect

the level of Uchl1 mRNA (187). According to their other study, HNRNPK and PTBP1 functioned as RNA binding proteins to interact with SINEUP, and thus contributing to subcellular distribution of SINEUP RNA and assembly of initiation complexes of translation (189). Synthetic SINEUPs were found to be the primary measurable tool to enhance the expression of a specific target gene. For example, SINEUP-cox7B transcribed *in vitro* is a synthetic SINEUP produced against endogenous cox7B mRNA, which can efficiently and specifically up-regulate the expression and translation of COX7B protein, leading to rescuing size of the brain and eye tissues in cox7B morphants (190). Collectively, SINEUPs contain significant treatment potential that can be used in different diseases due to inadequate protein production.

Although lncRNA is not translated into protein, it is still considered a functional molecule that regulates gene expression at multiple levels, including the chromatin, transcriptional, and post-transcriptional levels (191). Indeed, lncRNA is involved in cell differentiation, cell cycle regulation, stem cell pluripotency, and maintenance of various biological processes (192, 193). LncRNAs can affect different apoptotic pathways. For instance, lncRNA overexpression can reduce the expression of membrane surface receptors by affecting extrinsic apoptosis pathway (194). Autophagy not only promotes cell survival but also causes cell death in some conditions. LncRNA can activate autophagy by activating related enzymes (194). In addition, lncRNAs can protect tumor cells from necroptosis by inhibiting the expression of some related proteins (195). Some lncRNA types also act as competitive endogenous RNAs to prevent oxidation and inhibit ferroptosis (195). Increasing evidence shows that lncRNAs are closely related to PCD, and the relationship between lncRNA and PCD is associated with the occurrence of heart disease, cancer cell apoptosis, and cell survival (196). In this section, we summarize the role of lncRNAs in PCD to determine the relationship between lncRNAs and PCD of oral cancer cells.

The evasion of apoptosis has been classified as one of the hallmarks of cancer and is among the main causes of therapy failure. Most tumors are defective in the activation of apoptosis owing to the occurrence of genetic or epigenetic events that either inactivate the p53 pathway or provoke the aberrant expression of pro-survival BCL-2 family members including BCL-2, BCL-XL or MCL-1 (197). It has been shown that BCL-2 exerts a key role in tumorigenesis. In a mouse model of APC-loss-induced colorectal cancer, BCL-2-dependent impairment of apoptosis is required for carcinoma onset (198). Importantly, such unbalance in favor of the pro-survival side of the BCL-2 family confers resistance to radiation, chemotherapeutic agents, and many selective pathway inhibitors that induce apoptosis primarily through the activation of the mitochondrial death machinery (197). Multiple regulatory mechanisms targeting BCL-2 family members involve a different class of lncRNAs. Several lncRNAs have been reported to mediate escape from apoptosis through different mechanisms. For example, lncRNA HOTTIP (HOXA distal transcript antisense RNA) promotes BCL-2 expression and induces chemoresistance in small cell lung cancer by sponging miR-216a (199). In another study, knockdown of HOTTIP has been shown to induce apoptosis by increasing Bax expression and decreasing Bcl-2 expression in prostate cancer cells (200). Sun et al. revealed that HOTTIP acted as a competitive endogenous RNA for microRNA-216a, thus preventing Bcl-2 from binding microRNA-216a in lung cancer cells (199). Recently, Mu et al. (201) reported that lncRNA HOTTIP knockdown lead to restrained the cell proliferation and arrested the cell cycle at G1 phase in human TSCC cell lines (TSCCA and TCA8113 cells). Furthermore, the expression levels of cyclins B, D1, and E were downregulated in HOTTIP-silenced cells. Also, HOTTIP silencing suppressed the growth of xenograft tumors. Besides, they found that the silencing of HOTTIP cause triggered apoptosis in TSCCA and TCA8113 cells and altered the expression of a group of apoptosis-related molecules: downregulated Bcl-2, upregulated Bax, and enhanced the cleavage of caspase 3 and PARP. Knockdown of HOTTIP also suppressed the migration, invasion, and epithelial–mesenchymal transition (EMT) of both TSCCA and TCA8113 cell lines. Altogether, the results of their study suggested that HOTTIP plays a critical role in regulating cell proliferation, apoptosis, and tumorigenesis of TSCC cells and it may serve as a promising potential candidate for OTSCC therapy (201).

Disorder of cell proliferation, apoptosis, and metastasis is an important trigger of cancer occurrence and development. The PI3K/AKT signaling pathway is an important signaling pathway that regulates cell proliferation, apoptosis, and metastasis (202). Recent studies have shown that autophagy plays an important role in tumorigenesis (203). Moreover, mTOR, which is downstream of the PI3K/AKT signaling pathway, is a crucial negative regulator of autophagy (13). Studies on esophageal squamous cell carcinoma and hepatocellular carcinoma have shown that high expression of lncRNA-CASC9 activates the PI3K/AKT signaling pathway, promoting the proliferation, invasion, and metastasis of cancer cells (204, 205). Recently, Yang et al. (206) observed that increased CASC9 expression promotes OSCC cell proliferation. It is unclear whether the increased CASC9 expression in cancer cells regulates the expression of mTOR through the regulation of the PI3K/AKT signaling pathway to control autophagy. For this reason, they depleted lncRNA CASC9 in OSCC cells which led to the significantly decreased expression of p-AKT and p-mTOR, as well as increased autophagy. Also, CASC9 knockdown partially rescued the decreased p-mTOR expression and increased autophagy. Taken together, these findings demonstrated that CASC9, which is highly expressed in OSCC cells, inhibits autophagy by activating the AKT/mTOR pathway (206).

Autophagy plays an important role in the occurrence and development of tumors (207). There exists crosstalk between autophagy and apoptosis; autophagy can both inhibit and promote apoptosis to affect the occurrence and development of cancers (208). Due to the diversity of cells, conditions and stimulating factors, autophagy acts as a double-edged sword for apoptosis (209). For example, Zhao Z. et al. found that oxamate inhibits apoptosis by promoting autophagy to promote gastric cancer (210); in contrast, Yeh P.S. et al. found that honokiol can promote apoptosis by promoting autophagy to promote

neuroblastoma (211). As mentioned, Yang et al. (206) found that autophagy and apoptosis were both increased in cells with silenced CASC9. However, apoptosis is significantly reduced in the OSCC cells cotreated with silenced lncRNA-CASC9 and the autophagy inhibitor, indicating that silencing CASC9 induced autophagy as a pro-death response. This study suggested that autophagy can regulate early apoptosis. Their study also found that CASC9 knockdown in OSCC cells increased and decreased the early apoptosis and P62 protein expression, respectively (206). It is shown that P62 can regulate both autophagy and apoptosis, and many studies reported that P62 mediates apoptosis primarily through regulating autophagy (212). It has been reported that P62 is incorporated into autophagosomes through binding to LC3 in autophagy-activated cells, and subsequently P62 is degraded by autophagy (213); thus, P62 protein expression decreases, and reduced P62 protein expression increases cell apoptosis. Overall, Yang et al. (206) supposed that CASC9 depletion in OSCC cells might promote the binding of P62 to LC3, and then P62 is incorporated into autophagosomes, resulting in the degradation of P62; subsequently, reduction of P62 may increase the autophagy-mediated apoptosis (206). However, the detailed mechanism remains to be further studied.

Currently, for the treatment of OSCC, cisplatin (DDP) is the first-line chemotherapy agent, whereas acquired DDP resistance greatly diminishes drug efficacy and survival benefit. In DDP-resistant OSCC, Wang et al. reported the increased expression of lncRNA MALAT1. Specifically, by the activation of PI3K/AKT/mTOR signaling pathway, MALAT1 overexpression could lead to DDP resistance, whereas MALAT1 knockdown could effectively re-sensitize OSCC cells to DDP treatment, suggesting an instrumental role of MALAT1 in PI3K/AKT/mTOR signaling-associated DDP resistance development (214). Furthermore, PI3K/AKT/mTOR signaling is also known as a critical regulatory pathway of autophagy, a highly conserved catabolic process involving the lysosome-mediated degradation of intracytoplasmic components and participating in a variety of cellular biological activities (215). Autophagy may block or promote tumor survival, depending on the various tumor types and stages. Recently, in OSCC, another lncRNA CASC9 was found to promote cancer progression through suppressing autophagy-mediated cell apoptosis *via* inducing AKT phosphorylation and the subsequent activation of the AKT/mTOR pathway (206) (**Figure 2**). In contrast, the tumor-suppressive lncRNA GAS5 (growth-arrest-specific transcript 5) could suppress proliferation, migration, invasion, and epithelial-mesenchymal transition (EMT) in OSCC (216, 217). Mechanically, GAS5 has been reported to act as a miR-21 sponge in ovarian and cervical cancer. In OSCC, Zeng et al. observed that GAS5 most likely also functions in this way. By sequestering miR-21, GAS5 rescues the expression of PTEN, a negative regulator of PI3K signaling, from miR-21-mediated repression, and thereby inhibiting the PI3K/AKT pathway (216) (**Figure 2**). Taken together, accumulating reports have revealed the prominent involvement and implications of lncRNAs in regulating cellular proliferation, drug resistance, and apoptosis through targeting the PI3K/AKT/mTOR signaling cascade during oral carcinogenesis.

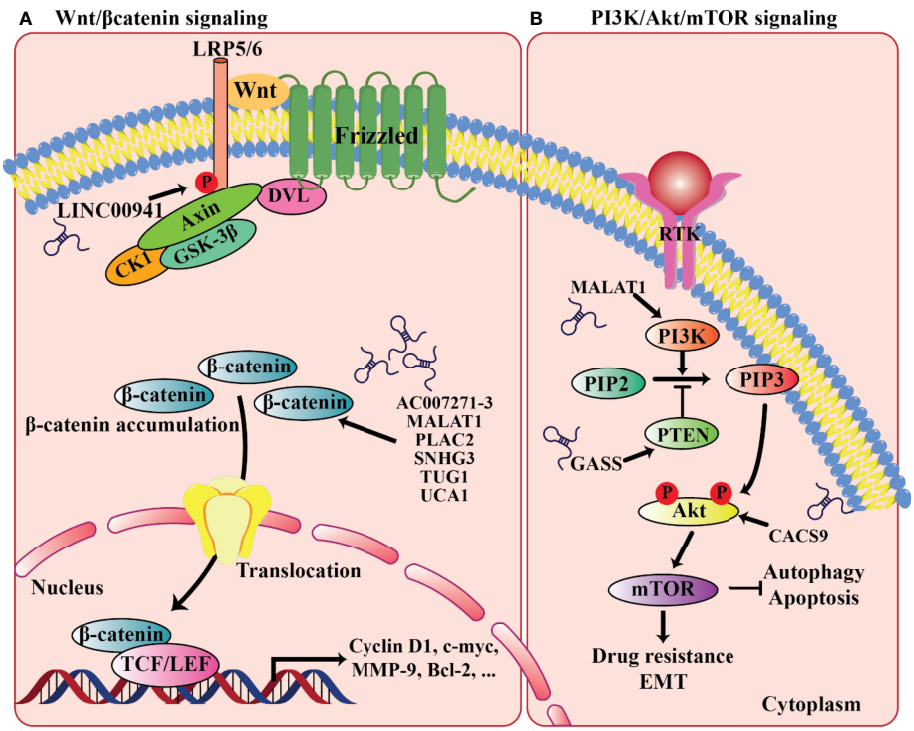

FIGURE 2 | LncRNAs involved in the relevant signaling pathways implicated in oral cancer progression. **(A)** Wnt/β-catenin signaling. **(B)** PI3K/AKT/mTOR signaling.

Autophagy suppresses tumor initiation and prevent s genomic instability. However, autophagy contributes to the progression of advanced cancer by rendering cancer cells resistant to therapeutic agent. Studies proved that the level of autophagy can be determined by monitoring its modulators, such as Beclin1, MAP1LC3B, mTOR, and P62 expressions (218, 219). Takamura et al. indicated that the deficiency of Beclin1/Atg6 could induce tumorigenesis of liver in mouse, and Atg5/Atg7 knockout mouse led to P62 gene deficiency and loss of autophagy. Abnormal accumulations of P62 inhibited NF -κB signing way and triggered inflammation, which promoted tumorigenesis. However, upon recovery of autophagy, inflammation was inhibited, thereby preventing tumorigenesis (220). Hu et al. reported that low expression of Beclin1 was related to poor differentiation, lymphatic metastasis, and TNM stag e and was a poor prognostic marker of OSCC (221). Increasing evidence s showed that autophagy can be regulated by HOTAIR (222). Yang L et al. found that in hepatocellular carcinoma, the overexpression of HOTAIR activate d autophagy by up -regulating ATG3 and ATG7, and the level of autophagy was inhibited when HOTAIR was knocked down (223). Luan W et al. reported that HOTAIR promoted the growth and metastasis of melanoma cells by competitively binding miR-152-3p and activating the downstream PI3k/Akt/mTOR signaling pathway (224). Wang et al. indicated that silencing of Beclin1 in OSCC promoted proliferation, inhibited apoptosis and enhanced chemosensitivity (225). However, whether HOTAIR could regulate autophagy was unclear. This researchers in another study found that HOTAIR interference could decrease the autophagosomes and the expression s of Beclin1, MAP1LC3B, ATG3 and ATG7 were down -regulated (226). Furthermore, it increased the expression of mTOR. So, HOTAIR could promote autophagy in OSCC cells. Besides, they observed that apoptosis rate accelerated in OSCC cells after HOTAIR was silenced, with increased expressions of bim, caspase 3, and caspase7 and decreased expressions of bcl - 2 and mcl -1 decreased. As result, HOTAIR acts as an oncogene in OSCC cells by accelerating autophagy and reducing apoptosis as well as silencing HOTAIR improves sensitivity to cisplatin for OSCC (226).

Maternally expressed 3 (MEG3), a long non-coding RNA, displays variety of biological functions, involved in diverse diseases. Researches have showed that MEG3 conferred endothelial cell aging and disturbed the regenerative angiogenesis (227). By negatively regulating notch pathway, MEG3 impaired the functional recovery after ischemic brain injury (228). The evidences indicated that MEG3 associate with vascular function pathological processes. MEG3 contributed to neurons apoptosis induced by hypoxia through miR-181b12/15-LOX axis (229), suggested that MEG3 may be infaust for neuroprotection. In the trophoblast cells of preeclampsia, level of MEG3 was down-expressed and resulted in abnormalities of apoptosis and migration. Although the functions of MEG3 were diversiform in nontumor disease, the tumor suppressor effect of MEG3 was concerned widely (230–232). In addition, recent studies have shown that the downregulation of MEG3 in lung cancer cells can activate the WNT pathway (230). The WNT/β-catenin signaling pathway, which regulates a variety of cellular processes, such as cell proliferation, apoptosis, and differentiation, is one of the classical pathways for signal transduction (233, 234). Liu and colleagues reported that lncRNA-MEG3 levels were negatively correlated with the WNT pathway. They reported also the expression level of MEG3 was significantly decreased in OSCC and overexpression of MEG3 inhibited the proliferation and metastasis of cancer cells and promoted apoptosis. Overall, they suggested that MEG3 inhibited OSCC cell proliferation, metastasis and promotes apoptosis by negatively regulating the WNT pathway (235). Recently, Tan et al. (236) reported lncRNA-MEG3 was downregulated in OSCC tissues, and the overexpression of MEG3 suppressed migration and promoted apoptosis in OSCC cell lines, while inhibition of MEG3 exhibited opposite effect. Also, they found that MEG3 could effectively sponge miR-548d-3p and decrease its expression level. Moreover, miR-548d-3p repressed the expression of SOCS5 and SOCS6 through binding their 3'UTR, thereby modulating the JAK–STAT signaling pathway and functioning as an oncogene in OSCC cells, as, overexpressed miR-548d-3p inhibits apoptosis by regulating the JAK–STAT Pathway. Importantly, overexpression of MEG3 enhanced the expression of SOCS5 and SOCS6 to regulate JAK–STAT pathway, whereas miR-548d3p overexpression decreased the effects of MEG3 on levels of SOCS5/SOCS6. Furthermore, upregulated expression of miR-548d-3p could abrogate the effect of MEG3 overexpression on migration and apoptosis in OSCC cell lines. In addition, the overexpression of MEG3 inhibited tumor migration and facilitated apoptosis *in vivo*. Together, the result of their study revealed that MEG3 could modulate JAK–STAT pathway *via* miR-548d3p/SOCS5/SOCS6 to suppresses migration and promote apoptosis in OSCC (236). Ferroptosis, an iron-dependent programmed cell death, can affect the prognosis of several tumors. A number of lncRNAs can alter the outcome of tumors by modulating the process of ferroptosis (237).In a study of Li et al. (238), the OSCC prognostic model was established on the basis of 8 frlncRNAs which have a prognostic role and expressed simultaneously with 25 mRNAs. Their study supported a prognostic model in patients with OSCC comprised of 8 different frlncRNAs, including MIAT,AC099850.3, STARD4-AS1, AC090246.1, AC021087.4, HOTARM1,ALMS1-IT1and AL512274.1., which can be used as a prognostic indicator and immune evaluation in OSCC patients and can be subsequently be used as promising therapeutic targets in these patients (238). However, little evidence is present considering the regulatory functions of ncRNAs in oral cancer by ferroptosis. The lncRNAs which regulate cell death pathways are listed in **Table 4**.

CIRCULAR RNA BIOGENESIS AND CIRCRNAS-MEDIATED PROGRAMMED CELL DEATH OF ORAL CANCER

Circular RNA (circRNA) is a subclass of non-coding RNA (ncRNA) (239–242). After long non-coding RNA (lncRNA) and microRNA (miRNA), it has developed into a new research hotspot in the field of cancer (243). CircRNAs are produced by reverse splicing and are characterized by a closed single-stranded structure and lack of 5′ cap and 3′ polyadenylation (poly(A)) tail,

which makes them more stable than lncRNA and miRNA. And circRNAs are highly conserved in eukaryotes, and their expression exhibits tissue- and developmental stage-specific. Numerous studies have revealed that circRNAs have an important effect on the progression and treatment of cancer and play a regulatory role in the tumor microenvironment (TME). Therefore, it suggests that circRNAs may serve as new cancer biomarkers as well as potential therapeutic targets (239, 240, 244, 245).

Back-splicing biogenesis of circRNAs varies from conventional splicing of linear RNAs, according to recent research. They are categorized as intronic-circRNAs, exonic-circRNAs and exon-intron circRNAs (246). Jeck et al. (247). Established two different models considering the circRNAs origination, known as intron-pairing-driven and lariat-driven circularization.Exon circularization is shown to be dependent on flanking intronic complementary sequences and alternate production of inverted repeating Alu pairs, resulting in several circular RNA transcripts being created from a single gene (248). Moreover, RBPs(RNA-binding proteins) function as inhibitors or activators of the circRNAs processing in some circumstances. It has been demonstrated that the generation of up to one-third of common circRNAs are consistently regulated by Quaking (QKI), an alternative splicing factor, and the insertion of QKI motifs are adequate to promote *de novo* synthesis of circRNAs from transcripts normally undergo linear splicing (249). However, by melting the stem's structure, ADAR1, the double-strand RNA-editing enzyme,inhibits the synthesis of circRNA (250). Nonetheless, the exact mechanism of generation of circRNAs remains poorly clarified.

circRNAs have been identified to be expressed widely in most organisms. The size of circRNAs ranges from <100 to several thousand nucleotides, and are produced by a non-canonical splicing event named back-splicing, during such event the downstream splice-donor site is covalently linked to upstream splice-acceptor site (251). The formed closed-loop structure of circRNAs makes them much more stable than linear RNAs, and their half-life is about 4 times longer than linear RNAs (252). In addition, back-splicing makes circRNAs lack 5' cap and 3′ tail, which enables them resistant to ribonuclease RNase R. This feature is usually used in experiments to distinguish circRNAs from linear counterparts (253). According to the sequences it contains, circRNA can be divided into three main different types: exon circRNA (EcRNA), intron circRNA (CiRNA) and exon-intron circRNA (EIcRNA) (242, 254). Among them, EcRNA is the most common and is mainly distributed in the cytoplasm, while circRNAs containing introns are distributed in the nucleus. CircRNAs exhibit widespread expression in different species and abundant expression in human tissues, especially in brain. And their sequences are highly conserved, and many studies have detected about 15,000 human circRNAs sequences in mice. Moreover, their expression exhibits in tissue-, cell- and developmental stage-specific manner, and partially dysregulated circRNAs have a close relationship with tumor pathological differentiation, TNM stage and Lei et al, indicating that they may be suitable candidates for cancer biomarkers (253, 255).

In 2000, Hanahan and Weinberg proposed six hallmarks of cancer that result in the progressive conversion of normal cells into cancerous cells (256). Most and perhaps all types of human cancer shared these acquired capabilities, including self-sufficiency in growth signals, evasion of antigrowth signals, resistance to cell death, limitless replicative potential, sustained angiogenesis, tissue invasion and metastasis. In recent years, some circRNAs have been shown to be involved in these properties of cancer (257).

As mentioned above, as a mechanism of cell death, apoptosis is significant for maintaining homeostasis of the internal environment. Tumor cells can often resist apoptosis, so that abnormal cells are not properly cleared. Abundant evidence supports the role of circRNAs in the evasion of apoptosis to promote cancer progression and blunt therapeutic responses. Cancer cells have developed various strategies to limit or evade apoptosis by upregulating anti-apoptotic components (e.g., Bcl-2, Bcl-xL, and Mcl-1) or decreasing the tumor-suppressive function of proapoptotic factors (e.g., Bax). These components involved in apoptosis are broadly inhibited or activated by circRNAs (258). In this section, we summarize the role of circRNAs in apoptosis to determine the relationship between circRNAs and the apoptosis of oral cancer cells (**Table 5**).

The p53 gene is a common tumor suppressor which is involved in cell cycle regulation *via* a variety of pathways and plays an important role in the development of various tumors, including OSCC (259). BAX is a water-soluble protein homologous to BCL-2 and promotes apoptosis. The overexpression of BAX can antagonize the protective effect of BCL-2 and cause cell death. It is located downstream of the p53 signaling pathway and is regulated by the p53 gene (260). Apoptotic protease activating factor-1 (Apaf-1) plays an important role in the mitochondrial apoptotic pathway, and its expression is regulated by the BAX gene. Apaf-1 ultimately mediates caspase family-related proteins, such as caspase-3, which is generally considered the most important terminal cleavage enzyme in apoptosis (261, 262). It has been shown that when hsa_circ_0055538 was overexpressed in OSCC cells (SCC9 and CAL27 cells), the expression levels of p53, p21, BAX, Apaf-1, caspase-3, and cleaved caspase-3 increased, while the expression of Bcl-2 decreased. Thus, upregulation of circ_0055538 promotes cell apoptosis. As well, downregulation of hsa_circ_0055538 in SCC9 and CAL27 cells using siRNA and obtained the opposite results. Hsa_circ_0055538 regulates the malignant biological behavior of oral squamous cell carcinoma through the p53/Bcl-2/caspase signaling pathway (263).

Circular RNA itchy E3 ubiquitin-protein ligase (circ-ITCH) was demonstrated to function as a tumor suppressor in multiple human cancers, such as lung cancer, ovarian carcinoma, and colorectal cancer (264). Recently, Hao et al. (265) investigated the functional role of circ-ITCH in OSCC. They found that the expression level of circ-ITCH was significantly downregulated in OSCC samples and reported the decreased expression of circ-

TABLE 4 | lncRNAs can regulate cell death pathways in oral cancer.

lncRNAs	Expression	Cancer cell	Target of miRNA	Inhibition/ Induction of Cell Death	Sample type	Note	Ref
LncRNA PANDAR	Up	OSCC	PIM1	Inhibition of apoptosis	*In vitro* (SAS cell line)	PANDAR inhibits apoptosis by overexpression of PIM1 through binding to SRSF7.	(51)
lncRNA GACAT1	Up	OSCC	miR-149	Inhibition of apoptosis and autophagy	Human (OSCC, n= 20), *In vitro* (PECAPJ41 and HSC-4 cells)	miR-149 induces apoptosis and in contrast, lncRNA GACAT1 inhibits apoptosis by sponging miR-149.	(10)
LncRNA PART1	Up	OSCC	FUS/EZH2 pathway	Inhibition of apoptosis	Human (OSCC, n= 36), *In vitro* (Tca-8113 and CAL27)	LncRNA PART1 inhibits apoptosis by binding to FUS and stabilizing EZH2 gene.	(52)
lncRNA PTSC3	Down	OSCC	–	Induction of apoptosis and autophagy	Human (OSCC, n=15), *In vitro* (SCC-1 and SCC-9 cells)	Overexpression of lncRNA PTSC3 induces apoptosis and autophagy.	(53)
LncRNA SCIRT	Down	OSCC	miR-221	Inhibition of apoptosis	*In vitro*	LncRNA SCIRT inhibits apoptosis through sponging miR-221 to upregulate lncRNA GAS5.	(54)
LncRNA LINC01207	Up	OSCC	miR-1301-3p	Inhibition of apoptosis and autophagy	Human (OSCC, n=30), *In vitro* (HSC-3 and HSC-4 cells)	LncRNA LINC01207 inhibits apoptosis and autophagy by regulating miR-1301-3p/LDHA axis.	(55)
LncRNA SNHG16	Up	OSCC	–	Inhibition of apoptosis	Huan (OSCC, n=50), *In vivo* (mice), *In vitro* (CAL27 and TCA8113)	LncRNA SNHG16 inhibits apoptosis.	(56)
lncRNA HOXA-AS2	Up	OSCC	EZH2	Inhibition of apoptosis	*In vitro* (Tca-8113 cells)	Downregulation of lncRNA HOXA-AS2 promotes apoptosis by regulating HOXA-AS2/EZH2 axis.	(57)
LncRNA HITTERS	Up	OSCC	MRE11-RAD50-NBS1 complex	Inhibition of apoptosis	Huan (primary OSCC, n=48), *In vitro* (SCC25 and CAL27)	lncRNA HITTERS can upregulate the expression level of proteins involved in DNA damage repair by binding to the MRE11-RAD50-NBS1 complex and as a result, attenuate endoplasmic reticulum stress-induced apoptosis.	(58)
lncRNA HOXA11-AS	Up	OSCC	miR-98-5p/YBX2 axis	Inhibition of apoptosis	*In vitro* (OSCC=15 and SCC-25 cells)	Downregulation of lncRNA HOXA11-AS promotes apoptosis by regulating miR-98-5p/YBX2 axis.	(59)
lncRNA DANCR	Up	OSCC	miR-216a-5p	Inhibition of apoptosis	Human (OSCC, n=86), *In vitro* (SCC15 and CAL-27)	Downregulation of DANCR induces apoptosis by targeting miR-216a-5p.	(60)
lncRNA PART1	Down	TSCC	miR-503-5p	Induction of apoptosis	Human (TSCC, n=40), *In vitro* (CAL-27 and SCC9 cells)	miR-503-5p prevent the effects of lncRNA-PART1 on the apoptosis, in return, overexpression of lncRNA-PART1 induces apoptosis by targeting miR-503-5p.	(61)
lncRNA PVT1	Up	OSCC	miR–150 –5p/GLUT –1	Inhibition of apoptosis	Human (OSCC, n=70), *In vitro* (SCC-090, SCC-25 and CAL-27)	miR-150-5p can induce apoptosis, in return, lncRNA PVT1 inhibits apoptosis by regulating the miR-150-5p/GLUT-1 axis.	(62)
Exosomal lncRNA HEIH	Up	TSCC	miR–3169-5p	Inhibition of apoptosis	*In vitro* (SCC4/DDP cells)	Exosomal HEIH inhibits apoptosis by sponging miR–3169-5p and increasing HDGF levels.	(63)
LncRNA NEAT1	Up	OSCC	Notch signaling pathway	Inhibition of apoptosis	*In vitro* (TSCC1 cell)	LncRNA NEAT1 inhibits apoptosis by activating Notch signaling pathway.	(64)
lncRNA XIST	Up	OSCC	miR-27b-3p	Inhibition of apoptosis	Human (OSCC tissue), *In vitro*	lncRNA XIST inhibits cell apoptosis in OSCC by regulating miR-27b-3p.	(65)
lncRNA AC007271.3	Up	OSCC	Slug and Wnt/β-catenin signaling pathway	Inhibition of apoptosis	Human (OSCC, n= 97), *In vitro* (SCC9, SCC15, SCC25)	lncRNA AC007271.3 inhibits apoptosis in OSCC cells *via* regulating Slug	(66, 67)

(Continued)

TABLE 4 | Continued

lncRNAs	Expression	Cancer cell	Target of miRNA	Inhibition/ Induction of Cell Death	Sample type	Note	Ref
LncRNA LINC00958	Up	OSCC	miR-185-5p/YWHAZ axis	Inhibition of apoptosis	*In vitro* (SCC 9 and CAL27)	LncRNA LINC00958 inhibits apoptosis through sponging miR-185-5p/YWHAZ axis	(68)
LncRNA LINC00958	Up	OSCC	Sirtuin1	Inhibition of apoptosis	*In vitro* (HSC4 cells)	LINC00958 increases anti-apoptosis protein Bcl-2 levels and decreases pro-apoptosis proteins Bax, c-casp-3. LINC00958 inhibits apoptosis of OSCC by targeting Sirtuin1.	(69)
lncRNA HOXA-AS2	Up	OSCC	–	Inhibition of apoptosis	*In vitro* (TCA-8113 cells)	Downregulation of lncRNA HOXA-AS2 induces apoptosis.	(70)
lncRNA SNHG20	Up	OSCC	miR-29a/ DIXDC1/ Wnt axis.	Inhibition of apoptosis	*In vitro* (SCC9 cells)	Downregulation of lncRNA SNHG20 promotes apoptosis through regulating the miR-29a/DIXDC1/Wnt axis.	(19)
lncRNA CASC9	Up	OSCC	AKT/ mTOR pathway	Inhibition of apoptosis/ autophagy	Human (OSCC, n=84), *In vitro* (SCC15 and CAL27)	lncRNA CASC9 inhibits autophagy-mediated cell apoptosis through the AKT/mTOR pathway.	(71)
lncRNA MEG3	down	OSCC	miR-548d-3p	Induction of apoptosis	*In vivo* (mice), *In vitro* (H157 and HSC-2 cells)	lncRNA MEG3 induces apoptosis through modulate JAK–STAT pathway by miR-548d-3p/SOCS5/SOCS6	(72)
lncRNA RP5-916L7.2	Up	TSCC	miR-328 and miR-939	Inhibition of apoptosis	Human (TSCC, n=30), *In vitro* (Tca-8113)	lncRNA RP5-916L7.2 suppresses cells apoptosis by targeting miR-939-5p and miR-328-5p.	(73)
lncRNA HOXA11-AS	Up	OSCC	miR-214-3p	Inhibition of apoptosis	Human (OSCC, n=31), *In vitro* (TSCCA and CAL-27)	LncRNA HOXA11-AS decreases apoptosis and caspase 3 activities by downregulation expression level of miR-214-3p.	(74)
ncRNA LEF1-AS1	Up	OSCC	–	Inhibition of apoptosis	Human (OSCC, n= 88), *In vitro* (SCC4 and SCC15 cells)	Downregulation LEF1-AS1 lead to induces apoptosis in OSCC cells.	(75)
lncRNA HULC	Up	OSCC	–	Inhibition of apoptosis	*In vitro* (SCC15 and SCC25)	Suppression of lncRNA HULC induces apoptosis in OSCC cells.	(76)
lncRNA CRNDE	Up	OSCC	–	Inhibition of apoptosis	Human (OSCC, n= 52), *In vitro* (CAL-27 and SCC-15 cells)	Suppression of lncRNA CRNDE induces the apoptosis of OSCC cells.	(77)
lncRNA KCNQ1OT1	Up	OSCC	miR-185-5p/Rab14 axis.	Inhibition of apoptosis	Human (OSCC, n= 60), *In vitro* (SCC15 and HSC-3 cells)	Suppression of lncRNA KCNQ1OT1 induces apoptosis by the regulation of miR-185-5p/Rab14 axis.	(78)
lncRNA GAS5	–	OSCC	miR-1297	Induction of apoptosis	*In vitro* (UM-SCC6 cells)	Overexpression of lncRNA GAS5 by propofol induces cell apoptosis. Besides, miR-1297 inhibits GSK3β expression. Upregulation of GSK3β levels by targeting miR-1297 through lncRNA GAS5 lead to enhances Mcl-1 degradation and induction of cell apoptosis.	(79)
LncRNA CASC2	Down	OSCC	miR-21	Induction of apoptosis	Human (OSCC, n=69), *In vitro* (Tca8113 and TSCCa)	LncRNA CASC2 promotes cell apoptosis by regulating of miR-21 expression.	(80)
LncRNA ENST00000 470447.1	Down	OSCC	–	Induction of apoptosis	*In vitro* (Tca-8113 cells)	ENST00000470447.1 promotes the apoptosis of Tca-8113 cells.	(81)
LncRNA LINC00961	Down	OSCC	PI3K/AKT signaling pathway	Induction of apoptosis	Human (OSCC, n=35), *In vitro* (OSC-4 and CAL-24)	LncRNA LINC00961 promotes apoptosis of OSCC cells by regulating the PI3K/AKT signaling pathway.	(82)
lncRNA ANRIL	Up	OSCC	TGF-β/ Smad pathway	Inhibition of apoptosis	Human (OSCC, n=35), *In vitro* (OSC-4 and CAL-24)	lncRNA ANRIL inhibits apoptosis of OSCC cells by regulating TGF-β/ Smad pathway.	(83)
LncRNA SNHG16	Up	OSCC	–	Inhibition of apoptosis	*In vitro* (CAL-27 and TSCCA cells)	LncRNA SNHG16 inhibits apoptosis of OSCC cells.	(84)
lncRNA XIST	Up	OSCC	miR-34a-5p	Inhibition of apoptosis	*In vitro* (Cal-27 and Tca-8113 cells)	Downregulation of lncRNA XIST promotes apoptosis of OSCC cells by regulating expression level of miR-34a-5p.	(85)

(Continued)

TABLE 4 | Continued

lncRNAs	Expression	Cancer cell	Target of miRNA	Inhibition/ Induction of Cell Death	Sample type	Note	Ref
lncRNA LINC00662	Up	OSCC	–	Inhibition of apoptosis	Human (OSCC, n=61), *In vitro* (ISG15 cell)	Downregulation of lncRNA LINC00662 promotes apoptosis of OSCC cells.	(86)
lncRNA HOTAIR	Up	OSCC	–	Inhibition of apoptosis and induction of autophagy	*In vitro* (CAL-27)	lncRNA HOTAIR can act as an oncogene lncRNA in OSCC cells by decreasing apoptosis and promoting autophagy.	(87)
LncRNA HOTAIR	Up	OSCC	–	Inhibition of apoptosis	Human (OSCC, n=76), *In vitro* (Tca8113 and TSCCA)	Downregulation of HOTAIR induces apoptosis of OSCC cells.	(88)
LncRNA HOTAIR	Up	OSCC	–	Inhibition of apoptosis	Human (OSCC, n=45), *In vitro* (Tca8113)	Downregulation of HOTAIR induces apoptosis of OSCC cells.	(89)
lncRNA HOTAIR	–	OSCC	–	Inhibition of apoptosis	*In vitro* (Tca8113 cells)	DNA damage promotes overexpression of lncRNA HOTAIR mRNA and it inhibits apoptosis of Tca8113 cells.	(90)
lncRNA LACAT1	Up	OSCC	miR-4301	Inhibition of apoptosis	*In vitro* (Cal-27 and Tca-8113 cells)	LACAT1 suppresses apoptosis of OSCC cells by targeting miR-4301.	(91)
lncRNA C5orf66 –AS1	Down	OSCC	–	Induction of apoptosis	Human (OSCC, n=30), *In vitro* (SCC9 cells)	Overexpression of lncRNA C5orf66–AS1 promotes apoptosis of OSCC cells.	(92)
lncRNA HOTTIP	Up	TSCC	–	Inhibition of apoptosis	Human (TSCC, n=30), *In vitro* (TSCCA and TCA8113 cells)	Downregulation of lncRNA HOTTIP promotes apoptosis of TSCC cell by regulation of apoptosis-related molecules	(93)
lncRNA NEAT1	Up	OSCC	miR-365	Inhibition of apoptosis	Human (OSCC, n=30), *In vitro* (SCC9 cells)	Downregulation of lncRNA NEAT1 promotes apoptosis in OSCC cells by regulating miR–365.	(94)
lncRNA KCNQ1OT1	Up	Tongue cancer	EGFR	Inhibition of apoptosis	Human (tongue cancer tissues, n=50), *In vitro* (UM1 and CAL-27 cells)	Downregulation of KCNQ1OT1 induces apoptosis of TSCC through intrinsic pathway and regulation of EGFR.	(62)
lncRNA CEBPA-AS1	Up	OSCC	CEBPA	Inhibition of apoptosis	Human (OSCC, n=60), *In vitro* (Tca8113 and Cal-27 cells)	Downregulation of lncRNA CEBPA-AS1 induces apoptosis of OSCC cell through pathway CEBPA/Bcl2 by targeting CEBPA.	(95)
lncRNA H19	Up	OSCC	miR-138	Inhibition of apoptosis	Human (OSCC, n=42), *In vitro* (HSC-2 and Ca9-22 cells)	lncRNA H19 inhibits apoptosis of OSCC cell through regulating miR-138 expression.	(96)
lncRNA TUC338	Up	TSCC	–	Inhibition of apoptosis	Human (TSCC, n=25) *In vitro* (CAL-27 and SCC-9 cells), *In vivo* (mice)	Downregulation of lncRNA TUC338 induces apoptosis of TSCC cell.	(97)
lncRNA MALAT	Up	TSCC	Wnt/β-catenin signaling pathway	Inhibition of apoptosis	Human (OSCC, n=42), *In vitro* (HSC-2 and Ca9-22 cells)	MALAT1 suppresses apoptosis of TSCC cells through modulating Wnt/β-catenin signaling pathway.	(98)
LncRNA TUG1		OSCC	Wnt/β-catenin signaling	Inhibition of apoptosis	*In vitro* (Tca8113 and TSCCA cells)	Downregulation of lncRNA TUG1 induces apoptosis of OSCC cells through modulating Wnt/β-catenin signaling pathway.	(99)
lncRNA UCA1	Up	OSCC	miR-184	Inhibition of apoptosis	Human (OSCC, n=30), *In vitro* (Tca8113-CDDP and TSCCA-CDDP cells)	lncRNA UCA1 knockdown promotes apoptosis rate of OSCC cell by sponging miR-184.	(100)
lncRNA MEG3	Down	OSCC	–	Induction of apoptosis	Human (OSCC, n=83), *In vitro*	lncRNA MEG3 induces apoptosis of OSCC cells	(101)

(Continued)

TABLE 4 | Continued

lncRNAs	Expression	Cancer cell	Target of miRNA	Inhibition/ Induction of Cell Death	Sample type	Note	Ref
					(Cal27 and SCC15 cells)		
lncRNA UCA1	Up	OSCC	WNT/β-catenin signaling pathway	Inhibition of apoptosis	*In vitro* (Cal27 and SCC15 cells)	Downregulation of lncRNA UCA1 promotes apoptosis of OSCC cell may be by regulating the WNT/β-catenin signaling pathway.	(102)
lncRNA TTN-AS1	Up	OSCC	miR-199a-3p	Inhibition of apoptosis	Human (OSCC tissue, n=36), *In vitro* (SCC-4 and HSC-3 cells)	Downregulation of lncRNA TTN-AS1 promotes apoptosis of OSCC cells by sponging miR-199a-3p.	(103)
lncRNA TTN-AS1	Up	OSCC	miR-411-3p	Inhibition of apoptosis	Human (OSCC tissue, n=50), *In vitro* (SCC-4 and SCC-9 cells)	lncRNA TTN-AS1 contribute to oral cancer development by inhibition of apoptosis in OSCC cells through regulating miR-411-3p/NFAT5 axis.	(20)
lncRNA TRG-AS1	Up	TSCC	miR-543/ YAP1 pathway	Inhibition of apoptosis	Human (TSCC, n= 57), *In vitro* (CAL-27 and SCC-15)	Downregulation of lncRNA TRG-AS1 induces apoptosis of TSCC cells by regulation of miR-543/YAP1 pathway.	(104)
LncRNA LINC00519	Up	TSCC	miR-876-3p	Inhibition of apoptosis	Human (TSCC, n= 52), *In vitro* (SCC-15 and CAL-27)	Downregulation of lncRNA LINC00519 induces apoptosis of TSCC cells by regulation of miR-876-3p/MACC1 axis.	(105)
LncRNA SNHG15	Down	OSCC	miR-188-5p	Inhibition of apoptosis	*In vitro* (SCC-9 and SCC-15)	LncRNA SNHG15 inhibits apoptosis of OSCC cells by sponging miR-188-5p	(19)
LncRNA FER1L4	Up	OSCC	miR-133a-5p	Inhibition of apoptosis	Human (OSCC tissue, n= 45), *In vitro* (SCC-9 and HN4 cells)	Downregulation of LncRNA FER1L4 induces apoptosis of OSCC cells by regulating the miR-133a-5p/Prx1 axis.	(106)

ITCH in OSCC is closely correlated with malignant progression and poor survival in OSCC patients. As well, the results of their study showed that circ-ITCH overexpression suppressed cell proliferation, but promoted apoptosis of OSCC cells *in vitro*. Also, they observed that the increased apoptosis rates of OSCC cells with circ-ITCH overexpression were notably diminished by co-transfection of miR-421, accompanied by the increased expression of Bcl-2 and the decreased levels of Bax, cleaved caspase-3 and PDCD4. Overall, the result of their research showed that circ-ITCH serves as a tumor suppressor in OSCC partly by suppressing cell proliferation and Inducing apoptosis in OSCC by regulating miR-421/PDCD4 Axis (265).

Baculoviral IAP repeat-containing 3 (BIRC3) belongs to the inhibitors of apoptosis (IAP) family of proteins, which suppress proapoptotic signaling. Several studies have reported that BIRC3 may also impair cancer cell susceptibility to chemotherapy (266). Recently, Wang et al. (267) built an apoptotic model with TNF-α, and then they confirmed a circRNA associated with the apoptosis of OSCC cells, circDOCK1 by comparing the expression profile of circRNAs in an apoptotic model with that in untreated OSCC cells. They observed that circDOCK1 is highly expressed in OSCC tissue and cell lines, and circDOCK1 is significantly downregulated in the apoptosis model. In order to further confirm the biological function of circDOCK1 in OSCC, they downregulated circDOCK1 expression using siRNAs and observed that the apoptosis rate increased. With the use of bioinformatics analysis, they surmised that circDOCK1 could serve as a miR-196a-5p sponge. Besides, miR-196a-5p may be implicated in cancer-associated pathways and regulate apoptosis-related genes (268, 269). In order to validate the circDOCK1/miR-196a-5p/mRNA axis, their results revealed that when the expression level of circDOCK1 is downregulated, miR-196-5p was upregulated while BIRC3 was downregulated accordingly. Moreover, when the expression level of miR-196-5p is upregulated, circDOCK1 and BIRC3 were downregulated accordingly, too. At the end of this study, they suggested that circDOCK1 suppresses cell apoptosis *via* inhibition of miR-196a-5p by targeting BIRC3 in OSCC (267).

It has been reported that TLR4 can mediate the immune escape of tumor cells and promote tumor cell to resist drug-induced apoptosis (270). Ai et al. (271) conducted a TNF-a induced apoptosis experiment in OSCC cells. The results of their study showed that TNF-a could induce apoptosis of OSCC cells, which was enhanced by knockdown of circ_0001461. In contrast, overexpression of circ_0001461 lead to inhibit the apoptosis of OSCC cells induced by TNF-a treatment. In addition, they reported that knockdown of circ_0001461 inhibited the expression of TLR4 and NF-kB, while overexpression of circ_0001461 promoted the protein level of TLR4 and NF-kB. Functionally, circ_0001461 directly targeted miR-145 and inhibited the proliferation, migration, and invasion of OSCC cells. TLR4, a direct target of miR-145, served as the key mediator of circ_0001461 function by promoting the resistance of immune induced apoptosis of OSCC cells. Together, their results suggested that circ_0001461 might promote OSCC cells to resist TNF-a induced apoptosis through TLR4 mediated NF-kB pathway (271).

Cetuximab is a recombinant human murine chimeric IgG1 monoclonal antibody, which has high affinity for EGFR, inhibits

TABLE 5 | Circular RNAs can regulate cell death pathways in oral cancer.

Circular-RNAs	Expression	Cancer cell	Target of miRNA	Inhibition/ Induction of Cell Death	Sample type	Note	Ref
circRNA_100533	Down	OSCC	miR-933	Induction of apoptosis	*In vitro* (CAL-27 and SCC-9 cell lines)	circRNA_100533 can induce apoptosis of OSCC cells by sponging miR-933, and then regulating GNAS expression.	(107)
circBICD2	Up	OSCC	miR-149-5p	Inhibition of apoptosis	Human (Tongue, n= 15; Buccal, n= 5; and gingival, n= 6), *In vitro* (SCC25 and CAL27 cells)	IGF2BP1 inhibits the apoptosis of OSCC cells by regulating the miR-149-5p/IGF2BP1 axis.	(108)
circFNDC3B	Up	OSCC	miR-520d-5p	Inhibition of apoptosis	*In vitro* (CAL27 and SCC15 cells)	Downregulation of circFNDC3B promotes apoptosis of OSCC cells by regulating the miR-520d-5p/SLC7A11 axis	(109)
circ_0109291	Up	OSCC	–	Inhibition of apoptosis	Human (OSCC tissue, n= 51), *In vitro* (CAL27 and SCC4 cells)	Downregulation of circ_0109291 induces apoptosis of OSCC cells.	(110)
circ_0002203	Down	OSCC	–	Induction of apoptosis	Human (OSCC tissue, n=40), *In vitro* (CAL27 and SCC15 cells)	Overexpression of circ_0002203 promotes apoptosis of OSCC cells.	(111)
circ_0055538	Down	OSCC	The p53/ Bcl-2/ caspase signaling pathway	Induction of apoptosis	Human (OSCC tissue, n= 44), *In vitro* (CAL27 and SCC9 cells)	Overexpression of circ_0055538 induces the apoptosis of OSCC cells by regulating the p53/Bcl-2/caspase signaling pathway.	(112)
circ_0007059	Down	OSCC	–	Induction of apoptosis	Human (OSCC tissue, n=52), *In vitro* (CAL27 and SCC15 cells)	Overexpression of circ_0007059 induces the apoptosis of OSCC cells maybe by remodulation of AKT/mTOR pathway.	(113)
circ_009755	Down	OSCC	–	Induction of apoptosis	Human (OSCC tissue, n=8), *In vitro* (CAL27 and SCC15 cells)	Decrease the expression level of circ_009755 suppresses the apoptosis of OSCC cells.	(114)
circATRNL1	Down	OSCC	miR-23a-3p	Induction of apoptosis	Human (OSCC, tissue, n= 48), *In vitro* (HSC3 and SCC25 cells)	Overexpression of circATRNL1 help to improved sensitivity of OSCC cells to radiotherapy by promotes apoptosis through sponging miR-23a-3p.	(115)
circ_0033144 (CircBCL11B)	Up	OSCC	miR-579/ LASP1 axis.	Inhibition of apoptosis	Human (OSCC, tissue, n= 50), *In vitro* (CAL27 and SCC15 cells)	Downregulation of cirCBCL11B promotes the apoptosis of OSCC cells by regulating miR-579/LASP1 axis.	(116)
CircSPATA6	Down	OSCC	miR-182/ TRAF6 axis	Induction of apoptosis	Human (OSCC, serum, n= 46), *In vitro* (CAL27 and SCC9 cells)	CircSPATA6 promotes apoptosis of OSCC cell by regulating the miR-182/TRAF6 axis.	(117)
Circ-BICD2	Up	OSCC	miR-296-5p	Inhibition of apoptosis	Human (OSCC tissue, n= 35), *In vitro* (CAL27 and SCC9 cells)	circ-BICD2 can promote apoptosis of OSCC cells might by the regulating the miR-296-5p/TAGLN2 axis.	(118)
Circ-ITCH	Down	OSCC	miR-421	Induction of apoptosis	Human (OSCC tissue, n=57), *In vitro* (SCC6 and HN4 cells)	Overexpression of circ-ITCH promotes apoptosis of OSCC cells through regulating miR-421/PDCD4 axis.	(119)
Circ-PVT1	Up	OSCC	–	Induction of apoptosis	Human (OSCC tissue, n=30), *In vitro* (SCC4 and CAL27 cells)	circ-PVT1 promotes apoptosis of OSCC cells.	(120)
Circ-KIAA0907	Down	OSCC	miR-96-5p	Induction of apoptosis	Human (OSCC tissue, n=59), *In vitro* (HSC6 and OECM1 cells)	circ-KIAA0907 induces apoptosis of OSCC cells through regulating the miR-96-5p/UNC13C axis.	(121)
circKRT1	Up	OSCC	miR-495-3p	Inhibition of apoptosis	Human (OSCC tissue, n=50), *In vitro* (Cal-27 and HSC-3)	Downregulation of circKRT1 inhibits the apoptosis of CD8+ T cells by regulating by the miR-495-3p/PDL1 axis and suggested that suppresses activity of CD8+ T-cell to induces immune evasion of OSCC cells.	(122)
circ_0000140	Down	OSCC	miR-31	Induction of apoptosis	Human (OSCC tissue, n=56), *In vitro* (Cal-27, HSC-3 and HOK cells)	circ_0000140 promotes apoptosis of OSCC cells by regulation of miR-31/LATS2 axis.	(123)
circRNA_043621	Up	OSCC	–	Inhibition of apoptosis	Human (OSCC tissue, n= 23), *In vitro* (TSCC1 cell)	The circRNA_043621 downregulation leads to induction of apoptosis in OSCC cells.	(124)
circRNA_102459	Down	OSCC	–	Induction of apoptosis	Human (OSCC tissue, n= 23), *In vitro* (TSCC1 cell)	The circRNA_102459 overexpression leads to induction of apoptosis in OSCC cells.	(124)
Circ-HIPK3	Up	OSCC	miR-381-3p	Inhibition of apoptosis	*In vitro* (SCC-4 and SCC-9 cells)	circ-HIPK3 inhibits apoptosis of OSCC cells through regulating miR-381-3p/YAP1 axis.	(125)

(Continued)

TABLE 5 | Continued

Circular-RNAs	Expression	Cancer cell	Target of miRNA	Inhibition/ Induction of Cell Death	Sample type	Note	Ref
CircRNA_10103	Down	OSCC	–	Induction of apoptosis	*In vitro* (OECM1 and HSC3 cells)	Overexpression of circRNA_10103 induces apoptosis of OECM1 and HSC3 cells.	(126)
circ_0001742	Up	TSCC	miR-431-5p	Inhibition of apoptosis	Human (TSCC tissue, n= 30), *In vitro* (CAL27 and SCC4 cells)	circ_0001742 inhibits apoptosis of TSCC cells by regulating the miR-431-5p/ATF3 axis.	(127)
circ_0005379	Down	OSCC	–	Induction of apoptosis	Human (OSCC tissue, n= 37), *In vitro* (SCC25 and CAL27 cells)	Overexpression of circ_0005379 induces apoptosis of OSCC cells might by regulating the EGFR pathway.	(128)
circ_0011946	Up	OSCC	miR-216a	Inhibition of apoptosis	Human (OSCC tissue, n= 30), *In vitro* (SCC25 and CAL27 cells)	Downregulation of expression level of circ_0011946 induces apoptosis of OSCC cells by the regulation of the miR-216a-5p/BCL2L2 axis.	(129)
Circ_0001461	Up	OSCC	miR-145	Inhibition of apoptosis	Human (OSCC tissue, n= 20), *In vitro* (CAL-27 and KB cells)	Circ_0001461 suppresses apoptosis of OSCC cells by regulating miR-145/TLR4/NF-κB axis.	(130)
circCDR1as	Up	OSCC	miR-876-5p	Induction of autophagy and inhibition of apoptosis	Human (OSCC tissue), *In vitro* (OSCC cells)	Upregulation of circCDR1as levels induces autophagy, and inhibits apoptosis in OSCC cells by targeting miR-876-5p.	(131)
circHIPK3	Up	OSCC	miR-637	Inhibition of apoptosis	Human (OSCC tissue, n= 40), *In vivo* (mice) *In vitro* (Tca8113 and SCC-9 cells)	CircHIPK3 inhibits apoptosis of OSCC cells through regulating the miR-637.	(132)
circDHTKD1	Up	OSCC	miR-326	Inhibition of apoptosis	Human (OSCC tissue, n= 56), *In vitro* (SCC9 and Cal27 cells)	circDHTKD1 inhibits apoptosis of OSCC cells by targeting miR-326	(133)
circ_0005623					Human (OSCC tissue, n= 56), *In vitro* (SCC-9 and CAL-27 cells).		
Circ_0002141	Up	OSCC		Inhibition of apoptosis	Human (OSCC tissue, n= 52), *In vitro* (OSCC cells)	Circ_0002141 inhibits apoptosis of OSCC cells by regulating miR-1231/EGFR axis	(134)
circ_0005379	Down	OSCC	miR-17-5p	Induction of apoptosis	Human (OSCC tissue), *In vitro* (SCC15 cells)	Overexpression of circ_0005379 promotes apoptosis of OSCC cells by regulating the miR-17-5p/ACOX1 axis.	(135)
circ-PKD2	Down	OSCC	miR-204-3	Induction of apoptosis	Human (OSCC tissue, n= 56), *In vitro* (SCC15 cells)	circ-PKD2 induces apoptosis of OSCC cell by suppressing of miR-204-3 activity.	(136)
circ_0001971 circ_0001874	–	OSCC	–	Inhibits of apoptosis	*In vitro* (SCC9 cells)	Upregulation of circ_0001971 and circ_0001874 synergistically inhibits apoptosis of OSCC cells.	(137)
Circ_0001971	Up	OSCC	miR-194 and miR-204	Inhibits of apoptosis	Human (OSCC tissue, n= 50), *In vitro* (CAL-27 and SCC9 cells)	Circ_0001971 inhibits apoptosis of OSCC by regulating miR-194 and miR-204.	(138)
Circ_0109291	Up	OSCC	miR-188-3p	Inhibits of apoptosis	Human (OSCC tissue, n= 60), *In vitro* (CAL-27/DDP and UM1/DDP cells)	Circ_0109291 was overexpressed in Cisplatin-resistant OSCC tissues and cells. Downregulation of circ_0109291 promotes apoptosis of OSCC cells by regulating the miR-188-3p/ABCB1 axis.	(139)
circ_0000745	Up	OSCC	miR-488	Inhibition of apoptosis	Human (OSCC tissue, n= 64), *In vitro* (Cal-27 and SCC9 cells)	circ_0000745 inhibits apoptosis of OSCC cells by regulating expression level of miR-488/CCND1.	(140)
Circ-SCMH1	Up	OSCC	miR-338-3p	Inhibition of apoptosis	Human (primary OSCC tissue, n= 62), *In vitro* (SCC-15/DDP and CAL-27/DDP)	Circ-SCMH1 was overexpressed in Cisplatin-resistant OSCC tissues and cells. Circ-SCMH1 contribute to oral cancer development by inhibition of apoptosis in OSCC cells through regulating miR-338-3p/LIN28B.	(141)

cell cycle progression, and induces tumor cell apoptosis by specifically binding to the extracellular EGFR domain. This reduces the production of MMPs and vascular endothelial growth factors, and inhibits tumor invasion and metastasis. Cetuximab has shown good clinical efficacy and tolerability for EGFR expression in head and neck cancers (272, 273). However, unresolved issues with this drug persist, such as acquired treatment resistance caused by mutations in KRAS and BRAF, both of which participate in the EGFR signaling pathway (274). It has been reported that ncRNAs can be regulated cetuximab sensitivity in cancer cells (275–277). Since cetuximab is a commonly used anticancer drug for OSCC treatment, recently Su et al. (278) performed a drug treatment experiment to investigate the effect of hsa_circ_0005379 on OSCC cell viability. In their study, apoptosis rates in hsa_circ_0005379 overexpression cells were measured by annexin V-FITC/PI dual-label flow cytometry and flow cytometry to detect apoptosis in different treatment groups of SCC25 and CAL27 (OSCC cell lines) was used. They found that early apoptotic rates in the mock group were 0.31 and 0.43% in SCC25 and CAL27 cells, respectively, while early apoptotic rates in the hsa_circ_0005379 group were 1.12 and 0.91% in SCC25 and CAL27 cells, respectively. Early apoptotic rates in the mock + cetuximab group were 17.88 and 15.22% in SCC25 and CAL27 cells, respectively, while early cell apoptotic rates in the circ_0005379 + cetuximab group increased to 38.35 and 35.77% in SCC25 and CAL27 cells, respectively. Their experimental results showed that changes in early apoptotic rates are not obvious in cells after high hsa_circ_0005379 expression in SCC25 and CAL27 cell lines. However, when cetuximab was added after overexpressing hsa_circ_0005379 in SCC25 and CAL27 cells, the early apoptotic rate of the cells significantly increased to 38.35 and 35.77%, respectively. This study indicated that high hsa_circ_0005379 expression increases cetuximab sensitivity and provides a new potential target for OSCC anticancer drugs design in the future (278). The occurrence of cisplatin (DDP) resistance in oral squamous cell carcinoma (OSCC) is a major challenge for OSCC treatment. Gao et al. reported that Circ_0109291 was higher expressed in DDP-resistant OSCC tissues and cells, and its knockdown suppressed resistance and enhanced the apoptosis of OSCC cells. They suggested that circ_0109291 could promote the DDP resistance and inhibit apoptosis of OSCC, and silenced circ_0109291 might be a key step to inhibit OSCC resistance (279). In another study, Tan and colleagues (280) found that circ_0001971 knockdown promoted chemosensitivity (DDP) and apoptosis in OSCC cells by interacting with miR-194 and miR-204 (280). Such studies show the circRNAs can serve as critical player in OSCC cell resistance and the functions of the circRNAs provide insight into their roles in oral cancer chemotherapy resistance. More studies about circRNAs-mediated PDC of oral cancer are listed in **Table 5**.

Recent studies have shown that autophagy plays a critical role in the occurrence of tumors and malignant transformation (101, 165, 281). In advanced stage tumors, cancer cells survive under low-nutrition and hypoxic conditions by inducing autophagy due to cancer cells have higher bioenergy requirements and nutritional needs than normal cells (165). The elucidation of the association between autophagy and poor survival in various cancers, suggested that autophagy may serve as a marker for both diagnostic and clinicopathological characteristics (282, 283). Thus, understanding the signaling pathways involved in the regulation of autophagy as well as its biological functions in OSCC represents new directions in the development of anticancer therapeutic strategies. Recently, Gao et al. (284) validated the functional roles of circCDR1as in regulation of autophagy in OSCC cells and further investigated how circCDR1as contributed to cell survival *via* up-regulating autophagy under a hypoxic microenvironment by using combination of human tissue model, *in vitro* cell experiments and *in vivo* mice model. They found that overexpression circCDR1as not only promoted OSCC cells proliferation *in vitro* and the growth of implanted tumors *in vivo* but also stimulated cells autophagy. The effects of circCDR1as on cellular autophagy contributed to OSCC progression and development. As well, hypoxia promoted the expression level of circCDR1as in OSCC cells and elevated autophagy. In addition, circCDR1as further increased hypoxia-mediated autophagy by targeting multiple key regulators of autophagy. They revealed that circCDR1as enhanced autophagy in OSCC cells *via* inhibition of rapamycin (mTOR) activity and upregulation of AKT and ERK½ pathways. Overexpression of circCDR1as enhances OSCC cells viability, endoplasmic reticulum (ER) stress, and inhibited cell apoptosis under a hypoxic microenvironment. Moreover, circCDR1as is promoted autophagy in OSCC cells by sponging miR-671-5p. Collectively, the results of their research revealed that high expression of circCDR1as enhanced the viability of OSCC cells under a hypoxic microenvironment by promoting autophagy, suggesting a novel treatment strategy involving circCDR1as and the inhibition of autophagy in OSCC cells (284) (**Figure 3**). Consistent with this studies, Cui et al. (285) reported overexpression of circCDR1as promoted autophagy, cell cycle, proliferation, and metastasis and repressed apoptosis in OSCC cells. CircCDR1as directly targeted miR-876-5p and miR-876-5p interacted with SLC7A11. MiR-876-5p overexpression was reversed the effects of circCDR1as elevation on OSCC cell autophagy, cell cycle, growth, motility, and apoptosis. In addition, circCDR1as knockdown blocked tumor growth *in vivo*. They suggested that circCDR1as acted as an oncogene in OSCC progression through elevating SLC7A11 by targeting miR-876-5p (285).

CONCLUSION

Apoptosis and autophagy are physiologically necessary pathways that are vital for cell homeostasis and as one of the major dysregulated processes in the carcinogenesis of oral cancer has been shown to be regulated by ncRNAs. In the current review, we have explained the impact of miRNAs, lncRNAs and circRNAs on apoptosis and autophagy in oral cancer. These ncRNAs interact with PI3K/Akt, NF-κB, Wnt/β-catenin, EGFR, TGF-β and other cancer-related pathways (**Tables 3**–**5**). Therefore, they not only regulate cell death pathway, but also influence other aspects of oral carcinogenesis.

Manipulation of expression of apoptosis-regulating circRNA, lncRNAs and miRNAs represent a strategy for combating carcinogenesis as well as resistance to chemo/radiotherapy. Some

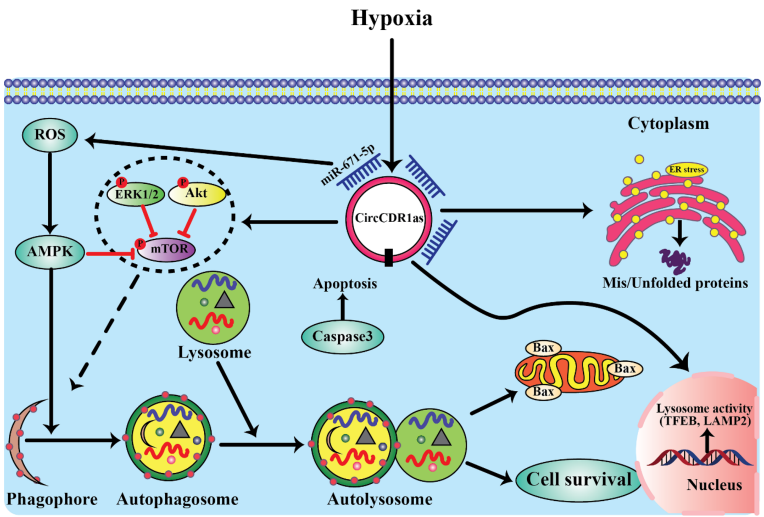

FIGURE 3 | The mechanism underlying the regulation of autophagy.

of the apoptosis-regulating circRNA/miRNA and miRNAs/lncRNAs have been shown to influence prognosis of lung cancer. The observed correlation between their expression and patients' survival is due to their impact on disease progression as well as response of patients to EGFR inhibitors and chemotherapeutic agents.

An acknowledged route of function of lncRNAs and circRNA in the regulation of apoptosis in oral cancer is their impact on expression of miRNAs. In fact, they can sponge or sequester miRNAs and release miRNA targets from their inhibitory effects. Circ-SCMH1/miR-338-3p, circ_0109291/miR-188-3p, circ_0001971/miR-194/miR-204, circ_0001874/miR-296, circ-PKD2/miR-204-3p, circ_0001461/miR-145, circ_0011946/miR-216a-5p, lncRNA-KCNQ1OT1/miR-185-5p, lncRNA RP5-916L7. 2/miR-328, LncRNA MEG3/miR-548d-3p, and LINC00958/miR-4306 are examples of circRNAs/miRNAs and lncRNAs/miRNAs interactions with verified roles in the control of oral cancer cells apoptosis. Based on the importance of apoptotic pathways in determination of response of oral cancer patients to conventional as well as targeted therapies, identification of the impacts of ncRNAs on apoptosis and prior profiling of these ncRNAs in clinical samples would help in prediction of response of patients to each therapeutic regimen and design of personalized treatment strategies. The advent of high throughput sequencing strategies has facilitated conduction of this approach in the clinical settings. Finally, the possibility of ncRNAs tracing in the peripheral blood of patients has opened a new opportunity for early detection of emergence of resistance to conventional or targeted therapies and modulation of therapeutic regimens to enhance the survival of affected individuals.

AUTHOR CONTRIBUTIONS

MT involved to conception, design, statistical analysis and drafting of the manuscript. LE and , AAS contributed to data collection and manuscript drafting. All authors contributed to the article and approved the submitted version

REFERENCES

1. Ferlay J, Colombet M, Soerjomataram I, Mathers C, Parkin DM, Piñeros M, et al. Estimating the Global Cancer Incidence and Mortality in 2018: GLOBOCAN Sources and Methods. *Int J Cancer* (2019) 144(8):1941–53. doi: 10.1002/ijc.31937
2. Wong T, Wiesenfeld D. Oral Cancer. *Aust Dental J* (2018) 63:S91–S9. doi: 10.1111/adj.12594
3. Bray F, Ferlay J, Soerjomataram I, Siegel RL, Torre LA, Jemal A. Global Cancer Statistics 2018: GLOBOCAN Estimates of Incidence and Mortality Worldwide for 36 Cancers in 185 Countries. *CA: Cancer J Clin* (2018) 68 (6):394–424. doi: 10.3322/caac.21492
4. Bossi P, Vullo SL, Guzzo M, Mariani L, Granata R, Orlandi E, et al. Preoperative Chemotherapy in Advanced Resectable OCSCC: Long-Term Results of a Randomized Phase III Trial. *Ann Oncol* (2014) 25(2):462–6. doi: 10.1093/annonc/mdt555
5. Zhong L-P, Zhang C-P, Ren G-X, Guo W, William WNJr., Sun J, et al. Randomized Phase III Trial of Induction Chemotherapy With Docetaxel, Cisplatin, and Fluorouracil Followed by Surgery Versus Up-Front Surgery in Locally Advanced Resectable Oral Squamous Cell Carcinoma. *J Clin Oncol* (2013) 31(6):744. doi: 10.1200/JCO.2012.43.8820
6. Sadighi S, Keyhani A, Harirchi I, Garajei A, Aghili M, Kazemian A, et al. Neoadjuvant Chemotherapy for Locally Advanced Squamous Carcinoma of Oral Cavity: A Pilot Study. *Acta Med Iranica* (2015) 53(6):380–6.
7. Valdez JA, Brennan MT. Impact of Oral Cancer on Quality of Life. *Dental Clinics* (2018) 62(1):143–54. doi: 10.1016/j.cden.2017.09.001
8. Ouyang L, Shi Z, Zhao S, Wang FT, Zhou TT, Liu B, et al. Programmed Cell Death Pathways in Cancer: A Review of Apoptosis, Autophagy and Programmed Necrosis. *Cell proliferation* (2012) 45(6):487–98. doi: 10.1111/j.1365-2184.2012.00845.x
9. Kerr JF, Wyllie AH, Currie AR. Apoptosis: A Basic Biological Phenomenon With Wideranging Implications in Tissue Kinetics. *Br J Cancer* (1972) 26 (4):239–57. doi: 10.1038/bjc.1972.33

10. Cohen GM, Sun X-M, Fearnhead H, MacFarlane M, Brown DG, Snowden RT, et al. Formation of Large Molecular Weight Fragments of DNA Is a Key Committed Step of Apoptosis in Thymocytes. *J Immunol* (1994) 153 (2):507–16.
11. Martin SJ, Green DR. Protease Activation During Apoptosis: Death by a Thousand Cuts? *Cell* (1995) 82(3):349–52. doi: 10.1016/0092-8674(95)90422-0
12. Galluzzi L, Green DR. Autophagy-Independent Functions of the Autophagy Machinery. *Cell* (2019) 177(7):1682–99. doi: 10.1016/j.cell.2019.05.026
13. He C, Klionsky DJ. Regulation Mechanisms and Signaling Pathways of Autophagy. *Annu Rev Genet* (2009) 43:67–93. doi: 10.1146/annurev-genet-102808-114910
14. Yun CW, Lee SH. The Roles of Autophagy in Cancer. *Int J Mol Sci* (2018) 19 (11):3466. doi: 10.3390/ijms19113466
15. Galluzzi L, Kepp O, Krautwald S, Kroemer G, Linkermann A. Molecular Mechanisms of Regulated Necrosis. *Semin Cell Dev Biol* (2014) 35:24–32. doi: 10.1016/j.semcdb.2014.02.006
16. Iyer MK, Niknafs YS, Malik R, Singhal U, Sahu A, Hosono Y, et al. The Landscape of Long Noncoding RNAs in the Human Transcriptome. *Nat Genet* (2015) 47(3):199–208. doi: 10.1038/ng.3192
17. Djebali S, Davis CA, Merkel A, Dobin A, Lassmann T, Mortazavi A, et al. Landscape of Transcription in Human Cells. *Nature* (2012) 489(7414):101–8. doi: 10.1038/nature11233
18. Nahand JS, Karimzadeh MR, Nezamnia M, Fatemipour M, Khatami A, Jamshidi S, et al. The Role of miR-146a in Viral Infection. *IUBMB Life* (2020) 72(3):343–60. doi: 10.1002/iub.2222
19. Letafati A, Najafi S, Mottahedi M, Karimzadeh M, Shahini A, Garousi S, et al. MicroRNA Let-7 and Viral Infections: Focus on Mechanisms of Action. *Cell Mol Biol Letters* (2022) 27(1):1–47. doi: 10.1186/s11658-022-00317-9
20. Tamtaji OR, Derakhshan M, Rashidi Noshabad FZ, Razaviyan J, Hadavi R, Jafarpour H, et al. Non-Coding RNAs and Brain Tumors: Insights Into Their Roles in Apoptosis. *Front Cell Dev Biol* (2021) 9:792185. doi: 10.3389/fcell.2021.792185
21. Mousavi SM, Derakhshan M, Baharloii F, Dashti F, Mirazimi SMA, Mahjoubin-Tehran M, et al. Non-Coding RNAs and Glioblastoma: Insight Into Their Roles in Metastasis. *Mol Ther Oncolytics* (2022) 24:262–87. doi: 10.1016/j.omto.2021.12.015
22. Dashti F, Mirazimi SMA, Rabiei N, Fathazam R, Rabiei N, Piroozmand H, et al. The Role of Non-Coding RNAs in Chemotherapy for Gastrointestinal Cancers. *Mol Ther Nucleic Acids* (2021) 26:892–926. doi: 10.1016/j.omtn.2021.10.004
23. Balandeh E, Mohammadshafie K, Mahmoudi Y, Hossein Pourhanifeh M, Rajabi A, Bahabadi ZR, et al. Roles of Non-Coding RNAs and Angiogenesis in Glioblastoma. *Front Cell Dev Biol* (2021) 9:716462. doi: 10.3389/fcell.2021.716462
24. Razavi ZS, Asgarpour K, Mahjoubin-Tehran M, Rasouli S, Khan H, Shahrzad MK, et al. Angiogenesis-Related Non-Coding RNAs and Gastrointestinal Cancer. *Mol Ther Oncolytics* (2021) 21:220–41. doi: 10.1016/j.omto.2021.04.002
25. Mahjoubin-Tehran M, Rezaei S, Jesmani A, Birang N, Morshedi K, Khanbabaei H, et al. New Epigenetic Players in Stroke Pathogenesis: From Non-Coding RNAs to Exosomal Non-Coding RNAs. *BioMed Pharmacother* (2021) 140:111753. doi: 10.1016/j.biopha.2021.111753
26. Geisler S, Coller J. RNA in Unexpected Places: Long Non-Coding RNA Functions in Diverse Cellular Contexts. *Nat Rev Mol Cell Biol* (2013) 14 (11):699–712. doi: 10.1038/nrm3679
27. Mirzaei H, Hamblin MR. Regulation of Glycolysis by Non-Coding RNAs in Cancer: Switching on the Warburg Effect. *Mol Therapy-Oncolytics* (2020) 19:218–39. doi: 10.1016/j.omto.2020.10.003
28. Hashemipour M, Boroumand H, Mollazadeh S, Tajiknia V, Nourollahzadeh Z, Borj MR, et al. Exosomal microRNAs and Exosomal Long Non-Coding RNAs in Gynecologic Cancers. *Gynecologic Oncol* (2021) 161(1):314–27. doi: 10.1016/j.ygyno.2021.02.004
29. Rahimian N, Razavi ZS, Aslanbeigi F, Mirkhabbaz AM, Piroozmand H, Shahrzad MK, et al. Non-Coding RNAs Related to Angiogenesis in Gynecological Cancer. *Gynecol Oncol* (2021) 161(3):896–912. doi: 10.1016/j.ygyno.2021.03.020
30. Saadat S, Noureddini M, Mahjoubin-Tehran M, Nazemi S, Shojaie L, Aschner M, et al. Pivotal Role of TGF-β/Smad Signaling in Cardiac Fibrosis: Non-Coding RNAs as Effectual Players. *Front Cardiovasc Med* (2020) 7:588347. doi: 10.3389/fcvm.2020.588347
31. Razavi ZS, Tajiknia V, Majidi S, Ghandali M, Mirzaei HR, Rahimian N, et al. Gynecologic Cancers and Non-Coding RNAs: Epigenetic Regulators With Emerging Roles. *Crit Rev Oncol Hematol* (2021) 157:103192. doi: 10.1016/j.critrevonc.2020.103192
32. Yousefi F, Shabaninejad Z, Vakili S, Derakhshan M, Movahedpour A, Dabiri H, et al. TGF-β and WNT Signaling Pathways in Cardiac Fibrosis: Non-Coding RNAs Come Into Focus. *Cell Commun Signal* (2020) 18(1):87. doi: 10.1186/s12964-020-00555-4
33. Hashemian SM, Pourhanifeh MH, Fadaei S, Velayati AA, Mirzaei H, Hamblin MR. Non-Coding RNAs and Exosomes: Their Role in the Pathogenesis of Sepsis. *Mol Ther Nucleic Acids* (2020) 21:51–74. doi: 10.1016/j.omtn.2020.05.012
34. Saadat S, Noureddini M, Mahjoubin-Tehran M, Nazemi S, Shojaie L, Aschner M, et al. Pivotal Role of TGF-β/Smad Signaling in Cardiac Fibrosis: Non-Coding RNAs as Effectual Players. *Front Cardiovasc Med* (2021) 7:256. doi: 10.3389/fcvm.2020.588347
35. Nahand JS, Rabiei N, Fathazam R, Taghizadieh M, Ebrahimi MS, Mahjoubin-Tehran M, et al. Oncogenic Viruses and Chemoresistance: What do We Know? *Pharmacol Res* (2021) 170:105730. doi: 10.1016/j.phrs.2021.105730
36. Irimie AI, Braicu C, Sonea L, Zimta AA, Cojocneanu-Petric R, Tonchev K, et al. A Looking-Glass of non-Coding RNAs in Oral Cancer. *Int J Mol Sci* (2017) 18(12):2620. doi: 10.3390/ijms18122620
37. Gomes CC, de Sousa SF, Calin GA, Gomez RS. The Emerging Role of Long Noncoding RNAs in Oral Cancer. *Oral Surg Oral Med Oral Pathol Oral Radiol.* (2017) 123(2):235–41. doi: 10.1016/j.oooo.2016.10.006
38. Zhang Z, Zhang J, Diao L, Han LJO. Small non-Coding RNAs in Human Cancer: Function. *Clin Utility Characterization* (2021) 40(9):1570–7.
39. Natsidis P, Schiffer PH, Salvador-Martínez I, Telford MJ. Computational Discovery of Hidden Breaks in 28S Ribosomal RNAs Across Eukaryotes and Consequences for RNA Integrity Numbers. *Scientific Reps* (2019) 9(1):1–10. doi: 10.1038/s41598-019-55573-1
40. Dahariya S, Paddibhatla I, Kumar S, Raghuwanshi S, Pallepati A, Gutti RK. Long NNon-Coding RNA: Classification, Biogenesis and Functions in Blood Cells. *Mol Immunol* (2019) 112:82–92. doi: 10.1016/j.molimm.2019.04.011
41. Gozuacik D, Akkoc Y, Ozturk DG, Kocak MJ. Autophagy-Regulating microRNAs and Cancer. *Front Oncol* (2017) 7:65. doi: 10.3389/fonc.2017.00065
42. Usman S, Jamal A, Teh M-T, Waseem A. Major Molecular Signalling Pathways in Oral Cancer Associated With Therapeutic Resistance. *Front Oral Health* (2020) 1:15.
43. Rivera C. Essentials of Oral Cancer. *Int J Clin Exp Pathology* (2015) 8 (9):11884.
44. Scully C, Porter S. Oral Cancer. *Western J Med* (2001) 174(5):348. doi: 10.1136/ewjm.174.5.348
45. van der Waal I, Scully C. Oral Cancer: Comprehending the Condition, Causes, Controversies, Control and Consequences. 4. Potentially Malignant Disorders of the Oral and Oropharyngeal Mucosa. *Dental Update* (2011) 38 (2):138–40.
46. Gupta N, Gupta R, Acharya A, Patthi B, Goud V, Reddy S, et al. Changing Trends in Oral Cancer–a Global Scenario. *Nepal J Epidemiol* (2016) 6 (4):613–9.
47. Jemal A, Bray F, Center MM, Ferlay J, Ward E, Forman D. Global Cancer Statistics. *CA: Cancer J Clin* (2011) 61(2):69–90. doi: 10.3322/caac.20107
48. Jadhav KB, Gupta N. Clinicopathological Prognostic Implicators of Oral Squamous Cell Carcinoma: Need to Understand and Revise. *North Am J Med Sci* (2013) 5(12):671. doi: 10.4103/1947-2714.123239
49. Hernandez BY, Zhu X, Goodman MT, Gatewood R, Mendiola P, Quinata K, et al. Betel Nut Chewing, Oral Premalignant Lesions, and the Oral Microbiome. *PLoS One* (2017) 12(2):e0172196. doi: 10.1371/journal.pone.0172196
50. Irfan M, Delgado RZR, Frias-Lopez J. The Oral Microbiome and Cancer. *Front Immunol* (2020) 11:591088. doi: 10.3389/fimmu.2020.591088

51. Kilian M, Chapple I, Hannig M, Marsh P, Meuric V, Pedersen A, et al. The Oral Microbiome–an Update for Oral Healthcare Professionals. *British Dental J* (2016) 221(10):657–66. doi: 10.1038/sj.bdj.2016.865
52. Kitamoto S, Nagao-Kitamoto H, Jiao Y, Gillilland MGIII, Hayashi A, Imai J, et al. The Intermucosal Connection Between the Mouth and Gut in Commensal Pathobiont-Driven Colitis. *Cell* (2020) 182(2):447–62. e14. doi: 10.1016/j.cell.2020.05.048
53. Kitamoto S, Nagao-Kitamoto H, Hein R, Schmidt T, Kamada N. The Bacterial Connection Between the Oral Cavity and the Gut Diseases. *J Dent Res* (2020) 99(9):1021–9. doi: 10.1177/0022034520924633
54. Zanoni DK, Patel SG, Shah JP. Changes in the 8th Edition of the American Joint Committee on Cancer (AJCC) Staging of Head and Neck Cancer: Rationale and Implications. *Curr Oncol Rep* (2019) 21(6):52. doi: 10.1007/s11912-019-0799-x
55. Müller S. Update From the 4th Edition of the World Health Organization of Head and Neck Tumours: Tumours of the Oral Cavity and Mobile Tongue. *Head Neck Pathol* (2017) 11(1):33–40. doi: 10.1007/s12105-017-0792-3
56. Sarradin V, Siegfried A, Uro-Coste E, Delord J-P. WHO Classification of Head and Neck Tumours 2017: Main Novelties and Update of Diagnostic Methods. *Bull du Cancer* (2018) 105(6):596–602. doi: 10.1016/j.bulcan.2018.04.004
57. Kennedy R. WHO Is in and WHO Is Out of the Mouth, Salivary Glands, and Jaws Sections of the 4th Edition of the WHO Classification of Head and Neck Tumours. *Br J Oral Maxillofac Surgery* (2018) 56(2):90–5. doi: 10.1016/j.bjoms.2017.12.009
58. Turner L, Mupparapu M, Akintoye SO. Review of the Complications Associated With Treatment of Oropharyngeal Cancer: A Guide to the Dental Practitioner. *Quintessence Int (Berlin Germany: 1985).* (2013) 44 (3):267.
59. Day TA, Davis BK, Gillespie MB, Joe JK, Kibbey M, Martin-Harris B, et al. Oral Cancer Treatment. *Curr Treat Options Oncol* (2003) 4(1):27. doi: 10.1007/s11864-003-0029-4
60. Ketabat F, Pundir M, Mohabatpour F, Lobanova L, Koutsopoulos S, Hadjiiski L, et al. Controlled Drug Delivery Systems for Oral Cancer Treatment—Current Status and Future Perspectives. *Pharmaceutics* (2019) 11(7):302.
61. Amelio I, Melino G, Knight RA. Cell Death Pathology: Cross-Talk With Autophagy and Its Clinical Implications. *Biochem Biophys Res Commun* (2011) 414(2):277–81. doi: 10.1016/j.bbrc.2011.09.080
62. Nahand JS, Shojaie L, Akhlagh SA, Ebrahimi MS, Mirzaei HR, Baghi HB, et al. Cell Death Pathways and Viruses: Role of microRNAs. *Mol Therapy-Nucleic Acids* (2021) 24:487–511. doi: 10.1016/j.omtn.2021.03.011
63. Eum K-H, Lee M. Crosstalk Between Autophagy and Apoptosis in the Regulation of Paclitaxel-Induced Cell Death in V-Ha-Ras-Transformed Fibroblasts. *Mol Cell Biochem* (2011) 348(1):61–8. doi: 10.1007/s11010-010-0638-8
64. Ghobrial IM, Witzig TE, Adjei AA. Targeting Apoptosis Pathways in Cancer Therapy. *CA: Cancer J Clin* (2005) 55(3):178–94. doi: 10.3322/canjclin.55.3.178
65. Mathew R, Karantza-Wadsworth V, White E. Role of Autophagy in Cancer. *Nat Rev Cancer* (2007) 7(12):961–7. doi: 10.1038/nrc2254
66. Choi KS. Autophagy and Cancer. *Exp Mol Med* (2012) 44(2):109–20. doi: 10.3858/emm.2012.44.2.033
67. Kundu M, Thompson CB. Autophagy: Basic Principles and Relevance to Disease. *Annu Rev Pathol Mech Dis* (2008) 3:427–55. doi: 10.1146/annurev.pathmechdis.2.010506.091842
68. Mohammadi AH, Seyedmoalemi S, Moghanlou M, Akhlagh SA, Talaei Zavareh SA, Hamblin MR, et al. MicroRNAs and Synaptic Plasticity: From Their Molecular Roles to Response to Therapy. *Mol Neurobiol* (2022). doi: 10.1007/s12035-022-02907-2
69. Mousavi SM, Amin Mahdian SM, Ebrahimi MS, Taghizadieh M, Vosough M, Sadri Nahand J, et al. Microfluidics for Detection of Exosomes and microRNAs in Cancer: State of the Art. *Mol Ther Nucleic Acids* (2022) 28:758–91. doi: 10.1016/j.omtn.2022.04.011
70. Ahmadpour S, Taghavi T, Sheida A, Tamehri Zadeh SS, Hamblin MR, Mirzaei H. Effects of microRNAs and Long Non-Coding RNAs on Chemotherapy Response in Glioma. *Epigenomics.* (2022) 14(9):549–63. doi: 10.2217/epi-2021-0439
71. Jafarzadeh A, Paknahad MH, Nemati M, Jafarzadeh S, Mahjoubin-Tehran M, Rajabi A, et al. Dysregulated Expression and Functions of microRNA-330 in Cancers: A Potential Therapeutic Target. *BioMed Pharmacother* (2022) 146:112600. doi: 10.1016/j.biopha.2021.112600
72. Dorraki N, Ghale-Noie ZN, Ahmadi NS, Keyvani V, Bahadori RA, Nejad AS, et al. miRNA-148b and Its Role in Various Cancers. *Epigenomics* (2021) 13 (24):1939–60. doi: 10.2217/epi-2021-0155
73. Jafarzadeh A, Naseri A, Shojaie L, Nemati M, Jafarzadeh S, Bannazadeh Baghi H, et al. MicroRNA-155 and Antiviral Immune Responses. *Int Immunopharmacol* (2021) 101(Pt A):108188. doi: 10.1016/j.intimp.2021.108188
74. Nahand JS, Mahjoubin-Tehran M, Moghoofei M, Pourhanifeh MH, Mirzaei HR, Asemi Z, et al. Exosomal miRNAs: Novel Players in Viral Infection. *Epigenomics* (2020) 12(4):353–70. doi: 10.2217/epi-2019-0192
75. Amiri A, Mahjoubin-Tehran M, Asemi Z, Shafiee A, Hajighadimi S, Moradizarmehri S, et al. Role of Resveratrol in Modulating microRNAs in Human Diseases: From Cancer to Inflammatory Disorder. *Curr Med Chem* (2021) 28(2):360–76.
76. Pourhanifeh MH, Mahjoubin-Tehran M, Shafiee A, Hajighadimi S, Moradizarmehri S, Mirzaei H, et al. MicroRNAs and Exosomes: Small Molecules With Big Actions in Multiple Myeloma Pathogenesis. *IUBMB Life* (2020) 72(3):314–33. doi: 10.1002/iub.2211
77. Aghdam AM, Amiri A, Salarinia R, Masoudifar A, Ghasemi F, Mirzaei H. MicroRNAs as Diagnostic, Prognostic, and Therapeutic Biomarkers in Prostate Cancer. *Crit Rev Eukaryot Gene Expr* (2019) 29(2):127–39. doi: 10.1615/CritRevEukaryotGeneExpr.2019025273
78. Masoudi MS, Mehrabian E, Mirzaei H. MiR-21: A Key Player in Glioblastoma Pathogenesis. *J Cell Biochem* (2018) 119(2):1285–90. doi: 10.1002/jcb.26300
79. Mirzaei H. Stroke in Women: Risk Factors and Clinical Biomarkers. *J Cell Biochem* (2017) 118(12):4191–202. doi: 10.1002/jcb.26130
80. Keshavarzi M, Sorayayi S, Jafar Rezaei M, Mohammadi M, Ghaderi A, Rostamzadeh A, et al. MicroRNAs-Based Imaging Techniques in Cancer Diagnosis and Therapy. *J Cell Biochem* (2017) 118(12):4121–8. doi: 10.1002/jcb.26012
81. Gholamin S, Mirzaei H, Razavi SM, Hassanian SM, Saadatpour L, Masoudifar A, et al. GD2-Targeted Immunotherapy and Potential Value of Circulating microRNAs in Neuroblastoma. *J Cell Physiol* (2018) 233 (2):866–79. doi: 10.1002/jcp.25793
82. Mirzaei H, Fathullahzadeh S, Khanmohammadi R, Darijani M, Momeni F, Masoudifar A, et al. State of the Art in microRNA as Diagnostic and Therapeutic Biomarkers in Chronic Lymphocytic Leukemia. *J Cell Physiol* (2018) 233(2):888–900. doi: 10.1002/jcp.25799
83. Saadatpour L, Fadaee E, Fadaei S, Nassiri Mansour R, Mohammadi M, Mousavi SM, et al. Glioblastoma: Exosome and microRNA as Novel Diagnosis Biomarkers. *Cancer Gene Ther* (2016) 23(12):415–8. doi: 10.1038/cgt.2016.48
84. Yan B, Gu W, Yang Z, Gu Z, Yue X, Gu Q, et al. Downregulation of a Long Noncoding RNA-Ncrupar Contributes to Tumor Inhibition in Colorectal Cancer. *Tumor Biol* (2014) 35(11):11329–35. doi: 10.1007/s13277-014-2465-0
85. Bohnsack MT, Czaplinski K, GÖRLICH D. Exportin 5 Is a RanGTP-Dependent dsRNA-Binding Protein That Mediates Nuclear Export of pre-miRNAs. *Rna.* (2004) 10(2):185–91. doi: 10.1261/rna.5167604
86. Yi R, Qin Y, Macara IG, Cullen BR. Exportin-5 Mediates the Nuclear Export of pre-microRNAs and Short Hairpin RNAs. *Genes Dev* (2003) 17(24):3011–6. doi: 10.1101/gad.1158803
87. Yang J-S, Phillips MD, Betel D, Mu P, Ventura A, Siepel AC, et al. Widespread Regulatory Activity of Vertebrate microRNA* Species. *RNA* (2011) 17(2):312–26. doi: 10.1261/rna.2537911
88. Yamada Y, Koshizuka K, Hanazawa T, Kikkawa N, Okato A, Idichi T, et al. Passenger Strand of miR-145-3p Acts as a Tumor-Suppressor by Targeting MYO1B in Head and Neck Squamous Cell Carcinoma. *Int J Oncol* (2018) 52 (1):166–78.
89. Lee HY, Zhou K, Smith AM, Noland CL, Doudna JA. Differential Roles of Human Dicer-Binding Proteins TRBP and PACT in Small RNA Processing. *Nucleic Acids Res* (2013) 41(13):6568–76. doi: 10.1093/nar/gkt361

90. Neilsen CT, Goodall GJ, Bracken CP. IsomiRs–The Overlooked Repertoire in the Dynamic Micrornaome. *Trends Genet* (2012) 28(11):544–9. doi: 10.1016/j.tig.2012.07.005
91. Ohanian M, Humphreys DT, Anderson E, Preiss T, Fatkin D. A Heterozygous Variant in the Human Cardiac miR-133 Gene, MIR133A2, Alters miRNA Duplex Processing and Strand Abundance. *BMC Genet* (2013) 14(1):1–10. doi: 10.1186/1471-2156-14-18
92. Meijer HA, Smith EM, Bushell M. Regulation of miRNA Strand Selection: Follow the Leader? *Biochem Soc Trans* (2014) 42(4):1135–40. doi: 10.1042/BST20140142
93. Filipowicz W, Bhattacharyya SN, Sonenberg N. Mechanisms of Post-Transcriptional Regulation by microRNAs: Are the Answers in Sight? *Nat Rev Genet* (2008) 9(2):102–14. doi: 10.1038/nrg2290
94. Shirjang S, Mansoori B, Asghari S, Duijf PH, Mohammadi A, Gjerstorff M, et al. MicroRNAs in Cancer Cell Death Pathways: Apoptosis and Necroptosis. *Free Radical Biol Med* (2019) 139:1–15. doi: 10.1016/j.freeradbiomed.2019.05.017
95. Fathullahzadeh S, Mirzaei H, Honardoost MA, Sahebkar A, Salehi M. Circulating microRNA-192 as a Diagnostic Biomarker in Human Chronic Lymphocytic Leukemia. *Cancer Gene Ther* (2016) 23(10):327–32. doi: 10.1038/cgt.2016.34
96. Salarinia R, Sahebkar A, Peyvandi M, Mirzaei HR, Jaafari MR, Riahi MM, et al. Epi-Drugs and Epi-miRs: Moving Beyond Current Cancer Therapies. *Curr Cancer Drug Targets*. (2016) 16(9):773–88. doi: 10.2174/1568009616666151207110143
97. Mohammadi M, Goodarzi M, Jaafari MR, Mirzaei HR, Mirzaei H. Circulating microRNA: A New Candidate for Diagnostic Biomarker in Neuroblastoma. *Cancer Gene Ther* (2016) 23(11):371–2. doi: 10.1038/cgt.2016.45
98. Mirzaei H, Khataminfar S, Mohammadparast S, Sales SS, Maftouh M, Mohammadi M, et al. Circulating microRNAs as Potential Diagnostic Biomarkers and Therapeutic Targets in Gastric Cancer: Current Status and Future Perspectives. *Curr Med Chem* (2016) 23(36):4135–50. doi: 10.2174/0929867323666160818093854
99. Davoodvandi A, Marzban H, Goleij P, Sahebkar A, Morshedi K, Rezaei S, et al. Effects of Therapeutic Probiotics on Modulation of microRNAs. *Cell Commun Signal* (2021) 19(1):4. doi: 10.1186/s12964-020-00668-w
100. Ashrafizadeh M, Zarrabi A, Hashemipour M, Vosough M, Najafi M, Shahinozzaman M, et al. Sensing the Scent of Death: Modulation of microRNAs by Curcumin in Gastrointestinal Cancers. *Pharmacol Res* (2020) 160:105199. doi: 10.1016/j.phrs.2020.105199
101. Pourhanifeh MH, Vosough M, Mahjoubin-Tehran M, Hashemipour M, Nejati M, Abbasi-Kolli M, et al. Autophagy-Related microRNAs: Possible Regulatory Roles and Therapeutic Potential in and Gastrointestinal Cancers. *Pharmacol Res* (2020) 161:105133. doi: 10.1016/j.phrs.2020.105133
102. Rezaei S, Mahjoubin-Tehran M, Aghaee-Bakhtiari SH, Jalili A, Movahedpour A, Khan H, et al. Autophagy-Related MicroRNAs in Chronic Lung Diseases and Lung Cancer. *Crit Rev Oncol Hematol* (2020) 153:103063. doi: 10.1016/j.critrevonc.2020.103063
103. Li C, Hashimi SM, Good DA, Cao S, Duan W, Plummer PN, et al. Apoptosis and Micro RNA Aberrations in Cancer. *Clin Exp Pharmacol Physiol* (2012) 39(8):739–46. doi: 10.1111/j.1440-1681.2012.05700.x
104. Su Z, Yang Z, Xu Y, Chen Y, Yu Q. MicroRNAs in Apoptosis, Autophagy and Necroptosis. *Oncotarget*. (2015) 6(11):8474. doi: 10.18632/oncotarget.3523
105. Yousefpouran S, Mostafaei S, Manesh PV, Iranifar E, Bokharaei-Salim F, Nahand JS, et al. The Assessment of Selected MiRNAs Profile in HIV, HBV, HCV, HIV/HCV, HIV/HBV Co-Infection and Elite Controllers for Determination of Biomarker. *Microb Pathog* (2020) 147:104355. doi: 10.1016/j.micpath.2020.104355
106. Donyavi T, Bokharaei-Salim F, Baghi HB, Khanaliha K, Janat-Makan MA, Karimi B, et al. Acute and Post-Acute Phase of COVID-19: Analyzing Expression Patterns of miRNA-29a-3p, 146a-3p, 155-5p, and Let-7b-3p in PBMC. *Int Immunopharmacol* (2021) 97:107641. doi: 10.1016/j.intimp.2021.107641
107. Visalli M, Bartolotta M, Polito F, Oteri R, Barbera A, Arrigo R, et al. miRNA Expression Profiling Regulates Necroptotic Cell Death in Hepatocellular Carcinoma. *Int J Oncol* (2018) 53(2):771–80. doi: 10.3892/ijo.2018.4410
108. Bader AG, Brown D, Winkler M. The Promise of microRNA Replacement Therapy. *Cancer Res* (2010) 70(18):7027–30. doi: 10.1158/0008-5472.CAN-10-2010
109. Ono K. Functions of microRNA-33a/B and microRNA Therapeutics. *J Cardiol* (2016) 67(1):28–33. doi: 10.1016/j.jjcc.2015.10.017
110. Lu J, Getz G, Miska EA, Alvarez-Saavedra E, Lamb J, Peck D, et al. MicroRNA Expression Profiles Classify Human Cancers. *Nature* (2005) 435(7043):834–8. doi: 10.1038/nature03702
111. Kumar MS, Lu J, Mercer KL, Golub TR, Jacks T. Impaired microRNA Processing Enhances Cellular Transformation and Tumorigenesis. *Nat Genet* (2007) 39(5):673–7. doi: 10.1038/ng2003
112. Esquela-Kerscher A, Slack FJ. Oncomirs—microRNAs With a Role in Cancer. *Nat Rev Cancer* (2006) 6(4):259–69. doi: 10.1038/nrc1840
113. Hayden EC. Cancer Complexity Slows Quest for Cure. *Nature* (2008) 455 (7210):148.
114. Yaacoub K, Pedeux R, Tarte K, Guillaudeux T. Role of the Tumor Microenvironment in Regulating Apoptosis and Cancer Progression. *Cancer letters* (2016) 378(2):150–9. doi: 10.1016/j.canlet.2016.05.012
115. Reed JC. Mechanisms of Apoptosis. *Am J pathology* (2000) 157(5):1415–30. doi: 10.1016/S0002-9440(10)64779-7
116. Chen Q, Gong B, Almasan A. Distinct Stages of Cytochrome C Release From Mitochondria: Evidence for a Feedback Amplification Loop Linking Caspase Activation to Mitochondrial Dysfunction in Genotoxic Stress Induced Apoptosis. *Cell Death Differentiation* (2000) 7(2):227–33. doi: 10.1038/sj.cdd.4400629
117. Ow Y-LP, Green DR, Hao Z, Mak TW. Cytochrome C: Functions Beyond Respiration. *Nat Rev Mol Cell Biol* (2008) 9(7):532–42. doi: 10.1038/nrm2434
118. Boulares AH, Zoltoski AJ, Yakovlev A, Xu M, Smulson ME. Roles of DNA Fragmentation Factor and Poly (ADP-Ribose) Polymerase in an Amplification Phase of Tumor Necrosis Factor-Induced Apoptosis. *J Biol Chem* (2001) 276(41):38185–92. doi: 10.1074/jbc.M100629200
119. Cui Z, Bao X, Liu Q, Li Q, Huang L, Wang H, et al. MicroRNA-378-3p/5p Represses Proliferation and Induces Apoptosis of Oral Squamous Carcinoma Cells *via* Targeting KLK4. *Clin Exp Pharmacol Physiol* (2020) 47(4):713–24. doi: 10.1111/1440-1681.13235
120. Pardini B, De Maria D, Francavilla A, Di Gaetano C, Ronco G, Naccarati A. MicroRNAs as Markers of Progression in Cervical Cancer: A Systematic Review. *BMC Cancer* (2018) 18(1):1–17. doi: 10.1186/s12885-018-4590-4
121. Wang Z, Yao W, Li K, Zheng N, Zheng C, Zhao X, et al. Reduction of miR-21 Induces SK-N-SH Cell Apoptosis and Inhibits Proliferation *via* PTEN/Pdcd4. *Oncol Letters* (2017) 13(6):4727–33. doi: 10.3892/ol.2017.6052
122. Hao Y, Huang J, Ma Y, Chen W, Fan Q, Sun X, et al. Asiatic Acid Inhibits Proliferation, Migration and Induces Apoptosis by Regulating Pdcd4 *via* the PI3K/Akt/mTOR/p70S6K Signaling Pathway in Human Colon Carcinoma Cells. *Oncol letters* (2018) 15(6):8223–30. doi: 10.3892/ol.2018.8417
123. Syed DN, Afaq F, Sarfaraz S, Khan N, Kedlaya R, Setaluri V, et al. Delphinidin Inhibits Cell Proliferation and Invasion *via* Modulation of Met Receptor Phosphorylation. *Toxicol Appl Pharmacol* (2008) 231(1):52–60. doi: 10.1016/j.taap.2008.03.023
124. Liu C, Tong Z, Tan J, Xin Z, Wang Z, Tian L. MicroRNA−21−5p Targeting PDCD4 Suppresses Apoptosis *via* Regulating the PI3K/AKT/FOXO1 Signaling Pathway in Tongue Squamous Cell Carcinoma. *Exp Ther Med* (2019) 18(5):3543–51.
125. Manasa V, Kannan SJTB. Impact of microRNA Dynamics on Cancer Hallmarks: An Oral Cancer Scenario. *Tumour Biol* (2017) 39 (3):1010428317695920. doi: 10.1177/1010428317695920
126. Li J, Huang H, Sun L, Yang M, Pan C, Chen W, et al. MiR-21 Indicates Poor Prognosis in Tongue Squamous Cell Carcinomas as an Apoptosis Inhibitor. *Clin Cancer Res* (2009) 15(12):3998–4008. doi: 10.1158/1078-0432.CCR-08-3053
127. Zhang X, Ng W-L, Wang P, Tian L, Werner E, Wang H, et al. MicroRNA-21 Modulates the Levels of Reactive Oxygen Species by Targeting SOD3 and Tnfα. *Cancer Res* (2012) 72(18):4707–13. doi: 10.1158/0008-5472.CAN-12-0639
128. Liu X, Wang A, Heidbreder CE, Jiang L, Yu J, Kolokythas A, et al. MicroRNA-24 Targeting RNA-Binding Protein DND1 in Tongue Squamous Cell Carcinoma. *FEBS Lett* (2010) 584(18):4115–20. doi: 10.1016/j.febslet.2010.08.040

129. Liu CJ, Lin SC, Yang CC, Cheng HW, Chang KW. Exploiting Salivary miR-31 as a Clinical Biomarker of Oral Squamous Cell Carcinoma. *Head Neck* (2012) 34(2):219–24. doi: 10.1002/hed.21713
130. Wong T-S, Ho W-K, Chan JY-W, Ng RW-M, Wei WIJT. Mature miR-184 and Squamous Cell Carcinoma of the Tongue. *Scientific World J* (2009) 9:130–2. doi: 10.1100/tsw.2009.12
131. Yu J, Ryan DG, Getsios S, Oliveira-Fernandes M, Fatima A, Lavker RM. MicroRNA-184 Antagonizes microRNA-205 to Maintain SHIP2 Levels in Epithelia. *Proc Natl Acad Sci U S A* (2008) 105(49):19300–5. doi: 10.1073/pnas.0803992105
132. Dai R, Li J, Liu Y, Yan D, Chen S, Duan C, et al. miR-221/222 Suppression Protects Against Endoplasmic Reticulum Stress-Induced Apoptosis *via* p27Kip1-and MEK/ERK-Mediated Cell Cycle Regulation. *Biol Chem* (2010) 391(7):791–801. doi: 10.1515/bc.2010.072
133. Philipp-Staheli J, Payne SR, Kemp CJ. p27Kip1: Regulation and Function of a Haploinsufficient Tumor Suppressor and Its Misregulation in Cancer. *Exp Cell Res* (2001) 264(1):148–68. doi: 10.1006/excr.2000.5143
134. Kudo Y, Kitajima S, Ogawa I, Kitagawa M, Miyauchi M, Takata T. Small Interfering RNA Targeting of S Phase Kinase–Interacting Protein 2 Inhibits Cell Growth of Oral Cancer Cells by Inhibiting P27 Degradation. *Mol Cancer Ther* (2005) 4(3):471–6. doi: 10.1158/1535-7163.MCT-04-0232
135. Fu S, Chen H, Cheng P, Zhang C, Wu Y. MiR-155 Regulates Oral Squamous Cell Carcinoma Tca8113 Cell Proliferation, Cycle, and Apoptosis *via* Regulating p27Kip1. *Eur Rev Med Pharmacol Sci* (2017) 21(5):937–44.
136. Tsai H-L, Pang S-Y, Wang H-C, Luo C-W, Li Q-L, Chen T-Y, et al. Impact of BMI1 Expression on the Apoptotic Effect of Paclitaxel in Colorectal Cancer. *Am J Cancer Res* (2019) 9(11):2544.
137. Haupt Y, Bath M, Harris A, Adams J. Bmi-1 Transgene Induces Lymphomas and Collaborates With Myc in Tumorigenesis. *Oncogene* (1993) 8(11):3161–4.
138. Venkataraman S, Alimova I, Fan R, Harris P, Foreman N, Vibhakar R. MicroRNA 128a Increases Intracellular ROS Level by Targeting Bmi-1 and Inhibits Medulloblastoma Cancer Cell Growth by Promoting Senescence. *PLoS One* (2010) 5(6):e10748. doi: 10.1371/journal.pone.0010748
139. He X, Dong Y, Wu CW, Zhao Z, Ng SS, Chan FK, et al. MicroRNA-218 Inhibits Cell Cycle Progression and Promotes Apoptosis in Colon Cancer by Downregulating BMI1 Polycomb Ring Finger Oncogene. *Mol Med* (2012) 18 (12):1491–8. doi: 10.2119/molmed.2012.00304
140. Kim JS, Choi DW, Kim CS, Yu SK, Kim HJ, Go DS, et al. MicroRNA-203 Induces Apoptosis by Targeting Bmi-1 in YD-38 Oral Cancer Cells. *Anticancer Res* (2018) 38(6):3477–85. doi: 10.21873/anticanres.12618
141. Jang CW, Chen CH, Chen CC, Chen JY, Su YH, Chen RH. TGF-Beta Induces Apoptosis Through Smad-Mediated Expression of DAP-Kinase. *Nat Cell Biol* (2002) 4(1):51–8. doi: 10.1038/ncb731
142. Huang C, Song H, Lai L. The Role and Mechanism of microRNA−18a−5p in Oral Squamous Cell Carcinoma. *Mol Med Rep* (2019) 20(2):1637–44.
143. Song L, Lin C, Wu Z, Gong H, Zeng Y, Wu J, et al. miR-18a Impairs DNA Damage Response Through Downregulation of Ataxia Telangiectasia Mutated (ATM) Kinase. *PLoS One* (2011) 6(9):e25454. doi: 10.1371/journal.pone.0025454
144. Liu WH, Yeh SH, Lu CC, Yu SL, Chen HY, Lin CY, et al. MicroRNA-18a Prevents Estrogen Receptor-α Expression, Promoting Proliferation of Hepatocellular Carcinoma Cells. *Gastroenterology* (2009) 136(2):683–93. doi: 10.1053/j.gastro.2008.10.029
145. Liang C, Zhang X, Wang H-M, Liu X-M, Zhang X-J, Zheng B, et al. MicroRNA-18a-5p Functions as an Oncogene by Directly Targeting IRF2 in Lung Cancer. *Cell Death Dis* (2017) 8(5):e2764–e. doi: 10.1038/cddis.2017.145
146. Guo Y, Shi W, Fang R. Mir−18a−5p Promotes Melanoma Cell Proliferation and Inhibits Apoptosis and Autophagy by Targeting EPHA7 Signaling. *Mol Med Rep* (2021) 23(1):1–. doi: 10.3892/mmr.2020.11717
147. Gao S, Zhu D, Zhu J, Shen L, Zhu M, Ren X. miR-18a-5p Targets FBP1 to Promote Proliferation, Migration, and Invasion of Liver Cancer Cells and Inhibit Cell Apoptosis. *Comput Math Methods Med* (2021) 2021:3334065. doi: 10.1155/2021/3334065
148. Cantile M, Schiavo G, Terracciano L, Cillo C. Homeobox Genes in Normal and Abnormal Vasculogenesis. *Nutr Metab Cardiovasc dis* (2008) 18 (10):651–8. doi: 10.1016/j.numecd.2008.08.001
149. Waltregny D, Alami Y, Clausse N, Jd L, Castronovo V. Overexpression of the Homeobox Gene HOXC8 in Human Prostate Cancer Correlates With Loss of Tumor Differentiation. *Prostate* (2002) 50(3):162–9. doi: 10.1002/pros.10045
150. McGonigle GJ, Lappin T, Thompson A. Grappling With the HOX Network in Hematopoiesis and Leukemia. *Front Biosci* (2008) 13:4297–308. doi: 10.2741/3006
151. Maroulakou IG, Spyropoulos DD. The Study of HOX Gene Function in Hematopoietic, Breast and Lung Carcinogenesis. *Anticancer Res* (2003) 23 (3A):2101–10.
152. Maeda K, Hamada JI, Takahashi Y, Tada M, Yamamoto Y, Sugihara T, et al. Altered Expressions of HOX Genes in Human Cutaneous Malignant Melanoma. *Int J Cancer* (2005) 114(3):436–41. doi: 10.1002/ijc.20706
153. Hassan NMM, Hamada J-I, Murai T, Seino A, Takahashi Y, Tada M, et al. Aberrant Expression of HOX Genes in Oral Dysplasia and Squamous Cell Carcinoma Tissues. *Oncol Res Featuring Preclinical Clin Cancer Ther* (2006) 16(5):217–24. doi: 10.3727/000000006783981080
154. De Souza Setubal Destro MF, Bitu CC, Zecchin KG, Graner E, Lopes MA, Kowalski LP, et al. Overexpression of HOXB7 Homeobox Gene in Oral Cancer Induces Cellular Proliferation and Is Associated With Poor Prognosis. *Int J Oncol* (2010) 36(1):141–9.
155. Wu X, Chen H, Parker B, Rubin E, Zhu T, Lee J. HOXB7, a Homeodomain Protein, Is Overexpressed in Breast Cancer and Confers Epithelial-Mesenchymal Transition. *Cancer Res* (2006) 66:9527. doi: 10.1158/0008-5472.CAN-05-4470
156. Chen H, Lee JS, Liang X, Zhang H, Zhu T, Zhang Z, et al. Hoxb7 Inhibits Transgenic HER-2/Neu–Induced Mouse Mammary Tumor Onset But Promotes Progression and Lung Metastasis. *Cancer Res* (2008) 68 (10):3637–44. doi: 10.1158/0008-5472.CAN-07-2926
157. Wang K, Jin J, Ma T, Zhai H. MiR-376c-3p Regulates the Proliferation, Invasion, Migration, Cell Cycle and Apoptosis of Human Oral Squamous Cancer Cells by Suppressing HOXB7. *Biomed Pharmacother* (2017) 91:517–25. doi: 10.1016/j.biopha.2017.04.050
158. Naqvi AR, Shango J, Seal A, Shukla D, Nares S. Herpesviruses and microRNAs: New Pathogenesis Factors in Oral Infection and Disease? *Front Immunol* (2018) 9:2099. doi: 10.3389/fimmu.2018.02099
159. Naqvi AR. Immunomodulatory Roles of Human Herpesvirus-Encoded microRNA in Host-Virus Interaction. *Rev Med Virol* (2020) 30(1):. doi: 10.1002/rmv.2081
160. Cai L, Lyu X, Luo W, Cui X, Ye Y, Yuan C, et al. EBV-miR-BART7-3p Promotes the EMT and Metastasis of Nasopharyngeal Carcinoma Cells by Suppressing the Tumor Suppressor PTEN. *Oncogene* (2015) 34(17):2156–66. doi: 10.1038/onc.2014.341
161. Cai L, Ye Y, Jiang Q, Chen Y, Lyu X, Li J, et al. Epstein–Barr Virus-Encoded microRNA BART1 Induces Tumour Metastasis by Regulating PTEN-Dependent Pathways in Nasopharyngeal Carcinoma. *Nat Commun* (2015) 6(1):1–13. doi: 10.1038/ncomms8353
162. Maclellan SA, Lawson J, Baik J, Guillaud M, Poh CF, Garnis C. Differential Expression of miRNAs in the Serum of Patients With High-Risk Oral Lesions. *Cancer Med* (2012) 1(2):268–74. doi: 10.1002/cam4.17
163. Ferre F, Colantoni A, Helmer-Citterich M. Revealing Protein–lncRNA Interaction. *Briefings Bioinf* (2016) 17(1):106–16. doi: 10.1093/bib/bbv031
164. Abbasi-Kolli M, Nahand JS, Kiani SJ, Khanaliha K, Khatami A, Taghizadieh M, et al. The Expression Patterns of MALAT-1, NEAT-1, THRIL, and miR-155-5p in the Acute to the Post-Acute Phase of COVID-19 Disease. *Braz J Infect Dis* (2022) 26(3):102354. doi: 10.1016/j.bjid.2022.102354
165. Shafabakhsh R, Arianfar F, Vosough M, Mirzaei HR, Mahjoubin-Tehran M, Khanbabaei H, et al. Autophagy and Gastrointestinal Cancers: The Behind the Scenes Role of Long non-Coding RNAs in Initiation, Progression, and Treatment Resistance. *Cancer Gene Ther* (2021) 28(12):1229–55. doi: 10.1038/s41417-020-00272-7
166. Vafadar A, Shabaninejad Z, Movahedpour A, Mohammadi S, Fathullahzadeh S, Mirzaei HR, et al. Long Non-Coding RNAs As Epigenetic Regulators in Cancer. *Curr Pharm Des* (2019) 25(33):3563–77. doi: 10.2174/1381612825666190830161528
167. Jarroux J, Morillon A, Pinskaya M. History, Discovery, and Classification of lncRNAs. *Adv Exp Med Biol* (2017) 1008:1–46. doi: 10.1007/978-981-10-5203-3_1

168. Losko M, Kotlinowski J, Jura J. Long Noncoding RNAs in Metabolic Syndrome Related Disorders. *Mediators Inflammation* (2016) 2016:5365209. doi: 10.1155/2016/5365209
169. Gonzalez I, Munita R, Agirre E, Dittmer TA, Gysling K, Misteli T, et al. A lncRNA Regulates Alternative Splicing *via* Establishment of a Splicing-Specific Chromatin Signature. *Nat Struct Mol Biol* (2015) 22(5):370–6. doi: 10.1038/nsmb.3005
170. Romero-Barrios N, Legascue MF, Benhamed M, Ariel F, Crespi M. Splicing Regulation by Long Noncoding RNAs. *Nucleic Acids Res* (2018) 46(5):2169–84. doi: 10.1093/nar/gky095
171. Chen W, Böcker W, Brosius J, Tiedge H. Expression of Neural BC200 RNA in Human Tumours. *J Pathol: A J Pathol Soc Great Britain Ireland* (1997) 183 (3):345–51. doi: 10.1002/(SICI)1096-9896(199711)183:3<345::AID-PATH930>3.0.CO;2-8
172. Hawkins PG, Morris KV. Transcriptional Regulation of Oct4 by a Long non-Coding RNA Antisense to Oct4-Pseudogene 5. *Transcription* (2010) 1 (3):165–75. doi: 10.4161/trns.1.3.13332
173. Dempsey JL, Cui JY. Long non-Coding RNAs: A Novel Paradigm for Toxicology. *Toxicolo Sci* (2017) 155(1):3–21. doi: 10.1093/toxsci/kfw203
174. Mariner PD, Walters RD, Espinoza CA, Drullinger LF, Wagner SD, Kugel JF, et al. Human Alu RNA Is a Modular Transacting Repressor of mRNA Transcription During Heat Shock. *Mol Cell* (2008) 29(4):499–509. doi: 10.1016/j.molcel.2007.12.013
175. Carrieri C, Cimatti L, Biagioli M, Beugnet A, Zucchelli S, Fedele S, et al. Long Non-Coding Antisense RNA Controls Uchl1 Translation Through an Embedded SINEB2 Repeat. *Nature* (2012) 491(7424):454–7. doi: 10.1038/nature11508
176. Jalali S, Jayaraj GG, Scaria V. Integrative Transcriptome Analysis Suggest Processing of a Subset of Long Non-Coding RNAs to Small RNAs. *Biol Direct* (2012) 7(1):1–13. doi: 10.1186/1745-6150-7-25
177. Peschansky VJ, Wahlestedt C. Non-Coding RNAs as Direct and Indirect Modulators of Epigenetic Regulation. *Epigenetics* (2014) 9(1):3–12. doi: 10.4161/epi.27473
178. Guttman M, Russell P, Ingolia NT, Weissman JS, Lander ES. Ribosome Profiling Provides Evidence That Large Noncoding RNAs Do Not Encode Proteins. *Cell* (2013) 154(1):240–51. doi: 10.1016/j.cell.2013.06.009
179. Gomes AQ, Nolasco S, Soares H. Non-Coding RNAs: Multi-Tasking Molecules in the Cell. *Int J Mol Sci* (2013) 14(8):16010–39. doi: 10.3390/ijms140816010
180. Chen J, Wang Y, Wang C, Hu J-F, Li W. LncRNA Functions as a New Emerging Epigenetic Factor in Determining the Fate of Stem Cells. *Front Genet* (2020) 11:277. doi: 10.3389/fgene.2020.00277
181. Kim DH, Marinov GK, Pepke S, Singer ZS, He P, Williams B, et al. Single-Cell Transcriptome Analysis Reveals Dynamic Changes in lncRNA Expression During Reprogramming. *Cell Stem Cell* (2015) 16(1):88–101. doi: 10.1016/j.stem.2014.11.005
182. Kanwal S, Guo X, Ward C, Volpe G, Qin B, Esteban MA, et al. Role of Long Non-Coding RNAs in Reprogramming to Induced Pluripotency. *Genomics Proteomics Bioinf* (2020) 18(1):16–25. doi: 10.1016/j.gpb.2019.06.003
183. Du Z, Jia L, Wang Y, Wang C, Wen X, Chen J, et al. Combined RNA-Seq and RAT-Seq Mapping of Long Noncoding RNAs in Pluripotent Reprogramming. *Sci data* (2018) 5(1):1–8. doi: 10.1038/sdata.2018.255
184. Chen N, Zhao G, Yan X, Lv Z, Yin H, Zhang S, et al. A Novel FLI1 Exonic Circular RNA Promotes Metastasis in Breast Cancer by Coordinately Regulating TET1 and DNMT1. *Genome Biol* (2018) 19(1):1–14. doi: 10.1186/s13059-018-1594-y
185. Dey BK, Mueller AC, Dutta A. Long non-Coding RNAs as Emerging Regulators of Differentiation, Development, and Disease. *Transcription* (2014) 5(4):e944014. doi: 10.4161/21541272.2014.944014
186. Fu D, Shi Y, Liu J-B, Wu T-M, Jia C-Y, Yang H-Q, et al. Targeting Long non-Coding RNA to Therapeutically Regulate Gene Expression in Cancer. *Mol Therapy-Nucleic Acids* (2020) 21:712–24. doi: 10.1016/j.omtn.2020.07.005
187. Toki N, Takahashi H, Zucchelli S, Gustincich S, Carninci P. Synthetic *In Vitro* Transcribed lncRNAs (SINEUPs) With Chemical Modifications Enhance Target mRNA Translation. *FEBS Letters* (2020) 594(24):4357–69. doi: 10.1002/1873-3468.13928
188. Liu Y, Ding W, Yu W, Zhang Y, Ao X, Wang J. Long non-Coding RNAs: Biogenesis, Functions, and Clinical Significance in Gastric Cancer. *Mol Therapy-Oncolytics* (2021) 23:458–76. doi: 10.1016/j.omto.2021.11.005
189. Toki N, Takahashi H, Sharma H, Valentine MN, Rahman F-UM, Zucchelli S, et al. SINEUP Long Non-Coding RNA Acts *via* PTBP1 and HNRNPK to Promote Translational Initiation Assemblies. *Nucleic Acids Res* (2020) 48 (20):11626–44. doi: 10.1093/nar/gkaa814
190. Indrieri A, Grimaldi C, Zucchelli S, Tammaro R, Gustincich S, Franco B. Synthetic Long Non-Coding RNAs [SINEUPs] Rescue Defective Gene Expression *In Vivo*. *Sci Rep* (2016) 6(1):1–8. doi: 10.1038/srep27315
191. Li G, Liu K, Du X. Long non-Coding RNA TUG1 Promotes Proliferation and Inhibits Apoptosis of Osteosarcoma Cells by Sponging miR-132-3p and Upregulating SOX4 Expression. *Yonsei Med J* (2018) 59(2):226–35. doi: 10.3349/ymj.2018.59.2.226
192. Yang M, Lu H, Liu J, Wu S, Kim P, Zhou X. Lncrnafunc: A Knowledgebase of lncRNA Function in Human Cancer. *Nucleic Acids Res* (2021). doi: 10.1093/nar/gkab1035
193. Zhu J, Fu H, Wu Y, Zheng X. Function of lncRNAs and Approaches to lncRNA-Protein Interactions. *Sci China Life Sci* (2013) 56(10):876–85. doi: 10.1007/s11427-013-4553-6
194. Xiong H, Ni Z, He J, Jiang S, Li X, Gong W, et al. LncRNA HULC Triggers Autophagy *via* Stabilizing Sirt1 and Attenuates the Chemosensitivity of HCC Cells. *Oncogene* (2017) 36(25):3528–40. doi: 10.1038/onc.2016.521
195. Tao H, Liu X, Liu X, Liu W, Wu D, Wang R, et al. LncRNA MEG3 Inhibits Trophoblast Invasion and Trophoblast-Mediated VSMC Loss in Uterine Spiral Artery Remodeling. *Mol Reprod Dev* (2019) 86(6):686–95. doi: 10.1002/mrd.23147
196. Jiang N, Zhang X, Gu X, Li X, Shang L. Progress in Understanding the Role of lncRNA in Programmed Cell Death. *Cell Death Discov* (2021) 7(1):1–11. doi: 10.1038/s41420-021-00407-1
197. Villanova L, Careccia S, De Maria R, Fiori ME. Micro-Economics of Apoptosis in Cancer: ncRNAs Modulation of BCL-2 Family Members. *Int J Mol Sci* (2018) 19(4):958. doi: 10.3390/ijms19040958
198. van der Heijden M, Zimberlin CD, Nicholson AM, Colak S, Kemp R, Meijer SL, et al. Bcl-2 Is a Critical Mediator of Intestinal Transformation. *Nat Commun* (2016) 7:10916. doi: 10.1038/ncomms10916
199. Sun Y, Hu B, Wang Q, Ye M, Qiu Q, Zhou Y, et al. Long Non-Coding RNA HOTTIP Promotes BCL-2 Expression and Induces Chemoresistance in Small Cell Lung Cancer by Sponging miR-216a. *Cell Death Dis* (2018) 9 (2):85. doi: 10.1038/s41419-017-0019-2
200. Zhang SR, Yang JK, Xie JK, Zhao LC. Long Noncoding RNA HOTTIP Contributes to the Progression of Prostate Cancer by Regulating HOXA13. *Cell Mol Biol (Noisy-le-grand)* (2016) 62(3):84–8.
201. Mu M, Li Y, Zhan Y, Li X, Zhang B. Knockdown of HOXA Transcript at the Distal Tip Suppresses the Growth and Invasion and Induces Apoptosis of Oral Tongue Squamous Carcinoma Cells. *Onco Targets Ther* (2018) 11:8033–44. doi: 10.2147/OTT.S174637
202. Martini M, De Santis MC, Braccini L, Gulluni F, Hirsch E. PI3K/AKT Signaling Pathway and Cancer: An Updated Review. *Ann Med* (2014) 46 (6):372–83. doi: 10.3109/07853890.2014.912836
203. Rangel M, Kong J, Bhatt V, Khayati K, Guo JY. Autophagy and Tumorigenesis. *FEBS J* (2021). doi: 10.1111/febs.16125
204. Liang Y, Chen X, Wu Y, Li J, Zhang S, Wang K, et al. LncRNA CASC9 Promotes Esophageal Squamous Cell Carcinoma Metastasis Through Upregulating LAMC2 Expression by Interacting With the CREB-Binding Protein. *Cell Death Differentiation.* (2018) 25(11):1980–95. doi: 10.1038/s41418-018-0084-9
205. Klingenberg M, Groß M, Goyal A, Polycarpou-Schwarz M, Miersch T, Ernst AS, et al. The Long Noncoding RNA Cancer Susceptibility 9 and RNA Binding Protein Heterogeneous Nuclear Ribonucleoprotein L Form a Complex and Coregulate Genes Linked to AKT Signaling. *Hepatology* (2018) 68(5):1817–32. doi: 10.1002/hep.30102
206. Yang Y, Chen D, Liu H, Yang K. Increased Expression of lncRNA CASC9 Promotes Tumor Progression by Suppressing Autophagy-Mediated Cell Apoptosis *via* the AKT/mTOR Pathway in Oral Squamous Cell Carcinoma. *Cell Death disease* (2019) 10(2):1–16. doi: 10.1038/s41419-018-1280-8
207. White E. The Role for Autophagy in Cancer. *J Clin Invest* (2015) 125(1):42–6. doi: 10.1172/JCI73941
208. Levine B. Autophagy and Cancer. *Nature* (2007) 446(7137):745–7. doi: 10.1038/446745a
209. Marino G, Niso-Santano M, Baehrecke EH, Kroemer G. Self-Consumption: The Interplay of Autophagy and Apoptosis. *Nat Rev Mol Cell Biol* (2014) 15 (2):81–94. doi: 10.1038/nrm3735

210. Zhao Z, Han F, Yang S, Wu J, Zhan W. Oxamate-Mediated Inhibition of Lactate Dehydrogenase Induces Protective Autophagy in Gastric Cancer Cells: Involvement of the Akt-mTOR Signaling Pathway. *Cancer Lett* (2015) 358(1):17–26. doi: 10.1016/j.canlet.2014.11.046
211. Yeh PS, Wang W, Chang YA, Lin CJ, Wang JJ, Chen RM. Honokiol Induces Autophagy of Neuroblastoma Cells Through Activating the PI3K/Akt/mTOR and Endoplasmic Reticular Stress/ERK1/2 Signaling Pathways and Suppressing Cell Migration. *Cancer Lett* (2016) 370(1):66–77. doi: 10.1016/j.canlet.2015.08.030
212. Islam MA, Sooro MA, Zhang P. Autophagic Regulation of P62 Is Critical for Cancer Therapy. *Int J Mol Sci* (2018) 19(5):1405.
213. Bjørkøy G, Lamark T, Brech A, Outzen H, Perander M, Overvatn A, et al. P62/SQSTM1 Forms Protein Aggregates Degraded by Autophagy and Has a Protective Effect on Huntingtin-Induced Cell Death. *J Cell Biol* (2005) 171(4):603–14.
214. Wang R, Lu X, Yu R. lncRNA MALAT1 Promotes EMT Process and Cisplatin Resistance of Oral Squamous Cell Carcinoma *via* PI3K/AKT/mTOR Signal Pathway. *Onco Targets Ther* (2020) 13:4049–61.
215. Lei CS, Kung HJ, Shih JW. Long Non-Coding RNAs as Functional Codes for Oral Cancer: Translational Potential, Progress and Promises. *Int J Mol Sci* (2021) 22(9):4903.
216. Zeng B, Li Y, Jiang F, Wei C, Chen G, Zhang W, et al. LncRNA GAS5 Suppresses Proliferation, Migration, Invasion, and Epithelial-Mesenchymal Transition in Oral Squamous Cell Carcinoma by Regulating the miR-21/PTEN Axis. *Exp Cell Res* (2019) 374(2):365–73.
217. Yang M, Xiong X, Chen L, Yang L, Li X. Identification and Validation Long Non-Coding RNAs of Oral Squamous Cell Carcinoma by Bioinformatics Method. *Oncotarget.* (2017) 8(64):107469–76. doi: 10.18632/oncotarget.18178
218. Furuya N, Yu J, Byfield M, Pattingre S, Levine B. The Evolutionarily Conserved Domain of Beclin 1 Is Required for Vps34 Binding, Autophagy and Tumor Suppressor Function. *Autophagy* (2005) 1(1):46–52. doi: 10.4161/auto.1.1.1542
219. Degenhardt K, Mathew R, Beaudoin B, Bray K, Anderson D, Chen G, et al. Autophagy Promotes Tumor Cell Survival and Restricts Necrosis, Inflammation, and Tumorigenesis. *Cancer Cell* (2006) 10(1):51–64. doi: 10.1016/j.ccr.2006.06.001
220. Takamura A, Komatsu M, Hara T, Sakamoto A, Kishi C, Waguri S, et al. Autophagy-Deficient Mice Develop Multiple Liver Tumors. *Genes Dev* (2011) 25(8):795–800. doi: 10.1101/gad.2016211
221. Hu Z, Zhong Z, Huang S, Wen H, Chen X, Chu H, et al. Decreased Expression of Beclin−1 Is Significantly Associated With a Poor Prognosis in Oral Tongue Squamous Cell Carcinoma. *Mol Med Rep* (2016) 14(2):1567–73. doi: 10.3892/mmr.2016.5437
222. Sun MY, Zhu JY, Zhang CY, Zhang M, Song YN, Rahman K, et al. Autophagy Regulated by lncRNA HOTAIR Contributes to the Cisplatin-Induced Resistance in Endometrial Cancer Cells. *Biotechnol Lett* (2017) 39(10):1477–84. doi: 10.1007/s10529-017-2392-4
223. Yang L, Zhang X, Li H, Liu J. The Long Noncoding RNA HOTAIR Activates Autophagy by Upregulating ATG3 and ATG7 in Hepatocellular Carcinoma. *Mol Biosyst* (2016) 12(8):2605–12. doi: 10.1039/C6MB00114A
224. Luan W, Li R, Liu L, Ni X, Shi Y, Xia Y, et al. Long Non-Coding RNA HOTAIR Acts as a Competing Endogenous RNA to Promote Malignant Melanoma Progression by Sponging miR-152-3p. *Oncotarget*. (2017) 8(49):85401–14. doi: 10.18632/oncotarget.19910
225. Wang X, Li S, Wu S, Xie L, Wang P. Silence of Beclin1 in Oral Squamous Cell Carcinoma Cells Promotes Proliferation, Inhibits Apoptosis, and Enhances Chemosensitivity. *Int J Clin Exp Pathol* (2017) 10(8):8424–33.
226. Wang X, Liu W, Wang P, Li S. RNA Interference of Long Noncoding RNA HOTAIR Suppresses Autophagy and Promotes Apoptosis and Sensitivity to Cisplatin in Oral Squamous Cell Carcinoma. *J Oral Pathol Med* (2018) 47(10):930–7. doi: 10.1111/jop.12769
227. Boon RA, Hofmann P, Michalik KM, Lozano-Vidal N, Berghäuser D, Fischer A, et al. Long Noncoding RNA Meg3 Controls Endothelial Cell Aging and Function: Implications for Regenerative Angiogenesis. *J Am Coll Cardiol* (2016) 68(23):2589–91. doi: 10.1016/j.jacc.2016.09.949
228. Liu J, Li Q, Zhang KS, Hu B, Niu X, Zhou SM, et al. Downregulation of the Long Non-Coding RNA Meg3 Promotes Angiogenesis After Ischemic Brain Injury by Activating Notch Signaling. *Mol Neurobiol* (2017) 54(10):8179–90. doi: 10.1007/s12035-016-0270-z
229. Liu X, Hou L, Huang W, Gao Y, Lv X, Tang J. The Mechanism of Long Non-Coding RNA MEG3 for Neurons Apoptosis Caused by Hypoxia: Mediated by miR-181b-12/15-LOX Signaling Pathway. *Front Cell Neurosci* (2016) 10:201. doi: 10.3389/fncel.2016.00201
230. Sun KX, Wu DD, Chen S, Zhao Y, Zong ZH. LncRNA MEG3 Inhibit Endometrial Carcinoma Tumorigenesis and Progression Through PI3K Pathway. *Apoptosis* (2017) 22(12):1543–52. doi: 10.1007/s10495-017-1426-7
231. Xia H, Qu XL, Liu LY, Qian DH, Jing HY. LncRNA MEG3 Promotes the Sensitivity of Vincristine by Inhibiting Autophagy in Lung Cancer Chemotherapy. *Eur Rev Med Pharmacol Sci* (2018) 22(4):1020–7.
232. Zhang Y, Zou Y, Wang W, Zuo Q, Jiang Z, Sun M, et al. Down-Regulated Long Non-Coding RNA MEG3 and Its Effect on Promoting Apoptosis and Suppressing Migration of Trophoblast Cells. *J Cell Biochem* (2015) 116(4):542–50. doi: 10.1002/jcb.25004
233. Su N, Wang P, Li Y. Role of Wnt/β-Catenin Pathway in Inducing Autophagy and Apoptosis in Multiple Myeloma Cells. *Oncol Lett* (2016) 12(6):4623–9. doi: 10.3892/ol.2016.5289
234. Taciak B, Pruszynska I, Kiraga L, Bialasek M, Krol M. Wnt Signaling Pathway in Development and Cancer. *J Physiol Pharmacol* (2018) 69(2).
235. Liu Z, Wu C, Xie N, Wang P. Long non-Coding RNA MEG3 Inhibits the Proliferation and Metastasis of Oral Squamous Cell Carcinoma by Regulating the WNT/β-Catenin Signaling Pathway. *Oncol Lett* (2017) 14(4):4053–8. doi: 10.3892/ol.2017.6682
236. Tan J, Xiang L, Xu G. LncRNA MEG3 Suppresses Migration and Promotes Apoptosis by Sponging miR-548d-3p to Modulate JAK-STAT Pathway in Oral Squamous Cell Carcinoma. *IUBMB Life* (2019) 71(7):882–90. doi: 10.1002/iub.2012
237. Zuo YB, Zhang YF, Zhang R, Tian JW, Lv XB, Li R, et al. Ferroptosis in Cancer Progression: Role of Noncoding RNAs. *Int J Biol Sci* (2022) 18(5):1829–43. doi: 10.7150/ijbs.66917
238. Li T, Wang Y, Xiang X, Chen C. Development and Validation of a Ferroptosis-Related lncRNAs Prognosis Model in Oral Squamous Cell Carcinoma. *Front Genet* (2022) 13. doi: 10.3389/fgene.2022.847940
239. Borran S, Ahmadi G, Rezaei S, Anari MM, Modabberi M, Azarash Z, et al. Circular RNAs: New Players in Thyroid Cancer. *Pathol Res Pract* (2020) 216(10):153217. doi: 10.1016/j.prp.2020.153217
240. Nahand JS, Jamshidi S, Hamblin MR, Mahjoubin-Tehran M, Vosough M, Jamali M, et al. Circular RNAs: New Epigenetic Signatures in Viral Infections. *Front Microbiol* (2020) 11:1853. doi: 10.3389/fmicb.2020.01853
241. Abbaszadeh-Goudarzi K, Radbakhsh S, Pourhanifeh MH, Khanbabaei H, Davoodvandi A, Fathizadeh H, et al. Circular RNA and Diabetes: Epigenetic Regulator With Diagnostic Role. *Curr Mol Med* (2020) 20(7):516–26. doi: 10.2174/1566524020666200129142106
242. Naeli P, Pourhanifeh MH, Karimzadeh MR, Shabaninejad Z, Movahedpour A, Tarrahimofrad H, et al. Circular RNAs and Gastrointestinal Cancers: Epigenetic Regulators With a Prognostic and Therapeutic Role. *Crit Rev Oncol Hematol* (2020) 145:102854. doi: 10.1016/j.critrevonc.2019.102854
243. Kristensen LS, Andersen MS, Stagsted LV, Ebbesen KK, Hansen TB, Kjems J. The Biogenesis, Biology and Characterization of Circular RNAs. *Nat Rev Genet* (2019) 20(11):675–91. doi: 10.1038/s41576-019-0158-7
244. Hallajzadeh J, Amirani E, Mirzaei H, Shafabakhsh R, Mirhashemi SM, Sharifi M, et al. Circular RNAs: New Genetic Tools in Melanoma. *Biomarkers Med* (2020) 14(7):563–71. doi: 10.2217/bmm-2019-0567
245. Zhang Q, Wang W, Zhou Q, Chen C, Yuan W, Liu J, et al. Roles of circRNAs in the Tumour Microenvironment. *Mol Cancer* (2020) 19(1):1–16. doi: 10.1186/s12943-019-1125-9
246. Hou LD, Zhang J. Circular RNAs: An Emerging Type of RNA in Cancer. *Int J Immunopathol Pharmacol* (2017) 30(1):1–6. doi: 10.1177/0394632016686985
247. Jeck WR, Sorrentino JA, Wang K, Slevin MK, Burd CE, Liu J, et al. Circular RNAs Are Abundant, Conserved, and Associated With ALU Repeats. *RNA* (2013) 19(2):141–57. doi: 10.1261/rna.035667.112
248. Zhang X-O, Wang H-B, Zhang Y, Lu X, Chen L-L, Yang L. Complementary Sequence-Mediated Exon Circularization. *Cell* (2014) 159(1):134–47. doi: 10.1016/j.cell.2014.09.001

249. Conn SJ, Pillman KA, Toubia J, Conn VM, Salmanidis M, Phillips CA, et al. The RNA Binding Protein Quaking Regulates Formation of circRNAs. *Cell* (2015) 160(6):1125–34. doi: 10.1016/j.cell.2015.02.014
250. Ivanov A, Memczak S, Wyler E, Torti F, Porath HT, Orejuela MR, et al. Analysis of Intron Sequences Reveals Hallmarks of Circular RNA Biogenesis in Animals. *Cell Rep* (2015) 10(2):170–7. doi: 10.1016/j.celrep.2014.12.019
251. Lasda E, Parker R. Circular RNAs: Diversity of Form and Function. *Rna.* (2014) 20(12):1829–42. doi: 10.1261/rna.047126.114
252. Li X, Yang L, Chen L-L. The Biogenesis, Functions, and Challenges of Circular RNAs. *Mol Cell* (2018) 71(3):428–42. doi: 10.1016/j.molcel.2018.06.034
253. Fan H-Y, Jiang J, Tang Y-J, Liang X-H, Tang Y-L. CircRNAs: A New Chapter in Oral Squamous Cell Carcinoma Biology. *OncoTar Ther* (2020) 13:9071. doi: 10.2147/OTT.S263655
254. Holdt LM, Kohlmaier A, Teupser D. Circular RNAs as Therapeutic Agents and Targets. *Front Physiol* (2018) 9:1262. doi: 10.3389/fphys.2018.01262
255. Shabaninejad Z, Vafadar A, Movahedpour A, Ghasemi Y, Namdar A, Fathizadeh H, et al. Circular RNAs in Cancer: New Insights Into Functions and Implications in Ovarian Cancer. *J Ovarian Res* (2019) 12 (1):1–12. doi: 10.1186/s13048-019-0558-5
256. Hanahan D, Weinberg RA. The Hallmarks of Cancer. *Cell* (2000) 100(1):57–70. doi: 10.1016/S0092-8674(00)81683-9
257. Su M, Xiao Y, Ma J, Tang Y, Tian B, Zhang Y, et al. Circular RNAs in Cancer: Emerging Functions in Hallmarks, Stemness, Resistance and Roles as Potential Biomarkers. *Mol cancer* (2019) 18(1):1–17. doi: 10.1186/s12943-019-1002-6
258. Li J, Sun D, Pu W, Wang J, Peng Y. Circular RNAs in Cancer: Biogenesis, Function, and Clinical Significance. *Trends Cancer* (2020) 6(4):319–36. doi: 10.1016/j.trecan.2020.01.012
259. Carlos de Vicente J, Junquera Gutierrez LM, Zapatero AH, Fresno Forcelledo MF, Hernández-Vallejo G, Lopez Arranz JS. Prognostic Significance of P53 Expression in Oral Squamous Cell Carcinoma Without Neck Node Metastases. *Head Neck: J Sci Specialties Head Neck* (2004) 26(1):22–30. doi: 10.1002/hed.10339
260. Youle RJ, Strasser A. The BCL-2 Protein Family: Opposing Activities That Mediate Cell Death. *Nat Rev Mol Cell Biol* (2008) 9(1):47–59. doi: 10.1038/nrm2308
261. Liu X, He Y, Li F, Huang Q, Kato TA, Hall RP, et al. Caspase-3 Promotes Genetic Instability and Carcinogenesis. *Mol Cell* (2015) 58(2):284–96. doi: 10.1016/j.molcel.2015.03.003
262. Wang Y, Cao Y, Zhu Q, Gu X, Zhu YZ. The Discovery of a Novel Inhibitor of Apoptotic Protease Activating Factor-1 (Apaf-1) for Ischemic Heart: Synthesis, Activity and Target Identification. *Sci Rep* (2016) 6(1):1–10. doi: 10.1038/srep29820
263. Su W, Sun S, Wang F, Shen Y, Yang H. Circular RNA Hsa_Circ_0055538 Regulates the Malignant Biological Behavior of Oral Squamous Cell Carcinoma Through the P53/Bcl-2/Caspase Signaling Pathway. *J Trans Med* (2019) 17(1):1–12. doi: 10.1186/s12967-019-1830-6
264. Li Y, Y-z Ge, Xu L, Jia R. Circular RNA ITCH: A Novel Tumor Suppressor in Multiple Cancers. *Life Sci* (2020) 254:117176. doi: 10.1016/j.lfs.2019.117176
265. Hao C, Wangzhou K, Liang Z, Liu C, Wang L, Gong L, et al. Circular RNA ITCH Suppresses Cell Proliferation But Induces Apoptosis in Oral Squamous Cell Carcinoma by Regulating miR-421/PDCD4 Axis. *Cancer Manage Res* (2020) 12:5651. doi: 10.2147/CMAR.S258887
266. Frazzi R. BIRC3 and BIRC5: Multi-Faceted Inhibitors in Cancer. *Cell Biosci* (2021) 11(1):1–14. doi: 10.1186/s13578-020-00521-0
267. Wang L, Wei Y, Yan Y, Wang H, Yang J, Zheng Z, et al. CircDOCK1 Suppresses Cell Apoptosis *via* Inhibition of Mir−196a−5p by Targeting BIRC3 in OSCC. *Oncol Rep* (2018) 39(3):951–66.
268. Ye Y, Yang S, Han Y, Sun J, Xv L, Wu L, et al. Linc00472 Suppresses Proliferation and Promotes Apoptosis Through Elevating PDCD4 Expression by Sponging miR-196a in Colorectal Cancer. *Aging (Albany NY)* (2018) 10(6):1523. doi: 10.18632/aging.101488
269. Luthra R, Singh R, Luthra M, Li Y, Hannah C, Romans A, et al. MicroRNA-196a Targets Annexin A1: A microRNA-Mediated Mechanism of Annexin A1 Downregulation in Cancers. *Oncogene* (2008) 27(52):6667–78. doi: 10.1038/onc.2008.256
270. Sun Z, Luo Q, Ye D, Chen W, Chen F. Role of Toll-Like Receptor 4 on the Immune Escape of Human Oral Squamous Cell Carcinoma and Resistance of Cisplatin-Induced Apoptosis. *Mol Cancer* (2012) 11(1):1–12. doi: 10.1186/1476-4598-11-33
271. Ai Y, Song J, Wei H, Tang Z, Li X, Lv X, et al. Circ_0001461 Promotes Oral Squamous Cell Carcinoma Progression Through miR-145/TLR4/NF-κb Axis. *Biochem Biophys Res Commun* (2021) 566:108–14. doi: 10.1016/j.bbrc.2021.06.009
272. Naruse T, Yanamoto S, Matsushita Y, Sakamoto Y, Morishita K, Ohba S, et al. Cetuximab for the Treatment of Locally Advanced and Recurrent/Metastatic Oral Cancer: An Investigation of Distant Metastasis. *Mol Clin Oncol* (2016) 5(2):246–52. doi: 10.3892/mco.2016.928
273. Dai W, Li Y, Zhou Q, Xu Z, Sun C, Tan X, et al. Cetuximab Inhibits Oral Squamous Cell Carcinoma Invasion and Metastasis *via* Degradation of Epidermal Growth Factor Receptor. *J Oral Pathol Med* (2014) 43(4):250–7. doi: 10.1111/jop.12116
274. Razis E, Pentheroudakis G, Rigakos G, Bobos M, Kouvatseas G, Tzaida O, et al. EGFR Gene Gain and PTEN Protein Expression are Favorable Prognostic Factors in Patients With KRAS Wild-Type Metastatic Colorectal Cancer Treated With Cetuximab. *J Cancer Res Clin Oncol* (2014) 140(5):737–48. doi: 10.1007/s00432-014-1626-2
275. Xu Y-J, Zhao J-M, Ni X-F, Wang W, Hu W-W, Wu C-P. LncRNA HCG18 Suppresses CD8+ T Cells to Confer Resistance to Cetuximab in Colorectal Cancer *via* miR-20b-5p/PD-L1 Axis. *Epigenomics* (2021) 13(16):1283–99. doi: 10.2217/epi-2021-0130
276. Suto T, Yokobori T, Yajima R, Morita H, Fujii T, Yamaguchi S, et al. MicroRNA-7 Expression in Colorectal Cancer Is Associated With Poor Prognosis and Regulates Cetuximab Sensitivity *via* EGFR Regulation. *Carcinogenesis.* (2015) 36(3):338–45. doi: 10.1093/carcin/bgu242
277. Zhang X, Wen L, Chen S, Zhang J, Ma Y, Hu J, et al. The Novel Long Noncoding RNA CRART16 Confers Cetuximab Resistance in Colorectal Cancer Cells by Enhancing ERBB3 Expression *via* miR-371a-5p. *Cancer Cell Int* (2020) 20(1):1–16. doi: 10.1186/s12935-020-1155-9
278. Su W, Wang Y, Wang F, Sun S, Li M, Shen Y, et al. Hsa_circ_0005379 Regulates Malignant Behavior of Oral Squamous Cell Carcinoma Through the EGFR Pathway. *BMC Cancer* (2019) 19(1):1–13. doi: 10.1186/s12885-019-5593-5
279. Gao F, Han J, Wang Y, Jia L, Luo W, Zeng Y. Circ_0109291 Promotes the Cisplatin Resistance of Oral Squamous Cell Carcinoma by Sponging miR-188-3p to Increase ABCB1 Expression. *Cancer Biother Radiopharm* (2020).
280. Tan X, Zhou C, Liang Y, Lai YF, Liang Y. Circ_0001971 Regulates Oral Squamous Cell Carcinoma Progression and Chemosensitivity by Targeting miR-194/miR-204 *In Vitro* and *In Vivo*. *Eur Rev Med Pharmacol Sci* (2020) 24(5):2470–81.
281. Pourhanifeh MH, Mahjoubin-Tehran M, Karimzadeh MR, Mirzaei HR, Razavi ZS, Sahebkar A, et al. Autophagy in Cancers Including Brain Tumors: Role of MicroRNAs. *Cell Commun Signaling* (2020) 18:1–22. doi: 10.1186/s12964-020-00587-w
282. Chang C-H, Bijian K, Wernic D, Su J, da Silva SD, Yu H, et al. A Novel Orally Available Seleno-Purine Molecule Suppresses Triple-Negative Breast Cancer Cell Proliferation and Progression to Metastasis by Inducing Cytostatic Autophagy. *Autophagy* (2019) 15(8):1376–90. doi: 10.1080/15548627.2019.1582951
283. Liu P-F, Chang H-W, Cheng J-S, Lee H-P, Yen C-Y, Tsai W-L, et al. Map1lc3b and Sqstm1 Modulated Autophagy for Tumorigenesis and Prognosis in Certain Subsites of Oral Squamous Cell Carcinoma. *J Clin Med* (2018) 7(12):478. doi: 10.3390/jcm7120478
284. Gao L, Dou Z-C, Ren W-H, Li S-M, Liang X, Zhi K-Q. CircCDR1as Upregulates Autophagy Under Hypoxia to Promote Tumor Cell Survival *via* AKT/ERK ½/mTOR Signaling Pathways in Oral Squamous Cell Carcinomas. *Cell Death Disease* (2019) 10(10):1–16. doi: 10.1038/s41419-019-1971-9
285. Cui L, Huang C, Zhou D. Overexpression of Circcdr1as Drives Oral Squamous Cell Carcinoma Progression. *Oral Dis* (2021). doi: 10.1111/odi.14085

Conflict of Interest: The authors declare that the research was conducted in the absence of any commercial or financial relationships that could be construed as a potential conflict of interest.

frontiers | Frontiers in Oncology

TYPE Original Research
PUBLISHED 24 August 2022
DOI 10.3389/fonc.2022.923681

OPEN ACCESS

EDITED BY
Monica Fedele,
Consiglio Nazionale Delle Ricerche (CNR), Italy

REVIEWED BY
Barbara Stecca,
Institute for Cancer Research, Prevention and Clinical Network, Italy
Sabrina Battista,
Consiglio Nazionale Delle Ricerche (CNR), Italy

*CORRESPONDENCE
Angel Ayuso-Sacido
ayusosa@vithas.es
Noemi Garcia-Romero
noemi.garcia@ufv.es

†These authors have contributed equally to this work

SPECIALTY SECTION
This article was submitted to Molecular and Cellular Oncology, a section of the journal Frontiers in Oncology

RECEIVED 20 April 2022
ACCEPTED 01 July 2022
PUBLISHED 24 August 2022

CITATION
Peris-Celda M, Carrión-Navarro J, Palacín-Aliana I, Sánchez-Gómez P, Acín RP, Garcia-Romero N and Ayuso-Sacido A (2022) Suppressor of fused associates with dissemination patterns in patients with glioma. *Front. Oncol.* 12:923681. doi: 10.3389/fonc.2022.923681

Suppressor of fused associates with dissemination patterns in patients with glioma

María Peris-Celda[1†], Josefa Carrión-Navarro[2†], Irina Palacín-Aliana[3,4,5], Pilar Sánchez-Gómez[6], Ricardo Prat Acín[7], Noemi Garcia-Romero[2*] and Angel Ayuso-Sacido[2,8,9*]

[1]Department of Neurosurgery, Mayo Clinic, Rochester, NY, United States, [2]Faculty of Experimental Sciences, Universidad Francisco de Vitoria, Madrid, Spain, [3]Atrys Health, Barcelona, Spain, [4]Fundación de Investigación HM-Hospitales, Madrid, Spain, [5]Faculty of Science, Universidad de Alcalá, Madrid, Spain, [6]Neurooncology Unit, Instituto de Salud Carlos III-Unidad Funcional de Investigación de Enfermedades crónicas (UFIEC), Madrid, Spain, [7]Departamento de Neurocirugía, Hospital Universitario La Fe, Valencia, Spain, [8]Brain Tumor Laboratory, Fundación Vithas, Grupo Hospitales Vithas, Madrid, Spain, [9]Faculty of Medicine, Universidad Francisco de Vitoria, Madrid, Spain

Gliomas are the most common brain tumors, which present poor prognosis, due, in part, to tumor cell migration and infiltration into distant brain areas. However, the underlying mechanisms causing such effects are unknown. Hedgehog (HH)–Gli axis is one of the signaling pathways involved, with a high number of molecular mediators. In this study, we investigated the association between HH-Gli intermediates and clinical parameters. We found that high levels of SuFu are associated with high dissemination patterns in patients with glioma. Therefore, we analyzed SuFu expression data in three glioma cohorts of surgical samples (N =1,759) and modified its expression in Glioblastoma Cancer Stem Cells (GB CSC) *in vitro* models. Our data reveal that SuFu overexpression increases cancer stemness properties together with a migratory phenotype. This work identifies SuFu as a new molecular player in glioma cell migration and a promising target to develop blocking agents to decrease GB dissemination.

KEYWORDS

glioma, brain tumors, SuFu = suppressor of fused, migration, hedgehog glioma-associated oncogene 1 (GLI1), glioblastoma

Introduction

Gliomas are the most common tumors of the central nervous system (CNS) with an incidence of 6.6 per 100,000 habitants, with a higher incidence in men (1). These heterogeneous tumors are divided into three groups by their glial cell composition: astrocytomas, oligodendrogliomas, and ependymomas (2). Tumor grade (I-IV) depends on

tumor malignancy and is defined and established by the World Health Organization (WHO) (3). Brain Magnetic Resonance Image (MRI) and histological evaluation are the gold standard techniques for glioma diagnostic (4); nonetheless, molecular analysis has been included in the last 5 years (3). Current glioma medical treatment is based on surgery, radiotherapy, and chemotherapy with the alkylating cytostatic agent temozolomide or with nitrosureas, depending on the tumor grade. The prognosis of patients with glioma is poor and the median overall survival of the most aggressive kind, glioblastoma (GB) (classified as grade IV), is less than 21 months (5). Despite advances in genomics, transcriptomics, and epigenetic characterization (6), few increases in survival rates have been observed in the last decades, highlighting the lack of knowledge about glioma tumor biology.

Tumor initiation, progression, relapse, and, in some cases, even therapy escape mechanisms are driven, in part, by the presence of a small subpopulation of cancer stem cells (CSCs) in the brain (7). CSC invasion capacity of the surrounding brain determines disease progression; however, the effect of this migration pattern in patients' prognosis is still unclear (8). One of the signaling pathways that has been suggested to be involved in gliomagenesis is the Hedgehog (HH)–Gli axis (9). This signaling cascade is active during the embryogenic development and normally is repressed in adult life, except in some pathologies like cancer, where it can be reactivated (10). Briefly, in humans, the activation of this pathway occurs when sonic HH binds to the transmembrane protein Patched 1 (Ptch1) and liberates Smoothened (Smo), which activates Gli transcription factors (11). The Gli complex is composed of three Gli proteins, normally suppressed by the negative regulator Suppressor of fused (SuFu) (12). Mutations on this gene are associated with some CNS tumors such as medulloblastoma or meningioma (13), and its loss appears to increase tumorigenesis (14). In an attempt to investigate HH-Gli pathway in gliomas, some assays have been developed (15, 16). However, the role of SuFu and its mechanism of action have not yet been elucidated. For this reason, and to investigate SuFu function in different grade glioma tumors, we analyzed its expression in three cohorts (N = 1,759) and established the correlation with migration and stemness patterns. Our data reveals that increased levels of SuFu correlate with high dissemination patterns in patients with glioma and in GB CSCs *in vitro* models.

Materials and methods

Human glioma and control samples

A total of 79 surgical samples were obtained from patients diagnosed with glioma. The brain tumors were classified by histology (astrocytoma, N = 10; oligodendrolgioma, N = 6; oligoastrocytoma, N = 1; and GB, N = 62) based on WHO criteria. Surgical procedures and MRI were conducted at Hospital La Fe (Valencia, Spain). All patients gave their informed patient consent in accordance with the medical and science ethics review board.

Cancer stem cell cultures

GB18 and GB27 CSCs were processed within 12 h of extraction, following the previously described protocol (17). Medium was replaced every 3 days. Sphere-like clusters were passaged before becoming necrotic by both enzymatic and mechanical disaggregation with polished Pasteur pipettes.

Vector construction

To induce the overexpression of SuFu in the CSCs, SuFu cDNA was PCR-amplified and cloned into the vector pWPI, which contains the GFP sequence following the internal ribosome entry site (Supplementary Figure 1A). Lentiviruses were generated by cotransfecting the backbone carrying SuFu along with pCMV AR8.2 and pMD2 VsVg into 293T cells. Transfection was performed using the CalPhos Kit (Calbiochem).

To induce the downregulation of SuFu, an entry vector for the expression of short hairpin RNA (shRNA) was designed with the BLOCK-iT^{TM} U6 Entry Vector Kit (Invitrogen) and was then transfected into 293FT cells using the BLOCK-iT^{TM} Lentiviral RNA Expression System (Invitrogen). The vector containing the shRNA was cloned into the pLenti6/BLOCK-iT^{TM} -DEST vector that contains Blasticidin resistance marker for the selection of infected cells (Supplementary Figure 1B). The corresponding empty vector was used as an internal control (shRC-).

Viral particles from both lentiviral systems were collected after 72 h. The viral particles were then purified by ultra-centrifugation at 26,000 rpm for 90 min at 4°C and resuspended in media. These viruses were used to infect CSCs with the use of Lipofectamine^{TM} 2000 (Invitrogen).

Development of infected CSCs

After infection with the upregulating lentiviral vector, CSCs were sorted by green fluorescent protein (GFP) expression using a MoFlo High Speed Cell Sorter (Beckman-Coulter). One cell per well was plated by Fluorescent Activated Cell Sorter (FACS)-automatic cell deposition in 96-well plates and allowed to expand clonally with the media being replaced every other day. The clone with the highest GFP expression, as confirmed by immunocytochemistry (Supplementary Figure 2), was used for all experiments. The level of GFP correlated with the level of transgene expression. However, with each successive passage, diminishing levels of either GFP or transgene were observed. To minimize variations in the transgene expression in subsequent passages, all experiments were carried out within the first 10 passages after clonal selection. As for the cells

infected with the downregulating vector, blasticidin (4 μg/ml) was used to select the infected cells. The antibiotic was kept in the media for at least 10 days, and a booster dose was given every couple of passages.

RNA extraction and cDNA synthesis

RNA extraction from tissues and CSCs was performed with TriReagent (Sigma) following the manufacturer's recommendations. RNA concentration was measured with a NanoDrop 2000 Spectrophotometer (Thermo Fisher Scientific). RNA was reverse-transcribed with the High-Capacity cDNA Reverse Transcription Kit (Applied Biosystems).

qRT-PCR

Resulting cDNA was diluted and analyzed by quantitative real-time PCR (qRT-PCR) using the Light Cycler 1.5 (Roche) sequence detection system with the SYBR Premix Ex Taq (Takara). Primers were designed using the Primer 3 software. Conditions were as follows: one cycle at 95°C for 10 min, followed by 45 cycles of 10 s at 95°C, 10 s at the primer hybridization temperature and 10 s at 72°C. $2^{-\triangle\triangle Ct}$ method was adopted to analyze the qRT-PCR results. Three housekeeping genes (Glyceraldehyde-3-phosphat dehydrogenase (GAPDH), β2-microglobuline, and β-actin) were used to normalize the data. All data are expressed as increased/decreased folds (relative units). Two replicates were set for each sample, and each reaction was repeated to ensure reproducibility. The information related to all the primers used can be found in Supplementary Table 1.

Cell-surface adhesion assay

Adhesion assays were carried out using different types of surfaces for optimum cell growth. Cell suspensions (2×10^4 cells per well) were seeded onto different extracellular matrix (ECM) components such as Matrigel™ (BD Biosciences), Laminin (Sigma-Aldrich), Fibronectin (Sigma-Aldrich), Gelatin (Sigma-Aldrich), synthetic Poly-D-Lysine (BD Biosciences), and Poly-L-Ornithine (Sigma-Aldrich)–coated surfaces.

Furthermore, polystyrene culture plates (BD Biosciences) were included as controls. Cells were cultured for 48 h, and then, images were taken with an Axiovert 40 CFL Carl Zeiss, microscope using a 20× objective.

Immunocytochemistry

All immunocytochemistry was performed on CSCs cultured in chamber slides and fixed with 4% paraformaldehyde (PFA) for 15 min at RT. Blocking was then performed with PBS with 2% BSA and 0.2% Triton X-100 for 1 h at RT. Primary antibodies mouse monoclonal anti-vinculin (1:300, Sigma-Aldrich), Alexa Fluor 647-Phalloidin (1:40, Invitrogen) and rabbit anti-SuFu (1:250, Abcam) were incubated overnight and 1 h at RT respectively. Secondary antibodies Alexa 488 anti-mouse (1:500 Invitrogen) and Alexa 488 anti- rabbit (1:500, Molecular Probe) were incubated for 1 h and nuclei were stained with DAPI (1:5000 Sigma-Aldrich). Slides were mounted with fluorescence mounting medium (Fluoromount™ Aqueous Mounting Medium, Sigma-Aldrich).

Fluorescence was observed under a Leica TCS SP5 - Inverted Confocal microscope, equipped with four laser lines to detect immunohistochemical signals. Each confocal micrograph consisted of 1024 (X) × 1024 (Y) x 16 (Z) pixels and all parameters were kept constant. Regions of Interest (ROIs) were defined, and quantification analysis was obtained with Leica Application Suite Advanced Fluorescence (LAS AF) software. The experiment was performed twice, with three images of the different type of cells taken in each event. Negative controls with the secondary antibodies were carried out in all cases.

Directional changes

5,000 CSCs per well were seeded on a Matrigel-coated 96-well plate. Changes in direction were tracked using an HCS IN Cell Analyzer 1000 (Cytiva, UK).

Spheres formation

After tumor sphere dissociation, CSCs were plated in 96-well plate at a density of 100 cells per well. One week later, spheres were counted and photographed. Sphere measures were obtained using ImageJ.

Cell viability assay

For cell viability assay, 3000 cells per well were plated in triplicates for each group (GB18wt, GB18SuFu and GB18sh5) on 96-well plates. Cell proliferation reagent MTS (CellTiter 96 Aqueous One Solution Reagent (Promega)) was added into wells and incubated for 3h at 37°C. Then, absorbance was measured at 490 nm and 630 nm to subtract background and non-specific absorbance in a plate reader (Varioskan Flash Multimode Reader, ThermoScientific). These experiments were performed four times and by triplicate for each time. Cell viability was expressed as percentage of viable cells.

Migration assays

To evaluate cell migration, a 24-well plate with 8-μm pore size polycarbonate membrane inserts was used. Cells were

resuspended in 100 µl serum-free DMEM medium and seeded in the upper chamber, and 500 µl of media with growth factors was added to the lower chamber. After 3 h, migrated cells were fixed with 4% PFA and stained with 0.1% crystal violet. All experiments were performed in triplicate.

Analysis of SuFu expression in publicly available glioma datasets

GlioVis data portal (http://gliovis.bioinfo.cnio.es) for visualization and analysis of brain tumor expression datasets was used to analyze gene expression data (18). Processed transcriptomic data from publicly available data cohorts [The Cancer Genome Atlas (TCGA) (N = 667) and Chinese Glioma Genome Atlas (CGGA) (N = 1013)] were used.

Statistical analysis

Quantitative variables were tested for normality using the Saphiro test. Under normally distributed conditions, mean differences were inferred using the two tailed t-test. The chi-squared test and Fisher's exact test were used to compare independent variables.

Statistical tests were performed using SPSS software version 20. The clinical variables studied were revised on three separate occasions for each patient and included an independent external review to minimize the error possibility.

Differences between groups were considered statistically significant when $p < 0.05$.

Results

High level of SuFu is associated with a high dissemination pattern in patients with glioma

With the aim of obtaining an overview of the HH-Gli pathway in glioma, we examined the association between pre-operative MRI clinical parameters and HH-Gli intermediates expression in tumoral tissue. Among the comparison test statistics, we found that the most significant corresponds to higher SuFu levels associated with increased dissemination at the time of diagnosis ($p < 0.01$) (Table 1).

For this reason, we decided to focus our study on elucidating SuFu's role in glioma tumors. An *in silico* study, as shown in Figure 1A, of the SuFu transcriptomic data obtained from TCGA (N = 667) and CGGA (N = 1,013) cohorts revealed that GB have lower SuFu expression levels than LGG. Then, we sought to examine SuFu expression in an external cohort. As presented in Figure 1B, we observed two defined subpopulations divided in high and low expression levels of SuFu. In addition, we visualized matched MRI images from the two most extreme datapoints, the two patients with the highest and the lowest SuFu. Figure 1C illustrates the differences between high (left) and low (right) grade of white matter infiltration, corresponding to SuFu gene expression.

SuFu upregulates stemness without an effect in CSCs growth/proliferation

To examine the role of SuFu in gliomas, we induced its upregulation and downregulation in GB18 and GB27 CSCs. In

TABLE 1 Comparison of clinical parameters among themselves and its association with HH-Gli intermediates expression.

Clinical Parameters		
Comparison	**Significance**	**Interpretation**
Tumor size–distance to ventricle (< or > 5 mm)	0.007	Higher tumor size was related with less distance to the ventricle
Mortality at 6 months after resection	0.009	More mortality →lower resection
Dissemination through white matter tracts-Resection	0.007	More dissemination →lower resection
Mortality at 6 months–distance to ventricle	0.04	More mortality →less distance
Mortality at 6 months–dissemination through white matter tracts	0.039	More mortality →high dissemination
HH-Gli intermediates expression and clinical parameters		
Comparison	**Significance**	**Interpretation**
Smo–tumor size	0.034	Higher Smo levels are associated to higher tumor size
SuFu–dissemination at diagnostic time	0.01	Higher SuFu overexpression is associated to increased dissemination
Glioma grade–Gli1 expression	0.016	Higher Gli1 levels are found in LGG[1]
Glioma grade–Gli1/SuFu	0.041	Higher Gli1/SuFu ratio in LGG
Glioma grade–Smo/Ptch1	0.038	Higher Smo/Ptch1 ratio in LGG

[1]LGG, low-grade glioma.
Significant data ($p < 0.05$) are shown.

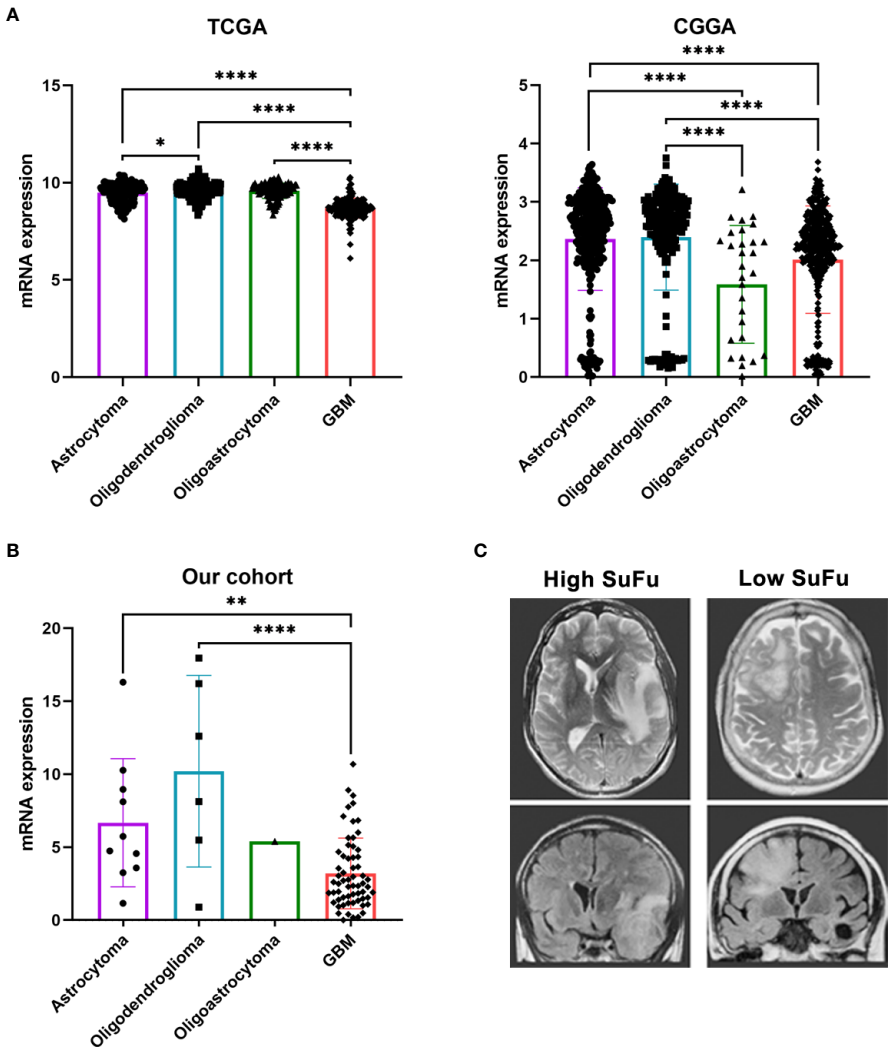

FIGURE 1
(A) SuFu mRNA expression analysis in TCGA (N = 667) and CGGA (N = 1,013) gliomas cohort, grouped according to histological type. **(B)** Quantitative RT-PCR analysis of SuFu in our cohort (N = 79). **(C)** Illustrative example of MRI, T2 axial (upper), and coronal T2 Flair Sequence right (bottom). *P < 0.05, **P < 0.01 and ****P < 0.0001.

an attempt to increase efficacy of downregulation, we tested two vectors (shR400 and shR537) and used the shR537 for the next assays due to its higher potency (Figure 2A and Supplementary Figure 3A). Then, we compared stemness and proliferation properties *in vitro*. SuFu overexpression resulted in increased spheroid formation (Figure 2B and Supplementary Figure 3) with a higher expression of pluripotency transcriptional factors, including *SOX2*, *OCT3/4*, and *BMI-1* (Figure 2C). These results led us to explore the effect of SuFu in GB CSCs proliferation. We first monitored spheres growth by measuring their diameter after a week in culture and no differences were noticed among groups, as shown in Figure 2D and Supplementary Figure 3.

Second, we added Sonic-Hedgehog (Shh) recombinant protein to the cell culture media, as it is one of the ligands that activate the Hedgehog signaling pathway. The three CSCs showed similar population doubling time (PDT) values (Figure 2E). Altogether, by the increased expression of pluripotency markers and sphere formation counts, these results suggest that SuFu is involved in GB CSC stemness potential.

SuFu expression influences cell–cell and cell–matrix adhesion protein profile

To interrogate about the involvement of SuFu mRNA levels in cell–cell and cell–ECM interactions, we performed an adhesion assay using different ECM compounds. As observed

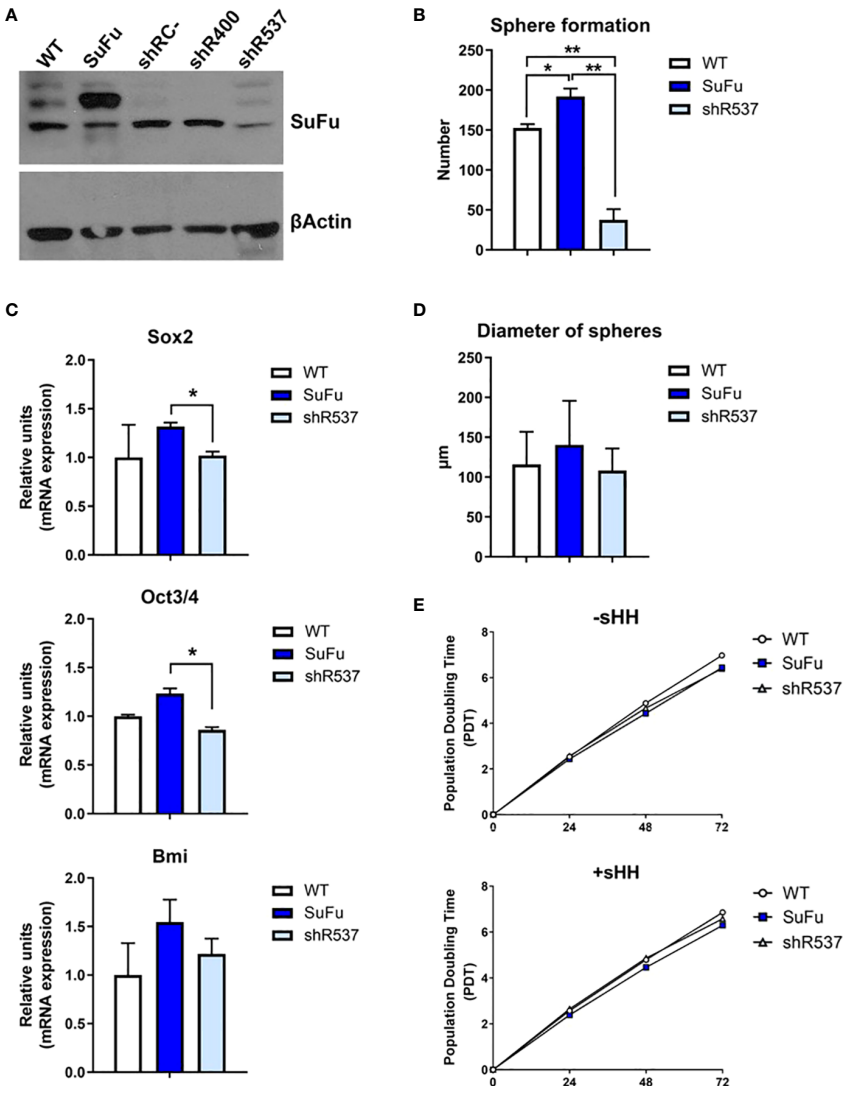

FIGURE 2
(A) Western blot analysis for SuFu using GB18 CSCs samples transfected with overexpression and downregulation vector. CSCs transfected with empty expression vector (shRC-) was used as control. **(B)** Number of spheres formed by GB18 CSCs **(C)** *Sox2*, *Oct3/4*, and *BMI* mRNA levels in GB18 CSCs by qRT-PCR. **(D)** Diameter of spheres of GB 18CSCs. **(E)** Duplication time in basal conditions (–sHH) and in the presence of ligand (+sHH). WT, SuFu, and shR537 CSCs were analyzed. Data are shown as mean ± S.D. and are representative of two independent experiments. P-values were calculated based on the two-tailed two-sample t test. *P < 0.05 and **P < 0.01.

in Figure 3A, we noticed higher adhesion in the SuFu overexpressed cell line in all materials analyzed. As these adhesive interactions are mostly mediated by the associated α and β transmembrane subunits of the integrins, we evaluated their expression. All β integrins expression levels were similar for each cell line except for the β5 subunit which was downregulated in the shRNA cell line (Figure 3B). On the contrary, all the α subunits were highly upregulated in the SuFu cell line (Figure 3C). These observations correlate with the adhesion patterns observed in the previous assays, because α3 and α5 bind fibronectin and α6 engages laminin which, together with collagen IV, are the main compounds of the Matrigel (19, 20).

As transmembrane integrins play a key role between cell and ECM interaction, we then investigated actin and vinculin cytoskeleton protein expression.

The quantification of fluorescence intensity showed a positive correlation between SuFu expression and actin levels, whereas SuFu upregulation decreases vinculin expression in GB CSCs (Figure 3D–G). These changes seem to also affect the number of directional changes performed by CSCs in culture (Figure 3H).

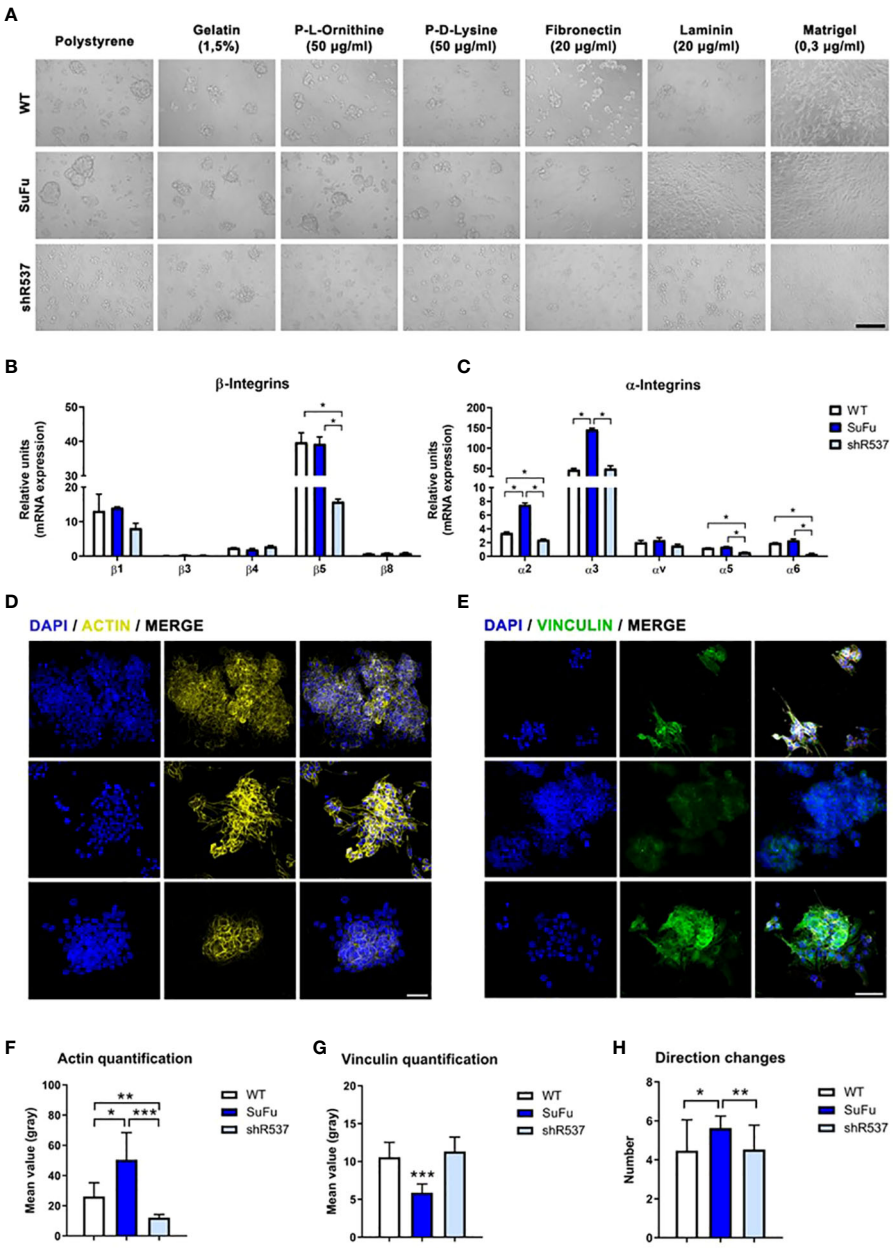

FIGURE 3
(A) Cell adhesion assay *in vitro*. **(B)** β-integrin subunits expression in GB18 CSCs. **(C)** α-integrin subunits expression in GB18 CSCs. **(D)** Representative image of actin immunofluorescence staining. **(E)** Immunofluorescence staining of vinculin. Scale bar represents 50 µm. **(F)** Immunofluorescence quantification of actin protein. **(G)** Immunofluorescence quantification of vinculin protein. **(H)** Movement of the cells measured by number of directional changes. *P < 0.05, **P < 0.01 and ***P < 0.001.

SuFu overexpression increases migratory phenotype in GB CSCs

The migration pattern was further confirmed by an *in vitro* transwell assay (Figure 4A). The number of migrating CSCs increased when SuFu was overexpressed in comparison with the other CSCs lines ($p < 0.05$) (Figure 4B). As it has been proved that the epithelial–mesenchymal transition (EMT) process contributes to the migration of GB tumors, we decided to evaluate several EMT-related markers (21). Consistent with previous observations, SuFu overexpression induces the transcription factor *Snail*, upregulates the expression of the mesenchymal marker *N-cadherin*, and downregulates *E-cadherin* levels (Figure 4C). All these changes seem to be induced by SuFu.

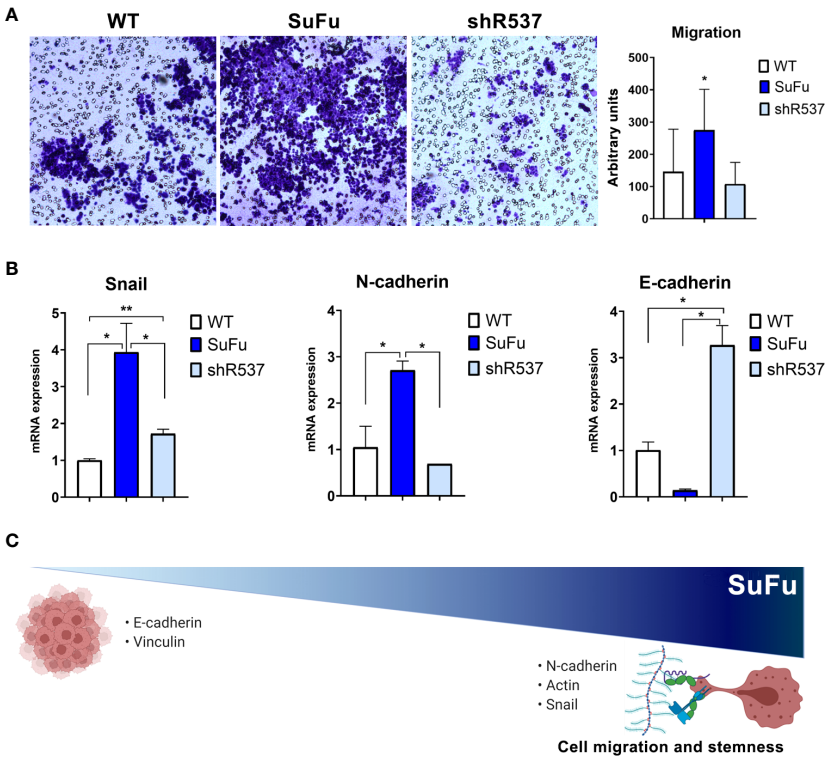

FIGURE 4
SuFu increases migration and mesenchymal phenotype. **(A)** Transwell migration assay. Relative migration of CSCs quantified with ImageJ. **(B)** Epithelial-to-mesenchymal transition expression genes. Data are shown as mean ± S.D. and are representative of two independent experiments. **(C)** Representative image of SuFu involvement in EMT. P-values were calculated based on the two-tailed two-sample t test. *P < 0.05 and **P < 0.01.

Discussion

The most prominent hallmarks of GB are its enhanced cell migration and invasiveness. Despite extensive research, the CSC ability to disseminate along the brain parenchyma presents an impediment for maximal surgical resection and radiotherapy (22). Unfortunately, the underlying mechanisms behind these processes still present a challenge for therapy effectiveness.

Cancer cell migration depends on an interplay between several factors and ECM compounds, and normally, correlates with the malignancy grade (23). We and others have demonstrated the association between high dissemination pattern, lower resection, and, consequently, a detriment in the overall postoperative survival (24–26). Elucidating the mechanisms through which glioma cells spread from the original site would lead to novel blocking compounds that could improve clinical outcomes (27).

In our cohort, SuFu levels appear to influence dissemination status at diagnostic time, which has been proposed as a factor related with stemness in GB and other tumors (28). In fact, our results indicate that the overexpression of SuFu upregulates GB stem cell and self-renewal properties without affecting proliferation rates. Although the dichotomy between migration and proliferation has generated intense controversy in glioma field (29), here, we found that both processes present mutually exclusive behaviors when we modulate SuFu expression. The "go or grow" phenomenon is observed in our CSCs with a tendency to the invasive phenotype.

Specifically, some canonical stem pathways such as Hedgehog, Wnt, and Notch play a key role in stemness regulation (30). In accordance with our attachment assay results, this stem phenotype has been previously accepted as a factor required for cell–cell and cell–ECM adhesion (31). The regulation of these interactions is mediated by the αβ heterodimeric transmembrane receptors called integrins (32). Although the interplay between SuFu and those molecules is still unknown, our experiments suggest that SuFu overexpression results in an incremental cell-mediated binding.

Several studies described that traction forces and focal adhesion generated by cells determine cell migration through the ECM (33, 34). In this sense, vinculin, in which its main function apart from focal adhesion creation is actin cytoskeleton regulation (35), is one of the most relevant molecules involved. In other tumors, such as breast, colorectal, and rhabdomyosarcomas cancer, it has been reported that loss of vinculin increases cell migration and correlates with poor prognosis (36–38). The dissemination pattern observed in our SuFu overexpressed population appears to be related to a loss

in vinculin and indirect upregulation of actin. The indicated effect has been observed in lung cancer, suggesting that it can directly enhance EMT (39), a fact that could be also influenced by β integrin activation, reducing E-cadherin and upregulating N-cadherin (40).

Although gliomas are not considered tumors with an epithelial origin, it has been widely accepted that EMT has an essential role in their development and spread (41). Our results indicate that SuFu is a key inductor of EMT in GB CSCs. Accordingly, it has been shown that EMT starts when cells lose their adhesions and then promote the tumor dissemination (42). The data presented here showcases that SuFu overexpression is linked to the ability of CSCs to undergo EMT and stemness. However, discordant results have been observed in the relation between EMT and stemness in other tumors, such as pancreas and breast cancer (43, 44). As, sometimes, mRNA abundance may not have a linear relationship with the translated protein expression level, further proteomic experiments are needed to corroborate these findings.

To the best of our knowledge, there is only one published study in which they attempted to elucidate the role of SuFu in gliomas. In addition, although they observed that SuFu ectopic expression restrains cell proliferation and invasion (15), they performed their experiments in established glioma cell lines with compromised stem properties, whereas our assays present a more realistic 3D model (45).

On the basis of our findings, we propose that SuFu could be used as an invasiveness prognosis biomarker, and it could be a promising target to develop blocking agents to decrease GB aggressiveness and dissemination. Indirectly, these treatments would in fact improve surgical resection efficacy by limiting dissemination through parenchyma. Even if these results are promising, in the future, we would need larger cohorts and further investigation to classify SuFu as a tumor dissemination molecular mediator.

Data availability statement

The raw data supporting the conclusions of this article will be made available by the authors, without undue reservation.

Ethics statement

The studies involving human participants were reviewed and approved by Hospital Universitario la Fe. The patients/participants provided their written informed consent to participate in this study.

Author contributions

Conceptualization: MP-C and AA-S. Methodology: NG-R and JC-N. Investigation: NG-R, JC-N, and IP-A. Writing—original draft preparation: NR. Writing—review and editing: NG-R, JC-N, and RPA. Supervision: AA-S. Funding acquisition: AA-S. All authors have read and agreed to the published version of the manuscript. All authors contributed to the article and approved the submitted version.

Funding

This research was funded by grants from the "Proyectos de Investigación en Salud" (PI21/01353) and La Universidad Francisco de Vitoria-Banco Santander (UFV2021-23).

Acknowledgments

We are especially grateful to Dr. Francisco Montes (Professor of Statistics and Operative Research at the University of Valencia) for his independent external review of the statistical analysis.

Conflict of interest

The authors declare that the research was conducted in the absence of any commercial or financial relationships that could be considered as a potential conflict of interest.

Publisher's note

Supplementary material

The Supplementary Material for this article can be found online at: https://www.frontiersin.org/articles/10.3389/fonc.2022.923681/full#supplementary-material

SUPPLEMENTARY FIGURE 1
Vector construction to induce SuFu overexpression **(A)** and downregulation **(B)**.

SUPPLEMENTARY FIGURE 2
SuFu immunofluorescence was achieved in GB 18.

SUPPLEMENTARY FIGURE 3
A. Western blot for SuFu using GB27 CSCs samples transfected with shRNA. Non-transfected cells were used as control. B. Number and diameter of spheres formed by GB27 CSCs.

SUPPLEMENTARY TABLE 1
Primer forward and reverse sequences.

References

1. Massara M, Persico P, Bonavita O, Poeta VM, Locati M, Simonelli M, et al. Neutrophils in gliomas. *Front Immunol* (2017) 8:1349. doi: 10.3389/fimmu.2017.01349

2. Weller M, Wick W, Aldape K, Brada M, Berger M, Pfister SM, et al. Glioma. *Nat Rev Dis Prim* (2015) 1. doi: 10.1038/nrdp.2015.17

3. Louis DN, Perry A, Reifenberger G, von Deimling A, Figarella-Branger D, Cavenee WK, et al. The 2016 world health organization classification of tumors of the central nervous system: a summary. *Acta Neuropathol* (2016) 131:803–20. doi: 10.1007/s00401-016-1545-1

4. Weller M, van den Bent M, Preusser M, Le Rhun E, Tonn JC, Minniti G, et al. EANO guidelines on the diagnosis and treatment of diffuse gliomas of adulthood. *Nat Rev Clin Oncol* (2021) 18:170–86. doi: 10.1038/s41571-020-00447-z

5. Stupp R, Taillibert S, Kanner A, Read W, Steinberg DM, Lhermitte B, et al. Effect of tumor-treating fields plus maintenance temozolomide vs maintenance temozolomide alone on survival in patients with glioblastoma a randomized clinical trial. *JAMA - J Am Med Assoc* (2017) 318:2306–16. doi: 10.1001/jama.2017.18718

6. Lathia J, Mack S. Cancer stem cells in glioblastoma. *Genes* (2015) 29 (12):1203–17. doi: 10.1101/gad.261982.115.tumors

7. Walcher L, Kistenmacher A-K, Suo H, Kitte R, Dluczek S, Strauß A, et al. Cancer stem cells–origins and biomarkers: Perspectives for targeted personalized therapies. *Front Immunol* (2020) 11:1280. doi: 10.3389/fimmu.2020.01280

8. Parsa AT, Wachhorst S, Lamborn KR, Prados MD, McDermott MW, Berger MS, et al. Prognostic significance of intracranial dissemination of glioblastoma multiforme in adults. *J Neurosurg* (2005) 102:622–8. doi: 10.3171/jns.2005.102.4.0622

9. Melamed JR, Morgan JT, Ioele SA, Gleghorn JP, Sims-Mourtada J, Day ES. Investigating the role of Hedgehog/GLI1 signaling in glioblastoma cell response to temozolomide. *Oncotarget* (2018) 9:27000–15. doi: 10.18632/oncotarget.25467

10. Barakat MT, Humke EW, Scott MP. Learning from Jekyll to control Hyde: Hedgehog signaling in development and cancer. *Trends Mol Med* (2010) 16:337–48. doi: 10.1016/j.molmed.2010.05.003

11. Maloverjan A, Piirsoo M, Kasak L, Peil L, Østerlund T, Kogerman P. Dual function of UNC-51-like kinase 3 (Ulk3) in the sonic hedgehog signaling pathway. *J Biol Chem* (2010) 285:30079–90. doi: 10.1074/jbc.M110.133991

12. Humke EW, Dorn KV, Milenkovic L, Scott MP, Rohatgi R. The output of hedgehog signaling is controlled by the dynamic association between suppressor of fused and the gli proteins. *Genes Dev* (2010) 24:670–82. doi: 10.1101/gad.1902910

13. Aavikko M, Li SP, Saarinen S, Alhopuro P, Kaasinen E, Morgunova E, et al. Loss of SUFU function in familial multiple meningioma. *Am J Hum Genet* (2012) 91:520–6. doi: 10.1016/j.ajhg.2012.07.015

14. Lee Y, Kawagoe R, Sasai K, Li Y, Russell HR, Curran T, et al. Loss of suppressor-of-fused function promotes tumorigenesis. *Oncogene* (2007) 26:6442–7. doi: 10.1038/sj.onc.1210467

15. Liu X, Wang X, Du W, Chen L, Wang G, Cui Y, et al. Suppressor of fused (Sufu) represses Gli1 transcription and nuclear accumulation, inhibits glioma cell proliferation, invasion and vasculogenic mimicry, improving glioma chemo-sensitivity and prognosis. *Oncotarget* (2014) 5:11655–68. doi: 10.18632/oncotarget.2585

16. Clement V, Sanchez P, de Tribolet N, Radovanovic I, Ruiz i Altaba A. HEDGEHOG-GLI1 signaling regulates human glioma growth, cancer stem cell self-renewal, and tumorigenicity. *Curr Biol* (2007) 17:165–72. doi: 10.1016/j.cub.2006.11.033

17. García-romero N, González-Tejedo C, Carrión-navarro J, La CD, Prat-acín R, Peris-Celda M, et al. Cancer stem cells from human glioblastoma resemble but do not mimic original tumors after *in vitro* passaging in serum-free media. *Oncotarget* (2016) 7(40):65888–901. doi: 10.18632/oncotarget.11676

18. Bowman RL, Wang Q, Carro A, Verhaak RGW, Squatrito M. GlioVis data portal for visualization and analysis of brain tumor expression datasets. *Neuro Oncol* (2017) 19:139–41. doi: 10.1093/neuonc/now247

19. Takada Y, Ye X, Simon S. The integrins. *Genome Biol* (2007) 8(5):215. doi: 10.1186/gb-2007-8-5-215

20. He Q, Johnston J, Zeitlinger J, City K, City K. Mammalian collagen IV jamshid. *Microscopy Research and Technique* (2015) 33:395–401. doi: 10.1002/jemt.20564.Mammalian

21. Takashima Y, Kawaguchi A, Yamanaka R. Promising prognosis marker candidates on the status of epithelial-mesenchymal transition and glioma stem cells in glioblastoma. *Cells* (2019) 8(11):1312. doi: 10.3390/cells8111312

22. Lara-Velazquez M, Al-Kharboosh R, Prieto L, Schiapparelli P, Quiñones-Hinojosa A. The study of brain tumor stem cell migration. *Methods Mol Biol* (2019) 1869:93–104. doi: 10.1007/978-1-4939-8805-1_9

23. Brockmann M-A, Ulbricht U, Grüner K, Fillbrandt R, Westphal M, Lamszus K. Glioblastoma and cerebral microvascular endothelial cell migration in response to tumor-associated growth factors. *Neurosurgery* (2003) 52:1391–9. doi: 10.1227/01.NEU.0000064806.87785.AB

24. Jiang H, Yu K, Li M, Cui Y, Ren X, Yang C, et al. Classification of progression patterns in glioblastoma: Analysis of predictive factors and clinical implications. *Front Oncol* (2020) 10:590648. doi: 10.3389/fonc.2020.590648

25. da Cunha MLV, Esmeraldo ACS, Leonardo AWH, Dos Santos MAM, Medeiros RTR, Botelho RV. Elderly patients with glioblastoma: the impact of the surgical resection extent on survival. *Rev Assoc Med Bras* (2019) 65:1433. doi: 10.1590/1806-9282.65.12.1433

26. Daigle K, Fortin D, Mathieu D, Saint-Pierre AB, Paré F-M, de la Sablonnière A, et al. Effects of surgical resection on the evolution of quality of life in newly diagnosed patients with glioblastoma: a report on 19 patients surviving to follow-up. *Curr Med Res Opin* (2013) 29:1307–13. doi: 10.1185/03007995.2013.823858

27. Kim Y. Regulation of cell proliferation and migration in glioblastoma: New therapeutic approach. *Front Oncol* (2013) 3:53. doi: 10.3389/fonc.2013.00053

28. Molina JR, Hayashi Y, Stephens C, Georgescu MM. Invasive glioblastoma cells acquire stemness and increased akt activation. *Neoplasia* (2010) 12:453–63. doi: 10.1593/neo.10126

29. Giese A, Loo MA, Tran N, Haskett D, Coons SW, Berens ME. Dichotomy of astrocytoma migration and proliferation. *Int J Cancer* (1996) 67:275–82. doi: 10.1002/(SICI)1097-0215(19960717)67:2<275::AID-IJC20>3.0.CO;2-9

30. Takebe N, Miele L, Harris PJ, Jeong W, Bando H, Kahn M, et al. Targeting notch, hedgehog, and wnt pathways in cancer stem cells: clinical update. *Nat Rev Clin Oncol* (2015) 12:445–64. doi: 10.1038/nrclinonc.2015.61

31. Osuka S, Zhu D, Zhang Z, Li C, Stackhouse CT, Sampetrean O, et al. N-cadherin upregulation mediates adaptive radioresistance in glioblastoma. *J Clin Invest* (2021) 131(6):e136098. doi: 10.1172/JCI136098

32. Giese A. Glioma invasion–pattern of dissemination by mechanisms of invasion and surgical intervention, pattern of gene expression and its regulatory control by tumorsuppressor p53 and proto-oncogene ETS-1. *Acta Neurochir Suppl* (2003) 88:153–62. doi: 10.1007/978-3-7091-6090-9_21

33. Thievessen I, Thompson PM, Berlemont S, Plevock KM, Plotnikov SV, Zemljic-Harpf A, et al. Vinculin-actin interaction couples actin retrograde flow to focal adhesions, but is dispensable for focal adhesion growth. *J Cell Biol* (2013) 202:163–77. doi: 10.1083/jcb.201303129

34. Cóndor M, Steinwachs J, Mark C, García-Aznar JM, Fabry B. Traction force microscopy in 3-dimensional extracellular matrix networks. *Curr Protoc Cell Biol* (2017) 75:10. doi: 10.1002/cpcb.24

35. Golji J, Mofrad MRK. The interaction of vinculin with actin. *PloS Comput Biol* (2013) 9:e1002995. doi: 10.1371/journal.pcbi.1002995

36. Li T, Guo H, Song Y, Zhao X, Shi Y, Lu Y, et al. Loss of vinculin and membrane-bound β-catenin promotes metastasis and predicts poor prognosis in colorectal cancer. *Mol Cancer* (2014) 13:1–15. doi: 10.1186/1476-4598-13-263

37. Meyer T, Brinck U. Immunohistochemical detection of vinculin in human rhabdomyosarcomas. *Gen Diagn Pathol* (1997) 142:191–8.

38. Somiari RI, Sullivan A, Russell S, Somiari S, Hu H, Jordan R, et al. High-throughput proteomic analysis of human infiltrating ductal carcinoma of the breast. *Proteomics* (2003) 3:1863–73. doi: 10.1002/pmic.200300560

39. Mitra P, Kalailingam P, Tan H, Thanabalu T. Overexpression of GRB2 enhances epithelial to mesenchymal transition of A549 cells by upregulating SNAIL expression. *Cells* (2018) 7:97. doi: 10.3390/cells7080097

40. Mamuya FA, Duncan MK. Av integrins and TGF-β-induced EMT: a circle of regulation. *J Cell Mol Med* (2012) 16:445–55. doi: 10.1111/j.1582-4934.2011.01419.x

41. Iwadate Y. Epithelial-mesenchymal transition in glioblastoma progression. *Oncol Lett* (2016) 11:1615–20. doi: 10.3892/ol.2016.4113

42. Brabletz T, Kalluri R, Nieto MA, Weinberg RA. EMT in cancer. *Nat Rev Cancer* (2018) 18:128–34. doi: 10.1038/nrc.2017.118

43. Rodriguez-Aznar E, Wiesmüller L, Sainz B, Hermann PC. EMT and stemness–key players in pancreatic cancer stem cells. *Cancers (Basel)* (2019) 11 (8):1136. doi: 10.3390/cancers11081136

44. Morel A-P, Lièvre M, Thomas C, Hinkal G, Ansieau S, Puisieux A. Generation of breast cancer stem cells through epithelial-mesenchymal transition. *PloS One* (2008) 3:e2888. doi: 10.1371/journal.pone.0002888

45. Kapałczyńska M, Kolenda T, Przybyła W, Zajączkowska M, Teresiak A, Filas V, et al. 2D and 3D cell cultures - a comparison of different types of cancer cell cultures. *Arch Med Sci* (2018) 14:910–9. doi: 10.5114/aoms.2016.63743

frontiers | Frontiers in Oncology

TYPE Review
PUBLISHED 02 September 2022
DOI 10.3389/fonc.2022.924553

OPEN ACCESS

EDITED BY
Shilpa S Dhar,
University of Texas MD Anderson Cancer Center, United States

REVIEWED BY
Elizabeth Martin,
Louisiana State University, United States
Banu Bayyurt –Kocabas,
National Heart, Lung, and Blood Institute (NIH), United States

*CORRESPONDENCE
Ana Popovic
Ana.POPOVIC@univ-cotedazur.fr
Sophie Tartare-Deckert
sophie.TARTARE-DECKERT@univ-cotedazur.fr

SPECIALTY SECTION
This article was submitted to Molecular and Cellular Oncology, a section of the journal Frontiers in Oncology

RECEIVED 20 April 2022
ACCEPTED 15 August 2022
PUBLISHED 02 September 2022

CITATION
Popovic A and Tartare-Deckert S (2022) Role of extracellular matrix architecture and signaling in melanoma therapeutic resistance. *Front. Oncol.* 12:924553. doi: 10.3389/fonc.2022.924553

Role of extracellular matrix architecture and signaling in melanoma therapeutic resistance

Ana Popovic[1,2]* and Sophie Tartare-Deckert[1,2]*

[1]Université Côte d'Azur, Institut National de la Santé et de la Recherche Médicale (INSERM), Centre Méditerranéen de Médecine Moléculaire (C3M), Nice, France, [2]Team Microenvironnement, Signaling and Cancer, Equipe Labellisée Ligue Contre le Cancer, Nice, France

The extracellular matrix (ECM) is critical for maintaining tissue homeostasis therefore its production, assembly and mechanical stiffness are highly regulated in normal tissues. However, in solid tumors, increased stiffness resulting from abnormal ECM structural changes is associated with disease progression, an increased risk of metastasis and poor survival. As a dynamic and key component of the tumor microenvironment, the ECM is becoming increasingly recognized as an important feature of tumors, as it has been shown to promote several hallmarks of cancer *via* biochemical and biomechanical signaling. In this regard, melanoma cells are highly sensitive to ECM composition, stiffness and fiber alignment because they interact directly with the ECM in the tumor microenvironment *via* cell surface receptors, secreted factors or enzymes. Importantly, seeing as the ECM is predominantly deposited and remodeled by myofibroblastic stromal fibroblasts, it is a key avenue facilitating their paracrine interactions with melanoma cells. This review gives an overview of melanoma and further describes the critical roles that ECM properties such as ECM remodeling, ECM-related proteins and stiffness play in cutaneous melanoma progression, tumor cell plasticity and therapeutic resistance. Finally, given the emerging importance of ECM dynamics in melanoma, future perspectives on therapeutic strategies to normalize the ECM in tumors are discussed.

KEYWORDS

tumor stroma cross-talk, ECM remodeling, ECM mediated therapeutic resistance, melanoma associated fibroblasts, melanoma progression and phenotypic switching

Introduction

Early-stage cutaneous melanoma (clinical stage I – II) that has not presented with nodal or distant metastasis is effectively treated with surgery (1). However, late-stage cutaneous melanoma (clinical stages III and IV) can present with metastases in the lymph nodes, microsatellite and in-transit metastatic lesions (stage III) or it can disseminate to distant

organs (stage IV) (1). It is therefore concerning that approximately 60% of melanoma patients present with metastatic lesions at the lymph nodes and 15% of patients experience metastases at distant organs including the lungs, liver, brain or bone (2, 3). Advanced melanoma is currently treated with chemo- and more recently, with immuno- and targeted therapies, however, it is often recalcitrant to these treatment regimens (2). Prognosis is poor for patients with advanced melanoma, as approximately 50-60% of these patients acquire drug resistance and go into therapeutic failure (3, 4). A possible reason for this, is that melanomas are highly heterogeneous within single tumors but also amongst different tumors at metastatic sites (5). This heterogeneity is in part caused by non-genetic mechanisms, which can drive melanoma cells to readily and reversibly switch between different phenotypic states (6, 7). The tumor microenvironment (TME) critically affects melanoma progression and tumor cell states at both the primary and secondary sites and has been shown to contribute to therapeutic resistance (8, 9).

The TME, which has been recognized as a hallmark of cancer, is a complex and evolving milieu that consists not only of tumor cells but also consists of non-malignant cell types, including fibroblasts, immune cells, nerve cells and endothelial cells, as well as the extracellular matrix (ECM) (10). Thus, the crosstalk between melanoma cells and their cellular and non-cellular surroundings plays a key role in disease progression and impacts the efficacy of anti-cancer therapies (6). The ECM is an important feature of the melanoma TME because ECM-derived biochemical and biomechanical cues have been shown to influence melanoma progression, tumor cell plasticity and therapeutic resistance (11, 12). The ECM is rich in proteins that form a 3D-meshwork of varying alignment and stiffness. Importantly, in cancers including melanoma, the ECM is drastically remodeled resembling fibrosis, especially during invasion and in response to therapies (12–15). This review begins with an overview of melanoma, including disease progression, current therapies and phenotypic plasticity, followed by a description of how ECM architecture is modified in the melanoma TME. Finally, we discuss the role of ECM signaling in melanoma progression, phenotypic plasticity and therapeutic resistance and give future perspectives on potential therapeutic strategies to normalize the melanoma TME.

Overview of melanoma

Melanoma progression

Cutaneous melanoma arises from neural-crest derived pigment producing melanocytes in the epidermis that have undergone genetic alterations, leading to aberrant growth and clonal expansion (16). While some melanomas arise from pre-existing naevi, the majority of melanomas arise *de novo* (17). The Clark model of cutaneous melanoma progression is a classical and well accepted model based on histopathological analyses of melanoma tissue samples at various stages of progression (18). This model begins with aggregated melanocytes forming a benign nevus in the epidermis that experience abnormal growth to form a dysplastic nevus, which can progress, upon clonal expansion, to the radial growth phase (RGP), where the melanoma cells are confined to the epidermis (18). Should the melanoma cells proliferate further and breach the basement membrane, they progress to the vertical growth phase (VGP), as the melanoma cells are able to invade the dermis (18). At the molecular level, melanocytic cells in the benign nevus, frequently have oncogenic mutations in the *BRAF* or *NRAS* genes. Furthermore, these lesions undergo dysplasia due to the loss of tumor suppressive signaling and the loss of expression of key cell cycle regulators. For example, the progression from a dysplastic nevus to the RGP occurs as a result of unchecked mutations and epigenetic changes in cell cycle and cell survival regulators including *PTEN*, *NF1*, *CDKN2A*, and *CCND1* that allow the melanoma cells to bypass senescence (18–20). Additionally, approximately 15% of melanomas occur due to a familial genetic predisposition, resulting in germline mutations in *CDKN2A* (most common) *CDK4*, *TERT*, *ACD*, *TERF2IP*, *POT1*, *MITF*, *MC1R*, and *BAP1* (21). The transition from the RGP to the VGP is characterized by an upregulation of mesenchymal markers such as N-cadherin, secreted protein acidic and cysteine rich (SPARC) and β-catenin, as well as the downregulation of the cell-cell adhesion molecule E-cadherin (18, 22, 23). Once the melanoma cells have invaded the dermis they can disseminate *via* lymphatic or blood vessels and metastasize to distant organs, which is considered the metastatic phase (18).

Although the Clark model has often been used as a reference for melanoma progression in studies investigating the molecular mechanisms that are driving melanoma progression, it is not routinely used for clinical melanoma diagnosis and classification. The first melanoma classification used by clinicians is the Breslow index, which measures the thickness of the tumor because a direct correlation exists between the depth of the melanoma in the skin and patient survival (24). Furthermore, the American Joint Committee on Cancer (AJCC) has recommended the use of the TNM (Tumor, Node, Metastasis) classification (stages 0 – IV), which grades the melanoma according to the thickness, the presence of ulceration in biopsies and any evidence of metastatic dissemination or lesions (25). More recently following the analysis of RNA, DNA and protein in 333 primary or metastatic samples from 331 melanoma patients, The Cancer Genome Atlas Network has proposed the classification of melanoma according to genetic mutations into 4 categories: BRAF, NRAS, NF-1 and triple negative (wild type) (20). The data indicated that mutations in *BRAF* are prevalent in 50% of melanoma patient samples, followed by *NRAS* (30%) and *NF1* (14%) and 15% of melanomas did not harbor somatic mutations in *BRAF, NRAS* or *NF1* (20).

Current therapies for melanoma treatment

Current FDA approved therapies for advanced melanoma include chemo-, immuno- and targeted therapies (2). The most commonly used chemotherapeutic drug used for melanoma treatment is Dacarbazine, which was initially approved for melanoma in the 1970s (26). However, as a monotherapy it was shown to have minimal efficacy in treating advanced melanoma, with the average response rate in patients being less than 5% and the 5 year survival of patients was suggested to be less than 6% (26–28). Furthermore, the combination of Dacarbazine treatment with earlier immunotherapies such as Interferon -2β and Interleukin-2 showed very little improvement in patient survival (2, 28). Notably, the landscape of advanced melanoma treatment has changed drastically in the last decade, following the FDA-approval of immune checkpoint/blockade inhibitors and targeted therapies (4, 29). It is important to note that the genetic classification of melanomas has become particularly important in determining whether a patient is eligible for immuno- or targeted therapy, as the administration of either immuno- or targeted therapy depends on the *BRAF* status (2). Should the patient have wild type *BRAF*, they are treated with immune check-point inhibitors and if a V600E/K mutation is identified in *BRAF*, they can be treated with BRAF and MEK inhibitors or with immunotherapy (2, 26).

Immunotherapy involves the administration of immune checkpoint inhibitors, which are antibodies against cytotoxic T-lymphocyte-associated antigen 4 (CTLA-4) and programmed cell death protein 1 (PD-1) receptor/PD-1 ligand (PD-L1) (2, 30). Mechanistically, the anti-CTLA-4 antibody binds to the inhibitory checkpoint CTLA-4 receptor that is present on the surface of regulatory T-cells, which prohibits the interaction of T-cells with antigen presenting cells that express the CTLA-4 ligand, B7 co-stimulatory molecule (31). The binding of anti-CTLA-4 antibodies to CTLA-4 promotes the activation of T-cells and the inhibition of the immune checkpoint blockade (30, 31). Activated T-cells are then able to illicit an immune response *via* cytokine secretion, clonal expansion and infiltration into the tumor leading to tumor regression (30, 31). To date, Ipilimumab is the only FDA approved anti- CTLA-4 antibody for the treatment of malignant melanoma and is used in clinics as a monotherapy or in combination with the anti-PD-1 antibody Nivolumab (2, 30). T-cell activation can also be suppressed *via* another receptor-ligand interaction, whereby ligands PD-L1 and PD-L2 can bind the PD-1 receptor, resulting in a co-inhibitory effect (2, 30). The anti-PD-L1 antibody prevents the binding of PD-L1 or PD-L2 to the PD-1 receptor, thereby promoting T-cell activation (32). The PD-1 receptor is expressed on the surface of immune cells including T-cells. Melanoma cells express the ligands PD-L1 and PD-L2 and fibroblasts present in the TME were shown to express the ligand PD-L2 (33, 34). In 2014, Nivolumab became the first FDA-approved anti-PD-1 antibody for the treatment of unresectable or metastatic melanoma and subsequently, Pembrolizumab was also approved by the FDA for malignant melanoma treatment in 2015 (2, 28, 30). Currently, Nivolumab and Pembrolizumab are administered as monotherapies or Ipilimumab can be administered in combination Nivolumab with as a combination therapy (2, 28, 35). Although immunotherapies have improved overall and relapse free survival in patients with late stage (stage III and IV) melanoma, immune-related adverse effects are particularly common in these patients including diarrhea, fatigue, skin rash, nausea, headaches and joint pain (2).

BRAF and MEK inhibitors, target the mitogen-activated protein kinase (MAPK)/ERK signaling pathway which is constitutively active in *BRAF* mutant melanoma (2, 30). *BRAF* encodes the rapidly accelerated fibrosarcoma (RAF) serine/threonine kinases (isoforms: ARAF, BRAF and CRAF) that constitutively dimerize due to the V600E mutation (36). Seeing as BRAF and its isoforms are upstream of the MAPK signaling cascade, they amplify its constitutive activation (37, 38). The MAPK signalling cascade has been shown to play a role in key processes of melanomagenesis such as differentiation, survival, proliferation, metastasis, invasion and angiogenesis (36). Briefly, this signaling pathway is activated by extracellular signals binding to G-coupled receptors or receptor tyrosine kinase (RTK) at the cell membrane, which then activates intracellular GTPase NRAS (also KRAS and HRAS) to NRAS-GTP that is able to further activate all 3 RAF protein isoforms, including BRAF (37, 39). This results in the phosphorylation of downstream MAP/ERK kinases (MEK) and the initiation of the MAPK signaling cascade by further phosphorylation of ERK1/2, which can induce transcriptional and translational signaling (37, 39). Vemurafenib was the first selective oral BRAF small molecule inhibitor, approved in 2011 by the FDA, for advanced melanoma treatment and in 2013 a second selective BRAF inhibitor, Dabrafenib, was approved by the FDA (2, 39). Furthermore, the MEK inhibitor Trametinib became FDA-approved in 2013. In clinical trials Trametinib was also partially successful in treating melanomas harbouring NRAS mutations (2, 40). Vemurafenib, Dabrafenib and Trametinib can all be administered as monotherapies and Dabrafenib and Trametinib can also be administered as a part of BRAF and MEK inhibitor combination therapy (2, 4). Furthermore, in 2015, the FDA approved the oral administration of the MEK inhibitor Cobimetinib in combination with Vemurafenib, as a combination therapy (2, 38).

Seeing as these immuno- and targeted therapies significantly improved overall response in approximately 40% of melanoma patients, they are fast becoming the standard of care for unresectable or metastatic melanoma in many countries including the United Kingdom, the United States, Australia and in Europe (2, 30). Approximately 50-60% of melanoma patients treated with the current FDA-approved immuno- and

targeted therapies respond transiently to treatment but unfortunately often progress to develop therapeutic resistance (4, 29). It is therefore not surprising that the resistant mechanisms employed by melanoma cells to circumvent these treatments constitute a major research area in the field of melanoma (3, 41).

Melanoma plasticity

It is fast becoming accepted that non-genetic heterogeneity is a key feature of melanomas that contributes to tumor progression and therapeutic resistance (3, 6, 41). Non-genetic heterogeneity is characterized by melanoma cell plasticity, as it has been shown that within a tumor. In order to adapt to changing pressure and various conditions in the TME, melanoma cells exist in different phenotypic states and can readily switch between distinct transcriptional programs, which are suggested to be distinct for different phenotypic states (3, 6, 41). For example, some melanoma cells might be highly differentiated, more proliferative and melanocytic, whereas some cells might be in a slow-cycling dedifferentiated and more invasive mesenchymal-like state (41). Phenotypic switching of melanoma cells has been shown to occur as a result of reversible epigenetic changes caused by but not limited to chromatin remodeling, microRNAs, long non-coding RNAs and histone modifications (3, 41). These transcriptional and epigenetic changes are thought to occur in melanoma cells as an adaptive response to cues in the TME such as hypoxia, glucose or amino acid deprivation, secreted and inflammatory factors, ECM mechano-signaling and in response to immuno- and targeted therapies (3, 7, 41, 42). In response to these cues, melanoma cells are able to temporarily reprogram their phenotype with regards to their proliferation, cell cycling, metabolic status and motility (7, 41).

To date, melanoma cells have been described to exist in several phenotypic states including the differentiated proliferative and melanocytic, the dedifferentiated invasive and mesenchymal-like, the dedifferentiated neural crest stem cell-like, starved, as well as transitory states (43–47). The melanocytic and invasive mesenchymal-like states were identified in melanoma patient tumors using RNA sequencing (44). Single-cell RNA sequencing further identified the differentiated, starved, neural crest-like states, as well as the melanocytic (more proliferative) and mesenchymal-like (more invasive) states in primary melanoma cells that were isolated from biopsies of melanoma patients, who were treated with BRAF or MEK inhibitors (45, 48). These phenotypic states have been linked to distinct transcriptomic profiles and gene signatures in melanoma cells (43–45, 47, 49, 50). More specifically, changes in the expression of the master regulator microphthalmia-associated transcription factor (MITF) has been associated with melanoma phenotypic switching (41, 49, 51).

Molecular signatures associated with drug resistant melanoma phenotypes

MITF is a key transcription factor that regulates melanocyte development, pigmentation and melanoma progression and has been implicated in cellular processes such as differentiation, survival, cell cycle regulation, senescence bypass, autophagy and lysosomal production and regulation (52). Furthermore, MITF plays a role in genetic processes such as DNA damage repair and chromosome stability (52). Interestingly, MITF was recently shown to directly repress genes associated with the expression of ECM and focal adhesion pathways, demonstrating its involvement in regulating cell-ECM interactions (53). With regards to melanoma phenotypic states, $MITF^{high}$ expressing melanoma cells have been associated with a more differentiated, melanocytic and proliferative state, whereas $MITF^{low}$ expressing melanoma cells have been characterized as more aggressive, dedifferentiated and mesenchymal-like and were found to be associated with invasion and therapeutic resistance (44, 49, 51).

A second transcriptomic signature that has been associated with the melanoma cell phenotypic switch that is inversely correlated to MITF expression, is the expression of the receptor tyrosine kinase AXL (50, 54). This receptor is expressed by cancer cells including melanoma cells and immune cells (55). The binding of AXL and its ligand growth arrest-specific protein 6 (GAS6) induces intracellular signaling that can affect cancer progression, metastasis and drug resistance (55). In melanoma, compared to the $MITF^{high}AXL^{low}$ signature, which promotes a more proliferative and drug sensitive phenotype, the $MITF^{low}AXL^{high}$ signature is specifically associated with an invasive, mesenchymal-like phenotype (50, 54). Importantly, $MITF^{low}AXL^{high}$ expression was shown to be common in *BRAF* mutated melanoma and has been identified in patients who relapsed following BRAF and MEK inhibitors treatment, thereby indicating that this signature results in a drug resistant phenotype (50).

Melanoma cells that have the $MITF^{low}AXL^{high}$ signature, which are associated with a more dedifferentiated phenotype can express epithelial to mesenchymal transition (EMT) molecular markers (3, 41, 56). It is important to note that melanoma cells cannot undergo EMT as melanocytes arise from the neuroectoderm but melanoma cells can be reprogrammed to mesenchymal-like cells (56, 57). In this regard, MITF/AXL expression was shown to correlate with SOX10 and SOX9 transcriptional signatures, which are molecular markers of epithelial-like and mesenchymal-like phenotypes, respectively (41). Therefore, $MITF^{low}AXL^{high}$ expressing melanoma cells have been associated with $SOX10^{low}SOX9^{high}$ expression and the opposite was shown for $MITF^{high}AXL^{low}$ expressing cells. Furthermore, lower levels of SOX10 have been shown to contribute to therapeutic resistance, in part, *via* the transcription factors JUN and/or AP-1 and TEAD (47, 58).

The SOX10^{low}SOX9^{high} signature has also been shown to induce a mesenchymal-like phenotype in melanoma cells with the increased expression of mesenchymal markers such as vimentin, platelet derived growth factor receptor-β (PDGFRβ) and α-smooth muscle actin (αSMA) (46, 59–61). Importantly, this signature has also been associated with drug resistance (12, 14).

Additionally, the HIPPO pathway, in particular the transcriptional co-activator yes-activated protein (YAP)-mediated signaling, has been implicated in the dedifferentiated, invasive mesenchymal-like phenotype (14, 41, 56). Accordingly, YAP and its downstream TEAD signature have been shown to be associated with melanoma metastasis and invasion (62–65). Importantly, there is also some evidence that in melanoma cells, the nuclear accumulation of the two transcriptional co-activator paralogs and mechanotransducers YAP and TAZ promotes resistance to BRAF inhibitors (65). More specifically, in MITF^{low}AXL^{high} melanoma cells that were resistant to the BRAF inhibitor Vemurafenib, increased actin stress-fiber formation and remodeling were observed, which were shown to be dependent on increased levels of nuclear YAP/TAZ (65). Furthermore, the pharmacological inhibition or knockdown of YAP in BRAF inhibitor resistant melanoma cells decreased ERK1/2 signaling, remodeling of the actin cytoskeleton and tumor growth and therefore enhanced BRAF inhibitor efficacy (14, 66). Importantly, this adaptive phenotypic transition of melanoma cells towards a dedifferentiated state, associated with upregulated expression of genes involved in EMT, ECM reprogramming, wound healing, cytoskeletal remodeling and YAP/TAZ/TEAD signatures has also been linked to immune evasion and resistance to PD-1 blockade immunotherapy (67, 68).

Interestingly, melanoma cells in a highly differentiated and melanocytic state, characterized by MITF^{high}, expression have also been shown to play a role in resistance to BRAF and MEK targeted therapies, *via* the rheostatic (on/off) regulation of the transcription factors, PAX3 and BRN2 (51, 69). Furthermore, it has been observed that BRAF inhibitor treatment led to the enrichment of a small population of melanoma cells in a dedifferentiated state, termed BRAF inhibitor persister cells. These persister cells constitutively expressed the Aryl hydrocarbon Receptor (AhR) transcription factor and were shown to promote relapse (21, 70). In addition, another population of persister melanoma cells was recently described to account for minimal residual disease (MRD), as this cell population had acquired tolerance to MAPK inhibitors *via* non-genetic mechanisms. This distinct phenotype was shown to be a transient neural crest stem cell (NCSC) population, which was shown to be dependent on the glial cell line-derived neurotrophic factor cascade that consequently resulted in AKT driven survival *via* focal adhesion kinase (FAK) signaling (71). To this end, the evidence for the role of phenotypic switching by melanoma cells, as an adaptive process involved in non-mutational resistance, is convincing but the investigation into other transitory phenotypic states and the factors that influence and regulate this phenotypic switching is ongoing (70). Given that melanoma cells can readily switch between these different phenotypic states in response to external cues from the TME or therapeutic insults, it is critical to improve our understanding of the biochemical and biomechanical signaling between melanoma cells and the tumorigenic ECM.

ECM architecture modification and therapeutic resistance

Key players in ECM modification

A major cause of altered ECM organization and dynamics during cancer is dysregulated ECM synthesis and remodeling by fibroblasts that have differentiated into cancer-associated fibroblasts (CAFs). ECM remodeling in the TME and organ fibrosis display striking similarities and are both considered to be dysregulated wound healing processes (12). CAFs are the predominant cells in the stroma that modify ECM architecture using several ECM remodeling mechanisms (72). Importantly, CAFs organize and rigidify the ECM by exuding mechanical and tractional forces, resulting in the deposition of ECM fibers that are radially aligned in a parallel fashion (73, 74). CAFs are activated fibroblasts that can originate from resident fibroblasts but may also arise from mesenchymal stem cells, endothelial cells and epithelial cancer cells that have undergone EMT (72, 75, 76). To date, there is no unique marker by which CAFs can be identified, as CAFs express a combination αSMA, fibroblast activation protein-α (FAPα), $\beta_1$integrin (CD29), fibroblast specific protein 1 (S100A4), caveolin 1, podoplanin and PDGFRβ (72, 76, 77). Furthermore, CAFs can express various combinations of these markers and at different levels (78). Given the numerous cells of origin of CAFs and their expression of various markers, it is not surprising that the CAF population in the TME is heterogeneous (72). Several studies have identified two key CAF phenotypically distinct clusters, inflammatory CAFs (iCAFs) and myofibroblastic CAFs (myCAFs), in the TME of breast cancer, pancreatic adenocarcinoma and melanoma (78–82). myCAFs exhibit myofibroblastic properties that are associated with increased levels of αSMA expression, ECM remodeling, actin-myosin adhesion, wound healing and transforming growth factor β (TGFβ) and interferon αβ (IFNαβ) signaling pathways (79, 82–84). Furthermore, myCAFs were found to be located in the vicinity of cancer cells suggesting that paracrine signaling between myCAFs and cancer cells is critical for ECM remodeling in the TME (78, 82).

In cutaneous melanoma, melanoma-associated fibroblasts (MAFs) are primarily responsible for depositing and remodeling ECM in the TME (85). Interestingly, in aged skin, ECM architecture was shown to be modified to a more aligned

organization by aged fibroblasts that produced less of the hyaluronic and proteoglycan link protein, HAPLN1. This aligned ECM in aged skin was shown to promote metastasis and influence therapeutic response and immune cell motility in the melanoma TME (86). ECM remodeling and fiber alignment by MAFs therefore play an important role in melanoma cell invasion and migration, immune escape, metastasis, intratumoral heterogeneity and therapeutic resistance (14, 56, 87–90).

ECM stiffness and fiber alignment in solid tumors, including breast carcinoma, sarcomas and melanoma, contribute to increased interstitial pressure, which results in blood vessel collapse and impaired blood supply, leading to hypoxic conditions (91). Importantly, variations in ECM biophysical properties and mechanical forces have been described to alter cellular metabolism in cancer cells (92, 93). Importantly, immunohistochemical analyses of primary and metastatic melanoma patient samples in a tissue microarray, showed that molecular markers of collagen levels were associated with the transcriptomic signature for melanoma cell phenotypic dedifferentiation *via* the YAP/PAX3/MITF axis (90). Furthermore, this dedifferentiated phenotype was found to be associated with increased collagen fiber abundance and correlated with poorer survival of melanoma patients (90).

Interestingly, we recently showed that melanoma cells that have the specific $MITF^{low}AXL^{high}$ transcriptomic signature and a dedifferentiated, invasive and mesenchymal-like phenotype, display the ability to autonomously deposit and remodel the ECM, resulting in a dense collagen rich and highly organized (aligned fibers) stiff ECM (14). Furthermore, mass spectrometry was used to compare the biochemical composition of 3D-ECM deposited by dedifferentiated, invasive and mesenchymal-like ($MITF^{low}AXL^{high}$) or differentiated and melanocytic ($MITF^{high}AXL^{low}$) melanoma cells. Matrices derived from dedifferentiated, melanoma cells were found to be enriched for key ECM structural proteins (e.g., fibronectin, laminin, collagen I, collagen IV, collagen VIII, tenascin) and proteins involved in ECM remodeling processes (e.g., Thrombospondin-1, Lysyl oxidase homolog 2 (LOXL2), ADAMTS-like protein 1 and Plasminogen activator inhibitor 1) (14).

MAFs and dedifferentiated mesenchymal-like melanoma cells can produce and remodel the ECM in response to cues from the TME such as secreted factors (e.g., TGFβ, PDGF, fibroblast growth factor 2), hypoxia, ECM mechanical signals and in response to BRAF inhibitor treatment (85). On the other hand, melanoma cells adhere to the ECM and interact directly with the ECM *via* cell surface receptors. Melanoma cells are therefore highly sensitive to the presence of specific ECM proteins, the alignment of ECM fibers and the mechanical stiffness of the ECM, which can all induce intracellular signaling and metabolic reprogramming, thereby altering melanoma cell behavior (3, 13, 14, 62). Furthermore, melanoma cells have been shown to reprogram fibroblasts in the lymph node to modify the biochemical properties and architecture of the ECM in the lymph node. This reprogramming of reticular fibroblasts is important for melanoma cell invasion at the metastatic site which is often the lymph node (94, 95). Thus, the role of the ECM in melanoma progression and therapeutic resistance resembles a feedback loop, which involves the interplay between fibroblasts, melanoma cells and ECM biochemical and biomechanical properties.

ECM remodeling mechanisms

ECM remodeling leads to alterations in ECM composition, fiber organization and stiffness that can influence melanoma progression, phenotypic switching and therapeutic response (96). The ECM is remodeled *via* three key mechanisms: i) ECM deposition and post translational modification, ii) degradation and iii) force-mediated ECM modification (97). The protein-rich ECM consists of approximately 300 macromolecules that are termed the core matrisome (98). Key matrisome components include collagens (e.g., collagen I, collagen IV), glycoproteins (e.g., fibronectin, laminin, elastin, tenascin), proteoglycans which are glycoproteins that have attached glycosaminoglycans (e.g., hyaluronan, perlecan). Furthermore, matrisome associated proteins include ECM-bound growth and secreted factors (e.g., vascular endothelial growth factor, hepatocyte growth factor, PDGF) and matricellular proteins (e.g., SPARC) (98, 99). ECM composition is dependent on the deposition and post-translational modification of ECM proteins (97).

During ECM deposition and post translational modification, ECM proteins are synthesized and translocated to the Golgi in the cytoplasm, where further post translational modifications can occur (97). For example, collagen is first synthesized as pre-collagen and is post translationally modified in the Golgi to a procollagen α-chain by glycosylation, pro-peptide alignment, disulphide bond formation and hydroxylation (97). Hydroxylation of the procollagen α-chain by lysyl hydroxylases results in triple helix formation of procollagen α-chains, which is followed by the secretion of procollagen α-helices into the extracellular space (97). In the extracellular space, collagen fibrils are formed by proteolytic cleavage of pro-peptides at the C and N terminals (97). Thereafter, the collagen fibrils are assembled *via* covalent cross-linking by lysyl oxidase (LOX) family members (97). For example, LOXL2 secreted by CAFs, crosslinks collagen and elastin fibers (100). The cross linking of ECM fibrils, in particular collagen fibers, is important for fiber assembly and also increases the tensile strength and stiffness of the ECM (97). Furthermore, collagen fibers are also cross linked to other ECM fibers such as fibronectin fibers by tissue transglutaminase 2, as the deposition of collagen I and III is dependent on the presence and stability of deposited fibronectin (97).

The second mechanism by which the ECM is modified is degradation, which involves the proteolytic cleavage of ECM components by proteases such as matrix metalloproteases (MMPs) (101). Proteolytic cleavage of ECM components promotes the release of ECM fragments, growth factors and cytokines in the ECM milleu, which promotes migration and infiltration of cells in the TME (102). ECM degradation therefore plays an important role in the crosstalk between the ECM, melanoma cells, MAFs and other cells present in the TME such as immune and endothelial cells (96, 97).

The third mechanism by which the ECM is remodeled, is force-mediated modification (96, 97). This involves the binding of cellular receptors such as integrins to ECM molecules including collagens and fibronectin. This leads to traction and mechanical forces, which are transduced to ECM molecules *via* integrins (96, 97). This results in conformational changes that expose binding sites on ECM molecules, which can then self-assemble into fibrils and create an ECM with aligned and parallel fibers (97). Seeing as melanoma cells interact directly with the ECM *via* cell membrane receptors at each stage of melanoma progression, ECM remodeling is tightly regulated during melanomagenesis (13). However, the role of ECM-derived mechanical signaling, which is called mechanotransduction, in melanoma biology is not entirely understood and is currently a dynamic and growing topic in the field.

ECM-mediated signaling in melanoma progression

ECM architecture has been shown to play important roles in melanoma phenotypic switching, metastasis and therapeutic resistance because ECM composition, alignment and stiffness directly affect intracellular signaling (96, 97, 103). These intracellular signaling cascades alter melanoma cell behavior and occur as a result of direct binding with the ECM *via* transmembrane receptors, including integrins and discoidin domain receptors (DDRs) (102). In this regard, fibrillar collagen I and non-fibrillar collagen IV, as well as fibronectin, play important roles in melanoma cell adhesion and migration, thereby promoting metastasis and invasion (13, 102). Melanoma cells were shown to directly interact with collagen IV in the TME *via* integrins ($\alpha_2\beta_1$ and $\alpha_3\beta_1$), which promoted melanoma cell spreading and motility, through the activation of MMP2 and MMP9 (104–107). Seeing as collagen IV is a found in basement membranes, integrin-mediated interaction of melanoma cells with collagen IV is necessary for melanoma cells to breach the basement membrane when progressing from the RGP to the VGP, where they invade into the dermis prior to disseminating to other organs *via* lymphatics and blood vessels (108, 109). Integrins have also been described to play an important role in melanoma cell adhesion to other ECM components including laminin, which is also found in basement membranes and fibronectin (108, 110). For example, integrins ($\alpha_4\beta_1$ and $\alpha_5\beta_1$) were found to be involved in promoting melanoma cell attachment to fibronectin fibers which promoted migration of melanoma cells (108).

The direct interaction of melanoma cells with fibrillar collagen I *via* DRR1 and DDR2 has also been shown to contribute to melanoma cell migration and invasion (111–113). For example, one study showed that in murine melanoma cells, the interaction of DDR2 with collagen I resulted in increased expression of MMP2 and MMP9 *via* the intracellular ERK/NF-κB signaling pathway and promoted melanoma cell invasion (112). Furthermore, the interaction of cancer cells with aligned ECM fibers promoted directional migration of cancer cells (102, 114). In this regard, melanoma cells were found to mimic the directional migration of fibroblasts along collagen fibrils in a 3D collagen ECM model (114, 115). Melanoma cells were described to elongate and migrate in parallel to collagen fibrils by extending actin-rich protrusions, called filapodia, which adhere to and detach from collagen fibrils in cycles, as the melanoma cells are migrating (115). Furthermore, fibronectin was found to be an essential ECM adhesive component required for the directional migration of pancreatic, prostate and head and neck squamous carcinoma cells (116). The fibronectin monomer consists of 15 domains and two extra domains and the extra domain A (EDA) has also been implicated in the activation of TGFβ signaling and its presence in tumors has been associated with increased ECM remodeling, MMP expression and actin cytoskeleton re-organization (117).

Interestingly, melanoma invasion is affected by both ECM fiber alignment and ECM stiffness, as the shape of melanoma cells was shown to change in response to stiffer and more fibrous substrates (118). For example, the elongation of melanoma cells along aligned collagenous fibers was observed and melanoma cell polarization was found to be directly proportional to collagen matrix fiber alignment (118). Several other studies support these findings, as aligned matrices were shown to promote carcinoma, pancreatic cancer and ovarian cancer cell elongation and invasion (87, 119, 120). Furthermore, ECM fiber alignment and stiffness have been reported to be critical for breast cancer invasion, which is reviewed in detail by Kai et al, 2019 (102, 121–123). Surprisingly in contrast to these studies, experiments using varying ECM stiffness models, suggested that the correlation between melanoma cell invasion and substrate stiffness might differ to what was observed for other cancer models. Melanoma cell invasion was shown to be restricted by both soft and highly stiff collagen substrates, suggesting a non-linear relationship between substrate stiffness and optimum invasion (14, 124). These findings are further supported by another group which showed that collagen matrices of an intermediate stiffness provided the optimal conditions for facilitating melanoma cell invasion (118). These differences might be related to the tissue origin of the breast cancer and

melanoma cells. Breast tissue is softer than the skin because breast tissue differs to the skin in term of its rigidity and elasticity. Thus, during malignancy, breast cancer cells initially progress in a softer matrix associated with the physiological breast tissue stiffness but require a stiffer matrix for invasion, whereas melanoma cells initially progress in a stiffer environment in the skin and require a softer and less dense matrix for invasion (125, 126).

It is important to note that the studies discussed in this section employed *in vitro* (e.g., hydrogels or decellularized matrices) or animal models to investigate the role of ECM alignment and stiffness in melanoma progression, in particular during melanoma cell migration and invasion. These findings have yet to be confirmed in clinical melanoma samples.

ECM architecture influences responses to targeted- and immuno-therapies

ECM stiffness and alignment, caused by collagen abundance and crosslinking in the TME, have been shown to contribute to melanoma cell phenotypic switching and therapeutic resistance by inducing mechanosignaling, which can alter cellular behavior to promote a mechanosensitive and resistant mesenchymal-like phenotype (14, 90). Collagen abundance and stiffness were shown to promote the nuclear localization of YAP, which regulated melanoma cell pigmentation and differentiation through the expression of MITF (90). Moreover, one study suggested that higher MITF levels in melanoma cells might be associated with the repression of ECM and focal adhesion genes (53). The effect of MITF repression of these genes was found to be reversible when MITF was knocked down in melanoma cells, resulting in increased focal adhesion complexes and resistance to BRAF inhibitor treatment (53). Interestingly, our group demonstrated that stiffer collagen substrates resulted in increased in mechanosensing *via* YAP and myocardin-related transcription factor (MRTF) in $MITF^{low}$, dedifferentiated, invasive mesenchymal-like melanoma cells, in response to BRAF inhibitor treatment (14). Furthermore, this mechanosensitivity promoted melanoma cells to deposit a stiff, organized and drug-protective ECM and these observations were further confirmed *in vivo* (14).

We also recently demonstrated that stiff and aligned collagen and fibronectin rich matrices deposited by MAFs protected melanoma cells from BRAF/MEK inhibitor treatment, when melanoma cells were cultured on top of these matrices (127). This matrix-mediated drug resistance was demonstrated to be DDR1 and DDR2 dependent and promoted melanoma cell survival *via* the NIK/IKKα/NF-κB2 signaling pathway (127). Therefore, the alignment of fibrils and ECM composition plays an important role in melanoma cell migration and contributes to melanoma cell escape mechanisms to targeted therapies. These studies therefore suggest that in melanoma cells, ECM topography plays important roles in MITF levels and therefore contribute to phenotypic switching and drug adaptive responses.

The induction of ECM-related signaling pathways is a mechanism that is implored by melanoma cells to evade BRAF inhibition and confers tolerance and resistance to BRAF inhibitor treatment (53, 71, 88, 127, 128). For example, one study described upregulated expression of the collagenase and metalloproteinase MT1-MMP in melanoma cells, which acquired resistance to the BRAF inhibitor Vemurafenib (128). Furthermore, this resistance mechanism involved $\beta_1$integrin/FAK signaling and was also dependent on the TGFβ cascade (128). Importantly, the inhibition of this ECM signaling cascade, using the MT1-MMP selective inhibitor ND322 restored melanoma cell sensitivity to BRAF inhibitor treatment (128). Interestingly, in PDX models treated with MAPK inhibitors, a subpopulation of drug-tolerant melanoma cells was described to be associated with the emergence of a transient neural crest stem cell (NCSC) state. The NCSC state was a persister state that most closely corresponds to the minimal residual disease (MRD) observed in clinics and displayed increased activation of FAK-dependent AKT survival signaling (71). Delaying the onset of this non-genetic resistance was achieved by FAK inhibition and the consequential targeting of NCSC-like melanoma cells (71).

Interestingly, BRAF inhibitor treatment has also been implicated in activating MAFs to remodel the ECM making it stiffer, which induced drug tolerance in melanoma cells (88). Furthermore, the direct interaction of melanoma cells *via* $\beta_1$integrin with the ECM deposited by MAFs, induced intracellular FAK signaling that consequently re-activated the ERK signaling pathway in melanoma cells, following BRAF inhibitor treatment (88). Importantly, a fibroblastic and remodeled ECM was observed in the tumoral stroma of melanoma tissue from Vemurafenib (BRAF inhibitor) treated patients (88). Additionally, myCAF (myofibroblastic MAF) clusters with distinguished ECM and TGFβ signaling signatures have been associated with primary resistance to immunotherapies in samples from non-responder melanoma patients (81).

These studies therefore provide some insight into the contribution of ECM signaling and remodeling in response to targeted- and immuno-therapies, in melanoma. However, these ECM-related resistance mechanisms employed by melanoma cells appear to be multifaceted and warrant further investigation.

Strategies to normalize the TME

Given that MAFs are the primary cells that remodel the ECM in the TME and that ECM composition, alignment and stiffness have been shown to promote metastasis, immunosuppression and therapeutic resistance, an obvious strategy to counteract this effect is to target MAF functions in the melanoma TME. However, it was reported that ablating CAFs in pancreatic ductal adenocarcinoma

(PDAC) mouse models resulted in invasive, dedifferentiated and highly hypoxic tumors (129). Furthermore, evidence of EMT and cancer stem cells were observed in tumors, which resulted in poor patient survival and immune suppression. Additionally, the authors also reported that lower myofibroblast number in PDAC patient tumors correlated with reduced patient survival (129). Interestingly, another study showed that targeting iCAFs by JAK inhibition shifted them to a myCAF phenotype *in vivo* (130). In contrast, another group reported that the blockade of CAF contractility by the JAK1/2 inhibitor, Ruxolitinib, counteracted CAF-dependent carcinoma cell invasion and ECM remodeling (131). Thus, the issue of functional complexity and phenotypic heterogeneity of CAFs must be taken into consideration for the development of effective anti-CAF therapies (78). Therefore, the current opinion in the field is to rather achieve normalization in the TME than completely ablate CAFs (132, 133). This approach focuses on restoring homeostasis in the TME, in particular with regards to the ECM, to resemble a non-tumorigenic normal tissue-like state (132, 133). One possible way to achieve this could be to reprogram MAFs to a normal fibroblast phenotype. However, this requires improved understanding of the mechanisms underpinning the activation and functional diversity of MAFs in the melanoma TME.

In light of the current opinion to rather normalize the fibrotic-like tumorigenic ECM than ablate CAFs in the TME, it might be worthwhile to investigate whether the repurposing of anti-fibrotic drugs that are used to treat idiopathic pulmonary fibrosis, such as the TGFβ regulator Pirfenidone or the triple tyrosine kinase inhibitor Nintedanib, in combination with current therapies, might disrupt MAF signaling and ECM-mediated resistance (62). Another strategy might be to identify novel druggable targets in melanoma cells that promote the ECM remodeling abilities associated with the dedifferentiated, mesenchymal-like and resistant phenotype in melanoma cells. We recently identified a fibrosis-associated miRNA cluster (miR-143/-145) that was shown to play an important role in driving the ECM program in dedifferentiated, invasive and mesenchymal-like melanoma cells (15). Furthermore, we also found that, in an allograft melanoma model, the anti-fibrotic drug Nintedanib was efficient in preventing miR-143/-145 cluster upregulation in melanoma cells and in combination with MAPK targeting therapy, normalized the tumoral ECM niche and delayed relapse (15).

Another approach might be to disrupt ECM fiber linearization in the melanoma TME by targeting the YAP mechanotransduction pathway and DDR1/2-dependent collagen signaling using Verteporfin and Imatinib, respectively (134, 135). This treatment strategy might prevent targeted therapy-induced collagen linearization and ECM remodeling, thereby potentially abrogating the permissive stroma and improve drug response. Interestingly, a recent study found that collagen linearization can be reversed and consequently metastasis can be hampered by genetically or pharmacologically restoring levels of the secreted factor WISP2. WISP2 and WISP1 are matricellular proteins secreted by cancer cells (136). WISP1 binds to linearized collagen type I, whereas WISP2 inhibits the binding of WISP1 to collagen type I and in turn inhibits collagen linearization. The authors found that in cancer patients, *WISP2* expression was lower in solid tumors. Therefore, the restoration of a higher WISP2:WISP1 ratio, in an *in vivo* cancer model, normalized collagen fibers in the TME and drastically inhibited metastasis (136). Therapeutically disrupting ECM fiber linearization might therefore prove to be a valuable strategy in achieving ECM normalization in the melanoma TME.

Approaches to normalize the fibrotic-like ECM in the TME have also been described to improve response to immunotherapy (137). One study showed that, in isogenic murine cancer models, including melanoma, targeting DDR2, using the tyrosine kinase inhibitor Dasatinib, in combination with anti-PD-1, improved therapeutic response to immunotherapy (137). Furthermore, another group showed that targeting collagen stabilization (crosslinking) using a LOX inhibitor in combination with anti-PD-1 *in vivo*, not only reduced overall tumor stiffness but also allowed for improved T-cell migration in the melanoma TME, thereby improving the overall efficacy of this immunotherapy (138). Furthermore, in a preclinical melanoma study, mouse survival was prolonged when CAFs were targeted with Nintedanib in combination with anti-PD-1 treatment. Tumor growth was described to be repressed due to the disruption the fibrotic-like ECM, which led to improved infiltration of CD8+ T cells and the production of granzyme B, therefore improving anti-tumor immunity and response to immunotherapy in tumor-bearing mice (139). Another potential therapeutic strategy to normalize the TME was suggested by a group that investigated the combination of shPD-L1 loaded nanoparticles and the ECM degradation enzyme hyaluronidase in an *in vivo* melanoma model (140). The authors found that the hyaluronidase degraded the hyaluronic acid in tumors, thereby increasing the infiltration of the shPD-L1 loaded nanoparticles in the TME and resulted in improved PD-L1 gene silencing (140). Additionally, another group carried out an epigenetic screen to identify novel druggable targets for melanoma treatment and identified TP-472 (targets bromodomain-7/9) as a potential drug, as it effectively inhibited melanoma cell proliferation (141). Interestingly, transcriptome-wide mRNA sequencing revealed that TP-472 treatment downregulated genes encoding various ECM proteins, such as integrins, collagens, and fibronectins in melanoma cells (141). Therefore, these studies suggest that normalizing the fibrotic and dense ECM in the melanoma TME might facilitate improved immune cell infiltration and overall immune anti-tumor response, which has the potential to significantly improve the efficacy of immunotherapies and patient prognosis.

Interestingly, there is some evidence that ECM molecules can serve as biomarkers and can predict the efficacy of immunotherapy treatment in melanoma patients (142, 143). For example, one study described that higher levels of ECM and tissue remodeling proteins such as MMP degraded type III and type IV collagens, quantified in patient serum from metastatic melanoma patients prior to immune

checkpoint inhibitor treatment, were predictors of poorer overall survival (143). Furthermore, another group recently demonstrated that levels of the ECM protein elastin microfibril interface-located protein 2 (EMILIN-2) vary amongst melanoma patients and that the absence of EMILIN-2 expression was shown to be associated with higher PD-L1 expression levels, that in turn, improved the efficacy of immunotherapy. A possible reason for this observation was suggested using an *in vivo* Emilin2-/- mouse model that showed improved vessel normalization and a decrease in hypoxia within tumors (142). Further investigation of ECM markers in melanoma patient serum might therefore be an interesting avenue to further explore, in order to identify novel melanoma prognostic biomarkers.

The normalization of the melanoma TME therefore has the potential to limit immune suppression, increase therapeutic responses and improve advanced melanoma patient prognosis. However, novel therapeutic strategies to prevent or reverse the altered ECM within tumors require further investigation.

Conclusion

The ECM is a dynamic feature of the TME that can dramatically influence cancer biology. Herein, we reviewed how melanoma ECM topology is remodeled by MAFs and dedifferentiated, invasive and mesenchymal-like melanoma cells. These remodeling changes result in ECM architectural modifications including changes in ECM deposition, composition, fiber alignment and mechanical stiffness. Importantly, these biophysical modifications influence melanoma cell, fibroblast and immune cell behaviors, generate intra-tumoral heterogeneity, promote metastasis and compromise anti-melanoma treatments. Furthermore, we give insight into how melanoma cells react to these architectural changes, as they interact directly with the ECM *via* transmembrane receptors, in a reciprocal manner, which influences melanoma cell migration, invasion and phenotypic tumor states. Notably, we provide evidence on how ECM composition, alignment and stiffness contribute to melanoma cells evading therapies and provide a perspective on current and future strategies to normalize the drug protective ECM in the TME.

Author contributions

AP and ST-D contributed equally to the conceptualization, writing and editing of this review. All authors contributed to the article and approved the submitted version.

Funding

AP is a postdoctoral research fellow whose fellowship is funded by the French National Institute for Cancer.

Acknowledgments

The authors acknowledge grant support from the French League for Cancer (équipe labellisée 2022), the French National Institute for Cancer (INCA N°12673) and the French-South African PHC PROTEA project (N° 46471YC).

Conflict of interest

The authors declare that the research was conducted in the absence of any commercial or financial relationships that could be construed as a potential conflict of interest.

Publisher's note

References

1. Ward WH, Lambreton F, Goel N, Yu JQ, Farma JM. Clinical presentation and staging of melanoma. In: *Cutaneous melanoma: Etiology and therapy*. CA, United States:Codon Publications (2017). p. 79–89.

2. Domingues B, Lopes J, Soares P, Populo H. Melanoma treatment in review. *ImmunoTargets Ther* (2018) 7:35–49. doi: 10.2147/ITT.S134842

3. Kozar I, Margue C, Rothengatter S, Haan C, Kreis S. Many ways to resistance: How melanoma cells evade targeted therapies. *Biochim Biophys Acta - Rev Cancer* (2019) 1871:3 13–22. doi: 10.1016/j.bbcan.2019.02.002

4. Robert C, Grob JJ, Stroyakovskiy D, Karaszewska B, Hauschild A, Levchenko E, et al. Five-year outcomes with dabrafenib plus trametinib in metastatic melanoma. *N Engl J Med* (2019) 381:7. doi: 10.1056/NEJMoa1904059

5. Grzywa TM, Paskal W, Włodarski PK. Intratumor and intertumor heterogeneity in melanoma. *Transl Oncol* (2017) 10:6. doi: 10.1016/j.tranon.2017.09.007

6. Arozarena I, Wellbrock C. Phenotype plasticity as enabler of melanoma progression and therapy resistance. *Nat Rev Cancer* (2019) 19:7. doi: 10.1038/s41568-019-0154-4

7. Kemper K, de Goeje PL, Peeper DS, van Amerongen R. Phenotype switching: Tumor cell plasticity as a resistance mechanism and target for therapy. *Cancer Res* (2014) 74:21. doi: 10.1158/0008-5472.CAN-14-1174

8. Quail DF, Joyce JA. Microenvironmental regulation of tumor progression and metastasis. *Nat Med* (2013) 19:11. doi: 10.1038/nm.3394

9. Farc O, Cristea V. An overview of the tumor microenvironment, from cells to complex networks. *Exp Ther Med* (2020) 21:1. doi: 10.3892/etm.2020.9528

10. Hanahan D, Weinberg RA. Hallmarks of cancer: The next generation. *Cell* (2011) 144:5. doi: 10.1016/j.cell.2011.02.013

11. Villanueva J, Herlyn M. Melanoma and the tumor microenvironment. *Curr Oncol Rep* (2008) 10:5. doi: 10.1007/s11912-008-0067-y

12. Diazzi S, Tartare-Deckert S, Deckert M. Bad neighborhood: Fibrotic stroma as a new player in melanoma resistance to targeted therapies. *Cancers* (2020) 12:6. doi: 10.3390/cancers12061364

13. Ju RJ, Stehbens SJ, Haass NK. The role of melanoma cell-stroma interaction in cell motility, invasion, and metastasis. *Front Med* (2018) 5:307. doi: 10.3389/fmed.2018.00307

14. Girard CA, Lecacheur M, Ben Jouira R, Berestjuk I, Diazzi S, Prod'homme V, et al. A feed-forward mechanosignaling loop confers resistance to therapies targeting the MAPK pathway in BRAF-mutant melanoma. *Cancer Res* (2020) 80:10. doi: 10.1158/0008-5472.CAN-19-2914

15. Diazzi S, Baeri A, Fassy J, Lecacheur M, Marin-Bejar O, Girard CA, et al. Blockade of the pro-fibrotic reaction mediated by the miR-143/-145 cluster enhances the responses to targeted therapy in melanoma. *EMBO Mol Med* (2022) 14:3. doi: 10.15252/emmm.202115295

16. Tsao H, Chin L, Garraway LA, Fisher DE. Melanoma: From mutations to medicine. *Genes Dev* (2012) 26:11. doi: 10.1101/gad.191999.112

17. Busse A, Keilholz U. Role of TGF-β in melanoma. *Curr Pharm Biotechnol* (2011) 12:12. doi: 10.2174/138920111798808437

18. Miller AJ, Mihm MC. Mechanisms of disease melanoma. *N Engl J Med* (2006) 1:55–65. doi: 10.1056/NEJMra052166

19. Greene MH, Elder DE, Guerry D, Epstein MN, Greene MH, Van Horn M. A study of tumor progression: The precursor lesions of superficial spreading and nodular melanoma. *Hum Pathol* (1984) 12:1147–65. doi: 10.1016/s0046-8177(84)80310-x

20. Akbani R, Akdemir KC, Aksoy BA, Albert M, Ally A, Amin SB, et al. Genomic classification of cutaneous melanoma. *Cell* (2015) 161:7. doi: 10.1016/j.cell.2015.05.044

21. Toussi A, Mans N, Welborn J, Kiuru M. Germline mutations predisposing to melanoma. *J Cutan Pathol* (2020) 47:7. doi: 10.1111/cup.13689

22. Girotti MR, Fernández M, López JA, Camafeita E, Fernández EA, Albar JP, et al. SPARC Promotes cathepsin b-mediated melanoma invasiveness through a collagen i/α2B1 integrin axis. *J Invest Dermatol* (2011) 131:12. doi: 10.1038/jid.2011.239

23. Bonitsis N, Batistatou A, Karantima S, Charalabopoulos K. The role of cadherin/catenin complex in malignant melanoma. *Exp Oncol* (2006) 3:187–93.

24. Breslow A. Thickness, cross-sectional areas and depth of invasion in the prognosis of cutaneous melanoma. *Ann Surg* (1970) 5:902–8. doi: 10.1097/00000658-197011000-00017

25. Balch CM, Gershenwald JE, Soong SJ, Thompson JF, Atkins MB, Byrd DR, et al. Final version of 2009 AJCC melanoma staging and classification. *J Clin Oncol* (2009) 27:36. doi: 10.1200/JCO.2009.23.4799

26. Eggermont AMM, Kirkwood JM. Re-evaluating the role of dacarbazine in metastatic melanoma: What have we learned in 30 years? *Eur J Cancer* (2004) 40:12. doi: 10.1016/j.ejca.2004.04.030

27. Shtivelman E, Davies MA, Hwu P, Yang J, Lotem M, Oren M, et al. Pathways and therapeutic targets in melanoma. *Oncotarget* (2014) 5:7. doi: 10.18632/oncotarget.1892

28. Fujimura T, Kambayashi Y, Ohuchi K, Muto Y, Aiba S. Treatment of advanced melanoma: Past, present and future. *Life* (2020) 10:9. doi: 10.3390/life10090208

29. Larkin J, Chiarion-Sileni V, Gonzalez R, Grob J-J, Rutkowski P, Lao CD, et al. Five-year survival with combined nivolumab and ipilimumab in advanced melanoma. *N Engl J Med* (2019) 381:16. doi: 10.1056/nejmoa1910836

30. Luke JJ, Flaherty KT, Ribas A, Long GV. Targeted agents and immunotherapies: Optimizing outcomes in melanoma. *Nat Rev Clin Oncol* (2017) 14:8. doi: 10.1038/nrclinonc.2017.43

31. Sullivan RJ, Atkins MB, Kirkwood JM, Agarwala SS, Clark JI, Ernstoff MS, et al. An update on the society for immunotherapy of cancer consensus statement on tumor immunotherapy for the treatment of cutaneous melanoma: Version. *J Immunother Cancer* (2018) 6:1. doi: 10.1186/s40425-018-0362-6

32. Mahoney KM, Freeman GJ, McDermott DF. The next immune-checkpoint inhibitors: Pd-1/pd-l1 blockade in melanoma. *Clin Ther* (2015) 37:4. doi: 10.1016/j.clinthera.2015.02.018

33. Yi M, Niu M, Xu L, Luo S, Wu K. Regulation of PD-L1 expression in the tumor microenvironment. *J Hematol Oncol* (2021) 14:1. doi: 10.1186/s13045-020-01027-5

34. Raskov H, Orhan A, Gaggar S, Gögenur I. Cancer-associated fibroblasts and tumor-associated macrophages in cancer and cancer immunotherapy. *Front Oncol* (2021) 11:668731. doi: 10.3389/fonc.2021.668731

35. Babacan NA, Eroglu Z. Treatment options for advanced melanoma after anti-PD-1 therapy. *Curr Oncol Rep* (2020) 22:4. doi: 10.1007/s11912-020-0894-z

36. Alqathama A. BRAF in malignant melanoma progression and metastasis: potentials and challenges. *Am J Cancer Res* (2020) 4:1103–14.

37. Poulikakos PI, Rosen N. Mutant BRAF melanomas-dependence and resistance. *Cancer Cell* (2011) 19(1):11–5. doi: 10.1016/j.ccr.2011.01.008

38. Eroglu Z, Ribas A. Combination therapy with BRAF and MEK inhibitors for melanoma: Latest evidence and place in therapy. *Ther Adv Med Oncol* (2016) 8:1. doi: 10.1177/1758834015616934

39. Kakadia S, Yarlagadda N, Awad R, Kundranda M, Niu J, Naraev B, et al. Mechanisms of resistance to BRAF and MEK inhibitors and clinical update of us food and drug administration-approved targeted therapy in advanced melanoma. *Onco Targets Ther* (2018) 11:7095–107. doi: 10.2147/OTT.S182721

40. Ascierto PA, Schadendorf D, Berking C, Agarwala SS, van Herpen CML, Queirolo P, et al. MEK162 for patients with advanced melanoma harbouring NRAS or Val600 BRAF mutations: A non-randomised, open-label phase 2 study. *Lancet Oncol* (2013) 14:3. doi: 10.1016/S1470-2045(13)70024-X

41. Rambow F, Marine JC, Goding CR. Melanoma plasticity and phenotypic diversity: Therapeutic barriers and opportunities. *Genes Dev* (2019) 33:19. doi: 10.1101/gad.329771.119

42. Friedl P, Alexander S. Review cancer invasion and the Microenvironment: Plasticity and reciprocity. *Cell* (2012) 147:5. doi: 10.1016/j.cell.2011.11.016

43. Hoek KS, Schlegel NC, Brafford P, Sucker A, Ugurel S, Kumar R, et al. Metastatic potential of melanomas defined by specific gene expression profiles with no BRAF signature. *Pigment Cell Res* (2006) 19:4. doi: 10.1111/j.1600-0749.2006.00322.x

44. Hoek KS, Eichhoff OM, Schlegel NC, Döbbeling U, Kobert N, Schaerer L, et al. *In vivo* switching of human melanoma cells between proliferative and invasive states. *Cancer Res* (2008) 68:3. doi: 10.1158/0008-5472.CAN-07-2491

45. Rambow F, Rogiers A, Marin-Bejar O, Aibar S, Femel J, Dewaele M, et al. Toward minimal residual disease-directed therapy in melanoma. *Cell* (2018) 174:4. doi: 10.1016/j.cell.2018.06.025

46. Wouters J, Kalender-Atak Z, Minnoye L, Spanier KI, De Waegeneer M, Bravo González-Blas C, et al. Robust gene expression programs underlie recurrent cell states and phenotype switching in melanoma. *Nat Cell Biol* (2020) 22:8. doi: 10.1038/s41556-020-0547-3

47. Tsoi J, Robert L, Paraiso K, Galvan C, Sheu KM, Lay J, et al. Multi-stage differentiation defines melanoma subtypes with differential vulnerability to drug-induced iron-dependent oxidative stress. *Cancer Cell* (2018) 33:5. doi: 10.1016/j.ccell.2018.03.017

48. Tirosh I, Izar B, Prakadan SM, Wadsworth MH, Treacy D, Trombetta JJ, et al. Dissecting the multicellular ecosystem of metastatic melanoma by single-cell RNA-seq. *Science* (2016) 352:6282. doi: 10.1126/science.aad0501

49. Carreira S, Goodall J, Denat L, Rodriguez M, Nuciforo P, Hoek KS, et al. Mitf regulation of Dia1 controls melanoma proliferation and invasiveness. *Genes Dev* (2006) 20:24. doi: 10.1101/gad.406406

50. Müller J, Krijgsman O, Tsoi J, Robert L, Hugo W, Song C, et al. Low MITF/AXL ratio predicts early resistance to multiple targeted drugs in melanoma. *Nat Commun* (2014) 5:1. doi: 10.1038/ncomms6712

51. Wellbrock C, Marais R. Elevated expression of MITF counteracts b-RAF-stimulated melanocyte and melanoma cell proliferation. *J Cell Biol* (2005) 170:5. doi: 10.1083/jcb.200505059

52. Goding CR, Arnheiter H. Mitf–the first 25 years. *Genes Dev* (2019) 33:15. doi: 10.1101/gad.324657.119

53. Dilshat R, Fock V, Kenny C, Gerritsen I, Lasseur RMJ, Travnickova J, et al. Mitf reprograms the extracellular matrix and focal adhesion in melanoma. *elife* (2021) 10. doi: 10.7554/eLife.63093

54. Sensi M, Catani M, Castellano G, Nicolini G, Alciato F, Tragni G, et al. Human cutaneous melanomas lacking MITF and melanocyte differentiation antigens express a functional axl receptor kinase. *J Invest Dermatol* (2011) . 131:12. doi: 10.1038/jid.2011.218

55. Zhu C, Wei Y, Wei X. AXL receptor tyrosine kinase as a promising anti-cancer approach: Functions, molecular mechanisms and clinical applications. *Mol Cancer* (2019) 18:1. doi: 10.1186/s12943-019-1090-3

56. Pedri D, Karras P, Landeloos E, Marine JC, Rambow F. Epithelial-to-mesenchymal-like transition events in melanoma. *FEBS J* (2022) 289:5. doi: 10.1111/febs.16021

57. Robert G, Gaggioli C, Bailet O, Chavey C, Abbe P, Aberdam E, et al. SPARC Represses e-cadherin and induces mesenchymal transition during melanoma development. *Cancer Res* (2006) 66:15. doi: 10.1158/0008-5472.CAN-05-3189

58. Shaffer SM, Dunagin MC, Torborg SR, Torre EA, Emert B, Krepler C, et al. Rare cell variability and drug-induced reprogramming as a mode of cancer drug resistance. *Nature* (2017) 546:7658. doi: 10.1038/nature22794

59. Li M, Zhang B, Wang X, Ban X, Sun T, Liu Z, et al. A novel function for vimentin: The potential biomarker for predicting melanoma hematogenous metastasis. *J Exp Clin Cancer Res* (2010) 29:1. doi: 10.1186/1756-9966-29-109

60. Shakhova O, Cheng P, Mishra PJ, Zingg D, Schaefer SM, Debbache J, et al. Antagonistic cross-regulation between Sox9 and Sox10 controls an anti-tumorigenic program in melanoma. *PloS Genet* (2015) 11:1. doi: 10.1371/journal.pgen.1004877

61. Cheng PF, Shakhova O, Widmer DS, Eichhoff OM, Zingg D, Frommel SC, et al. Methylation-dependent SOX9 expression mediates invasion in human melanoma cells and is a negative prognostic factor in advanced melanoma. *Genome Biol* (2015) 16:1. doi: 10.1186/s13059-015-0594-4

62. Nazemi M, Rainero E. Cross-talk between the tumor microenvironment, extracellular matrix, and cell metabolism in cancer. *Front Oncol* (2020) 10:239. doi: 10.3389/fonc.2020.00239

63. Verfaillie A, Imrichova H, Atak ZK, Dewaele M, Rambow F, Hulselmans G, et al. Decoding the regulatory landscape of melanoma reveals TEADS as regulators of the invasive cell state. *Nat Commun* (2015) 6:1. doi: 10.1038/ncomms7683

64. Zhang X, Yang L, Szeto P, Abali GK, Zhang Y, Kulkarni A, et al. The hippo pathway oncoprotein YAP promotes melanoma cell invasion and spontaneous metastasis. *Oncogene* (2020) 39:30. doi: 10.1038/S41388-020-1362-9

65. Kim MH, Kim J, Hong H, Lee S, Lee J, Jung E, et al. Actin remodeling confers BRAF inhibitor resistance to melanoma cells through YAP/TAZ activation. *EMBO J* (2016) 35:5. doi: 10.15252/embj.201592081

66. Wang C, Zhu X, Feng W, Yu Y, Jeong K, Guo W, et al. Verteporfin inhibits YAP function through up-regulating 14-3-3σ sequestering YAP in the cytoplasm. *Am J Cancer Res* (2016) 1:27–37.

67. Hugo W, Zaretsky JM, Sun L, Song C, Moreno BH, Hu-Lieskovan S, et al. Genomic and transcriptomic features of response to anti-PD-1 therapy in metastatic melanoma. *Cell* (2017) 168:3. doi: 10.1016/j.cell.2017.01.010

68. Orgaz JL, Crosas-Molist E, Sadok A, Perdrix-Rosell A, Maiques O, Rodriguez-Hernandez I, et al. Myosin II reactivation and cytoskeletal remodeling as a hallmark and a vulnerability in melanoma therapy resistance. *Cancer Cell* (2020) 37:1. doi: 10.1016/j.ccell.2019.12.003

69. Smith MP, Rana S, Ferguson J, Rowling EJ, Flaherty KT, Wargo JA, et al. A PAX3/BRN2 rheostat controls the dynamics of BRAF mediated MITF regulation in MITFhigh/AXLlow melanoma. *Pigment Cell Melanoma Res* (2019) 32:2. doi: 10.1111/pcmr.12741

70. Shen S, Faouzi S, Bastide A, Martineau S, Malka-Mahieu H, Fu Y, et al. An epitranscriptomic mechanism underlies selective mRNA translation remodelling in melanoma persister cells. *Nat Commun* (2019) 10:1. doi: 10.1038/s41467-019-13360-6

71. Marin-Bejar O, Rogiers A, Dewaele M, Femel J, Karras P, Pozniak J, et al. Evolutionary predictability of genetic versus nongenetic resistance to anticancer drugs in melanoma. *Cancer Cell* (2021) 39:8. doi: 10.1016/j.ccell.2021.05.015

72. Sahai E, Astsaturov I, Cukierman E, DeNardo DG, Egeblad M, Evans RM, et al. A framework for advancing our understanding of cancer-associated fibroblasts. *Nat Rev Cancer* (2020) 20:3. doi: 10.1038/s41568-019-0238-1

73. Calvo F, Ege N, Grande-Garcia A, Hooper S, Jenkins RP, Chaudhry SI, et al. Mechanotransduction and YAP-dependent matrix remodelling is required for the generation and maintenance of cancer-associated fibroblasts. *Nat Cell Biol* (2013) 15:6. doi: 10.1038/ncb2756

74. Liu T, Zhou L, Li D, Andl T, Zhang Y. Cancer-associated fibroblasts build and secure the tumor microenvironment. *Front Cell Dev Biol* (2019) 7:60. doi: 10.3389/fcell.2019.00060

75. Kuzet SE, Gaggioli C. Fibroblast activation in cancer: when seed fertilizes soil. *Cell Tissue Res* (2016) 365:3. doi: 10.1007/s00441-016-2467-x

76. Ganguly D, Chandra R, Karalis J, Teke M, Aguilera T, Maddipati R, et al. Cancer-associated fibroblasts: Versatile players in the tumor microenvironment. *Cancers* (2020) 12:9. doi: 10.3390/cancers12092652

77. Kalluri R, Zeisberg M. Fibroblasts in cancer. *Nat Rev Cancer* (2006) 6:5. doi: 10.1038/nrc1877

78. Mhaidly R, Mechta-Grigoriou F. Fibroblast heterogeneity in tumor micro-environment: Role in immunosuppression and new therapies. *Semin Immunol* (2020) 48:4. doi: 10.1016/j.smim.2020.101417

79. Costa A, Kieffer Y, Scholer-Dahirel A, Pelon F, Bourachot B, Cardon M, et al. Fibroblast heterogeneity and immunosuppressive environment in human breast cancer. *Cancer Cell* (2018) 33:3. doi: 10.1016/j.ccell.2018.01.011

80. Givel AM, Kieffer Y, Scholer-Dahirel A, Sirven P, Cardon M, Pelon F, et al. MiR200-regulated CXCL12β promotes fibroblast heterogeneity and immunosuppression in ovarian cancers. *Nat Commun* (2018) 9:1. doi: 10.1038/s41467-018-03348-z

81. Kieffer Y, Hocine HR, Gentric G, Pelon F, Bernard C, Bourachot B, et al. Single-cell analysis reveals fibroblast clusters linked to immunotherapy resistance in cancer. *Cancer Discovery* (2020) 10:9. doi: 10.1158/2159-8290.CD-19-1384

82. Öhlund D, Handly-Santana A, Biffi G, Elyada E, Almeida AS, Ponz-Sarvise M, et al. Distinct populations of inflammatory fibroblasts and myofibroblasts in pancreatic cancer. *J Exp Med* (2017) 214:3. doi: 10.1084/jem.20162024

83. Pelon F, Bourachot B, Kieffer Y, Magagna I, Mermet-Meillon F, Bonnet I, et al. Cancer-associated fibroblast heterogeneity in axillary lymph nodes drives metastases in breast cancer through complementary mechanisms. *Nat Commun* (2020) 11:1. doi: 10.1038/s41467-019-14134-w

84. Bonneau C, Eliès A, Kieffer Y, Bourachot B, Ladoire S, Pelon F, et al. A subset of activated fibroblasts is associated with distant relapse in early luminal breast cancer. *Breast Cancer Res* (2020) 22:1. doi: 10.1186/s13058-020-01311-9

85. Romano V, Belviso I, Venuta A, Ruocco MR, Masone S, Aliotta F, et al. Influence of tumor microenvironment and fibroblast population plasticity on melanoma growth, therapy resistance and immunoescape. *Int J Mol Sci* (2021) 22:10. doi: 10.3390/ijms22105283

86. Kaur A, Ecker BL, Douglass SM, Kugel CH, Webster MR, Almeida FV, et al. Remodeling of the collagen matrix in aging skin promotes melanoma metastasis and affects immune cell motility. *Cancer Discovery* (2019) 9:1. doi: 10.1158/2159-8290.CD-18-0193

87. Goetz JG, Minguet S, Navarro-Lérida I, Lazcano JJ, Samaniego R, Calvo E, et al. Biomechanical remodeling of the microenvironment by stromal caveolin-1 favors tumor invasion and metastasis. *Cell* (2011) .146:1. doi: 10.1016/j.cell.2011.05.040

88. Hirata E, Girotti MR, Viros A, Hooper S, Spencer-Dene B, Matsuda M, et al. Intravital imaging reveals how BRAF inhibition generates drug-tolerant microenvironments with high integrin β1/FAK signaling. *Cancer Cell* (2015) 27:4. doi: 10.1016/j.ccell.2015.03.008

89. Hutchenreuther J, Leask A. Why target the tumor stroma in melanoma? *Cell Commun Signal* (2018) 12:1. doi: 10.1007/s12079-017-0419-1

90. Miskolczi Z, Smith MP, Rowling EJ, Ferguson J, Barriuso J, Wellbrock C. Collagen abundance controls melanoma phenotypes through lineage-specific microenvironment sensing. *Oncogene* (2018) 7:23. doi: 10.1038/s41388-018-0209-0

91. Gilkes DM, Semenza GL, Wirtz D. Hypoxia and the extracellular matrix: drivers of tumour metastasis. *Nat Rev Cancer* (2014) 4:6. doi: 10.1038/nrc3726

92. Bertero T, Gaggioli C. Mechanical forces rewire metabolism in the tumor niche. *Mol Cell Oncol* (2019) 6:3. doi: 10.1080/23723556.2019.1592945

93. Romani P, Valcarcel-Jimenez L, Frezza C, Dupont S. Crosstalk between mechanotransduction and metabolism. *Nat Rev Mol Cell Biol* (2020) 22:1. doi: 10.1038/s41580-020-00306-w

94. Riedel A, Shorthouse D, Haas L, Hall BA, Shields J. Tumor induced stromal reprogramming drives lymph node transformation. *Nat Immunol* (2016) 17:9. doi: 10.1038/ni.3492

95. Rovera C, Berestjuk I, Lecacheur M, Tavernier C, Diazzi S, Pisano S, et al. Secretion of interleukin-1 by dedifferentiated melanoma cells inhibits JAK1-STAT3-driven actomyosin contractility of lymph node fibroblastic reticular cells. *Cancer Res* (2022) 82:9. doi: 10.1158/0008-5472.CAN-21-0501

96. Pickup MW, Mouw JK, Weaver VM. The extracellular matrix modulates the hallmarks of cancer. *EMBO Rep* (2014) 15:12. doi: 10.15252/embr.201439246

97. Winkler J, Abisoye-Ogunniyan A, Metcalf KJ, Werb Z. Concepts of extracellular matrix remodelling in tumour progression and metastasis. *Nat Commun* (2020) 11:1. doi: 10.1038/s41467-020-18794-x

98. Socovich AM, Naba A. The cancer matrisome: From comprehensive characterization to biomarker discovery. *Semin Cell Dev Biol* (2019) 89:5. doi: 10.1016/j.semcdb.2018.06.005

99. Hynes RO, Naba A. Overview of the matrisome-an inventory of extracellular matrix constituents and functions. *Perspect Biol* (2012) 4:1. doi: 10.1101/cshperspect.a004903

100. Wu L, Zhu Y. The function and mechanisms of action of LOXL2 in cancer. *Int J Mol Med* (2015) 36:5. doi: 10.3892/ijmm.2015.2337

101. Frantz C, Stewart KM, Weaver VM. The extracellular matrix at a glance. *J Cell Sci* (2010) 123:24. doi: 10.1242/jcs.023820

102. Kai FB, Drain AP, Weaver VM. The extracellular matrix modulates the metastatic journey. *Dev Cell* (2019) 49:3. doi: 10.1016/j.devcel.2019.03.026

103. Leight JL, Drain AP, Weaver VM. Extracellular matrix remodeling and stiffening modulate tumor phenotype and treatment response. *Annu Rev Cancer Biol* (2017) 1:1. doi: 10.1146/annurev-cancerbio-050216-034431

104. Kramer RH, Marks N. Identification of integrin collagen receptors on human melanoma cells. *J Biol Chem* (1989) 8:4684–8.

105. Chelberg MK, McCarthy JB, Skubitz APN, Furcht LT, Tsilibary EC. Characterization of a synthetic peptide from type IV collagen that promotes melanoma cell adhesion, spreading, and motility. *J Cell Biol* (1990) 1:261–70. doi: 10.1083/jcb.111.1.261

106. Pfaff M, Aumailley M, Specks U, Knolle J, Zerwes HG, Timpl R. Integrin and arg-Gly-Asp dependence of cell adhesion to the native and unfolded triple helix of collagen type VI. *Exp Cell Res* (1993) 1:167–76. doi: 10.1006/excr.1993.1134

107. Pasco S, Brassart B, Ramont L, Maquart FX, Monboisse JC. Control of melanoma cell invasion by type IV collagen. *Cancer Detect Prev* (2005) 29:3. doi: 10.1016/j.cdp.2004.09.003

108. Etoh T, Beyers HR, Mihm MC. Integrin expression in malignant melanoma and their role in cell attachment and migration on extracellular matrix proteins. *J Dermatol* (1992) 11:841–6. doi: 10.1111/j.1346-8138.1992.tb03794.x

109. Li C, McCarthy JB, Furcht LT, Fields GB. An all-d amino acid peptide model of α1(IV)531-543 from type IV collagen binds the α3β1 integrin and mediates tumor cell adhesion, spreading, and motility. *Biochemistry* (1997) 49:15404–10. doi: 10.1021/bi971817g

110. Kramer RH, Vu M, Cheng YF, Ramos DM. Integrin expression in malignant melanoma. *Cancer Metastasis Rev* (1991) 1:49–59. doi: 10.1007/BF00046843

111. Romayor I, Badiola I, Olaso E. Inhibition of DDR1 reduces invasive features of human A375 melanoma, HT29 colon carcinoma and SK-HEP hepatoma cells. *Cell Adh Migr* (2020) 14:1. doi: 10.1080/19336918.2020.1733892

112. Poudel B, Lee YM, Kim DK. DDR2 inhibition reduces migration and invasion of murine metastatic melanoma cells by suppressing MMP2/9 expression through ERK/NF-κB pathway. *Acta Biochim Biophys Sin* (2015) 47:4. doi: 10.1093/abbs/gmv005

113. Reger de Moura C, Battistella M, Sohail A, Caudron A, Feugeas JP, Podgorniak MP, et al. Discoidin domain receptors: A promising target in melanoma. *Pigment Cell Melanoma Res* (2019) 32:5. doi: 10.1111/pcmr.12809

114. Ray A, Morford RK, Ghaderi N, Odde DJ, Provenzano PP. Dynamics of 3D carcinoma cell invasion into aligned collagen. *Integr Biol* (2018) 10:2. doi: 10.1039/c7ib00152e

115. Xie R, Li B, Jia L, Li Y. Identification of core genes and pathways in melanoma metastasis *via* bioinformatics analysis. *Int J Mol Sci* (2022) 23:2. doi: 10.3390/ijms23020794

116. Erdogan B, Ao M, White LM, Means AL, Brewer BM, Yang L, et al. Cancer-associated fibroblasts promote directional cancer cell migration by aligning fibronectin. *J Cell Biol* (2017) 216:11. doi: 10.1042/BST20160387

117. Su S, Chen J, Yao H, Liu J, Yu S, Lao L, et al. CD10+GPR77+ cancer-associated fibroblasts promote cancer formation and chemoresistance by sustaining cancer stemness. *Cell* (2018) 172:4. doi: 10.1016/j.cell.2018.01.009

118. Ahmadzadeh H, Webster MR, Behera R, Valencia AMJ, Wirtz D, Weeraratna AT, et al. Modeling the two-way feedback between contractility and matrix realignment reveals a nonlinear mode of cancer cell invasion. *Proc Natl Acad Sci* (2017) 114:9. doi: 10.1073/pnas.1617037114

119. Lee HO, Mullins SR, Franco-Barraza J, Valianou M, Cukierman E, Cheng JD. FAP-overexpressing fibroblasts produce an extracellular matrix that enhances invasive velocity and directionality of pancreatic cancer cells. *BMC Cancer* (2011) 11:1. doi: 10.1186/1471-2407-11-245

120. Kwon Y, Cukierman E, Godwin AK. Differential expressions of adhesive molecules and proteases define mechanisms of ovarian tumor cell matrix Penetration/Invasion. *PloS One* (2011) 6:4. doi: 10.1371/journal.pone.0018872

121. Acerbi I, Cassereau L, Dean I, Shi Q, Au A, Park C, et al. Human breast cancer invasion and aggression correlates with ECM stiffening and immune cell infiltration. *Integr Biol* (2015) 7:10. doi: 10.1039/c5ib00040h

122. Berger AJ, Renner CM, Hale I, Yang X, Ponik SM, Weisman PS, et al. Scaffold stiffness influences breast cancer cell invasion *via* EGFR-linked mena upregulation and matrix remodeling. *Matrix Biol* (2020) 85:1. doi: 10.1016/j.matbio.2019.07.006

123. Koorman T, Jansen KA, Khalil A, Haughton PD, Visser D, Rätze MAK, et al. Spatial collagen stiffening promotes collective breast cancer cell invasion by reinforcing extracellular matrix alignment. *Oncogene* (2022) 41(17):2458–69. doi: 10.1038/s41388-022-02258-1

124. Rathore M, Girard C, Ohanna M, Tichet M, Ben Jouira R, Garcia E, et al. Cancer cell-derived long pentraxin 3 (PTX3) promotes melanoma migration through a toll-like receptor 4 (TLR4)/NF-κB signaling pathway. *Oncogene* (2019) 38:30. doi: 10.1038/s41388-019-0848-9

125. Kaushik S, Pickup MW, Weaver VM. From transformation to metastasis: deconstructing the extracellular matrix in breast cancer. *Cancer Metastasis Rev* (2016) 35:4. doi: 10.1007/S10555-016-9650-0

126. Pfisterer K, Shaw LE, Symmank D, Weninger W. The extracellular matrix in skin inflammation and infection. *Front Cell Dev Biol* (2021) 9:682414. doi: 10.3389/fcell.2021.682414

127. Berestjuk I, Lecacheur M, Carminati A, Diazzi S, Rovera C, Prod'homme V, et al. Targeting discoidin domain receptors DDR1 and DDR2 overcomes matrix-mediated tumor cell adaptation and tolerance to BRAF-targeted therapy in melanoma. *EMBO Mol Med* (2022) 14:2. doi: 10.15252/emmm.201911814

128. Marusak C, Thakur V, Li Y, Freitas JT, Zmina PM, Thakur VS, et al. Targeting extracellular matrix remodeling restores BRAF inhibitor sensitivity in BRAFi resistant melanoma. *Clin Cancer Res* (2020) 26:22. doi: 10.1158/1078-0432.CCR-19-2773

129. Özdemir BC, Pentcheva-Hoang T, Carstens JL, Zheng X, Wu CC, Simpson TR, et al. Depletion of carcinoma-associated fibroblasts and fibrosis induces immunosuppression and accelerates pancreas cancer with reduced survival. *Cancer Cell* (2014) 25:6. doi: 10.1016/j.ccr.2014.04.005

130. Biffi G, Oni TE, Spielman B, Hao Y, Elyada E, Park Y, et al. Il1-induced Jak/STAT signaling is antagonized by TGFβ to shape CAF heterogeneity in pancreatic ductal adenocarcinoma. *Cancer Discovery* (2019) 9:2. doi: 10.1158/2159-8290.CD-18-0710

131. Albrengues J, Bourget I, Pons C, Butet V, Hofman P, Tartare-Deckert S, et al. LIF mediates proinvasive activation of stromal fibroblasts in cancer. *Cell Rep* (2014) 7:5. doi: 10.1016/j.celrep.2014.04.036

132. Abyaneh HS, Regenold M, McKee TD, Allen C, Gauthier MA. Towards extracellular matrix normalization for improved treatment of solid tumors. *Theranostics* (2020) 10:4. doi: 10.7150/thno.39995

133. Zheng J, Gao P. Toward normalization of the tumor microenvironment for cancer therapy. *Integr Cancer Ther* (2019) 18. doi: 10.1177/1534735419862352

134. Dong L, Lin F, Wu W, Liu Y, Huang W. Verteporfin inhibits YAP-induced bladder cancer cell growth and invasion *via* hippo signaling pathway. *Int J Med Sci* (2018) 15:6. doi: 10.7150/ijms.23460

135. Olsson PO, Gustafsson R, In't Zandt R, Friman T, Maccarana M, Tykesson E, et al. The tyrosine kinase inhibitor imatinib augments extracellular fluid exchange and reduces average collagen fibril diameter in experimental carcinoma. *Mol Cancer Ther* (2016) 15:10. doi: 10.1158/1535-7163.MCT-16-0026

136. Janjanam J, Pano G, Wang R, Minden-Birkenmaier BA, Breeze-Jones H, Baker E, et al. Matricellular protein WISP2 is an endogenous inhibitor of collagen linearization and cancer metastasis. *Cancer Res* (2021) 81:22. doi: 10.1158/0008-5472.CAN-20-3982

137. Tu MM, Lee FYF, Jones RT, Kimball AK, Saravia E, Graziano RF, et al. Targeting DDR2 enhances tumor response to anti–PD-1 immunotherapy. *Sci Adv* (2019) 5:2. doi: 10.1126/sciadv.aav2437

138. Nicolas-Boluda A, Vaquero J, Vimeux L, Guilbert T, Barrin S, Kantari-Mimoun C, et al. Tumor stiffening reversion through collagen crosslinking inhibition improves T cell migration and anti-PD-1 treatment. *elife* (2021) 10. doi: 10.7554/eLife.58688

139. Kato R, Haratani K, Hayashi H, Sakai K, Sakai H, Kawakami H, et al. Nintedanib promotes antitumour immunity and shows antitumour activity in combination with PD-1 blockade in mice: potential role of cancer-associated fibroblasts. *Br J Cancer* (2021) 124:5. doi: 10.1038/s41416-020-01201-z

140. Guan X, Lin L, Chen J, Hu Y, Sun P, Tian H, et al. Efficient PD-L1 gene silence promoted by hyaluronidase for cancer immunotherapy. *J Control Release* (2019) 293:104–12. doi: 10.1016/j.jconrel.2018.11.022

141. Mason LD, Chava S, Reddi KK, Gupta R. The BRD9/7 inhibitor TP-472 blocks melanoma tumor growth by suppressing ECM-mediated oncogenic signaling and inducing apoptosis. *Cancers* (2021) 13:21. doi: 10.3390/cancers13215516

142. Fejza A, Polano M, Camicia L, Poletto E, Carobolante G, Toffoli G, et al. The efficacy of anti-PD-L1 treatment in melanoma is associated with the expression of the ECM molecule EMILIN2. *Int J Mol Sci* (2021) 22:14. doi: 10.3390/ijms22147511

143. Jensen C, Madsen DH, Hansen M, Schmidt H, Svane IM, Karsdal MA, et al. Non-invasive biomarkers derived from the extracellular matrix associate with response to immune checkpoint blockade (anti-CTLA-4) in metastatic melanoma patients. *J Immunother Cancer* (2018) 6:1. doi: 10.1186/s40425-018-0474-z

Glossary

ACD	Adrenocortical dysplasia protein homolog
AhR	Aryl hydrocarbon receptor
AJCC	American Joint Committee on Cancer
AKT	Protein kinase B
AP-1	Activator protein 1
AXL	AXL receptor tyrosine kinase
BAP1	ubiquitin carboxyl-terminal hydrolase BAP1
BRAF	B-Raf proto-oncogene
BRN2	POU domain
class 3	transcription factor 2
CAFs	Cancer associated fibroblasts
CCND1	Cyclin D1
CDK4	Cyclin-dependent kinase 4
iCAFs	Inflammatory cancer associated fibroblasts
myCAFs	Myofibroblast cancer associated fibroblasts
CD29	$\beta_1$integrin
CDKN2A	Cyclin Dependent Kinase Inhibitor 2A
CTLA-4	Cytotoxic T-lymphocyte-associated protein 4
DDRs	Discoidin domain receptors
ECM	Extracellular matrix
EDA	Extra domain
EMILIN-2	Elastin microfibril interface-located protein 2
EMT	Epithelial to mesenchymal transition
ERK	Extracellular signal-regulated kinase
FAK	Focal adhesion kinases
FAPα	Fibroblast activation protein-α
FDA	Food and Drug Administration
GAS6	Gamma-carboxyglutamic acid (Gla)-containing protein
IKKα	IkB kinase α
LOX	Lysyl oxidase
MAFs	Melanoma associated fibroblasts
MAPK	Mitogen-activated protein kinase
MEK	Mitogen-activated protein kinase kinase
MC1R	Melanocortin 1 Receptor
miRNA	MicroRNA
MITF	Melanocyte inducing transcription factor
MMPs	Matrix metalloproteinases
MRD	Minimum residual disease
MRTF	Myocardin-related transcription factor A
NCSC	Neural crest stem cell
NF-1	Neurofibromin 1
NF-kB2	Nuclear factor kappa B subunit 2
NIK	NF-k-B-inducing kinase
NRAS	NRAS Proto-Oncogene GTPase
PAX3	Paired box gene 3
PDAC	Pancreatic ductal adenocarcinoma
PDGFRβ	Platelet derived growth factor receptor-β
PD-1	Programmed cell death protein 1
PD-L1	Programmed death-ligand 1
PDX	Patient derived xenograft
POT1	Protection of telomeres 1
PTEN	Phosphatase and tensin homolog
RGP	Radial Growth Phase αSMA α smooth muscle actin
SOX9/SOX10	SRY-Box Transcription Factor 9/10
SPARC	Secreted protein acidic and cysteine rich
S100A4	Fibroblast specific protein 1
TAZ	Transcriptional coactivator with PDZ-binding motif
TEAD	TEA domain transcription factor 1
TERF2IP	Telomeric repeat-binding factor 2-interacting protein 1
TERT	Telomerase reverse transcriptase
TNM	tumor
nodes	and metastases
TME	Tumor microenvironment
VGP	Vertical growth phase
YAP	Yes-associated protein

frontiers | Frontiers in Oncology

TYPE Original Research
PUBLISHED 21 September 2022
DOI 10.3389/fonc.2022.890825

OPEN ACCESS

EDITED BY
Deilson Elgui De Oliveira,
São Paulo State University, Brazil

REVIEWED BY
Tadashi Watanabe,
University of the Ryukyus, Japan
Alexander Hahn,
Deutsches Primatenzentrum, Germany

*CORRESPONDENCE
Omar Coso
omar.coso@gmail.com

SPECIALTY SECTION
This article was submitted to Molecular and Cellular Oncology, a section of the journal Frontiers in Oncology

RECEIVED 06 March 2022
ACCEPTED 31 August 2022
PUBLISHED 21 September 2022

CITATION
Sapochnik D, Raimondi AR, Medina V, Naipauer J, Mesri EA and Coso O (2022) A major role for Nrf2 transcription factors in cell transformation by KSHV encoded oncogenes. *Front. Oncol.* 12:890825. doi: 10.3389/fonc.2022.890825

A major role for Nrf2 transcription factors in cell transformation by KSHV encoded oncogenes

Daiana Sapochnik[1,2], Ana R. Raimondi[1,3], Victoria Medina[1,3], Julian Naipauer[1,3,4], Enrique A. Mesri[3,4] and Omar Coso[1,2,3]*

[1]CONICET-Universidad de Buenos Aires, Instituto de Fisiología, Biología Molecular y Neurociencias (IFIBYNE), Buenos Aires, Argentina, [2]Departamento de Fisiología, Biología Molecular y Celular, Universidad de Buenos Aires, Facultad de Ciencias Exactas y Naturales, Buenos Aires, Argentina, [3]University of Miami- Center for AIDS Research (UM-CFAR)/Sylvester Comprehensive Cancer Center (CCC) Argentina Consortium for Research and Training in Virally Induced AIDS-Malignancies, University of Miami Miller School of Medicine, Miami, FL, United States, [4]Viral Oncology Program, Sylvester Comprehensive Cancer Center, Miami Center for AIDS Research, Department of Microbiology & Immunology, University of Miami, Miami, FL, United States

Kaposi's sarcoma (KS) is the most common tumor in AIDS patients. The highly vascularized patient's skin lesions are composed of cells derived from the endothelial tissue transformed by the KSHV virus. Heme oxygenase-1 (HO-1) is an enzyme upregulated by the Kaposi´s sarcoma-associated herpesvirus (KSHV) and highly expressed in human Kaposi Sarcoma (KS) lesions. The oncogenic G protein-coupled receptor (KSHV-GPCR or vGPCR) is expressed by the viral genome in infected cells. It is involved in KS development, HO-1 expression, and vascular endothelial growth factor (VEGF) expression. vGPCR induces HO-1 expression and HO-1 dependent transformation through the Ga13 subunit of heterotrimeric G proteins and the small GTPase RhoA. We have found several lines of evidence supporting a role for Nrf2 transcription factors and family members in the vGPCR-Ga13-RhoA signaling pathway that converges on the HO-1 gene promoter. Our current information assigns a major role to ERK1/2MAPK pathways as intermediates in signaling from vGPCR to Nrf2, influencing Nrf2 translocation to the cell nucleus, Nrf2 transactivation activity, and consequently HO-1 expression. Experiments in nude mice show that the tumorigenic effect of vGPCR is dependent on Nrf2. In the context of a complete KSHV genome, we show that the lack of vGPCR increased cytoplasmic localization of Nrf2 correlated with a downregulation of HO-1 expression. Moreover, we also found an increase in phospho-Nrf2 nuclear localization in mouse KS-like KSHV (positive) tumors compared to KSHV (negative) mouse KS-like tumors. Our data highlights the fundamental role of Nrf2 linking vGPCR signaling to the HO-1 promoter, acting upon not only HO-1 gene expression regulation but also in the tumorigenesis induced by vGPCR. Overall, these data pinpoint this transcription factor or its associated proteins as putative pharmacological or therapeutic targets in KS.

KEYWORDS
Nrf2, HO-1 (heme oxygenase-1), gene expression regulation, KSHV-vGPCR, signal transduction

Introduction

Exposure of cells to environmental toxicants and potential carcinogens has been linked to pathologic processes, including neurodegenerative and cardiovascular diseases, as well as to cancers (1). Eukaryotic cells have developed complex responses to detoxify potentially harmful substances and maintain cellular redox homeostasis in which different signaling cascades participate. The response involves the induction of cytoprotective and detoxifying enzymes consisting of phase I (cytochrome P450s) and phase II (detoxifying and antioxidant proteins) enzymes (2). The expression of these genes attempts to restore the cell to a basal state, preventing damage to cellular components sensitive to redox changes (i.e., proteins, lipids, and DNA) (3). One such enzyme is Heme oxygenase-1 (HO-1), an inducible and ubiquitous 32-kDa enzyme that regulates heme metabolism and iron levels by catalyzing the degradation of the heme group. The products of this enzymatic reaction are carbon monoxide, free iron, and biliverdin. This final product is subsequently reduced to the antioxidant bilirubin (4). HO-1 activity can be regulated at different levels, but it depends primarily on the control of HO-1 expression at the transcriptional level (4–6). A variety of stress-inducing stimuli, antioxidants, growth factors, and hormones can induce HO-1 expression (7–10). HO-1 has been considered a cytoprotective molecule because of heme metabolism products' antioxidant properties. It has been involved in several physiological responses against oxidative and cellular stress and inflammation (5). However, several studies have now expanded this notion and defined HO-1 as an important regulator of the physiology of the vasculature, vascular endothelial growth factor (VEGF) secretion, endothelial cell cycle control, proliferation, angiogenesis, and tumorigenesis (6, 11–14).

The transcriptional regulation of HO-1 is mainly controlled by Nrf2, a transcription factor of the leucine zipper-type, a cap'n'collar bZip protein ubiquitously expressed and responsible for the basal and inducible expression of proteins involved in the oxidative stress response, drug metabolism, cytoprotection, apoptosis, differentiation, proliferation, and growth (15). Nrf2 undergoes spatial-temporal regulation switched on and off by tightly regulated mechanisms. Proteasomal degradation regulates the cell's response to inflammatory, hypoxic, oxidative, and xenobiotic stimuli. In unstressed conditions or resting cells, the level of Nrf2 protein is maintained at very low levels by its inhibitor Keap1 which sequesters Nrf2 in the cytosol and facilitates its degradation *via* the proteasome. Several mechanisms by which Nrf2 can be regulated independently of Keap1 were described (16, 17). In the presence of Nrf2 inducers, Nrf2 is liberated from Keap, translocates to the nucleus, and forms a heterodimer with small masculoaponeurotic fibrosarcoma (Maf) binding to the Antioxidant Response Element (ARE), a cis-acting enhancer sequence (TCAG/CXXXGC) (15, 18, 19). The genes that are Nrf2-regulated can be classified into phase II enzymes, antioxidants, molecular chaperones, DNA repair enzymes, and anti-inflammatory response proteins (20). Importantly, the Nrf2 promoter displays an ARE sequence within its promoter region to initiate its transcription further enhancing the adaptive cell defense response (15). Nrf2 seems to play a dual role in cancer, potentially acting as both a tumor suppressor and an oncogenic factor. Raised Nrf2 levels have been detected in an array of cancer tissues including lung (21, 22) and pancreas (23, 24). It is proposed that this provides cells with enhanced chemo-resistance as well as supports increased proliferation thus promoting cancer growth and development (23). Nrf2-deficient mice are more susceptible to toxicity by compounds such as paracetamol and tobacco smoke and too many diseases. Interestingly, Nrf2 $^{-/-}$ mice do survive and can procreate which suggests that Nrf2 is not necessarily vital for survival in unstressed cells and is only called upon in the presence of stress or insult (25). However, Nrf2 plays a major role in health and disease and therefore is a potential therapeutic target. This fact highlights the need to understand and determine whether gene expression regulation of Nrf2 would be beneficial in both the short and long-term and its intermediate signaling mediators.

The most frequent type of tumor in AIDS patients is Kaposi sarcoma (KS), formed by spindle cells derived from endothelial cells transformed by KSHV (26, 27). The product of orf 74 in the KSHV genome is a constitutively active G protein-coupled receptor (vGPCR) that plays an important role in the development of KSHV-induced oncogenesis (26, 28–31). Only a few cells in KS-like lesions express vGPCR (28), however, down-regulation of the receptor in these cells results in a decreased expression of angiogenic factors and tumor regression (32, 33). vGPCR is homologous to the mammalian interleukin-8 receptor. A mutation confers vGPCR its constitutive, ligand-independent activity (34–36). It has been shown that the expression of vGPCR in fibroblasts induces transformation, angiogenesis in endothelial cells (EC), and angioproliferative KS-like

lesions in mice (28, 31, 37). HO-1 expression is induced during KSHV infection of human dermal microvascular endothelial cells (DMVEC) and is highly expressed in biopsy tissues from oral AIDS-Kaposi sarcoma lesions (38). Moreover, KSHV induction of HO-1 in lymphatic EC (LEC) occurs in two distinct phases, a transient phase upon acute infection and a sustained phase coincident with the establishment of viral latency (39). Previous work from our laboratory and collaborators shows that vGPCR induces HO-1 mRNA and protein levels in fibroblasts and endothelial cells and that these facts correlate with increased cell proliferation, survival, and VEGF-A expression, one of the determinant events in KS development. Inhibition of HO-1 expression or activity impairs the tumorigenesis induced by vGPCR in allograft tumor animal models (40). Several studies show that vGPCR contributes to KS development by switching on a complex network of signaling pathways (29, 41). vGPCR activates downstream effectors by coupling to different subunits of heterotrimeric G proteins (42–44). We have shown that the expression of both Ga12 and Ga13 subunits mimicked vGPCR-induced HO-1 expression and transformation through the small GTPase RhoA. Reduced expression of RhoA impairs vGPCR-induced VEGF expression and secretion, cell survival and proliferation, and transformation both in cell culture and in a murine allograft tumor model (40, 45). Despite the implication of HO-1 as a vGPCR downstream target, the nature of the molecular pathways connecting the receptor to HO-1 expression regulation remains unknown.

Previous reports have shown that KSHV *de novo* infection of HMVEC-d requires ROS for Nrf2 activation during the early stages of infection and establishment of latency and observed activated Nrf2 levels in KSHV positive KS and Primary Effusion Lymphoma (PEL) lesion cells (46). Moreover, two simultaneous Nrf2 activation pathways necessary for the sustained expression of the Nrf2 target gene have been shown to occur in KSHV-infected long-term-infected telomerase-immortalized endothelial (TIVE-LTC) cells (47).

In this study, using a combination of biological models that include cells transformed by vGPCR in culture, tumors in mice, and KSHV full genome-bearing cells, including KSHV-Bac16 based mutant system with vGPCR deletion, we have shown that the effect of vGPCR signaling on HO-1 expression and tumorigenesis is mediated by ARE sites and its associated transcription factor Nrf2. Moreover, vGPCR not only affects the transcriptional activation of Nrf2 but also induces Nrf2 nuclear translocation. Nrf2 transcriptional activity and nuclear translocation are mainly mediated by vGPCR-induced activation of the Gα12/13-RhoA-ERK1/2 signaling pathway.

Experimental procedures

DNA constructs

The plasmid pHO-1-Luc was provided by J. Alam and contained a 15- kb murine HO-1 promoter upstream of a luciferase gene (reporter gene vector pSK-luc) as described previously (48). pCEFL-AU5-vGPCR was constructed in Dr. Gutkind's laboratory introducing vGPCR cDNA as a Bgl2/Not1 fragment in pCEFLAU5 (28). The reporter construct pGL3_Nrf2-3xARE-Luc (minimum promoter containing three ARE sites in tandem, T/CGCTGAGTCA) was a gift of M. Marinissen, and the pG5 Luc (minimum promoter containing 5 sites for GAL4 binding) was purchased from Promega. The expression plasmid for Nrf2 WT, pCDNA3 His B – V5 Nrf2 (Wild Type), was a kind gift from M. McMahon y J. Hayes and previously described (49). Briefly, the PCR amplification of the murine Nrf2 coding sequence and 50 nucleotides of the 5′-untranslated region was ligated into EcoRV-digested pcDNA3.1/V5HisB (Invitrogen), allowing expression of mNrf2-V5-his fusion protein from a CMV promoter. The expression plasmid for Nrf2 Dominant Negative (Nrf2 DN) (reporter gene vector pEF) was provided by J. Alam and described previously (48). The expression plasmids pCDNA3_Gα12-QL and pCEFL_HA_Gα13-QL were obtained by cloning the constitutively active forms of both cDNAs and cloned as Bgl2/Not1 fragments into pCDNA3 and pCEFL-HA, respectively. pCEFL_AU5_RhoA-QL and pCEFL_Rho-N19 Dominant Negative were cloned as BamH1/EcoR1 fragments and introduced in the respective vectors in Dr. Gutkind's laboratory who provided them as a gift (40, 50, 51). The expression vectors for the MEKs were previously described (52).

Cell lines and transfections

NIH3T3 fibroblasts were received from Dr. S. Gutkind's laboratory and maintained in Dulbecco's modified Eagle's medium (DMEM) (Invitrogen) supplemented with 10% calf serum. Stable transfections of NIH3T3 for vGPCR were received from Dr. S. Gutkind's laboratory and described previously (40). Stable transfections of NIH3T3_vGPCR for different shRNAs were performed using the Lipofectamine Plus Reagent (Invitrogen). NIH3T3_vGPCR cells were plated at 60% confluence in 10 cm plates and transfected with 2ug of shRNA (shScramble and shRNAs targeted against Nrf2 - GIPZ Nfe2l2 shRNA Thermo RMM4532-EG18024). Transfected cells were selected with 750 ug/ml G418 (Promega Corp., Madrid, Spain) and 0.4ug/ml Puromycin (Invitrogen). mECs were obtained from Balb/C mice (NCI, Bethesda, MD) as previously described (33). By transfection with KSHVBac36, the vector containing the insert with the genome of KSHV in Bacterial Artificial Chromosome (KSHVBac36), mECK36 cells were generated. mECKnull is a variant of the latter that lost the plasmid and was subsequently used as the source for the generation of mECK16-delta-Revertant or mECK16-delta–vGPCR cell lines, which express reinstalled KSHV genomes in its complete or devoid of vGPCR versions, respectively (53).

Luciferase reporter assays

Cells were transfected with different expression plasmids together with 1ug of the indicated reporter plasmid per well in 6-well plates. In all cases, the total amount of plasmid DNA was adjusted with pcDNA3 empty and 0.2ug of pCDNA3-b-galactosidase. *Firefly* luciferase activity in cellular lysates was assayed using the luciferase reporter system catalog number E1500 (Promega Corp.), and light emission was quantified using a luminometer (Junior Berlthold). To study transcriptional activation domains of transcription factors, we used the Luciferase GAL4 reporter system, where a Gal4 DBD – Nrf2 TAD vector expresses a fusion protein containing the DNA binding domain of GAL4 and the transactivation domain of Nrf2, is co-transfected with the pG5 Luc. When co-transfected in the same cell, these two constructs allow for the assessment of the regulation of gene expression by signal transduction pathways that impinge on the transcription factor Nrf2 using luciferase as a reporter gene. All assays were performed in three biological replicates and measured in triplicates for quantification.

RT-qPCR

Total cellular RNA was isolated using TRIReagent (Genbiotech-MRC) using the manufacturer's protocols. RNA concentration was measured by Nanodrop™ (Thermo Fisher), and 2ug of RNA was treated with RNase-free DNase I (Invitrogen). DNase treatment was performed for 15 min at room temperature, followed by EDTA treatment for 10 minutes at 65 ° to stop the DNase. After DNase treatment, the samples were incubated for 5 minutes at 65 ° in the presence of 500ng OligodT (Genbiotech). cDNA synthesis was performed using MMLV (Moloney murine leukemia virus) reverse transcriptase (RT) (Promega) with RNaseOUT (Invitrogen) for 50 minutes at 37°. qPCR was performed using 1ul of cDNA in a BioRad CFX96 instrument with 9ul of the Master Mix qPCR 2.0 (PB-L, Productos Bio-Logicos), including SYBR Green detection. qPCR cycles: STEP 1 95° 3min; STEP 2 (x40) 95° 20seg, 62° 20 seg and 72° 30 seg with reading; STEP 3 95° 1 min; STEP 4 Melting curve 60° 30seg, 95° 30seg (temperature of the sample is then increased incrementally as the instrument continues to measure fluorescence). Luciferase mRNA was quantified by qPCR using the following primer set: forward (5-CCGCCGTTGTTGTTTTG- 3) and reverse (5-ACACAACTCCTCCGCGC-3). For vGPCR, the primer sequences were: forward (5-AGGAGCGATAGATATACTG-3) and reverse (5-CAACACTTCTGCCAATAG-3). Luciferase and vGPCR mRNA expression were normalized against the Beta-galactosidase mRNA, in which primer sequences were: forward (5-CCACGGAGAATCCGACG-3) and reverse (5-GCGAGGCGGTTTTCTCC-3). In every run, melting curve analysis was performed to verify the specificity of products and water and No–RT controls. Three biological replicates were used for each sample and measured in triplicates in the qPCR analysis. Data were analyzed using the ΔΔCT method previously described (54); we used this method because the genes were amplified with comparable efficiencies. Target gene expression was normalized to Beta-galactosidase by taking the difference between CT values for target genes and Beta-galactosidase (ΔCT value). These values were then calibrated to the control sample to give the ΔΔCT value. The fold target gene expression is given by the formula: 2–ΔΔCT. We used Beta-galactosidase as a reference gene to normalize transfected cells.

Western blot

Nrf2 and phospho-Nrf2 were detected by Western blotting with anti-Nrf2 (Abcam ab89443) and anti-phospho-Nrf2 (Abcam ab76026). For kinase analysis, we used anti-ERK2 (Santa Cruz: sc-154), Anti-Phospho–ERK1/2 (Santa Cruz sc-7383), Anti-p38 (Santa Cruz sc-535-G), Anti-Phospho-p38 (Cell Signaling 9211), Anti-JNK (Santa Cruz sc- 474-G), Anti-Phospho–JNK (Cell Signaling 9255S), Anti-Akt1 (Santa Cruz sc-1618), Anti-Phospho-Akt1/2/3 (Santa Cruz sc-16646-R), Anti-Keap1 (Cell Signaling 8047) and anti-HO-1 (Cell Signaling 43966). Proteins were visualized by enhanced chemiluminescence detection (Amersham Biosciences) using secondary antibodies coupled to horseradish peroxidase or secondary antibodies coupled to fluorophores and detected using an Odyssey System (Li-cor). The MEK inhibitor PD98059 (catalog number 513000) was purchased from Calbiochem (San Diego, California).

Indirect immunofluorescence

NIH3T3, NIH3T3_vGPCR, NIH3T3_Gα12-QL, NIH3T3 Gα13-QL, and NIH3T3 RhoA-QL cells were seeded on glass coverslips. Cells were serum-starved for 24 h, washed twice with 1ml PBS, and then fixed and permeabilized with 4% formaldehyde and 0.05% Triton X-100 in 1ml PBS for 10 min. After washing with PBS, cells were blocked with 1% bovine serum albumin and incubated with anti Nrf2 (Abcam) as primary antibody O.N. at 4C°. Following incubation, cells were washed three times with 1ml PBS and then incubated for an additional hour with the corresponding secondary antibody (1:1000) conjugated with fluorescein isothiocyanate (Molecular Probes). Cells were washed three times with 1ml PBS and stained with Propidium Iodide (1 ug/ml) (Molecular Probes) in the last wash. Coverslips were mounted in Mowiol mounting medium (Sigma) and viewed using a confocal microscope (Fluoview FV300, Olympus, Japan). For nucleus/cytoplasm ratio quantification of protein localization, we used ImageJ and the results were displayed in the graph as fluorescence intensity

ratio. Values near one indicate homogenous protein localization, while values over one indicate mainly nuclear localization, and values below one indicate localization mainly cytoplasmically. For mouse-KS tumor immunofluorescence analysis, we used frozen mouse KSHV (+) and KSHV (–) tumor samples obtained as previously described (33, 55). Briefly, mECK36 KSHV (+) cells injected subcutaneously into the flanks of nude mice form mouse KSHV (+) tumors 5 weeks after injection. KSHV (–) tumor cells injected subcutaneously into the flanks of nude mice form KSHV (–) tumors 3 weeks after injection. Immunofluorescence assay (IFA) of mECK16-deltavGPCR, mECK16Δ-Revertant, Mouse KSHV-positive, and KSHV-negative tumors was performed as previously described (56). Briefly, cells were fixed in 4% paraformaldehyde for 10 min and washed with PBS. Cells were permeabilized in 0.2% Triton-X/PBS for 20 min at 4°C. After blocking with 3% of BSA in PBS and 0.1% Tween 20 for 60 min, samples were incubated with primary antibodies overnight at 4C. After PBS washing, samples were incubated with fluorescent secondary antibodies for 1 hour (Molecular Probes), washed, and mounted with ProLong Gold antifade reagent with DAPI (Molecular Probes).

Tumor xenografts in athymic nude mice and antitumor effect of Nrf2 silencing

NIH3T3, NIH3T3_vGPCR, NIH3T3_vGPCR_shScramble, NIH3T3_vGPCR_shNrf2 stable cell lines were used to induce tumor allografts in 7-week athymic (*nu/nu*) nude mice. Cells were harvested, washed, counted, and resuspended in PBS. 1 X 10^6 NIH3T3_vGPCR (control) or NIH3T3_vGPCR_shNrf2 cells were injected subcutaneously in the right flank of six and five nude mice, respectively. Mice were monitored twice weekly until each animal developed one tumor in the area of the cell injection. Tumor volume and body weight were measured every other day during the investigation period. Tumor volumes (V) were determined by the formula V=L$x$$W^2$x0.5, with L being the longest cross-section and W the shortest. Data are mean ± S.E.M expressed as tumor volume (cm^3), calculated as described above. Animals from each group were euthanized for tissue retrieval at the various time points indicated in the study. Using standard protocols, the tissues were fixed in 4% buffered paraformaldehyde overnight, dehydrated, and embedded in paraffin. H&E-stained sections were used for diagnostic purposes.

All animal studies were carried out according to the Institutional Animal Care and Use Committee of the Facultad de Ciencias Exactas y Naturales (FCEN) the University of Buenos Aires approved protocol, and local government regulations (Servicio Nacional de Sanidad y Calidad Agroalimentaria, RS617/2002, Argentina). All mice were maintained under a 12:12 h dark/light cycle with food and water *ad libitum*. They were grouped-housed (3-5 mice per cage). Male and female mice were used and randomly assigned to the different experimental groups. All mice were euthanized by Carbon Dioxide inhalation using especially appropriate equipment of the Animal Facility.

Statistical analysis

Sample sizes were estimated based on variance obtained from previous studies, an alpha level of 0.05, and statistical power >0.8. To minimize any possible bias during tumor measurements, mice from both experimental groups were housed together and were evaluated in random order by experimenters blinded to the treatment conditions. No exclusion criteria were *a priori* established, and all injected mice were included in the analysis. Normality of data distributions was estimated with Shapiro-Wilk tests, two-tailed parametric statistics were used in all cases, and the threshold for significance was set at p = 0.05. The *p* values are indicated along with statistical parameters, such as the number of cells and animals used in each experiment in the results and the figure legends. Statistical analysis was performed with GraphPad Prism 9 software. Group differences were analyzed by student t-test or ANOVA followed by Dunnet Test. Experimental groups are compared to the control. Two-way repeated measures ANOVA was used for tumor volume analysis. A *p-value* <0.05 (*) was considered statistically significant.

Image analysis and quantification

Different band intensities corresponding to Western blot detection of protein samples were quantified using the ImageJ software.

Results

ARE elements are involved in the vGPCR-mediated activation of HO-1

We performed Luciferase Reporter Assays to identify the elements within the HO-1 promoter responsible for vGPCR activation. For this aim, we used a reporter construct containing 4.9Kb of the HO-1 promoter (HO-1 4.9 Luc) and serial deletions (HO-1 3.8 Luc, HO-1 1.4 Luc, and HO-1 0.3 Luc) (Figure 1A). As shown in Figure 1B, the loss of the proximal ARE reduces the transcriptional activity of the HO-1 (4.9Kb) promoter. This result suggests that the ARE sequence might be responsible for HO-1 promoter activation by vGPCR. Next, we used a minimum promoter containing three ARE sites in tandem (3xARE Luc) to determine the role of the HO-1 ARE sites in activating the HO-1 promoter by vGPCR. We co-transfected this reporter with expression plasmids for Nrf2 WT and Nrf2 Dominant Negative (DN), lacking the Nrf2 transactivation

domain as control of responsiveness of the reporter (Supplementary Figure 1). To evaluate the effect of over-expression of vGPCR, we co-transfected the 3xARE Luc reporter with expression plasmids for vGPCR. As seen in Figure 1C, vGPCR produced an increment in the reporter activity, indicating that vGPCR may activate ARE sites in target genes. To determine if the transcription factor Nrf2 mediated this effect, we co-transfected vGPCR with plasmids that express Nrf2 WT or Nrf2 DN. Interestingly co-transfection with vGPCR and Nrf2 WT produce a higher induction than the observed for vGPCR alone, suggesting that vGPCR and Nrf2 may be linked by a common signaling pathway. The induction produced by vGPCR was abolished by Nrf2 DN. Altogether, these results (Figure 1C) suggest that vGPCR activates ARE sites through Nrf2. These results were confirmed by RT-qPCR analysis of Luciferase mRNA expression (Figure 1D). vGPCR over-expression was confirmed by RT-qPCR (Figure 1E).

Like many GPCRs, vGPCR activates downstream effectors like Gα12, Gα13, and RhoA. To determine if those proteins were involved as mediators in the activation mechanism of the ARE sites by vGPCR, we performed luciferase assays with the 3xARE Luc construct co-transfected with expression vectors for vGPCR and downstream effectors. As shown in Figure 1F, vGPCR and its downstream effectors activate transcriptional response at the ARE sites. Moreover, the activation of ARE sites by vGPCR, Gα12, and Gα13 are RhoA dependent, as the co-transfection with RhoA Dominant Negative (RhoAN19) produces a decrease in the activation of the reporter when compared with the effect produced by vGPCR, Gα12 and Gα13 alone (Figure 1G). These results suggest that vGPCR, Gα12, and Gα13 activate ARE sites through RhoA.

Key role of Nrf2 on HO-1 activation by vGPCR

To evaluate the role of Nrf2 in the induction of the HO-1 promoter by vGPCR, we performed Luciferase Reporter Assays. We used a reporter with the luciferase gene upstream of the murine HO-1 promoter. As seen in Figure 2, vGPCR induces an increment in the activity of the HO-1 promoter when compared to cells transfected with a control plasmid (pCDNA3.1 empty). To demonstrate that this effect was mediated through Nrf2, we co-transfected vGPCR with Nrf2 WT or with Nrf2 DN. The effect of co-transfection of vGPCR and Nrf2 WT in HO-1 promoter was bigger than the effect of vGPCR alone. Interestingly, the co-transfection of vGPCR with Nrf2 DN produced a decrease of about 30% respective to the effect of vGPCR alone. These results suggest that Nrf2 plays a key role in activating the HO-1 promoter by vGPCR (Figure 2A). These results were confirmed by RT-qPCR analysis of Luciferase mRNA expression (Figure 2B).

vGPCR activates Nrf2 TAD and induces Nrf2 nuclear translocation

Like many transcription factors, Nrf2 has to be activated on its Transcriptional Activated Domain (TAD) to recruit the transcriptional machinery needed to activate the transcription of target genes. To determine if vGPCR affects TAD activation, we performed luciferase assays. We co-expressed a Gal4DBD–Nrf2TAD fusion protein and a Gal4 Binding Element upstream luciferase and evaluated reporter activity in control cells and cells overexpressing vGPCR, Gα12-QL, Gα13-QL, or RhoAQL. As shown in Figure 3A, vGPCR and the downstream signaling components can activate this promoter, suggesting that Nrf2-TAD targets vGCPR-triggered signaling. In basal conditions, Nrf2 localizes in the cytoplasm, and Keap1 drives it to proteasomal degradation, whereas in stimulated conditions, the complex Nrf2-Keap1 is dissociated, and Nrf2 translocated to the nucleus. To determine if vGPCR affects Nrf2 nuclear translocation, we performed immunofluorescence assays using a specific Nrf2 antibody on NIH3T3, NIH3T3_vGPCR, NIH3T3_Gα12-QL, NIH3T3_Ga13-QL and NIH3T3_RhoA-QL (all stable cell lines). As shown in Figure 3B, in NIH3T3 cells, Nrf2 has a predominantly cytoplasmic localization whereas, in the four stable cell lines that express vGPCR, Gα12-QL, Gα13-QL, or RhoA-QL, Nrf2 is found predominantly in the nucleus (Figures 3B–C). These results suggest that vGPCR and its effectors downstream have the same effect on Nrf2 nuclear translocation.

vGPCR increases expression levels and phosphorylation of Nrf2

Given that it has been reported that Nrf2 is directed to proteasomal degradation and that in-stimulated conditions, it can be phosphorylated; we wondered if overexpression of vGPCR could stabilize the protein levels of Nrf2 and affect its phosphorylation levels. For this purpose, we performed Western Blots using lysates of NIH3T3 and NIH3T3_vGPCR cells and evaluated the levels of total and phosphorylated Nrf2 proteins in both cell lines. As seen in Figure 4A, vGPCR augments the level of total and phosphorylated Nrf2. These results suggest that vGPCR not only stabilizes Nrf2, but it also induces Nrf2 phosphorylation levels.

It is known that different post-translational modifications such as phosphorylation, ubiquitination, sumoylation, and many others can modify Nrf2 and Keap1. We evaluated different kinase activation pathways in our model to determine if phosphorylation on the Nrf2-Keap1 complex is a mediator of the vGPCR effect. We performed Western Blot assays with specific antibody pairs (phospho-protein and total protein) for four different relevant kinases, ERK1/2 (Figure 4B), p38

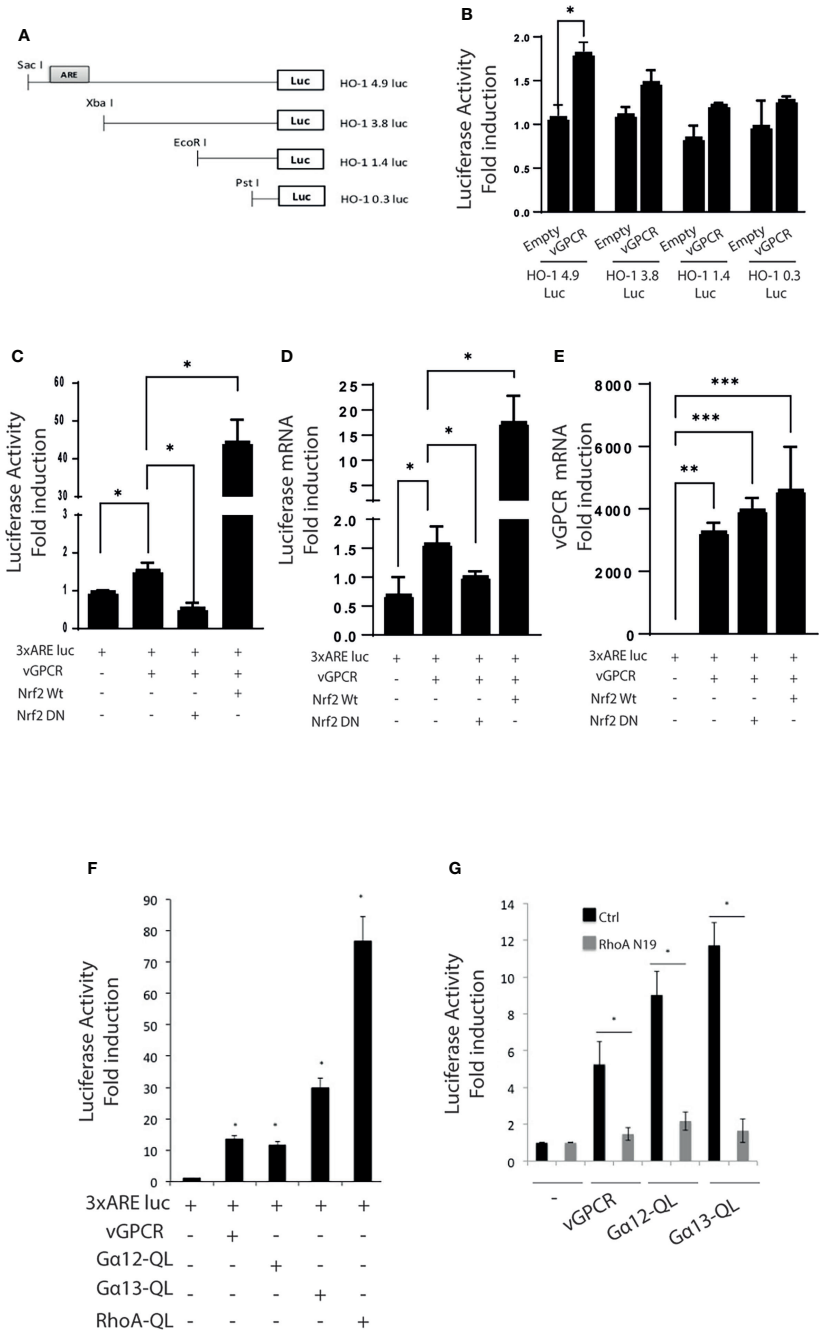

FIGURE 1
(A) Serial deletions of the 4.9Kb region of the HO-1 promoter. **(B)** Luciferase activity of serial deletions of the HO-1 promoter after co-transfection of the reporter construct with a plasmid that expresses vGPCR. The results are expressed as fold induction relative to cells transfected with the 4.9Kb promoter construct. **(C)** Luciferase activity of a minimum promoter with three ARE sites in tandem (3xARE Luc) after transfection of vGPCR; effect of co-transfection with vGPCR and Nrf2 WT, and effect of co-transfection with vGCPR and Nrf2 DN. The results are expressed as fold induction relative to control cells (transfected with the reporter and an empty vector). **(D)** Fold-changes of Luciferase mRNA expression were assessed by RT-qPCR in triplicate and are presented as means ± SD. **(E)** Fold-changes of vGPCR mRNA expression were assessed by RT-qPCR in triplicate and are presented as means ± SD. **(F)** Luciferase activity of the 3xARE Luc reporter constructs after transfection with plasmids expressing vGPCR, Gα12-QL, Gα13-QL, and RhoA-QL (constitutively active forms of Gα12, Gα13, and RhoA, respectively). The results are expressed as fold induction relative to control cells (transfected with the reporter and an empty vector). **(G)** Luciferase activity of the 3xARE Luc after co-transfection with vGPCR, Gα12-QL, and Gα13-QL with or without RhoA-N19 (a dominant negative form of RhoA). The results are expressed as fold induction relative to control cells (transfected with the reporter and an empty vector). *P-value* <0.05 (*). P-value <0.002 (**). P-value <0.0002 (***).

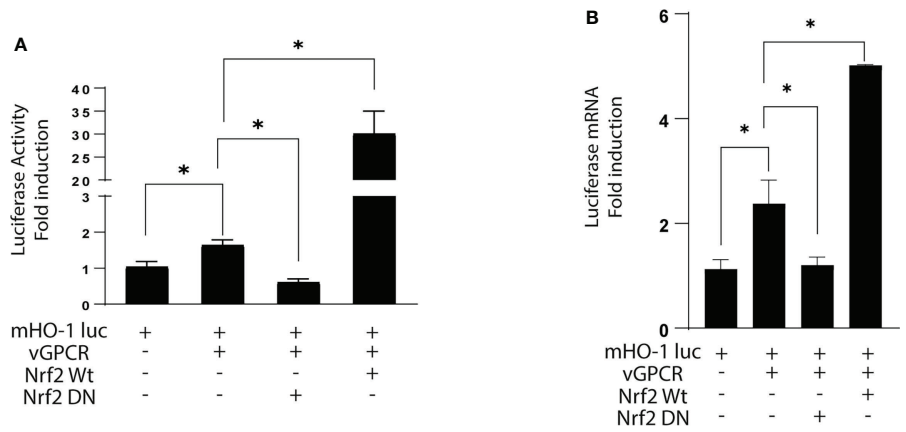

FIGURE 2
(A) Luciferase activity of the murine HO-1 promoter after transfection with vGPCR; co-transfection with Nrf2 WT and the dominant negative Nrf2 DN. The results are expressed as fold induction relative to control cells (transfected with the reporter and an empty vector). **(B)** Fold-changes of Luciferase mRNA expression were assessed by RT-qPCR in triplicate and are presented as means ± SD. (*P <0.05).*p-value* <0.05 (*).

(Figure 4C), AKT (Figure 4D), and JNK (Figure 4E). In all cases, we evaluated NIH3T3, NIH3T3_vGPCR, and an appropriate positive control (see Figures 4B–E). As seen in Figure 4, vGPCR can activate ERK1/2 and p38 but not AKT and JNK in our model.

vGPCR effects on Nrf2 transcriptional activity are mediated by ERK1/2

As we showed, vGPCR affects Nrf2 transcriptional activity, so we wanted to know if the ERK1/2 pathway mediated this effect. For this aim, we performed Luciferase assays with the murine HO-1 promoter (Figure 5A), the 3xARE Luc (Figure 5B), and the GAL4–Nrf2TAD reporter system (Figure 5C). We transfected NIH3T3_vGPCR cells with the reporter construct. We activated the ERK1/2 pathway co- transfecting with expression plasmids for MEK-EE (constitutive activated) or inhibited the pathway co-transfecting with MEK-AA (dominant negative). Figure 5A shows that co-transfection of vGPCR and MEK-EE did not produce a higher effect in HO-1 promoter activation compared to vGPCR alone. This might be due to a saturation of the system when activation of the signaling axis to this particular reporter construct is already ignited by vGPCR. On the other hand, co-transfection of vGPCR with MEK-AA diminished the effect observed with vGPCR alone. Figures 5B, C showed a higher effect when co-transfecting vGPCR with MEK-EE than vGCPR alone. According to this result, co-transfection with vGPCR and MEK-AA produced a decrease in reporter activation concerning vGPCR alone. These results suggest that the ERK1/2 pathway mediates the vGCPR effect on Nrf2 transcriptional activity, which might have participated in HO-1 promoter activation.

vGPCR effect on Nrf2 nuclear translocation is mediated by ERK1/2

To evaluate the ability of vGPCR to induce Nrf2 nuclear translocation by ERK1/2 signaling, we performed immunofluorescence assays using an Nrf2-specific antibody treating NIH3T3_ vGPCR cells with or without the MEK inhibitor PD98059 (20uM) for 2hs. Figure 6 shows that the inhibition of the ERK1/2 pathway by PD98059 impairs the nuclear translocation of Nrf2. The ratio of Nuclear Fluorescence/Cytoplasm Fluorescence drops from 2.5 in NIH3T3_vGCPR cells, which indicates nuclear localization to 0.5, indicative of cytoplasmic localization. This result suggests that the effect of vGPCR on Nrf2 nuclear localization is mediated by ERK1/2. Whereas vGPCR increases Nrf2 stability and phosphorylation and considering that vGCPR activates the ERK1/2 pathway, we wanted to test if the ERK1/2 pathway has a role in Nrf2 phosphorylation. As seen in Supplementary Figure 2, the inhibition of the ERK1/2 pathway did not produce a decrease in the phosphorylation levels of Nrf2 induced by vGPCR, suggesting that the effect of ERK1/2 may not be through direct phosphorylation of Nrf2 (Supplementary Figure 2).

Silencing of Nrf2 impairs vGPCR-induced tumorigenesis in mice

Whereas parental NIH3T3 cells are non-transformed, they acquire the capability to form foci in cell culture models and to induce tumors in nude mice when transfected by a plasmid construct expressing an oncogene. Thus, vGPCR-overexpressing NIH3T3 cells, but not the parental cells, have been reported to induce tumors when injected into nude mice (57). Prompted by

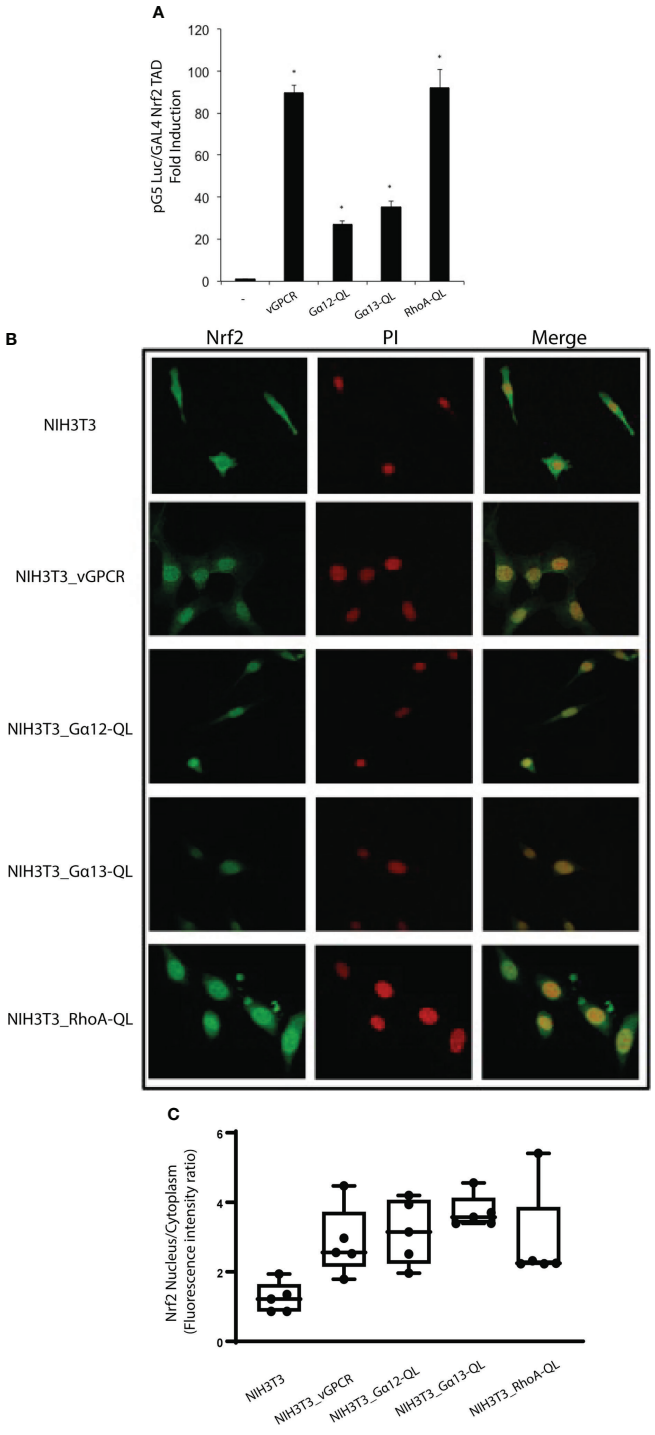

FIGURE 3
(A) Luciferase activity of the GAL4 reporter system to study transcriptional activation domains of transcription factors. pG5Luc and pGAL4_Nrf2TAD reporter plasmids were co-transfected with plasmids expressing vGPCR, Gα12-QL, Gα13-QL, and RhoA-QL. The results are expressed as fold induction relative to control cells (transfected with the reporter and an empty vector). **(B)** vGPCR, Gα12-QL, Gα13-QL, and RhoA-QL induced nuclear translocation of Nrf2. Confocal microscopy of NIH3T3 stable cell lines for the expression of vGPCR, Gα12-QL, Gα13-QL, and RhoA-QL were incubated with anti-Nrf2 and anti-rabbit FITC. For visualizing the nucleus, propidium iodide was used. Magnification 40X. **(C)** Quantification of fluorescence intensity for the nucleus/cytoplasm localization of Nrf2 in the different conditions from **(B)**. *p-value* <0.05 (*).

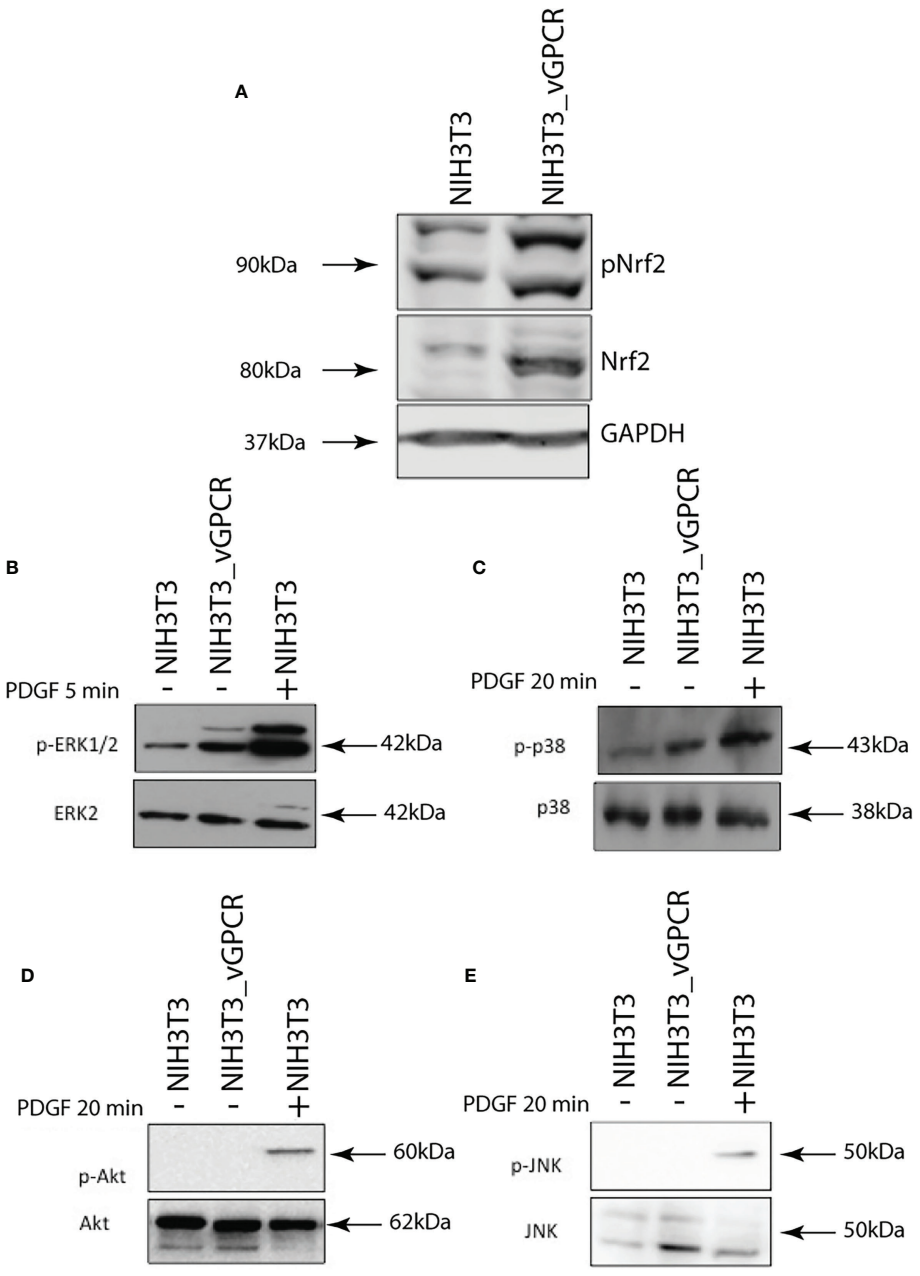

FIGURE 4
(A) Western Blot Assays performed in NIH3T3 and NIH3T3_vGPCR were evaluated for Nrf2 levels and Nrf2 phosphorylation using anti-phospho Nrf2 and anti- Nrf2. As loading control we used GAPDH. **(B)** Western Blot Assays performed in lysates of NIH3T3 and NIH3T3_vGPCR cells were evaluated for activation of ERK using anti-phospho ERK1/2 and anti-ERK2; as a control, we used NIH3T3 cells treated with PDGF 5 minutes. **(C)** Activation p38 using anti-phospho p38 and anti-p38; as control, we used NIH3T3 cells treated with Anisomycin for 20 minutes. **(D)** Activation of AKT using anti-phospho AKT and anti-AKT as a control, we used NIH3T3 cells treated with PDGF for 20 minutes. **(E)** Activation of JNK using anti-phospho JNK and anti-JNK as a control, we used NIH3T3 cells treated with PDGF for 20 minutes.

our findings, we used these models to investigate whether silencing Nrf2 could affect vGPCR-induced tumorigenesis *in vivo*. For this aim, we transfected the NIH3T3_vGPCR cell line with different shRNAs directed against Nrf2 (NIH3T3_vGCPR–shNrf2) and with a control shRNA (NIH3T3_vGPCR–shScramble). We generated stable cell lines and evaluated them for Nrf2 expression levels. As shown in Figure 7A, stable cell lines named NIH3T3_vGPCR-shNrf2-2 and NIH3T3_vGPCR-shNrf2-2.1 showed lower levels of Nrf2 expression when compared with NIH3T3_vGPCR. We

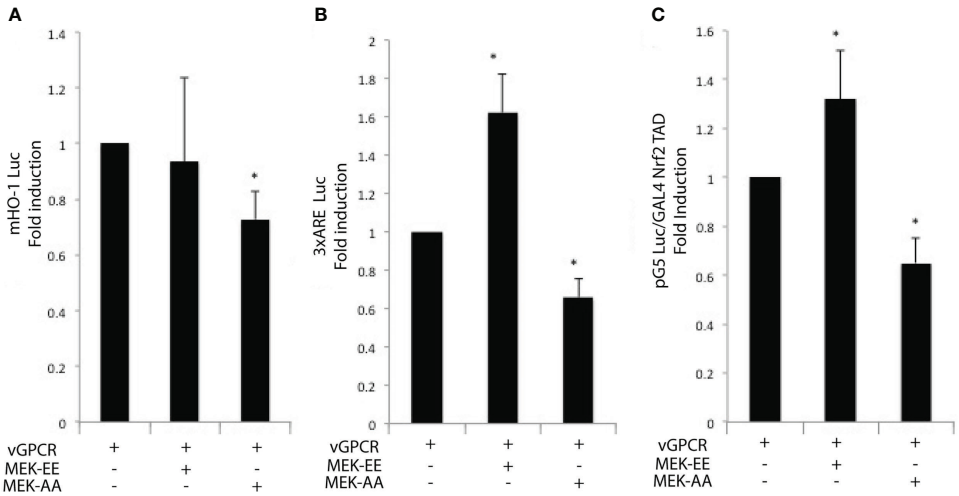

FIGURE 5
Luciferase activity of the murine HO-1 promoter **(A)**; 3xARE Luc **(B)** and the GAL4 – Nrf2 TAD reporter system **(C)** of NIH3T3 cells after transfection of vGPCR alone (bar one in each set); co-transfection of vGPCR and MEK-EE (bar 2 in each set) and co-transfection of vGPCR and MEK-AA (bar three in each set). *P-value* <0.05 (*).

injected 1x10^6 NIH3T3_vGPCR (control) or NIH3T3_vGPCR–shNrf2-2.1 cells into the right flank of six and five nude mice, respectively, and observed the mice twice a week. In concordance with the *in vitro* described effects upon HO-1 expression, silencing Nrf2 by shRNA strongly impacts the tumorigenic behavior of transformed cells *in vivo*. Tumors produced by NIH3T3_vGPCR–shNrf2_2.1 tend to be smaller than the ones observed in the NIH3T3_vGPCR group (Figures 7B–C); probably due to the significant delay in tumor onset found for Nrf2 silenced cells (Figure 7D).

Nrf2 subcellular localization and activation by vGPCR in full KSHV genome bearing cells and KS-like mouse tumors

To determine the specific contribution of vGPCR signaling to the subcellular localization of Nrf2 in the context of full KSHV genome-bearing cells, we used a previously described Bac16-delta vGPCR mutant or its revertant in mECK36 cells that have lost the Bac36 episome by lack of antibiotic selection, mECK16-

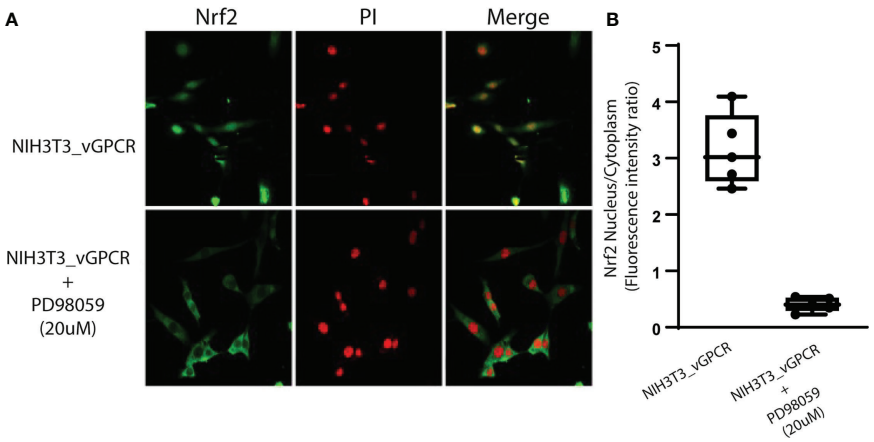

FIGURE 6
Inhibition of ERK1/2 activity block Nrf2 nuclear translocation. **(A)** Confocal microscopy of NIH3T3 stable cell lines for vGPCR control or treated with PD98059 20uM and incubated with anti-Nrf2 and anti-rabbit FITC. For visualizing the nucleus, propidium iodide was used. Magnification 40X. **(B)** Quantification of fluorescence intensity for the nucleus/cytoplasm localization of Nrf2 in the different conditions from **(A)**.

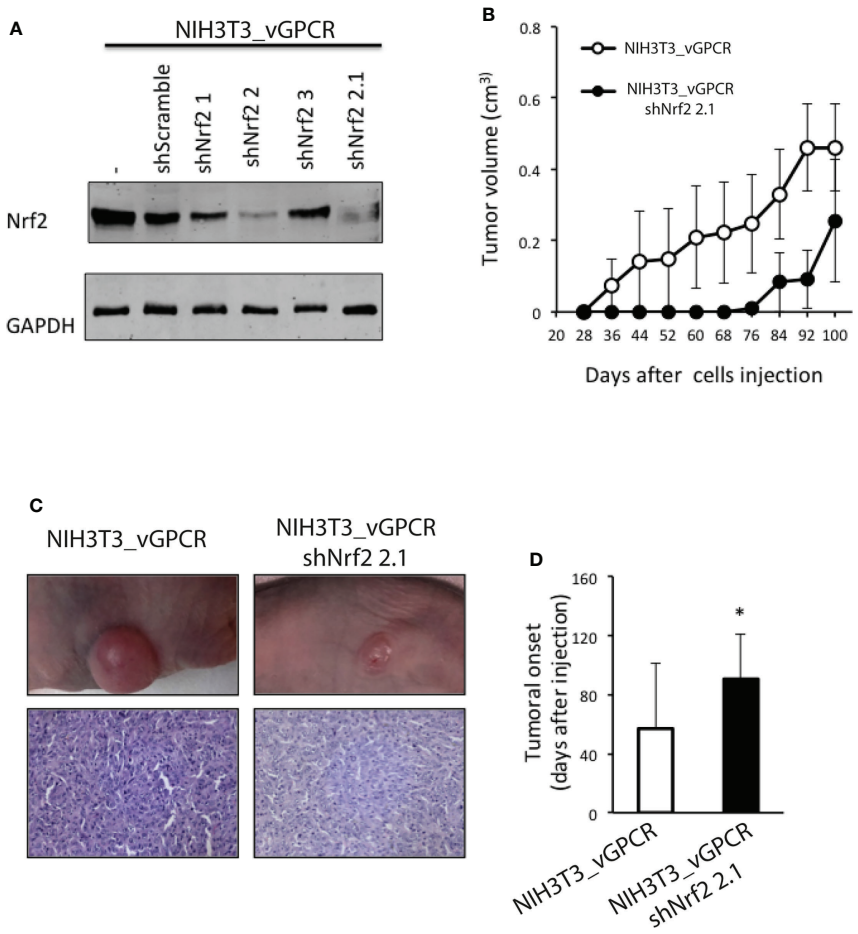

FIGURE 7
(A) Western Blot Assays performed in NIH3T3_vGPCR or different NIH3T3_vGPCR stable cell lines for the expression of shRNAs targeting Nrf2. We used an anti-Nrf2 antibody to detect Nrf2 levels in the different cell lines. **(B)** 1 X 10^6 NIH3T3_vGPCR (control) or NIH3T3_vGPCR_shNrf2 2.1 cells were injected subcutaneously in the right flank of six and five nude mice respectively. Data are mean ± S.E.M expressed as tumor volume (cm^3), calculated as Materials and Methods described. (Two-way repeated measures ANOVA, treatment factor $F_{1, 81} = 2.47$ p = 0.15). **(C)** An example of tumor-bearing mice from each group is depicted. H&E staining from representative tumors from mice injected with NIH3T3_vGPCR or NIH3T3_vGPCR_shNrf2 cells, respectively. **(D)** The tumor onset was defined as the first day of appearance of a measurable tumor. Data are mean ± S.E.M. NIH3T3_vGPCR: 57± 44.33; NIH3T3 _vGPCR_shNrf2: 90.6 ± 30.56. *p-value* <0.05 (*).

deltavGPCR, and mECK16-revertant, respectively (53). In Figure 8A, top panel, Nrf2 subcellular localization is mainly nuclear in cells infected with the complete KSHV genome (mECK16-revertant cells), but in cells infected with a KSHV virus lacking vGPCR (mECK16-deltavGPCR cells) the Nrf2 subcellular localization shift to a more cytoplasmic signal (Figure 8A bottom panel). Moreover, western blot analysis of these cells showed that the cytoplasmic subcellular localization of Nrf2 in vGPCR mutant cells correlates with increased expression of Keap1 and decreased expression of HO-1, Figure 8B. Finally, we were able to show that in KSHV-positive [KSHV (+)] mouse KS-like tumors, Nrf2 activation (Nrf2 phosphorylation) and subcellular localization is mainly nuclear in contrast with that observed in KSHV-negative [KSHV (–)] mouse tumors, Figure 8C.

Discussion

Kaposi's sarcoma (KS) is the most common tumor in AIDS patients, and the highly vascularized patient's skin lesions are composed of the cells that derive from the endothelial tissue transformed by the KSHV virus (58). In previous works from our laboratory and collaborators, we have contributed to showing how the expression of vGPCR in fibroblasts produces transformation with foci formation in Petri dishes and tumors in nude mice. The lesions produced by these tumors in animals are rich in vessel irrigation, which resembles those of human patients with KS (31, 57). In addition, we have demonstrated that vGPCR induces the gene coding for HO-1 in both fibroblasts and endothelial cells and that this increase in HO-

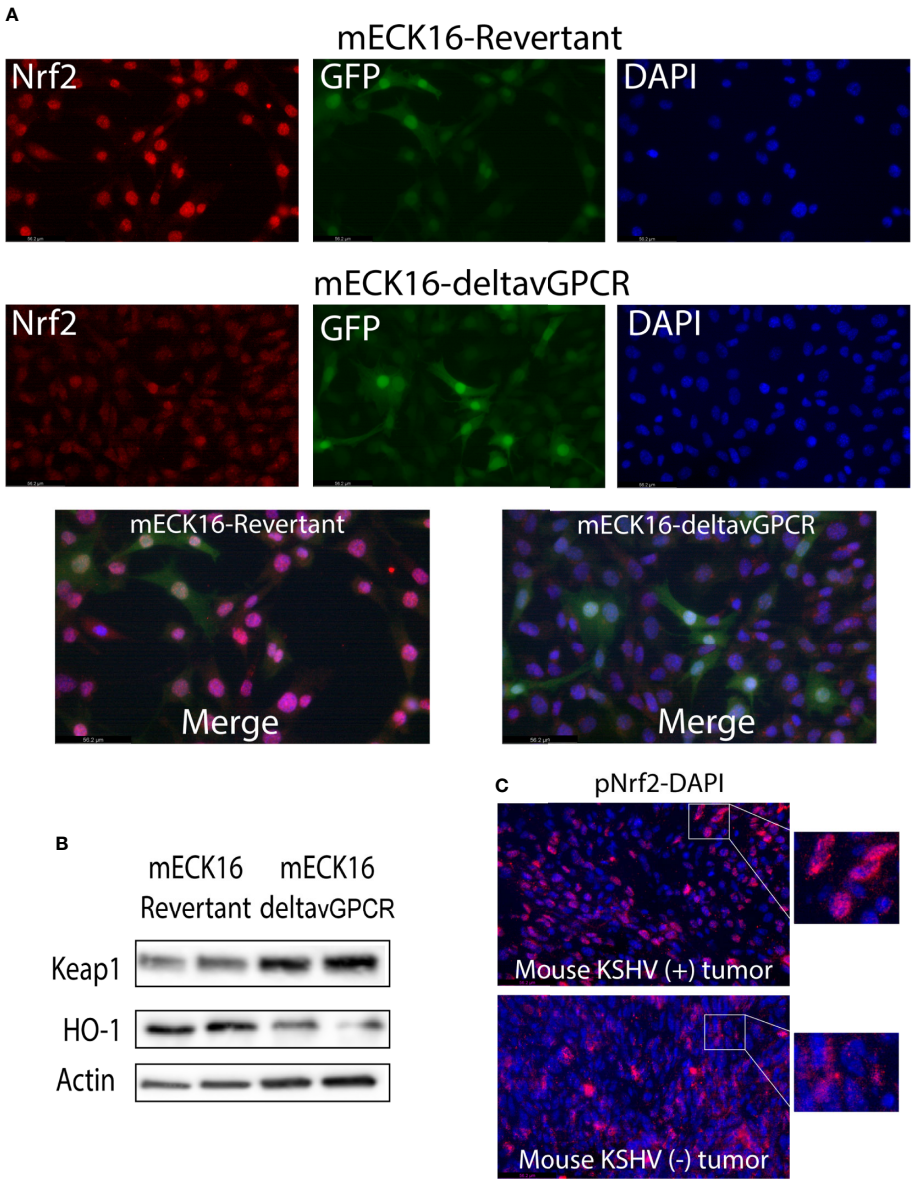

FIGURE 8
(A) Immunofluorescence analysis of mECK16-revertant and mECK16-ΔvGPCR cells to evaluate Nrf2 expression (red), GFP signal comes from the BAC16 plasmid (green), and nuclei were counterstained with DAPI (blue). **(B)** Western Blot Assays were performed in mECK16-revertant and mECK16-ΔvGPCR cell lines for the expression of Keap1 and HO-1; Actin was used as a loading control. **(C)** Immunofluorescence analysis of mouse KSHV (+) and mouse KSHV (–) tumors to evaluate Nrf2 phosphorylation (red), nuclei were counterstained with DAPI (blue).

1 expression levels correlates with and is necessary for increased proliferation and cell survival. On the other hand, we have shown that the inhibition of HO-1 expression or its activity causes a reduction in the size of the vGPCR- induced tumors in mice (40). In cells transformed by vGPCR, it has been reported the activation of at least three major signal transduction pathways MAPKS ERK1/2, JNK, and p38 (59, 60). In addition, the cascade of PI3K/Akt has been reported as activated by the viral oncogene vGPCR. Activation of Akt would be dependent on PI3K and would have beta and gamma subunits of G proteins as intermediates (61). Small GTP binding proteins of the Rho family, such as RhoA and Rac1, as well as alpha subunits of heterotrimeric G proteins, increase their GTP loading in cells expressing vGPCR with their subsequent activation (40, 45). We have shown that vGPCR induces HO-1 expression and cell transformation using a pathway that sequentially includes the Gα12/13 and RhoA proteins (40, 45) Figure 9.

Regarding the role of HO-1 in the development of tumors, some results suggest that HO-1 can act as a cytoprotective enzyme, reducing the risk of developing some types of tumors. However, HO-1 is given a "dual" role. On one hand, it acts as a protective agent in healthy tissues, but on the other hand, it can act as an antiapoptotic and proangiogenic mediator. In one way or another, although the role of HO-1 as a target of vGPCR is clear, we still do not entirely know the mechanism that regulates its promoter expression. The transcription factors that bind to the HO-1 promoter are still poorly characterized as the signal transduction pathways that regulate them. The transcriptional regulation at the ARE site level is mainly controlled by Nrf2, a transcription factor of the leucine zipper-type (6) Figure 9.

According to our previous results and current global knowledge, we hypothesize that Nrf2 acts as a key factor in regulating the promoter of HO-1 by vGPCR. We contribute new data that links vGPCR with the promoter of HO-1, highlighting the fundamental role of Nrf2 as a mediator not only in the regulation of HO-1 but also in the tumorigenesis induced by vGPCR. We have described that the loss of the ARE element (located at the -4 Kb position) from the HO-1 promoter results in a decrease in reporter activity, indicating that this site is important in vGPCR mediated activation of HO-1 (Figure 1B).

We have determined the relevance of ARE sites on vGPCR-mediated activation. On one hand, we show that the deletion of a promoter region containing this sequence produces a decrease in the activation of the HO-1 promoter (Figure 1B) and, on the other hand, that vGPCR can activate a minimal promoter with ARE sites in tandem (3xARE Luc) (Figures 1C–D). Regarding the downstream elements of vGPCR, it was described by our group and co-workers, that vGPCR activates the HO-1 promoter through the small Gα12/13 G protein and RhoA (40, 45). In the present report, we demonstrated that both vGPCR and Gα12/13 activate ARE sites through RhoA and that they are not independent pathways since when co-transfected with a dominant negative form of RhoA, the effect produced by vGPCR and Gα12/13 was hampered (Figures 1F–G). This suggests that these elements are key in the activation of Nrf2. Once this was demonstrated, we considered it important to study the role of the transcription factor protein Nrf2. Figures 1, 2 show that Nrf2 is key for activating the HO-1 promoter and the ARE sites. We showed that Nrf2 can recruit the transcriptional machinery and induce expression of a reporter gene in response to vGPCR and downstream elements.

vGPCR activates different transcription factors that control different genes. In our model, although vGPCR can induce NF-κB through Rac1, and the HO-1 promoter has binding sites for this transcription factor, we provide evidence that Nrf2 has a key role as a transcription factor in the regulation of HO-1 mediated by vGPCR. Nrf2 activation seems to proceed *via* RhoA and not Rac1, although a more thorough study is currently being followed to determine the nature of Rac1 involvement. This suggests a fine regulation by a complex network of proteins that are differentially activated in different models and regulate gene

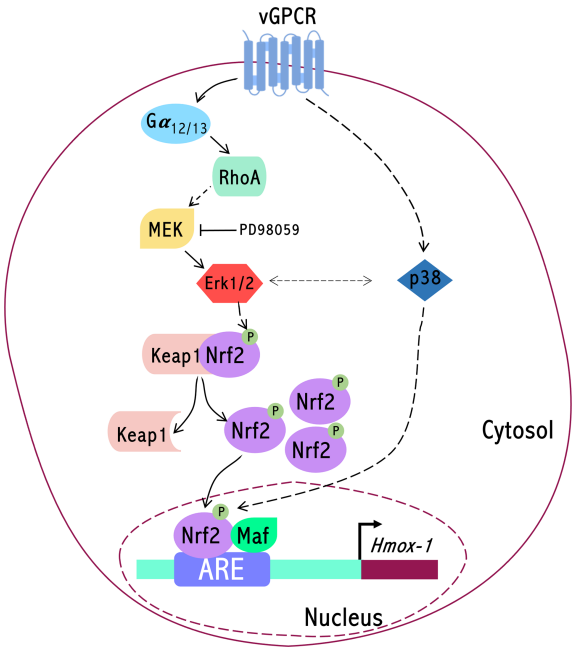

FIGURE 9
Signaling axis connecting the KSHV encoded oncogene vGPCR to the HO-1 promoter (Hmox-1) involves Gα12/13 and RhoA dependent Erk1/2 MAPK mediated activation of the transcription factor Nrf2.

expression orchestrating the biological response (proliferation, angiogenesis).

Another key aspect is the subcellular localization of Nrf2. It must be translocated to the nucleus to act as a transcription factor. We demonstrate here that both vGPCR and downstream elements can induce nuclear translocation of Nrf2 (Figure 3). This suggests that vGPCR is not only capable of inducing translocation to the nucleus of Nrf2 but that it may bind ARE elements and recruit the transcriptional machinery necessary for transcription initiation.

Work from different groups shows that vGPCR can activate different signaling pathways in different models. For example, Bais et al. have demonstrated that vGPCR activates the JNK and p38 pathways (57). In endothelial cells, vGPCR activates multiple pathways, including AMPc and AKT (41, 61, 62). The activation of this pathway has also been described in NIH3T3 cells. In this report, even using the same cell line, we have not seen AKT activation (Figure 4D), but we confirm that vGPCR activates the ERK1/2 and p38 pathways, as shown in Figures 4B–C. Numerous studies suggest that phosphorylation of Nrf2 may contribute to its regulation. Nrf2 contains serines, threonines, and tyrosines that can provide phosphorylation sites for various kinases. For example, it has been shown that PKC can phosphorylate Nrf2 in serine 40 (Neh2) and disrupt the association between Nrf2/Keap1, thus promoting the translocation of Nrf2 to the nucleus (63). Keum et al. demonstrated that p38 could phosphorylate Nrf2, promote its association with Keap1 and thus prevent its nuclear translocation (64). We have shown that vGPCR stabilizes and increases the phosphorylation levels of Nrf2 (Figure 4A).

Furthermore, vGPCR activates the ERK1/2 pathway and influences Nrf2 transcriptional activation (Figure 5) and nuclear translocation (Figure 6). However, we observed no effect on Nrf2 phosphorylation when we treated NIH3T3_vGPCR cells with the MEK inhibitor PD98059 (Supplementary Figure 2). This could be due, for example, to the fact that Nrf2 is being phosphorylated in several residues and that inhibition of the ERK pathway affects only certain amino acids, among which Serine 40 is not found to recognize the antibody used herein. Another possibility that justifies this result would be that vGPCR activates the phosphorylation of Nrf2 by an ERK-independent pathway and that ERK is regulating some proteins related to the import of Nrf2 to the nucleus. In this way, the inhibition of the ERK pathway would impede the translocation to the nucleus of Nrf2 in an indirect fashion. We cannot determine with the techniques performed whether the increase of Nrf2 is due to an increase in the half-life of Nrf2 or if it is due to an increase in the expression of the Nrf2 gene. However, our results clearly show the involvement of ERK1/2 as an intermediary between the vGPCR-Gα12/13-RhoA axis and nuclear translocation of Nrf2, as well as its transcriptional activation.

By performing experiments in nude mice, we show that the tumorigenic effect of vGPCR is affected by the silencing of Nrf2 (Figure 7). Cells that clearly show a decrease in Nrf2 expression by Western Blot were able to form tumors but with a markedly significant delay. Interestingly, the immunohistochemical analysis of control and experimental groups has shown detectable Nrf2 levels. However, experimental groups have shown only residual expression levels. This data tells us about a positive selection of cells expressing Nrf2 produced *in vivo* on the population of injected cells and provides extra data regarding the importance of expressing Nrf2 so that these cells can develop a tumor.

Studies published by Gjyshi et al. have shown that *de novo* infection of endothelial cells by KSHV leads to an increase in Nrf2 expression, an increase in the nuclear fraction of Nrf2, and an increase in phosphorylation levels of Nrf2 (46, 47). In addition, they have demonstrated that the increase in Nrf2 stability is not due directly to the dissociation of Nrf2 from Keap1 but also increases the expression of Nrf2 and, consequently, HO-1. It is noteworthy that those works used the complete genome of KSHV so that different proteins may be involved in regulating HO-1. To test the relevant oncogenic role of vGPCR in Nrf2 activation in the context of the complete KSHV genome, we used a deletion mutant of vGPCR and showed the lack of vGPCR induced an increase in cytoplasmic localization of Nrf2 correlated with a downregulation of HO-1 expression. Moreover, when we compare mouse KS-like KSHV (positive) tumors with KSHV (negative) tumors, we also show an increase in phospho-Nrf2 nuclear localization in KSHV (positive) tumors (Figure 8).

Many of the experiments in this study are performed using NIH3T3 cells as a biological scenario. These cells are widely used for validating oncogene activity, allowing consistency with our previous signaling studies (40, 45). Anyway, to test an environment more related to cells infected with KSHV, we have performed experiments that show vGPCR-dependent control of HO-1 expression under the control of Nrf2, with a model developed in Dr. Mesri's laboratory using mouse bone marrow cells of the endothelial cell lineage expressing the complete KSHV genome in its wild type form or variants.

It is also important to note that many pathways begin to interact when infected with the complete genome of KSHV. For example, regarding the increase of HO-1, we mention that KSHV increases the stability and phosphorylation of Nrf2, but it is also known that the BACH1 (repressor of HO-1 expression) mRNA is negatively regulated by viral miRNA miR-K12-11 (65, 66). This might imply that the expression of vGPCR and miR-K12-11 are two independent mechanisms that converge on the increase of HO-1.

We have previously shown that vGPCR is one of the key genes for tumor development induced by infection with KSHV (56). Our laboratory had previously reported that vGPCR targeted the HO-1 promoter through the Gα12/13-RhoA proteins and that the development of these tumors was mediated by HO-1; we have also demonstrated that pharmacological inhibition or decreased HO-1 expression produced a decrease in tumor size (40). Throughout this work,

we have been able to deepen the study on the effects of vGPCR on the expression of HO-1. We have shown that vGPCR not only activates Gα12/13-RhoA, but these proteins are signaling towards ARE sites present in the HO-1 promoter and that the transcription factor Nrf2 is key in this regulation. We have also shown that vGPCR-Gα12/13-RhoA signal to MAPK ERK1/2 and that vGPCR activates p38 MAPK. Regarding the role of ERK, we have demonstrated that it affects translocation to the nucleus of Nrf2 and the transcriptional activation of its transactivation domain. Finally, experiments in nude mice show that the tumorigenic effect of vGPCR is affected by the silencing of Nrf2 since mice injected with NIH3T3_vGPCR-shNrf2 cells showed a delay in tumor development. Altogether, our results show that vGPCR signals through Gα12/13, RhoA, and Erk1/2 to the HO-1 promoter in an Nrf2-dependent manner, as sketched in Figure 9. Our report points out Nrf2 and its associated factors as a putative pharmacological target for controlling cell growth in cells transformed by KSHV oncogenes providing the basis to focus our efforts in considering Nrf2 and associated proteins as therapeutic targets in KS treatment.

Data availability statement

The original contributions presented in the study are included in the article/Supplementary Material. Further inquiries can be directed to the corresponding author.

Ethics statement

All animal studies were carried out according to Institutional Animal Care and Use Committee of the Facultad de Ciencias Exactas y Naturales (FCEN) University of Buenos Aires approved protocol and local government regulations (Servicio Nacional de Sanidad y Calidad Agroalimentaria, RS617/2002, Argentina).

Author contributions

SD: Conceptualization, data curation, formal analysis, methodology, validation, visualization, investigation, writing-original draft; RA: Conceptualization, data curation, formal analysis, methodology, validation, investigation; MV: Conceptualization, data curation, formal analysis, methodology, validation, investigation; NJ: Conceptualization, data curation, formal analysis, methodology, validation, investigation, writing-original draft, writing-review, and editing; ME: Conceptualization, investigation, supervision, funding acquisition, project administration; CO: Conceptualization, data curation, methodology, investigation, writing-original draft, writing-review and editing, supervision, funding acquisition, project administration. All authors contributed to the article and approved the submitted version.

Funding

This work was supported by the NIH grants CA136387 (to ME) and CA221208 (to ME and CO); by the Florida Biomedical Foundation, Bankhead Coley Foundation grant 3BB05 (to ME), by Ubacyt Grant 20020150100200BA (to CO), Ubacyt Grant Proyecto # 01/W949.20020100100949 (to CO) and by National Agency of Scientific and Technological Promotion: PICT 2015-3436 (to CO).

Acknowledgments

We are thankful to Dr. Maria Julia Marinissen and Dr. Tamara Beatriz Tanos for insightful discussions that fueled the early stages of the work presented in this manuscript.

In memoriam

Dr. Enrique Mesri, inspiring artist and teacher, outstanding investigator, sadly passed away days before acceptance of this manuscript. We are indebted to him for his guidance, his energetic commitment to work, his willingness to share enthusiasm and remarkable scientific contributions.

Conflict of interest

The authors declare that the research was conducted in the absence of any commercial or financial relationships that could be construed as a potential conflict of interest.

Publisher's note

Supplementary material

The Supplementary Material for this article can be found online at: https://www.frontiersin.org/articles/10.3389/fonc.2022.890825/full#supplementary-material

References

1. Osburn WO, Kensler TW. Nrf2 signaling: An adaptive response pathway for protection against environmental toxic insults. *Mutat Res* (2008) 659(1-2):31–9. doi: 10.1016/j.mrrev.2007.11.006

2. Miao W, Hu L, Scrivens PJ, Batist G. Transcriptional regulation of NF-E2 p45-related factor (NRF2) expression by the aryl hydrocarbon receptor-xenobiotic response element signaling pathway: Direct cross-talk between phase I and II drug-metabolizing enzymes. *J Biol Chem* (2005) 280(21):20340–8. doi: 10.1074/jbc.M412081200

3. Wang XJ, Zhang DD. Ectodermal-neural cortex 1 down-regulates Nrf2 at the translational level. *PloS One* (2009) 4(5):e5492. doi: 10.1371/journal.pone.0005492

4. Maines MD, Gibbs PE. 30 some years of heme oxygenase: from a "molecular wrecking ball" to a "mesmerizing" trigger of cellular events. *Biochem Biophys Res Commun* (2005) 338(1):568–77. doi: 10.1016/j.bbrc.2005.08.121

5. Alam J, Igarashi K, Immenschuh S, Shibahara S, Tyrrell RM. Regulation of heme oxygenase-1 gene transcription: Recent advances and highlights from the international conference (Uppsala, 2003) on heme oxygenase. *Antioxid Redox Signal* (2004) 6(5):924–33. doi: 10.1089/ars.2004.6.924

6. Dulak J, Loboda A, Zagorska A, Jozkowicz A. Complex role of heme oxygenase-1 in angiogenesis. *Antioxid Redox Signal* (2004) 6(5):858–66. doi: doi: 10.1089/ars.2004.6.858

7. Salinas M, Diaz R, Abraham NG, Ruiz de Galarreta CM, Cuadrado A. Nerve growth factor protects against 6-hydroxydopamine-induced oxidative stress by increasing expression of heme oxygenase-1 in a phosphatidylinositol 3-kinase-dependent manner. *J Biol Chem* (2003) 278(16):13898–904. doi: 10.1074/jbc.M209164200

8. Martin D, Rojo AI, Salinas M, Diaz R, Gallardo G, Alam J, et al. Regulation of heme oxygenase-1 expression through the phosphatidylinositol 3-kinase/Akt pathway and the Nrf2 transcription factor in response to the antioxidant phytochemical carnosol. *J Biol Chem* (2004) 279(10):8919–29. doi: 10.1074/jbc.M309660200

9. Malaguarnera L, Imbesi RM, Scuto A, D'Amico F, Licata F, Messina A, et al. Prolactin increases HO-1 expression and induces VEGF production in human macrophages. *J Cell Biochem* (2004) 93(1):197–206. doi: 10.1002/jcb.20167

10. Medina MV, Sapochnik D, Garcia Sola M, Coso O. Regulation of the expression of heme oxygenase-1: Signal transduction, gene promoter activation, and beyond. *Antioxid Redox Signal* (2020) 32(14):1033–44. doi: 10.1089/ars.2019.7991

11. Kiemer AK, Bildner N, Weber NC, Vollmar AM. Characterization of heme oxygenase 1 (heat shock protein 32) induction by atrial natriuretic peptide in human endothelial cells. *Endocrinology.* (2003) 144(3):802–12. doi: 10.1210/en.2002-220610

12. Poss KD, Tonegawa S. Reduced stress defense in heme oxygenase 1-deficient cells. *Proc Natl Acad Sci U S A.* (1997) 94(20):10925–30. doi: 10.1073/pnas.94.20.10925

13. Amersi F, Buelow R, Kato H, Ke B, Coito AJ, Shen XD, et al. Upregulation of heme oxygenase-1 protects genetically fat zucker rat livers from ischemia/reperfusion injury. *J Clin Invest.* (1999) 104(11):1631–9. doi: 10.1172/JCI7903

14. Otterbein LE, Soares MP, Yamashita K, Bach FH. Heme oxygenase-1: unleashing the protective properties of heme. *Trends Immunol* (2003) 24(8):449–55. doi: 10.1016/S1471-4906(03)00181-9

15. Tonelli C, Chio IIC, Tuveson DA. Transcriptional regulation by Nrf2. *Antioxid Redox Signal* (2018) 29(17):1727–45. doi: 10.1089/ars.2017.7342

16. Yamamoto M, Kensler TW, Motohashi H. The KEAP1-NRF2 system: a thiol-based sensor-effector apparatus for maintaining redox homeostasis. *Physiol Rev* (2018) 98(3):1169–203. doi: 10.1152/physrev.00023.2017

17. Baird L, Yamamoto M. The molecular mechanisms regulating the KEAP1-NRF2 pathway. *Mol Cell Biol* (2020) 40(13):e00099-20. doi: 10.1128/MCB.00099-20

18. Nguyen T, Sherratt PJ, Pickett CB. Regulatory mechanisms controlling gene expression mediated by the antioxidant response element. *Annu Rev Pharmacol Toxicol* (2003) 43:233–60. doi: 10.1146/annurev.pharmtox.43.100901.140229

19. Itoh K, Chiba T, Takahashi S, Ishii T, Igarashi K, Katoh Y, et al. An Nrf2/small maf heterodimer mediates the induction of phase II detoxifying enzyme genes through antioxidant response elements. *Biochem Biophys Res Commun* (1997) 236(2):313–22. doi: 10.1006/bbrc.1997.6943

20. Hayes JD, McLellan LI. Glutathione and glutathione-dependent enzymes represent a co-ordinately regulated defence against oxidative stress. *Free Radic Res* (1999) 31(4):273–300. doi: 10.1080/10715769900300851

21. Singh A, Misra V, Thimmulappa RK, Lee H, Ames S, Hoque MO, et al. Dysfunctional KEAP1-NRF2 interaction in non-small-cell lung cancer. *PloS Med* (2006) 3(10):e420. doi: 10.1371/journal.pmed.0030420

22. Ohta T, Iijima K, Miyamoto M, Nakahara I, Tanaka H, Ohtsuji M, et al. Loss of Keap1 function activates Nrf2 and provides advantages for lung cancer cell growth. *Cancer Res* (2008) 68(5):1303–9. doi: 10.1158/0008-5472.CAN-07-5003

23. Lister A, Nedjadi T, Kitteringham NR, Campbell F, Costello E, Lloyd B, et al. Nrf2 is overexpressed in pancreatic cancer: Implications for cell proliferation and therapy. *Mol Cancer.* (2011) 10:37. doi: 10.1186/1476-4598-10-37

24. DeNicola GM, Karreth FA, Humpton TJ, Gopinathan A, Wei C, Frese K, et al. Oncogene-induced Nrf2 transcription promotes ROS detoxification and tumorigenesis. *Nature.* (2011) 475(7354):106–9. doi: 10.1038/nature10189

25. Kensler TW, Wakabayashi N, Biswal S. Cell survival responses to environmental stresses *via* the Keap1-Nrf2-ARE pathway. *Annu Rev Pharmacol Toxicol* (2007) 47:89–116. doi: 10.1146/annurev.pharmtox.46.120604.141046

26. Flore O, Rafii S, Ely S, O'Leary JJ, Hyjek EM, Cesarman E. Transformation of primary human endothelial cells by kaposi's sarcoma-associated herpesvirus. *Nature.* (1998) 394(6693):588–92. doi: 10.1038/29093

27. Cesarman E, Damania B, Krown SE, Martin J, Bower M, Whitby D. Kaposi sarcoma. *Nat Rev Dis Primers.* (2019) 5(1):9. doi: 10.1038/s41572-019-0060-9

28. Montaner S, Sodhi A, Molinolo A, Bugge TH, Sawai ET, He Y, et al. Endothelial infection with KSHV genes *in vivo* reveals that vGPCR initiates kaposi's sarcomagenesis and can promote the tumorigenic potential of viral latent genes. *Cancer Cell* (2003) 3(1):23–36. doi: 10.1016/S1535-6108(02)00237-4

29. Montaner S, Sodhi A, Ramsdell AK, Martin D, Hu J, Sawai ET, et al. The kaposi's sarcoma-associated herpesvirus G protein-coupled receptor as a therapeutic target for the treatment of kaposi's sarcoma. *Cancer Res* (2006) 66(1):168–74. doi: 10.1158/0008-5472.CAN-05-1026

30. Sodhi A, Montaner S, Gutkind JS. Does dysregulated expression of a deregulated viral GPCR trigger kaposi's sarcomagenesis? *FASEB J* (2004) 18(3):422–7. doi: 10.1096/fj.03-1035hyp

31. Bais C, Van Geelen A, Eroles P, Mutlu A, Chiozzini C, Dias S, et al. Kaposi's sarcoma associated herpesvirus G protein-coupled receptor immortalizes human endothelial cells by activation of the VEGF receptor-2/KDR. *Cancer Cell* (2003) 3(2):131–43. doi: 10.1016/S1535-6108(03)00024-2

32. Jensen KK, Manfra DJ, Grisotto MG, Martin AP, Vassileva G, Kelley K, et al. The human herpes virus 8-encoded chemokine receptor is required for angioproliferation in a murine model of kaposi's sarcoma. *J Immunol* (2005) 174(6):3686–94. doi: 10.4049/jimmunol.174.6.3686

33. Mutlu AD, Cavallin LE, Vincent L, Chiozzini C, Eroles P, Duran EM, et al. *In vivo*-restricted and reversible malignancy induced by human herpesvirus-8 KSHV: a cell and animal model of virally induced kaposi's sarcoma. *Cancer Cell* (2007) 11(3):245–58. doi: 10.1016/j.ccr.2007.01.015

34. Arvanitakis L, Geras-Raaka E, Varma A, Gershengorn MC, Cesarman E. Human herpesvirus KSHV encodes a constitutively active G-protein-coupled receptor linked to cell proliferation. *Nature.* (1997) 385(6614):347–50. doi: 10.1038/385347a0

35. Cesarman E, Nador RG, Bai F, Bohenzky RA, Russo JJ, Moore PS, et al. Kaposi's sarcoma-associated herpesvirus contains G protein-coupled receptor and cyclin d homologs which are expressed in kaposi's sarcoma and malignant lymphoma. *J Virol* (1996) 70(11):8218–23. doi: 10.1128/jvi.70.11.8218-8223.1996

36. Gershengorn MC, Geras-Raaka E, Varma A, Clark-Lewis I. Chemokines activate kaposi's sarcoma-associated herpesvirus G protein-coupled receptor in mammalian cells in culture. *J Clin Invest.* (1998) 102(8):1469–72. doi: 10.1172/JCI4461

37. Yang TY, Chen SC, Leach MW, Manfra D, Homey B, Wiekowski M, et al. Transgenic expression of the chemokine receptor encoded by human herpesvirus 8 induces an angioproliferative disease resembling kaposi's sarcoma. *J Exp Med* (2000) 191(3):445–54. doi: 10.1084/jem.191.3.445

38. McAllister SC, Hansen SG, Ruhl RA, Raggo CM, DeFilippis VR, Greenspan D, et al. Kaposi sarcoma-associated herpesvirus (KSHV) induces heme oxygenase-1 expression and activity in KSHV-infected endothelial cells. *Blood.* (2004) 103(9):3465–73. doi: 10.1182/blood-2003-08-2781

39. Botto S, Totonchy JE, Gustin JK, Moses AV. Kaposi sarcoma herpesvirus induces HO-1 during *De novo* infection of endothelial cells *via* viral miRNA-dependent and -independent mechanisms. *mBio.* (2015) 6(3):e00668. doi: 10.1128/mBio.00668-15

40. Marinissen MJ, Tanos T, Bolos M, de Sagarra MR, Coso OA, Cuadrado A. Inhibition of heme oxygenase-1 interferes with the transforming activity of the kaposi sarcoma herpesvirus-encoded G protein-coupled receptor. *J Biol Chem* (2006) 281(16):11332–46. doi: 10.1074/jbc.M512199200

41. Polson AG, Wang D, DeRisi J, Ganem D. Modulation of host gene expression by the constitutively active G protein-coupled receptor of kaposi's sarcoma-associated herpesvirus. *Cancer Res* (2002) 62(15):4525–30.

42. Cannon ML, Cesarman E. The KSHV G protein-coupled receptor signals *via* multiple pathways to induce transcription factor activation in primary effusion lymphoma cells. *Oncogene.* (2004) 23(2):514–23. doi: 10.1038/sj.onc.1207021

43. Dadke D, Fryer BH, Golemis EA, Field J. Activation of p21-activated kinase 1-nuclear factor kappaB signaling by kaposi's sarcoma-associated herpes virus G protein-coupled receptor during cellular transformation. *Cancer Res* (2003) 63 (24):8837–47.

44. Shepard LW, Yang M, Xie P, Browning DD, Voyno-Yasenetskaya T, Kozasa T, et al. Constitutive activation of NF-kappa b and secretion of interleukin-8 induced by the G protein-coupled receptor of kaposi's sarcoma-associated herpesvirus involve G alpha(13) and RhoA. *J Biol Chem* (2001) 276(49):45979–87. doi: 10.1074/jbc.M104783200

45. Martin MJ, Tanos T, Garcia AB, Martin D, Gutkind JS, Coso OA, et al. The Galpha12/13 family of heterotrimeric G proteins and the small GTPase RhoA link the kaposi sarcoma-associated herpes virus G protein-coupled receptor to heme oxygenase-1 expression and tumorigenesis. *J Biol Chem* (2007) 282(47):34510–24. doi: 10.1074/jbc.M703043200

46. Gjyshi O, Bottero V, Veettil MV, Dutta S, Singh VV, Chikoti L, et al. Kaposi's sarcoma-associated herpesvirus induces Nrf2 during *de novo* infection of endothelial cells to create a microenvironment conducive to infection. *PloS Pathog* (2014) 10(10):e1004460. doi: 10.1371/journal.ppat.1004460

47. Gjyshi O, Flaherty S, Veettil MV, Johnson KE, Chandran B, Bottero V. Kaposi's sarcoma-associated herpesvirus induces Nrf2 activation in latently infected endothelial cells through SQSTM1 phosphorylation and interaction with polyubiquitinated Keap1. *J Virol* (2015) 89(4):2268–86. doi: 10.1128/JVI.02742-14

48. Alam J, Wicks C, Stewart D, Gong P, Touchard C, Otterbein S, et al. Mechanism of heme oxygenase-1 gene activation by cadmium in MCF-7 mammary epithelial cells. role of p38 kinase and Nrf2 transcription factor. *J Biol Chem* (2000) 275(36):27694–702. doi: 10.1074/jbc.M004729200

49. McMahon M, Itoh K, Yamamoto M, Hayes JD. Keap1-dependent proteasomal degradation of transcription factor Nrf2 contributes to the negative regulation of antioxidant response element-driven gene expression. *J Biol Chem* (2003) 278(24):21592–600. doi: 10.1074/jbc.M300931200

50. Chikumi H, Vazquez-Prado J, Servitja JM, Miyazaki H, Gutkind JS. Potent activation of RhoA by galpha q and gq-coupled receptors. *J Biol Chem* (2002) 277 (30):27130–4. doi: 10.1074/jbc.M204715200

51. Marinissen MJ, Servitja JM, Offermanns S, Simon MI, Gutkind JS. Thrombin protease-activated receptor-1 signals through gq- and G13-initiated MAPK cascades regulating c-jun expression to induce cell transformation. *J Biol Chem* (2003) 278(47):46814–25. doi: 10.1074/jbc.M305709200

52. Coso OA, Chiariello M, Yu JC, Teramoto H, Crespo P, Xu N, et al. The small GTP-binding proteins Rac1 and Cdc42 regulate the activity of the JNK/SAPK signaling pathway. *Cell.* (1995) 81(7):1137–46. doi: 10.1016/S0092-8674(05)80018-2

53. Medina MV, DA A, Ma Q, Eroles P, Cavallin L, Chiozzini C, et al. KSHV G-protein coupled receptor vGPCR oncogenic signaling upregulation of cyclooxygenase-2 expression mediates angiogenesis and tumorigenesis in kaposi's sarcoma. *PloS Pathog* (2020) 16(10):e1009006. doi: 10.1371/journal.ppat.1009006

54. Bryan HK, Olayanju A, Goldring CE, Park BK. The Nrf2 cell defence pathway: Keap1-dependent and -independent mechanisms of regulation. *Biochem Pharmacol* (2013) 85(6):705–17. doi: 10.1016/j.bcp.2012.11.016

55. Ma Q, Cavallin LE, Leung HJ, Chiozzini C, Goldschmidt-Clermont PJ, Mesri EA. A role for virally induced reactive oxygen species in kaposi's sarcoma herpesvirus tumorigenesis. *Antioxid Redox Signal* (2013) 18(1):80–90. doi: 10.1089/ars.2012.4584

56. Cavallin LE, Ma Q, Naipauer J, Gupta S, Kurian M, Locatelli P, et al. KSHV-induced ligand mediated activation of PDGF receptor-alpha drives kaposi's sarcomagenesis. *PloS Pathog* (2018) 14(7):e1007175. doi: 10.1371/journal.ppat.1007175

57. Bais C, Santomasso B, Coso O, Arvanitakis L, Raaka EG, Gutkind JS, et al. G-Protein-coupled receptor of kaposi's sarcoma-associated herpesvirus is a viral oncogene and angiogenesis activator. *Nature.* (1998) 391(6662):86–9. doi: 10.1038/34193

58. Mesri EA, Cesarman E, Boshoff C. Kaposi's sarcoma and its associated herpesvirus. *Nat Rev Cancer.* (2010) 10(10):707–19. doi: 10.1038/nrc2888

59. Sodhi A, Montaner S, Patel V, Zohar M, Bais C, Mesri EA, et al. The kaposi's sarcoma-associated herpes virus G protein-coupled receptor up-regulates vascular endothelial growth factor expression and secretion through mitogen-activated protein kinase and p38 pathways acting on hypoxia-inducible factor 1alpha. *Cancer Res* (2000) 60(17):4873–80.

60. Couty JP, Geras-Raaka E, Weksler BB, Gershengorn MC. Kaposi's sarcoma-associated herpesvirus G protein-coupled receptor signals through multiple pathways in endothelial cells. *J Biol Chem* (2001) 276(36):33805–11. doi: 10.1074/jbc.M104631200

61. Montaner S, Sodhi A, Pece S, Mesri EA, Gutkind JS. The kaposi's sarcoma-associated herpesvirus G protein-coupled receptor promotes endothelial cell survival through the activation of akt/protein kinase b. *Cancer Res* (2001) 61 (6):2641–8.

62. Pati S, Foulke JSJr., Barabitskaya O, Kim J, Nair BC, Hone D, et al. Human herpesvirus 8-encoded vGPCR activates nuclear factor of activated T cells and collaborates with human immunodeficiency virus type 1 tat. *J Virol* (2003) 77 (10):5759–73. doi: 10.1128/JVI.77.10.5759-5773.2003

63. Huang HC, Nguyen T, Pickett CB. Phosphorylation of Nrf2 at ser-40 by protein kinase c regulates antioxidant response element-mediated transcription. *J Biol Chem* (2002) 277(45):42769–74. doi: 10.1074/jbc.M206911200

64. Keum YS, Yu S, Chang PP, Yuan X, Kim JH, Xu C, et al. Mechanism of action of sulforaphane: Inhibition of p38 mitogen-activated protein kinase isoforms contributing to the induction of antioxidant response element-mediated heme oxygenase-1 in human hepatoma HepG2 cells. *Cancer Res* (2006) 66 (17):8804–13. doi: 10.1158/0008-5472.CAN-05-3513

65. Skalsky RL, Samols MA, Plaisance KB, Boss IW, Riva A, Lopez MC, et al. Kaposi's sarcoma-associated herpesvirus encodes an ortholog of miR-155. *J Virol* (2007) 81(23):12836–45. doi: 10.1128/JVI.01804-07

66. Qin Z, Freitas E, Sullivan R, Mohan S, Bacelieri R, Branch D, et al. Upregulation of xCT by KSHV-encoded microRNAs facilitates KSHV dissemination and persistence in an environment of oxidative stress. *PloS Pathog* (2010) 6(1):e1000742. doi: 10.1371/journal.ppat.1000742

frontiers | Frontiers in Oncology

TYPE Original Research
PUBLISHED 23 September 2022
DOI 10.3389/fonc.2022.927140

OPEN ACCESS

EDITED BY
Sharon Prince,
University of Cape Town, South Africa

REVIEWED BY
Anca Maria Cimpean,
Victor Babes University of Medicine and Pharmacy, Romania
Navnath S. Gavande,
Wayne State University, United States

*CORRESPONDENCE
Christiane Kuempers
christiane.kuempers@uksh.de

SPECIALTY SECTION
This article was submitted to Molecular and Cellular Oncology, a section of the journal Frontiers in Oncology

RECEIVED 10 May 2022
ACCEPTED 02 September 2022
PUBLISHED 23 September 2022

CITATION
Kuempers C, Jagomast T, Heidel C, Paulsen F-O, Bohnet S, Schierholz S, Dreyer E, Kirfel J and Perner S (2022) CDK7 is a prognostic biomarker for non-small cell lung cancer. *Front. Oncol.* 12:927140. doi: 10.3389/fonc.2022.927140

CDK7 is a prognostic biomarker for non-small cell lung cancer

Christiane Kuempers[1*], Tobias Jagomast[1], Carsten Heidel[1,2], Finn-Ole Paulsen[1,3], Sabine Bohnet[4], Stefanie Schierholz[5], Eva Dreyer[1], Jutta Kirfel[1] and Sven Perner[1,6,7]

[1]Institute of Pathology, University Hospital Schleswig-Holstein, Luebeck, Germany, [2]Department of Surgery, Schoen Klinik Neustadt, Holstein, Germany, [3]Department of Oncology, Hematology and Bone Marrow Transplantation with Division of Pneumology, University Medical Center Hamburg-Eppendorf, Hamburg, Germany, [4]Department of Pulmonology, University Hospital Schleswig-Holstein, Luebeck, Germany, [5]Department of Surgery, Medical University of Schleswig-Holstein, Luebeck, Germany, [6]Pathology, Research Center Borstel-Leibniz Lung Center, Borstel, Germany, [7]German Center for Lung Research (DZL) Department Borstel, Borstel, Germany

Aim: Non-small cell lung cancer (NSCLC) remains the leading cause of cancer-related death globally despite promising progress of personalized therapy approaches. Cyclin-dependent kinase 7 (CDK7) is a kinase involved in transcription, overexpressed in a broad spectrum of cancer types and found to be associated with an unfavourable prognosis. In this study, we aimed to investigate the protein expression of CDK7 in a large cohort of NSCLC incorporating adenocarcinomas (adNSCLC) and squamous cell carcinomas (sqNSCLC) and to correlate its expression with clinicopathological data.

Methods: We performed immunohistochemical staining of CDK7 on our cohort of NSCLC including 258 adNSCLC and 101 sqNSCLC and measured protein expression *via* a semi-automated read out. According to the median value of CDK7 the cohort was stratified in a CDK7 high and low expressing group, respectively, and results were correlated with clinico-pathological data.

Results: CDK7 was significantly higher expressed in sqNSCLC than in adNSCLC. In the group of sqNSCLC, CDK7 expression was significantly higher in sqNSCLC with lymph node metastases than in sqNSCLC with N0 stage. We found a significantly worse overall survival and disease-free survival for patients with CDK7 high expressing NSCLC.

Conclusion: Since a high CDK7 expression seems to be linked with a poor prognosis it might serve as a promising novel prognostic biomarker and its assessment could be implied in future routine diagnostic workup of NSCLC samples. Considering that CDK7 inhibitors are currently tested in several trials for advanced solid malignancies, it may also be a new target for future anti-cancer therapy.

10.3389/fonc.2022.927140

KEYWORDS
CDK7, non-small cell lung cancer (NSCLC), prognostic, biomarker, immunohistochemistry

Introduction

Non-small cell lung cancer (NSCLC) remains, despite promising progress of personalized therapy approaches, the leading cause of cancer-related death globally (1).

The cyclin-dependent kinases (CDK) are a family of several serine/threonine kinases that regulate essential cellular processes. They are broadly divided into the two major

Subclasses of cell cycle–associated CDKs and transcription-associated CDKs, the latter group including CDK7. The transcription-associated CDKs play major roles in the multistep process of RNA polymerase II transcription. CDK7 is a 346 amino acid protein that binds to cyclin H and the accessory protein MAT1 to function as a CDK-activating kinase. CDK7 regulates the initiation of transcription and promoter escape by phosphorylating the carboxy-terminal domain of RNA Pol II and therefore has a general role in transcription (2). Overexpression of CDK7 is commonly observed in a broad spectrum of human cancers for example breast cancer, hepatocellular carcinoma, gastric cancer, colorectal cancer, squamous cell carcinomas of the oral cavity, head and neck (HNSCC) and esophagus, as well as ovarian cancer (3–10). Here, it was found to associate with aggressive clinicopathological features and unfavourable prognosis, except for ER+ breast cancer where its overexpression is linked with a better prognosis (11).

Due to CDKs control processes critical for cancer cell survival and growth, they have been discussed as promising therapeutic targets. Elevated CDK7 expression in tumor cells compared with their normal counterparts raise the possibility that tumors with increased expression of CDK7 may be more sensitive to CDK7 inhibition, particularly in the case of ER+ breast cancer, where the CDK7-activated nuclear receptor, ERα, drives tumor progression (12). However, there does not seem to be clear evidence in the literature regarding the question of whether protein expression of CDK7 is related to sensitivity towards CDK7 inhibitors.

Until now, even multiple CDK inhibitors (CDKIs) have been developed and tested in different cancer types (2, 12). CDKIs, specifically the ones that block the enzyme activity of CDK4 and CDK6, have been approved by FDA for the treatment of metastatic hormone receptor-positive breast cancer (13).

Concerning lung cancer, THZ1, a selective CDK7 covalent inhibitor, has recently been shown to be effective in reducing the expression of superenhancer-associated genes and inhibiting growth of small cell lung cancer (SCLC) (14). The more specific CDK7 inhibitor YKL-5–124 was found to predominately disrupt cell cycle progression while simultaneously triggering immune response signaling in SCLC, which provides a rationale for new combination regimens consisting of CDK7 inhibitors and immunotherapy (15).

There are also some studies on CDK7 inhibition for NSCLC (1, 16–18). Cheng et al. (16) could show that treatment with THZ1 suppressed proliferation and migration of human NSCLC cell lines, arrested cell cycle at G2/M phase and induced apoptosis. They found that CDK7 inhibition blocked the glycolysis pathway without affecting glutamine metabolism, suggesting that the inhibitory effect of THZ1 is due in part to an impairment of cancer metabolism. Hur et al. (18) investigated the effects of THZ1 in squamous cell carcinoma cell lines with SOX2 amplification and also found that THZ1 treatment led to suppression of cell growth and apoptotic cell death. They conclude that THZ1 may effectively control the proliferation and survival of SOX2-amplified squamous cell carcinoma cells through a decrease in global transcriptional activity. Ji et al. (17) found that THZ1-tolerant cells partially recovered their sensitivity to 3rd generation EGFR-TKIs and conclude that CDK7 inhibitors could potentially be used as a therapeutic strategy to overcome EMT-associated EGFR-TKI resistance in NSCLC.

However, the CDK7-mediated mechanisms involved in progression of NSCLC are not fully understood and protein expression of CDK7 in NSCLC has not extensively been studied so far.

In this study, we aimed to investigate the protein expression of CDK7 in a huge cohort of NSCLC incorporating pulmonary adenocarcinomas (adNSCLC) and pulmonary squamous cell carcinomas (sqNSCLC) and to correlate its expression with clinicopathological data and survival.

Abbreviations: adNSCLC, pulmonary lung adenocarcinoma; CDKIs, CDK inhibitors; CDK7, Cyclin-depending Kinase 7; DFS, disease-free survival; ESCC, esophageal squamous cell carcinomas; FFPE, Formalin-fixed paraffin-embedded; HNSCC, head and neck squamous cell carcinomas; IHC, Immunohistochemistry; OD, optical density; OS, overall survival; OSCCs, oral squamous cell carcinomas; SCC, squamous cell carcinoma; sqNSCLC, pulmonary squamous cell carcinoma; TMA, tissue microarrays.

Material and methods

Cohort

359 patients with lung cancer (258 adNSCLC, 101 sqNSCLC) undergoing surgical resection were enrolled in this study. The median age of the patients (157 female, 202 male) at initial diagnosis was 67 years. At the time of the last follow-up, 56 patients were alive and 294 were deceased. Tumors were graded according to the 2015 World Health Organization Classification of Lung Tumors. 6 of the primary tumors were graded as G1 (1.7%), 176 as G2 (49%), and 175 as G3 (48.7%). In 3 cases (0.8%) grading was not provided. For determination of tumor state, the 8th Edition of UICC/TNM staging system was used. From primary tumors, 160 (44.6%), 95 (26.5%), 59 (16.4%) and 43 (12%) were classified as pT1, pT2, pT3 and pT4, respectively. In 2 cases (0.6%) note concerning T-stage was missing. In 31 cases (23 adNSCLC and 8 sqNSCLC, respectively) note concerning N-stage was missing. Archived tissue blocks and slides were collected from 2005 to 2017. All data were anonymized before inclusion in this retrospective study cohort.

This study was approved by the Internal Review Board of the University of Luebeck (file number 16-277, 16-278).

Immunohistochemistry (IHC)

IHC staining was performed according to the manufacturer's instructions, using the Ventana Discovery (Ventana Medical System) automated staining system. In brief, slides were incubated with a primary CDK7- antibody (mouse monoclonal, CDK7 (MO1) Mouse mAb #2916, 1:100, Cell Signaling, Danvers, MA, USA).

For IHC, tissue microarrays (TMA) were constructed from formalin-fixed paraffin-embedded (FFPE) tumor blocks as described previously (19). In short, for TMA construction each sample was represented in triplicates of 0.6 mm diameter cores. A tumor sample was incorporated in further analysis if at least one core was evaluable. Staining was considered positive if staining was nuclear.

Stained slides were scanned (Panoramic Desk, 3DHistech) and evaluation of the staining intensity was performed with the bioimage analysis software *QuPath*, short for Quantitative Pathology (20, 21). This software allows objective assessment of the staining intensity in different cellular compartments within specified regions of interest (ROI). ROIs were defined as tumor cell areas that were annotated in each TMA core to exclude stromal cells and benign areas from evaluation (Supplement Figure 1). Due to nuclear staining of CDK7, mean Nuclear DAB optical density (OD) of each core was automatically calculated. This resulted in continuous arbitrary variables to reflect protein expression of the tumor cells. For further analysis, mean value of the patients' triplets was obtained. A representative subset of the cores was reviewed by two independent pathologists (CK and SP) with regard to a meaningful evaluation performed by the software. This ensured that expression above the calculated median corresponded conventional-morphologically to moderate to strong nuclear staining, and expression below the median to an absent or weak nuclear staining. Median of nuclear DAB OD (0.2497) from all samples was used to dichotomize the cohort into CDK7 high and low expressing group. On basis of this dichotomization, the statistical analysis concerning survival and correlation with other clinicopathological data was carried out.

Statistical analyses

For the statistical analyses and data visualization, R software (version 4.0.2, R Foundation, Vienna, Austria; http://www.R-project.org) was used. T-tests were used to associate CDK7 expression with tumor entity and to examine differences between primary tumors with and without nodal metastases. To analyze a correlation of CDK7 expression with clinicopathological characteristics T-tests were applied. Chi-square tests were used to distinguish whether there were differences in clinicopathological features of the CDK7 low and CDK7 high expressing groups, which we considered in the survival analyses. Kaplan-Meier curves were used to illustrate overall survival (OS) and disease-free survival (DFS) in dependency of CDK7 expression and were statistically proved by log-rank tests. All tests were two-tailed and p-values of < 0.05 were considered statistically significant.

Results

CDK7 expression pattern in primary NSCLC

CDK7 showed nuclear staining. Expression pattern for CDK7 between the cores originating from one tumor sample was homogenous meaning that the intratumoral difference in expression of the cells was neglectable. Figure 1 provides pictures of immunohistochemical stainings. However, the overall expression between patients varied with a range of expression intensities from absent to strong immunoreactivity.

For further analyses, the cohort was divided in a CDK7 low and a CDK7 high expressing group by stratifying samples according to the median OD value of CDK7 (n= 179 each).

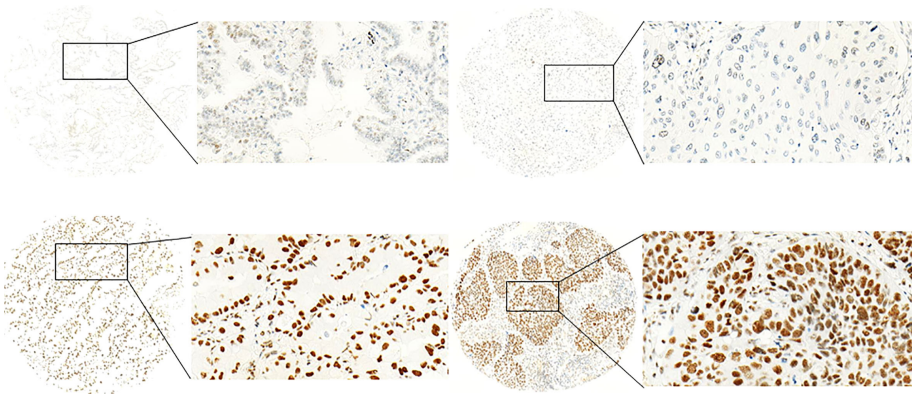

FIGURE 1
Exemplary pictures of CDK7 expression patterns in NSCLC. Left: adNSCLC with low (top) and high (below) expression (nuclear DAB OD 0.1547 and 0.5006, respectively). Right: sqNSCLC with low (top) and high (below) expression (nuclear DAB OD 0.1524 and 0.3969, respectively) of CDK7. Median nuclear DAB OD = 0.2497). The figures demonstrate specific nuclear staining that appears homogenous within the cores. (Objective magnification ×100 and 400, respectively).

Considering the two groups of adNSCLC and sqNSCLC separately, one striking result was that CDK7 was significantly higher expressed in sqNSCLC than in adNSCLC ($p < 0.0001$; Figure 2). Of the 101 sqNSCLC, 70 (69.3%) were CDK7 high and 31 (30.7%) were CDK7 low expressing tumors. Of the 258 adNSCLC instead, 109 (42.2%) were CDK7 high and 149 (57.8%) were CDK7 low expressing tumors.

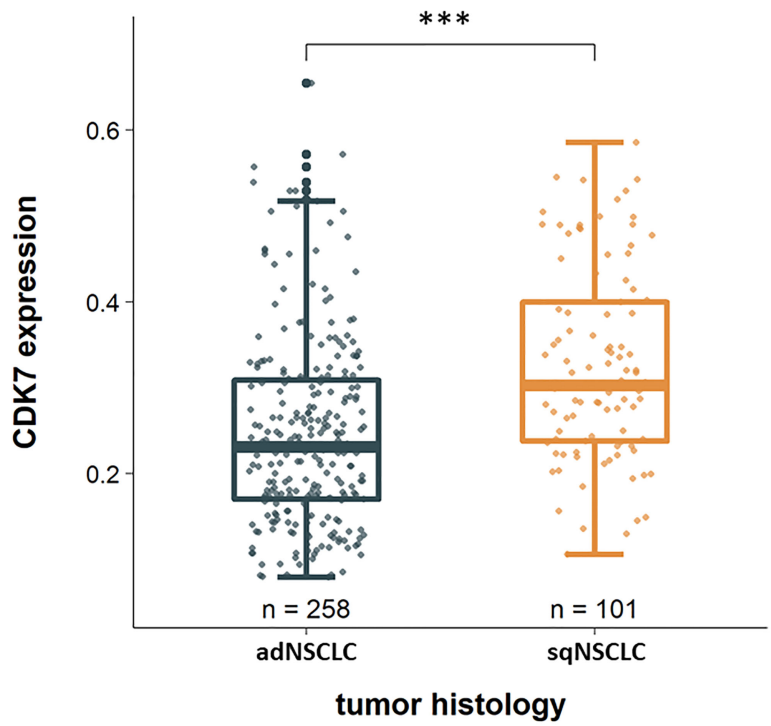

FIGURE 2
CDK7 expression in dependency of tumor histology. CDK7 is significantly higher expressed in sqNSCLC compared to adNSCLC (*** $p < 0.0001$).

Correlation of CDK7 expression with clinicopathological characteristics

Concerning the whole cohort, there was no significant correlation of CDK7 expression concerning T-status, N-status, M-status, and UICC-status, grading, or time to recurrence. However, there was a trend for a higher UICC-stage (p 0.32) and worse grading (p 0.24) with increasing CDK7 expression (data not shown). Furthermore, CDK7 expression tended to be higher in primary carcinomas that later recurred compared to primary tumors that showed no relapse (p 0.34). One significant result was observed with regard to sex meaning that CDK7 was higher expressed in NSCLC of male patients (p=0.0274).

Considering these parameters in the two groups of adNSCLC and sqNSCLC separately, we observed that CDK7 expression was significantly higher in sqNSCLC with lymph node metastases than in sqNSCLC with N0 stage (p 0.039; Figure 3). This could not be stated for the group of adNSCLC (p 0.086; not shown). There were no further significant differences concerning T-status, M-status, and UICC-status, grading or time to recurrence between the two entities with regard to CDK7 expression.

Correlation of CDK7 expression with survival

We analyzed whether CDK7 expression could predict OS. Required follow-up data were available for the majority of the cohort of 346 cases (96.4%). By stratifying samples according to the median, two equal-size groups (high CDK7 expressing tumors above median (n=173) and low CDK7 expressing tumors below median (n=173)) were created (Table 1).

Concerning the whole cohort, Kaplan-Meier curve indicates a significantly worse OS for patients with CDK7 high expressing NSCLC than for patients with CDK7 low expressing NSCLC (log-rank test p 0.0036; Figure 4A). For OS, the 5-year survival rates were estimated at 58% for CDK7 high expression and 78% for low expression, respectively.

Due to expression of CDK7 was significantly different between adNSCLC and sqNSCLC, we assessed OS between both entities. We arrived at the same result for the subcohort of adNSCLC meaning that patients with CDK7 high expressing adNSCLC showed a significantly worse OS (p 0.0046; Figure 4B). 5-year survival rates were estimated at 55% for CDK7 high expressing adNSCLC and 80% for low CDK7 expressing adNSCLC.

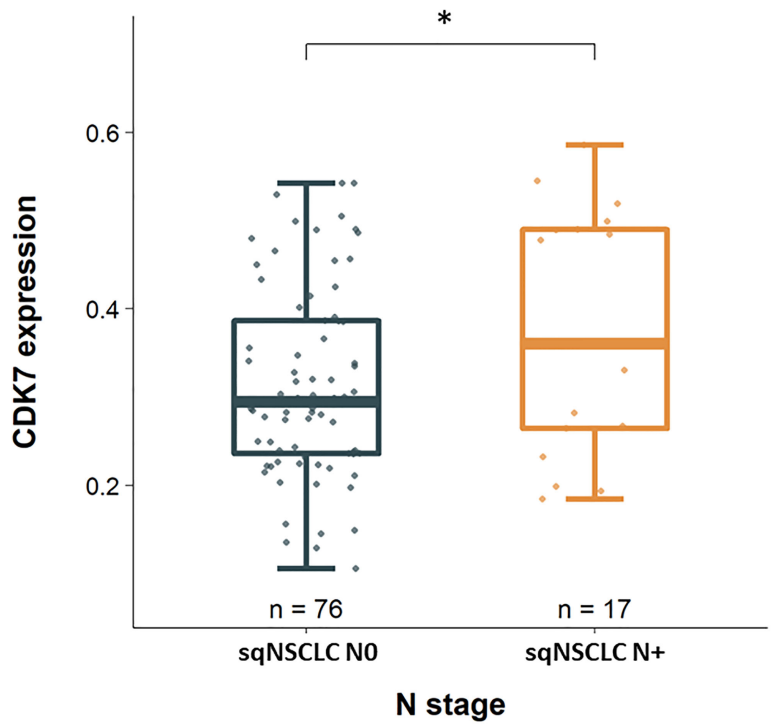

FIGURE 3
CDK7 expression between sqNSCLC with and without lymph node metastases. Compared to sqNSCLC with a pN0 stage, sqNSCLC with lymph node metastases show a significant higher CDK7 expression (* p 0.039).

10.3389/fonc.2022.927140

TABLE 1 Overview of clinico-pathological characteristics of CDK7 high and low expressing group.

	CDK7 low (n=173)	CDK7 high (n=173)	total (n=346)	p-value
Sex				0,159
female	82 (47.4%)	69 (39.9%)	151 (43.6%)	
male	91 (52.6%)	104 (60.1%)	195 (56.4%)	
Age				0,747
> median	84 (48.6%)	87 (50.3%)	171 (49.4%)	
< median	89 (51.4%)	86 (49.7%)	175 (50.6%)	
T-stage				0,517
missing	0	2	2	
T(1,2)	121 (69.9%)	125 (73.1%)	246 (71.5%)	
T(3,4)	52 (30.1%)	46 (26.9%)	98 (28.5%)	
N-Stage				0,29
missing	6	22	28	
N(0)	125 (74.9%)	105 (69.5%)	230 (72.3%)	
N(1,2)	42 (25.1%)	46 (30.5%)	88 (27.7%)	
M-Stage				0,814
missing	129	120	249	
M(0)	41 (93.2%)	50 (94.3%)	91 (93.8%)	
M(1)	3 (6.8%)	3 (5.7%)	6 (6.2%)	
UICC-Stage				0,507
missing	2	17	19	
Mean (SD)	1.719 (0.842)	1.782 (0.867)	1.749 (0.853)	
Range	1.000 - 4.000	1.000 - 4.000	1.000 - 4.000	
Median (Q1, Q3)	1.000 (1.000, 2.000)	2.000 (1.000, 2.250)	1.000 (1.000, 2.000)	
Grading				0,786
missing	1	2	3	
G(1,2)	87 (50.6%)	89 (52.0%)	176 (51.3%)	
G(3,4)	85 (49.4%)	82 (48.0%)	167 (48.7%)	

For the subcohort of sqNSCLC there was no difference concerning OS in dependency of CDK7 expression (p 0.55; not shown).

In the following, we investigated if CDK7 expression has also an implication regarding DFS thereby taking the whole cohort as well as the subcohorts separately into consideration. Survival analysis was restricted to 202 patients with required follow-up data. According to the median, Kaplan-Meier curve indicates a significantly worse DFS for patients with CDK7 high expression

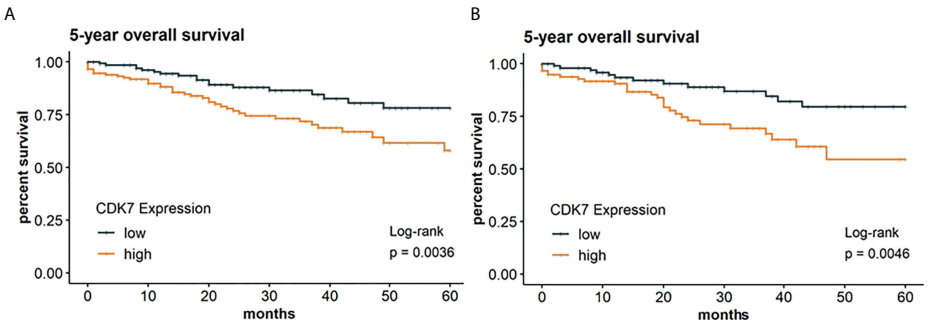

FIGURE 4
Kaplan Meier graphs with a p-value of Log-rank test of **(A)** 5-year overall survival of the whole cohort and **(B)** 5-year overall survival of the subcohort of adNSCLC. Median of CDK7 expression was used to stratify the cohort in two groups with expression above median considered as high expression and expression below median considered as low expression. Upregulation of CDK7 correlated significantly with a shorter OS for the whole cohort and group of adNSCLC (p=0.0036 and p=0.0046, respectively).

in NSCLC than for patients with CDK7 low expression in NSCLC (log-rank test p 0.022; Figure 5A). 5-year disease-free survival rates were 32% and 56% for high and low CDK7 expression, respectively.

The same applies to the group of adNSCLC (p 0.027; Figure 5B). Here, 5-year survival rates were estimated at 31% for CDK7 high expressing adNSCLC and 64% for low CDK7 expressing adNSCLC.

As for OS, we also found no difference of DFS in dependency of CDK7 expression for the subcohort of sqNSCLC (p 0.15; not shown).

To assess if the prognostic value of CDK7 expression was independent of other prognostic factors for 5-year OS and 5-year DFS, at first univariable followed by multivariable cox regression was performed. It was found that high CDK7 expression was not an independent prognostic factor neither for OS nor for DFS (OS: HR=4.92 (95% CI 0.92-26.41), p=0.063; DFS: HR= 0.94 (95% CI 0.47-1.89), p=0.858).

Discussion

Despite promising advances in the therapy of NSCLC, the identification of new prognostic and therapeutically targetable biomarkers is needed. Molecular targeted therapy has improved the survival of adNSCLC patients, while less advances have been made in the treatment of sqNSCLC (18). Recently, transcription-associated CDKs, to which CDK7 also belongs, have emerged as an exciting area of great promise in oncology. Various studies demonstrate that cancers depend on oncogenic transcription factors and their downstream networks can be therapeutically targeted by CDK7 inhibitors of which THZ1 is the best known (2). The role of CDK7 in NSCLC has not yet been investigated as thoroughly as in other malignancies, and concerning lung cancer, there are already more insights for SCLC than for NSCLC. However, for NSCLC, there are few *in vitro* studies using cell lines from pulmonary adenocarcinoma and squamous cell carcinoma demonstrating that THZ1 effectively inhibits cell proliferation and migration, causes cell-cycle arrest, induces apoptosis, and suppresses glycolysis (1, 16–18). Wang et al. (1) have conducted extensive *in vitro*- and *in vivo*- studies and could demonstrate that CDK7 silencing and inhibition with THZ1 elicited apoptosis and suppressed tumor growth of NSCLC. Moreover, THZ1 boosted antitumor immunity by recruiting infiltrating CD8+ T cells and synergized with anti-PD-1 therapy. The authors conclude that the combined CDK7 inhibition and anti-PD-1 therapy could be an effective treatment of NSCLC.

However, no direct link between protein expression of CDK7 and sensitivity towards CDK7 inhibition is mentioned in the studies. There are only few studies dealing with protein expression of CDK7 on lung cancer. To the best of our knowledge, this should be the first study to investigate protein expression of CDK7 in a large cohort of NSCLC containing both adNSCLC and sqNSCLC, which represent the two major subtypes of NSCLC (approx. 60 and 30%, respectively) (18, 22).

CDK7 expression pattern

Concerning evaluation of expression pattern, we set a high and low expressing group according to the median nuclear DAB OD value of CDK7 resulting in two groups of equal size (n=179 each). Automatically calculated values reflecting protein expression of the tumor cells were reviewed with regard to a meaningful evaluation by two pathologists. Expression values above the calculated median corresponded conventional-morphologically to moderate to strong

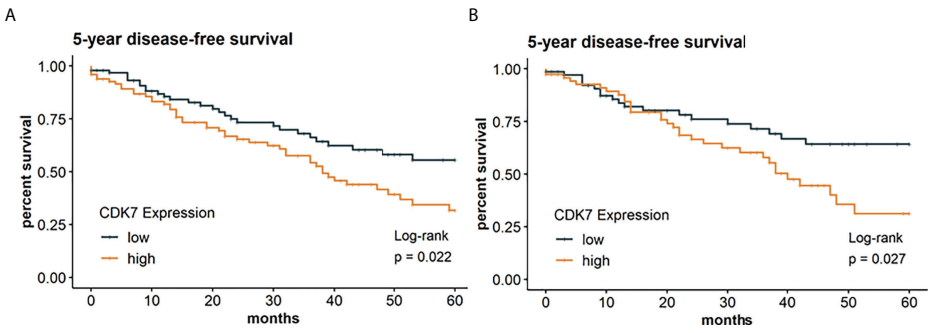

FIGURE 5
Kaplan Meier graphs with a p-value of Log-rank test of **(A)** 5-year disease-free survival of the whole cohort and **(B)** 5-year disease-free survival of the subcohort of adNSCLC. Median of CDK7 expression was used to stratify the cohort in two groups with expression above median considered as high expression and expression below median considered as low expression. Upregulation of CDK7 correlated significantly with a shorter DFS for the whole cohort and group of adNSCLC (p=0.0022 and p=0.0027, respectively).

nuclear staining, and expression below the median to an absent or weak nuclear staining.

Our observed expression pattern fits into data in literature. For example, in a study by Wang et al., the group sizes of CDK7 low and high expressing adNSCLC in two independent cohorts were also approximately equal (cohort 1: CDK7 low n=52 (56.5%), CDK7 high n=40 (43.5%); cohort 2: CDK7 low n=118 (53.2%), CDK7 high n=104 (46.8%)). In this regard, assessment of immunohistochemical staining must be taken into account. In above-mentioned study, evaluation of CDK7 staining pattern is comparable to ours. CDK7 staining was semi-quantified scored as 0 to 3+ using signal intensity in the tumor cell nuclei (no staining = 0, weak = 1, moderate = 2, strong = 3). CDK7 score ≥ 2 was used as cut-off for dividing the samples into a high and low expression group. In another study dealing with CDK7 expression on adNSCLC corresponding group sizes are not explicitly stated (22).

There are seemingly so far no published studies concerning protein expression of CDK7 in sqNSCLC. However, there are studies that have investigated squamous cell carcinomas (SCC) of other sites. Jiang et al. examined protein expression of CDK7 in oral squamous cell carcinomas (OSCCs) (n=113). Immunoreactivity was evaluated using the immunoreactive score reaching from 0 to 12 (intensity score × proportion score defining intensity score as 0 = negative, 1 = weak, 2 =moderate, 3= strong and defining proportion score as 0 = negative, 1= <10%, 2 = 11-50%, 3 = 51-80%, 4 = >80% positive cells). The distribution of the samples in a CDK7 low and high expressing group was 54.8% (n=62) and 45.2% (n=51), respectively and was thus also even. Zhang et al. who examined protein expression of CDK7 in 98 esophageal squamous cell carcinomas (ESCC) used the same score and with that found a higher proportion of CDK7 high expressing tumors (81.6%, n=80).

We found that CDK7 was significantly higher expressed on sqNSCLC than on adNSCLC (Figure 2). Since there are no other studies that have comparatively investigated the protein expression of CDK7 on both entities, our results are not comparable one to one.

Prognostic significance

Concerning survival data, we found a high CDK7 protein expression to be associated with a poor OS and DFS for the whole cohort and the group of adNSCLC (Figures 4 and 5). This finding is in line with that of Wang et al. In this already above-mentioned study, two independent cohorts of pure adNSCLC (n = 92 and 222, respectively) were investigated (1). The authors stated a significantly poorer OS (p 0.036 and 0.003, respectively) in adNSCLC with high CDK7 protein expression. Bian et al. (22) examined 100 samples of adNSCLC *via* immunohistochemistry and also found a significantly poorer OS for patients with high expression of CDK7 ($p < 0.0001$).

In agreement with these findings, studies investigating protein expression of CDK7 in squamous cell carcinomas stated a relationship of increased CDK7 expression with poor prognosis. Since no studies concerning protein expression of CDK7 in sqNSCLC are published so far, literature regarding CDK7 expression on squamous cell carcinomas (SCC) of other sites is discussed. Jiang et al. found an elevated CDK7 expression on OSCCs to be significantly associated with a reduced OS as well as DFS (p 0.022 and 0.010, respectively) (7). Zhang et al. (9) stated that patients with CDK7 high expressing ESCC had a significantly shorter OS (p 0.01) and identified CDK7 as an independent prognostic indicator of OS. Jagomast et al. (8) also noted that CDK7 overexpression resulted in significantly worse 5-year OS as well as DFS rates for HNSCC patients (p 0.037 and 0.016, respectively). Since aetiological factors for sqNSCLC include first of all smoking which also applies to OSCC, ESCC, and HNSCC a comparison of CDK7 expression between these carcinoma entities is justified.

Just mentioned results are in contrast to our finding that there was no significant association of CDK7 expression with regard to OS and DFS in the subcohort of sqNSCLC. Here, the relatively smaller number of cases compared to the number of adNSCLC in our cohort (n= 101 vs. 258) should be taken into consideration. Still, the reasons are not entirely comprehensible especially since the group size of sqNSCLC (n=101) is comparable to SCC cohorts in literature and since etiologic factors overlap (7, 9). Possible reasons could be different definitions for high vs. low expressing tumors (cf (7, 9).) and a smaller cohort size compared to the study of Jagomast et al. (n=419) who used the same definition for CDK7 low vs. CDK7 high (8). Whether CDK7 is indeed no prognostic for sqNSCLC should be investigated on independent and larger sqNSCLC cohorts.

Interestingly, we found an overall higher expression of CDK7 for sqNSCLC than for adNSCLC (Figure 2), for which we could not demonstrate an association with survival data. In addition, for sqNSCLC we found a higher expression of CDK7 in primary tumors that were nodally metastatic than in non-metastatic sqNSCLC (Figure 3). The results were significant (p 0.039) even though the proportion of sqNSCLC with metastases was smaller than the proportion of sqNSCLC without metastases (n=17 (18.3%) vs n=76 (81.7%), Figure 3). Since metastasis generally results in poorer survival, the data appear contradictory. Here, it should be taken into account that the group of sqNSCLC (n=101) might be too small to provide an association with survival data. However, this finding may suggest that immunohistochemically detected overexpression of CDK7 on sqNSCLC is indicative of lymph node metastasizing and thus greater aggressiveness. These findings need further analysis on larger cohorts of sqNSCLC. Studies investigating CDK7 expression on SCC did not discover a significant correlation with N-Stage (7–9).

There was no significant association of CDK7 expression in dependency of lymph node metastasizing in the subcohort of adNSCLC (p 0.086) although the proportion of metastatic adNSCLC (n=77; 32.8%) among adNSCLC was higher than the proportion of metastatic sqNSCLC among sqNSCLC. Studies that have investigated CDK7 expression on adNSCLC do not address correlation with metastasis, so no comparison with our data can be made here.

Correlation of CDK7 Expression with other clinicopathological variables

The only significant correlation was found in relation to sex meaning that CDK7 was higher expressed in NSCLC from male patients (p=0.0274). This observation should however be primarily a coincidence without having a causal relationship. Our observation that CDK7 expression does actually not associate with clinicopathological data other than survival broadly fits with those from cited literature. However, for example, Jiang et al. found an elevated CDK7 expression on OSCCs to be significantly associated with higher T-stage (p 0.009) (7) and Zhang et al. stated that overexpression of CDK7 was significantly associated with worse tumor grade (p<0.01). Studies on protein expression of CDK7 on adNSCLC do not explicitly address its correlation with clinic-pathological parameters on which we focused (1, 22).

In summary, to our knowledge, we are seemingly the first to examine CDK7 protein expression on a cohort of NSCLC containing both adNSCLC and sqNSCLC. These data are of interest due to promising *in vitro* studies on CDK7 and its inhibition in NSCLC exist already. We found CDK7 be to significantly higher expressed on sqNSCLC than on adNSCLC. CDK7 expression was significantly higher in sqNSCLC with lymph node metastases than in sqNSCLC with N0 stage, indicating a greater aggressiveness. We found a significantly worse OS and DFS for CDK7 high expressing tumors in the whole NSCLC cohort and subcohort of adNSCLC.

Our findings suggest that the CDK7 protein expression status could offer valuable information about prognosis of NSCLC patients and thereby it could serve as indicator for a meaningful follow-up management. Therefore, its involvement in routine diagnostic workup of NSCLC samples could be meaningful in the future. Additionally, due to its clear nuclear staining, expression pattern would be effortless to evaluate.

Our study has the major limitation that our results are not validated with an independent cohort. Since the results of a single biomarker study have limited value, validation from other researchers on independent cohorts is required.

Given promising previous findings of *in vitro* studies with CDK7 inhibitors on NSCLC cells together with our findings and assuming that protein expression of CDK7 in the large cohort of NSCLC might indicate sensitivity to CDK7 inhibition, one could suggest that CDK7 might serve as a novel prognostic biomarker and additionally as therapeutic target.

Finally, prospective studies are necessary to validate our findings on independent cohorts, to investigate a correlation between CDK7 protein expression and sensitivity towards CDK7 inhibition, and to unravel molecular mechanisms by which CDK7 contributes to poor prognosis in NSCLC.

Data availability statement

The raw data supporting the conclusions of this article will be made available by the authors, without undue reservation.

Ethics statement

The study was conducted in accordance with the Declaration of Helsinki, and the protocol was approved by the local ethics council at the University of Lübeck (file number 16-277, 16-278). For the present study, the retrospective part (16-277) of the ethics application applies. It stipulates that statement on consent of the patients for research purposes is required for samples from 2018 onwards. The samples examined in this study originated from earlier years (2005-2017).

Author contributions

SP and CK planned the research project. ED performed the immunohistochemical stainings. TJ performed the statistical analysis. CH, F-OP, SB, and SS provided patients' follow-up data. CK, TJ, CH, F-OP, SB, SS, JK, and SP wrote and/or revised the manuscript. All authors have read and agreed to the published version of the manuscript.

Funding

Supported with funds from the Section of Medicine at the University of Luebeck J18-2020.

Conflict of interest

SP is a consultant of Ventana, Roche, Novartis, Astellar, Astrazeneca, Bristol-Myers Squibb, Merck Serono and MSD. JK is a consultant of Roche, AMGEN and BMS.

The remaining authors declare that the research was conducted in the absence of any commercial or financial relationships that could be construed as a potential conflict of

interest. The above-mentioned companies had no influence on the study design, acquisition of data, or writing of the manuscript.

Publisher's note

All claims expressed in this article are solely those of the authors and do not necessarily represent those of their affiliated organizations, or those of the publisher, the editors and the reviewers. Any product that may be evaluated in this article, or claim that may be made by its manufacturer, is not guaranteed or endorsed by the publisher.

Supplementary material

The Supplementary Material for this article can be found online at: https://www.frontiersin.org/articles/10.3389/fonc.2022.927140/full#supplementary-material

SUPPLEMENTARY FIGURE 1
Exemplary TMA core of a CDK7 stained sqNSCLC segmented automatically by QuPath (tumor cells are annotated with yellow/orange depending on chromogenic intensity, immune cells are annotated with purple/blue, stroma with green, pigment with black). Tumor cells were defined as regions of interest.

References

1. Wang J, Zhang R, Lin Z, Zhang S, Chen Y, Tang J, et al. CDK7 inhibitor THZ1 enhances antiPD-1 therapy efficacy *via* the p38α/MYC/PD-L1 signaling in non-small cell lung cancer. *J Hematol Oncol J Hematol Oncol* (2020) 13:99. doi: 10.1186/s13045-020-00926-x

2. Chou J, Quigley DA, Robinson TM, Feng FY, Ashworth A. Transcription-associated cyclin-dependent kinases as targets and biomarkers for cancer therapy. *Cancer Discovery* (2020) 10:351–70. doi: 10.1158/2159-8290.CD-19-0528

3. Li B, Ni Chonghaile T, Fan Y, Madden SF, Klinger R, O'Connor AE, et al. Therapeutic rationale to target highly expressed CDK7 conferring poor outcomes in triple-negative breast cancer. *Cancer Res* (2017) 77:3834–45. doi: 10.1158/0008-5472.CAN-16-2546

4. Huang J-R, Qin W-M, Wang K, Fu D-R, Zhang W-J, Jiang Q-W, et al. Cyclin-dependent kinase 7 inhibitor THZ2 inhibits the growth of human gastric cancer *in vitro* and *in vivo*. *Am J Transl Res* (2018) 10:3664–76.

5. Wang C, Jin H, Gao D, Wang L, Evers B, Xue Z, et al. A CRISPR screen identifies CDK7 as a therapeutic target in hepatocellular carcinoma. *Cell Res* (2018) 28:690–2. doi: 10.1038/s41422-018-0020-z

6. Zhou Y, Lu L, Jiang G, Chen Z, Li J, An P, et al. Targeting CDK7 increases the stability of snail to promote the dissemination of colorectal cancer. *Cell Death Differ* (2019) 26:1442–52. doi: 10.1038/s41418-018-0222-4

7. Jiang L, Huang R, Wu Y, Diao P, Zhang W, Li J, et al. Overexpression of CDK7 is associated with unfavourable prognosis in oral squamous cell carcinoma. *Pathol (Phila)* (2019) 51:74–80. doi: 10.1016/j.pathol.2018.10.004

8. Jagomast T, Idel C, Klapper L, Kuppler P, Offermann A, Dreyer E, et al. CDK7 predicts worse outcome in head and neck squamous-cell cancer. *Cancers* (2022) 14:492. doi: 10.3390/cancers14030492

9. Zhang J, Yang X, Wang Y, Shi H, Guan C, Yao L, et al. Low expression of cyclinH and cyclin-dependent kinase 7 can decrease the proliferation of human esophageal squamous cell carcinoma. *Dig Dis Sci* (2013) 58:2028–37. doi: 10.1007/s10620-013-2597-x

10. Zhang Z, Peng H, Wang X, Yin X, Ma P, Jing Y, et al. Preclinical efficacy and molecular mechanism of targeting CDK7-dependent transcriptional addiction in ovarian cancer. *Mol Cancer Ther* (2017) 16:1739–50. doi: 10.1158/1535-7163.MCT-17-0078

11. Patel H, Abduljabbar R, Lai C-F, Periyasamy M, Harrod A, Gemma C, et al. Expression of CDK7, cyclin h, and MAT1 is elevated in breast cancer and is prognostic in estrogen receptor-positive breast cancer. *Clin Cancer Res Off J Am Assoc Cancer Res* (2016) 22:5929–38. doi: 10.1158/1078-0432.CCR-15-1104

12. Sava GP, Fan H, Coombes RC, Buluwela L, Ali S. CDK7 inhibitors as anticancer drugs. *Cancer Metastasis Rev* (2020) 39:805–23. doi: 10.1007/s10555-020-09885-8

13. Zhang M, Zhang L, Hei R, Li X, Cai H, Wu X, et al. CDK inhibitors in cancer therapy, an overview of recent development. *Am J Cancer Res* (2021) 11:1913–35.

14. Christensen CL, Kwiatkowski N, Abraham BJ, Carretero J, Al-Shahrour F, Zhang T, et al. Targeting transcriptional addictions in small cell lung cancer with a covalent CDK7 inhibitor. *Cancer Cell* (2014) 26:909–22. doi: 10.1016/j.ccell.2014.10.019

15. Zhang H, Christensen CL, Dries R, Oser MG, Deng J, Diskin B, et al. CDK7 inhibition potentiates genome instability triggering anti-tumor immunity in small cell lung cancer. *Cancer Cell* (2020) 37:37–54.e9. doi: 10.1016/j.ccell.2019.11.003

16. Cheng Z-J, Miao D-L, Su Q-Y, Tang X-L, Wang X-L, Deng L-B, et al. THZ1 suppresses human non-small-cell lung cancer cells *in vitro* through interference with cancer metabolism. *Acta Pharmacol Sin* (2019) 40:814–22. doi: 10.1038/s41401-018-0187-3

17. Ji W, Choi YJ, Kang M-H, Sung KJ, Kim DH, Jung S, et al. Efficacy of the CDK7 inhibitor on EMT-associated resistance to 3rd generation EGFR-TKIs in non-small cell lung cancer cell lines. *Cells* (2020) 9:E2596. doi: 10.3390/cells9122596

18. Hur JY, Kim HR, Lee JY, Park S, Hwang JA, Kim WS, et al. CDK7 inhibition as a promising therapeutic strategy for lung squamous cell carcinomas with a SOX2 amplification. *Cell Oncol Dordr* (2019) 42:449–58. doi: 10.1007/s13402-019-00434-2

19. Ribbat-Idel J, Dressler FF, Krupar R, Watermann C, Paulsen F-O, Kuppler P, et al. Performance of different diagnostic PD-L1 clones in head and neck squamous cell carcinoma. *Front Med* (2021) 8:640515. doi: 10.3389/fmed.2021.640515

20. Bankhead P, Loughrey MB, Fernández JA, Dombrowski Y, McArt DG, Dunne PD, et al. QuPath: Open source software for digital pathology image analysis. *Sci Rep* (2017) 7:16878. doi: 10.1038/s41598-017-17204-5

21. Jagomast T, Idel C, Klapper L, Kuppler P, Proppe L, Beume S, et al. Comparison of manual and automated digital image analysis systems for quantification of cellular protein expression. *Histol Histopathol* (2022) 37(6):18434. doi: 10.14670/HH-18-434

22. Bian Y, Sui Q, Bi G, Zheng Y, Zhao M, Yao G, et al. Identification and validation of a proliferation-associated score model predicting survival in lung adenocarcinomas. *Dis Markers* (2021) 2021:3219594. doi: 10.1155/2021/3219594

frontiers | Frontiers in Oncology

TYPE Original Research
PUBLISHED 23 November 2022
DOI 10.3389/fonc.2022.969396

OPEN ACCESS

EDITED BY
Xiuwei Yang,
University of Kentucky, United States

REVIEWED BY
Jorge Melendez-Zajgla,
Instituto Nacional de Medicina Genómica (INMEGEN), Mexico
Rongbo Han,
Nanjing Medical University, China

*CORRESPONDENCE
Magaly Martínez-Ferrer
magaly.martinez1@upr.edu

†These authors have contributed equally to this work and share first authorship

SPECIALTY SECTION
This article was submitted to Molecular and Cellular Oncology, a section of the journal Frontiers in Oncology

RECEIVED 15 June 2022
ACCEPTED 27 October 2022
PUBLISHED 23 November 2022

CITATION
García-Vargas AM, Roque-Reyes YM, Arroyo-Villegas DM, Santiago-Negron D, Sánchez-Vázquez MM, Rivera-Torres A, Reyes-Meléndez AC, Cardona-Berdecía V, García-Maldonado M, Víquez OM and Martínez-Ferrer M (2022) HLA-BAT1 alters migration, invasion and pro-inflammatory cytokines in prostate cancer. *Front. Oncol.* 12:969396. doi: 10.3389/fonc.2022.969396

HLA-BAT1 alters migration, invasion and pro-inflammatory cytokines in prostate cancer

Aileen M. García-Vargas[1,2†], Yarelis M. Roque-Reyes[2,3†], Desiree M. Arroyo-Villegas[2,4], Daniel Santiago-Negron[2,5], María M. Sánchez-Vázquez[2], Alejandro Rivera-Torres[2,4], Andrea C. Reyes-Meléndez[2,3], Valerie Cardona-Berdecía[2,4], Miosotis García-Maldonado[6], Olga M. Víquez[7] and Magaly Martínez-Ferrer[2,5*]

[1]Department of Pharmacology and Toxicology, School of Medicine, University of Puerto Rico, Medical Sciences Campus, San Juan, PR, United States, [2]Division of Cancer Biology, University of Puerto Rico Comprehensive Cancer Center, San Juan, PR, United States, [3]Department of Biology, University of Puerto Rico, Rio Piedras Campus, San Juan, PR, United States, [4]Department of Chemistry, University of Puerto Rico, Rio Piedras Campus, San Juan, PR, United States, [5]Department of Pharmaceutical Sciences, School of Pharmacy, University of Puerto Rico, Medical Sciences Campus, San Juan, PR, United States, [6]Research Biobank, University of Puerto Rico Comprehensive Cancer Center, San Juan, PR, United States, [7]Division of Nephrology and Hypertension, Department of Medicine, Vanderbilt University, Nashville, TN, United States

Prostate cancer (PCa) accounts for more than 1 in 5 diagnoses and is the second cause of cancer-related deaths in men. Although PCa may be successfully treated, patients may undergo cancer recurrence and there is a need for new biomarkers to improve the prediction of prostate cancer recurrence and improve treatment. Our laboratory demonstrated that HLA-B-associated transcript 1 (BAT1) was differentially expressed in patients with high Gleason scores when compared to low Gleason scores. BAT1 is an anti-inflammatory gene but its role in PCa has not been identified. The objective of this study is to understand the role of BAT1 in prostate cancer. *In vitro* studies showed that BAT1 down-regulation increased cell migration and invasion. In contrast, BAT1 overexpression decreased cell migration and invasion. RT-PCR analysis showed differential expression of pro-inflammatory cytokines (TNF-α and IL-6) and cell adhesion and migration genes (MMP10, MMP13, and TIMPs) in BAT1 overexpressed cells when compared to BAT1 siRNA cells. Our *in vivo* studies demonstrated up-regulation of TNF-α, IL-6, and MMP10 in tumors developed from transfected BAT1 shRNA cells when compared to tumors developed from BAT1 cDNA cells. These findings indicate that BAT1 down-regulation modulates TNF-α and IL-6 expression which may lead to the secretion of MMP-10 and inhibition of TIMP2.

KEYWORDS

prostate cancer, animal models, migration, invasion, inflammation, cytokines

1 Introduction

Prostate cancer (PCa) accounts for more than 1 in 5 diagnoses of cancer in the United States and is the second leading cause of cancer-related deaths in men in the country (1). PCa may be successfully treated with radical prostatectomy, radiation therapy, and other treatments (2). However, patients may undergo cancer recurrence. There is a need for the development of new biomarkers to improve the prediction of cancer recurrence and treatment. Previous findings in our laboratory demonstrated that Human Leukocyte Antigen (HLA)-B Associated Transcript 1 (BAT1) or DDX39B was differentially expressed in patients with high Gleason scores when compared to low Gleason scores. The characterization of biomarkers in PCa may lead to a better prognosis and outcome for PCa patients.

BAT1 is a member of the DEAD-box family of RNA-dependent ATPases. BAT1 is located on the short arm of chromosome 6 in the region of the major histocompatibility complex (MHC) III and is about ~40kb telomeric of tumor necrosis factor-alpha (TNF-α) (3). Its role in splicing is to transfer pre-mRNA from the nucleus to the cytoplasm (4). Studies have shown that unidentified MHC class III genes play a role in inflammatory and immunopathological responses in diseases such as ulcerative colitis, diabetes, rheumatoid arthritis, and multiple sclerosis (5–12). Specifically, HLAs that are located on chromosome 6 and are part of the major histocompatibility complex are highly polymorphic in humans leading to increase immune response through inflammatory cytokine expression (12–14). BAT1 was identified as an anti-inflammatory gene through the modulation of pro-inflammatory cytokines tumor necrosis factor-alpha (TNF-α), interleukin-1 (IL-1), and interleukin-6 (IL-6) in diabetes, Chagas cardiomyopathy, and Plasmodium vivax malaria. Patients that had Chagas cardiomyopathy or Plasmodium vivax malaria and presented polymorphisms in the -22C/G and -348C/T promoter region of BAT1, lead to the increased expression on pro-inflammatory cytokines, specifically, TNF-α and IL-6 when compared to patients that did not have polymorphisms in the promoter region of BAT1 (15–20). The presence of inflammatory components plays a pivotal role in the cancer tumor microenvironment and favors metastasis/cell invasion thus, promoting oncogenesis. The identification of BAT1 as an anti-inflammatory gene in other types of diseases suggests that BAT1 is playing a role in immune response (21). The objective of this study was to identify the biological role of BAT1 in prostate cancer.

In this study, we evaluated the role of BAT1 in migration, invasion, and inflammation using *in vitro* and *in vivo* models of PCa. We demonstrated that BAT1 down-regulation leads to an increase in PCa cell migration and invasion *in vitro*. In contrast, BAT1 overexpression decreased PCa cell migration and invasion *in vitro*. We studied alternative pathways associated with migration and invasion. We focused on matrix metalloproteinases (MMPs) and tissue inhibitors of matrix metalloproteinases (TIMPs). MMP dysregulation in cancer leads to the degradation of the extracellular matrix (ECM) during tissue remodeling and inflammation, which leads to metastasis (22–24). MMPs are proteolytic enzymes that remodel the microenvironment and are present during an event of wound healing and inflammation (25–27). MMPs are highly expressed in diverse types of cancer including breast, prostate, bronchial, and squamous cell carcinoma (28–32). Studies have shown that MMPs are expressed in different prostatic cell types, suggesting that the proteolytic axis during prostate cancer invasion and metastasis is coordinated by stromal and epithelial components (29–31). TIMPs are natural inhibitors of MMPs and their loss of inhibition leads to tumor progression and inflammation in PCa (32, 33). MMPs have been found to be involved in epithelial-mesenchymal transition (EMT). EMT is the transition from epithelial cells to mesenchymal cells and it is characterized by the changes in cell morphology that decrease adhesiveness caused by rearrangements of the cytoskeletal system of tumor cells and this allows them to invade and metastasize surrounding tissues. In addition, it has been shown that EMT is related to the invasion and metastasis ability of tumors in the liver, breast, prostate, and colorectal cancer (32). In our study, BAT1 overexpression decreased TNF-α, IL-6, and MMP mRNA expression when compared to BAT1 down-regulation in PCa cells *in vitro*. Concurrently, BAT1 overexpression increased TIMP RNA expression when compared to BAT1 down-regulation in PCa cells *in vitro*. *In vivo* studies demonstrated that BAT1 down-regulation increased TNF-α, IL-6, and MMP-10 expression. These findings suggest that BAT1 down-regulation causes inflammation and promotes cell migration and invasion. BAT1 overexpression may decrease PCa progression through the modulation of inflammation and migration. BAT1 may serve as a potential biomarker for PCa recurrence.

2 Materials and methods

2.1 I*n vitro* experiments

2.1.1 Cell culture

Human prostate cancer cell lines, 22RV1 and PC3 obtained from American Type Culture Collection (ATCC, VA, USA) were cultured in RPMI-1640 medium (Hyclone, Waltham, MA, USA) containing 5% penicillin-streptomycin (Pen Strep) (Gibco, Life Technologies, Carlsbad, CA, USA) and 10% fetal bovine serum (FBS) (Hyclone, Waltham, MA, USA). Cells were incubated at 37°C and 5% CO2 in a humidified incubator.

2.1.2 RNAi-mediated transfection

Prostate cancer cells, PC3 and 22RV1, were seeded and transfected with BAT1 siRNA (si-BAT1) (Sigma, St. Louis, MO) using Lipofectamine RNAiMAX transfection reagent (Invitrogen, Carlsbad, CA) and OPTI-MEM Reduced Serum Medium (Life Technologies, Carlsbad, CA) following the manufacturer's protocol. These cells were used for *in vitro* experiments for transient transfection.

The BAT1 siRNA sequence used was: sense 5'-CUUUC UCGGUAUCAGCAGUdTdT-3' and anti-sense 5'-ACU GCUGAUACCGAGAAAGdTdT-3'. The control for this transfection was PC3 or 22RV1 cells transfected with the Mission Negative Universal Control siRNA sequence targeting no gene (Sigma, St. Louis, MO).

2.1.3 BAT1 cDNA prostate cancer cells

Prostate cancer cells, PC3 and 22RV1, were seeded and transfected with BAT cDNA-GFP tagged lentiviral particles (BAT1cDNA) (pLenti-C-mGFP vector) (Origene, Rockville, MD, USA) using Polybrene transfection reagent (EMD Millipore, Burlington, MA) and OPTI-MEM Reduced Serum Medium. Cells were selected by culturing in the presence of puromycin. These cells were used for *in vitro* and *in vivo* experiments for stable cell line transfection. The control for this transfection was PC3 or 22RV1 with no transfection.

2.1.4 BAT1 shRNA prostate cancer cells

Prostate cancer 22RV1 cells were seeded and transfected with BAT1 shRNA lentiviral particles (shBAT1) (pLKO.1 vector) (Clone ID: TRCN0000074383) (Sigma, St. Louis, MO) using Polybrene transfection reagent (EMD Millipore, Burlington, MA) and OPTI-MEM Reduced Serum Medium. Cells were selected by culturing in the presence of puromycin. These cells were used for *in vivo* experiments for stable cell line transfection. The control was mice that had 22RV1 cells with no transfection. The BAT1 shRNA lentiviral particle (pLKO.1 vector) sequence used was: CCGGCCTCAACCTC AAACACATTAACTCGAGTTAATGTGTTTGAGGTTGAGG TTTTT.

2.1.5 Western blot

Cells were trypsinized, lysed using cell lysis buffer, and centrifuged. Protein concentration was determined using the Bio-Rad DC Protein Assay Kit and a spectrophotometer at 750 nm to obtain the quantity of protein in ug/uL. Forty (ug) of protein were loaded and separated using 12% SDS-PAGE and transferred onto a PVDF membrane (Bio-Rad, Hercules, CA, USA), followed by blocking in 5% BSA (Fisher Scientific, Fair Lawn, NJ, USA) for 1 hour at room temperature. BAT1 rabbit monoclonal antibody (1:1000 dilution) (Epitomics, Burlingame, CA) and anti-GFP (1:10000 dilution) (Abcam, Cambridge, MA, USA) were added and incubated overnight at 4 °C. Detection was achieved with the appropriate secondary antibody and enhanced chemiluminescence (ECL) kit (Bio-Rad, Hercules, CA, USA). Image J software (NIH, Bethesda, MD, USA) was used to quantitatively analyze the protein expression levels. β-actin (Sigma, A5441, Monoclonal Anti- β Actin Mouse) protein expression was used as the loading control.

2.1.6 Migration assay

Cell migration was assayed using the wound healing method. Control PC3, siBAT1 PC3 or BAT1cDNA PC3 cells were seeded at a density of $2x10^5$ cells/mL and grown in a monolayer in six-well dishes until 95% confluent. Cells were serum starved in RPMI medium overnight. Cells were wounded in the center of the well using a 200 µL pipette tip, washed with 1X PBS, and incubated with RPMI-1640 serum-containing medium. Images of the wound were obtained at 0, 12, and 24 hours after wounding at a 4X magnification using a Nikon Eclipse TS100 microscope (Nikon, Tokyo, Japan). Wound width was measured using the Image Pro Plus Software (Meyer Instruments, Inc., Houston, TX, USA). 22RV1 cells were not used for the migration assay because these cells do not grow in a confluent monolayer.

2.1.7 Invasion assay

Cell invasion assay was performed using the Boyden chamber method. siBAT1 or BAT1cDNA PC3 and 22RV1 cells were seeded at a density of $5x10^4$ cells/mL in serum-free RPMI-1640 medium in the upper chamber membrane of 24-well Transwell inserts (Corning, Corning, NY, USA) previously coated with laminin (Becton Dickinson, Franklin Lakes, NJ, USA). The lower chamber contained 600 µL of RPMI-1640 medium with 10% FBS and 5% Pen Strep. Cells were incubated at 37°C and 5% CO2 for 12 and 24 hours. Cells that did not invade the membrane from the insert were removed with a cotton swab dipped in 1X PBS. The membrane was then fixed by submerging the insert in 10% formalin (Thermo Scientific Waltham, MA, USA) and counterstained with hematoxylin (American Master Tech, Lodi, CA, USA). The Boyden membrane was removed and mounted on a glass slide. Images were obtained using 4X magnifications with a Nikon Eclipse TS100 microscope (Nikon, Tokyo, Japan). Invasive cells were counted using the Image Pro Plus Software (Meyer Instruments, Inc., Houston, TX, USA).

2.1.8 Cell proliferation

PC3 and 22RV1 siBAT1 or BAT1cDNA cells were seeded at a density of $1x10^4$ cells/well in a 96-well plate. Cell proliferation was assayed at 24 hours using 20 µL of CellTiter 96® AQueous One Solution Reagent (Promega, Madison, WI, USA) and 100 µL of RPMI medium, and incubated for 2 hours at 37°C and 5% CO2 in a humidified incubator. The plates were read at 490 nm using the xMarkTM Microplate Absorbance Spectrophotometer (Bio-Rad, Hercules, CA, USA).

2.1.9 Cell viability

Cell viability and apoptosis assays were performed using flow cytometry (FACs analysis) with the Muse Cell Analyzer (EMD Millipore Merck KGaA, Darmstadt, Germany). PC3 and 22RV1 cells were seeded and grown in a 6-well cell culture plate, transfected with either siBAT1 or BAT1cDNA, and collected into tubes 24 hours after transfection. Cells were suspended in 1X PBS and 1 mL was transferred to a new tube. Twenty µL of cell suspension were stained with 380 µL of the Muse Count and Viability reagent and incubated (protected from light) for 5 minutes at room temperature. For 22RV1 cells, the protocol was the same with the exception that 20 µL of the Muse cell dispersal reagent (EMD Millipore Merck KGaA, Darmstadt, Germany) was added to 20 µL cells with 380 µL of the Muse Count and Viability reagent to each sample.

2.1.10 Apoptosis

siBAT1 or BAT1cDNA PC3 cells ($1x10^7$) were resuspended in 1X PBS, stained with 100 µL of annexin-V, and incubated and protected from light for 20 minutes at room temperature. For 22RV1 cells, $2x10^5$-$2x10^7$ cells/1mL was added to tubes, 50 µL of cell suspension was mixed with 50 µL of the Muse cell dispersal reagent and were incubated protected from light for 20 minutes at room temperature. Cell populations were gated using the Muse software.

2.1.11 RNA isolation and qRT-PCR

Total RNA was extracted from siBAT1 or BAT1cDNA PC3 and 22RV1 cells using the RNeasy Mini Isolation Kit (Qiagen, Venlo, The Netherlands) following the manufacturer's protocol. cDNA was synthesized using the iScript cDNA Synthesis Kit (Bio-Rad, USA) according to the manufacturer's instructions. PCR amplification was done using real-time PCR with the iQ SYBR Green Supermix (Bio-Rad, USA) and the Step One Plus Real-time PCR System (Applied Biosystems, Carlsbad; CA, USA) as follows: 95 °C for 5 min, 95 °C for 15 seconds and 60 °C for 1 min at 40 cycles. Changes in mRNA expression were analyzed using the ΔΔCt method and the Step One Software. Negative fold changes were determined by dividing 1/Average Fold Change obtained. Expression levels were normalized to GAPDH expression.

2.2 *In vivo* experiments

2.2.1 Orthotopic mouse model

For *in vivo* experiments, human prostate cancer 22RV1 cells (250,000 cells contained in 70 µL) transfected with shBAT1 (n=5 mice) or BAT1cDNA (n=5 mice) were mixed with 30 uL collagen and injected into the anterior prostate lobules of 7–8-week-old male ICR-SCID mice (Taconic, Germantown, NY, USA) to generate 2 tumors (one per each prostate lobule). Our control mice (n=6) were injected with non-transfected 22RV1 cells. Mice were kept in a pathogen-free environment under the Institutional Animal Care and Use Committee regulations at The University of Puerto Rico Medical Sciences Campus animal facility (Protocol #A8700110). Mice were anesthetized and sacrificed. Furthermore, prostate tumors and livers were collected, weighed, and used for histologic analysis.

2.2.2 Tissue collection and histological examination

Tumors collected were fixed in 10% buffered formalin and embedded in paraffin. Formalin-fixed paraffin-embedded (FFPE) tumors were cut at 5 µm sections using a microtome (Leica Microsystems, Wetzlar, Germany) and mounted on slides. Slides were deparaffinized in xylene, hydrated using serial descending concentrations of alcohol, stained with hematoxylin, followed by stain differentiation with eosin, and dehydrated with increasing serial dilutions of ethanol and xylene. Slides were mounted with coverslips using permount-mounting medium. As described by Lsaacs and Hukku (33) tumors were classified into four categories by a degree of differentiation: well differentiated, moderately differentiated, poorly differentiated, and anaplastic. Well-differentiated tumors are characterized by the presence of glandular structures, lumen, basement membrane, and stroma. Moderately differentiated tumors are characterized by smaller glandular structures with the lumen obstructed by tumor cells. However, the basement membrane and stroma remained intact. Tumors classified as poorly differentiated have an absence of glandular structures, and basement membrane, and do not show a consistent relationship between tumor cells and stroma. Individual tumor cells, however, still show a normal nucleus to cytoplasm ratio. Tumors classified as anaplastic lack appearance of tissue organization and individual tumor cells show irregular nucleus size and abnormal nucleus to cytoplasm ratio. Our tumors collected represent n=6 tumors for control, n=5 tumors for BAT1cDNA, and n=3 tumors for shBAT1.

2.2.3 Immunohistochemistry

Formalin-fixed paraffin-embedded (FFPE) mice tumor tissues were dewaxed in xylene and rehydrated in descending concentrations of alcohol and deionized water. Antigen retrieval was performed using the Antigen Unmasking Solution (Vector Laboratories, Burlingame, CA, USA) followed by quenching of endogenous peroxidase with 3% v/v H_2O_2. Sections were blocked for 1 hour with horse serum (R.T.U Vectastain Kit, Vector Laboratories, Burlingame, CA, USA) and left overnight with the primary antibody at 4°C in a humidified chamber. The primary antibodies used were: BAT1 (1:50 dilution) (Epitomics, Burlingame, CA, USA), Cleaved Caspase-3 (1:200 dilution) (Cell Signaling, Danvers, MA, USA), Ki67 (1:1000 dilution) (Vector Laboratories, Burlingame, CA, USA), TNF-α (1:100 dilution)

(Abcam, Cambridge, MA, USA), IL-6 (1:25 dilution) (Novus Biologicals, Littleton, CO, USA), and MMP10 (1:100 dilution) (Abcam, Cambridge, MA, USA). Protein expression was detected with the peroxidase substrate kit (ImmPACT DAB) (Vector Laboratories, Burlingame, CA, USA). Hematoxylin was used as a counterstain. Digital images were obtained using an Olympus IX71 Inverted microscope (Olympus America, Melville, NY, USA) at a 20x magnification. To quantify BAT1, Cleaved Caspase-3 expression, and Ki67 expression, a set of 5 random fields per slide were chosen and the number of total cells, negative cells, and positive cells were quantified. The number of positive cells in response to the primary antibody was divided over the number of total cells and a percentage per field was determined. The 5 total fields per slide were then averaged to generate a percentage of positive cells. To quantify MMP10, TNF-α, and IL-6 expression, a subjective scale from 1-4 was used. In this scale, we gave a score of one (1) if 25% or less of the tumor cells were stained, a score of two (2) if 26% to 50% of the tumor cells were stained, a score of three (3) if 51% to 75% of the tumor cells were stained, and a score of four (4) if more than 75% of the tumor cells were stained. The score was given in a blind manner. All images were analyzed using Image the Pro Plus Software (Meyer Instruments, Inc., Houston, TX, USA).

2.2.4 Immunofluorescence

Paraffin-embedded tissue (FFPE) was dewaxed in xylene (x2) and rehydrated in descending concentrations of alcohol and deionized water. Antigen retrieval was performed using the Antigen Unmasking Solution (Vector Laboratories, Burlingame, CA, USA) and the heat was applied using a microwave. Slides were placed on ice and then followed by quenching of endogenous peroxidase with 3% v/v H_2O_2. Sections were blocked for 1 hour with 10% FBS and left overnight with the primary antibody at 4°C in a humidified chamber. The primary antibody used was CD31 (1:50 dilution) (Abcam, Cambridge; MA, USA). The secondary antibody used was Alexa-Fluor 594 (anti-rabbit) 1:1000 (Molecular Probes, Life Technologies, Carlsbad, CA, USA) and, nuclei were stained with DAPI 1:5000 (Santa Cruz Biotechnology, Santa Cruz, CA, USA). Digital images were obtained using an Olympus IX71 Inverted microscope (Olympus America, Melville, NY, USA) at a 20X magnification. To quantify CD31, sets of 5 random fields were chosen per slide and the total number of blood vessels was counted and averaged per slide.

2.2.5 Statistical analysis

All *in vitro* experiments were performed in triplicates (n=3). Results represent the mean ± standard error of the mean (SEM). Differences between treatments were analyzed using the Student's t-test at a 95% confidence interval. P-values <0.05 were considered statistically significant. Statistical analysis was done using GraphPad Prism Software (GraphPad Software, CA, USA). For *in vivo* statistical analysis was done using the analysis of variance (ANOVA) and the GraphPad Prism Software (GraphPad Software, CA, USA).

3 Results

3.1 BAT1 expression was decreased after siRNA transfection and increased after cDNA transfection in PC3 and 22RV1 cells

To investigate the role of BAT1 in prostate cancer cells, we transfected PC3 and 22RV1 cells with siBAT1 to down-regulate BAT1 expression or BAT1cDNA to overexpress BAT1 expression. Protein and RNA extraction from transfected cells were obtained and subjected to SDS-PAGE western blot analysis or qRT-PCR to determine efficient transfection. siBAT1 PC3 cells showed significantly less expression of BAT1 by western blot analysis and qRT-PCR when compared to control (Figures 1A, B). Additionally, siBAT1 22RV1 cells showed significantly less expression of BAT1 by western blot analysis and qRT-PCR when compared to control (Figures 1E, F). In contrast, BAT1cDNA PC3 and 22RV1 cells showed a significant increase in BAT1 expression by western blot and qRT-PCR analysis when compared to control (Figures 1C, D, G, H).

3.2 BAT1 down-regulation significantly increased cell migration and BAT1 overexpression significantly decreased cell migration in PC3 cells

The ability of PC3 cells to migrate after BAT1 expression was altered. Results showed that siBAT1 PC3 cells had a significant increase in migratory potential at 12 hours and at 24 hours when compared to control (Figures 2A, B). Conversely, BAT1cDNA PC3 cells showed a significant decrease in migratory potential of 37% at 12 hours and 44% at 24 hours when compared to control (Figures 2C, D). 22RV1 cells were not used for the migration assay because these cells do not grow in a confluent monolayer.

3.3 BAT1 down-regulation significantly increased cell invasion and BAT1 overexpression significantly decreased cell invasion in PC3 and 22RV1 cells

The effects of BAT1 expression in invasion were examined using the Transwell assay siBAT1 PC3 cells significantly increased cell invasion at 12 hours and 24 hours when

10.3389/fonc.2022.969396

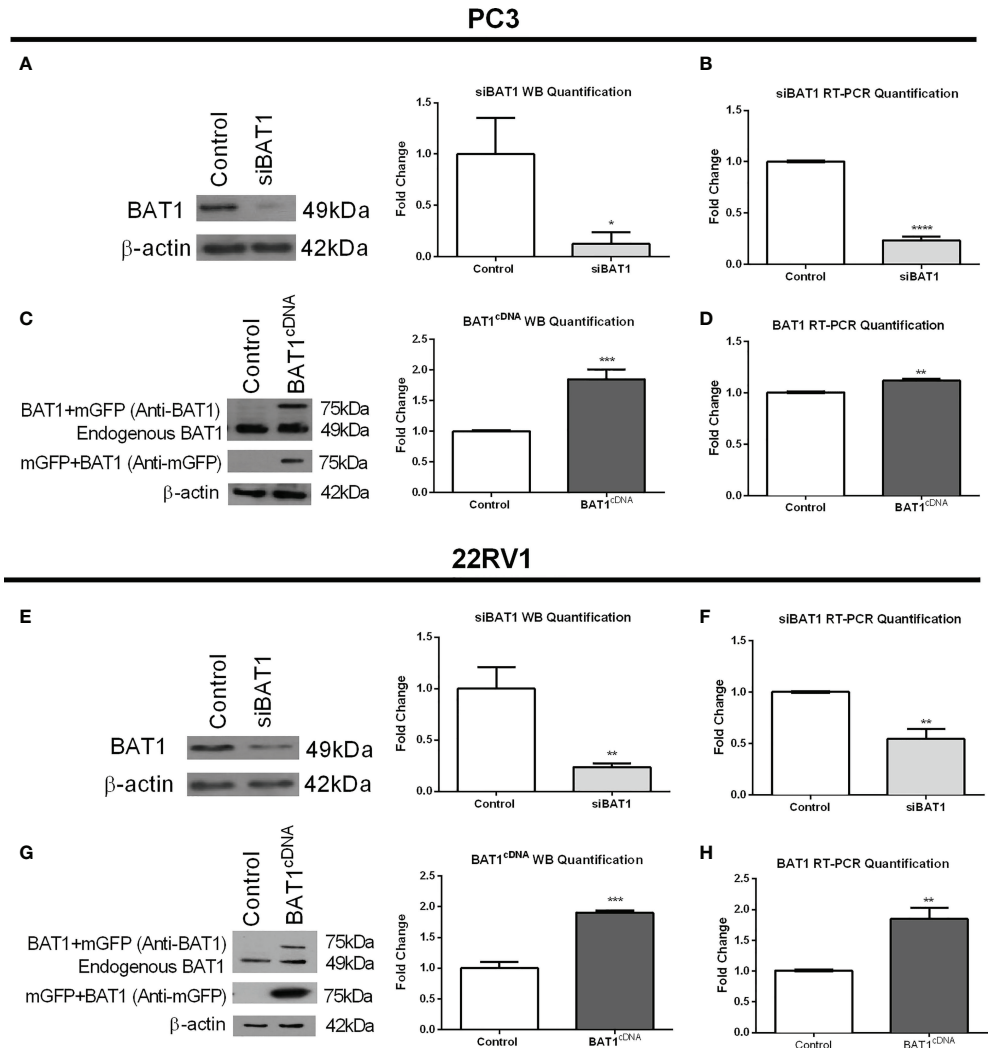

FIGURE 1
BAT1 Expression was decreased after siRNA Transfection and increased after cDNA Transfection in PC3 and 22RV1 cells. The samples were collected for a period of 24 hours. **(A)** Representative images and quantification of BAT1 protein expression in PC3 prostate cancer cells using western blot analysis showed a significant decrease in siBAT1 transfected cells when compared to control (*P<0.05). **(B)** Quantification of BAT1 RNA expression using RT-PCR in PC3 prostate cancer cells showed a significant decrease in BAT1 expression in siBAT1 transfected cells when compared to control (****P < 0.0001). **(C)** Representative images and quantification of BAT1 protein expression in PC3 prostate cancer cells using western blot analysis showed a significant increase in protein expression in BAT1cDNA when compared to control (***P < 0.001). **(D)** Quantification of BAT1 RNA expression using RT-PCR in PC3 prostate cancer cells showed a significant increase in BAT1 protein expression in BAT1cDNA cells when compared to control (**P < 0.01). **(E)** Representative images and quantification of BAT1 protein expression in 22RV1 prostate cancer cells using western blot analysis showed a significant decrease in siBAT1 transfected cells when compared to control (**P < 0.01). **(F)** Quantification of BAT1 RNA expression using RT-PCR in 22RV1 prostate cancer cells showed a significant decrease in BAT1 expression in siBAT1 transfected cells when compared to control (**P < 0.01) **(G)** Representative images and quantification of BAT1 protein expression in 22RV1 prostate cancer cells using western blot analysis showed a significant increase in BAT1cDNA when compared to control (***P < 0.001). **(H)** Quantification of BAT1 RNA expression using RT-PCR in 22RV1 prostate cancer cells showed a significant increase in BAT1 protein expression in BAT1cDNA cells when compared to control (**P < 0.01).

compared to control (Figures 3A, C). Moreover, siBAT1 22RV1 cells significantly increased cell invasion at 12 hours and 24 hours when compared to control (Figures 3B, D). On the contrary, BAT1cDNA PC3 cells significantly decreased cell invasion at 12 hours and 24 hours when compared to control (Figures 3E, G). Furthermore, cell invasion significantly decreased in BAT1cDNA 22RV1 cells at 12 hours and 24 hours when compared to control (Figures 3F, H). Also, to determine if changes in migration and invasion were due to changes in proliferation and apoptosis, we performed a proliferation assay using MTT and an apoptosis assay using FACs analysis. Results showed no significant changes in these

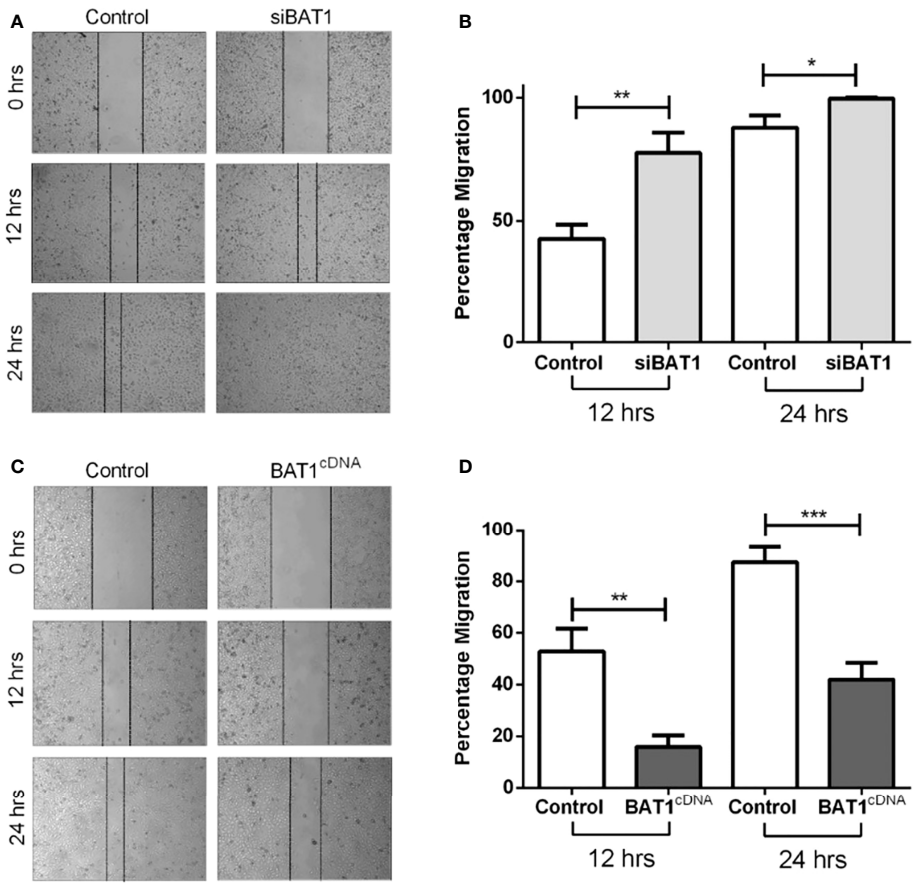

FIGURE 2
BAT1 down-regulation increased PC3 prostate cancer cell migration and BAT1 overexpression decreased PC3 prostate cancer cell migration. **(A)** Representative images of Control PC3 and siBAT1 PC3 cells using 4X magnification. **(B)** Relative invasion of siBAT1 PC3 cells caused a significant increase in migration at 12hrs (**P < 0.01) and 24hrs (*P < 0.05) when compared to control. **(C)** Representative images of Control PC3 and BAT1cDNA PC3 cells using 4X magnification. **(D)** Relative invasion of (+) BAT1cDNA PC3 cells caused a significant decrease in migration at 12hrs (**P < 0.01) and 24hrs (***P < 0.001) when compared to control.

molecular hallmarks of cancer (Supplemental Figures S1–S3). These data suggest that BAT1 suppresses cell migration and invasion without altering proliferation or apoptosis *in vitro*.

3.4 Alteration of BAT1 expression showed changes in genes associated with inflammation, adhesion, and metastasis in PC3 and 22RV1 cells using qRT-PCR

Previous studies have associated the role of BAT1 as an anti-inflammatory gene in diseases such as Chagas cardiomyopathy and *Plasmodium vivax* malaria through the modulation of tumor necrosis factor-alpha (TNF-α) and interleukin-6 (IL-6) (16, 18). It is known that inflammation can eventually lead to cell migration and metastasis (34, 35). Thus, we wanted to identify a detailed signaling pathway that might be involved with BAT1 expression in PCa cell progression using qRT-PCR. Results demonstrated significant changes in TNF-α, IL-6, MMP-10, and TIMP2 expression. BAT1cDNA PC3 cells significantly decreased TNF-α, IL-6, and matrix metallopeptidase 13 (MMP-13) expression when compared to siBAT1 PC3 cells (Figure 4 and Table 1). Results showed significant decreases in TNF-α, IL-6, and matrix metallopeptidase 10 (MMP-10) expressions in BAT1cDNA 22RV1 cells when compared to siBAT1 22RV1 cells (Figures 4C, D, F). Additionally, tissue inhibitor of metalloproteinase 2 (TIMP2) expression, was significantly increased in BAT1cDNA 22RV1 cells when compared to siBAT1 22RV1 cells. These results suggest that BAT1 is altering inflammatory cytokine expression and metastatic gene expression.

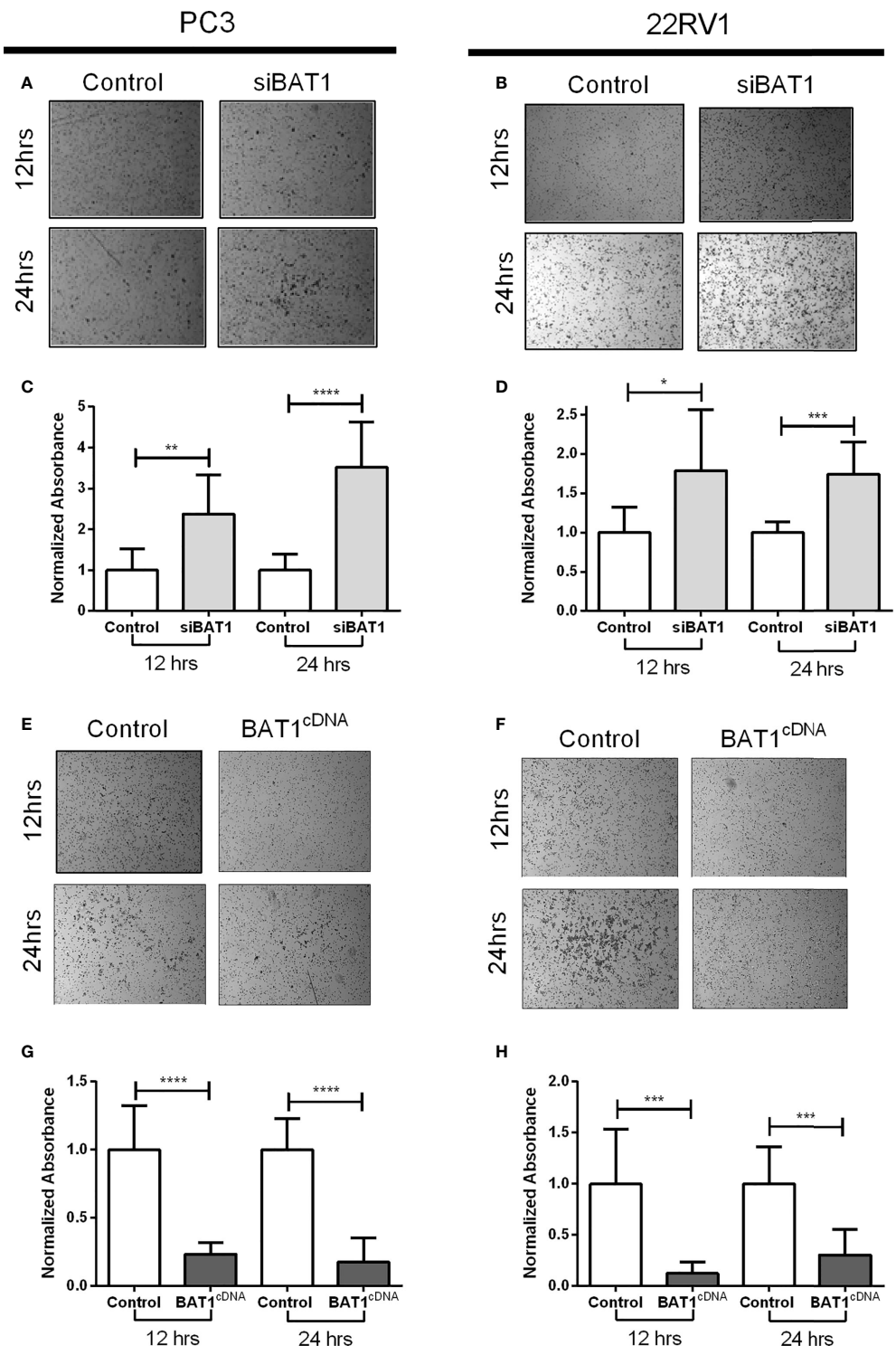

FIGURE 3
BAT1 down-regulation increased PC3 and 22RV1 prostate cancer cell and BAT1 overexpression decreased PC3 and 22RV1 prostate cancer cell invasion. **(A, B)** Representative images of invasive siBAT1 PC3 and 22RV1 cells at a 4X magnification. **(C)** Relative invasion of siBAT1 PC3 cells caused a significant increase in invasion when compared to control at 12hrs (**P < 0.01) and 24hrs (****P < 0.0001). **(D)** Relative invasion of siBAT1 22RV1 cells caused a significant increase in invasion when compared to control at 12hrs (*P < 0.05) and 24hrs (***P < 0.001). **(E, F)** Representative images of invasive BAT1cDNA PC3 and 22RV1 cells at a 4X magnification. **(G)** Relative invasion of BAT1cDNA PC3 cells caused a significant decrease in invasion when compared to control at 12hrs (****P < 0.0001) and 24hrs (****P < 0.0001). **(H)** Relative invasion of BAT1cDNA 22RV1 cells caused a significant decrease in invasion when compared to control at 12hrs (***P < 0.001) and 24hrs (***P < 0.001).

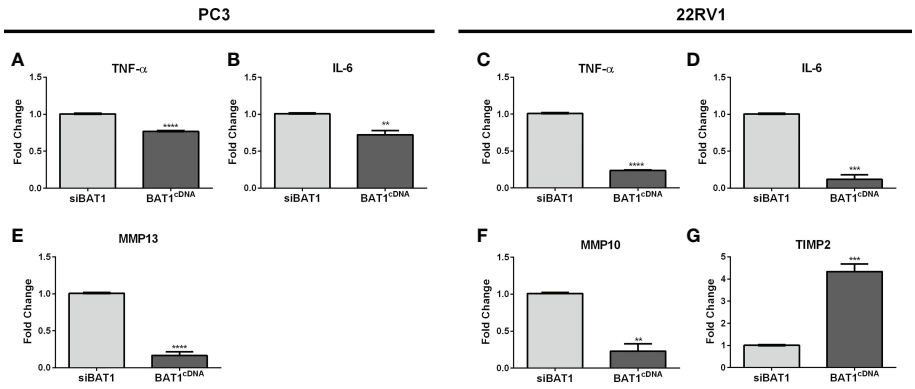

FIGURE 4
BAT1 expression showed changes in genes associated with inflammation, adhesion, and metastasis in PC3 and 22RV1 cells using qRT-PCR. The samples were collected for a period of 24 hours. **(A, C)** BAT1cDNA PC3 and 22RV1 cells showed a significant decrease in TNF-α expression when compared to siBAT1 (****P < 0.0001). **(B, D)** BAT1cDNA PC3 and 22RV1 cells showed a significant decrease in IL-6 expression when compared to siBAT1 (**P < 0.01) (***P < 0.001). **(E)** BAT1cDNA PC3 cells showed a significant decrease in MMP13 expression when compared to siBAT1 (****P < 0.0001). **(F)** BAT1cDNA 22RV1 cells showed a significant decrease in MMP10 expression when compared to siBAT1 (**P < 0.01). **(G)** BAT1cDNA 22RV1 cells showed a significant increase in TIMP2 expression when compared to siBAT1 (***P < 0.001).

TABLE 1 Alteration of BAT1 expression showed changes in genes associated with inflammation, adhesion and metastasis in PC3 and 22RV1 cells using qRT-PCR.

Cell Line Transfected	Gene	Function	Fold Change
PC3 $BAT1^{cDNA}$ vs PC3 siBAT1	TNF-α	Involved in systemic inflammation	-1.35
PC3 $BAT1^{cDNA}$ vs PC3 siBAT1	IL-6	Pro-inflammatory cytokine	-0.92
PC3 $BAT1^{cDNA}$ vs PC3 siBAT1	MMP13	Involved in cancer migration	-6.25
22RV1 $BAT1^{cDNA}$ vs 22RV1 siBAT1	TNF-α	Involved in systemic inflammation	-4.34
22RV1 $BAT1^{cDNA}$ vs 22RV1 siBAT1	IL-6	Pro-inflammatory cytokine	-9.09
22RV1 $BAT1^{cDNA}$ vs 22RV1 siBAT1	TIMP2	Directly suppress the proliferation of endothelial cells	4.33
22RV1 $BAT1^{cDNA}$ vs 22RV1 siBAT1	MMP10	Involved in cancer migration	-4.00

3.5 *In vivo* expression of BAT1, Ki-67, TNK- α, IL-6 and MMP10

Prior to 22RV1 prostate cancer cells injection into SCID mice prostate lobules, we confirmed transfection of BAT1 expression using western blot analysis (Supplemental Figure S4). PC3 cells were not used for *in vivo* experiments because they do not grow properly in these models. Tumors developed in SCID mice were examined by immunohistochemistry. H&E sections were evaluated by a pathologist for the observation of inflammation and histological classification. The tumors were classified as poorly differentiated or anaplastic. (Supplemental Figure S5). BAT1 expression was significantly increased in BAT1cDNA prostate tumors when compared to control and shBAT1 prostate tumors (Figures 5A, B). Although tumors from shBAT1 transfected mice showed no statistical significance in BAT1 expression when compared to control, results represent a tendency to decrease expression.

To evaluate whether BAT1 expression altered proliferation, apoptosis, or angiogenesis *in vivo*, mice prostate tumor sections were examined by immunohistochemistry or immunofluorescence. The nuclear marker Ki67 was used to determine changes in proliferation. Mice prostate tumors developed from BAT1cDNA and shBAT1 transfected cells significantly decreased cell proliferation when compared to control (Figure 5C). shBAT1 tumors showed an increase in TNF-α expression when compared to control and BAT1cDNA (Figure 5D). Apoptosis using the pro-apoptotic marker cleaved caspase-3 showed no change in expression for all groups (Supplemental Figure S6). To determine if BAT1 expression plays a role in angiogenesis, mice prostate tumor sections were subjected to immunofluorescence using the

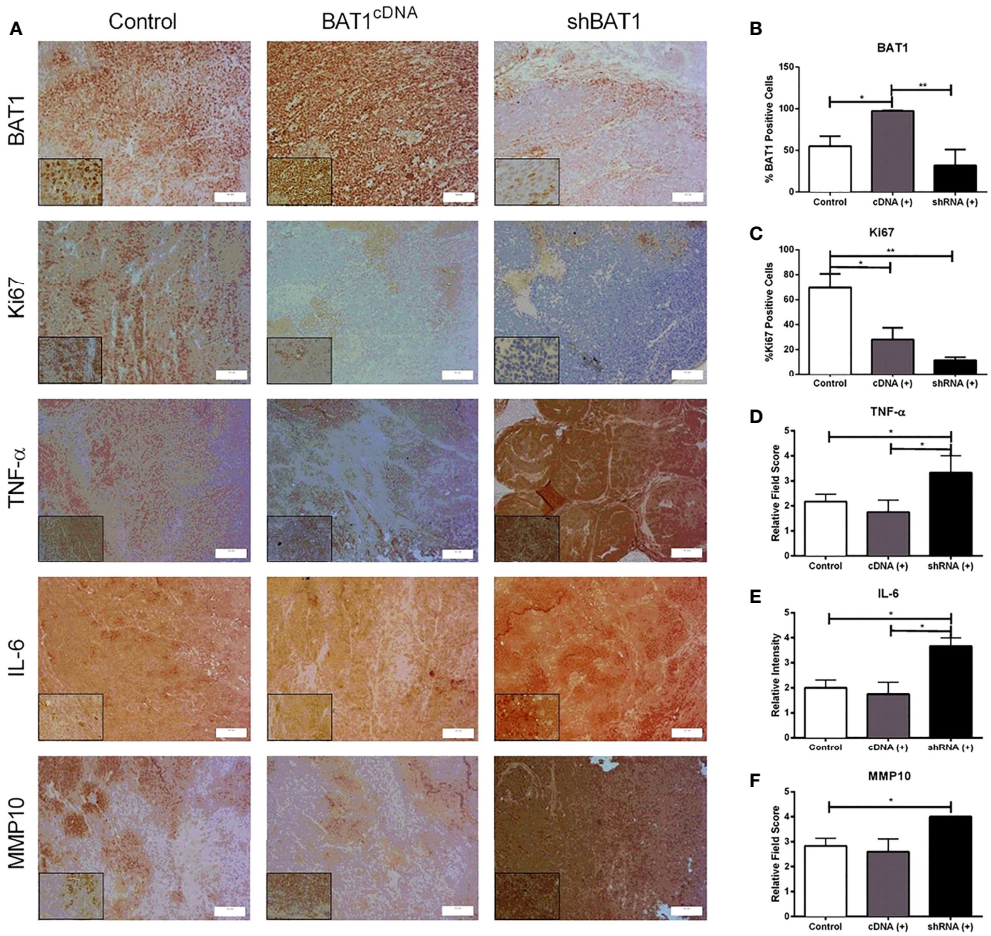

FIGURE 5
In vivo expression of BAT1, Ki67, TNF-α, IL-6, and MMP10. All of the samples were collected for a period of 24 hours. **(A)** Representative images of immunohistochemical staining BAT1 expression in mice prostate tumors previously injected with 22RV1 cells, BAT1cDNA 22RV1 cells, or shBAT1 22RV1 cells at a 20X (50μm) or 60X magnification (10μm) magnification. **(B)** Quantification mice prostate tumors obtained from BAT1cDNA mice prostate tumors showed a significant increase in BAT1 expression using immunohistochemistry when compared to control (*P < 0.05) and shBAT1 (**P < 0.01). **(C)** shBAT1 (**P < 0.01) and BAT1cDNA (*P < 0.05) tumors showed a significant decrease in Ki67 expression when compared to control. **(D)** shBAT1 tumors showed a significant increase in TNF-α expression when compared to control and BAT1cDNA (*P < 0.05). **(E)** shBAT1 tumors showed a significant increase in IL-6 expression when compared to control and BAT1cDNA mice prostate tumors (*P < 0.05). **(F)** shBAT1 tumors showed a significant increase in MMP10 expression when compared to control (*P < 0.05).

angiogenesis marker CD31. Results showed no significant change in the number of blood vessels for all groups (Supplemental Figure S7).

In vitro results showed changes in cell invasion, migration, and genes associated with inflammation and metastasis. In an inflammatory event, the downregulation of BAT1 may stimulate increases in pro-inflammatory cytokines, TNF-α and IL-6. Cells may lose their ability to maintain tight junctions and cell-cell adhesion leading to invasive potential through the secretion of MMPs and the inhibition of TIMPs. MMPs degrade the extracellular matrix leading to invasion of mesenchymal cells into the bloodstream, thus promoting metastasis. Based on this signaling pathway, we identified significant changes in TNF-α, IL-6, and matrix metallopeptidase 10 (MMP-10) gene expression when we performed RT-PCR in PC3 and 22RV1 prostate cancer cells, thus, we wanted to determine if there would be significant changes in expression in an *in vivo* mouse model. Immunohistochemistry analysis in mice prostate tumors showed that shBAT1 significantly increased TNF-α and IL-6 expression when compared to control and BAT1cDNA tumors (Figures 5D, E). Additionally, MMP-10 expression was significantly increased in shBAT1 mice prostate tumors when compared to control (Figure 5F). These findings suggest that BAT1 down-regulation leads to activation of pro-inflammatory cytokines TNF-α and IL-6, which leads to the secretion of MMP-10, inhibition of TIMP2, and promotion of invasion and migration (Figure 6).

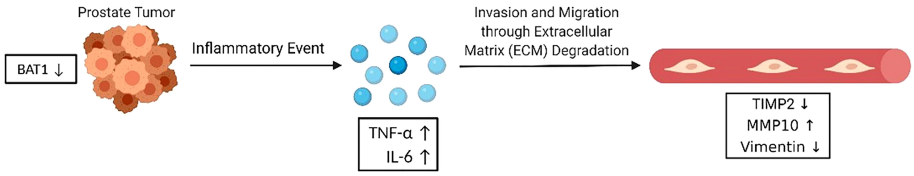

FIGURE 6
BAT1 promotes *in vitro* invasion and migration. BAT1 down-regulation leads to activation of pro-inflammatory cytokines TNF-α and IL-6, which leads to the secretion of MMP-10 and inhibition of TIMP2. MMP-10 may degrade the ECM and promote PCa invasion and migration through extracellular matrix degradation.

4 Discussion

Studies have shown that unidentified MHC class III genes play a role in inflammatory and immunopathological responses in diseases such as ulcerative colitis, diabetes, rheumatoid arthritis, and multiple sclerosis (5–12). The RNA helicase and MHC class III gene, BAT1, has been identified as an anti-inflammatory gene in diseases such as Chagas cardiomyopathy, Plasmodium vivax malaria, multiple sclerosis, and insulin dependent diabetes mellitus by the modulation of the pro-inflammatory cytokines TNF-α, IL-6 and IL-1 expression (12–14, 36). Nevertheless, the functional role of BAT1 in PCa recurrence has not been revealed. Immunohistochemical analysis demonstrated that BAT1 expression was differentially expressed in patients with high Gleason scores when compared to PCa patients with low Gleason scores. In this work, we determined the role of BAT1 in migration, invasion, and gene expression using *in vitro* and *in vivo* PCa models.

In this study, genetic down-regulation of BAT1 significantly increased cell migration, invasion, and expression of TNF-α, IL-6, MMP10, and MMP13 while it decreased the expression of TIMP2. Conversely, overexpression of BAT1 significantly decreased cell migration, invasion, and expression of TNF-α, IL-6, MMP10, and MMP13 while it increased the expression of TIMP2. However, apoptosis and cell proliferation were not affected in either group due to no significant changes observed in the proliferation and apoptosis assays using FACs analysis. The results suggest that BAT1 mechanisms do not involve changes in proliferation or apoptotic pathways. Taken together, these data indicate that BAT1 overexpression may function as an anti-inflammatory gene and suppressor of metastasis and invasion in PCa. Since metastasis and invasion eventually may promote recurrence, understanding and identifying the mechanisms by which BAT1 functions may lead to better treatment options for recurrent PCa patients.

Cancer cell invasion is an important hallmark of cancer and an essential step toward metastasis (37, 38). In our study, we observed increases in cell migration and invasion in PCa cells transfected with siBAT1 and decreases in cell migration and invasion in PCa cells transfected with BAT1cDNA. Based on these results, we wanted to determine changes in genes that were associated with invasion, adhesion, and metastasis. We expected to detect changes in matrix metalloproteinases (MMPs) and its inhibitor, tissue inhibitors of matrix metalloproteinases (TIMPs). Significant changes were determined in MMP-10, MMP-13, and TIMP2. These results were expected due to previously published data that have identified MMPs to be involved in EMT, which is related to the invasion and metastasis ability of tumors in various types of cancer, including PCa.

BAT1 expression has been implicated in alterations of inflammation, specifically, through the modulation of TNF-α and IL-6 expression in inflammatory diseases (15–18). In a tumor microenvironment or inflammatory event, mesenchymal cells can secrete TNF-α and IL-6 (32, 39). The pro-inflammatory cytokine TNF-α can subsequently lead to the release of MMPs (32). To study the functional role of BAT1 in inflammatory cytokine secretion, qRT-PCR was performed to confirm mRNA expressions of TNF-α and IL-6 *in vitro*. Results showed decreases in TNF-α and IL-6 expression in PCa cells treated with BAT1cDNA when compared to siBAT1. These results were expected due to studies identifying BAT1 polymorphisms (decreases in BAT1 expression) with inflammation in patients that had an immune response disease. These findings also may explain why we found changes in migratory and invasive potential. We subsequently measured changes in cell migration and invasion *in vitro*, which may be contributed to the expression of TNF-α and IL-6 in PC3 and 22RV1 cells. Based on these results, we hypothesized that the secretion of pro-inflammatory cytokines may lead to metastatic potential through EMT. To verify our hypothesis, Western Blot analysis was performed to confirm the overexpression of Vimentin and N-Cadherin proteins. However, results showed no significant changes in Vimentin and N-cadherin protein expression in siBAT1 PCa cells compared to control cells (Figure S9).

IHC analysis showed that shBAT1 mice prostate tumors increased TNF-α, IL-6, and MMP-10 expression. These findings correlated to our qRT-PCR results demonstrating an increase in MMP-10 expression *in vitro*. Additionally, MMP-10 (stromelysin-2) has been overexpressed in various cancers including gastric,

bladder, renal, esophageal, skin, and non-small cell lung cancer (40, 41). MMP-10 plays an important role in the development and progression of malignant tumors. MMP-10 expression has been implicated in the modulation of invasion, apoptosis, angiogenesis, and cell proliferation in cancer (42).

This study has some limitations including that no migration and invasion studies were performed in the *in vivo* models, and additional experiments need to be performed to supplement and conclude that the promotion of invasion and migration is present in the *in vivo* model possibly due to the changes described on TNF- α, IL-6, MMP-10, and TIMP2 in this manuscript. Another limitation was that the migration assays *in vitro* were only performed using the PC3 cell line because the 22RV1 cell line grows in clusters and are not appropriate for the wound healing test. Lastly, for the *in vivo* experiments, only the 22RV1 cell line was used because previous studies in our laboratory had shown that they grow better in mice in comparison with the PC3 cell line.

Data availability statement

The original contributions presented in the study are included in the article/Supplementary Material. Further inquiries can be directed to the corresponding author.

Ethics statement

All animal experiments were performed by a protocol approved by the Institutional Animal Care and Use Committee (IACUC) at the University of Puerto Rico, Medical Sciences Campus.

Author contributions

Conceptualization, MM-F and MS-V. Methodology: MM-F, OV, MS-V, MG-M. Software: AG-V, YR-R, DA-V, MS-V, AR-T, AR-M, VC-B, DN. Validation: MM-F. and MS-V. Formal analysis: MM-F, OV, and MS-V. Investigation: AG-V, YR-R, DA-V, MS-V, AR-T, AR-M, VC-B, DN. Resources: MM-F, MG-M, and MS-V. Data curation: MM-F and MS-V. Writing—original draft preparation: A G-V, YR-R, DA-V. Writing—review and editing: AG-V, YR-R, DA-V, MS-V, AR-T, AR-M, VC-B, DN, OV, MG-M. Visualization: MM-F and MS-V. Supervision: MM-F and MS-V. Project administration: MM-F. Funding acquisition: MM-F. All authors contributed to the article and approved the submitted version.

Funding

This research was funded by Institutional funds from the University of Puerto Rico Comprehensive Cancer Center, the NIGMS-RISE Program (Grant Number #R25GM061838), the RCMI Pilot Project (Grant Number #8G12MD007600 and NIMHD: U54-MD007600), and the National Center Institute of the National Institutes of Health (Award Grant Number # U54CA096297/CA096300).

Conflict of interest

The authors declare that the research was conducted in the absence of any commercial or financial relationships that could be construed as a potential conflict of interest.

Publisher's note

All claims expressed in this article are solely those of the authors and do not necessarily represent those of their affiliated organizations, or those of the publisher, the editors and the reviewers. Any product that may be evaluated in this article, or claim that may be made by its manufacturer, is not guaranteed or endorsed by the publisher.

Supplementary material

The Supplementary Material for this article can be found online at: https://www.frontiersin.org/articles/10.3389/fonc.2022.969396/full#supplementary-material

References

1. Siegel RL, Miller KD, Fuchs HE, Jemal A. Cancer statistics, 2022. *CA: A Cancer J Clin* (2022) 72(1):7–33. doi: 10.3322/caac.21708

2. Siegel RL, Miller KD, Jemal A. Cancer statistics, 2020. *CA: A Cancer J Clin* (2020) 70(1):7–30. doi: 10.3322/caac.21590

3. Allcock RJN, Price P, Gaudieri S, Leelayuwat C, Witt CS, Dawkins RL. Characterisation of the human central MHC gene, BAT1: Genomic structure and expression. *Exp Clin Immunogenetics* (1999) 16(2):98–106. doi: 10.1159/000019100

4. Momose F, Basler CF, O'Neill RE, Iwamatsu A, Palese P, Nagata K. Cellular splicing factor RAF-2P48/NPI-5/BAT1/UAP56 interacts with the influenza virus nucleoprotein and enhances viral RNA synthesis. *J Virology* (2001) 75(4):1899–908. doi: 10.1128/JVI.75.4.1899-1908.2001

5. Okamoto K, Makino S, Yoshikawa Y, Takaki A, Nagatsuka Y, Ota M, et al. Identification of IKBL as the second major histocompatibility complex–linked susceptibility locus for rheumatoid arthritis. *Am J Hum Genet* (2003) 72(2):303–12. doi: 10.1086/346067

6. Kilding R, Iles MM, Timms JM, Worthington J, Wilson AG. Additional genetic susceptibility for rheumatoid arthritis telomeric of the DRB1 locus. *Arthritis Rheumatism* (2004) 50(3):763–9. doi: 10.1002/art.20043

7. Barrett JC, Clayton DG, Concannon P, Akolkar B, Cooper JD, Erlich HA, et al. Genome-wide association study and meta-analysis find that over 40 loci affect risk of type 1 diabetes. *Nat Genet* (2009) 41(6):703–7. doi: 10.1038/ng.381

8. Boodhoo A, Wong AM-L, Williamson D, Voon D, Lee S, Allcock RJ, et al. A promoter polymorphism in the central MHC gene, *ikbl*, influences the binding of transcription factors USF1 and E47 on disease-associated haplotypes. *Gene Expression* (2004) 12(1):1–11. doi: 10.3727/000000004783992206

9. De La Concha EG, Fernandez–Arquero M, Lopez–Nava G, Martin E, Allcock RJ, Conejero L, et al. Susceptibility to severe ulcerative colitis is associated with polymorphism in the central MHC gene IKBL. *Gastroenterology* (2000) 119 (6):1491–5. doi: 10.1053/gast.2000.20258

10. Ota M, Katsuyama Y, Kimura A, Tsuchiya K, Kondo M, Naruse T, et al. A second susceptibility gene for developing rheumatoid arthritis in the human MHC is localized within a 70-kb interval telomeric of the TNF genes in the HLA class III region. *Genomics* (2001) 71(3):263–70. doi: 10.1006/geno.2000.6371

11. Shin HD, Yang SW, Kim DH, Park Y. Independent association of tumor necrosis factor polymorphism with type 1 diabetes susceptibility. *Ann New York Acad Sci* (2008) 1150(1):76–85. doi: 10.1196/annals.1447.059

12. Shiina T, Inoko H, Kulski JK. An update of the HLA genomic region, locus information and disease associations: 2004. *Tissue Antigens* (2004) 64(6):631–49. doi: 10.1111/j.1399-0039.2004.00327.x

13. Choo SY. The HLA system: Genetics, immunology, clinical testing, and clinical implications. *Yonsei Med J* (2007) 48(1):11. doi: 10.3349/ymj.2007.48.1.11

14. Price P, Witt C, Allock R, Sayer D, Garlepp M, Kok CC, et al. The genetic basis for the association of the 8.1 ancestral haplotype (A1, B8, DR3) with multiple immunopathological diseases. *Immunol Rev* (1999) 167(1):257–74. doi: 10.1111/j.1600-065x.1999.tb01398.x

15. Allcock RJ, Williams JH, Price P. The central MHC gene, BAT1, may encode a protein that down-regulates cytokine production. *Genes to Cells* (2001) 6(5):487–94. doi: 10.1046/j.1365-2443.2001.00435.x

16. Mendonça VRR, Souza LCL, Garcia GC, Magalhães BML, Lacerda MVG, Andrade BB, et al. DDX39B (BAT1), TNF and IL6 gene polymorphisms and association with clinical outcomes of patients with plasmodium vivax malaria. *Malaria J* (2014) 13(1):1–14. doi: 10.1186/1475-2875-13-278

17. Quiñones-Lombraña A. BAT1 promoter polymorphism is associated with rheumatoid arthritis susceptibility. *J Rheumatol* (2008) 35(701):4.

18. Ramasawmy R, Cunha-Neto E, Faé KC, Müller NG, Cavalcanti VL, Drigo SA, et al. *bat1*, a putative anti-inflammatory gene, is associated with chronic chagas cardiomyopathy. *J Infect Diseases.* (2006) 193(10):1394–9. doi: 10.1086/503368

19. Wong AM-L, Allcock RJ, Cheong KY, Christiansen FT, Price P. Alleles of the proximal promoter of BAT1, a putative anti-inflammatory gene adjacent to the TNF cluster, reduce transcription on a disease-associated MHC haplotype. *Genes to Cells* (2003) 8(4):403–12. doi: 10.1046/j.1365-2443.2002.00641.x

20. Price P. Polymorphisms at positions -22 and -348 in the promoter of the BAT1 gene affect transcription and the binding of nuclear factors. *Hum Mol Genet* (2004) 13(9):967–74. doi: 10.1093/hmg/ddh113

21. Degli-Esposti MA, Leelayuwat C, Dawkins RL. Ancestral haplotypes carry haplotypic and haplospecific polymorphisms of BAT1: Possible relevance to autoimmune disease. *Eur J Immunogenetics.* (1992) 19(3):121–7. doi: 10.1111/j.1744-313X.1992.tb00051.x

22. Roche J. The epithelial-to-Mesenchymal transition in cancer. *Cancers (Basel)* (2018) 10:52. doi: 10.3390/cancers10020052

23. Gilles C, Newgreen DF, Sato H, Thompson EW. *Matrix metalloproteases and epithelial-to-mesenchymal transition: Implications for carcinoma metastasis*. Austin, TX: Landes Bioscience (2013). pp. 297–315.

24. Moustakas A, De Herreros AG. Epithelial–mesenchymal transition in cancer. *Mol Oncol* (2017) 11:715–7. doi: 10.1002/1878-0261.12094

25. Nissisen L, Kahari V. Matrix metalloproteinases in inflammation. *Biochim Biophys Acta (BBA) - Gen Subj* (1840) 2014:2571–80. doi: 10.1016/j.semcdb.2007.07.003

26. Manicone A, Mcguire J. Matrix metalloproteinases as modulators of inflammation. *Semin Cell Dev Biol* (2008) 19(1):34–41. doi: 10.3389/fphar.2012.00140

27. Noël A, Gutiérrez-Fernández A, Sounni NE, Behrendt N, Maquoi E, Lund IK, et al. New and paradoxical roles of matrix metalloproteinases in the tumor microenvironment. *Front Pharmacol* (2012) 3. doi: 10.1002/pros.10194

28. Jung M, Römer A, Keyszer G, Lein M, Kristiansen G, Schnorr D, et al. MRNA expression of the five membrane-type matrix metalloproteinases MT1-MT5 in human prostatic cell lines and their down-regulation in human malignant prostatic tissue. *Prostate* (2003) 55(2):89–98. doi: 10.1038/sj.pcan.4500609

29. Daja MM, Niu X, Zhao Z, Brown JM, Russell PJ. Characterization of expression of matrix metalloproteinases and tissue inhibitors of metalloproteinases in prostate cancer cell lines. *Prostate Cancer Prostatic Diseases* (2003) 6(1):15–26. doi: 10.1158/0008-5472.CAN-09-3515

30. Littlepage LE, Sternlicht MD, Rougier N, Phillips J, Gallo E, Yu Y, et al. Matrix metalloproteinases contribute distinct roles in neuroendocrine prostate carcinogenesis, metastasis, and angiogenesis progression. *Cancer Res* (2010) 70 (6):2224–34. doi: 10.1158/0008-5472.CAN-09-3515

31. Escaff S, Fernández JM, González LO, Suárez A, González-Reyes S, González JM, et al. Comparative study of stromal metalloproteases expression in patients with benign hyperplasia and prostate cancer. *J Cancer Res Clin Oncol* (2010) 137 (3):551–5. doi: 10.2741/2161

32. Le NTV. The dual personalities of matrix metalloproteinases in inflammation. *Front Bioscience.* (2007) 12(1):1475. doi: 10.1002/pros.23056

33. Adissu HA, McKerlie C, Di Grappa M, Waterhouse P, Xu Q, Fang H, et al. Timp3 loss accelerates tumour invasion and increases prostate inflammation in a mouse model of prostate cancer. *Prostate* (2015) 75(16):1831–43. doi: 10.1002/pros.23056

34. Isaacs JT, Hukku B. Nonrandom involvement of chromosome 4 in the progression of rat prostatic cancer. *Prostate* (1988) 13(2):165–88. doi: 10.1002/pros.2990130208

35. Wu Y, Zhou BP. Inflammation: a driving force speeds cancer metastasis. *Cell Cycle* (2009) 8(20):3267–73. doi: 10.4161/cc.8.20.9699

36. Galarza-Muñoz G, Briggs FBS, Evsyukova I, Schott-Lerner G, Kennedy EM, Nyanhete T, et al. Human epistatic interaction controls IL7R splicing and increases multiple sclerosis risk. *Cell* (2017) 169(1):72–84.e13. doi: 10.1016/j.cell.2017.03.007

37. Hanahan D, Weinberg RA. Hallmarks of cancer: the next generation. *Cell* (2011) 144(5):646–74. doi: 10.1016/j.cell.2011.02.013

38. Hanahan D, Weinberg RA. The hallmarks of cancer. *Cell* (2000) 100(1):57–70. doi: 10.1016/s0092-8674(00)81683-9

39. Shang GS, Liu L, Qin YW. IL-6 and TNF-α promote metastasis of lung cancer by inducing epithelial-mesenchymal transition. *Oncol Lett* (2017) 13 (6):4657–60. doi: 10.3892/ol.2017.6048

40. Aung PP, Oue N, Mitani Y, Nakayama H, Yoshida K, Noguchi T, et al. Systematic search for gastric cancer-specific genes based on SAGE data: melanoma inhibitory activity and matrix metalloproteinase-10 are novel prognostic factors in patients with gastric cancer. *Oncogene* (2006) 25(17):2546–57. doi: 10.1038/sj.onc.1209279

41. Zhang X, Yin P DID, Luo G, Zheng L, Wei J, Zhang J, et al. IL-6 regulates MMP-10 expression *via* JAK2/STAT3 signaling pathway in a human lung adenocarcinoma cell line. *Anticancer Res* (2009) 29(11):4497–501. doi: 10.1186/1471-2407-14-310

42. Zhang G, Miyake M, Lawton A, Goodison S, Rosser CJ. Matrix metalloproteinase-10 promotes tumor progression through regulation of angiogenic and apoptotic pathways in cervical tumors. *BMC Cancer* (2014) 14:310. doi: 10.1186/1471-2407-14-310

Frontiers in Oncology

Advances knowledge of carcinogenesis and tumor progression for better treatment and management

The third most-cited oncology journal, which highlights research in carcinogenesis and tumor progression, bridging the gap between basic research and applications to imrpove diagnosis, therapeutics and management strategies.

Discover the latest Research Topics

See more →

Frontiers

Avenue du Tribunal-Fédéral 34
1005 Lausanne, Switzerland
frontiersin.org

Contact us

+41 (0)21 510 17 00
frontiersin.org/about/contact